SRFME is a joint venture
between CSIRO and the
Western Australian government

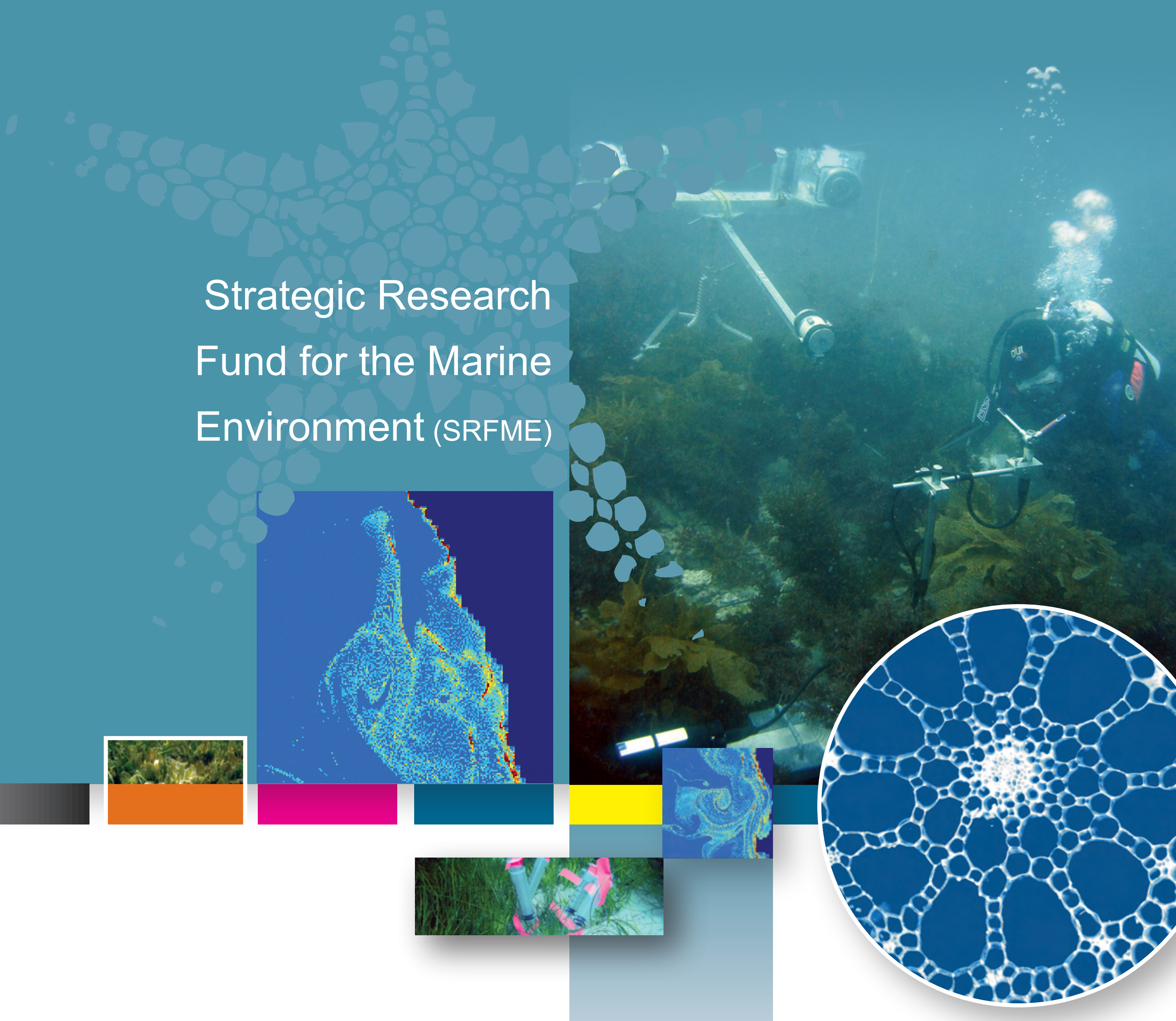

Strategic Research Fund for the Marine Environment (SRFME)

Final report volume two

December 2006

the SRFME core projects

Edited by John K. Keesing, John N. Heine, Russell C. Babcock, Peter D. Craig and J. Anthony Koslow **CSIRO** Marine and Atmospheric Research

Strategic Research Fund for the Marine Environment (SRFME)

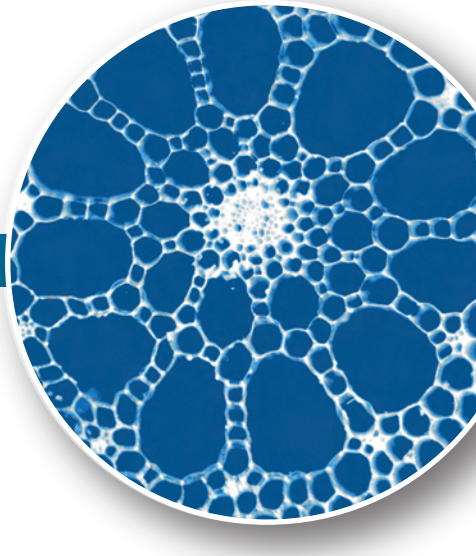

Final report **December 2006**
volume **two**

Edited by John K. Keesing, John N. Heine,
Russell C. Babcock, Peter D. Craig and J. Anthony Koslow **CSIRO** Marine and Atmospheric Research

© Copyright Strategic Research Fund for the Marine Environment 2006

This book may be used for research or individual study and educational purposes. Properly acknowledged quotations may be made, but enquiries regarding the republication of any material or requests for additional copies of this report should be addressed to:

Strategic Research Fund for the Marine Environment
CSIRO Marine and Atmospheric Research
Private Bag 5 Wembley 6913 AUSTRALIA

Full copies of this report may also be downloaded from www.srfme.com.au

National Library of Australia
Cataloguing-in-Publication data:

Strategic Research Fund for the Marine Environment (SRFME) :

final report. Vol. 2, The SRFME core projects.

ISBN 1 921061 93 6

1. CSIRO - Appropriations and expenditures. 2. Marine

sciences - Research - Western Australia - Finance. 3.

Marine resources - Research - Western Australia - Finance.

I. Keesing, John K. II. CSIRO.

354.5709941

Published by Strategic Research Fund for the Marine Environment, CSIRO, Australia

For bibliographic purposes, this report may be cited either as an entire volume, eg.:

Keesing J.K, Heine, J.N, Babcock, R.C., Craig, P.D. and Koslow, J.A. (2006). Strategic Research Fund for the Marine Environment Final Report. Volume 2: the SRFME core projects 274p. Strategic Research Fund for the Marine Environment, CSIRO, Australia.

or where referring to specific sections we would encourage the following form of citation; eg.:

Wild-Allen, K and Rosebrock, R. (2006). A Regional 3-D hydrodynamic-coupled biogeochemical model. pp 166-183. In: Keesing J.K, Heine, J.N, Babcock, R.C., Craig, P.D. and Koslow, J.A. Strategic Research Fund for the Marine Environment Final Report. Volume 2: the SRFME core projects 274p. Strategic Research Fund for the Marine Environment, CSIRO, Australia

Preface

The Strategic Research Fund for the Marine Environment (SRFME) was established as a joint venture by the Western Australian State Government and the CSIRO in 2001 with the aims of building capability and capacity in marine science in Western Australia through the reestablishment of CSIRO's marine research capability and the training of postgraduate students, facilitating strong collaboration among the Western Australian marine science community, and conducting strategic research that is of benefit to Western Australia.

These two volumes comprise the Final Report of SRFME. Volume 1 outlines the establishment of SRFME, the development of its research framework and research portfolio as well as its structure and governance in chapter 1 and details the SRFME Collaborative Linkages Program which was comprised of a set of PhD Scholarship Projects (chapter 2), SRFME Collaborative Projects (chapter 3) and SRFME State Linkage Projects (chapter 4). Volume 1 also introduces the SRFME Core Projects (chapter 5) and concludes with a list of publications arising from SRFME (chapter 6). Volume 2 of the SRFME Final Report comprises an overview summary (chapter 1), followed by detailed chapters on the scientific research conducted in the areas of physical oceanography (chapter 2), coastal and continental shelf pelagic community structure (chapter 3), coastal and continental shelf biogeochemistry and modelling (chapter 4), coastal benthic ecosystem structure and dynamics (chapters 5 and 6) and concludes with a description of the data archiving systems and the interactive data and model output visualisation software developed in SRFME (chapter 7).

A list of acknowledgements to the many people who have contributed to the success of SRFME is included elsewhere in this final report, but I would like to make special mention of a few in particular, whose support to me in my role as SRFME Research Director has been invaluable. I would like to thank Dr Nan Bray (CSIRO) and Dr Sue Meek (WA Government) who had the vision to develop and establish SRFME, and subsequent senior people in the WA State Government; Dr Bruce Hobbs, and CSIRO; Dr Greg Ayers, John Gunn, Dr Tony Haymet, Tim Moltmann, Dr John Parslow, Dr Ian Poiner and Craig Roy who all provided tremendous support. I would also like to thank other members of the SRFME Joint Venture Management Committee and Technical Advisory Committee, especially Dr Ray Masini, Peter Millington, Phillip Murray, Linda Penny and Dr Chris Simpson for their support and advice, CSIRO project Leaders; Dr Russ Babcock, Dr Peter Craig, and Dr Tony Koslow for their excellent science leadership, Lucy Kay for her tireless work for SRFME and John Heine for producing the final report.

Dr John Keesing

Research Director
Strategic Research Fund for the Marine Environment

31 December 2006

Foreword

Premier of Western Australia

FOREWORD BY THE PREMIER OF WESTERN AUSTRALIA
HON ALAN CARPENTER MLA

The $20 million Strategic Research Fund for the Marine Environment (SRFME) was established as a joint venture between the State Government of Western Australia and the CSIRO. Through this partnership, each invested $10 million to build capability and capacity in marine science in Western Australia, facilitate strong collaboration among the Western Australian marine science community, and conduct strategic research that is of benefit to Western Australia.

The outcomes described in these two volumes of the SRFME Final Report, even at over 500 pages, seek only to summarise the vast amount of work undertaken in SRFME by CSIRO and its collaborators in Western Australian universities, State agencies and Museum. From this report, it is apparent that the goals for SRFME have been impressively exceeded.

Encouraged by the track record of success in SRFME, the State Government has recently announced investment of a further $21 million to establish the Western Australian Marine Science Institution (WAMSI). In doing so, they have demonstrated the Government's commitment to ensuring the capability and capacity for marine science in Western Australia is maintained and grown. Through WAMSI, the strategic research needs of the State will continue to be addressed and the strong partnerships, such as those established with the CSIRO through SRFME, will endure.

Through WAMSI, the Western Australian State Government looks forward to further outstanding marine science outcomes, from CSIRO and its collaborators, which contribute to the wise management of Western Australia's marine environment and the sustainable development of its natural resources.

Alan Carpenter MLA
PREMIER

30 JAN 2007

197 St George's Terrace, Perth, Western Australia 6000
Telephone (08) 9222 9888 Facsimile (08) 9322 1213 Email: wa-government@dpc.wa.gov.au
www.premier.wa.gov.au

Acknowledgements

Many people have contributed to the establishment and management of SRFME and the development of its research portfolio. Many more have participated in the many research projects funded by SRFME. In addition to the SRFME research teams, SRFME PhD students and their supervisors whose names are listed with their contributions to each of the chapters of this volume of the SRFME Final Report, we thank the following people who have contributed to the SRFME Joint Venture in a number of ways over the period of 2000 to 2006.

Kim Anderson, Department of Industry and Resources

Simon Allen, CSIRO

Dr Greg Ayers, CSIRO

Arthur Banks, CSIRO

Louise Bell, CSIRO

Pru Bonham, CSIRO

Dr Bernard Bowen, Chairman Marine Research Taskforce

Dr Nan Bray, CSIRO

Dr Alan Butler, CSIRO

Dr Ed Butler, CSIRO

Dr Nick Caputi, Department of Fisheries

Gary Carroll, CSIRO

Celine Chan, CSIRO

Graham Cobby, Department of Industry and Resources

Ian Cook, CSIRO

Dr Scott Condie, CSIRO

Jeff Cordell, CSIRO

Richard Craddock, Department of Industry and Resources

Dr George Cresswell, CSIRO

Lea Crosswell, CSIRO

Dr Nick D'Adamo, Department of Conservation and Land Management

Carl Davies, CSIRO

Peter Dunn, CSIRO

Siobhan Duffy, CSIRO

John Gunn, CSIRO

Peter Green, CSIRO

Kim Grey, CSIRO

Michael Harrison, CSIRO

Dr Tony Haymet, CSIRO

Dr Chad Hewitt, CSIRO

Dr Bruce Hobbs, Department of the Premier and Cabinet

Dr John Huisman, Murdoch University

Tennille Irvine, CSIRO

Neale Johnston, CSIRO

Lucy Kay, CSIRO

Hiski Kippo, CSIRO

Mark Lewis, CSIRO

Craig McCauley, CSIRO

James McLaughlin, CSIRO

Dr Mike Mackie, Department of Fisheries

Dr Ray Masini, Department of the Environment

Dr Sue Meek, Department of Commerce and Trade

Peter Millington, Department of Fisheries

Dr Des Mills, Department of the Environment

Don Michel, CSIRO

Toni Moate, CSIRO

Tim Mangan, CSIRO

Tim Moltmann, CSIRO

Michael Mulligan, Geraldton Port Authority

Phillip Murray,
Department of the Premier and Cabinet

Tim O'Sullivan, CSIRO

Angela Palmer, CSIRO

Dr John Parslow, CSIRO

Val Pearce, CSIRO

Lindsay Pender, CSIRO

Dr Jim Penn, Department of Fisheries

Ms Linda Penny,
Department of the Premier and Cabinet

Ron Plashke, CSIRO

Dr Ian Poiner, CSIRO

Jane Pollock, CSIRO

Pam Powell, CSIRO

Dr Andrew Revill

Craig Roy, CSIRO

Dr Keith Sainsbury, CSIRO

Dr Cameron Sim, Department of the Environment

Dr Chris Simpson, Department of Conservation and Land Management

Dirk Slawinski, CSIRO

Dr Peter Thompson, CSIRO

Paul Tzaikos, Department of Industry and Technology

Dr Paul Vogel, Department of Environment and Water

Bernadette Waugh, CSIRO

Dr Paul Wellings, CSIRO

Dr Fred Wells, WA Museum

Dr Kate Wilson, CSIRO

Dr Jackie Zanetti, CSIRO

Contents - volume two

CHAPTER 1

1. INTRODUCTION AND SYNOPSIS

Investigators / Institutions

John Keesing, Russ Babcock, Peter Craig, Tony Koslow

CSIRO Marine and Atmospheric Research

Introduction

The research projects in the Strategic Research Fund for the Marine Environment (SRFME) have contributed significantly to our understanding of the marine environment of south-western Australia. Combining physical and biological oceanography with marine chemistry, biology and ecology, this research, and the future studies and publications that arise from it, will better inform decisions in managing, developing and protecting the WA marine environment.

In this volume we provide an overview of the research conducted by CSIRO and its collaborators in WA Universities and State government agencies in SRFME. Most of this research was conducted from 2002 to 2005. This volume comprises 7 chapters. Following this introduction and summary, chapter 2 covers the physical oceanography of the south-western Australian shelf region, and chapter 3 outlines the results of our extensive biophysical characterisation of the pelagic components of the ecosystem off southwestern Australia. Chapter 4 covers coastal and shelf biogeochemistry and modelling and seeks to integrate and synthesize much of the work in earlier chapters. Chapter 5 explores the structure of the benthic ecosystem off southwestern Australia including the spatial and temporal variability in marine animal and plant diversity. Chapter 6 then describes the dynamics of these benthic environments and the processes that give rise to the observed spatial patterns. Finally, in chapter 7, we outline how the data collected during these studies is archived and describe the innovative tools that have been developed to help visualize the data and model outputs.

The Leeuwin Current

In structuring this overview, we start with the physical oceanographic influences on the Western Australian marine ecosystems before moving on to examine the biogeochemical components of the pelagic and benthic parts of the ecosystem, including aspects of their dynamics and ecological interactions. Western Australian marine ecosystems are directly, and measurably, affected by hydrodynamic processes at a wide range of scales, from the circulation in the Pacific and Indian Oceans, down to turbulence from individual waves crossing the reefs. Time-scales range from the seconds associated with breaking waves up to the decades associated with climate change. Research in SRFME has increased our understanding of the oceanography at all of these scales. At decadal to century time-scales, the water temperature at coastal stations in the region has risen by around 0.017 ºC per year over the last 50 years, consistent with the global temperature rise attributed to climate change. At the same time, salinity off the WA coast has also increased. Sea-level at Fremantle is rising at about 1.5 mm per year. There is also a clear suggestion of a lengthening warm season. As in other parts of the world, Western Australia will need to determine how it will respond to a changed climate, and marine studies will be vital to ensure that industry and the community have adequate time and information to adapt. How the Western Australian marine environment will change as a result of climate change remains a great unknown.

The Leeuwin Current is profoundly influential on the marine ecosystems of Western Australia. As one of very few poleward-flowing eastern boundary currents in the world, it has been the subject of much research. SRFME studies have quantified both the annual and ENSO-related interannual variations of the Leeuwin Current, and the relationship between the Fremantle sea level and the strength (volume transport) of the Current. These results justify the usage of the Fremantle sea-level as an index for the Leeuwin Current, that has been widely used in fisheries management in Western Australia, especially for predicting western rock lobster recruitment. The Leeuwin Current is about 40% stronger during a La Nina year than during an El Nino. The Current responds as well to a smaller signal called the Pacific Decadal Oscillation, which can also be monitored by the Fremantle sea-level.

The average flow rate of the Leeuwin Current, estimated from long-term, ship-based measurements, is about 3.4×10^6 m^3s^{-1}. An increase in the flow rate of 1 million m^3s^{-1} is reflected by an increased Fremantle sea-level of about 7.5 cm. The strength of the current varies by about a factor of 2 over the year, being strongest in winter and weakest in summer, when it is opposed by southerly winds. These summertime winds may generate northward coastal currents that have been given local names such as the Capes and Abrolhos Currents.

SRFME research has determined that the extent of influence of the Leeuwin Current is much greater than previously envisaged. During the winter, the Leeuwin Current turns east past Cape Leeuwin, and can be tracked, in satellite images of surface temperature and height, all the way to southern Tasmania, a distance of 5500 km from North West Cape, making it the world's longest current. Its name changes to the South Australian Current, and then the Zeehan Current, over this distance.

Eddies form south of the Abrolhos Islands (29ºS) from meanders of the Leeuwin Current. The eddies are studied primarily from satellite altimetry, and are more intense when the Leeuwin Current is strongest, in the winter and in La Nina years. Warm-core eddies drift from the shelf offshore and may persist for months. Approximately six warm-core eddies form each year, carrying a total volume of water roughly equivalent to flushing the southern shelf twice per year. The eddies are believed to carry nutrients and phytoplankton from inshore waters, significantly enhancing offshore primary production, and probably play a significant role in the advection of larvae. Significant advances in the understanding of these eddies and their importance to the southwestern Australian continental shelf ecosystem have resulted from SRFME studies. This work is described in part in both volumes 1 and 2 of the SRFME Final Report and is to be documented in a special issue of the journal *Deep Sea Research.*

The Leeuwin Current is apparent in images of both sea-surface temperature and sea-surface height. As part of SRFME, an accurate numerical (hydrodynamic) model of the Leeuwin Current has been developed, at 10 km horizontal resolution, by forcing it with the surface observations, and using the model equations to calculate the 3-dimensional current and density fields. The model has been validated against ship-based observations of eddies, and inshore moorings.

Three moorings were deployed across the shelf from Two Rocks in water depths of 20 m, 40 m and 100 m, and maintained for a year, primarily recording currents and water temperature. At the innermost mooring (approx. 5 km offshore), the currents follow the wind direction, principally north in the summer and south in the winter, with the current speed close to 3% of the wind speed. At the 100 m mooring, about 50 km offshore, surface waters tend to follow the wind direction, while waters below 50 m flow south under the influence of the Leeuwin Current. The water is warmer and saltier inshore during the summer, but during the winter the Leeuwin Current keeps the offshore water warmer. In summer, the surface water in 100 m is about 2 ºC warmer than the bottom, but the water is well-mixed during the winter.

Biogeochemistry

Two Rocks was also the base for a major SRFME measurement program along a transect from nearshore to the outer continental shelf (100 m water depth). The transect was occupied monthly from 2002 – 2004, with a quarterly extension to offshore waters (1000 m depth). Cruise sampling was combined with satellite observations of sea-surface temperature (SST), ocean colour and altimetry, and subsurface measurements of currents and temperature from the moorings to provide both a cross-sectional description of the physics and productivity, and verification data for the modelling.

The Two Rocks transect data reveal that summer conditions on the shelf and offshore were oligotrophic, characterized by a shallow upper mixed layer, with a strong thermocline and well stratified water column. Surface waters were nitrate-depleted and generally contained low phytoplankton biomass levels (< 0.2 mg m^{-3}), overlying a deep chlorophyll maximum (DCM) layer located between the 0.1% and 1.0% light levels. The DCM was frequently associated with a deep nitracline (between 100 and 150 m water depth). By contrast, in late autumn and winter, the upper mixed layer deepened and stratification weakened, leading to shoaling of the nitracline and DCM. Except within the lagoon, where no clear seasonal cycle was observed, phytoplankton biomass integrated through the water column was generally twice as high from April – September as in the spring and summer (October – February).

Satellite data reveal the spatial extent of the dynamics observed at the transect. Near-surface chlorophyll-*a*, an indicator of phytoplankton biomass, can be inferred from ocean-colour sensors mounted on satellites. Over the continental shelf, phytoplankton production appears to peak during the late autumn and early winter, corresponding to the onset of winter storms and the seasonal strengthening of the Leeuwin Current and its eddy field. Further offshore, the phytoplankton biomass peaks in late winter, assisted by the eddies' transport of both nutrients and phytoplankton from the shelf. Deeper mixing during winter is also likely to enhance nutrient levels. The offshore flux of phytoplankton biomass by the warm-core eddies is estimated as equivalent to about 4×10^5 tonnes of carbon per year.

A relatively simple, one-dimensional, biophysical model has been developed during SRFME to demonstrate the importance of spinup over the shelf for warm-core eddies. The model represents an eddy as a trapped body of water and follows it as it detaches from the Leeuwin current and moves offshore. Given appropriate density and nutrient properties during eddy formation, the model successfully distinguishes between the productivity of the warm and cold-core eddies as they evolve. Cold-core eddies tend to spin up on the low-nutrient, seaward side of the Leeuwin Current.

High-nutrient water below the nutricline is not considered to contribute directly to the shelf, because the Leeuwin Current inhibits upwelling. However, vertical mixing, associated both with storms and the increased intensity of the Leeuwin Current, is thought to bring nutrients locally towards the surface, into the photic zone, during autumn and winter.

The role of vertical mixing on the biogeochemistry was also tested with a simplified one-dimensional biogeochemical model. The model was set up to simulate the upper 200 m at station E, the outermost station on the transect, 85 km offshore and in 1000 m of water, for the year 2003. Vertical mixing due to atmospheric conditions and the Leeuwin Current was simulated by forcing ("relaxing") the vertical temperature and salinity profiles to synTS (a technique which, given the surface height and temperature, derives T and S profiles from historical data sets).

There were only 5 transects to Station E during 2003, providing limited data for comparison. The model appears to predict well (given only 5 comparison points) the measured seasonal cycle of temperature. It predicts the stable summertime nutrient profile with a deep (100 m) chlorophyll maximum, and the transition to a surface bloom in autumn. It failed to predict the deep chlorophyll maximum observed in late winter. The winter observation corresponded to an exceptional cold event (2 °C cooler at 100 m depth), relative to synTS predictions, and may have been associated with an eastward migration of the Leeuwin Current, obviously beyond the scope of a 1-d model.

Thus, the late-autumn and early-winter bloom appears to be at least partially explained by enhanced vertical mixing, and the transport, by eddies, of nutrient-rich water from the shelf. It is also possible that the intensified Leeuwin may entrain nutrients in the north, where the nutricline is shallower, and advect them southward.

One of the main roles of the SRFME hydrodynamic model was to provide the ocean-forcing for a fully 3-dimensional biogeochemical model. The biogeochemical model simulates the cycling of carbon, nitrogen and oxygen through the water column and sediments. Its primary output is phytoplankton biomass, and its key initial challenge is to represent the seasonal cycle of phytoplankton productivity as observed from satellites and measurements from the Two Rocks transect. The model appears to simulate the large-scale variability, with low productivity in the summer and blooms in the late autumn and winter. However, it does not reproduce the high inshore productivity visible in satellite images for autumn and winter.

Nutrient sources remain a significant unknown for the coastal and shelf biogeochemistry. The inshore productivity is assumed to be due to onshore or nearshore sources that are not sufficiently identified or quantified to be included in the model. Nutrients will also be stored in coastal and shelf sediments, and presumably released during high wave and swell conditions. Sensitivity tests with the model indicate the likely importance of nutrient storage in the sediments, but the magnitude of the store is unquantified. Further, the large-scale nutrient distribution, required for both initialising the model, and for its open boundary conditions, is not well established. The hydrodynamic model currently uses temperature and salinity fields predicted from synTS. The model can also access CSIRO's global BLUElink model for initial and open boundary conditions. Equivalent fields for nutrients do not yet exist.

Plankton Ecology

Measurements along the Two Rocks transect indicate that phytoplankton biomass and production integrated through the water column were generally several-fold higher offshore, although maximum volumetric chlorophyll concentrations were observed inshore. Depth-integrated chlorophyll concentrations on the shelf and offshore generally ranged from 20 – 40 mg chl *a* m^{-2}, compared to 5 – 15 mg chl *a* m^{-2} inshore. This difference was considerably reduced in spring and summer, because the seasonal cycle was less pronounced in the lagoon environment. Annual phytoplankton production over the study period was 46 g C$\cdot$m$^{-2}\cdot$yr^{-1} inshore and about 115 g C$\cdot$m$^{-2}\cdot$yr^{-1} on the shelf and offshore—relatively oligotrophic for a coastal environment. Not unexpectedly, given the nutrient depleted conditions generally observed in the euphotic zone, biomass and production were far greater in the small phytoplankton size fraction (< 5 μm): the median percentage of biomass and primary productivity in the small size fraction was 5 and 12%, respectively. Based on analysis of HPLC pigments, the outer shelf and offshore stations were characterised by high prochlorophyte and unicellular cyanobacteria populations. Small flagellates were most prevalent on the shelf, and periodic blooms of larger diatoms dominated inshore waters. Small haptophytes were ubiquitous.

Zooplankton biomass was also generally greatest in late autumn and winter. The assemblages differed significantly in nearshore and shelf/offshore waters and between winter and other seasons, following patterns among species groups observed elsewhere in coastal waters.

Microzooplankton biomass peaked in winter, consistent with the winter peak in chlorophyll. Species richness was significantly higher on the shelf and offshore than nearshore, which was ascribed to the generally less stable inshore environment. Dilution experiments indicated that the microzooplankton consumed, on average, 60% of primary production. Growth of the picoplankton was particularly closely coupled with microzooplankton grazing.

The impact of grazing of mesozooplankton on the phytoplankton was generally low, but the impact on the microzooplankton increased with distance offshore. Incubation experiments showed that increased densities of mesozooplankton grazed down an increased proportion of the microzooplankton, which led to a decrease in grazing on phytoplankton.

Particularly clear trends in onshore-offshore and seasonal assemblages were seen in the ichthyoplankton. These trends were related to water mass structure and the seasonal characteristics of spawning in the region. The inshore region was characterized by reef fishes, such as gobies, clinids, blennies and tripterygiids, whereas pelagic fishes, such as clupeids and carangids, dominated over the shelf. Oceanic fishes, such as myctophids, phosichthyids and gonostomatids dominated the ichthyoplankton at the shelf break and over the slope. However the changing seasonal dynamics of the Leeuwin and Capes Currents were clearly reflected in the ichthyofauna assemblages.

Benthic Ecology

Towards the coastline, the seabed falls within the photic layer, and macrophyte productivity begins to dominate phytoplankton productivity. SRFME made significant advances in our knowledge of the patterns found in the benthic components of Western Australia's marine ecosystems and the underlying processes and dynamics that give rise to these patterns and the variability exhibited in benthic communities. Western Australia is unusual in possessing high-biomass, high-productivity benthic ecosystems despite the relatively low-nutrient levels that result from the low-rainfall climate and the influence of the Leeuwin Current.

SRFME focused on improving understanding of one major habitat type – coastal rocky reefs – that had previously received relatively little attention. Rocky reefs are an important habitat type in nearshore coastal waters, supporting a diverse assemblage of benthic macroalgae and associated fish and invertebrates. The rocky reef communities are a key component of coastal productivity, provide habitat and food for marine fauna, contribute to biogeochemical cycles, and can exert influence over nearby habitats such as seagrass meadows. Despite their recognised importance, comparatively little is known of the ecology of rocky reef habitats along the lower west coast of Western Australia.

SRFME research incorporated the first quantitative, broad-scale investigations of several key ecological processes on the reef benthos of south-western Australia. Major findings were that spatial gradients in wave exposure were significantly correlated with spatial patterns in the species richness and composition of macroalgae, that the rates of some ecological processes (e.g. algal productivity) and the abundances of both mobile and sessile fauna vary significantly between inshore and offshore reefs, and that consumers (including humans) exert a significant influence on some reef-associated biota. The understanding of both pattern and process is essential to achieving the ultimate goal of modelling the coastal ecosystem and gaining the ability to predict ecosystem behaviour.

The benthic field sites were categorized into 3 "regions" – Jurien, Perth and Geographe Bay – within each of which there were two "locations" – Green Head and Jurien Bay, Two Rocks and Marmion, and Bunbury and Cape Naturaliste, respectively. Each location had two measurement "sites", within which quadrats were sampled.

There is a strong seasonal signal in algal biomass in all regions, but processes underlying this pattern varied for different locations, or for particular sites within locations depending on the dominant algal habitat type. Most locations (e.g. Jurien Bay, Marmion, Two Rocks and Bunbury) showed lowest biomass in winter. The proximal factors that drive these variations also differ among locations. Erosion of biomass is most likely to be driving changes in *Ecklonia*-dominated sites (Marmion, Two Rocks, Perth) while light-limitation is likely to be a major factor at Bunbury. Here, seasonal resuspension of particulate matter and sediment by winter and spring storms and swell appears to affect the entire algal community, which is largely made up of foliose red and brown algae. At sites where *Sargassum* dominates (Green Head), there is a summer minimum in biomass because of the algal phenology. In contrast to the pattern for biomass, algal community structure showed no seasonal trend.

Among the study regions, the overall number of algal species recorded was similar. In all the regions, by far the largest contribution to overall species diversity was made by the red algae. While variations in species richness were not large, more species were recorded at the lower latitude sites, and fewer recorded in the Perth region. This may be explained by variation in the relative dominance of large brown algae in the different regions, since there is an inverse relationship between *Ecklonia* biomass and that of red algae. The highest densities of *Ecklonia* were found at reefs in the Perth region.

Macroalgal community structure varied at all the spatial scales we examined, but was strongest at the site level. In fact, at the site level, the differences between sites, even within locations, was greater than the differences between sites at the most widely separated regions. This strongly suggests that, for algal community structure, processes operating or varying across relatively small scales may be responsible for much of the observed variation observed. Assemblages not dominated by *Ecklonia* or other canopy species were most often composed of a diverse mixture of medium to small sized foliose algae, mainly red and brown, although green algae were occasionally dominant. Our study has shown that these habitats can on average form almost 50% of all algal communities, and are likely to be of greater importance than previously assumed in WA.

Since the nature of this variation was often associated with clear qualitative differences in community structure, for example, the presence or absence of a canopy, we developed a method to classify algal communities based on a semi-quantitative mix of structural and taxonomic attributes. The system was accurate in 75% of cases and offers a means of classifying algal assemblages for use in higher-level analysis of patterns at the landscape scale, and as a rapid system for visual quantification of habitats for mapping and ground-truthing (for example, in hyperspectral mapping).

A statistical model relating algal-assemblage structure to physical environmental variables in the Jurien region showed that the two factors most strongly associated with community structure were seabed roughness at the 1 m and 10 m scales, and modelled seabed orbital velocity. Wave-generated water movement across the seabed and small-scale seabed topography interact very strongly, further reinforcing the conclusion that small scale variations in ecological processes are likely to be of prime importance in determining the structure of benthic reef assemblages. Processes controlled by interactions of topography and water motion include physical disturbance (dislodgement), diffusive processes (gas and nutrient exchange) and sediment transport (scour and burial). It is important for us to understand this small scale variation in algal assemblages, as a basis for future work and for scaling up results to larger areas.

For invertebrates, weaker patterns in community structure were present, particularly for the algal-associated epifauna. Some pattern was present in the larger sessile and solitary fauna, but levels of similarity/dissimilarity did not vary markedly across scales. The lack of pattern suggests that the spatial scales encompassed in the sampling (regions, locations, sites), which was designed primarily to quantify algal assemblages, did not adequately capturing variation in the invertebrate assemblages.

However, informative patterns did emerge at different spatial scales. Species number varied according to the algal habitat type with epifaunal invertebrate species richness (at the scale of 0.25 m^2 quadrats) higher for turf habitats, followed by *Caulerpa*, *Ecklonia* forest, *Sargassum*, low algae, red foliose and mixed brown habitats. A higher number of solitary and sessile invertebrates (1 m^2 quadrat) were found to be associated with low algae and red foliose habitats, followed by mixed brown, turf, *Sargassum*, *Ecklonia* forest and *Caulerpa* habitats. As for the algae, the highest number of invertebrate species was recorded at Jurien, and Perth had the lowest numbers of species although numbers were only marginally greater at Geographe Bay. While the magnitude of the differences is relatively small, it is once again interesting that the region with the most *Ecklonia*-dominated sites had the lowest number of species.

For larger sessile invertebrates, belt transects revealed strong trends for coral and sponge abundance, within low algae and red foliose algal habitat types. Brown algal dominated habitats totalled 53% of habitats covered by transects at Marmion, yet within these transects only 22% of sponges and 7% of corals were recorded. These patterns essentially reflect algal habitat structure and coverage, and its patchiness or variability, not just at the site level but within sites. Interestingly a coral species (*Plesiastrea*) was one of the taxa most responsible for dissimilarity among sessile and solitary invertebrate assemblages at the site level. Sessile invertebrates such as corals and sponges may achieve a higher larval settlement rate, and/or higher subsequent survival and growth, in habitat that is lower and more sparsely covered by algae, in contrast to the typically dense, canopy forming brown algae species.

At the scale of individual quadrats, there were significant patterns in the overall abundance of mobile invertebrates, particularly molluscs and crustaceans. Most of these animals are relatively small and likely to be key contributors to secondary production in the reef ecosystem. This pattern resulted from a significant negative correlation between invertebrate abundance and the biomass of *Ecklonia radiata*, that has a key indirect influence on invertebrate assemblages.

Fish assemblages showed a contrasting pattern to those of algae and invertebrates, with a high level of variation among assemblages at the regional level and virtually none at the location level. However, at the site level there was once again significant variation in fish assemblages. We attribute this consistent variation at the site level to the association of fish assemblages with definable algal habitat types that tend to dominate at particular sites. While large brown algal assemblages dominated at just over half the sites, nearly as many sites were instead characterized by a diverse assemblage of foliose and filamentous red and brown algae.

At small scales across all three major groups we have studied, algae, invertebrates and fish, we see the importance, even dominance, of processes operating at distances of metres to tens of metres for structuring variation in benthic assemblages. This variation has important implications for understanding which ecological processes structure these communities. As noted, analysis of algal community structure strongly suggests that some aspect of wave action, coupled with the nature of the substratum, interact to determine the characteristics of the algal community. The characteristics of the algal community in turn appear to strongly determine the nature of invertebrate assemblages. For fish, these aspects of habitat also appear to be important, although in their case there may also be stronger large-scale biogeographic factors influencing distribution across the west coast region.

At the regional level, some locations have physical characteristics that mean larger-scale processes play a more important role. Variation in water quality in eastern Geographe Bay creates conditions that result in a seasonal change in algal biomass, quite distinct from other parts of the west coast. The implications of this unusual pattern merit further exploration. It is possible that elevated nitrogen levels in Perth metropolitan waters are linked in some way to the abundance of *Ecklonia*-dominated habitats at Marmion. For most of the coast, smaller-scale studies focused on the impact of environmental factors at the site, or even quadrat, scale are likely to lead to a broader general understanding of key ecological processes across the coastal ecosystem as a whole. The role of such small-scale processes, and of nutrients in coastal reef systems, remains an important area of research yet to be fully explored.

In December 2005, 4 acoustic doppler velocimeters, capable of measuring wave orbital velocities, were deployed across the Marmion reef to measure the cross-shore change in wave signature. The amplitude diminished by up to 1/3 as the waves travelled 1500 m across the reef. This behaviour was reproduced by a standard wave model (SWAN), but with enhanced bottom friction attributed to the reef roughness.

In these shallower waters, the water movement tends to be dominated by the effect of surface waves. The 20-m mooring on the Two Rocks transect included a pressure sensor to measure waves, and an acoustic doppler current profiler, which could be used to infer the sediment suspended from the seabed by the waves. The data were used to calibrate a sediment-transport model. They show that, at this inshore location, the waves are sufficiently energetic to keep medium-sized sand mobile most of the time.

South and north of Perth, the sediment mobility was examined by nesting a local wave model (SWAN) inside a global model (WAVEWATCH 3). The modelling suggests high levels of sand mobility (>60% of the time) in Geographe Bay throughout the year, with an increase (to 80%) in the winter. There is a small area in the lee of Cape Naturaliste where the mobility is much reduced. Mobility rates are also similar off Geraldton.

Exposure to waves affects the distribution of macroalgal species on the reefs. For Jurien Bay, the wave model was used to estimate exposure to large wave events at the 26 sites sampled during the benthic field program. The species diversity at the sites was positively correlated with wave disturbance; that is, the more exposed the site to large wave events, the higher the diversity. Presumably, the breakage and removal of plants by big waves increases opportunities for new species to establish. There is a suggestion that, at the highest exposure, diversity begins to diminish again, presumably because only the hardiest species survive under the most extreme conditions. This increase, and subsequent decrease in species diversity with increasing disturbance rate is a well-documented phenomenon, generally known as the *intermediate disturbance hypothesis.*

Accumulated wave exposure over an 8 year period provided a significantly better explanation of species richness patterns than wave-energy over a single year. This suggests that species richness of macroalgae might be the result of integration of processes occurring over years, rather than the result of short-term responses to disturbance.

The consequences of wave action for an individual alga include detachment from the substrate on which it grows. Our research showed that, once detached, kelps may drift for many kilometres. Substantial accumulations of detached reef algae occurred at an inshore reef, coinciding with high densities of sea urchins, which eat mainly detached fragments of algae. Analyses of the morphology of individual kelps at this location indicate that a large proportion originate from reefs several kilometres further offshore. These results demonstrate large-scale trophic linkages across the lagoon that are a result of wave action.

Trophic linkages such as these are likely to have profound implications for the function of WA's coastal ecosystems at broad scales. For example, differences between inshore and offshore reefs were observed for densities of sea urchins (higher densities inshore) and grazing on drift kelp by sea urchins (higher inshore), as well as for algal productivity and diversity. This overall trend might be a result of the gradient in wave action, and gradients in ecological processes that occur due to physical disturbance by waves, such as detachment and export of reef algae. Our measurements of rates of recruitment to collectors indicated that while rates were higher inshore, they were also highly variable. This suggests that densities of adult urchins inshore were not due to higher recruitment, but to the higher availability of food (drifting fragments of algae).

Primary productivity of *Ecklonia* was greater at Jurien than in the Perth Region. In addition, productivity was higher offshore at Jurien, but not in the Perth Region. These results suggest that nitrogen *per se* might not be limiting for growth of macroalgae on this coast since these productivity patterns are directly opposite to the C:N trends found in *Ecklonia* plants from these sites. The C:N values were far lower at Perth, than at Jurien — yet production was higher at Jurien. There is potential for anthropogenic nitrogen sources in the Perth region to enhance the growth of macroalgae which is worthy of further investigation. Nutrient levels offshore from Perth seem to be elevated and to carry a high level of $\delta^{15}N$, a sign of terrestrial effluent origins for this nitrogen. In addition, C:N ratios of kelps from both regions were lower inshore than offshore — yet production tended to be higher offshore, at least at Jurien. The most common paradigm for marine algae of all types is that their growth is nitrogen limited, yet our data contradict this assumption. The suggestion that availability of nitrogen might not be limiting growth of *Ecklonia* on the WA coast requires investigation through controlled experiments. Other potential influences on the rate of N uptake, such as light availability, and the role of wave-driven turbulence, must also be investigated.

Little of the *Ecklonia* primary productivity was directly consumed. The only direct grazing was by herbivorous fish. However, densities of herbivorous fish, and rates of grazing by herbivorous fishes, varied from reef to reef, and showed no broad trends. The highest rates of consumption of tethered kelps were on drifting fragments, and mainly by sea urchins. Similar observations have also been made in seagrass and intertidal habitats in the region. It is clear that detached macroalgae are ubiquitously important in sustaining coastal food webs on the Western Australian coast.

Humans can exert a strong influence on the structure of communities through harvesting of key species. For example, in several parts of the world, hunting and fishing has reduced predators of sea urchins to ecologically trivial abundances, resulting in increases in sea urchin density and landscape-scale decreases in canopy-forming primary producers due to grazing. Similar processes are possible in WA, and are a potential explanation for variation in the structure of assemblages of reef algae. SRFME research included the first assessment of the effects of a 16-year fishing closure (the Kingston Sanctuary at Rottnest Island) on assemblages of fish and invertebrates. The overall abundance of fish, abundance of predatory fish and western rock lobster (*Panulirus cygnus*) was higher inside the Kingston Sanctuary than at adjacent fished reefs. For fish, two popular angling species and four by-catch species were more abundant inside the sanctuary, while some bycatch species showed opposite patterns.

The differences in abundance of predatory fishes and lobsters were reflected by experimental predation rates on small and medium size invertebrates. The intensity of predation on tethered sea urchins was higher in the sanctuary. However, there were no simple trends in the abundance of prey: the abundance of one species of sea urchin (***Heliocidaris erythrogramma***) was lower in the area protected from fishing, consistent with the pattern predicted if predation was a strong influence, but the abundance of a second species (***Centrostephanus tenuispinus***) was higher. There was also no evidence of trophic-cascade effects outside the protected area as a result of lower abundance of predators, with no difference in assemblages of macroalgae between the sanctuary and fished areas.

The correlation between wave energy and both algal diversity, and community structure, plus the patchy nature of macroalgal assemblages, suggests that physical disturbance may have much more pervasive and important influences on benthic communities of WA coastal reefs than do top-down effects resulting from variations in predation. Curiously, bottom-up effects (supply of nutrients) also appear to have less influence on the structure of benthic assemblages than might be predicted in what has been assumed to be a nutrient-limited coastal ecosystem. The dynamics of patches and the influence of varying nutrient availability require more detailed investigation before we can be certain of their impact on the dynamics of WA coastal ecosystems.

Data storage and access

As a by-product of its research, SRFME has set high standards in the archiving and documentation of data collected and has developed innovative tools for the visualisation and analysis of data and model outputs.

The SRFME field and model data have been stored in standard formats (mostly NetCDF and ASCII column-files) in a data repository that is accessible for visualisation by the software DIVE (Data Interrogation and Visualisation Environment). DIVE enables data from different sources (such as models, vessels, moorings and diving), to be overlaid and compared in up to 4 dimensions. The DIVE software has been supplied to State Agencies to give them direct access to the SRFME data set.

DIVE is supplemented by other software tools developed during SRFME. WebOLIVE is a web-based visualisation program for regularly gridded data such as model output and climatology. WebOLIVE is installed on the SRFME website. Aus-Connie (The Australian Connectivity Interface, *http://www.per.marine.csiro.au/aus-connie*) allows users to investigate large-scale patterns of spatial connectivity around Australia. It provides estimates of the probability that any two regions are connected by ocean circulation. Meanwhile, the Argo website (*http://www.per.marine.csiro.au/argo*) provides an interactive data explorer to display tracks and vertical profiles from over 100 Argo vertical profiling floats which have been deployed in the Indian and Southern Oceans.

SRFME also constructed high-resolution climatology for temperature, salinity, nitrate, phosphate, oxygen and silicate off the Western Australian coast. The SRFME-CSIRO Atlas for Regional Seas (CARS) covers the domain 110E-130E, 40S-10S at one-eighth-degree resolution, with data at 56 standard depths. SRFME CARS is available at *http://www.per.marine.csiro.au/SRFME-modelling/olive_atlas.html*

Conclusion

While SRFME has made very significant advances in our understanding of many aspects of Western Australian marine ecosystems, much remains to be done. The area is known for its unique oceanography, productive benthic ecosystems and as a biodiversity “hotspot” worthy of significant conservation measures. However, the area is also one that creates great wealth for Australia through the exploitation of its natural resources and, increasingly, nature-based tourism. Achieving the right balance of these activities and ensuring their sustainability is a major challenge, particularly as the population of Western Australia's coastal regions is growing rapidly. As the coastal population grows, so too will pressures on the coastal region. The range of often competing uses and cumulative impacts has the potential to degrade Western Australia's unique marine environment, if the coasts are not managed with care.

Continued high-quality strategic research like that conducted over the five years of SRFME can ensure that decision-making in the marine environment is based on continually improving knowledge of these marine systems. Thus, while this report closes a successful chapter in marine science in Western Australia, the need for strategic marine science remains as great today as when SRFME began. The chapters in this report outline where SRFME has advanced our knowledge of Western Australian marine ecosystems. In addition, the chapters set out a path for future strategic research to further understanding of these systems. In many cases, the new research needs to test hypotheses that have arisen in SRFME. It should also target our need to describe key processes in the marine environment, to enable us to better predict the response to future anthropogenic change.

CHAPTER 2

2. PHYSICAL OCEANOGRAPHY OF THE SOUTH WESTERN AUSTRALIAN SHELF

Investigators / Institutions

Ming Feng, Peter Craig (Project Leader), Chris Fandry, Jim Greenwood,
Nugzar Margvelashvili, Alan Pearce, Graham Symonds

CSIRO Marine and Atmospheric Research

Outline

Executive Summary

Executive Summary

The coastal marine region of southwestern Australia is affected by the very large scales of the Pacific and Indian Oceans, down to the small scales of waves crossing the reefs. There are significant time-scales from the seconds associated with breaking waves up to the decades associated with climate change. Capturing this range of scales involves a diversity of data sets collected from ships, moorings, and satellites, and generated by models.

At long time scales, the water temperature at coastal stations in the region rose by around 0.017 ^{o}C per year over the last 50 years, consistent with the global temperature rise attributed to climate change. At the same time, salinity off the WA coast has also increased. Sea-level at Fremantle is rising at about 1.5 mm per year. There is also a clear suggestion of a lengthening warm season.

The southward-flowing Leeuwin Current conveys much of the large-scale influence on the shelf/coast. The Fremantle sea-level is an indicator of the strength of the Leeuwin Current on timescales from days to years. The average flow rate of the current is about 3.4 x 10^6 m^3s^{-1}. An increase in the flow rate of 1 million m^3s^{-1} will be reflected by an increased Fremantle sea-level of about 7.5 cm. The strength of the current varies by about a factor of 2 over the year, being weakest in summer, when it is opposed by southerly winds, and strongest in winter. It is also about 40% stronger during a La Nina year than during an El Nino. The La Nina-El Nino oscillation is principally based in the Pacific Ocean, with a time-scale of several years. The Leeuwin Current also responds to a smaller signal called the Pacific Decadal Oscillation, which can also be monitored by the Fremantle sea-level.

Eddies form south of the Abrolhos Islands (29ºS) from meanders of the Leeuwin Current. The eddies are more intense when the Leeuwin Current is flowing strongest, in the winter and in La Nina years. Warm-core eddies drift from the shelf offshore and may persist for months. The eddy drift carries a volume of water roughly equivalent to flushing the southern shelf twice per year. The eddies are believed to carry nutrients and phytoplankton from inshore waters, significantly enhancing offshore primary production, and probably play a significant role in the advection of fish larvae.

Satellite technology enables the Leeuwin Current and its eddies to be observed at large scale, at least at the surface. The current is apparent in images of both sea-surface temperature and sea-surface height. The satellite data have been augmented by subsurface and inshore data collected from vessels, and by the deployment of moorings.

Three moorings were maintained for a year off the coast at Two Rocks. The moorings were at water depths of 20 m, 40 m and 100 m, and primarily recorded currents and temperature. At the innermost mooring (approx. 5 km offshore), the currents follow the wind direction, principally north in the summer and south in the winter, with the water speed close to 3% of the wind speed. At the 100 m mooring, about 50 km offshore, surface waters tend to follow the wind direction, while waters below 50 m flow south under the influence of the Leeuwin Current. Water temperatures are warmer inshore during the summer, but during the winter the Leeuwin Current keeps the offshore water warmer. The surface water in 100 m is about 2 ºC warmer than the bottom, but the water is well-mixed during the winter.

As the water shallows toward the shoreline, the water movement is increasingly dominated by the effect of surface waves. The 20-m mooring included a pressure sensor to measure waves, and an acoustic doppler current profiler, which could be used to infer the sediment suspended from the seabed by the waves and currents. The data were used to calibrate a sediment-transport model, which indicates that, at this inshore location, the waves are sufficiently energetic to keep the medium-sized sand particles mobile most of the time.

South and north of Perth, the sediment mobility was examined by nesting a local wave model (SWAN) inside a global model (WAVEWATCH 3). The modelling suggests high levels of sand mobility (>60% of the time) in Geographe Bay throughout the year, with an increase (to 80%) in the winter. There is a small area in the lee of Cape Naturaliste where the mobility is much reduced. Mobility rates are similar off Geraldton, although the high-mobility region is more limited in area during the summer.

In December 2005, 4 acoustic doppler velocimeters, capable of measuring wave orbital velocities, were deployed across the Marmion reef to measure the cross-shore change in wave signature. The amplitude diminished by up to 1/3 as the waves travelled 1500 m across the reef. This behaviour was reproduced by a standard wave model (SWAN). The longer-term intention is to quantify the relationship between the varying wave environment and the benthic habitat.

2.1 Introduction

Physical oceanography determines the environment in which marine organisms live. Ocean currents change the environment by moving constituents like heat, salt and nutrients. Currents also obviously carry drifting organisms themselves, including propagules. The fate of propagules in part determines the distribution of species along the coastline.

At large scale, the most prominent feature along the WA coastline is the Leeuwin Current, a warm, low-salinity current that flows southward along the shelf-break, strengthening in the winter, and weakening in summer. The Leeuwin Current responds to the very large-scale dynamics of the Indian and Pacific Oceans, and is strongest in the La Nina phase of the El Nino cycle. South of Geraldton, the current meanders and sheds eddies that may last for months as they drift offshore into the Indian Ocean. The eddies are thought to be a major mechanism for carrying nutrients and organisms across the continental shelf.

A well-known consequence of the Leeuwin Current is the high level of correlation between the Southern Oscillation Index (SOI, a measure of the El Nino cycle), the Fremantle sea-level and lobster larval recruitment on the WA coast (Pearce and Phillips, 1988). When the SOI is high (a La Nina), the Leeuwin Current is flowing strongly, Fremantle sea-level is up, and there is above-average recruitment of larval rock lobsters.

A key objective of SRFME was to better understand and characterise the Leeuwin Current. The results of this study are contained in the following sections. Section 2.2 describes the Leeuwin Current in detail, quantifying its flow rate and variability within the year and from year to year. It describes the connection to Fremantle sea-level, and the extension of the current that extends to western Tasmania. It also introduces the eddy energetics associated with the current, and the way this varies seasonally and interannually.

Section 2.3 considers the role of the Leeuwin Current eddies in transporting water and its constituents across the shelf. Warm-core (clockwise-rotating) eddies tend to be the most productive waters off the southwestern coast. They are formed over the shelf, principally in autumn and winter, and are thought to contribute to the general productivity of the Indian Ocean in this region. Chapters 3 and 4 deal in more detail with the primary productivity of the shelf and slope waters.

There are 2 sources of local long-term marine measurements. The first is Fremantle sea-level, which has been monitored since the late 19th century. The second is CSIRO's Rottnest station, in 50 m of water, which has been occupied, discontinuously, since 1951. Water level from the former, and temperature from the latter, reflect a signal that is attributed to climate change. The data also reveal the so-called Pacific Decadal Oscillation in the tropical Pacific. These long timescale events are discussed in Section 2.4. This is followed, in Section 2.5, by a brief discussion of a shorter-timescale (1-2 year) event called the Indian Ocean Dipole, which appears to be triggered by external forcing, e.g. the El Nino-Southern Oscillation in the Pacific.

On the inner continental shelf, the influence of the Leeuwin Current becomes less pronounced, and the local effects of wind, solar heating and evaporation become more important. The inshore physics were measured in SRFME on the regular Two Rocks transect (described in detail in Chapter 3), and particularly by the year-long deployment of three moorings across the shelf, to measure currents, temperature and salinity. The results of these studies, focussed more on the inner shelf, are presented in Section 2.6.

While wind, particularly, plays an increasingly important role in the ocean dynamics in shallower water, close inshore, surface waves also begin to dominate. If the waves actually break on fringing reefs, they will be almost totally responsible for pumping water into and out of the reef lagoon. Waves are likely to have a dramatic effect on benthic habitat, especially over the reefs. The characterisation of the wave dynamics, both at shelf and nearshore scales, was begun relatively late in SRFME, with the implementation of both measurement and modelling studies. The results to date are presented in Section 2.7.

The use of numerical models has been a key feature of the SRFME physical oceanography. Much of the analysis of the Leeuwin Current and its eddies is based on a relatively simple (geostrophic) model interpretation of satellite altimeter data. Further, as part of the study, a 10-km-resolution, fully 3-dimensional hydrodynamic model was implemented for the SRFME region. The primary role of this model has been to provide the physical setting for a biogeochemical model describing the nutrient dynamics and primary production over the SW WA continental shelf and slope. Details of the model are presented in Chapter 4.

A sediment model also forms part of the modelling package, as described in Section 2.8. Sea-bed sediments are lifted by waves, and then carried by currents. Sediment movement may result in change in substrate, light exclusion from the water, and redistribution of chemicals, including nutrients, that adsorb onto the particles. Understanding of sediment dynamics is essential for predicting, and managing, inshore waters.

2.2 The Leeuwin Current

The Leeuwin Current is a narrow and meandering eastern boundary current that flows southward along the continental shelf break off the Western Australian coast (Cresswell and Golding, 1980). An anomalously large meridional pressure gradient, set up by the warm, low-density tropical Pacific Ocean water entering the Indian Ocean through the Indonesian Archipelago (the Indonesian Throughflow) is believed to account for the existence of the Leeuwin Current (Godfrey and Ridgway, 1985). The meanders and eddies in the Leeuwin Current system are likely due to the instability of the current (e.g. Feng *et al.* 2005). The El Niño/Southern Oscillation (ENSO) related upper ocean variations propagate poleward as coastally-trapped waves along the northwest to western Australian coast as illustrated in Fig. 2.1 (Feng *et al.* 2003). The waves transmit high coastal sea-levels during the La Niña years and low sea levels during the El Niño years.

Pearce and Phillips (1988) hypothesized that coastal sea level at Fremantle could be a proxy for the Leeuwin Current strength. Interannual variability of the Fremantle sea level is highly correlated to the recruitment to a number of local fisheries, including the western rock lobster, Australia's most valuable single species fishery. Thus, the Fremantle sea level is used in fishery recruitment research to represent the Leeuwin Current strength (Caputi *et al.* 1995). However, the relationship between the Fremantle sea level and the Leeuwin Current still needs to be established, as does the effect of the Leeuwin Current variability on ecosystem processes and fisheries recruitment off Western Australia. The role of both eddies in the marine ecosystem off Western Australia, and the eddy-induced cross-shelf transport, have not been carefully quantified. Thus, there is a need to understand the annual and interannual variability of the Leeuwin Current and its eddy field, as well as their impacts on regional marine ecosystems and fisheries off Western Australia.

The aims of this study are two-fold: to understand and characterize the natural variability of the Leeuwin Current system, the mean flow and the eddy field, and the ENSO influence; and to understand and characterize the influences of the Leeuwin Current and its eddy field on the marine ecosystem off the southwest Western Australia coast.

The contribution from this study toward the understanding of the biophysical coupling off the southwest Western Australia coast is reported in more detail in the Chapters 3 and 4, and in the collaborative project report by Waite *et al.* (Vol. 1, Sec. 3.3.1). More detailed analysis of a data-assimilating model output in the Leeuwin Current region can be found in the collaborative project report by Berthot *et al.* (Vol. 1, Sec. 3.3.3).

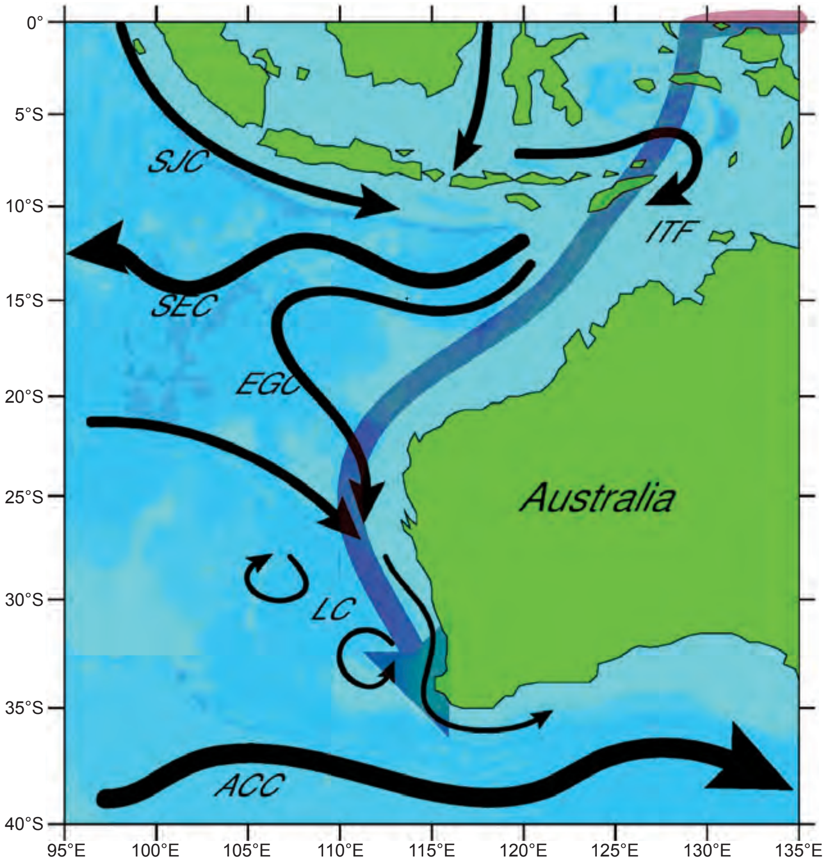

Figure 2.1: Schematic of the major surface currents in the east-southeast Indian Ocean. ITF: Indonesian Throughflow; SEC: South Equatorial Current; SJC: South Java Current; EGC: East Gyral Current; LC: Leeuwin Current; ACC: Antarctic Circumpolar Current. A transparent arrow is used to highlight the wave guide along which the Pacific ENSO signals propagate (from Feng *et al.* 2003).

Annual and interannual variations of the Leeuwin Current

Through the SRFME research, significant progress has been made in understanding the annual and interannual variations of the Leeuwin Current by constructing a monthly upper ocean thermal climatology off southwest Western Australia. Using 300 m as the reference depth, the annual mean volume transport of the Leeuwin Current is estimated to be 3.4 Sv (10^6 m^3s^{-1}). On the annual cycle, the Leeuwin Current is stronger during austral autumn to winter with peak transport of about 5 Sv during May-July, and is weak during austral spring-summer with transport of 2-3 Sv (Fig. 2.2; Feng *et al.* 2003). The seasonal variation of the Leeuwin Current induces a 20 cm seasonal variation of the steric height on the inshore side of the current, consistent with the annual variation of the Fremantle sea level. Thus, the annual variation of the Fremantle sea level can be mostly explained by the annual variation of the Leeuwin Current.

The wind forcing not only plays a crucial role in the annual cycle of the Leeuwin Current, but is also responsible for forcing coastal current systems on a variety of temporal and spatial scales, such as coastal upwelling and vertical mixing of the water column. Wind data for the period 2000 to 2004 have been acquired from the Bureau of Meteorology stations at Rottnest Island (assumed representative of the offshore waters) and on the coast at Ocean Reef. The original wind measurements at the two weather station sites are at 1-minute intervals but these have been converted to hourly values for the present analysis, and monthly averages have also been derived to more clearly show the seasonal wind fields. The overall mean wind speed over the 5-year period at Rottnest Island was 7.5 m s^{-1}, and marginally weaker at 6.2 m s^{-1} at Ocean Reef. As a result of the annual meridional migration of the subtropical high-pressure belt, a pronounced seasonal cycle is evident in the monthly mean wind vectors at the two sites (Fig. 2.3). Through much of the year, the meridional wind stress is dominantly northward, albeit with a weak southward component in winter. During the summer months when the high-pressure belt is furthest south, the zonal wind stress is westward (offshore) but as the belt moves northwards in winter, this switches to a strong eastward, or onshore, component.

During the austral winter, a continuous current, extending from its origin at North West Cape to the southern tip of Tasmania, with a total distance of 5500-km, is portrayed in the satellite-derived altimetry data and sea surface temperature (Fig. 2.4), as well as in the SRFME-CARS climatology (Ridgway and Condie, 2004). Surface buoy tracks confirm the location and continuity of the current trajectory. A naming convention is proposed for the boundary flow, with the Leeuwin Current representing flow from North West Cape to the Great Australian Bight (GAB), The South Australian Current denoting the current between the eastern GAB and western Bass Strait, and the Zeehan Current located off western Tasmania. The poleward penetration of the warm, low-salinity waters of the Leeuwin Current is the underlying mechanism for the migration, and subsequent distribution, of many marine pelagic fauna from the tropical northern waters to the temperate shelves of western and southern Australia, and west coast of Tasmania. The connection of the shelf currents during the austral winter may also be responsible for spawning behaviours of the Australian salmon species *Arripis trutta.*

From the upper ocean climatology, the Leeuwin Current is stronger during the La Niña years, with a mean transport of 4.2 Sv, and weaker during the El Niño years with a mean transport of 3 Sv (Fig. 2.2; Feng *et al.* 2003). The interannual variations of the Leeuwin Current influence the interannual variations of the Fremantle sea level. The Fremantle sea level is 3.4 cm lower than the climatological mean in an El Niño year, while it is 5.6 cm higher in a La Niña year. The linear relationship between the Fremantle sea-level and the volume transport of the Leeuwin Current across 32°S on the annual and interannual time scales (Fig. 2.2, lower panel) supports the use of Fremantle sea-level to represent the strength of the Leeuwin Current in fisheries management practices.

The transmission of the ENSO signals along the coastal wave guide, as illustrated in Fig. 2.1, is further demonstrated in the correlations between regional altimeter sea-level anomalies and the Southern Oscillation index (SOI) for the years 1992-2002 (Fig. 2.5; Feng *et al.* 2003). The correlations are generally 0.6-0.7 along the northwest and west Australian coast. The correlation is also significant along the southern coast. The high correlation between the Fremantle and altimeter sea-level anomalies along the coasts (Fig. 2.5) suggests that the Fremantle sea-level index may apply to a large geographic range of the Leeuwin Current, although the calibration to the current strength will vary with locations.

There are differences in the responses of the Fremantle sea-level to ENSO in different seasons, as revealed by a partial least square regression (PLSR) analysis to model the relationship between Fremantle sea-level anomalies and sea-surface temperatures of the Indo-Pacific Ocean (Fig. 2.6). The PLSR has advantage over the frequently used empirical orthogonal function (EOF) analysis in reducing spatial dimensions, because it takes into account the variance in the responsible variable, in this case the Fremantle sea-level. The PLSR reveals that two leading SST patterns together account for more than 65% of total Fremantle sea-level variances in all the seasons. The first pattern was related to equatorial Pacific ENSO, and the second pattern is similar to the global warming signatures in the Indo-Pacific. The time-series of the first pattern explains a significant portion of the interannual variability of the Fremantle sea-level in all seasons, with the highest explained variance in the austral spring-summer.

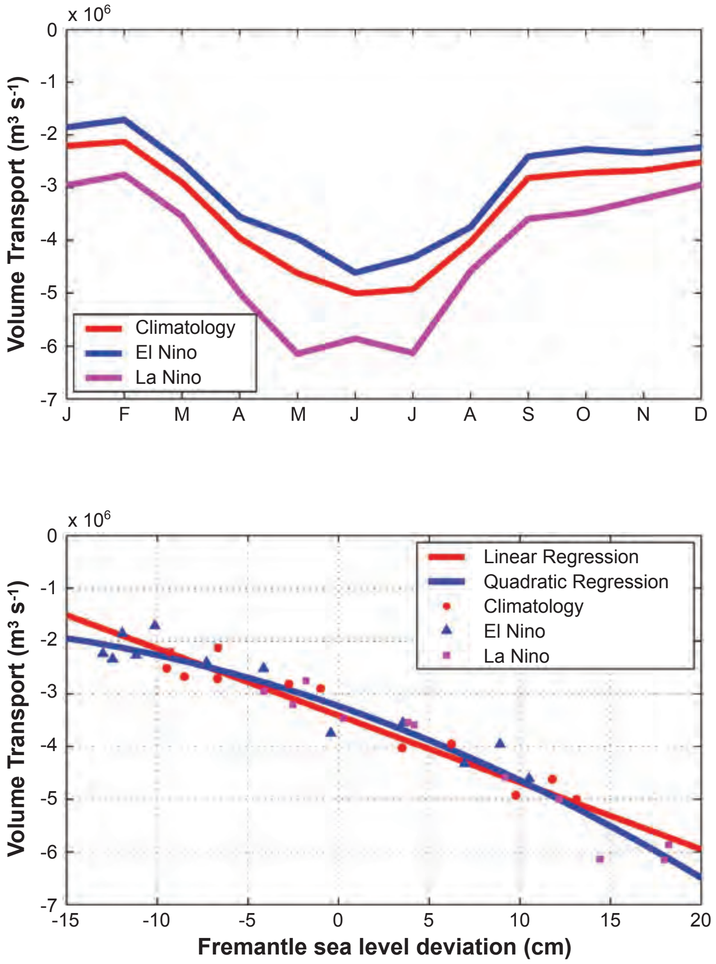

Figure 2.2: (upper panel) Monthly climatology, El Niño and La Niña scenarios of the Leeuwin Current volume transport and (lower panel) the quasi-linear relationship between the monthly Fremantle sea-level anomalies and the volume transport of the Leeuwin Current (from Feng *et al.* 2003).

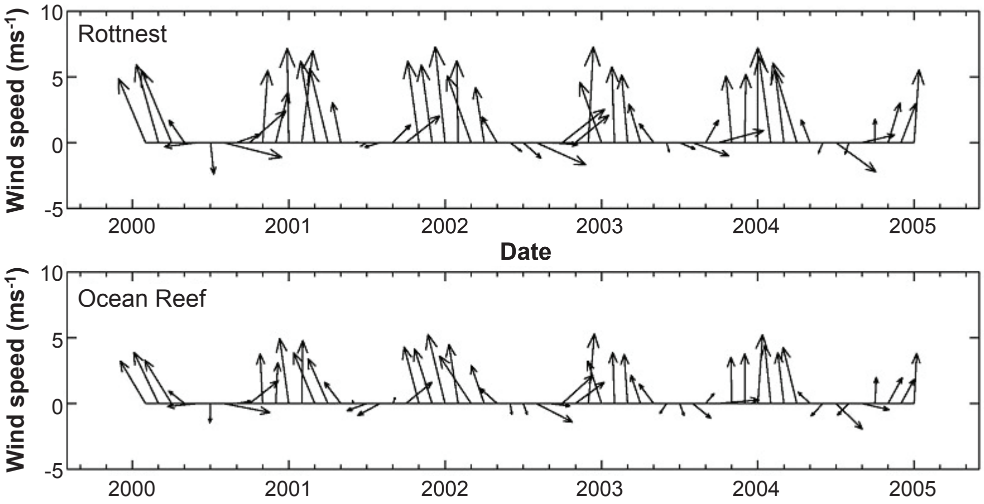

Figure 2.3: Monthly mean wind vectors from Rottnest Island (representing open-shelf conditions) and Ocean Reef (coastal). North is upwards (A. Pearce).

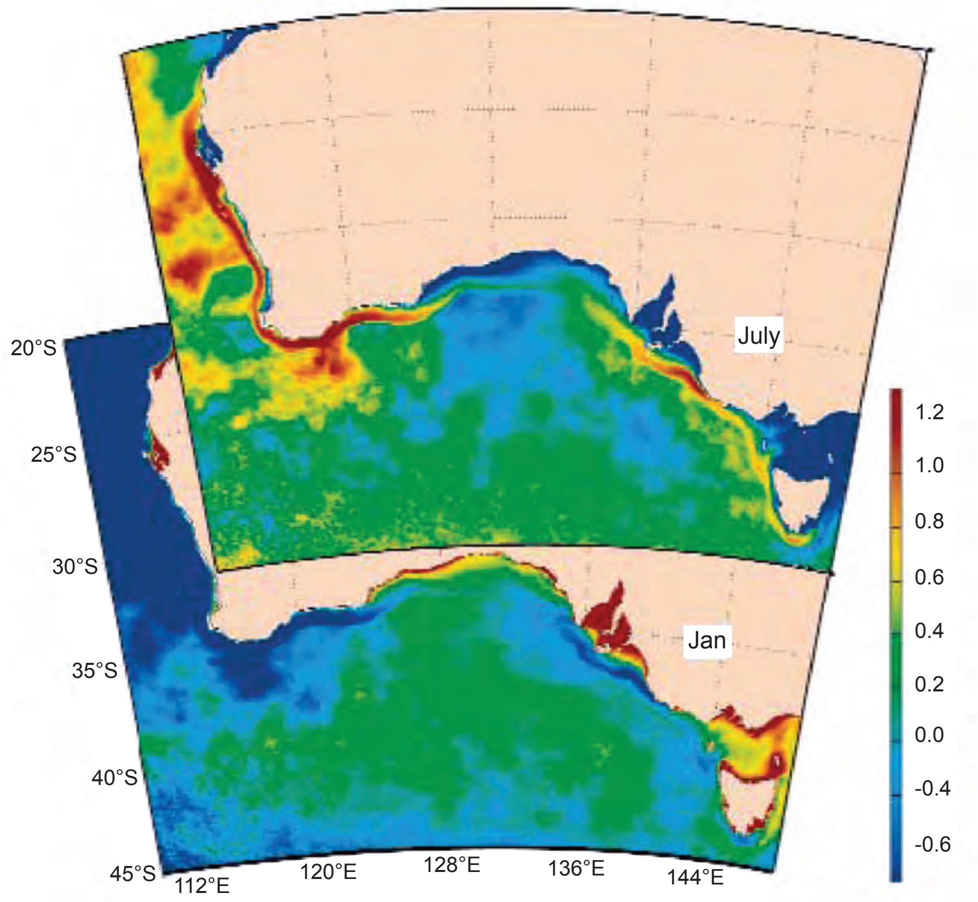

Figure 2.4: Sea surface temperature anomalies during January and July in a high resolution climatology (from Ridgway and Condie, 2004).

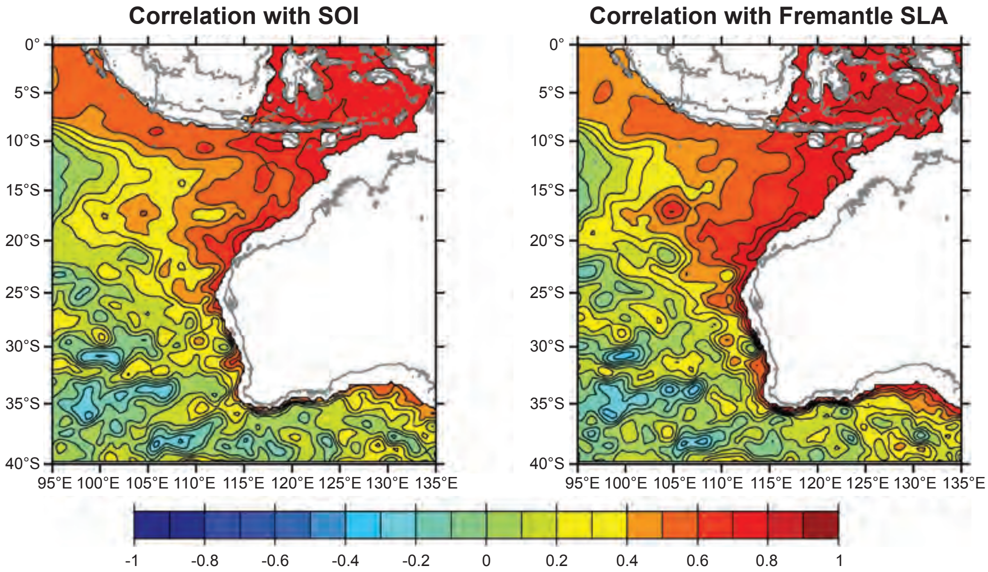

Figure 2.5: (left panel) Correlations between the satellite altimeter sea level anomaly in the east-southeast Indian Ocean and the SOI, and (right panel) between the altimeter and the Fremantle sea level anomalies (from Feng *et al.* 2003).

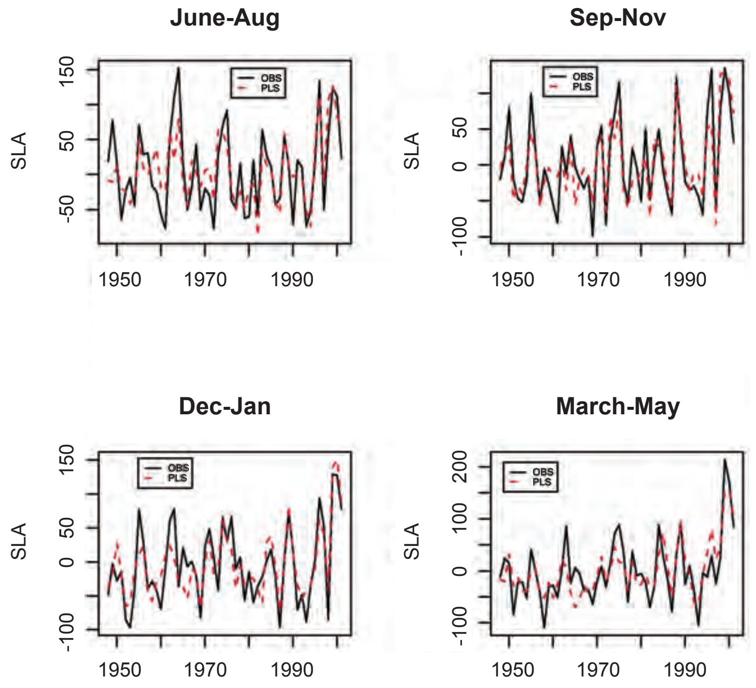

Figure 2.6: Interannual variations of seasonal Fremantle sea level anomalies and the reconstruction from the first two partial least square regression modes (from Y. Li, manuscript).

Annual and interannual variations of the eddy energetics in the Leeuwin Current system

The anomalous large-scale pressure gradient in the East Indian Ocean, which drives the Leeuwin Current, also fuels an eddy kinetic energy level in the Leeuwin Current system which is the strongest of all the mid-latitude eastern-boundary currents (Fig. 2.7a; Feng *et al.* 2005). A revisit of the momentum balance of the Leeuwin Current shows that, north of the Abrolhos Islands, the alongshore momentum balance is between the pressure gradient and northward wind stress (Table 2.1). South of the Abrolhos Islands, the Leeuwin Current is highly unstable and strong eddy kinetic energy is observed offshore of the current axis (Fig. 2.7a). The longshore momentum balance on the offshore side of the current reveals an increased alongshore pressure gradient, weakened longshore wind stress, and a significant Reynolds stress exerted by mesoscale eddies (Table 2.1). The Reynolds stress term indicates a significant offshore transfer of the southward momentum of the Leeuwin Current by the formation of mesoscale eddies (Fig. 2.7b). As shown later, the formation of the Leeuwin Current eddies also carries a significant amount of the Leeuwin Current and shelf water, heat, and plankton biomass offshore (Feng *et al.* 2006).

The eddy field in the Leeuwin Current has a strong seasonality, as derived from satellite altimetry data (Fig. 2.8). The Leeuwin Current eddies tend to be less energetic during the austral spring-summer. The Leeuwin Current increases its current speed and volume transport in the austral autumn due to the relaxation of the opposing longshore wind. Intense current instability and large meanders are observed along the path of the current during May-July, as indicated by the high eddy kinetic energy off the southwest Australian coast (Fig. 2.8). Long-lived warm-core eddies tend to form from meanders of the Leeuwin Current during the austral autumn, and then propagate offshore during the austral winter (Fang and Morrow, 2003), as indicated by the offshore migration of the high eddy kinetic energy region with seasons (Fig. 2.8).

Interannual variations of the Leeuwin Current eddy field are also derived from the satellite altimetry data. There have been 12 years of continuous satellite altimeter measurements since 1993. The May to October average sea-surface eddy kinetic energy in the individual year is highly related to the Fremantle sea-level (not shown), or the strength of the Leeuwin Current.

There are stronger eddy kinetic energies during the La Niña years such as 1999 and 2000, and weaker energies during the El Niño years such as 1994, 1997, 2002, and 2004 (Fig. 2.9). Note that 2002 and 2004 are classified as weak El Niño years. An interesting observation is that when the overall energy level is high, the region with high eddy energy extends to further south.

Mesoscale eddies are an integral part of the ocean circulation. The roles of mesoscale eddies in enhancing ocean production have been identified in recent years. Eddy-induced upwelling, vertical mixing, horizontal stirring, and cross-shelf exchange could all affect the ocean production. Recognition of the ENSO-related variability of eddy energetics in the Leeuwin Current system is a first step in studying their impacts on both the interannual variations in the ocean production off the Western Australia coast, and the latitudinal distribution of the rock lobster recruitment (N. Caputi, personal communication, 2005).

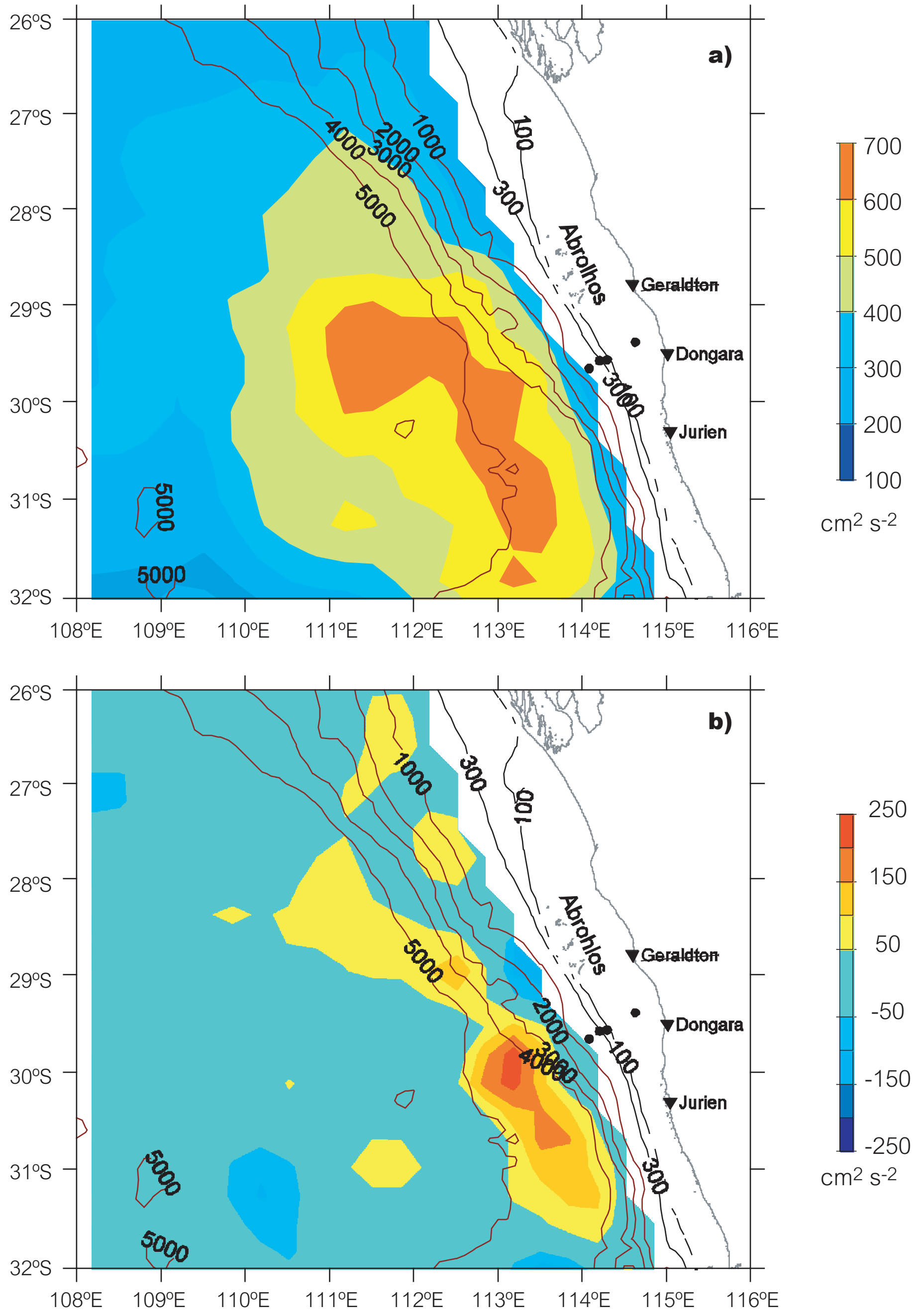

Figure 2.7: (a) Sea surface eddy kinetic energy and (b) cross-product between the zonal and meridional velocity anomalies estimated from altimeter sea surface height anomalies. Bottom bathymetry is shown as contours. The black dots off Dongara denote the LUCIE mooring positions (from Feng *et al.* 2005).

Table 2.1: Vertically integrated longshore momentum balance of the Leeuwin Current (From Feng *et al.* 2005)

	North	South
Orientation	**247T**	**252.4T**
Integrated Pressure Gradient	-1.00†	-1.51
Wind Stress	0.92 (0.87)*	0.65 (0.62)
Reynolds Stress Divergence (offshore side of the LC axis)	--	-1.00

†unit: 10^{-4} m^2s^{-2}.

*numbers in the parentheses are from the scatterometer wind stress climatology.

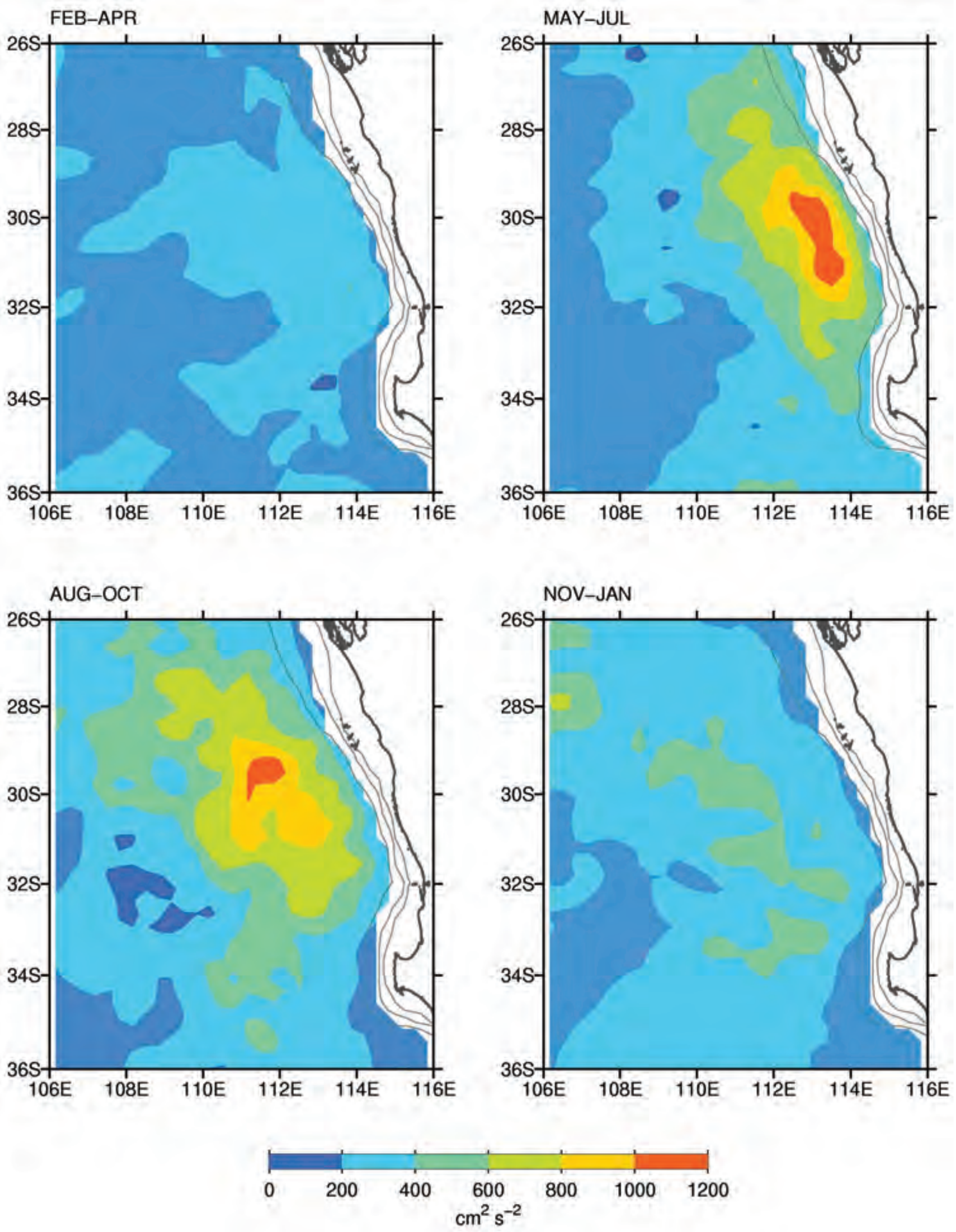

Fig. 2.8: Seasonal evolution of the surface eddy kinetic energy off SW Western Australia inferred from satellite altimeter data (from Feng *et al.* 2006).

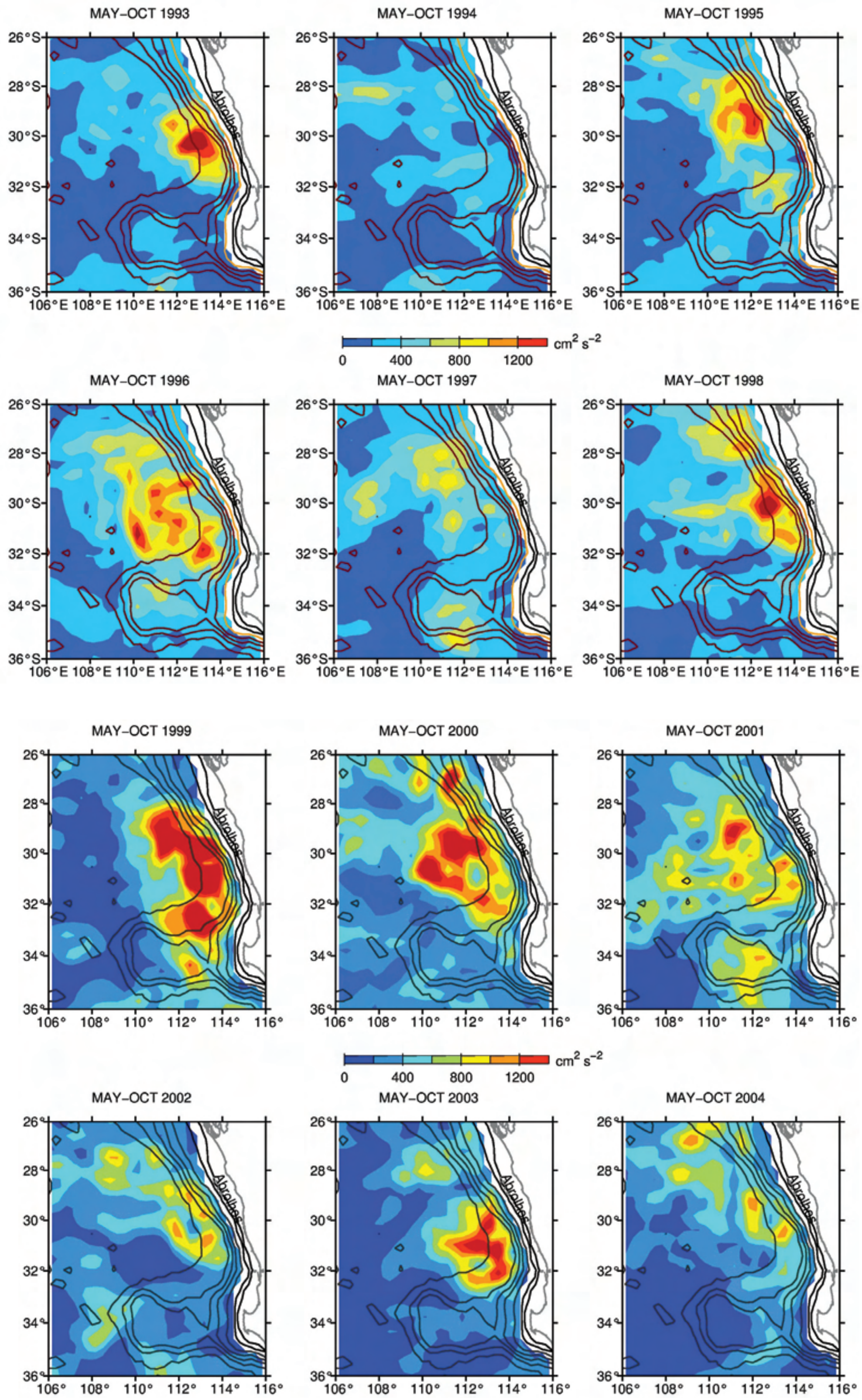

Figure 2.9: Interannual variations of eddy energetics during May-October in the Leeuwin Current system (M. Feng).

2.3 Seasonal chlorophyll a pattern and eddy-driven cross-shelf transport

Off the southwest Western Australian coast, seasonal blooms of sea-surface chlorophyll *a*, which is an indicator of phytoplankton biomass, can be derived from multi-year SeaWIFS satellite data (Fig. 2.10). The chlorophyll *a* peaks during the late austral autumn to early winter (May-July) on the shelf and shelf break, leading the general late-winter peak in the open ocean. The late autumn-early winter chlorophyll *a* blooms on the shelf and shelf break are in phase with the seasonal strengthening of the Leeuwin Current and its eddy field, and are consistent with the phytoplankton biomass on the shelf and shelf break observed during over 3-years along the biophysical transect from Two Rocks (see Chapter 3). Hypotheses for the phytoplankton cycle behaviour are introduced in Chapter 3.

Cross-shelf exchange due to warm-core eddies is common along the western boundaries of the ocean basins. In recent years, warm-core eddies generated on the eastern boundaries of the ocean basins have also been recognized to cause cross-shelf transport of nutrient/ phytoplankton. Cross-shelf transport due to the formation of the Leeuwin Current eddies has also been hypothesized (Feng *et al.* 2006).

To identify the pathways of the cross-shelf transport, the finite-size Lyapunov Exponent (FSLE) method is used to calculate the manifolds in the surface flow field. The stable and unstable manifolds are convergence and divergence trajectories of particles in a 2-dimensional flow field. The stable and unstable manifolds form strong constraints to the flow field so that the cross-over points of stable and unstable manifolds, called hyperbolic point, are key locations for cross-frontal exchange.

The manifold structure of the 2-dimensional current field derived from the altimeter data is used to characterize the horizontal stirring by mesoscale eddies during 2003 off southwest Western Australia. High stirring is generally observed in the region of high eddy kinetic energy and the manifolds of the current field tend to follow the southward meandering path of the Leeuwin Current (Fig. 2.11). Hyperbolic points are identified in the flow field between the Leeuwin Current eddies and the shelf. High-biomass waters from the continental shelf are drawn into a warm-core eddy following the pathway defined by the manifolds and the hyperbolic points, as evidenced in the satellite chlorophyll a images (Fig. 2.11).

Given that six similar warm-core eddies may form off the southwest coast each year (Fang and Morrow, 2003), the exchange between the shelf and open ocean is estimated to be 1.4×10^{12} m^3 year^{-1}. Based on this crude estimate, the shelf off the southwest Western Australia can be flushed twice a year by the formation of the mesoscale eddies. The entrained shelf water would make up a few percent of the volume, but contribute nearly 20% of the phytoplankton biomass, within the warm-core eddies. The impact of the cross-shelf exchange may be two-fold: on the one hand, high production waters are carried offshore with the formation of the eddies, and are important for the ocean production in the oligotrophic subtropical marine environment. On the other hand, the exchange may lead to loss of teleost eggs and larvae, and have negative impact on the teleost recruitment on the shelf (D. Gaughan, personal communication).

As these warm-core eddies eventually detach from the Leeuwin Current, they carry a significant amount of water, heat, and biomass from the Leeuwin Current and shelf region into the open ocean. One of the warm-core eddies was surveyed during a Southern Surveyor cruise in October 2003. The research results from this cruise are reported in the collaborative project (Vol 1, Sec. 3.3.1). Here, one figure from Feng *et al.* (2006) highlights the impacts of the mesoscale eddies. From the cruise data (Fig. 2.12), the chlorophyll *a* concentration in the surface layer of the warm-core eddy (a mixture of Leeuwin Current water and shelf water) was higher than in a cold-core eddy (open ocean water); the warm-core eddy is more productive than the cold-core eddy. Overall the offshore transport by the warm-core eddies is estimated to be 20% of the Leeuwin Current's annual mean transport. The long-lived eddies of the Leeuwin Current off the southwest coast can also transport 0.004 PW (10^{15} W) of heat and about 10^9 g of chlorophyll *a* biomass offshore annually. Adding the contribution from short-lived eddies, the total offshore transport of phytoplankton biomass could add to up to 4×10^{11} g carbon every year along the whole WA coast.

The reason for the enhanced productivity and high chlorophyll concentration of the warm-core eddy has been closely investigated using a coupled physical-biological numerical model (Greenwood *et al.* 2006). The model considers eddies as a trapped body of water and follows them as they detach from the Leeuwin current and move offshore. With specification of the appropriate density and nutrient properties during eddy formation, the model could successfully distinguish between productivity in the warm and cold-core eddies. This is the first time that this has been attempted for a warm and cold-core eddy pair and has provided important insight into the role of vertical mixing and nutrient regeneration. The primary mechanisms supporting production were found to be different in the two eddies. While production in the cold eddy was consistent with a balance between vertical nitrate flux and gravitational settling, the enhanced production of the warm eddy resulted from a combination of elevated initial nutrient concentrations, and increased mixed-layer nutrient recycling efficiency. Most importantly, the nutrient content of the surface water during the formation of the warm–core eddy in May 2003 was found to make a considerable contribution to its enhanced productivity up to six months later (Fig. 2.13). This result emphasises the importance of understanding offshore transport during eddy formation for its role in biological production in this region.

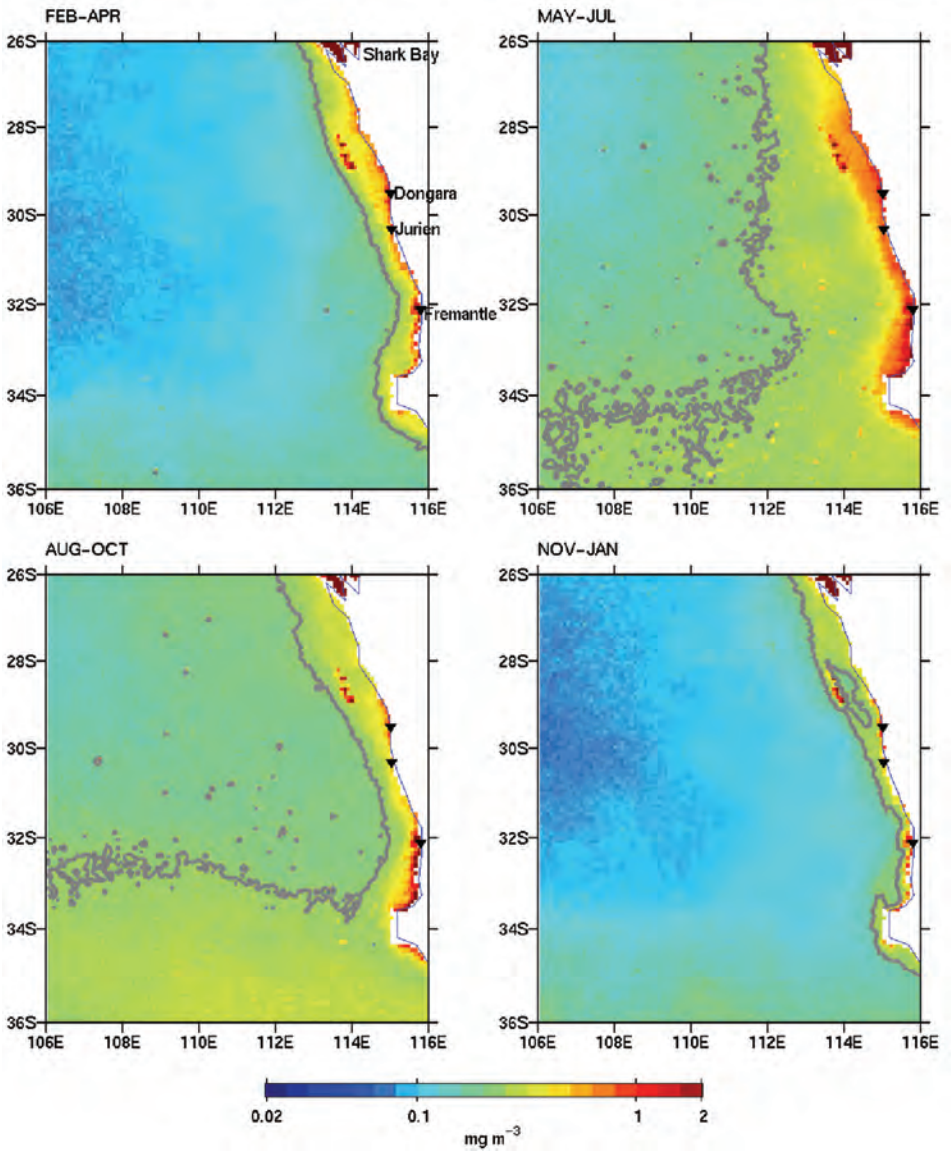

Figure 2.10: Seasonally-averaged sea surface chlorophyll *a* concentration in the southeast Indian Ocean calculated from multi-year SeaWIFS satellite data. The unit is mg m^{-3} (from Feng *et al.* 2006).

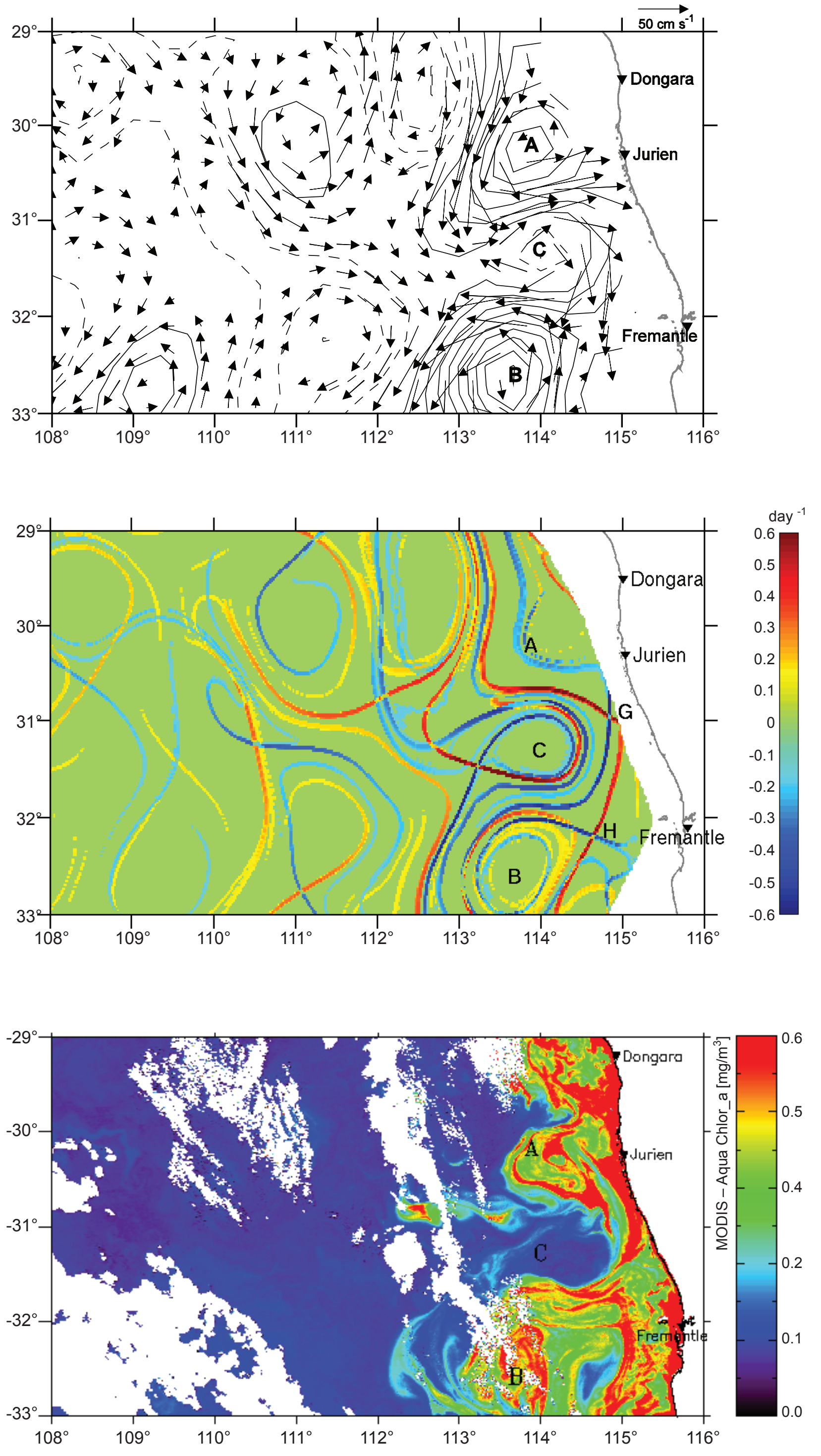

Fig 2.11: (a) Surface geostrophic current anomaly on 25 May 2003 off southwest Western Australia. *A* and *B* are two anticyclonic structures and *C* is a cyclonic structure. The contours denote the sea surface height anomalies with a 5 cm interval. (b) Spatial distribution of the forward (positive) and backward (negative) FSLE, indicating the stable and unstable manifolds of the current field. *G* and *H* are the two hyperbolic points mentioned in the text. (c) MODIS sea surface chlorophyll *a* image on 25 May 2003 (from Feng, manuscript; the MODIS image is contributed by L. Majewski).

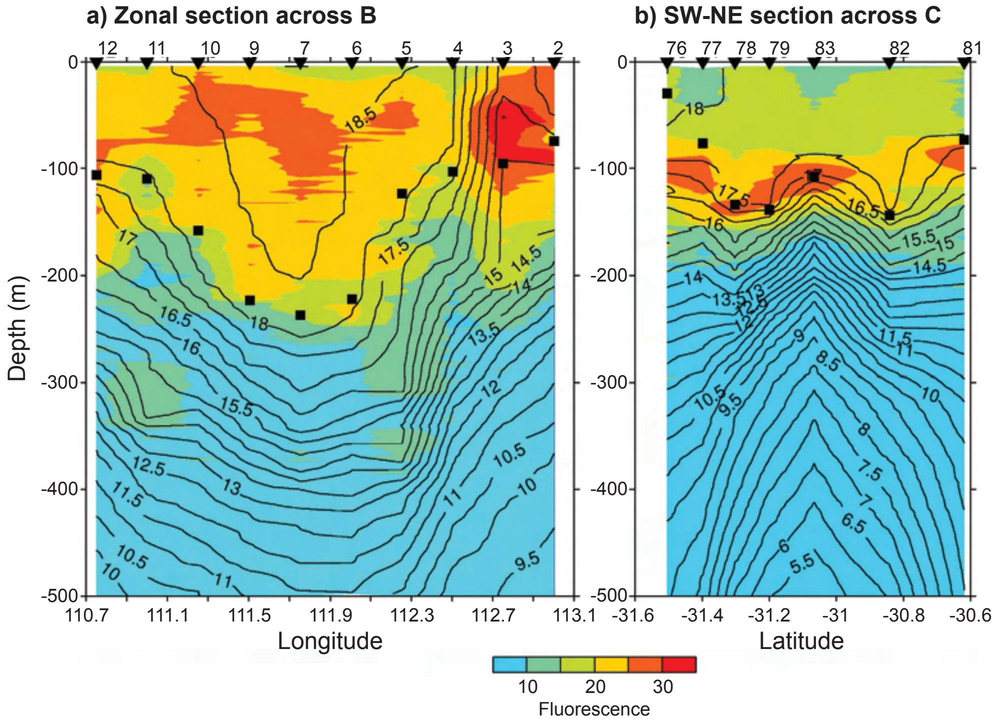

Figure 2.12: Vertical temperature structures along two transects across the warm-core eddy (a) and the cold-core eddy (b) during the October 2003 Southern Surveyor cruise. The colour shadings denote the fluorescence measurements and the solid squares denote the depth of the mixed layer (defined by a density increase of 0.125 kg m^{-3} from 10 m). The station numbers of the CTD casts are denoted on the tops of the panels (from Feng *et al.* 2006)

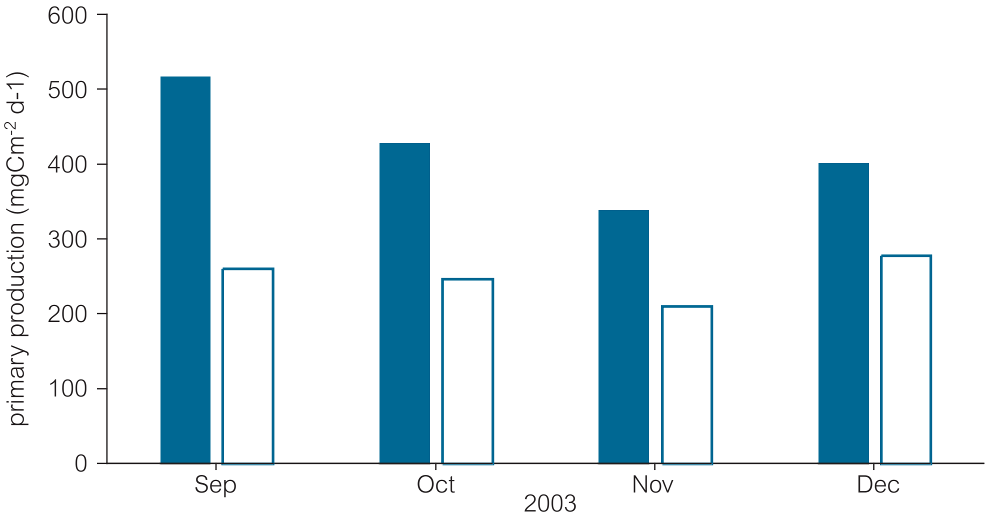

Fig 2.13: Enhanced production of warm core eddy (between September and December 2003) when nutrient content of surface water during eddy formation (in May 2003) is high, and representative of productive shelf water (filled bars), compared with that when nutrient content is low, and more representative of off-shore water (open bars) (from Greenwood *et al.* 2006).

2.4 Decadal and climate-change signals on the WA coast

Decadal variations of the Fremantle sea-level

In addition to the ENSO variability, Fremantle sea-level also experiences variability on decadal time-scales, related to Pacific Decadal Oscillation (PDO) in the tropical Pacific (Fig. 2.14). The PDO has similar spatial sea surface temperature anomaly patterns as ENSO. The PDO-caused upper-ocean anomalies transmit a high sea-level anomaly to Fremantle during its cool phase due to enhanced trade winds in the Pacific (e.g. 1950's—mid 1970's), and transmit a low sea-level anomaly during the warm phase of the PDO due to slackened trade winds (e.g. mid 1970's—mid 1990's). This is demonstrated in the detrended Fremantle sea-level (Fig. 2.14). Thus, the Fremantle sea-level can be used as an index for low-frequency climate variability in the tropical Pacific. The multi-decadal variation in the Fremantle sea-level anomaly helps explain its slower rising trend relative to the global average value from 1950's to 1990's (Feng *et al.* 2004).

The decadal variations of the Fremantle sea-level may also be a signature of a decadal variability in the strength of the Leeuwin Current. During a PDO cool phase, when high temperature water accumulates off north-west Western Australia, via the Indonesian throughflow, the slope in the sea-surface height extending from north-west to the south-west of Western Australia increases. Reduced slope is observed during a PDO warm phase (Fig. 2.15). The forcing of the Leeuwin current therefore increases (decreases) during a PDO cool phase (warm phase).

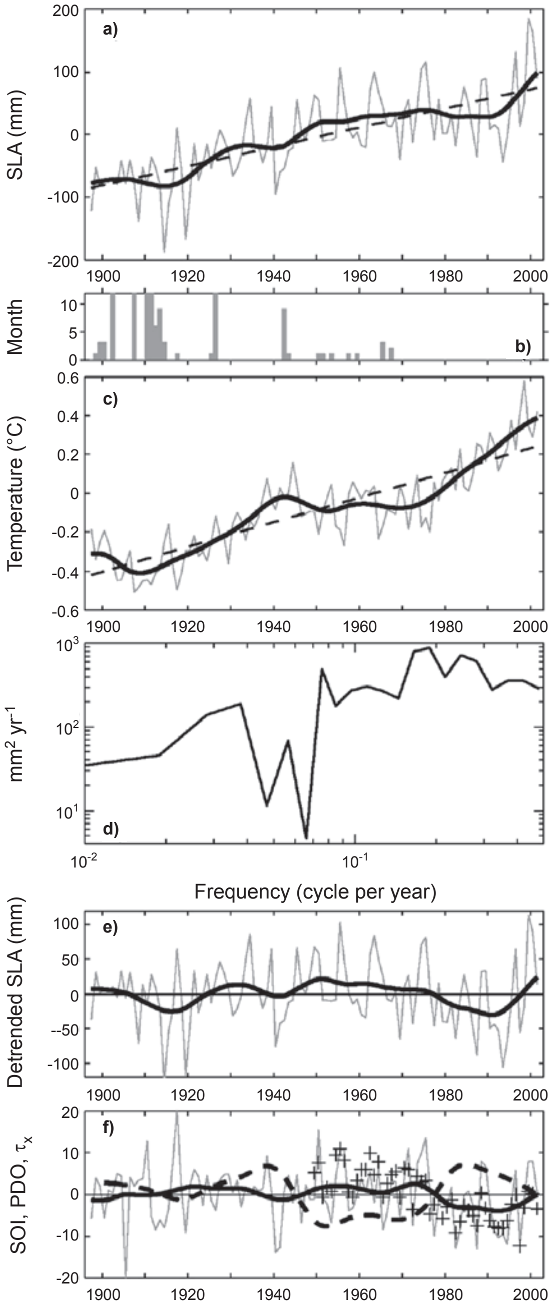

Figure 2.14: (a) Annual mean Fremantle sea level anomaly, (b) numbers of months with missing sea level data, (c) global average surface temperature, (d) power spectrum of the Fremantle sea level anomaly, (e) annual mean detrended sea level anomaly, and (f) annual mean Southern Oscillation Index and average easterly wind stress anomaly at the equatorial Pacific (crosses, unit: 10^{-3} Nm^{-2}). The heavy lines in (a), (c), (e), and (f) are smoothed time series using a 19-year Hanning filter. The dashed lines in (a) and (c) show the linear trends, and the dashed line in (f) is the smoothed Pacific Decadal Oscillation index (from Feng *et al.* 2004).

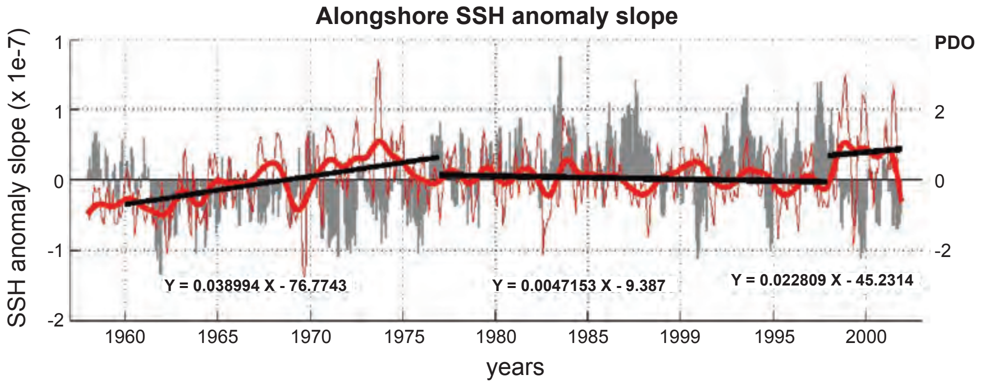

Figure 2.15: Pacific Decadal Oscillation (grey bars) and Sea Surface height slope anomaly (red line). The thick Red line represents the SSH slope anomalies filtered with a 19-years Hanning filter. Black lines represent linear trends during the different PDO phases (from Berthot *et al.* manuscript).

Climate change signals along the Western Australian coast

A long-term rising trend of 1.54 mm per year is observed in the Fremantle sea-level in the 20th century, corresponding to the warming in the global average surface temperature (Fig. 2.14). This rising trend is not obvious during the decades from 1950's to mid 1990's due to the multi-decadal variation. Similar rising trends in coastal sea-level can derived for other shorter time-series along the Western Australian coast, after removing the multi-decadal signals from them, and are consistent with the trends in the global sea-level.

In the decade of 1991–2000, the average SST in the Indian Ocean was 0.6°C warmer than the 1900-1960 base, and continued to warm in 2001-2004. The largest increase is located in the Southern Ocean south of Madagascar, with secondary maxima off Somalia and the northwest of Western Australia (Fig. 2.16). In the Leeuwin Current, the temperature change is less than that further offshore and closer to the global average SST increase. This is due to the influence of El Niño/Southern Oscillation on the coast of Western Australia. Since the mid-1970's, the Leeuwin Current is likely to have been weaker, and the SST warming is damped by a shallow inshore thermocline.

As examples, the seasonal cycle of decadal sea-surface temperature variations (from the Hadley Centre for Climate Prediction and Research dataset) are shown off Ningaloo reef, the Houtman Abrolhos Islands, and Rottnest Island (Fig. 2.17). There is an expansion of the warm season in the annual cycle, especially in the southern latitudes at the Abrolhos and Rottnest. This could be due to the influence of the Leeuwin Current. Thus, in additional to the general temperature rise in the recent decades, there is also a change of seasonal cycle, most dramatically observed in 1970's-1980's. Off Rottnest, the warm season extends by almost two months into the autumn.

The CSIRO commenced a series of coastal monitoring stations around Australia in the early 1950s, including six along the Western Australian continental shelf, but most ran for only a few years. The site off Rottnest Island is the only surviving site off the west coast, operating from 1951 to 1956 and then 1970 to the present. The water depths at these stations are about 55m and sampling was undertaken approximately fortnightly to monthly. Temperature, salinity and selected nutrients were measured at 10m depth-intervals between the water surface and the seabed using classical oceanographic methods (reversing thermometers and Nansen/Niskin bottles, with the salinities being analysed on an Autolab salinometer). The number of yearly samples at the Rottnest station varied between 5 and over 30 depending on personnel and boat availability. The annual mean temperatures and salinities were derived as the simple depth-averages of all available sampling days in each calendar year for those years where there were more than 6 sampling days fairly evenly spread through the year to reduce possible seasonal bias. There has been a clear and consistent upward trend in the annual temperatures of this coastal station over the past 5 decades, with ENSO-related variability superimposed (Fig. 2.18). The coastal time-series off Rottnest Island matches both the linear trend and the interannual variability of the global dataset very well.

In the upper 150 m, the Indian Ocean is becoming more saline at all latitudes (Boyer *et al.* 2005). There is a reasonably consistent rise in salinity in both the World Ocean Database and the Rottnest station data (Fig. 2.19). It is unfortunate that the World Ocean Database salinities did not extend beyond 1996, as there was a dramatic and sudden fall in salinity of over 0.5 psu off Rottnest Island between 1998 and 1999. This was apparently associated with the reduced salinities observed to the northwest of Australia at the time by Phillips *et al.* (2005), and presumably transported southwards by the Leeuwin Current. The salinity drop in the mid-1970s was also reflected in both datasets but was of much shorter duration near the coast. The linear trend at the Rottnest station for the period up to 2004 (which includes the dramatic salinity decrease) is 0.0036 psu/year, which agrees closely with the rate of 0.0040 psu/year for the World Ocean Database. The rate rises appreciably to 0.0066 at Rottnest if we take the period 1951 to 1998 before the salinity drop. The mechanism for the salinity rise in the coastal region off WA still needs further research.

The rising trend of water temperature off the Western Australia coast is further demonstrated by the reconstructed sea surface temperature anomalies from coral oxygen isotope data at Ningaloo reef and Houtman Abrolhos Islands (Fig. 2.20). From the coral records, the temperatures at Ningaloo and Abrolhos are rising at the rate of 0.0158 and 0.0177 degree C per year over the second half of 20th century, respectively. By comparison, the temperatures from the adjacent grids of Hadley Centre data have trends of similar magnitude. The CSIRO Mark-3 coupled ocean-atmosphere model (MK3) was run for 1990-2100 under the IPCC A2 greenhouse gas scenario (SRESA2) to assess future global climate changes. Although the model does not resolve the shelf current off the coast, it still produces similar rising temperature r trends as in the data. This suggests that the long-term trend in the surface temperature on the shelf is likely due to local air-sea fluxes, rather than the detailed structure of the ocean currents. The research on climate change impact on the Western Australia coastal sea-level and temperature, and current will be a continuing effort of CSIRO research in WA. Both the rising temperature and the shift in seasonal cycle would have important implications for the marine ecosystem.

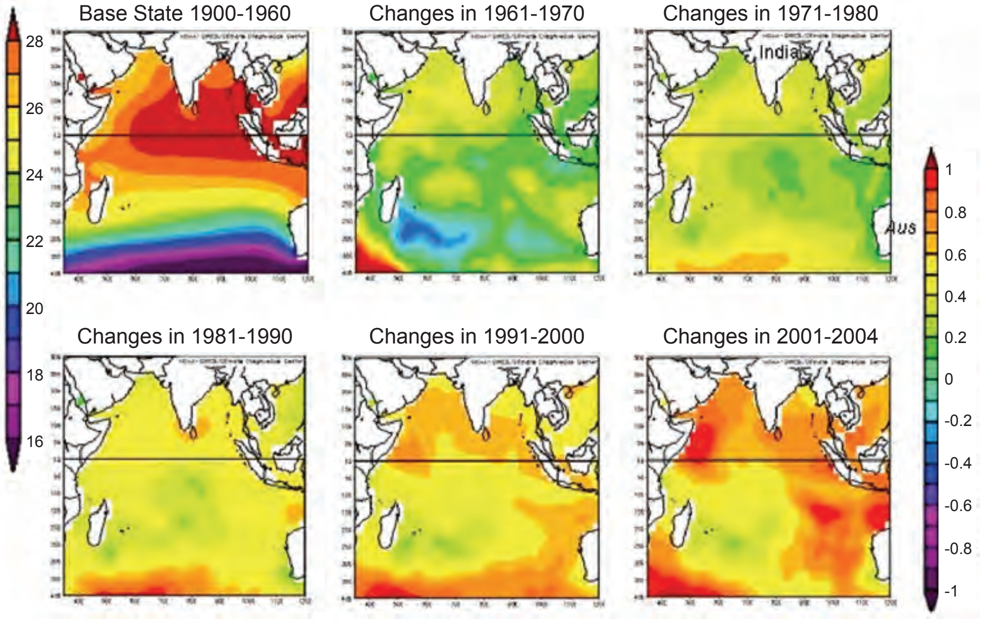

Figure 2.16: Decadal changes in the sea surface temperatures in the Indian Ocean from the 1900-1960 mean over the subsequent decades. The key on the left-hand-side is for mean temperature during 1900-1960 and that on the right-hand-side is for temperature change (from Feng *et al.* 2005).

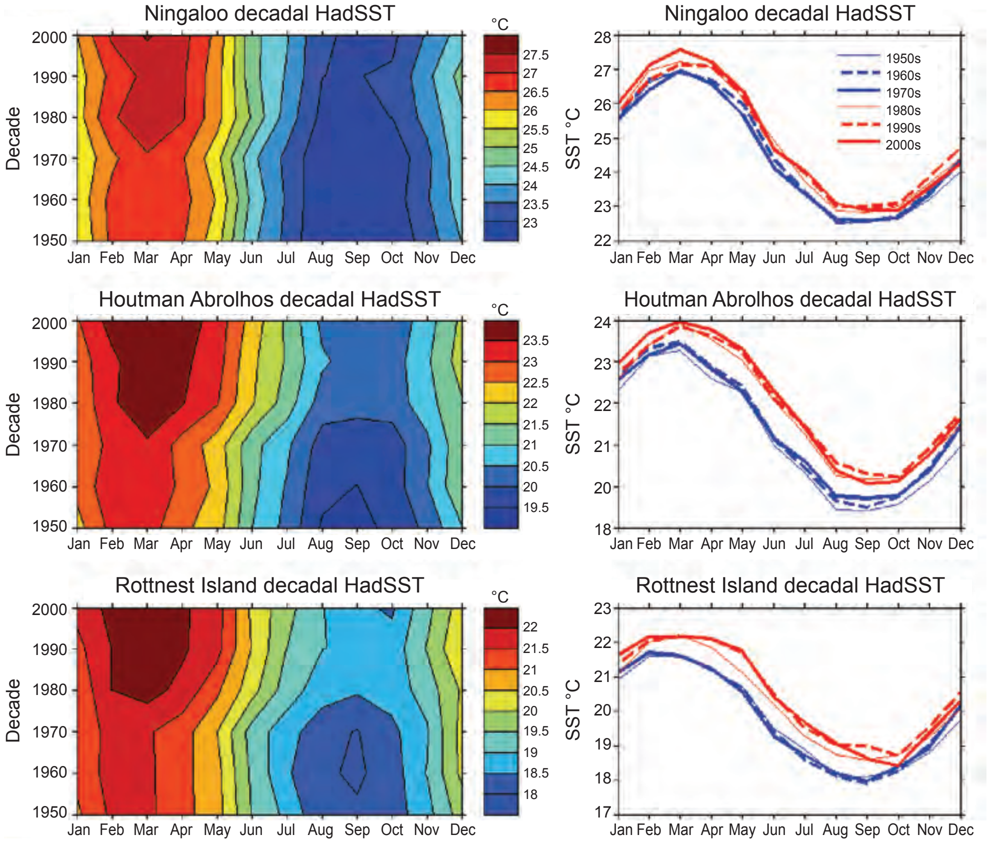

Figure 2.17: Seasonal cycle of the decadal mean sea surface temperatures off Ningaloo Reef, Houtman Abrolhos Islands, and Rottnest Island from the Hadley Centre for Climate Prediction and Research dataset. The left panels provide a contour view of the same data to highlight the lengthening of the warm season (Slawinski and Feng 2006, informal SRFME report).

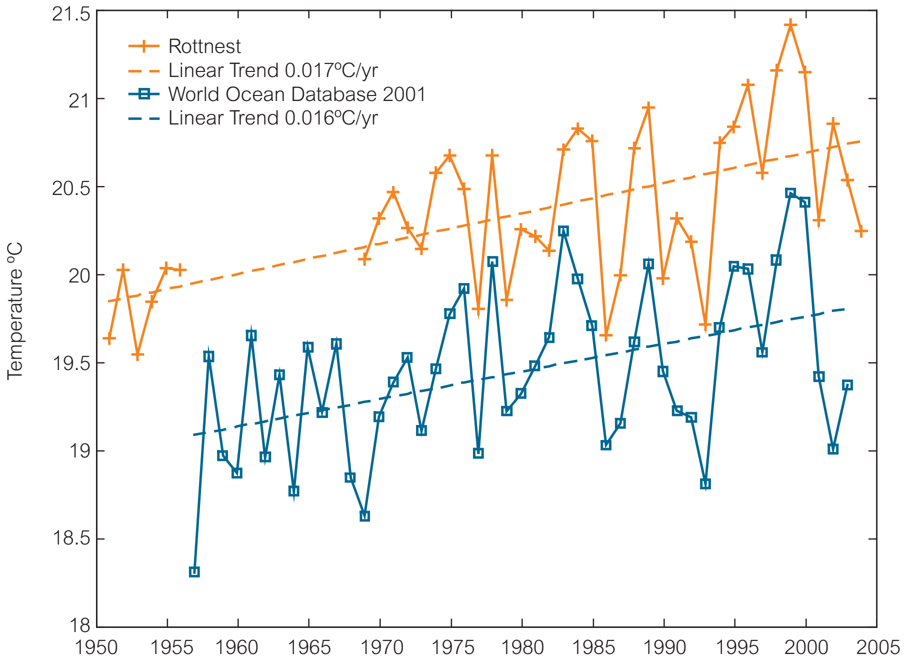

Figure 2.18: Annual mean temperatures off Rottnest from the World Ocean Database (WOD) global datasets and the Rottnest station time series. The WOD data are offset by 1°C to separate the two time series (from Pearce and Feng 2006, manuscript).

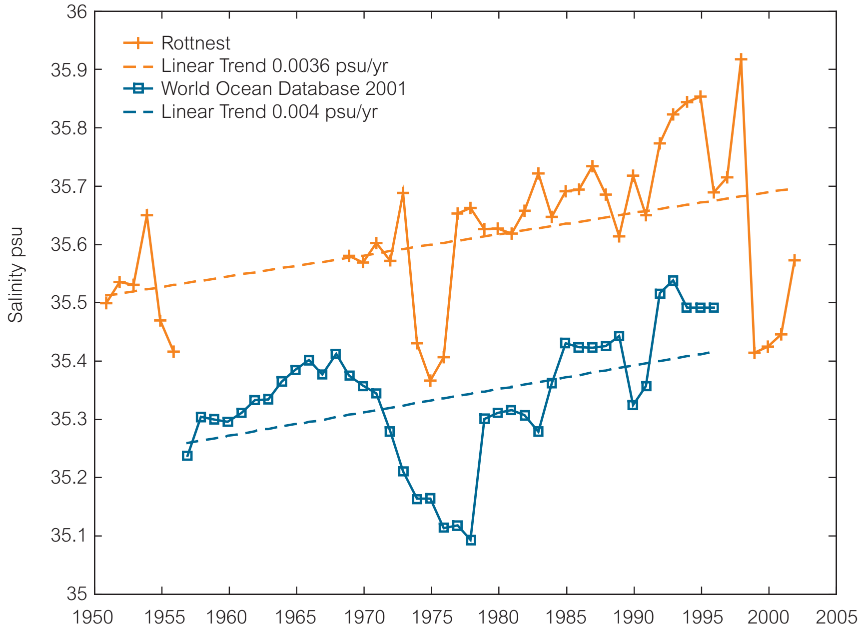

Figure 2.19: Annual mean salinities from the World Ocean Dataset (blue) global dataset, with the Rottnest station salinity shown in orange. The WOD data are offset by 1°C to separate the two time series (from Pearce and Feng 2006, manuscript).

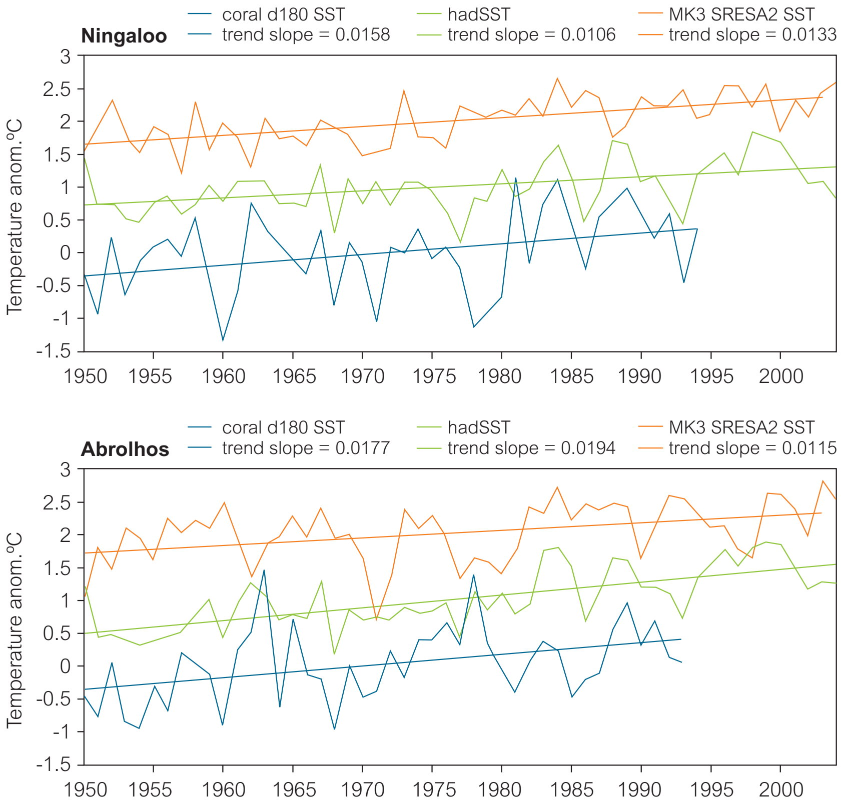

Figure 2.20: Sea surface temperature anomalies at Ningaloo and Abrolhos from coral oxygen isotope data, Hadley Centre data, and CSIRO Mark-3 model output. The unit for the trend is degree C per year (Slawinski and Feng, informal SRFME report).

2.5 Indian Ocean Dipole

In recent years, there have been a growing number of studies of interannual variability in the tropical Indian Ocean, especially of the Indian Ocean Dipole (IOD) events. An IOD event starts with anomalous SST cooling along the Sumatra-Java coast in the eastern Indian Ocean during May-June. The normal equatorial westerly winds during June-August weaken and reverse direction. An IOD event peaks near September-October, with warmer than usual SST over large parts of the western basin. Because there is non-negligible correlation between ENSO and IOD indices, there is a vigorous scientific debate over whether or not IOD is in any way independent of ENSO.

The SRFME contribution to IOD research results from examination of the evolution of subsurface ocean temperature in the tropical Indian Ocean during IOD events (Feng and Meyers, 2003). Here we only show the dominant empirical orthogonal function (EOF) patterns from the altimetry sea-level anomaly in the whole tropical Indian Ocean, and from the upper-ocean temperatures along two XBT sections in the Indian Ocean (Fig. 2.21). The dominant EOF pattern in sea-level anomaly exhibits an east-west dipole. Negative sea-level anomaly (a shallow thermocline) appears in the eastern Indian Ocean with peak values of about 6 cm along the Sumatra-Java coast, extending northward into the Bay of Bengal and southward to northwest Australia, likely along the coastal wave guides. The western Indian Ocean has dominantly positive anomaly (a deep thermocline), with peak values of more than 6 cm at the South Equatorial Current/South Equatorial Counter Current ridge. The dominant EOF pattern in the XBT temperature data is consistent with that of the sea level anomaly (Fig. 2.21, lower panels). Along the IX1 section in the eastern Indian Ocean, the dominant EOF pattern shows mostly negative temperature anomaly, with a peak value of -1.2^{o}C near the Sumatra-Java coast. Along the IX12 section in the western to central Indian Ocean, the dominant EOF pattern shows positive temperature anomaly with a peak value of 1^{o}C near 6-12^{o}S in the South Equatorial Current/South Equatorial Counter Current ridge. The dominant EOF patterns in sea-level anomaly and XBT temperature represent the peak phase of an IOD event, on the basis of comparing the temporal evolution with the index of the IOD (the zonal wind in the equatorial Indian Ocean). Thus, the ocean dynamics in the Indian Ocean have an influence on the evolution of the IOD events, which may have independence from Pacific ENSO.

To further clarify this, a partial correlation analysis is carried out. The subsurface evolution in the tropical Indian Ocean (indexed by the zonal equatorial wind) is strongly affected by the Indian Ocean SST zonal gradient, and to a lesser extent by the El Niño-Southern Oscillation. The correlation between inverted SOI and SST difference is 0.56. The wind-index correlation with the inverted SOI is 0.67. Both the SST difference and the wind index have dissimilarity with inverted SOI. On the other hand, the wind index is highly correlated with the interannual SST difference across the tropical Indian Ocean, with a zero-lag correlation of 0.82 (Fig. 2.22) and a lag correlation of 0.86 (SST difference leading by 1 month). The observed behaviour of the tropical Indian Ocean and the role of internal ocean dynamics suggest a coupled ocean/atmosphere instability which may be initiated by ENSO or other anomalies during the early Sumatra-Java upwelling season; however, proof of its existence will require further research, including modelling and model validation with these observations. The impact of the IOD on the Australian climate is demonstrated in Meyers *et al.* (manuscript).

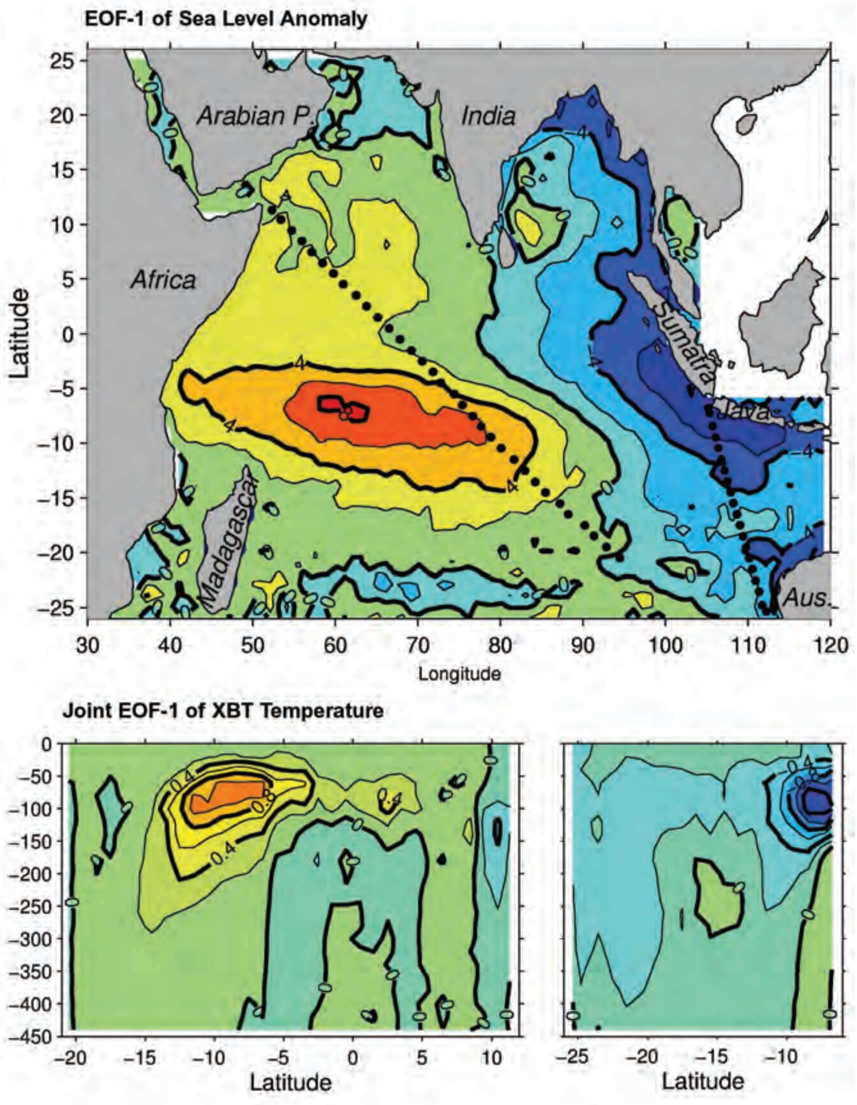

Figure 2.21: Empirical orthogonal function (EOF) analysis of altimeter sea level anomaly (SLA) and upper ocean temperature along two frequently repeated XBT sections. Dominant EOF loadings for sea level anomaly (top panel), and temperature anomaly along the two XBT sections (lower panel: right, IX1; left, IX12). The unit for sea level anomaly loading is cm and the contour interval is 2 cm. The unit for temperature loading is ˚C and the contour interval is 0.1˚C. The locations of the XBT sections are denoted with black dots in the upper panel (from Feng and Meyers, 2003).

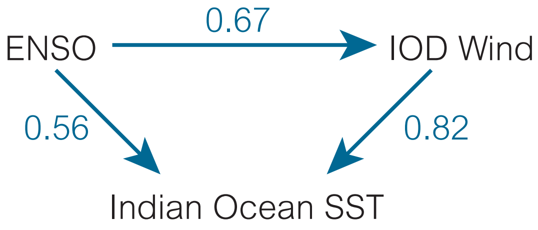

Figure 2.22: Sketch of the partial explanation relationship between SOI, SST difference in the tropical Indian Ocean, and the IOD wind index. The arrows denote influence and the numbers are correlation coefficients (from Feng and Meyers, 2003).

2.6 Inshore Dynamics

Much of the SRFME field research was focused on a transect seaward from Two Rocks (see Figs 3.2 and 3.3). The transect was based on 5 stations, A to E, in nominal depths of 15, 40, 100, 300 and 1000 m. The three inshore stations were occupied approximately monthly from 2002 to 2004, with the outer two stations visited approximately every 3 months. In addition, moorings were deployed at stations A, B and C for the period July 2004- July 2005. Each mooring was planned to contain an ADCP (acoustic doppler current profiler) and CTD (conductivity-temperature-depth) sensor, in addition to tide gauges and chemical sensors. The Two-Rocks transect is described in detail in chapter 3, and the mooring data in a separate report (Fandry, *et al.* 2006). In this section, we review the inshore physical oceanography inferred from the data.

Currents

Longshore currents near the coast at the shallow (20m deep) site, A, are strongly correlated with the longshore component of wind (Fig. 2.23) which reveals a close dynamical balance between wind stress and bottom stress which means that the longshore current, V, can be estimated by the following formula

$$V = (\tau^W / C_D \rho_{water})^{1/2}$$

where τ^W is the wind stress, C_D the coefficient of bottom friction (~0.003) and ρ_{water} the density of water (1024 kg m^{-3}). (Strictly, this relationship assumes that the cross-shore component of current is much smaller than the longshore component, which is a generally safe assumption near-shore.)

Another relationship, consistent with the above formulae, and often used as a rule of thumb, estimates the current speed as 3% of the wind speed. In fact, a linear relationship with the longshore current given by between 2.5% and 3% of the longshore wind speed has a correlation coefficient of at least 0.87 (Fig. 2.24, Table 2.2). The northward coastal current driven by winds during summer was identified by Cresswell *et al.* (1989), and later named the Capes Current by Pearce and Pattiaratchi (1999).

Table 2.2: Linear regression analysis for Station A for the relationship, V=aW+b, where V is the depth-averaged longshore current speed (m/s) and W is the longshore wind speed (m/s).

Measurement Period	a	b	Correlation Coefficient, r
July 04 to Oct 04	0.0281	-0.0358	0.87
Oct 04 to Jan 05	0.0253	-0.0161	0.87
Jan 05 to June 05	0.0295	-0.0566	0.88

By contrast with the shallow site A, currents at the deeper offshore site C (100m deep), are generally not well correlated with wind (Fig. 2.25), even during summer when the Leeuwin Current is at its weakest. Currents below 50m are generally southwards, indicating the influence of the Leeuwin Current. Monthly averaged current profiles at sites A and C (Fig. 2.26) show important differences that are related to the relative influence of the wind near the coast and the Leeuwin current offshore. The current at site A is northwards during the months October to April and southwards during the months May to September. This is in direct response to the prevailing winds. At site C, however, the Leeuwin current is evident in the southward flow during all months except January and February. In fact in depths below 50m, the current is always southwards.

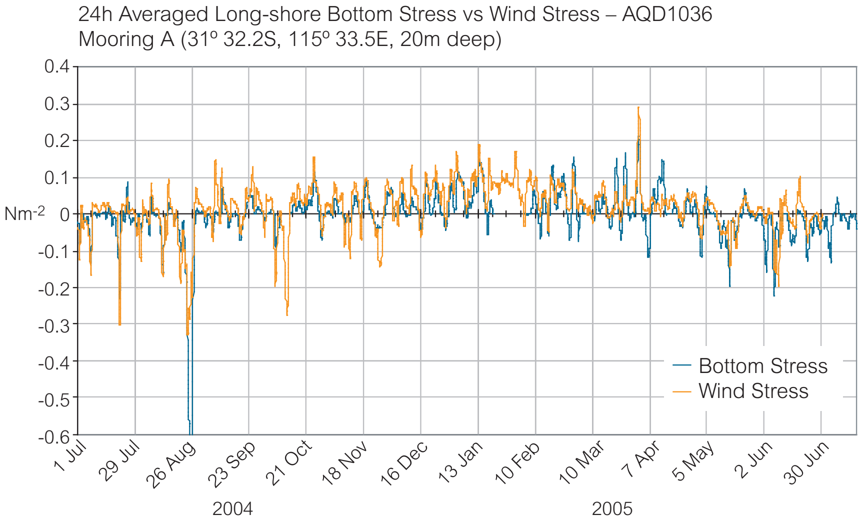

Figure 2.23: Longshore wind stress vs bottom stress at mooring A

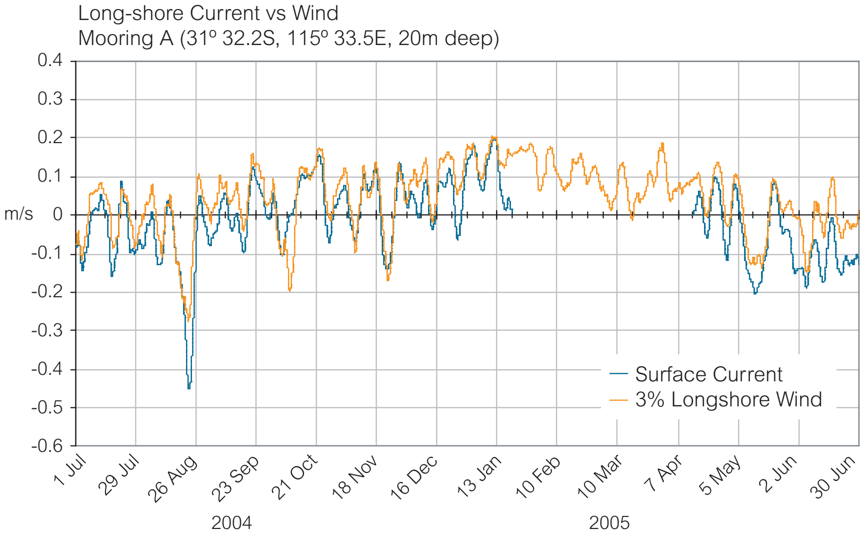

Figure 2.24: Long-shore surface currents vs 3% of longshore wind speed at mooring A

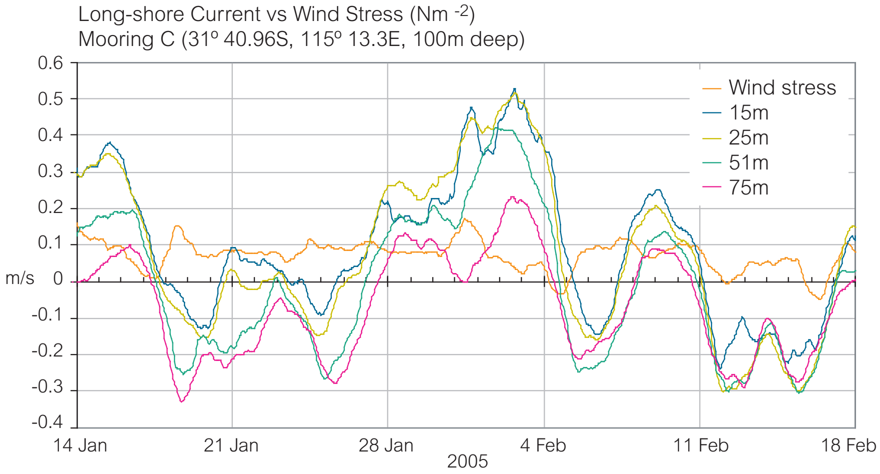

Figure 2.25: Longshore currents and wind stress at mooring C

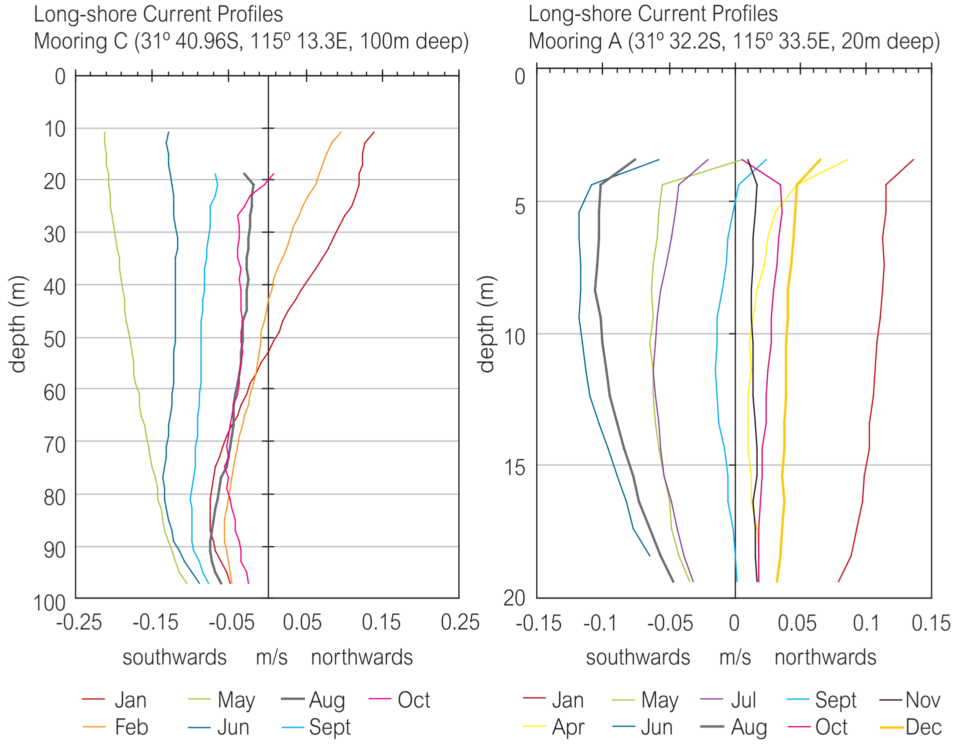

Figure 2.26: Monthly averaged longshore current profiles observed at moorings C and A

Temperature and salinity

The influence of the Leeuwin Current is also evident in the temperature data (Fig. 2.27). Near-shore waters are warmer than offshore waters during the summer months as expected, but this is reversed in winter due to the influence of the warm Leeuwin Current offshore. However, periodic storm events cause strong horizontal and vertical mixing and inshore waters mix with warmer Leeuwin Current offshore waters with a consequent rise in near-shore temperatures.

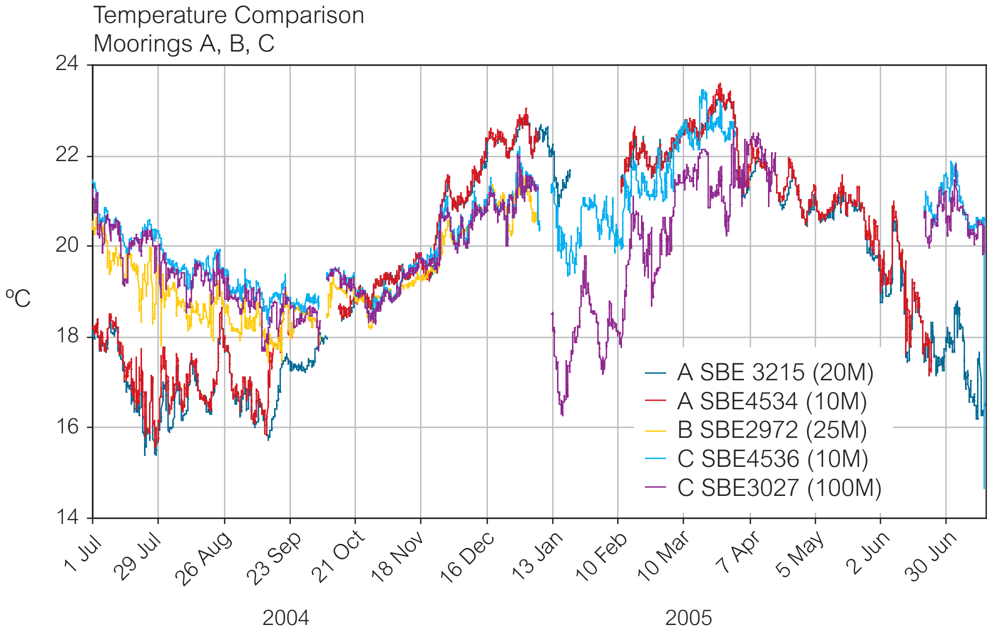

Figure 2.27: Comparison of water temperatures at all mooring sites

The near-surface temperatures from the transect stations (Fig. 2.28), and derived from satellite data (Fig. 2.29) show a similar annual cycle to the moorings data reflecting the seasonal presence of water in the Leeuwin Current (offshore) and the exchange of heat-with the atmosphere (especially inshore).

Consistent with the mooring data, the greatest variability occurred in the shallow coastal waters at the inshore Station A. Monthly mean nearshore temperatures varied from about 17°C in August/September to 23°C in mid-summer (Fig. 2.29); on occasion, however, individual nearshore temperatures from the mooring fell below 16°C between July and September (Fig. 2.27).

At the offshore stations, monthly-averaged, near-surface temperatures peak perhaps a month later than inshore (March rather than February, Fig. 2.30). Inshore waters cool much more rapidly, from March to August, while offshore surface temperatures, maintained by the Leeuwin Current, stay above 20°C through to June or July (Fig. 2.30C). Offshore, the winter trough of 19°C occurs as late as September/October. The seasonal temperature range at stations D and E is therefore only 4°C while close inshore it is 6 to 7°C, with a seasonally-reversing cross-shelf temperature gradient.

The cross-shelf temperature structure in summer results from coastal heating (a narrow band of warm nearshore water in the coastal boundary layer: Zaker *et al.* submitted, Pearce *et al.* submitted), slightly cooler water in the north-going Capes Current, and then warming again into the (weak) Leeuwin Current. With the rapid loss of heat to the atmosphere in autumn/winter from the shallow nearshore waters, coincident with the inflow of warmer water in the strengthening Leeuwin Current along the outer shelf, there can be a marked temperature gradient of up to 5°C between the shore and the shelf-break.

According to the transect data (Fig. 2.31), inshore salinities rose from 35.4 in winter (due to precipitation and coastal run-off) to 36.4 in summer (due to evaporation) in the shallow water, an annual range of 1 psu, while the corresponding near-surface range in the Leeuwin Current was between 35.4 and 35.8 (only 0.4 psu). The elevated salinities >36 psu between January and April did not extend as far offshore as the inner-shelf station B (25 km offshore).

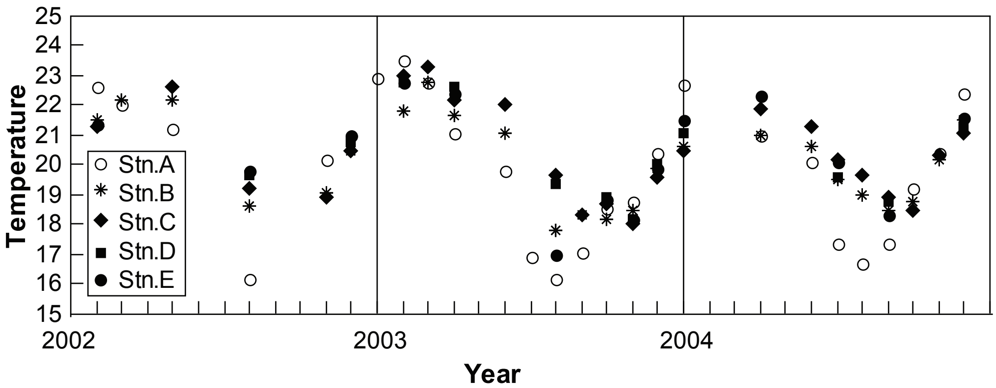

Figure 2.28: Near-surface (5 m depth) temperature from the CTD profiles at the Two Rocks Transect stations over the 3-year period.

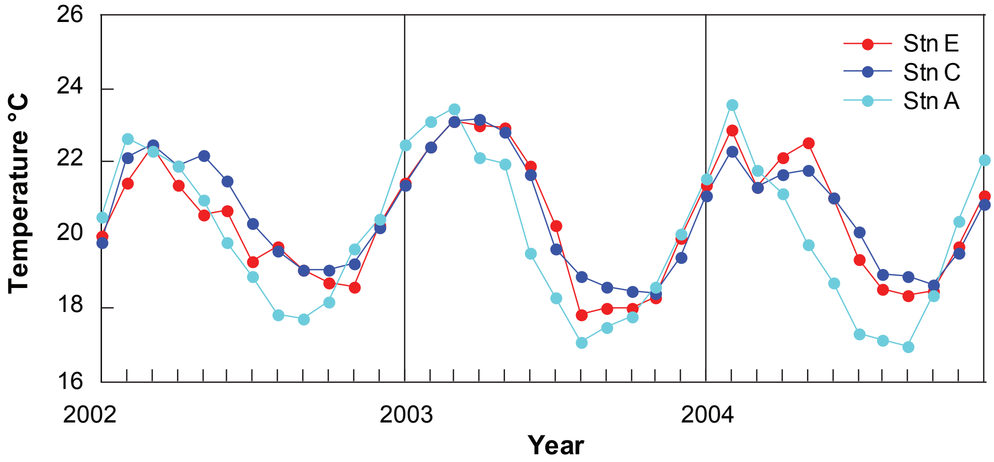

Figure 2.29: Monthly-mean SST derived from satellite data for the Two Rocks stations A, C and E between 2002 and 2004.

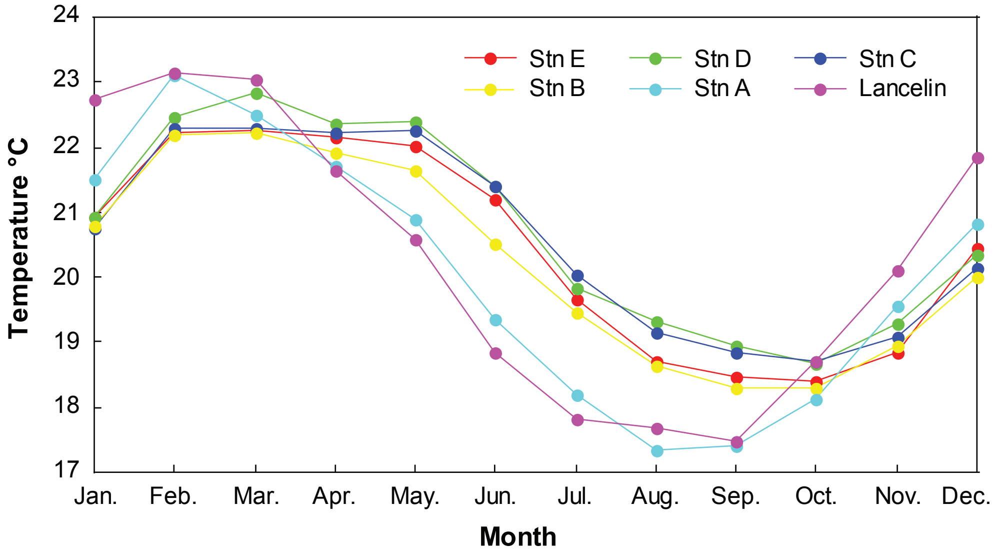

Figure 2.30: The mean annual sea-surface temperature cycle at the Two Rocks stations A to E derived from the AVHRR (2002 to 2004) together with temperatures from shallow nearshore waters off Lancelin (2003 to 2005) for comparison with station A.

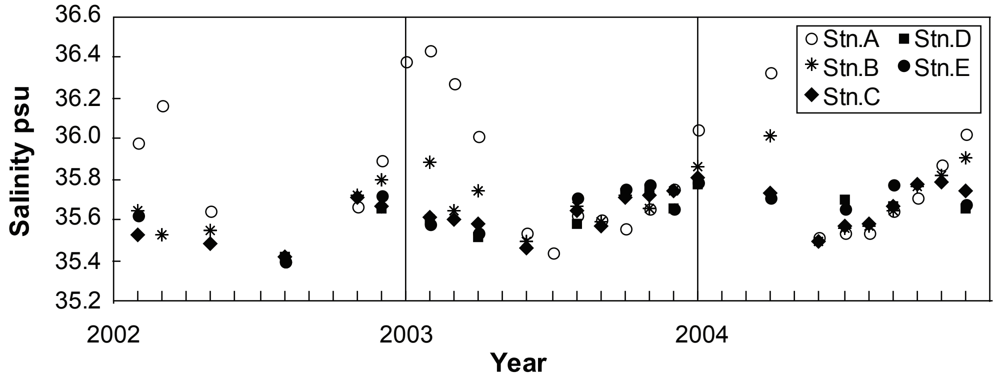

Figure 2.31: Near-surface (5 m depth) salinity from the CTD profiles at the Two Rocks Transect stations over the 3-year period.

2.7 Wave Propagation and Dissipation

As waters shallow across the continental shelf towards the shore, surface waves become increasingly important for both the physics and ecology. Offshore regions of the South West Australian Shelf are dominated by oceanic swell and seas with an average significant wave height about 3 m and period from 5 to 20 s. Most of the year the waves arrive from the south-west, though winter storms often result in waves from the west and north-west bringing high energy conditions to the coast for short periods. Inshore, much of the coastline is sheltered from the direct impact of the swell-wave activity by an extensive chain of reefs, which cause significant attenuation of the ocean waves (Steedman 1993; Sanderson and Eliot 1999). In open areas with little or no presence of reefs, ocean waves propagating inshore experience much less dissipation than in a reef protected areas and any alterations in the offshore wave conditions may have direct impact on the coast.

The high productivity of reef environments has been attributed to direct and indirect affects of waves associated with the oscillatory water motion, turbulent fluxes across wave boundary layers, and wave driven mean flows. Wave exposure has also been linked to habitat type, species diversity and patchiness in algal distribution. The attenuation of wave height, in the absence of breaking, provides a measure of dissipation due to bottom friction over rough reefs, high friction implying a more turbulent bottom boundary layer. Higher turbulence in turn has implications for turbulent fluxes of particles and nutrients between the water column and the underlying plant canopy, and bottom stress affecting habitat, diversity and patchiness.

Modelling waves in open coastal waters

Wave dynamics have been assessed for both open and reef waters along the SW WA coast using both measurement and modelling. The model is SWAN (Simulating Waves Nearshore), which is described and validated in Booij *et al.* (1999) and Ris *et al.* (1999). SWAN includes wave dissipation due to bottom friction, wave breaking and white-capping. For open waters, the wave studies are motivated primarily by the role of waves in sediment dynamics (Section 2.8).

The offshore boundary conditions for the wave modelling are supplied by the 9-year record of significant wave height, period and direction (Fig 2.32), obtained from global simulations with the model WAVEWATCH III (WW3) (Tolman, 1999). To assess the accuracy of the WW3 predictions in the study area, the modelled waves were tested against wave measurements from a site located north-west from Cape Naturaliste near the shelf break at 50 m depth (Fig 2.33a). As shown in figure 2.34, the modelled wave heights tend to exceed the measurements. This discrepancy may be attributable to wave attenuation over the shelf, not properly represented in the coarse resolution (1^ox1^o) WW3 model. However, subsequent numerical experiments, conducted with a fine-resolution implementation of the SWAN model have indicated that the wave attenuation over the shelf would account for only 7 % of the required wave height decline at the Cape Naturaliste site (Fig 2.33b), insufficient to match the model to data.

Based on these and similar experiments with the Rottnest wave station, we conclude that the global-scale WW3 model may systematically overestimate offshore wave height in this region. Scaling of the wave height by a factor of 9/11 matches the model to data (Fig. 2.34). Similar scaling (9/12) fits the model to measurement at Rottnest Island site (Fig. 2.35).

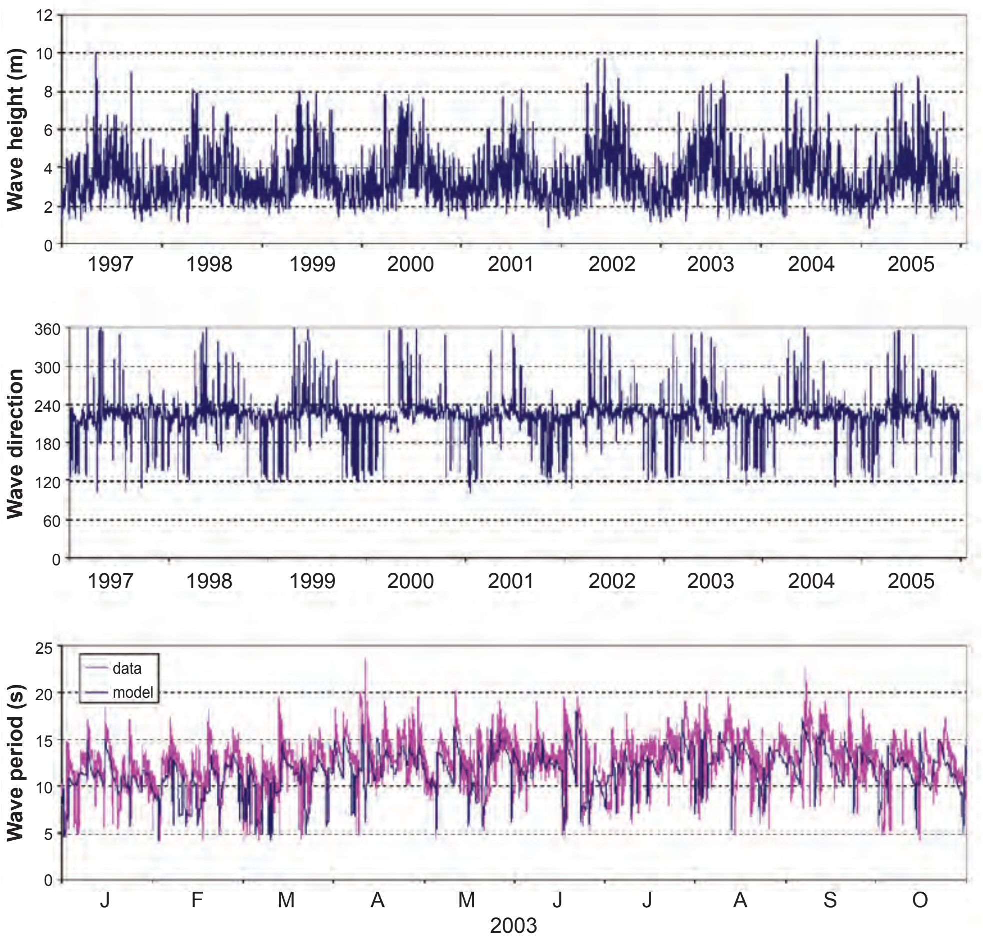

Figure 2.32: Wave characteristics near the Geographe Bay as predicted by WAVEWATCH III model.

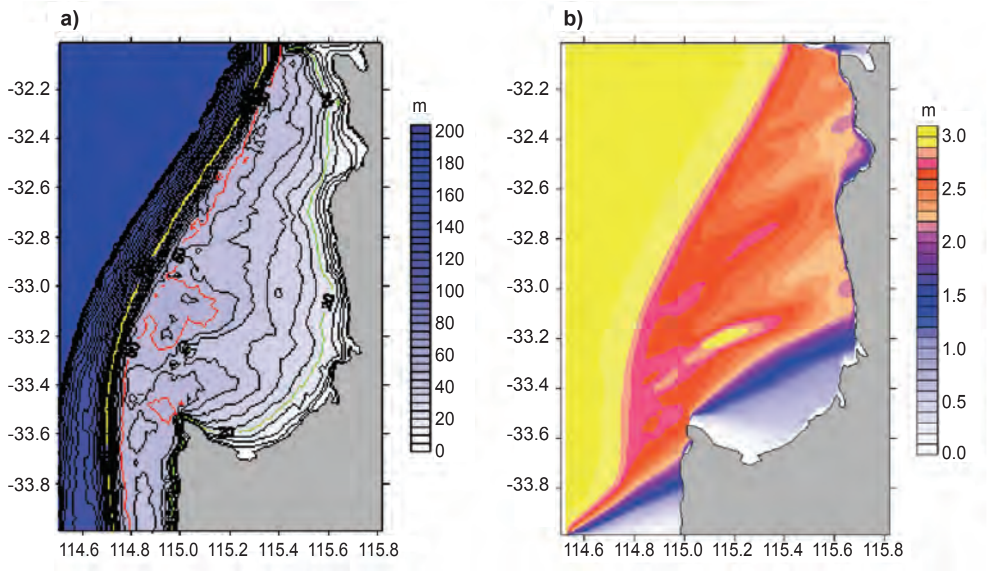

Figure 2.33: Geographe Bay (a) bathymetry and (b) simulated significant wave height for south-westerly waves (SWAN model). The square dot in (a) indicates location of the measurement site.

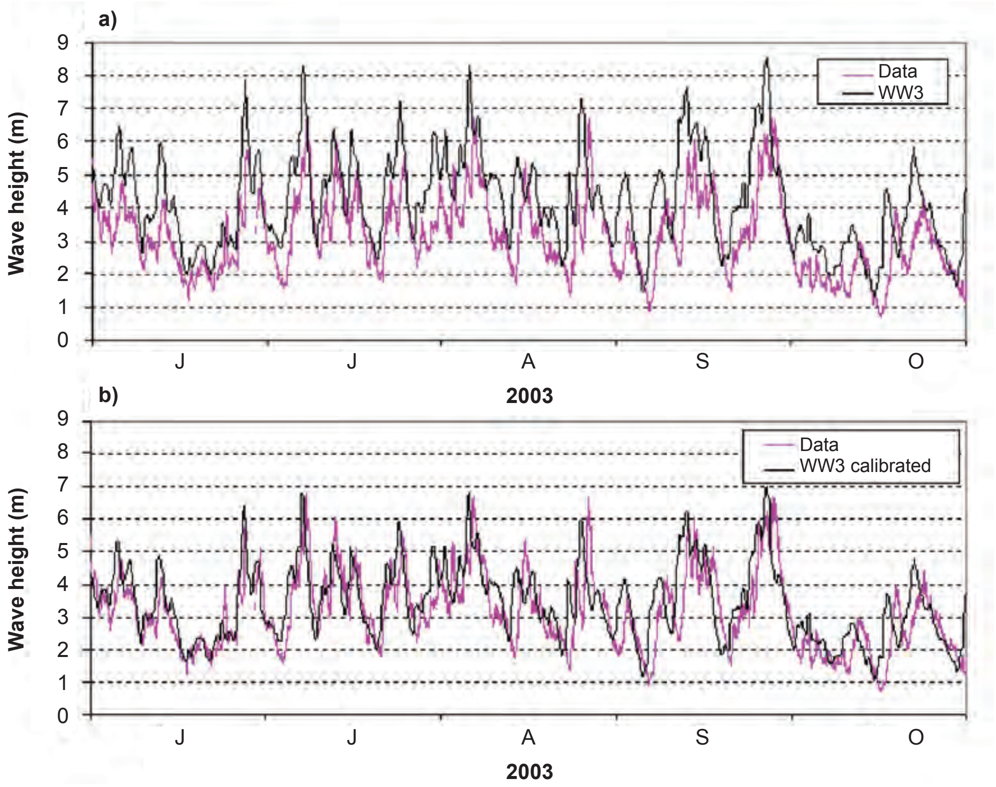

Figure 2.34: Significant wave height predicted by WAVEWATCH III model vs measurements at Cape Naturaliste Station (a) original model output (b) the model output scaled by factor 9/11.

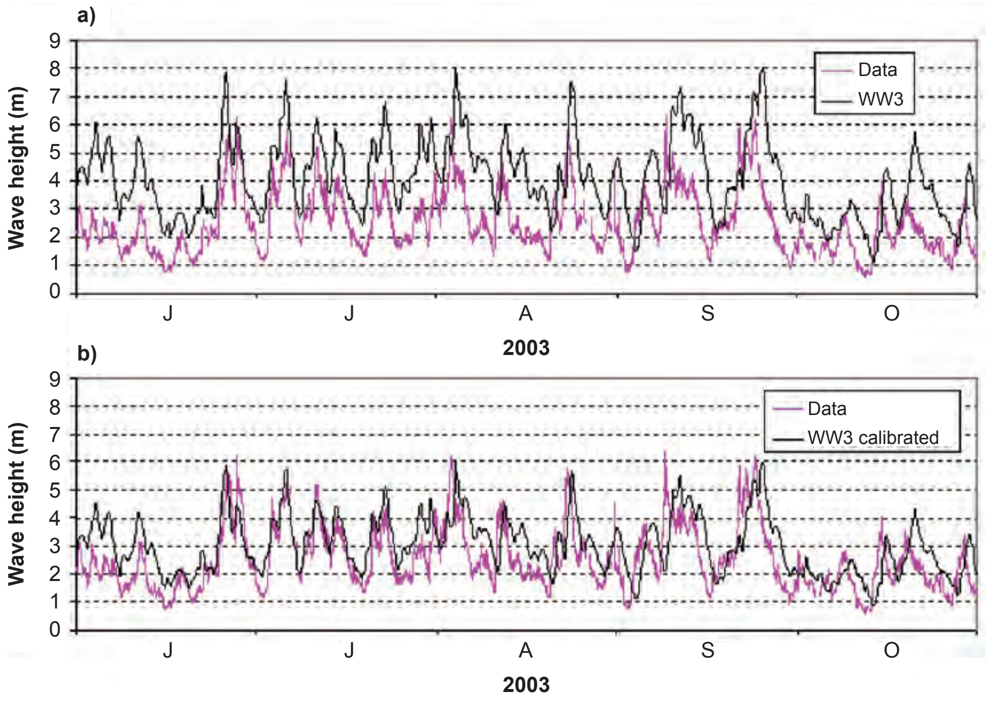

Figure 2.35: Significant wave height predicted by WAVEWATCH III model vs measurements at Rottnest Island Station (a) original model output (b) the model output scaled by factor 9/12.

Wave measurement over Marmion reef

As a first step towards quantifying wave dissipation due to bottom friction over reefs, direct measurements of wave attenuation were made. Four, 3D acoustic doppler velocimeters, were deployed across a section of the reefs off Marmion, south of the Hillary's boat harbour, as shown in Figure 2.36. The bathymetry shown in figure 2.36 was derived from soundings provided by the W.A. Department of Planning and Infrastructure and gridded to 30m horizontal resolution.

The velocimeters were set to record at 2Hz for two hours every four hours and were deployed for the period December 2-19, 2005. The current meters were bottom mounted on rigid frames and measured the three components of velocity at a height of 0.6m above the bottom. Corresponding pressure measurements were made 0.1m above bottom. The measurement site was chosen because very high resolution (sub-metre horizontal) bathymetry was available from a multi-beam survey undertaken by Fugro Pty Ltd allowing the opportunity to quantify bottom roughness. The bathymetry measured by Fugro (decimated to 2.5m horizontal resolution) is shown in Figure 2.37 which also shows the measurement locations and the depth profile along the instrument transect. The instruments had to be separated far enough that we might hope to see measurable attenuation in wave height, yet not so far apart that other effects such as refraction might dominate changes in wave height. The reef crests in this region are also deep enough to avoid any dissipation due to depth-induced wave breaking, which to a first approximation is where the wave height is 0.8 times the water depth. In the absence of any previous measurements, the maximum distance between velocimeters was determined by the size of the Fugro survey region. Instruments ADV1, ADV3 and ADV4 were located on and near the base of reefs in depths of 10.4m, 10.5m and 9m, respectively. ADV2 was located near the top of a reef in a depth of 7.8m.

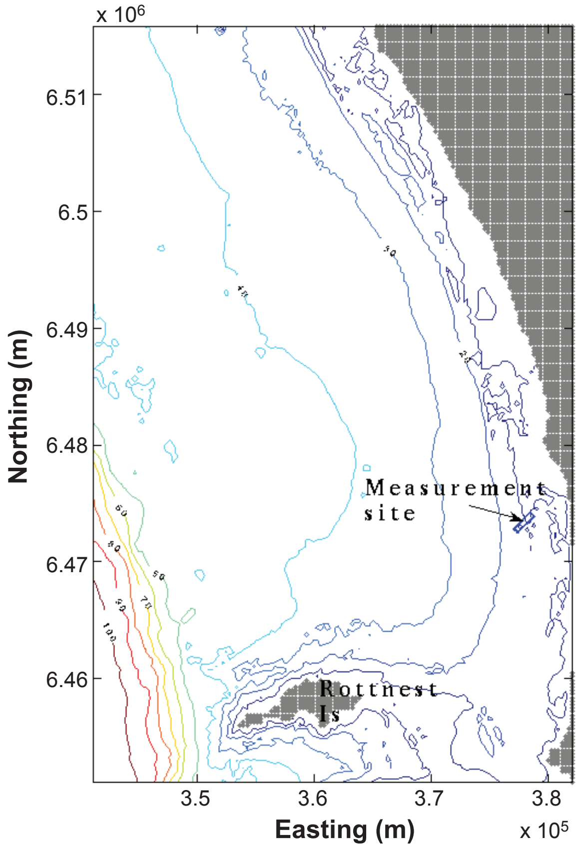

Figure 2.36: Map showing the location of the ADV deployments in the blue box labelled measurement site. See figure 2.37 for detail.

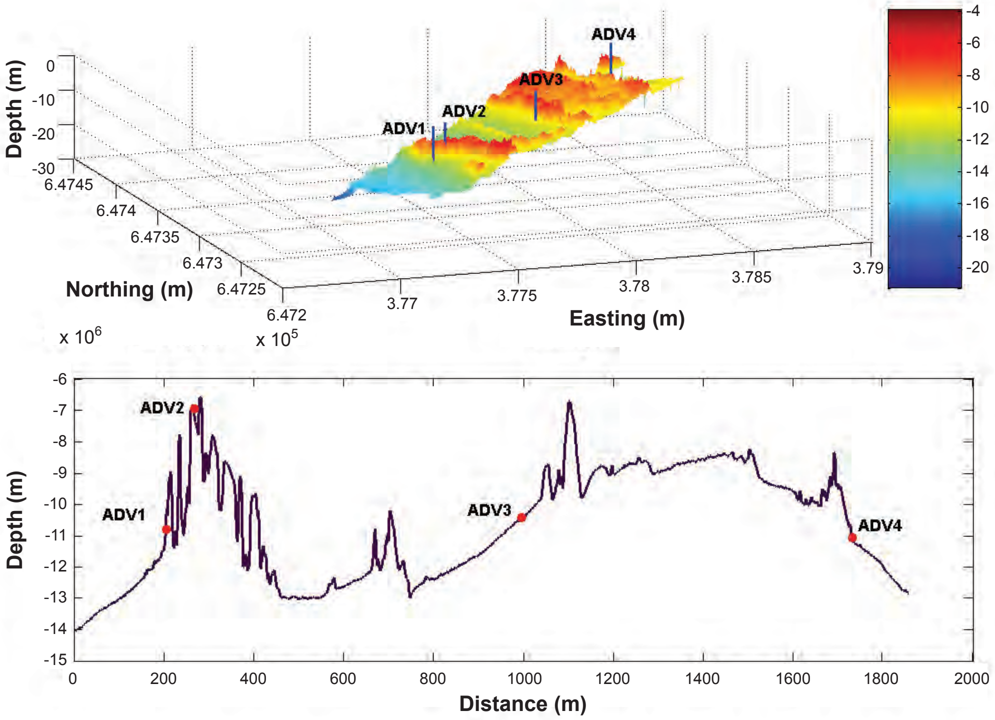

Figure 2.37: Locations of the four Nortek Vector Velocimeters plotted on the multibeam bathymetry, decimated to 2.5m horizontal resolution. (bathymetry courtesy of Fugro Pty Ltd).

The significant wave height (H_s) is calculated from the zeroth moment of the sea surface elevation spectrum calculated from the measurements according to

$$H_s = 4\int_{f_1}^{f_2} E_\eta(f)df \qquad (3)$$

Where $E_\eta(f)$ is the spectrum of sea-surface elevation, f_1 and f_2 were set at .05 and 0.15 Hz, respectively, and a trapezoidal method used to integrate the spectrum. Time-series of the significant wave height for each two-hour measurement period, calculated from the observed pressure at each of the ADVs, are shown in Figure 2.38. Also shown in Figure 2.38 is the time-series of significant wave height from the Rottnest Island wave buoy located in 80m water depth about 30km south west of the Marmion reefs.

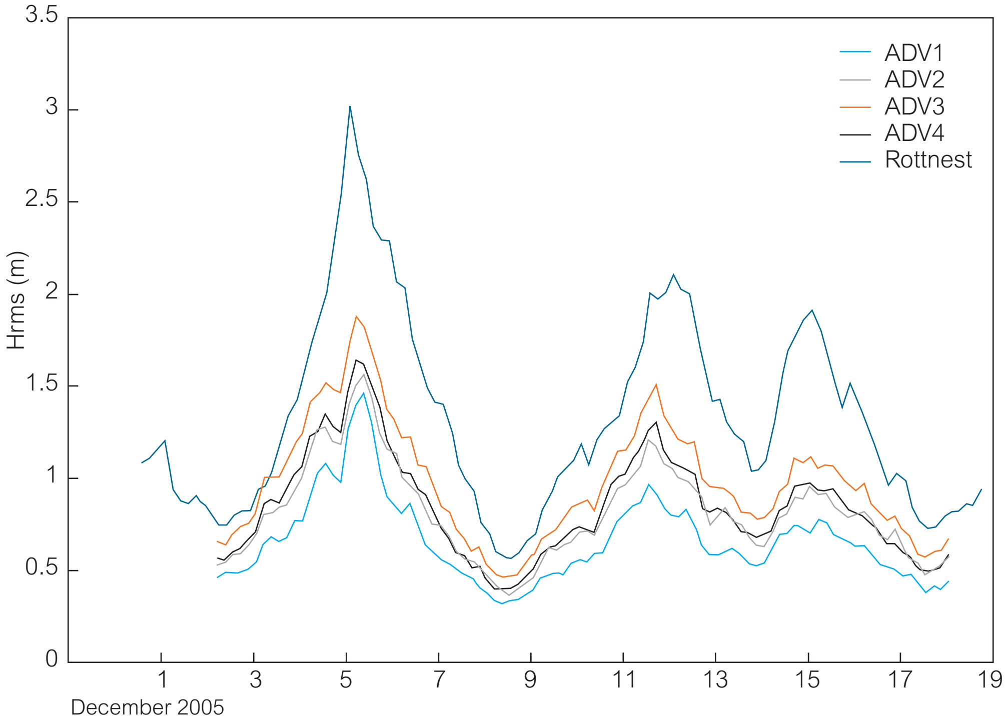

Figure 2.38: Time series of significant wave height (Hs) derived from adv measurements and Rottnest wave buoy.

The velocity measurements are not reported here because the velocity range was set too low to accommodate the larger than expected wave heights. Velocities that exceed the set range are wrapped back into the range and can in principle be unwrapped. However, this has not been attempted.

Moving inshore from the outermost location, the wave height increases at the reef top (ADV2) as the waves shoal over the shallow reef. The wave height then decreases to ADV3 where the wave height is similar to the offshore site (ADV1). Between ADV3 and ADV4 there is a significant reduction in wave height. Though not shown, power spectra showed little evidence of any frequency dependence in dissipation.

Modelling waves over the Marmion reef

To assess the relative importance of dissipation through bottom friction the wave model SWAN was used to simulate wave propagation across the instrument array. Two cases were considered, distinguished by the size of the model domain and the forcing along the offshore boundary.

Case 1.

In this case the model domain stretched from Rottnest Island in the south to Two Rocks, about 40km north of Hillary's boat harbour with bathymetry specified on a 300m grid. The model was forced along the offshore boundary with the observed wave heights and directions from the Rottnest wave buoy. Nested within the 300m grid, and centred over the instrument array, was a smaller 30m grid, where the forcing at the three open boundaries was provided from the larger scale model.

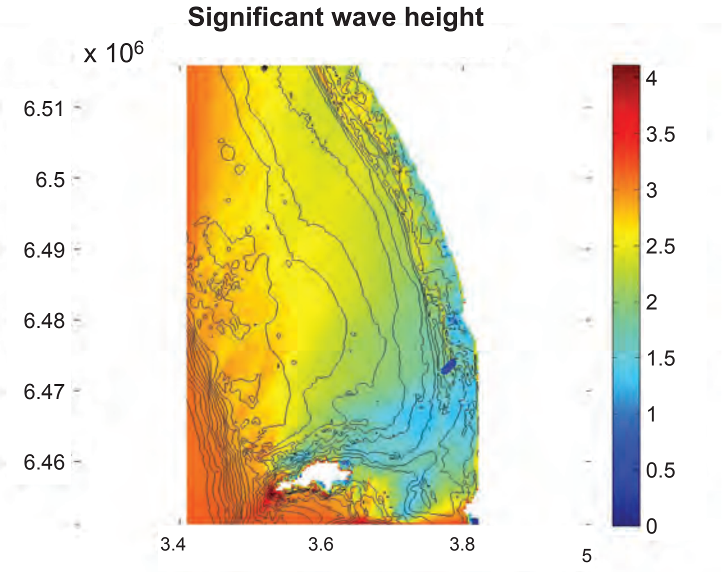

Figure 2.39: Model predicted significant wave height ($H_s = H_{rms}\sqrt{2}$) on the 300m grid. The location of the ADV's is indicated by the small blue squares.

An example of the model predicted significant wave height is shown in Figure 2.39 for the offshore forcing conditions: H_s=3.7m, T=15s and dir=71°. Wave heights at the measurement site are seen to be reduced in part by refraction and the presence of Rottnest Island. A series of model runs was done, each run being forced by the Rottnest wave height, period and direction corresponding to each two-hour measurement period at the Marmion site. The model was run with the Madsen *et al.* (1988) formulation of bottom friction using the default bottom roughness length-scale k_n= 0.05, which is consistent with relatively smooth sandy bottoms. Over rough reefs, it was expected that a significant increase in the roughness length would be needed to match model and observations. However, a comparison of the predicted and observed wave heights in Figure 2.40 clearly shows the model underestimates the wave heights, suggesting that friction in the model might be too high, or that some other aspect of the model is causing an anomalous decrease in wave height.

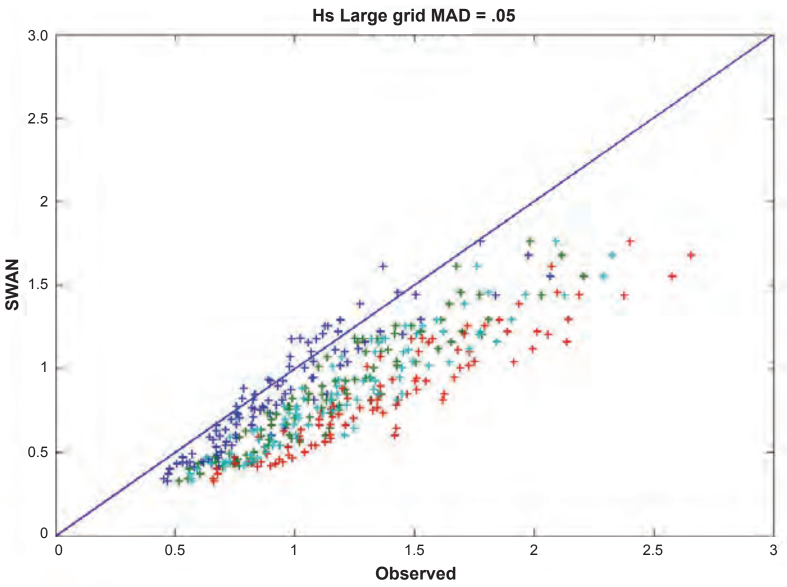

Figure 2.40: Observed H_s versus model forced by Rottnest wave buoy observations. Colour code same as legend in figure 2.38.

Case 2.

In this case a smaller model domain was centred on the instrument array with bathymetry specified on a 30m grid everywhere. The offshore boundary was located close to the position of the offshore ADV. A series of model runs was done, each run being forced by the measured wave height, period and direction at the offshore ADV.

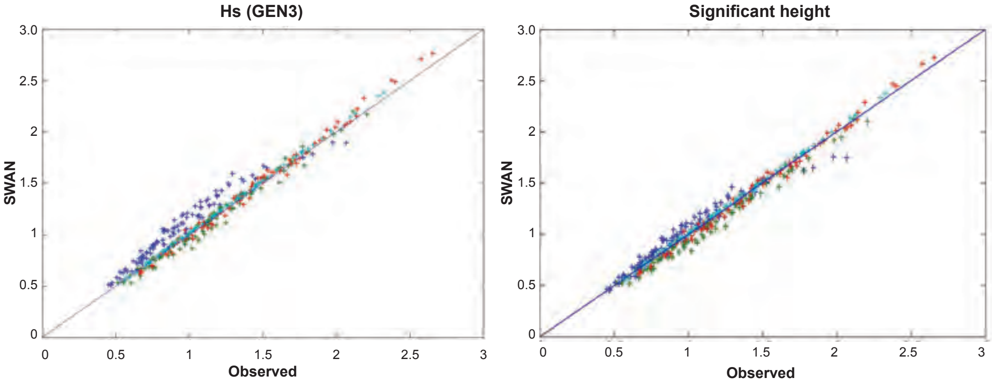

Figure 2.41: Observed H_s versus model with offshore boundary at the location of ADV1. left panel, Madsen friction coefficient 0.05, right panel, Madsen friction coefficient 0.16. Colour code same as legend in figure 2.38.

A comparison of predicted and observed wave heights using k_n=0.05 is shown in Figure 2.41. Clearly the agreement between model and data is much better since the forcing is given by the offshore ADV. With the instruments relatively close together, a surface gravity wave will take approximately 3 minutes to propagate from the offshore to the inshore ADV. However the observations from the inner ADV are consistently above the line, suggesting bottom friction may be too low. Results for a model run with k_n=0.16 are also shown in Figure 2.41. While the reduction in wave height is relatively small it has been achieved with a significant increase in bottom roughness length scale, three times higher than accepted values for sandy bottoms.

This required increase in friction is consistent with recent observations of frictional dissipation of waves propagating over coral reefs reported by Lowe *et al.* (2005). This in turn implies a more turbulent bottom boundary layer which will affect the turbulent transfer of water and particles between the water column and the underlying canopy. Enhanced bottom stress in the presence of waves can increase the rate of nutrient uptake (Falter *et al.* 2004). Hearn *et al.* (2001) suggest that uptake rates are a function of the rate at which wave energy is dissipated by bottom friction.

2.8 Sediment dynamics

Sediment transport is significant for the ecology of the SW Australian coast in a number of ways. Occasional resuspension of sediments can be very effective at reducing the light necessary for the growth of phytoplankton or benthic primary producers (microphytobenthos, macroalgae, sea grass). Many pollutants and nutrients are sediment reactive, and their transport is directly influenced by the sediment dynamics. In open coastal areas, exposed to strong wind and wave currents, intensive bed load transport and resuspension may lead to physical disruption of benthic habitats as well as to enhanced cycling of nutrients across water and sediments. The implications and relative significance of these processes for the ecology of the SW Australian shelf are still not well understood. This is partly due to complexity of the coupled physical and biological systems and partly due to lack of understanding of the sediment dynamics itself.

Sediment transport in coastal water can be driven by both waves and stationary currents, which exert frictional forces on the sea-bed, dislodging sediment grains and entraining them into the water column. For a typical shelf environment, the bottom boundary-layer generated by stationary currents, and often associated with tides or wind-driven flow, may be several meters thick, while the turbulent boundary-layer generated by wind-waves is often confined within a few cm of the sea-bed. Because of this, much smaller boundary-layer size, the bottom friction generated by oscillating wave-currents will be much higher than the friction due to stationary currents of comparable magnitude. On a shelf with a relatively small tidal range and energetic waves, such as SW Australian Shelf, the waves are likely to be a key agent influencing sediment stability, while currents would play more important role in driving transport of the suspended materials.

In open coastal waters of the SW Australian Shelf, swell waves are the key influence on sediment dynamics (Harris *et al.* 1998). Inshore, in areas sheltered from the direct impact of the swell waves, non-tidal variations in sea-level, locally generated waves, and wind-driven water circulation play a more significant role in sediment resuspension and transport (Pattiaratchi *et al.* 1997). Previous studies suggest highly mobile sediments on the shelf inshore (Searle and Logan 1978; Rosich *et al.* 1994) as well as offshore (Harris *et al.* 1998). In areas with an extensive meadow, the profuse foliage may absorb a significant part of the wave energy, with roots and rhizomes of the sea-grass stabilising otherwise mobile substrates. The main sources of contemporary sediments for the coastal environment are expected to be due to bioproduction in sea-grass meadows, reef erosion in the offshore regions, and erosion of cliffs and sandy shorelines with little contribution from river loads (Hodgkin and Hesp 1998; Frances *et al.* 2001).

In this section we investigate spatial, seasonal and inter-annual variability of the sediment mobility on the shelf. A 1-d vertical model, tested against measurements, is employed to assess the sediment mobility at Two Rocks site. A 2-d wave model (SWAN), combined with an empirical formulation for the sediment stability, is applied to the Geraldton shelf, an area influenced by dredging operations, and Geographe Bay, which is characterised by a distinct geomorphological features including migrating erosional patches (Searle and Logan 1978).

Two Rocks

During the project, significant wave height and mean wave period have been recorded inshore at mooring site A (20 m depth). Fig. 2.42 shows an example of the measurements from the first deployment. The wave period varies from 5 to 8 seconds suggesting (as expected) little contribution from the high-energy swell waves. Most of the time, the significant wave height exceeds 1 m, and reaches ~5.8 m during the storm event. The mooring was also equipped with an acoustic Doppler current profiler (ADCP), which provided data for currents and acoustic backscatter signal intensity.

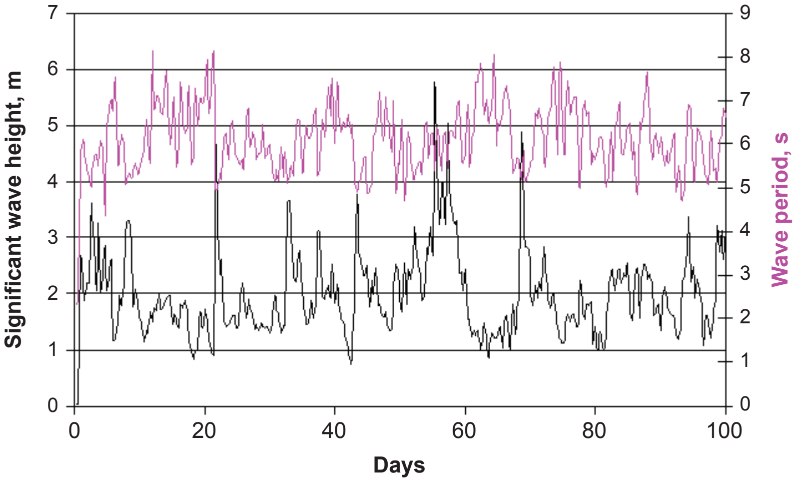

Figure 2.42: Significant wave-height and wave period as measured at the deployment site A (July-October 2004).

The measured waves and currents were used to drive a 1-d vertical sediment transport model. A log-profile is used to extrapolate ADCP currents to the near-bottom region, and linear wave theory assumed to estimate the near-bottom oscillating velocities from the measured significant wave height and wave period. The model simulates bottom exchanges due to resuspension and deposition, and utilises the Grant and Madsen (1986) approach for calculating bottom friction under combined waves and currents. The modelled sediments, resuspended from the sea-bed, are entrained into the water column due to turbulent mixing, which is parameterised using the Mellor-Yamada turbulence closure scheme. The model was tested against suspended sediment concentrations inferred from the strength of the backscatter signal (Margvelashvili and Slawinski, 2004). As can be seen from Fig. 2.43, the range of uncertainty in the concentration estimates covers a factor of about 3, and the modelled data fall neatly into the range estimated from the backscatter. Comparison of the modelled shear stresses with the critical shear, required for initiation of motion of sediments with 0.4 mm grain size (Rosich *et al.* 1994) suggests that, for the most of the modelled period, the wave and current environment at the deployment site are strong enough to maintain a highly mobile near-bed region with appreciable movement of sand particles (Fig. 2.44). The critical shear stresses, during these calculations, were estimated using Yalin's formula as cited in van Rijn (1993).

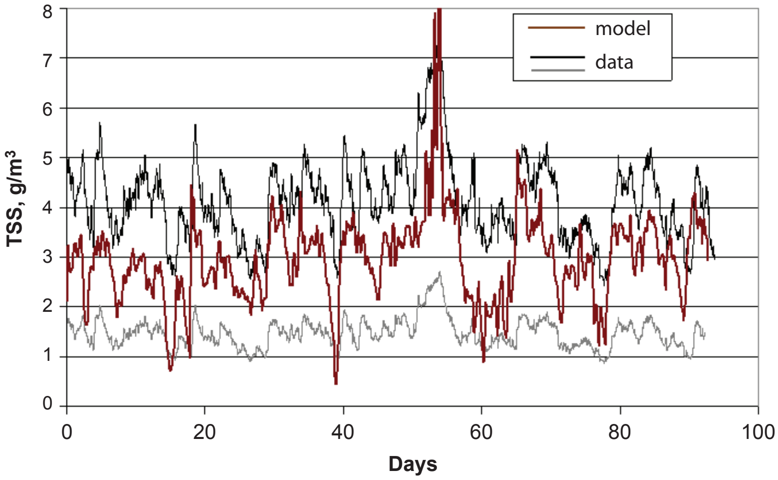

Figure 2.43: Modelled total suspended solids (TSS) vs data (the data show estimates of the maximum and minimum concentration of sediments as derived from ADCP backscatter).

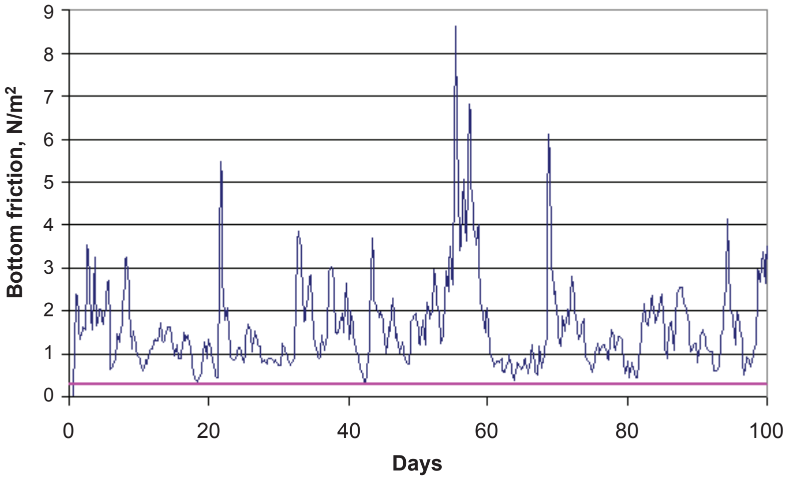

Figure 2.44: Simulated bottom friction at the deployment site A, in July-October 2004. (The red line shows the bottom stress required for initiation of motion of sand particles with 0.4mm diameter).

Geographe Bay

As discussed in Section 2.7, for Geographe Bay, scaled WW3 data have been used to provide offshore boundary conditions for modelling sediment mobility from 1997 to 2005. The wave attenuation over the shelf has been accounted for by calculating, at every cell of the computational grid the attenuation coefficient obtained from the fine-resolution SWAN model simulations. To reduce model runtime, the SWAN runs were driven by the mean wave amplitude and period at the western boundary, and with varying incident-wave direction. The attenuation coefficients, varying with the direction of the offshore waves, are defined by the ratio of the incident wave height to the modelled heights inshore. The near-bottom wave orbital velocities were calculated from WW3 data using linear wave approximations and the wave heights scaled by the attenuation coefficients. From the near-bottom orbital velocities, the bottom friction was calculated as a function of the sediment grain size (Johnson 1966; Li and Amos 2001). The Shields formula (Fredsoe & Deigaard, 1992) was used to estimate the critical shear stress at which sediments with 1mm grain-size become mobile. This modelling assumes that the sediment stability on the shelf is controlled primarily by swell waves, and stationary currents or seas make only a minor contribution to the bottom friction.

The modelling results suggest that, during winter, sediments in most of Geographe Bay are mobile for more than 60 % of time (Fig. 2.45). An area with a relatively low mobility of sediments is located in a southern region of the bay, which is sheltered from the south-westerly waves by the Cape Naturaliste coastline. The model predicts very high mobility rates for sediments in water less than ~20 m deep along the coastline. This may be an overestimate, since the modelling does not account for attenuation of the waves by sea-grass. However, the model also does not account for wave diffraction, and may underestimate the wave amplitude behind the Cape Naturaliste for south-westerly swell.

The predicted high mobility rates do not imply that particles are resuspended for the same fraction of time. The sediment grains may roll over the sea-bed or drift along the bottom by more-or-less regular jumps, spending a relatively small fraction of time in water column. This motion is called “saltation”. To resuspend saltating particles from the sea-bed, and entrain them into the bottom-boundary layer generated by stationary currents, the shear stress needs to be increased, to counterbalance gravitational settling of particles by the enhanced turbulent mixing.

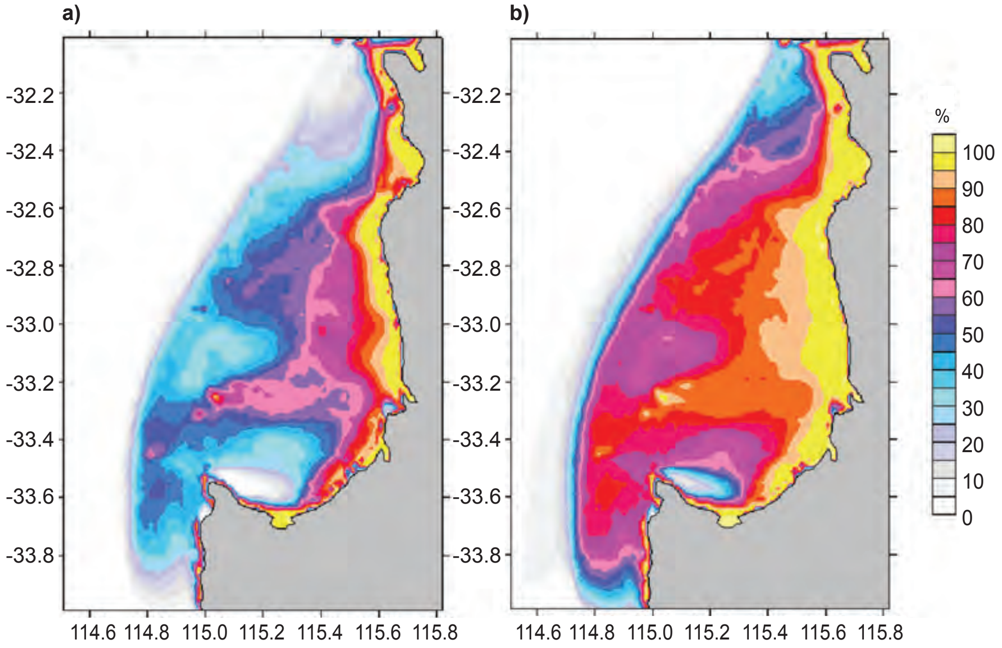

Figure 2.45: Sediment mobility in Geographe Bay (a) summer (b) winter.

Geraldton

The simulations conducted in Geographe Bay have been replicated for the Geraldton area shelf. The Geraldton shelf is characterised by complex bathymetry with a number of shoals and islands near the shelf edge, sheltering the mid-shelf environment from ocean swell (Fig. 2.46). The modelled, area-averaged, sediment mobility in the Geraldton was about 6% lower that that in the Geographe Bay. Figure 2.47 shows annual variations of the sediment mobility over the Geographe Bay and Geraldton shelves for winter and summer seasons, indicating large seasonal variations in sediment dynamics and little annual changes with no clear trends in sediment mobility over the 9 years of the modelling period.

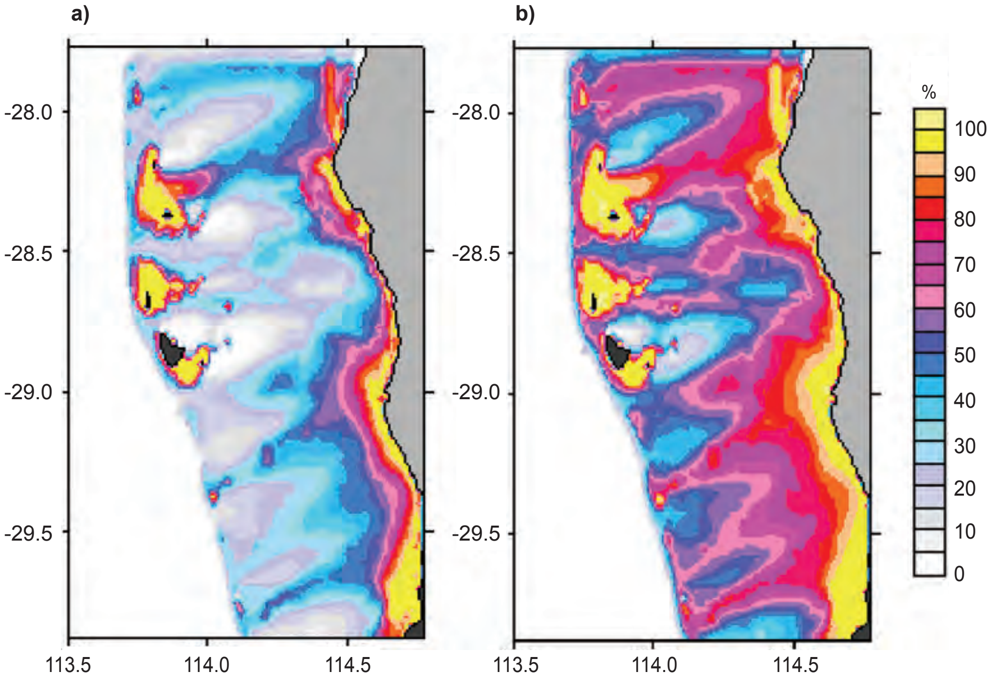

Figure 2.46: The same as in Figure 2.45 for Geraldton site.

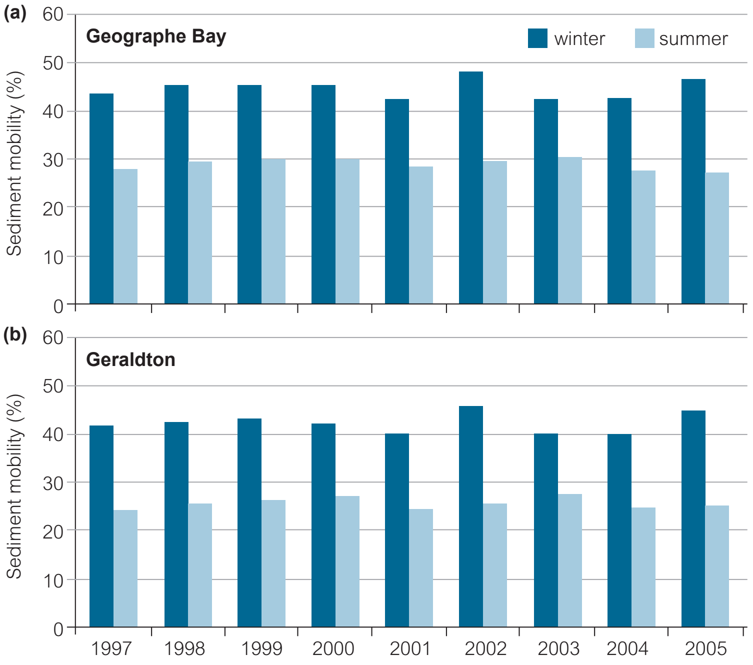

Figure 2.47: Sediment mobility in (a) Geographe Bay (b) Geraldton.

2.9 Summary and conclusions

Probably the most fundamental question for SRFME has been: what determines the offshore, pelagic dominated, and inshore, benthic dominated, marine productivity? This question is pursued in following chapters. The physical environment, discussed in the present chapter, is obviously key to this question. Where are recruits carried by currents? How are nutrients carried from their source? What affects the water temperature? Does sediment resuspension enhance nutrient supply or limit light? How severe are the wave stresses on benthic habitat?

SRFME physical oceanographic studies have placed emphasis on implementation of models, for hydrodynamics (currents, temperature, salinity and mixing), waves and sediments. Models are intended ultimately to provide a predictive capability, for scenarios of, say, climate change or coastal development. For the physics, the most important prediction is usually one of fate: if an individual, or dissolved substance, begins in a certain place at a certain time, where will it travel to. If the individual is negatively buoyant, then it may travel like sediment, falling to the seabed under calm conditions, and being resuspended by storms.

The physical environment off Western Australia is particularly challenging because it is exposed to open-ocean dynamics, incorporating the influence of the Indian and Pacific Oceans. The present study has made extensive use of satellite data, most importantly from altimeters, and historical research data to assess the magnitude of the current systems and their variability. It has quantified the annual and ENSO-related interannual variations of the Leeuwin Current and established a linear relationship between the Fremantle sea-level and the strength (volume transport) of the Leeuwin Current. These results justify the usage of the Fremantle sea-level as an index for the Leeuwin Current, as has been widely used in fisheries management of Western Australia, especially for the western rock lobster recruitment.

Analysis of the Leeuwin dynamics has led to a better understanding of the physical drivers of the seasonal phytoplankton blooms off the southwest Western Australia coast. The Leeuwin Current may draw nutrients from low-latitude to the south when it is stronger during the austral autumn to winter and during the La Niña years. The two unique features of the Leeuwin Current, the largest eddy kinetic energy among all mid-latitude eastern boundary currents and the significant surface heat loss along the path the Leeuwin Current, also facilitate the nutrient uptake off the coast. Eddy induced cross-shelf transport transfers productive water from the shelf to the open ocean, which could affect the western rock lobster recruitment process.

Meanwhile, from the historical in-water data, we have constructed a high resolution climatology for temperature, salinity, and nutrients off the Western Australian coast, the SRFME-CSIRO Atlas for Regional Seas. From this climatology, the Leeuwin Current, the South Australian Current, and the Zeehan Current off western Tasmania are found to be joined, during the austral winter, into the longest eastern boundary current in the world, which has an important effect on poleward transport of tropical biota along the west and south coasts of Australia.

In analysis of cross-shore transect and moorings data, we have observed the transition from Leeuwin-dominated to locally-forced physics. At the offshore site (Station C, 100 m deep), currents predominantly follow the Leeuwin Current. Inshore (Station A, 20 m), currents follow the longshore wind, at close to 3% of the wind speed. Offshore, too, the temperature and salinity are closely tied to Leeuwin Current values, while inshore the water properties are more variable, responding to local heating, evaporation and land runoff.

Further, the inshore dynamics are affected by surface waves, particularly over reefs. The dominant waves are generated as swell in the Southern and Indian Oceans, and increase in amplitude as they shoal toward the coast. By comparison with wave-rider data, publicly-available, global wave model data (in this case WAVEWATCH III) appear to represent the incoming waves reasonably well, and thus supply reasonable boundary conditions for high-resolution coastal models. Our measurements of wave dynamics across the Marmion reef indicate that wave energy dissipates rapidly (requiring a factor of 3 increase in bottom friction in the model). This result has implication for reef productivity, because increased dissipation is considered to enhance nutrient uptake by macroalgae.

High (orbital) velocities under waves cause resuspension of sediments, that may lead to substrate change, reduced light in the water, and movement of nutrients and other chemicals. Our sediment modelling suggests that, for the SW shelf region during the winter, sand-sized sediments are mobile for between 50 and 60% of the time.

The implications of the physical oceanography are pursued in following chapters. In particular, in Chapter 4, hydrodynamic and sediment models are combined with biogeochemical models to describe the shelf-scale biogeochemistry. Then, Chapter 6 explores the interaction between waves and benthic habitat. These are preliminary investigations. With improved understanding of the physical environment across the shelf, we are now much better placed to explore cross-disciplinary links, through better design of interdisciplinary experiments, and the continued implementation of coupled models.

References

Berthot, A., Pattiaratchi, C., Feng, M., Meyers, G., Li, Y. (2006). Latitudinal response of the Leeuwin Current to Interannual forcings using SODA reanalysis data. Manuscript to be submitted.

Booij, N., Ris, R. C., and Holthuijsen, L. H., (1999). A Third generation wave model for coastal regions 1. Model description and validation, *J. Geophys. Res.*, 104(C4), 7649-7666.

Caputi, N., Chubb, C. F., and Brown, R. S. (1995). Relationship between spawning crop, environment, recruitment and fishing effort for the western rock lobster, Panulirus Cygnus, fishery in Western Australia, *Crustaceana*, 68, 213-226.

Cresswell G.R., Boland F.M., Peterson J.L. and Wells G.S., 1989 Continental shelf currents near the Abrolhos Islands, Western Australia. *Austr. J. Mar. Freshw. Res*. 40. 113-128.

Falter, J. L., Atkinson, M. J., and Merrifield, M., (2004). Mass transfer limitation of nutrient uptake by a wave dominated reef flat community, *Limnol. Oceanogr.*, 49, 1820-1831.

Fandry, C.B., Slawinski, D. and Pender, L. (2006) Two Rocks Moorings Data Report. CSIRO Marine and Atmospheric Research Paper 005.

Fang, F., and Morrow, R. (2003). Evolution, movement and decay of war-core Leeuwin Current eddies. *Deep-Sea Research II*,50, 2245-2262.

Feng, M., and Meyers, G. (2003). Interannual variability in the tropical Indian Ocean: A two-year time scale of Indian Ocean Dipole. *Deep-Sea Research II*, 50, 2263-2284.

Feng, M., Meyers, G., Pearce, A., Wijffels, S. (2003). Annual and Interannual Variations of the Leeuwin Current at 32°S. *Journal of Geophysical Research*, 108(11), 3355, doi:10.1029/2002JC001763.

Feng, M., Meyer, G. Church, J. (2005). How our sea temperature has changed? IOCI Note Series.

Feng, M., Wijffels, S., Godfrey, S. and Meyers, G. (2005). Do eddies play a role in the momentum balance of the Leeuwin Current? *J. Phys. Oceanogr.*, 35, 964-975.

Feng, M., Fandry, C., Majewski, L., Waite, A. (2006). Characteristics of two counter-rotating eddies in the Leeuwin Current system off the Western Australian coast. *Deep-Sea Research II*, accepted.

Frances, M., Prosser I., Hughes A., Hua Lu, Stevenson J. (2001). Waterborne erosion – an Australian story. *CSIRO Land & Water, Technical report* 17/01, 50 p.

Fredsoe, J., Deigaard, R. (1992). Mechanics of coastal sediment transport. *World Scientific, Advanced series on Ocean Engineering, v. 3*, 369 p.

Godfrey, J. S., and K. R. Ridgway, (1985). The large-scale environment of the poleward-flowing Leeuwin Current, Western Australia: Longshore steric height gradients, wind stresses, and geostrophic flow, *Journal of Physical Oceanography,* 15, 481-495.

Grant, D., Madsen, O. (1986). The continental shelf bottom boundary layer. *Ann. Rev. Fluid Mech.* 18, p 265-305.

Greenwood, J., Feng, M., Waite, A. (2006). The influence of vertical mixing on biological production in two contrasting mesoscale eddies in the south eastern Indian Ocean. *Deep-Sea Research II*, submitted.

Harris, P., Coleman, R. (1998). Estimating global shelf sediment mobility due to swell waves. *Marine Geology* 150, 171-177.

Hearn, C. J., Atkinson, M. J., Falter, J. L., (2001). A physical derivation of nutrient uptake rates in coral reefs: Effects of roughness and waves, *Coral Reefs*, 20, 347-356.

Hodgkin, E., Hesp, P. (1998). Estuaries to salt lakes: Holocene transformation of the estuarine ecosystems of south-western Australia. *Mar. Freshwater Res.*, 49, 183-201.

Johnson I. (1966). Wave boundary layer and friction factors. *Proc. of 10th Int. Conf. On Coastal Engng*, Tokyo, pp 127-148.

Li M., Amos, C. (2001). SEDTRANS96: the upgraded and better calibrated sediment transport model for continental shelves. *Computers and Geosciences* 27, pp. 619-645.

Lowe, R. J., Falter, J. L., Bandet, M. D., Pawlak, G., Atkinson, M. J., Monismith, S. G., and Kosef, J. R., (2005). Spectral wave dissipation over a barrier reef, *J. Geophys. Res.*, 110, C04001, doi:10.1029/2004JC002711.

Madsen, O. S., Poon, Y –K., and Graber, H. C., (1988). Spectral wave attenuation by bottom friction: Theory, *Proc 21st Int Conf. Coastal Engineering*, ASCE, 492-504.

Margvelashvili, N., Slawinski, D. (2004). Sediment model development data availability and calibration plans. *SRFME Integrated Modelling Project, 2004 Annual Report*, 25-37.

Pattiaratchi, C., Hegge, B., Gould, J., Eliot, I. (1997). Impact of sea-breeze activity on nearshore and foreshore processes in southwestern Australia. *Continental Shelf Research,* v. 17, N 13, pp 1539-1560.

Pearce, A.F. and Pattiaratchi, C.B. (1999). The Capes Current: a summer countercurrent flowing past Leeuwin and Cape Naturaliste, Western Australia. *Cont. Shelf Res.*,19, 401-420.

Pearce, A. F., and B. F. Phillips, (1988). ENSO events, the Leeuwin Current and larval recruitment of the western rock lobster, *J. Cons. Int. Explor. Mer.*, 45, 13-21.

Phillips H. E., Wijffels, S. E., Feng, M. (2005). "Interannual variability in the freshwater content of the Indonesian-Australian Basin", *Geophysical Research Letters 32* (3): L03603.

Ridgway, K., Condie. S., (2004). The 5500-km-long boundary flow off western and southern Australia. *Journal of Geophysical Research*, 109(C4), C04017.

Ris, R. C., Holthuijsen, L. H., and Booij, N., (1999). A Third generation wave model for coastal regions 2. Verification, *J Geophys. Res.*, 104(C4), 7667-7681.

Rosich R., Bastyan, G., Paling, E., Van Seden, D. (1994). Perth Coastal Water Study. Sediment Nutrient Processes. *Project E3.4, No. SSB* 15/94.

Sanderson P., Eliot I. (1999). Compartmentalisation of beachface sediments along the southwestern coast of Australia. *Marine Geology* 162, p. 145-164.

Searle, J., Logan B. (1978). Sedimentation in Geographe Bay. Report to Public Works Dep. Of Western Australia. *Research Project R.T.2595, WA, Nedlands*, 41 p.

Steedman R. (1993). Collection of wave data and the role of waves in nearshore circulation. Report prepared for water authority of Western Australia.

Tolman, H. L., (1999). User manual and system documentation of WAVEWATCH-III version 1.18. NOAA / NWS / NCEP / OMB technical note 166, 110 pp.

van Rijn L. C. (1993). Principles of sediment transport in rivers, estuaries and coastal seas. Aqua Publications.

CHAPTER 3

3. COASTAL AND SHELF PELAGIC COMMUNITY STRUCTURE: PATTERN AND PROCESSES

Investigators / Institutions

Tony Koslow (Project Leader), Peter Fearns, Ming Feng, Jim Greenwood, Christine Hanson, Tim Harriden, Martin Lourey, Nick Mortimer, Alan Pearce, Joanna Strzelecki

CSIRO Marine and Atmospheric Research, Floreat, WA

Lesley Clementson, Rudy Kloser, Tim Ryan, Peter Thompson, Karen Wild-Allen

CSIRO Marine and Atmospheric Research, Hobart, TAS

Harriet Paterson, Stephane Pesant, Anya Waite

University of Western Australia

Barbara Muhling, Lynnath Beckley

Murdoch University

Leon Majewski	Curtin University
Ashrafi Begum	Department of Environment

Outline

Executive Summary

A significant aim of SRFME was to characterize the continental shelf/slope pelagic ecosystem off southwestern WA in terms of its productivity and dynamics, and the physical, chemical and

biological factors driving variability along dominant spatial and temporal scales. To achieve this, we took a number of approaches which included field sampling, instrument deployment and remote sensing studies between Jurien Bay in the north and Geographe Bay in the south. We used a range of conventional oceanographic methods as well as developing and testing new methodologies using *in situ* benthic chambers to measure sediment-nutrient flux and hydroacoustics to estimate the distribution, abundance and biomass of nektonic fauna. The most significant field undertaking was monthly sampling from 2002 – 2004 along a transect off Two Rocks from nearshore to the outer continental shelf (100 m water depth), which we extended quarterly to offshore waters (1000 m depth). Cruise sampling was combined with satellite observations of sea surface temperature (SST), ocean colour and altimetry, and subsurface measurements of currents and temperature from moorings. The Two Rocks transect field program involved six core research components:

1) The physical structure and nutrient dynamics within the water column
2) Phytoplankton community composition, biomass and productivity
3) Microzooplankton communities and their grazing dynamics (reported in detail in Volume 1 – Section. 2.2.9)
4) Mesozooplankton communities and their grazing dynamics
5) Ichthyoplankton community composition and ecology (reported in detail in Volume 1 – Section 2.2.8)
6) Spatial structure of zooplankton and micronekton communities

Along the Two Rocks transect, standard sampling protocols included: meteorological (wind, air temperature) observations from coastal stations; vertical CTD (conductivity-temperature-depth) casts with concurrent measurement of *in situ* fluorescence, dissolved oxygen and subsurface irradiance; discrete water column samples for analysis of salinity, dissolved nutrients (nitrate+nitrite, ammonium, phosphate and silicate), chlorophyll *a*, HPLC pigments, particulate organic carbon, phytoplankton and microzooplankton species composition and abundance, primary production, and microzooplankton grazing; sediment trap deployments for measurement of vertical carbon fluxes; bongo net samples for mesozooplankton biomass, species composition, grazing rates and secondary production; low-frequency acoustic transects, and high-frequency acoustic vertical profiles in combination with targeted water column zooplankton sampling. Nutrient regeneration within the sediments and exchange with the water column was measured seasonally at a range of spatial scales within Marmion Lagoon, in Geographe Bay and Jurien Bay. Benthic chambers were used to measure *in situ* flux rates.

The study resulted in an unprecented level of information of the biological oceanography of the region and clearly identified patterns of seasonal variability which can largely be explained by the region's unique oceanography. In addition we established important cross shelf variability in the dominant functional groups of phytoplankton and zooplankton. The study provided important parameters for the biogeochemical modeling undertaken in SRFME and reported in Chapter 4.

The main findings of the study are summarized as follows.

The nutrient flux from sandy sediments to the water column was highly variable, with greater variability among stations within a location than among seasons. The seasonal cycle of total carbon content in the sediments was not reflected in the nutrient flux. The lack of a clear seasonal signal may have resulted from most of the nutrient flux occurring in pulses during extreme events, which was not captured by the sampling. Far higher levels of ammonium were released into the water column than nitrate, and the N:P ratio was far lower (~2 – 2.8) than the expected Redfield ratio of 16.

Distinct surface phytoplankton assemblages were observed on the inner shelf and further offshore, and between summer and winter. The outer shelf and offshore stations were characterised by high prochlorophyte and unicellular cyanobacteria populations, while small flagellates and periodic diatom blooms dominated inshore waters. Small haptophytes were ubiquitous. Cell count and HPLC analyses proved complementary, with the cell counts emphasizing the larger phytoplankton — mostly diatoms and large filamentous cyanobacteria — and the HPLC focusing on the smaller pico- and nanophytoplankton.

Extensive measurements were undertaken to validate and calibrate the standard algorithms used to assess chl *a* from remotely sensed ocean colour. The standard ocean colour algorithms used by sensors such as SeaWiFS and MODIS appear to produce accurate estimates of chl *a*, and hence phytoplankton biomass, most of the time. Although the absorption properties of the different in-water components were all considered low for coastal waters, at times there is a higher contribution of CDOM than phytoplankton to the total absorption which results in an over-estimate of the *in situ* chl *a*.

Zooplankton biomass was generally greatest in late autumn and winter. The assemblages differed significantly in nearshore and shelf/offshore waters and between winter and other seasons, following patterns among species groups observed elsewhere in coastal waters.

Mesozooplankton community grazing was examined with a newly modified analytical method that enabled meso- and microzooplankton grazing to be simultaneously estimated, along with phytoplankton production. Mesozooplankton grazing on both total phytoplankton and on the microzooplankton was lowest inshore and increased with distance offshore. The increased predation on the microzooplankton offshore was consistent with the smaller phytoplankton and increased role of microzooplankton grazing generally observed offshore. Grazing by mesozooplankton on phytoplankton was low, and the proportion of primary production removed by microzooplankton decreased with increasing mesozooplankton biomass.

We used three methods to estimate secondary production: copepod egg production rates, a biochemical assay related to rates of protein synthesis, and simple non-food-limited production models based on copepod abundance and size. Secondary production was low in comparison with productive marine environments, but comparable to estimates off the North West Cape. There was no correlation between phytoplankton biomass and secondary production. Secondary production was at times a very high proportion of primary production, in relation to the contribution by large phytoplankton alone.

Low frequency acoustic data were used to characterize the distribution of micronekton across the transect. Seasonal patterns were seen, with the main pattern (principal component 1, which explained 31% of the variability) based on inshore backscattering peaking in autumn, with an opposite pattern in winter. Principal component 2, which explained 19% of the variability, highlighted the inner and outer shelf. Increased backscattering on the inner shelf (15 – 20 km offshore) and on the outer shelf just offshore of the 100 m depth station was observed on virtually all summer cruises.

A high frequency acoustic system (TAPS) was used to examine the vertical distribution of zooplankton through the water column. The instrument proved capable of detecting zooplankton even at the relatively low plankton densities in our region.

3.1 Introduction

Investigator / Institution

Tony Koslow	CSIRO Marine and Atmospheric Research

Background

The dominant oceanographic influence on the pelagic ecosystem off the west coast of WA is the Leeuwin Current, the world's only poleward-flowing eastern boundary current (Cresswell and Golding 1980) (see Fig. 2.1). The Leeuwin Current (LC) flows predominantly along the shelf break, bringing warm, nutrient-poor water in its surface layer southward and, as a downwelling current, is generally held to be responsible for the region's low pelagic productivity, relative to other eastern boundary current regions (e.g. the California, Peru and Benguela Current regions) (Pearce 1991). The Leeuwin Current is highly seasonal, peaking in the autumn and winter and reduced in summer when it flows against the prevailing monsoonal southerly 'sea breeze,' which drives north-flowing counter-currents inshore of the LC over the shelf—the Ningaloo Current in the north and Capes Current in the south. Leeuwin Current flow is also closely linked with the ENSO cycle, being weaker during El Niño years when the Indonesian Throughflow is reduced: the Throughflow sets up the meridional pressure gradient that drives the Leeuwin Current (Feng *et al.* 2003, 2004). SRFME has succeeded in verifying the assumed relationship between the Leeuwin Current and Fremantle sea level and in quantifying annual variability and ENSO related variability in Leeuwin Current transport (see Ch. 2).

Recruitment to the western rock lobster (*Panulirus cygnus*) fishery, Australia's most valuable single-species fishery, is closely correlated to the Leeuwin Current and ENSO cycle (Caputi *et al.* 2001), along with recruitment to other fisheries such as whitebait and pilchard (Caputi *et al.* 1996). A model of larval transport indicates that differential transport is probably not responsible for the correlation with western rock lobster recruitment, suggesting that it is based on changes in biological productivity (Griffin *et al.* 2001). Interestingly, rock lobster recruitment is higher during La Niña years, when flow of nutrient-poor LC water is enhanced. However until recently the biophysical dynamics of this system were virtually unstudied: the seasonal cycles of the plankton in coastal, shelf and Leeuwin Current waters were not described, and the potential links between climate variability and biological productivity were not known. As recently as 1998, the plankton cycle off WA was mistakenly believed to follow the typical temperate shelf pattern characterised by a strong spring bloom and low productivity in summer and winter (Longhurst 1998).

Management of marine resources and habitats requires that we distinguish the effects of natural climate variability and climate change from anthropogenic effects. Understanding how climate forcing influences nutrient, phytoplankton, zooplankton and micronekton dynamics across the shelf in southwestern Australia has important application to fisheries resource assessment and management of the marine environment. The overall aims of SRFME were to describe seasonal cycles in the physical structure of the water column, nutrient profiles and plankton communities and their dynamics across the shelf and Leeuwin Current and to assess the mechanisms driving these patterns.

Objectives

The objectives of this component of the SRFME study were to:

- Describe biophysical ocean structure, its seasonal cycle and interannual variability based on remote sensing data and monitoring temperature, salinity, nutrients, phytoplankton (chlorophyll and other pigments) and zooplankton along an onshore-offshore transect north of Perth (Two Rocks).
- Assess the nutrient flux across the sediment-water interface.
- Measure primary productivity and parameters related to zooplankton grazing and productivity at selected stations.
- Apply acoustic methods to monitor zooplankton and higher trophic levels and assess fine-scale distributions based on Tracor Acoustic Profiling System (TAPS) (6 frequencies, 300 kHz - 3 megaHz) and underway 38 and 120kHz frequencies.
- Provide input data and collaborate in development of biogeochemical and nutrient-phytoplankton-zooplankton (NPZ) models for the coastal zone and continental shelf.

Field program

An extensive field research program was undertaken over a 3-year period (2002 – 2004) off the southwestern coast of Western Australia. The study was conducted along an 85 km oceanographic transect off Two Rocks, WA (Fig. 3.1).

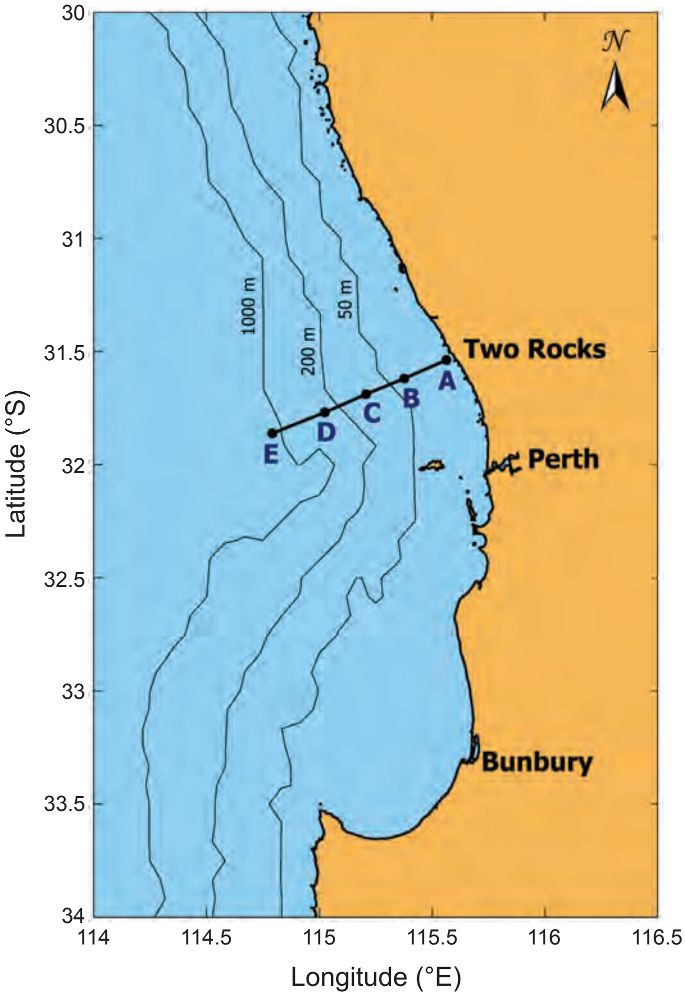

Figure 3.1: Location of the Biophysical Oceanography 'Two Rocks Transect', north of Perth, Western Australia and regularly-sampled stations.

Five core stations (A to E; Table 3.1) were sampled on a monthly to quarterly basis, and encompassed coastal 'lagoon' (Stn A: 15 m depth), inner shelf (Stn B: 40 m), outer shelf (Stn C: 100 m), shelf-break (D: 300 m) and offshore (Stn E: 1000 m) regions (Figs. 3.1, 3.2). In addition to the full sampling programs at these five stations, between-station CTD (conductivity-temperature-depth) profiles were undertaken during the quarterly cruises of 2003 and 2004 (stations AB, BC, CE and DE; Table 3.1). Complete details of the sampling program and methodologies used are included in succeeding sections. Over the duration of the study, 27 research cruises were successfully completed (Table 3.2), resulting in a comprehensive temporal dataset of integrated biological, chemical and physical oceanography within the southwestern Australian region.

Table 3.1. Location, nominal water depth and distance offshore of the Two Rocks Transect stations.

Station	Latitude (°S)	Longitude (°E)	Depth (m)	Distance (km)
A	31.5195	115.5980	15	4
AB	31.5363	115.5594	36	14
B	31.5772	115.4632	40	27
BC	31.6183	115.3652	50	32
C	31.6484	115.2956	100	40
CD	31.6799	115.2210	150	50
D	31.7215	115.1230	300	61
DE	31.7650	115.0198	700	73
E	31.8118	114.9092	1000	85

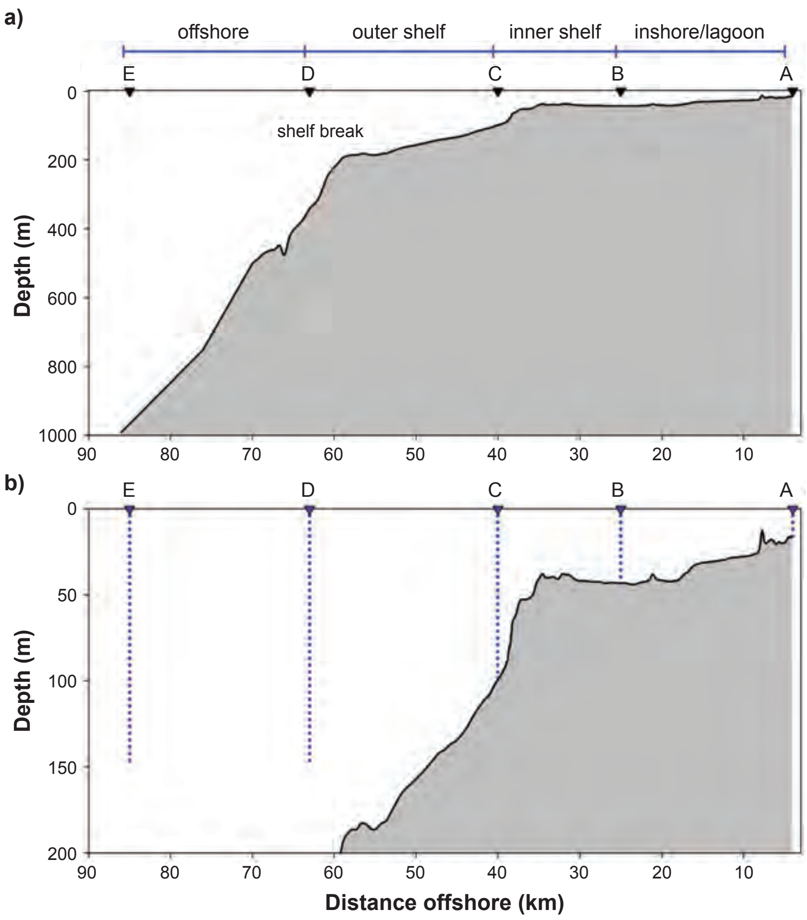

Figure 3.2: Cross-shelf profile of the Two Rocks Transect stations (A to E), illustrating a) large scale bathymetry (to 1000 m water depth) overlaid with region labels, and b) detailed bathymetry (to 200 m water depth) with an indication of maximum sampling depths.

Table 3.2. Summary of the Biophysical Oceanography surveys undertaken during the 3-year field program off Two Rocks, WA.

Voyage	Month	Year	Season	Vessel	Stations
MI200201	Feb	2002	Summer	Maritime Image	A, B, C, E
MC200202	Mar	2002	Fall	Mesocat	A, B
MC200203	May	2002	Fall	Mesocat	A, B, C
NA200204	Aug	2002	Winter	Naturaliste	A, B, C, D, E
MC200205	Nov	2002	Spring	Mesocat	A, B, C
MI200206	Dec	2002	Summer	Maritime Image	A, B, C, D, E
MC200301	Jan	2003	Summer	Mesocat	A
NA200302	Feb	2003	Summer	Naturaliste	A, B, C, D, E
MC200303a	Mar	2003	Fall	Mesocat	C
MC200303	Apr	2003	Fall	Mesocat	A, B, C
NA200304	Apr	2003	Fall	Naturaliste	A, B, C, D, E
MC200305	Jun	2003	Winter	Mesocat	A, B, C
MC200306	Aug	2003	Winter	Mesocat	A
SS200307	Aug	2003	Winter	Southern Surveyor	A, B, C, D, E
MC200308	Sep	2003	Winter	Mesocat	A, B, C
SS200309	Oct	2003	Spring	Southern Surveyor	A, B, C, D, E
NA200311	Dec	2003	Summer	Naturaliste	A, B, C, D, E
SS200401	Jan	2004	Summer	Southern Surveyor	A, B, C, D, E
MC200402	Apr	2004	Fall	Mesocat	A, B, C
MI200403	Apr	2004	Fall	Maritime Image	A, E
MC200404	Jun	2004	Winter	Mesocat	A, B, C
MI200405	Jul	2004	Winter	Maritime Image	A, B, C, D, E
MC200406	Aug	2004	Winter	Mesocat	A, B, C
NA200407	Sep	2004	Spring	Naturaliste	A, B, C, D, E
MC200408	Oct	2004	Spring	Mesocat	A, B, C
MC200409	Nov	2004	Spring	Mesocat	A, B, C
NA200410	Dec	2004	Summer	Naturaliste	A, B, C, D, E

Seven primary tasks were established to meet the objectives of determining the spatial (onshore-offshore) and temporal (seasonal and interannual) patterns of variability in the biological oceanography of southwestern Australia, and of describing and modeling regional biogeochemical processes. These included measurement of:

1) Physical structure and nutrient dynamics within the water column

2) Phytoplankton community composition, biomass and productivity

3) Microzooplankton communities and their grazing dynamics

4) Mesozooplankton communities and their grazing dynamics

5) Ichthyoplankton community composition and ecology

6) Spatial structure of zooplankton and micronekton communities

7) Modeling biogeochemical processes in the inshore lagoon and across the continental shelf and Leeuwin Current

Tasks 3 and 5 (microzooplankton and ichthyoplankton dynamics) formed the basis for two PhD projects, undertaken by Harriet Paterson (UWA) and Barbara Muhling (Murdoch), respectively. The findings from these student components are reported in Volume I of the SRFME Final Report.

Nutrient regeneration across the sediment-water interface was examined as well at three sites along the coast: within Marmion Lagoon and in Geographe and Jurien Bays.

3.2 Temporal and Spatial Variability in Biophysical Oceanography Across the Continental Shelf and Slope

3.2.1 Nearshore Sediment/Water Column Exchange Processes

Investigator / Institution

Martin Lourey and Paul Dean	CSIRO Marine and Atmospheric Research

Introduction

The microbial remineralisation of organic matter and flux of the released nutrients back to the water column may be an important component of coastal nutrient budget. Phytoplankton fix water column nutrients (including those from anthropogenic sources) into organic matter, some of which is deposited on the sea floor. Once incorporated into the sediments it may be remineralised and released across the sediment water interface to maintain water column productivity. Some sediment processes play an important role in moderating the amount of organic matter that is recycled across the sediment water interface. For instance, the bacterial conversion of nitrate to N_2 gas (denitrification) removes nitrate from the system to the extent that this process limits algal growth in some systems with high endogenous nutrient loads (Berelson *et al.* 1998). Variations in organic matter loads, benthic metabolism and processes such as denitrification may therefore lead to shifts in pelagic primary productivity.

Despite the potential contribution that variations in sediment nutrient processes make to the Western Australian coastal nutrient budget, to date temporal and spatial variations in this region and in sandy sediments generally are largely unknown. Furthermore, the response of these processes to human influences, such as input of anthropogenic nutrients, habitat alteration and marine bio-invasions have also not been studied. This study makes the first attempt to quantify the resupply of nutrients from the sediments to the water column in WA and improve our understanding of the physical, chemical and biological processes that control the magnitude of these important nutrient processes.

Materials and methods

Study sites

Field work was conducted between January, 2005 and January 2006. *In situ* benthic chambers were deployed and cores collected from nine sites distributed between Bunbury in the South and Jurien Bay in the North (Fig. 3.3). Sites were clustered about the three core research stations of the SRFME Coastal Ecosystems and Biodiversity project, namely Perth Coastal, Geographe Bay adjacent the town of Bunbury, and Jurien Bay located well to the north of metropolitan Perth. A nested hierarchical sampling design was employed in order to estimate the variability at the following spatial scales: 10m, 1,000m and 10,000m (Fig. 3.3). At each station or geographic region, three sites were selected, each separated by around 10 km. Within each of these sites two locations separated by 1,000m were sampled. At each location replicate benthic chambers were deployed <10m apart (Fig 3.3). Sediment nutrient pools and fluxes were measured along the 10m depth contour.

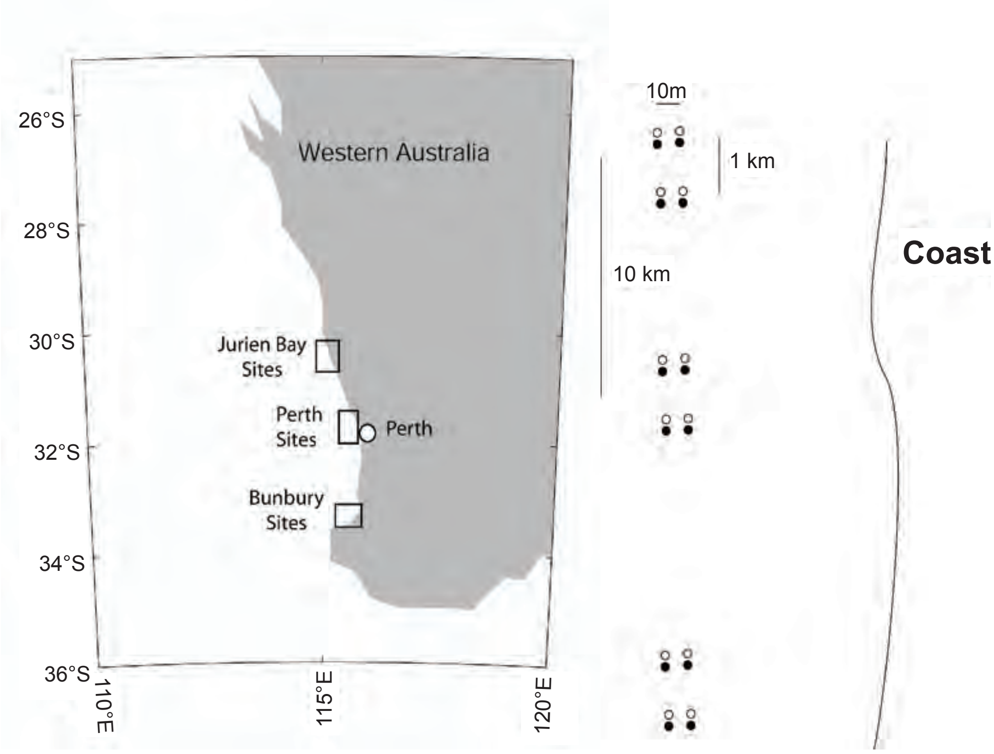

Figure 3.3: Map of WA indicating the location of the core SRFME stations and schematic outlining the nested sampling design. The open and closed circles represent light and dark chambers.

Chambers

Each CSIRO benthic lander consists of paired dark and light acrylic chambers (Fig 3.4). The chambers are lowered slowly and settled into the sediment surface by venting water through a number of one-way valves trapping a nominal volume of 12.5 litres against 0.075 m^2 of the sediment surface. Seating of the chambers into the sandy sediments was confirmed by divers. Each chamber was stirred slowly to break up concentration gradients within the chamber. Stirring commenced at the beginning of each deployment. A known volume of CsCl was injected into each chamber, the dilution of this Cs spike at the first sampling was used to determine the volume of water trapped in the chamber and as an indication of exchange between the chamber and surrounding water. Five water samples were drawn into 60ml syringes at regular intervals throughout the deployment. Oxygen concentration was recorded at 10 minute intervals using a pulsed oxygen probe tapped into the lid of each chamber. These chambers were deployed for around 5.5 hours at each location, a time period generally sufficient to record a discernable dissolved oxygen flux in the dark chambers without completely depleting the oxygen. Our aim was to not deplete the dissolved oxygen by any greater than 20% and avoid artificially promoting anaerobic processes. After recovery, the syringes were subsampled for dissolved nutrients (filtered through a 0.45um membrane), and stored frozen until analysis.

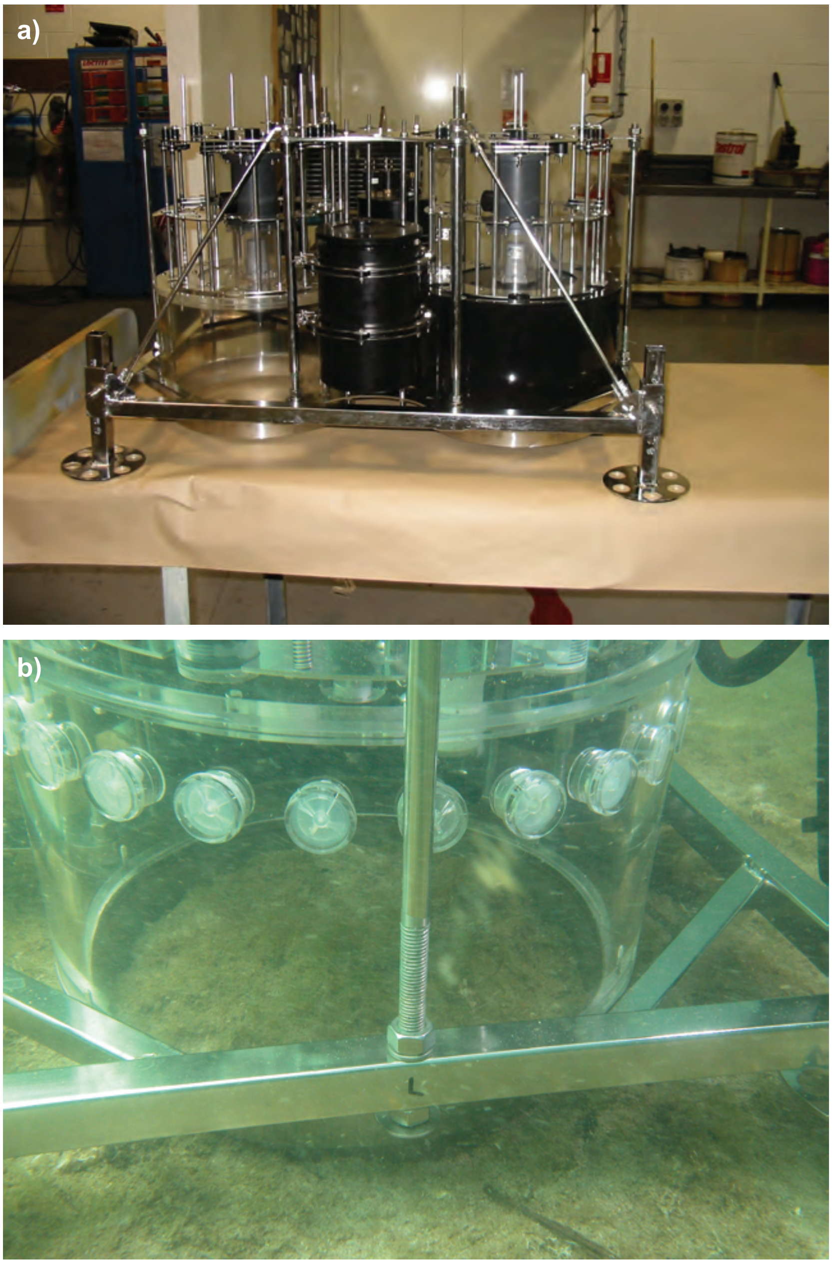

Fig 3.4: CSIRO benthic landers.

Cores

At each sampling location four sediment cores were collected by divers using 10cm diameter acrylic tubes. After retrieval, the overlying water was carefully siphoned off two of the cores and subsamples of the surface sediment collected for pigment analyses (cryovials, stored frozen at -86°C), moisture content (preweighed petri dish, stored frozen), particulate nutrients and organic carbon (25 ml plastic vials, stored frozen until dried) and sediment grain size (zip lock bag, stored frozen until dried). The water was drained from the other two cores and the top 1cm collected for lipid analyses (solvent washed glass jars, stored frozen).

Sample analyses

Dissolved nutrients, phosphate, nitrate, nitrite and silicic acid (silicate) were determined colorometrically by flow injection analysis using standard methods. The ammonium channel of the same instrument was modified to measure that species fluorometrically for improved sensitivity. Dissolved oxygen concentration was measured at 10 minute intervals inside each chamber with a pulsed dissolved oxygen probe tapped into the lid. Each electrode was regularly calibrated against 0% and 100% dissolved oxygen standards prepared using treatments of sodium sulphite (0%) and aerated (100%) seawater samples.

Particulate nitrogen and carbon were determined using CHN analysis on bulk sediment samples dried at 60°C and ground to a fine powder. The particulate organic carbon fraction was determined by subtracting the total carbon from the particulate organic carbon fraction (determined after acidification to drive off the carbonates).

Results

Fluxes of all species (determined by linear regression) were highly variable between stations (and replicate deployments) in each of the study regions (Marmion, Jurien and Bunbury). The spatial variability between stations was generally greater than the variability between seasons (Figs. 3.5, 3.6 and 3.7). Mean dark dissolved nitrogen fluxes ranged from –428 µmol m^{-2} day^{-1} in Geographe Bay during summer to 1304 µmol m^{-2} day^{-1} in Marmion during winter (Figs. 3.6 and 3.7). Both the light and dark dissolved nitrogen fluxes were dominated by ammonium flux. Nitrate fluxes (consumption or release) were generally low (<20% of the magnitude of the ammonium flux), with the exception of Jurien in summer (70% of the ammonium flux) and Bunbury in autumn where the nitrate flux was greater than ammonium (Figs. 3.5 and 3.6). Because of the variability there were no obvious significant differences between light and dark fluxes. Mean silicate and phosphate fluxes were similarly variable with no obvious seasonal trend (Figs. 3.5, 3.6 and 3.7). For example, mean phosphate flux in the dark chambers decreased during the course of the year between winter and spring in Jurien (Fig. 3.5) but increased over the same period in Marmion (Fig. 3.6).

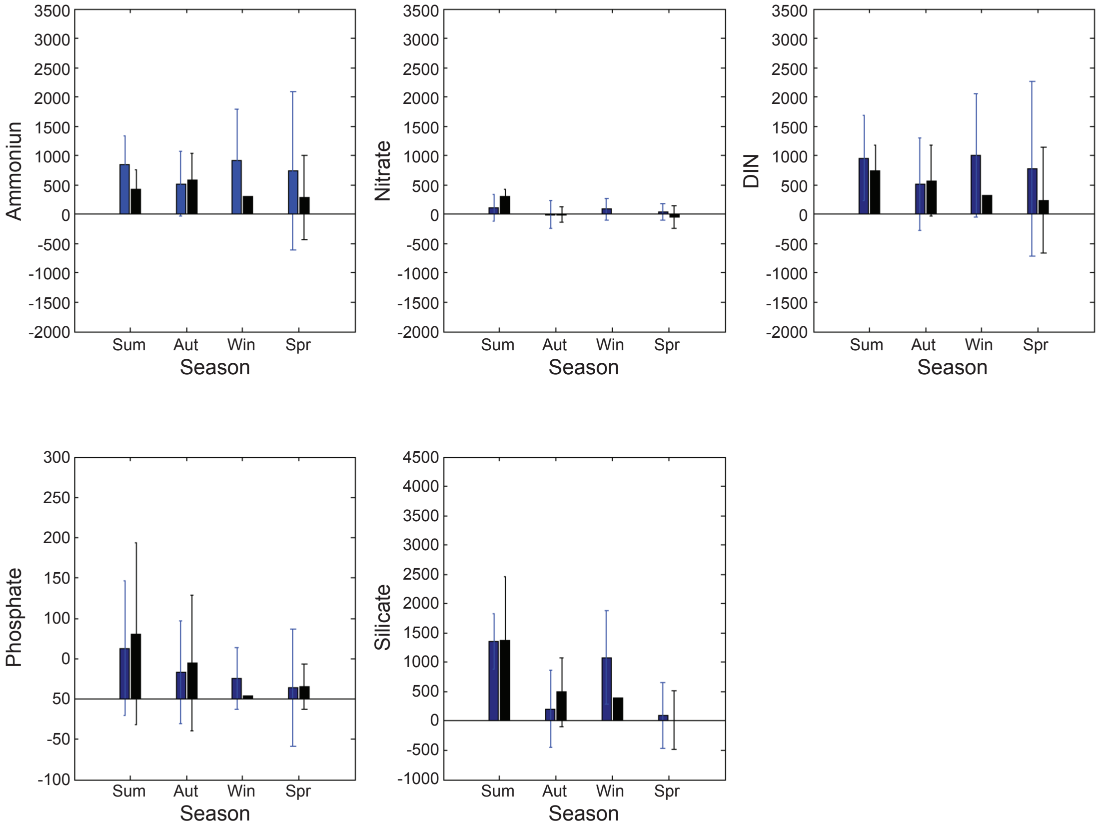

Fig 3.5: Mean (and standard deviation) seasonal variation of sediment nutrient flux (µmol m^{-2} day^{-1}) measured in clear (blue bars) and opaque (black bars) benthic chambers in Jurien.

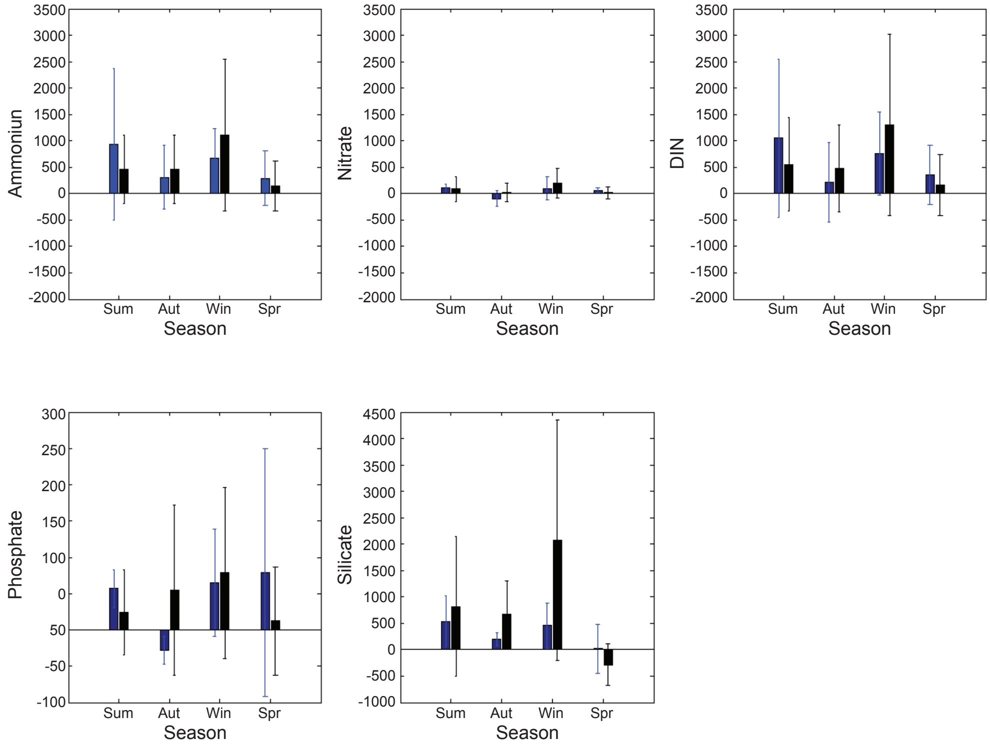

Fig 3.6: Mean (and standard deviation) seasonal variation of sediment nutrient flux (μmol m^{-2} day^{-1}) measured in clear (blue bars) and opaque (black bars) benthic chambers in Marmion.

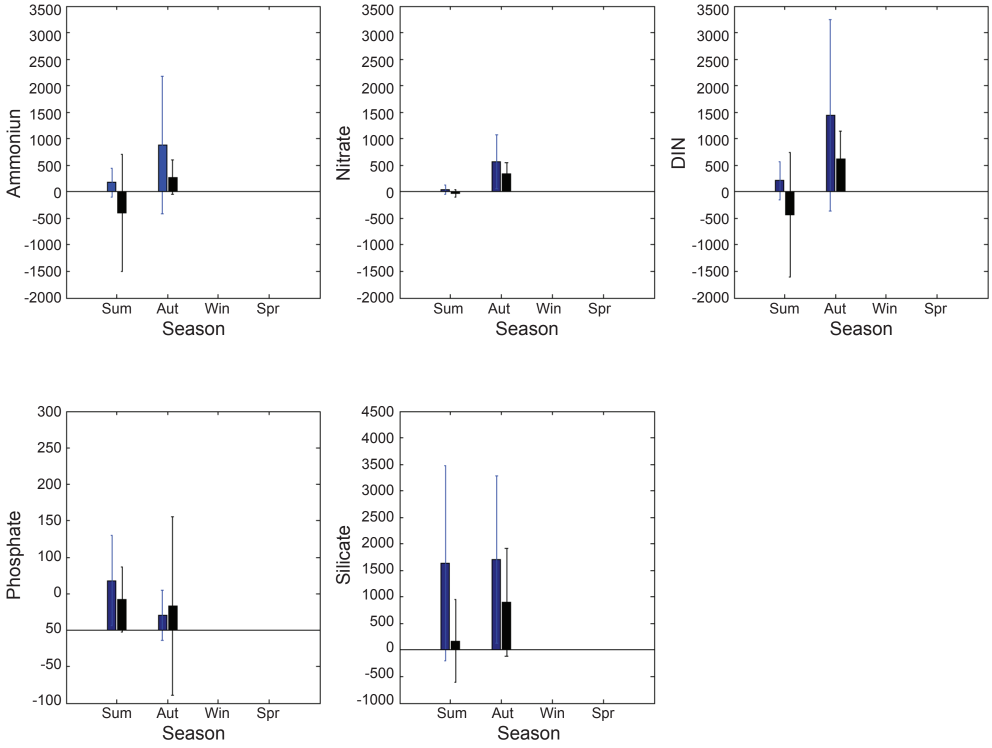

Fig 3.7: Mean (and standard deviation) seasonal variation of sediment nutrient flux (μmol m^{-2} day^{-1}) measured in clear (blue bars) and opaque (black bars) benthic chambers in Bunbury.

The ratio of dissolved nitrogen (ammonium + nitrate flux) to phosphate flux (N to P ratio) was considerably lower than what we would expect from the remineralisation and resupply of marine phytoplankton (an N to P ratio of 16, Redfield *et al.* 1963). The highest N to P ratio observed here is for samples collected in Jurien averaging around 4.5 in both light and dark treatments (Fig. 3.8). The lowest values are from Bunbury (-2.6 and -1.2 for light and dark treatments, however, this relationship is uncertain due to scant data from this area and the relationship is strongly influenced by a small number of the data points (Fig. 3.8). Combining all the data the N to P ratio is around 2.0 in the light and 2.8 in the dark treatments, respectively (Fig. 3.8).

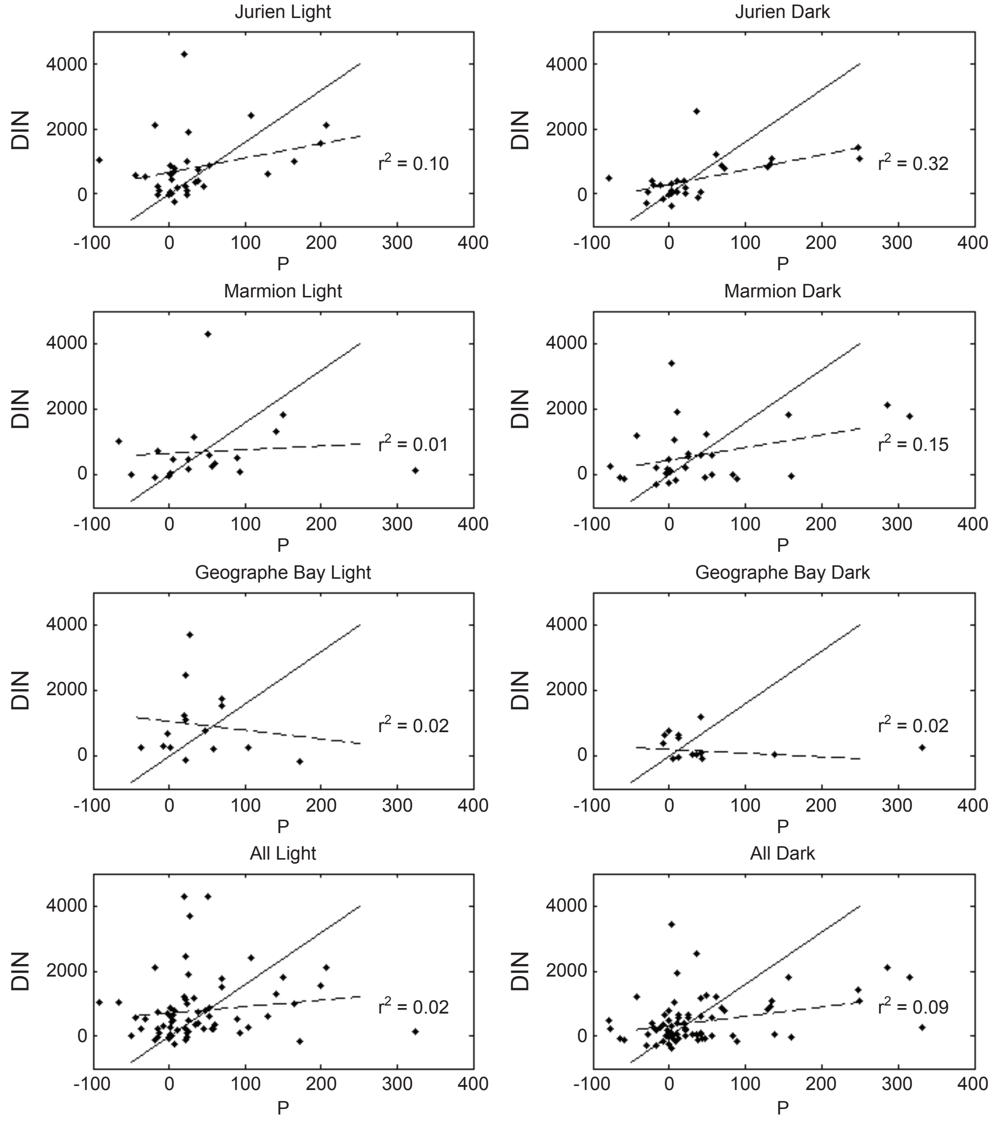

Fig. 3.8: Dissolved inorganic nitrogen flux (DIN) to phosphate flux (P) ratio in light (left) and Dark (right) treatments (μmol m^{-2} day^{-1}). The solid line is the Redfield N:P ratio.

Sediment organic carbon content (and nitrogen content) in Marmion increased from around 0.2% C by dry wt (0.014% N by dry wt) in summer to peak of 0.5% C by dry wt (0.03% N by dry wt) in winter before falling back to 0.25 C by dry wt (0.02 N by dry wt) in autumn (Fig. 3.9). However, a similar seasonal pattern observed in the total carbon content (dominated by carbonate concentration) suggests there may have been some variation in the sediment composition between surveys, possibly due to physical sorting (Fig. 3.9). In Jurien where the total carbon content was the same throughout the season, the organic carbon content was highest in summer and autumn and lowest in winter and spring, coinciding roughly with variations in biomass (Fig. 3.9).

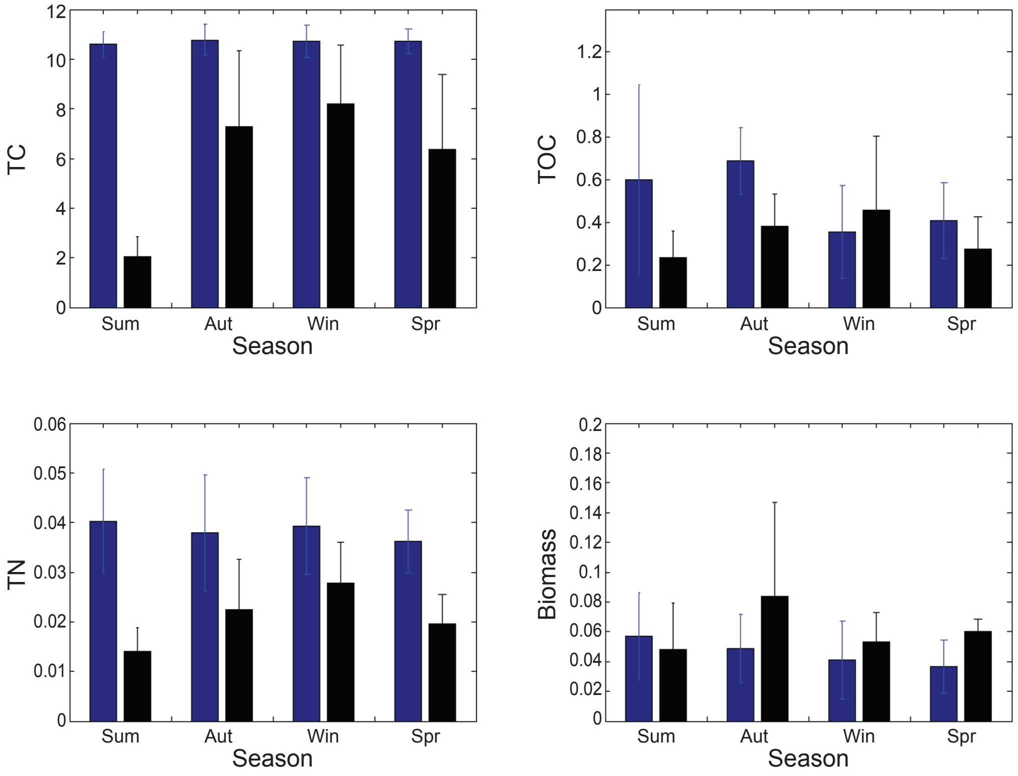

Figure 3.9: Seasonal (mean and standard deviation) variation in sediment carbon and nitrogen content (% of dry weight) as well as benthic microalgal biomass estimated from chlorophyll a concentration (µg g^{-1} of wet weight).

Discussion

Spatial variability

The inner shelf region of the WA shelf is dynamic. Waves and currents resuspend and sort sediments releasing trapped organic material and porewaters (Fanning *et al.* 1982; Kendrick *et al.* 1998). As such the physical composition (grain size), benthic algal community and supply and distribution of particulate organic matter in marine sediments is heterogeneous (Kendrick *et al.* 1998; van Keulen and Borowitzka 2003). The dynamic nature of the system and heterogeneous sediment distribution drives considerable spatial variability in sediment nutrient processes. Here the spatial variability in sediment nutrient fluxes at each station was greater than the average variation between seasons. Variations in the hydrodynamic forcing between the stations (and at a smaller scale between replicate deployments) will control the accumulation of organic carbon and in turn the macroinvertebrate community present (Witte 2000; Lennon and Pfaff, 2005). Long periods of accumulation of organic matter that might be expected between storm events or in sheltered areas will increase nutrient concentration in porewaters and possibly diffusive fluxes in chambers. Organic rich or sheltered sediments will also have a higher population of macroinvertebrate grazers (polychaete worms, molluscs etc) which could increase non-diffusive nutrient fluxes by increasing carbon turnover (Arzayus and Canuel, 2004; Wenzhofer and Glud 2004).

Benthic nitrogen fluxes are not well correlated to the concentration of particulate nitrogen (or total organic carbon) in the sediments. However, this does not immediately suggest that accumulation of organic material does not make an important contribution to sediment nutrient fluxes. It is likely that the labile particulate organic nitrogen fraction or the fraction that is vulnerable to bacterial remineralisation makes most of the contribution to the observed nutrient fluxes (Cowan *et al.* 1996). Our measurements of total particulate nitrogen include both the labile fraction and the refractory material. Because it is relatively impervious to bacterial activity it is probable that the refractory component dominates over the labile fraction. Sediment trap measurements of the rate of supply of fresh organic carbon to the sediments may be a better mechanism for determining spatial variations in the supply of labile organic carbon to the sediments.

Non-diffusive fluxes may significantly alter observed sediment nutrient fluxes. Non-diffusive fluxes include the contribution made to the observed nutrient flux by hydrodynamic and biotic processes (Arzayus and Canuel, 2004). These processes may contribute to the fluxes, but mostly reduce the apparent fluxes by transporting water out of the chamber during the deployment (Webb and Eyre 2004). Sandy sediments such as those in our study region may be more susceptible to the influence of non-diffusive sources of exchange than finer grained sediments. For example, water movement across the sediment and pressure variations associated with waves may advect water through permeable sediments resulting in exchange with the chamber waters (Precht *et al.* 2004). This will reduce the magnitude of the observed nutrient fluxes. The reduction in the observed nutrient flux by non diffusive processes can be estimated by observing the extinction of an inert tracer (CsCl) from the chambers (Webb and Eyre 2004). While the non-diffusive fluxes estimated from caesium extinction varied widely (due to differences in bioirrigation and porosity of the sediments), they were not correlated directly to the magnitude of the nutrient fluxes.

Some of the spatial variability between replicate deployments at the same station may be due to the positioning of the chambers themselves. The composition of the sediments does vary on spatial scales of approximately the size of the benthic chamber footprint. Specifically, there are significant differences in the physical and chemical characteristics of the peaks of sand ridges compared to the depressions in between (Rosich *et al.* 1994). In most cases the large footprint afforded by the benthic chamber approach is sufficient to average across the sand ridges. However, there are cases where the ridging is large enough for the chamber to land on or between the features. Therefore, random variations in the positioning of the chambers in these locations will contribute to the spatial variability observed.

Temporal variability

The mechanical disturbance of sediments and release of sediment organic matter and nutrients during resuspension events such as storms may contribute significant nutrients to coastal regions and moderate nutrient levels in the sediments (Fanning *et al.* 1982; Kendrick *et al.* 1998). While such events and the resulting nutrient pulses may be short lived because coastal regions are strongly nitrogen limited and nutrients released will undoubtedly be consumed rapidly as the storm passes, there are important consequences for sediment nutrient fluxes. Firstly, the resupply and rapid fixing of nutrients will ultimately result in a brief period of higher than usual export as the phytoplankton cells die or are grazed. Short term increases in nutrient flux may be expected to coincide with these short term increases in export. Secondly, the frequency and intensity of these events will ultimately control how much nitrogen can accumulate in surface sediments and porewaters before being stripped away into the water column. As such the timing of deployments about these events will also contribute to variations in diffusive sediment nutrient fluxes.

In Marmion there is a seasonal variation in mean total carbon content of the sediments suggesting there may be a seasonal variation in the composition of the sediment. Some of this variability may be attributed to our ability to relocate stations between cruises (to within the accuracy of a GPS) but it is likely that there was reworking and redistribution of the sediments between cruises. During high energy periods wave energy resuspends material and currents redistribute sediments potentially stripping away the finer fractions (van Keulen and Borowitzka, 2003). These seasonal variations in the physical nature of the sediments may contribute to seasonal variations in nutrient fluxes by reducing the amount of fine organic particles in the sediment and reducing the stability of the biotic community. In Jurien the total carbon is the same suggesting the sediments were more stable over time and that the observed trends were related to biotic processes.

N to P

The N to P flux ratio was considerably lower than 16, which would be expected where phytodetritus is being remineralised (Redfield *et al.* 1963). The deviation of the N to P relationship away from Redfield *et al.* (1963) is primarily due to stations with a high phosphate flux (>100 μmol m^{-2} day^{-1}), but a lower than expected nitrogen flux. There are three possible reasons for this. Firstly, low N to P ratio may reflect rapid preferential consumption of nitrogen within the chambers by nitrogen limited benthic algae. The low nitrogen flux relative to phosphate was evident in both light and dark chambers. This may appear unexpected as we may not expect photosynthesis in the dark treatment. However, dark uptake of nitrogen has been observed in phytoplankton communities, especially during periods of nitrogen limitation. Secondly, it is possible that phytodetritus is not the dominant source of labile organic matter to the sediments in this region. The shelf in this region supports abundant seagrass beds (Kirkman and Kuo, 1990) and macroalgal communities (Kirkman, 1981) and biomass based estimates suggest that macroalgal and seagrass primary productivity is considerably greater than pelagic phytoplankton communities. However, N to P ratios for the dominant macroalgal and seagrass species in the region are higher than that of phytoplankton and would presumably generate a larger N to P ratio than Redfield. Thirdly, denitrification (the microbial conversion of NO_3- to N_2 gas) could reduce nitrogen efflux relative to phosphate. We consider this unlikely as denitrification rates measured in the region (Cockburn Sound) are low (Forehead, 2006).

Comparison to other Australian Estimates

Published estimates of the dissolved inorganic nitrogen flux in Australian estuaries and coastal waters are presented in Table 3.3. From the few estimates it is evident that the level of variability encountered here is a common feature of Australian marine and estuarine environments. Our dissolved inorganic nitrogen flux values compare favourably with the estimates that have been made previously in our study area (Rosich *et al.* 1994) and the measurements collected in the nearby semi enclosed lagoon, Cockburn Sound (Forehead 2006). While our higher flux rates were similar to the upper limits observed in the Perth Coastal Waters Study by Rosich *et al.* (1994) our lowest values are considerably lower. The lower estimates recorded here are from our Bunbury stations, which were not considered by the Perth Coastal Waters Study, and appear to be considerably different to our measurements in Perth. Of the studies listed above, the Bremmer River is unique, in that the DIN fluxes were always negative (consumption) reflecting the unique nature (turbid and high nitrate) of this system (Cook *et al.* 2004a).

Summary

This preliminary investigation into sediment nutrient fluxes in sandy sediments of the WA shelf reveals that within a region spatial variations in sediment nutrient fluxes are as large as regional and seasonal differences. The source of this spatial variability is likely to be due to the complex interactions between the physical and biological attributes of the sediments. Additional sediment flux deployments and focused laboratory incubations accompanied by statistical and modelling approaches as part of WAMSI Node 1 will help isolate the key mechanisms that contribute to the relationship between nutrient fluxes and sediment characteristics.

Table 3.3. Summary of average DIN fluxes (μmol m^{-2} day^{-1}) from a number of Australian coastal and estuarine benthic flux studies. The studies in bold were conducted in Western Australian Waters.

Location	DIN flux	Source
Australian Estuaries		
Swan River, WA	**100**	**Douglas** *et al.* **1996**
Wilson Inlet, WA	**1720**	**Fredricks** *et al.* **1999**
Gippsland Lakes, Vic	-540 - 12000	Longmore *et al.* 1998
Huon R. Mud Flats, Tas	-960 – 2448	Cook *et al.* 2004b
3 estuaries, SE QLD	-2690 – 1080	Ferguson *et al.* 2004
6 coastal lagoons, SE QLD	-7800 – 2640	Eyre and Ferguson 2002
Bremmer River, SE QLD	-3300 - -600	Cook *et al.* 2004a
Australian Marine		
Port Phillip Bay, Vic	700-1243	Berelson *et al.* 1998
Moreton Bay, QLD	-500 – 6000	Dennison and Abal 1999
Coastal GBR, QLD	245-820	Alongi and McKinnon 2005
Bowling Green Bay GBR, QLD	-154 – 890	Ullman and Sandstrom 1987
Reef GBR, QLD	140 – 540	Hansen *et al.* 1987
Inner GBR shelf, QLD	36 – 720	Lourey *et al.* 2001
Cockburn Sound, WA	**up to1450**	**Forehead 2006**
Perth Coastal Waters, WA	**571 – 2142**	**Rosich** *et al.* **1994**
Perth, Jurien and Bunbury, WA	**-428 - 1304**	**This study**

3.2.2 Phytoplankton Community Structure

Investigator / Institution

Christine Hanson, Lesley Clementson, Peter Thompson

CSIRO Marine and Atmospheric Research

Introduction

Assessment of phytoplankton species composition is of high importance in studies of pelagic ecology. Standard methods for identification and enumeration of phytoplankton have primarily involved light microscopic examination of preserved cells (Utermohl, 1958; Willen, 1976), with the picoplanktonic fraction (cells < 3 μm) analysed using epi-fluorescence microscopy (Murphy and Haugen, 1985) and/or flow cytometry (Olson *et al.* 1985; Simon *et al.* 1994). These are often one of the more time consuming data sets to obtain and can have a high coefficient of variation associated with the cells counted. Pigment analysis (via High Performance Liquid Chromatography or HPLC) and diagnostic pigments are also used to estimate community composition and concentration with a higher degree of reproducibility than microscopic methods. Pigments which relate specifically to an algal class are termed marker or diagnostic pigments (Jeffrey and Vesk, 1997; Jeffrey and Wright, 2006) and some of these diagnostic pigments are found exclusively in one algal class (e.g. prasinoxanthin which is only found in prasinophytes) while others are the principal pigments of one class but are also found in other classes (e.g. fucoxanthin in diatoms and some haptophytes; 19'-butanoyloxyfucoxanthin (19BF) in chrysophytes and some haptophytes). The presence or absence of these diagnostic pigments can provide a crude guide to the composition of a phytoplankton community including identifying classes of small flagellates that cannot be determined by light microscopy techniques, and drastically reduce sample processing time compared to microscopic methods (as discussed in Hill *et al.* 2005; Wanstrand and Snoeijs, 2006).

Methodology

Phytoplankton community composition was assessed at five stations along the Two Rocks Transect (Fig. 3.1), with samples obtained monthly to quarterly (depending on station) over approximately 3 years (February 2002 to December 2004). Community structure was quantified using two methods: 1) Cell counts, using light microscopy, were completed on samples preserved in acidic-Lugol's solution. Phytoplankton cells > 5 μm in size were identified and counted within ten major taxonomic groups: diatoms, dinoflagellates, cyanobacteria, chlorophytes, cryptophytes, euglenophytes, chrysophytes, silicoflagellates, raphidophytes and haptophytes. 2) Detailed pigment analyses, using High Performance Liquid Chromatography (HPLC), were performed on phytoplankton collected on glass-fibre filters. Methods used to analyse water samples for pigment composition and concentration can be found in Keesing and Heine (2005). Marker pigments were analysed for trends, and in this study the presence of fucoxanthin has been used to indicate diatoms; peridinin – dinoflagellates; 19'-hexanoyloxyfucoxanthin (19HF) – haptophytes; 19'-butanolyoxyfucoxanthin (19BF) – chrysophytes; alloxanthin – cryptophytes; prasinoxanthin – prasinophytes; zeaxanthin – cyanophytes; chlorophyll b – chlorophytes/green algae and divinyl (DV) chlorophyll a – prochlorophytes.

Cell count data tended to be non-normal regardless of transformation, and so statistical assessment was limited to a single factor non-parametric technique (Kruskal-Wallis One Way Analysis of Variance on Ranks). Pigment concentrations were log transformed prior to statistical analysis allowing simultaneous assessment of temporal and spatial variation using a general linear model.

Microscopic assessment

The variation in abundance of major taxonomic groups was very high: across all stations and all sample periods the across taxon mean co-efficient of variation was 328%. In spite of the high variability significant differences were found in both spatial and temporal distributions of phytoplankton based on cell counts from surface samples. High numbers of filamentous cyanobacteria occasionally dominated the counts (Fig. 3.10), and on average accounted for 39.4% of all cells. Bacillariophytes (diatoms) were similarly abundant (39.2%), followed by cryptophytes (10.1%) dinophytes (dinoflagellates, 6.7%) and chlorophytes (1.7%).

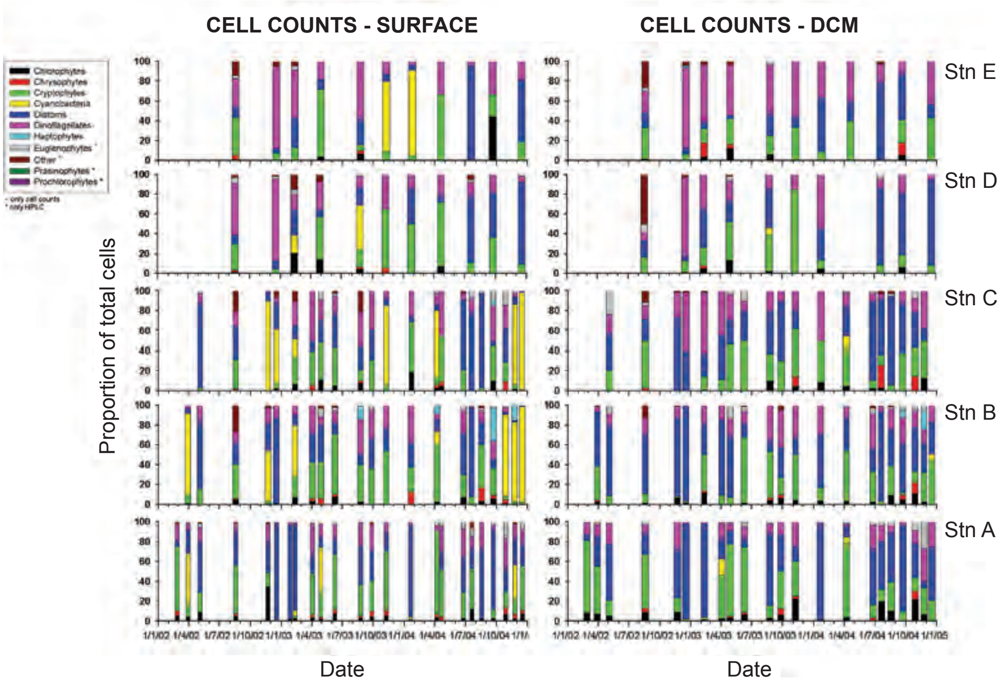

Figure 3.10: Phytoplankton community composition as determined by cell counts using light microscopy, where dominant genera were identified and counted within eight major taxonomic groups.

Diatoms ($p = 0.003$), chlorophytes ($p = 0.001$) and cryptophytes ($p = 0.001$) all showed significant spatial trends with surface cell densities declining with distance offshore (Fig. 3.11). Diatom densities were found to decrease in abundance from 91×10^3 cells L^{-1} to 3.3×10^3 cells L^{-1} or by a factor of 30 moving from the coastal lagoon (Stn A) to the most offshore station (E, 1000 m water depth). Diversity (Shannon-Weaver index) tended to be greater inshore rather than offshore although this trend was not statistically significant ($p > 0.05$). This research represents the first time an offshore-onshore gradient in algal class abundance has been demonstrated for waters off the Western Australia coast. While some spatial patterns have been reported (e.g. Hanson *et al. in press*), the systematic sampling undertaken in SRFME provides the first evidence of strong onshore-offshore gradients in the abundance of a number of key taxa persisting over a multiyear time scale. Silicoflagellates, which were identified as a possible ecological concern in 1996 (DEP 1996) due to their relatively high abundance and potential to kill fish, were found to be ~ 0.1% of all enumerated cells. Significant seasonal changes in surface cell abundance were evident within the diatoms and cyanobacteria. Diatoms reached a peak ($p = 0.013$) in median cell density while cyanobacteria tended ($p = 0.033$) to be least abundant during winter. A winter peak in community dominance by diatoms was also noted by Thompson and Waite (2003) in the nearshore region of Perth's coastal waters.

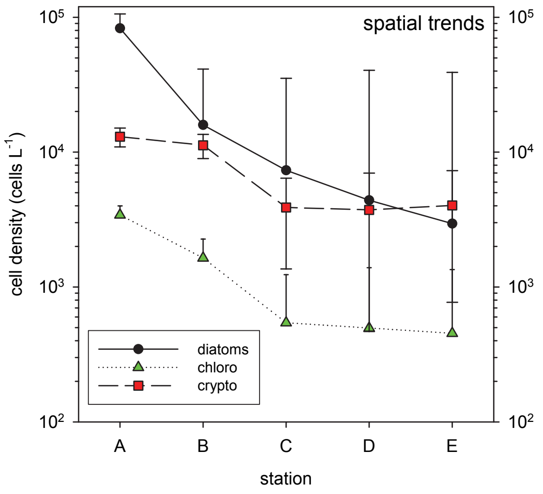

Figure 3.11: Surface densities of selected phytoplankton taxa; diatoms (●), chlorophytes (▲) and cryptophytes (■) at each of five stations across the onshore (station A) to offshore (station E) transect at Two Rocks, WA. Standard errors of the means from 2 way ANOVA are shown; to improve figure clarity sometimes as upper bounds only.

Pigment assessment

Surface waters

In general, phytoplankton biomass (as indicated by chlorophyll *a* concentration) showed strong spatial variation across the transect and strong temporal variation throughout the study period. In surface waters, phytoplankton biomass decreased from inshore (Stn A) to offshore (Stn E; Fig 3.12). At all stations, except the most inshore station, there was a clear seasonal cycle in the biomass signal with a maximum chlorophyll *a* concentration usually in the austral winter (August) of each year (Fig. 3.13a for representative data from Stn B). The lack of seasonality in chlorophyll *a* concentration within inshore waters is also confirmed by a 7-year time series analysis of SeaWiFS satellite imagery (see Section 4.2, Fig. 4.17).

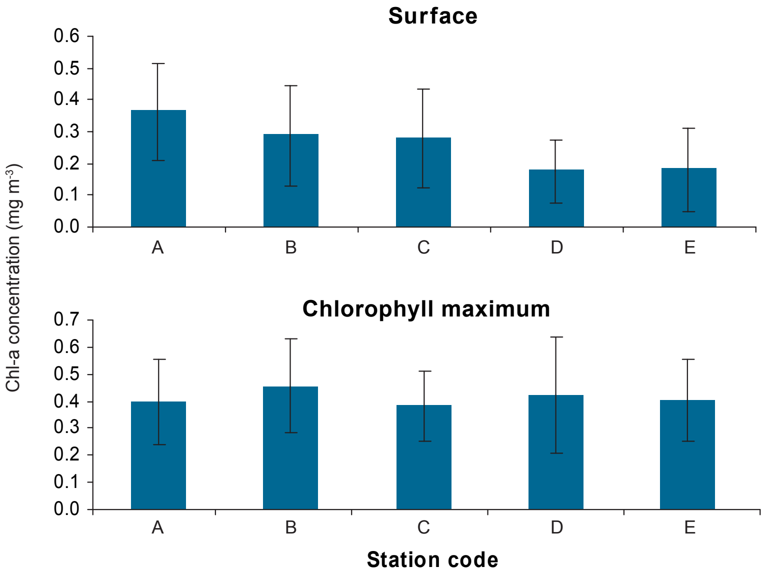

Figure 3.12: Mean (± s.d.) phytoplankton biomass (as total chlorophyll *a*) from onshore (Stn A) to offshore (Stn E) over the three-year study period. The upper graph represents the surface waters and the lower graph represents the values from the depth of the chlorophyll maximum.

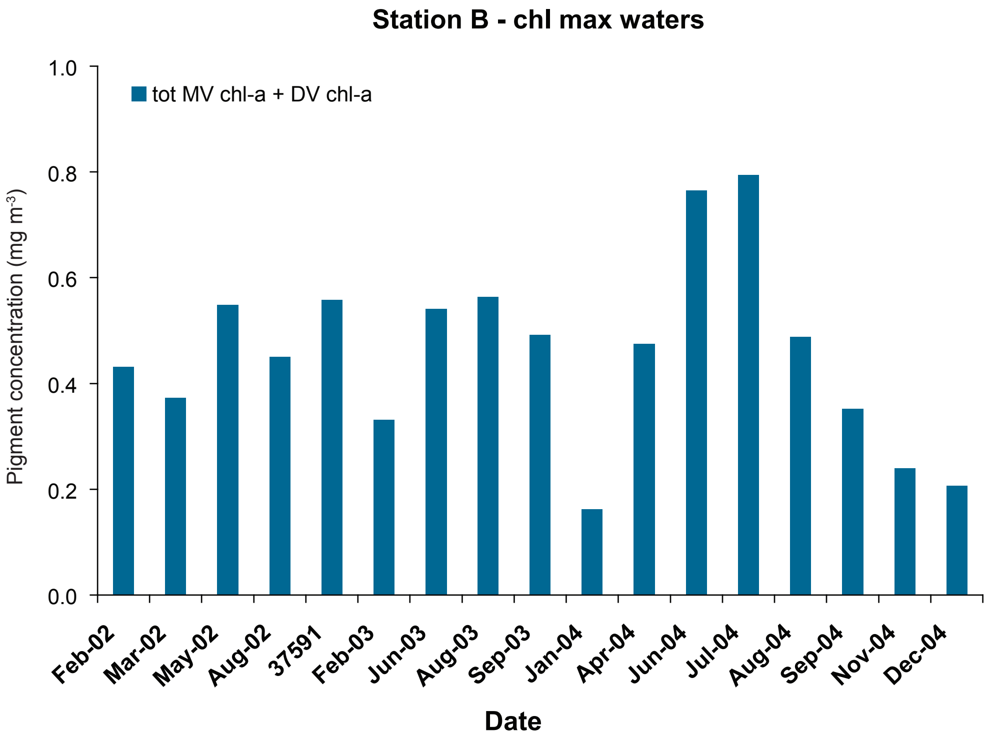

Figure 3.13: Phytoplankton biomass (as total chlorophyll-a; that is MV + DV chlorophyll *a*) over the three-year study period.

Pigment to chlorophyll *a* ratios were used to determine the dominant pigments and hence indicate the dominant algal group(s) at each station. Variation in these ratios across the transect indicated different phytoplankton communities existed on and off the shelf. The two most inshore stations (A, B) have a diverse pigment composition indicating a phytoplankton community composition of diatoms, chlorophytes and/or euglenophytes, haptophytes, prasinophytes, cryptophytes and cyanophytes, with photosynthetic dinoflagellates and chrysophytes present infrequently throughout the study (Fig. 3.14a). Dinoflagellates (as indicated by the presence of peridinin) were not found at stations further offshore. Diatom abundance (indicated by the presence of fucoxanthin) diminished with distance from the shore, with few if any diatoms present at Station E. At Station A, fucoxanthin was 17.2% of the total accessory pigments compared with 6% at Station E. Chlorophytes (indicated by chlorophyll *b* and lutein) also decreased with distance from the shore and were present infrequently at stations D and E, generally only during the winter months (Fig. 3.14a).

As a percentage of the total accessory pigments, chlorophyll *b* was 26.6% at Station A compared to < 0.2% at Station E. Cyanophytes (indicated by the presence of zeaxanthin) were the dominant algal group at Stations C, D and E, with 42% zeaxanthin of the total accessory pigments at Station E compared to 7% at Station A and 19% at Station B. Zeaxanthin also exhibited a strong seasonal cycle with a maximum during the summer months, again at all locations except the most inshore station (A; Fig 3.14a). Zeaxanthin is a photoprotective pigment and an increase in its concentration during summer may in part be due to a reaction to increased irradiance. However nitrogen-fixing cyanobacteria may be expected to predominate under the highly stratified, nutrient-limited conditions prevailing offshore during summer. Prochlorophytes (indicated by the presence of DV chlorophyll *a*) were present at Stations D and E generally only during the summer months. The concentration of DV chlorophyll *a* indicated greater abundance of prochlorophytes at Station E. The pigment composition observed at the offshore stations is consistent with observations of pigment composition at similar latitudes throughout the Indian Ocean (Barlow *et al. in review*).

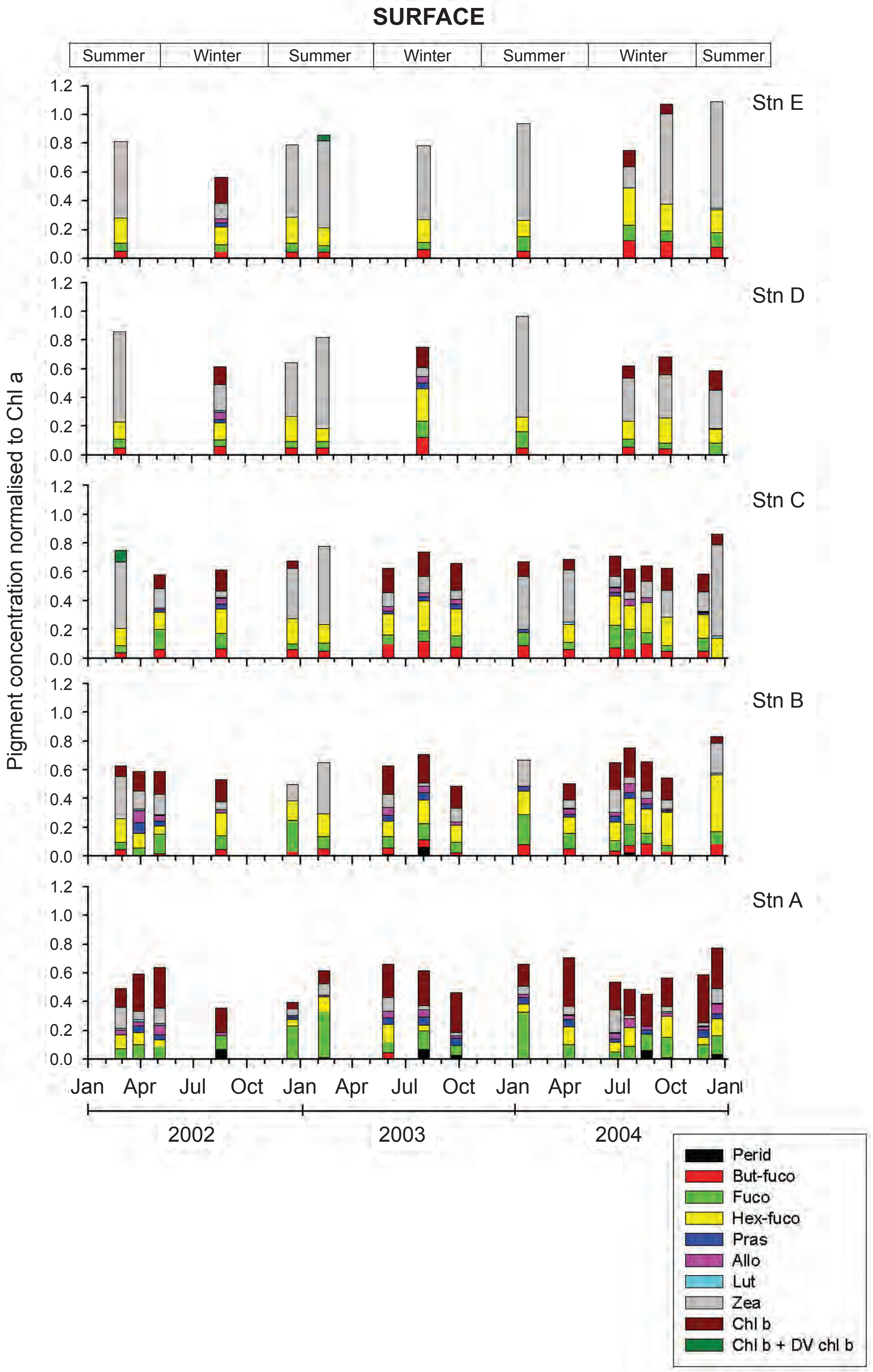

Figure 3.14a: Composition of diagnostic pigments measured, by HPLC, in surface waters from inshore (Station A) to offshore (Station E) along the Two Rocks transect.

Chlorophyll maximum

Unlike surface waters, total biomass did not show a distinct onshore/offshore pattern (Fig. 3.12). Also different from surface waters, where phytoplankton biomass (as indicated by chlorophyll *a* concentration) showed a clear seasonal cycle, with a maximum chlorophyll *a* concentration in the austral winter (August) of each year (Fig. 3.13), there was no such signal observed for the chlorophyll maximum waters (see Fig. 3.13 for representative data from Stn B). Differences in the phytoplankton composition between the surface and chlorophyll maximum depth were most notable at Stations D and E (Fig. 3.14a,b). By contrast, the two most inshore stations (A, B) showed similar phytoplankton compositions at both surface and chlorophyll maximum depths (Fig. 3.14a,b), possibly because the water column was generally well-mixed. Station C fluctuated between the two extremes; at times having a similar phytoplankton composition at both depths and at other times each depth having a notably different composition. Cyanophyte abundance (indicated by the presence of zeaxanthin) was greatly reduced at the chlorophyll maximum depth (23%) compared to the surface (42%) at Station E. Similar results were observed at all stations, except the most inshore station (A). By contrast, chlorophytes (indicated by chlorophyll *b*) increased in abundance at the chlorophyll maximum depth most notably at Stations D and E (Fig. 3.14b). At Station E, as a percentage of the total accessory pigments, chlorophyll *b* was 12% at the chlorophyll maximum depth compared to < 0.2% in the surface waters. Prochlorophytes (indicated by the presence of DV chlorophyll *a*) were present at stations D and E generally only during the summer months and on two occasions were observed at station C.

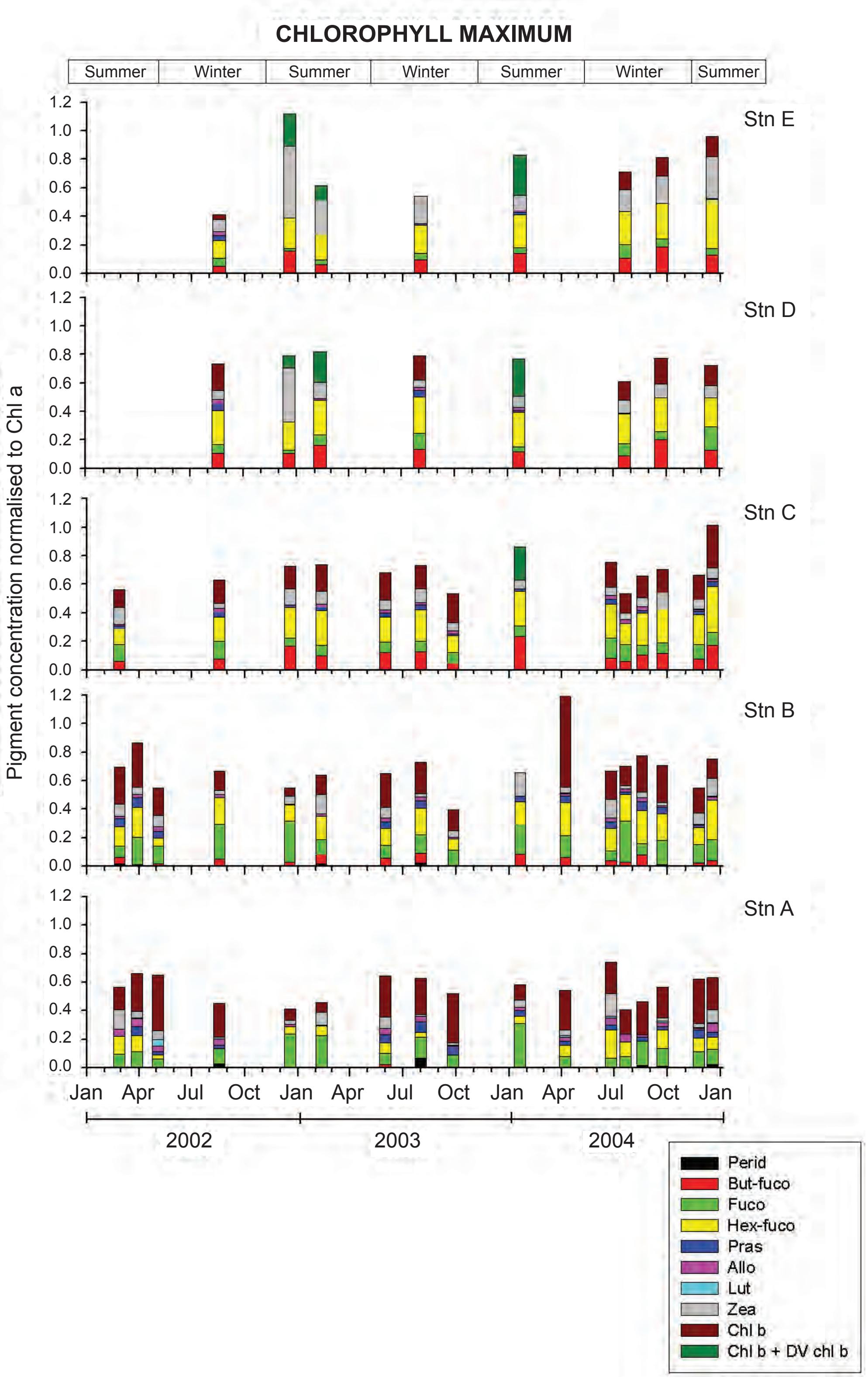

Figure 3.14b: Composition of diagnostic pigments measured, by HPLC, in chlorophyll maximum depths from inshore (Station A) to offshore (Station E) along the Two Rocks transect.

Statistical analyses

Statistical analysis using a four-season model confirmed some strong patterns of distribution in time and space (Table 3.4) with many marker pigments showing onshore-offshore gradients and seasonal patterns in concentrations when the three years of data were averaged together (Fig. 3.15a). Three different spatial patterns were evident. The most common spatial pattern was a decrease in pigment concentration with distance offshore which was shown for all pigments except β,ε-carotene and lutein. A similar result was noted for chlorophyll *a* in the summary data above, and also by Pearce *et al.* (2000). The pigment results support and extend those from the cell counts. Onshore-offshore gradients include a general decline in total phytoplankton density as well as a reduction in densities of diatoms, chlorophytes, cryptophytes, prasinophytes and haptophytes. Contrasting spatial patterns were observed in zeaxanthin and 19-BF. Zeaxanthin concentrations rose with distance offshore while 19-BF peaked at Stn C. From these we concluded that cyanobacteria dominance increases with distance offshore while chrysophytes and silicoflagellates achieve their greatest abundance midshelf.

Table 3.4. Statistical analysis of surface pigments for spatial and temporal patterns. Probabilities (P) of the null hypothesis (no difference in time or space) being correct are reported*.

	Marker for:	**Spatial (onshore-offshore)**	**Temporal (seasonal)**
MV chla	All photosynthetic phytoplankton except prochlorophytes	0.001	0.001
Carotenoid β,ε	widespread	0.137	0.006
Carotenoid β,β	widespread	0.006	0.144
Chl*b*	Chlorophytes	<0.001	<0.001
zeaxanthin	Cyanophytes and prochlorophytes	<0.001	0.001
alloxanthin	Cryptophytes	<0.001	0.969
19’-hexanoyloxy fucoxanthin	Haptophytes	0.006	0.097
prasinoxanthin	Prasinophytes	<0.001	<0.001
neoxanthin	Chlorophytes	0.048	0.743
fucoxanthin	Diatoms, haptophytes and chrysophytes	<0.001	<0.001
19’-butanoyloxy fucoxanthin	Haptophytes and chrysophytes	<0.001	<0.001
chl c_3	Prymnesiophytes and chrysophytes	0.002	<0.001
Lutein	Chlorophytes	0.351	0.002
Alloxanthin	Cryptophytes	<0.001	<0.001
Violoxanthin	Chlorophytes and eustigmatophytes	<0.001	0.040

*Log transformation was used to improve homoscedasticity and normality * Interactions were not assessed as no ‘autumn’ samplings were conducted on stations D & E.

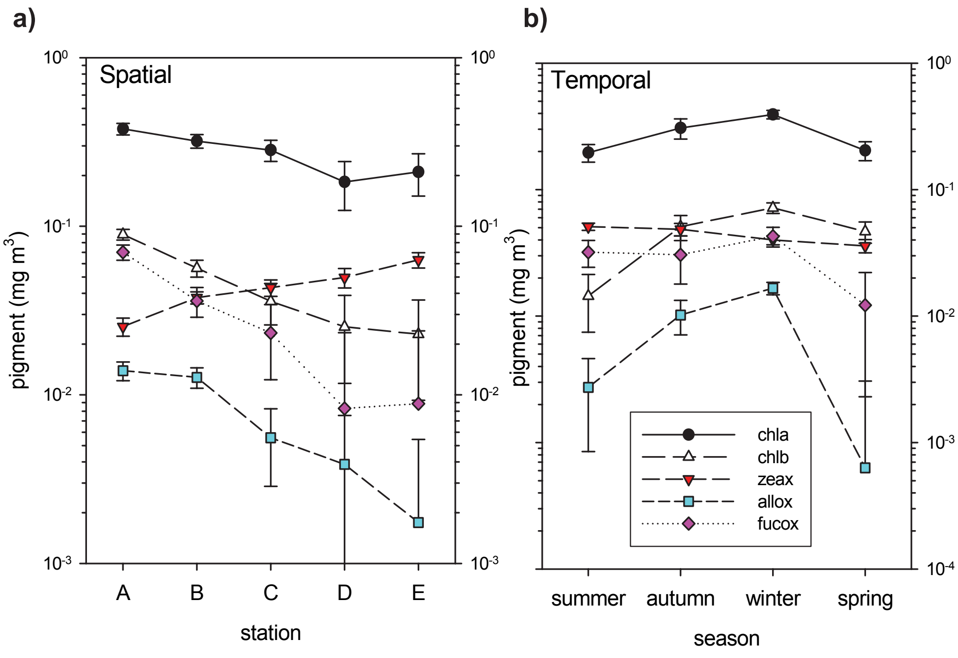

Figure 3.15: (a) Surface concentrations of selected pigments at each of five stations across the onshore (station A) to offshore (station E) transect at Two Rocks, WA and (b) their seasonal variation.

Data were also analysed using a two season model, with summer as Nov – Apr and winter as May – Oct (as utilised in Section 3.2.3; Bio-optics and Remote Sensing). A single factor ANOVA on the zeaxanthin:chl-a ratio indicated a significant difference between seasons for Stations B – E ($p < 0.05$), and also within Stn B itself ($p < 0.05$; Stn B chosen for analysis as it had the largest temporal dataset), indicating a seasonal cycle in cyanophyte abundance.

Almost all pigments peaked in abundance (annual bloom) in winter and declined significantly into summer. A similar winter peak of inshore phytoplankton biomass was also noted in Thompson and Waite (2003). Relative to other pigments, fucoxanthin and alloxanthin declined rapidly from their mid winter peaks suggesting greater rates of loss from the water column possibly due to faster sinking or greater predation. Unusual temporal patterns were observed in concentrations of lutein, β,ε-carotene and zeaxanthin with peak concentrations reached in summer or autumn. The general decrease in phytoplankton biomass during summer combined with a peak in zeaxanthin concentrations suggests the influence of increased stratification and nutrient limitation on the regional phytoplankton community at this time. Peridinin, the marker pigment for dinoflagellates, was only present at very low concentrations at stations A and B, indicating the large number of dinoflagellates (~ 7%) observed under the microscope at all stations (Fig. 3.10) were almost exclusively heterotrophic (i.e. lacking in photosynthetic pigments), and therefore most closely affiliated with the grazing microzooplankton community.

3.2.3 Bio-optics and Remote Sensing

Investigators / Institution

Lesley Clementson, Peter Fearns and Tim Harriden

CSIRO Marine and Atmospheric Research

Introduction

An increasing use of remote sensing products by managers of marine environments to further their understanding of ecosystem dynamics on increasing spatial and temporal scales, is dependent on a thorough understanding of the contribution and variation in the spectral absorption and scattering properties of the regional waters of interest (Harriden *et al.* 2004).

Standard algorithms used to estimate chlorophyll *a* concentration for the SeaWiFS and MODIS sensors have been developed from large datasets of bio-optical data collected primarily in the Northern Hemisphere. These Northern Hemisphere conditions (atmospheric and in-water) are not always applicable to regions in the southern hemisphere (Takashima *et al.* 2003), leading to inaccurate estimates of retrieved parameters and limited use of remote sensing as a tool for environmental managers (Majewski *et al.* 2004).

Open-ocean (case 1) waters are considered to be well-defined optically with total absorption generally dominated by the phytoplankton component that correlates well with the concentration of chlorophyll *a* (Morel and Maritorena, 2001). Coastal and estuarine (case 2) waters, by comparison, often have significant contributions to the total absorption from the detrital/non-algal and chromophoric dissolved organic matter (CDOM) components, causing retrieved estimates of chlorophyll *a* concentration to be over estimated (Babin *et al.* 2003).

Here we report on a dataset which was developed to determine if and/or how the strong seasonal features observed in the climatology and oceanography off Western Australia affect the bio-optical characteristics of the shelf waters in this region. The dataset will also be used to determine the validity of the standard algorithms used by the SeaWiFS, MODIS and MERIS ocean colour sensors for Western Australian waters and, if necessary, will provide a strong base for developing an algorithm that captures the particular features of this region.

Methodology

In January 2003 collection of an extensive set of inherent and apparent optical properties at three sites – Bunbury, Two Rocks and Jurien Bay (see Fig. 5.2) – along the Western Australian coast began (samples were collected for pigment analysis at the Two Rocks site from February 2002).

At each site, samples were collected at 5 km intervals (stations 1-6) along a transect that extended from inshore to approximately 25-30 km offshore where the water column depth was about 40–50 m. The outer-most station at each site (T6 at Two Rocks, B6 at Bunbury and J5 at Jurien Bay) was used as the main validation station for that site and was always occupied within 2 hours either side of midday local time. In addition to this, at the two Rocks site, samples for pigment analysis were collected at stations C, D and E, further off shore (see Fig. 3.1). Note that station B is the same location as station T6. At each station, profiles of temperature, salinity and fluorescence were collected using a SeaBird 19plus conductivity – temperature – depth (CTD) sensor with a General Oceanics 12 bottle rosette equipped with 10 L Niskin bottles. The system also incorporated a flow through fluorometer (WETStar), an oxygen sensor (SeaBird) and a PAR sensor (Biospherical Instruments). Downward spectral irradiance and upward spectral radiance profiles were collected using a HydroRad-2 (HOBILabs) and PRR-600 radiometer (BSI); water leaving radiance was also measured using a Zeiss radiometer (from Curtin University) and profiles of total spectral absorption and attenuation coefficients were measured with an ac-9 (WETLabs). More detailed information on the deployment and operation protocols for all instruments can be found in Keesing and Heine (2005). In addition, water samples were collected from the surface and the Secchi depth of the water column (these depths were chosen as they matched the depths in the MERIS validation protocols) for the determination of total suspended matter, the concentration and composition of phytoplankton pigments and the absorption coefficients of phytoplankton, detritus and CDOM. Aboard the vessel water samples were transferred from the Niskin bottles to 5 litre plastic carboys and stored in the cool and the dark until return to the land base (approx. 4 hours) for filtering. In general sample collection and analysis followed the protocols outlined in Ocean Optics Protocols for Satellite Ocean Colour Validation revision 5 (Mueller *et al.* 2003). Methods used to analyse water samples for pigment composition and concentration and for the absorption coefficients of the dissolved and particulate fractions can be found in Keesing and Heine (2005).

SeaWiFS data are received in Perth by WASTAC and processed routinely using SeaDAS version 4.6 (July 2004) to provide level 2 (eg. Chlorophyll *a* concentration) Local Area Coverage (LAC) data. SeaWiFS images were also provided by the SeaWiFS Project, NASA/Goddard Space Flight Centre and Orbimage. Remote sensing estimates of chlorophyll *a* concentration were extracted from the

LAC data for comparison to the *in-situ* chlorophyll *a* concentration measurements. Only retrieved chlorophyll *a* values that fell within 4 hours of the *in situ* sample being collected and within 2 km of the sample station were used. Mean values of retrieved chlorophyll *a* were the average of the eight closest pixels that complied with both the time and distance requirements. Remote sensing data have had standard projections applied and been composited into datasets for inclusion in the SRFME database (see Ch. 7).

Sample location

Jurien Bay, the northern-most sampling location lies 275 km to the north of Perth and is contained within the Jurien Bay Marine Park. A string of islands and reefs lie just off the coast sheltering the inshore waters of Jurien Bay. The first two stations on the sampling transect are inshore of the reefs while the remaining three sampling stations are in the more exposed waters outside of the reefs. Jurien Bay is a site for recreational fishing and the professional Western rock lobster industry. The Hill River, the smaller of two main rivers in the Moore – Hill River basin catchment area, discharges directly to the ocean just south of Jurien Bay. Flow in the Hill River is highly seasonal, only flowing during winter or after heavy rain within the catchment area. Much of the catchment area, inland of Jurien Bay, has been cleared for agricultural purposes.

Two Rocks lies 66 km north of Perth in a predominately light urban environment. There are no rivers or significant industrial or urban sources discharging to the ocean within several km to the north or south of this sampling site.

Bunbury represents the southern most sampling site, lying 185 km to the south of Perth on the shoreline of Geographe Bay. Bunbury is an urban area (population in excess of 50,000) with a deepwater port and recreational marinas. The first station on the sampling transect lies within the port area, close to the outlet of the Leschenault Inlet which drains the Collie River basin catchment area. The remaining five stations are located offshore in Geographe Bay.

Results and Discussion

Validation

Surface data from stations T6, B6, J5 and B, C, D and E were used to determine the relationship between *in situ* and satellite-retrieved chlorophyll *a* concentration with a total of 62 matching data pairs. The relationship between *in situ* and retrieved chlorophyll *a* is strong with a slope of ca. 1 and an R^2 of 0.72 (Fig. 3.16a). Removal of the very high concentration point reduces the slope to ca. 0.90 and the R^2 to 0.69 When the samples are separated into seasons (winter: May-October; summer: November-April), then most of the variability is associated with the winter samples (Fig. 3.16b). There is a clear distinction between the chlorophyll *a* concentration during the designated summer and winter seasons; the *in situ* chlorophyll *a* concentration ranges from 0.146 to 0.810 (mean 0.397) mg m^{-3} during winter and from 0.067 to 0.332 (mean 0.160) mg m^{-3} during summer. Similar results have been obtained from the archive of SeaWiFS images for the Western Australian coastal region, showing retrieved chlorophyll *a* concentration to begin to increase in May and reaching a maximum, usually in August of each year (Moore *et al.* 2006). (See Section 4.2 in this report for more discussion of the seasonal cycles.)

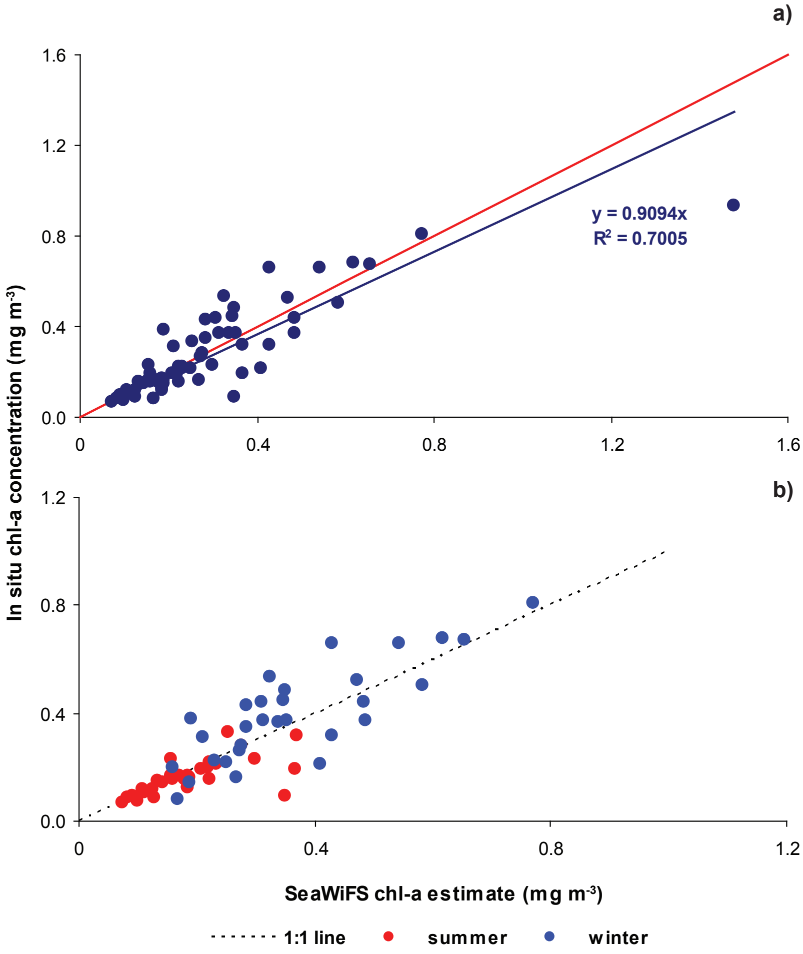

Figure 3.16: (a) The relationship between *in situ* chlorophyll *a* (measured by HPLC) with the retrieved chlorophyll a estimates from the SeaWiFS standard algorithm for stations T6, B, C, D and E (Two Rocks), B6 (Bunbury) and J5 (Jurien Bay). (b) Data shown in (a) separated into summer and winter seasons (the outlying data point in (a) was removed from plot (b)).

In situ measurements - TSM

At each site, samples for all *in situ* measurements were collected at 5 km intervals (stations 1-6) along a transect that extended from inshore to approximately 25-30 km offshore (T6 at Two Rocks, B6 at Bunbury and J5 at Jurien Bay) where the water column depth was about 40–50 m.

Total suspended matter is the sum of all particulate matter in the water sample – live and senescent phytoplankton cells and inorganic and organic minerals. In most coastal areas, it may be expected that during winter there would be a correlation between a shallower Secchi depth and storm events causing resuspension of bottom sediments and increased land runoff; that is the TSM would be largely composed of inorganic and organic minerals. The lower sun angle in winter will also contribute to a shallower Secchi depth. In this study at stations 3 – 6 Bunbury and Two Rocks and stations 3 – 5 Jurien Bay, the Secchi depth was shallower in winter than summer and corresponded well with an increase in total suspended matter (TSM) in surface waters. In Western Australian coastal waters, *in situ* sampling and SeaWiFS imagery has shown an increase in phytoplankton biomass during winter which often correlates with the highest TSM values being recorded over the same months and may indicate that the majority of TSM in winter is algal material.

TSM can be used as an indicator of water clarity, but provides no information as to what type of particulate material is affecting the clarity of the water. For remote sensing purposes there is a need to understand which component(s) are dominating the water column and potentially affecting the accurate retrieval of remotely sensed products such as chlorophyll *a*, TSM and CDOM concentration.

In situ measurements - Pigments

Pigment analysis and diagnostic pigments have been used in this study to estimate the phytoplankton community composition and concentration at all stations and sites. Pigments that relate specifically to an algal class are termed marker or diagnostic pigments (Jeffrey & Vesk, 1997) and some of these diagnostic pigments are found exclusively in one algal class (e.g. prasinoxanthin which is only found in prasinophytes) while others are the principal pigments of one class but are also found in other classes (e.g. fucoxanthin in diatoms and some haptophytes; 19'-butanoyloxyfucoxanthin (19BF) in pelagophytes and some haptophytes). The presence or absence of these diagnostic pigments can provide a simple guide to the composition of a phytoplankton community including identifying classes of small flagellates that cannot be determined by light microscopy techniques. In this study the presence of fucoxanthin has been used to indicate diatoms; peridinin – dinoflagellates; 19'-hexanoyloxyfucoxanthin (19HF) – haptophytes; alloxanthin – cryptophytes; prasinoxanthin – prasinophytes; zeaxanthin – cyanophytes and chlorophyll *b* – green algae.

The composition of only the diagnostic pigments for the outermost station of the Two Rocks transect is shown in Fig. 3.17, but is representative of the pigment/phytoplankton composition at the Bunbury and Jurien sites. This pigment composition reveals that the phytoplankton community is quite diverse, but extremely stable, and indicates that diatoms, haptophytes, cyanophytes, chrysophytes and chlorophytes or green algae are present in the phytoplankton community all through the sampling period (Feb 2002 – Dec 2004), while cryptophytes and prasinophytes are present most of the time. Dinoflagellates are present infrequently and except for cyanophytes, the pigment data indicates that the ratio of the different algal groups changes little with the seasons. Cyanophytes show a significant increase during summer.

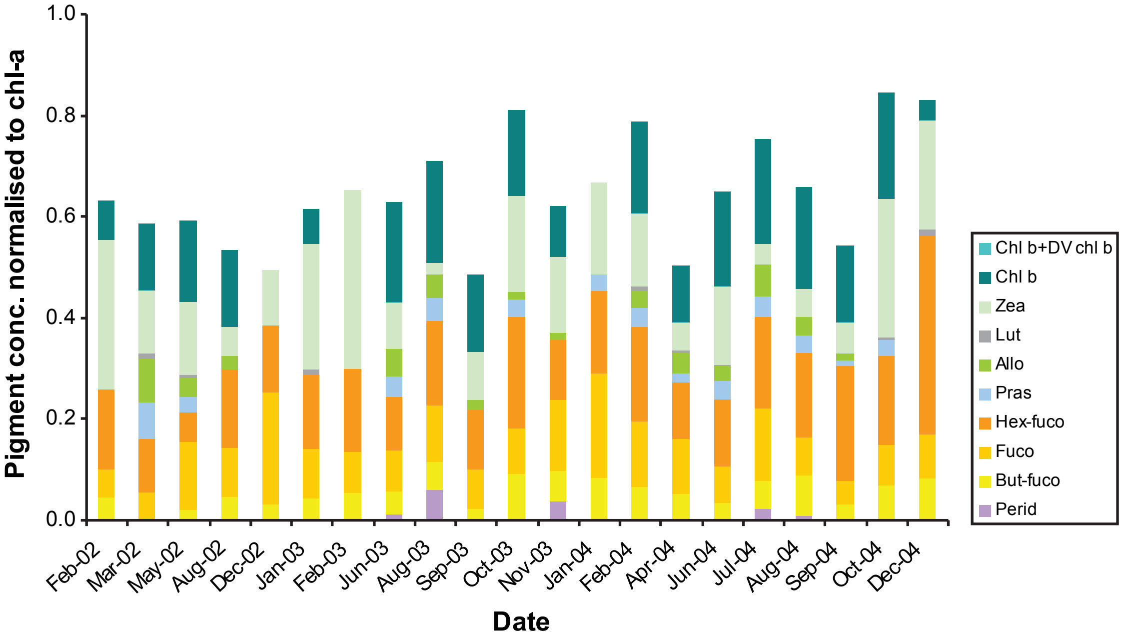

Fig. 3.17: Pigment composition (diagnostic pigments only) plotted against time for the surface waters of station T6 on the Two Rocks transect.

These results indicate that there is no significant difference in the phytoplankton community composition along the Western Australian coast from Bunbury to Jurien Bay and that there is also little seasonal succession within the phytoplankton community. The increase in cyanophytes could be due to either *Synechoccocus* spp. or *Trichodesmium* spp. cells or a combination of both species. Both of these species are commonly found in tropical and subtropical waters, such as the Leeuwin Current. The summer increase in cyanophytes is consistent with conditions of increased stratification, a deeper mixed layer depth, and decreased N in the upper mixed layer found during summer along the Western Australian coast (see Section 4.1).

In situ measurements – Absorption coefficients

One of the suite of measurements made during this project is the absorption coefficients of the different components in the water column. Absorption coefficients for CDOM (a_{CDOM}), detrital (a_d) and phytoplankton (a_{ph}) components are determined for each sample thus indicating the contribution of the different components to the total absorption of the water column at the different stations and sites. SeaWiFS and MODIS ocean colour sensors have 8 channels or wavelength bands in the visible and near infra-red region of the spectrum where data is collected. The second channel is centered on 443 nm to detect maximum contribution from chl-a. All results presented from this study will refer to values at 440 nm to coincide with data collected by the sensor.

At the Two Rocks and Bunbury sites there is a clear decrease in the value of $a_d(440)$ from inshore to offshore, while at Jurien Bay the $a_d(440)$ value is relatively constant along the entire transect (Fig. 3.18). There is no discharge of rivers or urban/industrial sources near the Two Rocks site that could explain the higher $a_d(440)$ values at the inshore stations. However the higher $a_d(440)$ values could be due to macro-algal and seagrass debris accumulating in the surface inshore waters, as well as resuspended sediment material. It should be noted that due to the shallowness of station T1, this station was sampled infrequently and the few results have not been included in the following results.

At Bunbury the innermost station (B1) is within the port area and close to the outlet of the Leschenault Inlet and station B2 is just outside the port area. It is likely that stations B1 and B2 are influenced by the detrital matter from the inlet and the river basin that it drains. At Jurien Bay there appears not to be any difference in the $a_d(440)$ values between the innermost stations (J1 and J2) inside the reefs and the other stations outside the reefs. A single factor ANOVA test ($p < 0.05$) shows that there is no significant difference between the $a_d(440)$ values at the three locations when the most inshore station (T1, B1, J1) and station B2 is excluded from the analysis and that there is also no significant difference between the $a_d(440)$ values during the summer and winter seasons as previously defined.

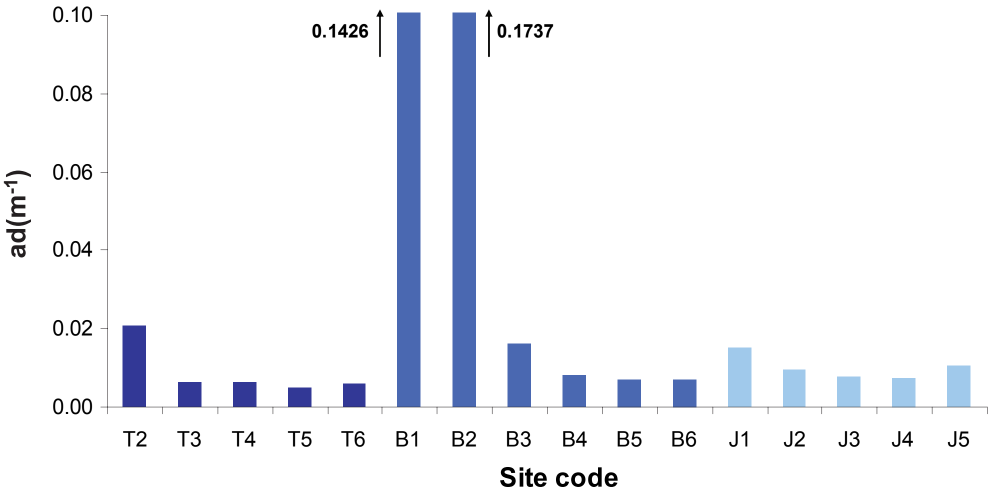

Fig. 3.18: The absorption coefficient for the detrital or non-algal component of the particulate matter at each station on the transect at each site.

Similar to the $a_d(440)$ values, the values of $a_{CDOM}(440)$ also decrease from inshore to offshore, but for this component the effect is observed at all three sites. At Jurien Bay the $a_{CDOM}(440)$ values are higher at the two inshore stations, inside the reefs, than at the stations outside the reefs, suggesting the inner two stations are probably affected by a terrestrial source. The Bunbury site also shows increases in $a_{CDOM}(440)$ values at those stations closest to the inlet.

Excluding the inner-most stations, these $a_{CDOM}(440)$ values fall within the range suggested for case 1 waters (Kirk, 1983) and would be considered low in most coastal waters. Single factor ANOVA tests ($p < 0.05$) show similar results to those for the detritus component in that there is no significant difference between the $a_{CDOM}(440)$ values at the three locations when the most inshore station (T1, B1, J1) is excluded from the analysis and that there is also no significant difference between the $a_{CDOM}(440)$ values during the summer and winter seasons.

Unlike the other components the $a_{ph}(440)$ values do not show an inshore to offshore decrease, showing instead similar values at all stations on a transect within any one trip at all sites. On occasion, higher values of $a_{ph}(440)$ are recorded at the inshore station on the Two Rocks and Bunbury site. At Jurien Bay, the phytoplankton community composition does not seem to be affected by the location of the reefs on the transect as $a_{ph}(440)$ values are similar at the stations inside and outside the reefs. As for the other components the values of $a_{ph}(440)$ would be considered low for a coastal region. Again single factor ANOVA tests ($p < 0.05$) show there is no significant difference between the $a_{ph}(440)$ values at the three locations when the most inshore station (T1, B1, J1) is excluded from the analysis, but there is a significant difference between the $a_{ph}(440)$ values during the summer and winter seasons.

Values of a(440) from the offshore station (T6) on the Two Rocks site has been compared with a(440) values from three coastal sites off Tasmania, two open-ocean sites in the Southern Ocean, and two sites off Heron Island in oligotrophic Great Barrier Reef waters (Fig. 3.19). The Two Rocks a(440) values represent the range of values that were observed over the seasons within a year and are compared to a(440) values taken at just one point in time. However the values from the three Tasmanian sites were observed in summer when the a(440) values for all components are likely to be at their lowest and the a(440) values for CDOM and detritus at the Southern Ocean sites would show less variability over the seasons than a coastal site. The comparison between the four sites does confirm that the a(440) values observed in Western Australian coastal waters are low and comparable to values found in open-ocean or oligotrophic waters. This result suggests that the reasonably good relationship between *in situ* chlorophyll *a* and retrieved estimates of chlorophyll *a* using the standard algorithm of the SeaWiFS sensor (Fig. 3.16) is due to the coastal waters of Western Australia being characterized optically as closer to case 1 waters than case 2 waters. Although the absorption properties of the different components of the water column are low in Western Australian waters, the proportion of absorption due to each component can still affect the accuracy of the retrieved chlorophyll *a* estimate. The percentage of absorption due to each component, including the water itself, has been calculated for all stations, except the most inshore station (T1, B1, J1) in the surface waters on each transect (Fig. 3.20). There are clearly times where the CDOM is the dominant component, contributing more to the total absorption than the phytoplankton. Under these circumstances, the satellite sensors would retrieve a chlorophyll *a* value which would be an over-estimate of the *in situ* chlorophyll *a*.

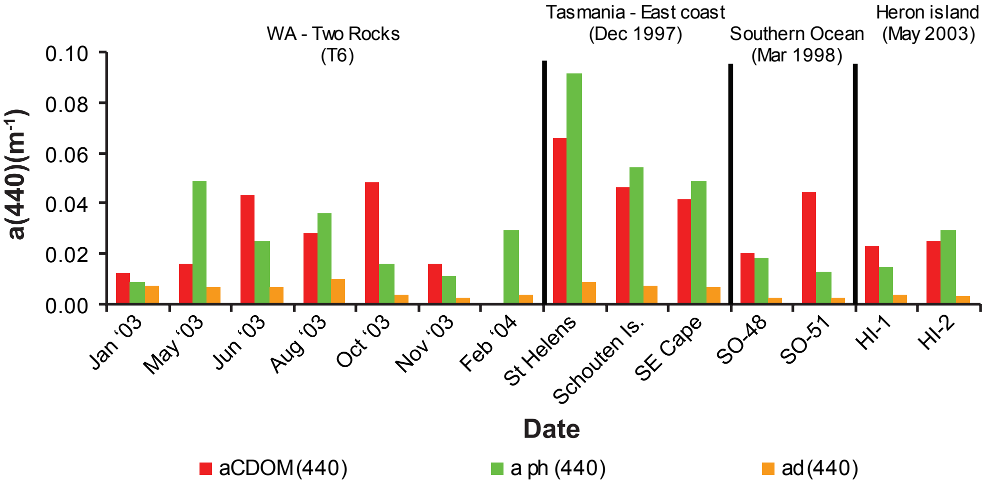

Figure 3.19: Comparison of a(440) values from a typical site in Western Australian coastal waters with other sites in Australian waters.

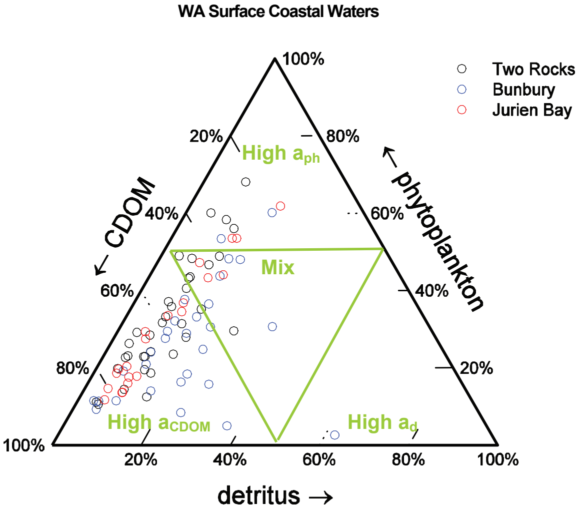

Figure 3.20: The relative contributions of phytoplankton, detritus and CDOM to the total absorption at 440 nm in the surface waters (sites T1, B1, J1 excluded) from the three locations.

Summary

Coastal areas of southern Western Australia are unlike many other Australian coastal areas in which the absorbance and scattering properties can be dominated by high sediment loadings or by high concentrations of CDOM. By comparison, the coastal waters of Western Australia have very low absorption properties. The phytoplankton community composition appears to remain stable throughout the year, however there is a significant increase in phytoplankton biomass at all locations during the winter months (May – October) (Clementson *et al.* 2004). Results from this study suggest that the strong seasonal features seen in the climatology and oceanography of this region are not reflected in the bio-optical characteristics of the coastal waters inshore of the 50 m contour. The standard ocean colour algorithms used by sensors such as SeaWiFS and MODIS appear to produce accurate estimates of chlorophyll *a*, and hence phytoplankton biomass, most of the time. Although the absorption properties of the different in-water components are all considered low for coastal waters, at times, there is a higher contribution of CDOM than phytoplankton to the total absorption which results in the retrieved chl *a* estimate to be an over-estimate of the *in situ* chlorophyll *a* as has been observed on occasion.

This study has provided one of the most detailed spatial and temporal studies of bi-optical parameters for any area in Australia. The results suggest that standard ocean colour algorithms and the resulting ocean colour products can be used within the coastal region from Bunbury to Jurien Bay, providing an important tool for scientists and managers of this marine environment. Whether the standard algorithms can provide accurate results beyond the regional extent of this study will be determined by future work in areas to the North and south of this study area.

3.2.4 Mesozooplankton

Investigators / Institution

Joanna Strzelecki and Tony Koslow	CSIRO Marine and Atmospheric Research

Introduction

The plankton of Australian coastal waters is poorly known, particularly around the western half of the continent. The only offshore seasonal survey of the eastern Indian Ocean was conducted in 1962-1963, when bi-monthly sampling was carried out in open oceanic waters on a transect along 110˚ E longitude (Zeitzschel, 1973, Tranter, 1977). In coastal waters, the zooplankton has only been systematically sampled in nearshore areas, bays and estuaries, and more recently along the Hillary's transect (e.g. SMCWS, 1996, Helleren and John, 1997). Limited observations of the macrozooplankton distribution off Hillarys and on the continental shelf around Albany, Bremer Bay and Esperance demonstrated that the composition and distribution of carnivorous macrozooplankton was influenced by the Leeuwin Current (Gaughan and Fletcher, 1997, Gaughan *et al.* submitted). These studies focused on the adults and larger size classes of zooplankton, but recent work has shown that smaller copepods and juvenile stages can not only be important numerically but can sometimes dominate in terms of biomass and grazing pressure (Dam *et al.* 1993, Gasol *et al.* 1997, Galienne and Robins, 2001). In an oligotrophic system such as the SRFME region, smaller species and juveniles can be an important trophic link between classical and microbial food webs (Calbet *et al.* 2001).

The mesozooplankton studies had two aims:

1) To describe spatial (particularly onshore-offshore) and seasonal patterns in abundance and biomass, and

2) To assess seasonal and cross-shelf patterns in secondary productivity and in the role of the zooplankton in pelagic biogeochemistry through their grazing on phytoplankton and the smaller zooplankton, and the export of carbon to depth.

The first aim was achieved through characterisation of the biological communities and their variability along temporal and spatial scales. Because the community was sampled monthly over three years (quarterly for offshore stations) and the turnover rate of zooplankton is approximately of that order, it was possible to observe the seasonal dynamics of important species, including the seasonally varying influence of the Leeuwin Current.

The mesozooplankton was also studied in a pair of anticyclonic and cyclonic eddies during a cruise of the R/V *Southern Surveyor*. The Leeuwin current has the highest eddy kinetic energy of any eastern boundary current in the world, and thus generates a significant number of eddies. The influence of eddies on production and transport of higher trophic levels is potentially of commercial as well as scientific interest. To date there has been no investigation of zooplankton in these mesoscale features off the coast of Western Australia.

Mesozooplankton production is often viewed as a key link between physical processes and their influence on primary production at the base of the food chain and the feeding, growth and survival of larval and juvenile fish, which regulates fishery recruitment. We therefore examined both the grazing dynamics of the zooplankton and their productivity.

The paradigm regarding the role of mesozooplankton in marine food webs has been fundamentally revised in the past 20 years (Azam *et al.* 1983). Previously, the 'classic' view of pelagic food chains was relatively straightforward, with the mesozooplankton (mostly copepods) serving as a direct link between the primary producers (mostly diatoms and dinoflagellates) and planktivorous fishes, such as clupeoids. It is now recognized that pico- and nanophytoplankton are responsible for most primary production in marine systems, particularly in oligotrophic regions. These phytoplankton are too small to be effectively grazed by copepods. Microzooplankton (mostly protists) are the dominant grazers, and they in turn, along with the larger phytoplankton, are the main prey of the mesozooplankton. As a result, trophic cascades are often observed, whereby increased mesozooplankton in an experiment may lead to decreased grazing on the phytoplankton, because increased grazing on the microzooplankton may release grazing pressure on the phytoplankton. This is most often observed in systems dominated by small phytoplankton, as is the case off Western Australia. Prior to this project, there had been no studies of the roles of micro- and mesozooplankton in pelagic food webs from our region.

Contemporary views of the marine planktonic food web are vastly more complicated today than they were a few decades ago. With a view to these issues, SRFME scholar Harriet Paterson examined the role of microzooplankton in the waters off Western Australia (see volume 1). Investigation of plankton trophodynamics now typically requires separate feeding experiments for the micro- and mesozooplankton. In order to simplify the experimental methods, we have proposed a modified experimental procedure, which enables the role of the micro- and mesozooplankton to be evaluated from a single set of grazing experiments. We also expanded the conventional Frost (1972) equations to estimate the micro- and mesozooplankton grazing on the phytoplankton and mesozooplankton predation on the microzooplankton from one feeding experiment.

There are routine methods in estimating primary production, but no commonly accepted and routine method for measuring secondary production. The ‘egg production method’ is the most commonly employed, but it is tedious and time consuming. New approaches related to studies of specific enzyme activity are being developed but still require testing against more routine methods like egg production. There are also global models of growth based on temperature dependent and weight specific physiological parameters (Runge and Roff 2000). However, these models assume that food is unlimited. The relative dependence of growth and reproduction in marine copepods upon temperature and chlorophyll (as a proxy for food) seems to vary, depending upon whether they are juveniles or adults, broadcast spawners, which tend to be more herbivorous, or sac-spawners, which are more omnivorous (Hirst and Bunker 2003). Our project examined the utility of egg production, enzyme assays and empirical models to estimate secondary production. Work in these areas is ongoing.

Mesozooplankton communities: abundance, biomass and community structure

Methods

Mesozooplankton was collected monthly at stations A to C and quarterly at D and E along the Two Rocks transect (Fig. 3.1). Replicate double-oblique bongo net tows were carried out with 355µm and 100µm mesh nets to sample the relatively small mesozooplankton that often predominates in oligotrophic regions. Sampling was not conducted within one hour of sunrise and sunset. Biomass was estimated based on measurement of dry weight. The 100 µm tow was split on board, filtered through 80 µm mesh and dried at 60º C to constant weight. Plankton samples were fixed with 10% sodium tetraborate-buffered formalin immediately after collection. Preserved samples were returned to the laboratory for identification. The samples were quantitatively sub-sampled using a Stempel pipette to obtain at least 100 adult copepods (0.5% to 2% of the total sample).

Community structure was analysed using nonparametric multivariate methods (Primer v.6). Prior to analysis, data were square root transformed to allow the intermediately abundant or intermediately large species to contribute more to the analyses. The Bray-Curtis similarity matrix which reflects changes in relative abundance as well as species composition was used as the basis of Multi-Dimensional Scaling (MDS) ordinations, and community relationships were examined with two-dimensional plots. The MDS was repeated until the same lowest stress was achieved. The simulation/permutation test ANOSIM (Warwick and Clarke, 1991) was used to compare the separation between groups. To determine the species contributing most to dissimilarities among groups, the program SIMPER (Warwick and Clarke, 1991) was used. Organisms with high average contribution and a large ratio of average contribution to standard deviation of contribution were considered good discriminating organisms (Clarke, 1993). They not only contributed most to dissimilarity but did so consistently. A permutational distance-based MANOVA (PERMANOVA, Anderson, 2005) based on the Bray-Curtis distance measure was used to test if there was a significant multivariate difference between assemblages in summer (December, January and February) and winter (June, July and August). Shannon's diversity index was used to compare species diversity along the Two Rocks transect. Shannon's index was chosen to account for both species richness (total number of species) and equitability (how evenly species are distributed).

Abundance and biomass

The total abundance of mesozooplankton ranged from 500 to 12,000 individuals m^{-3} (Fig. 3.21).

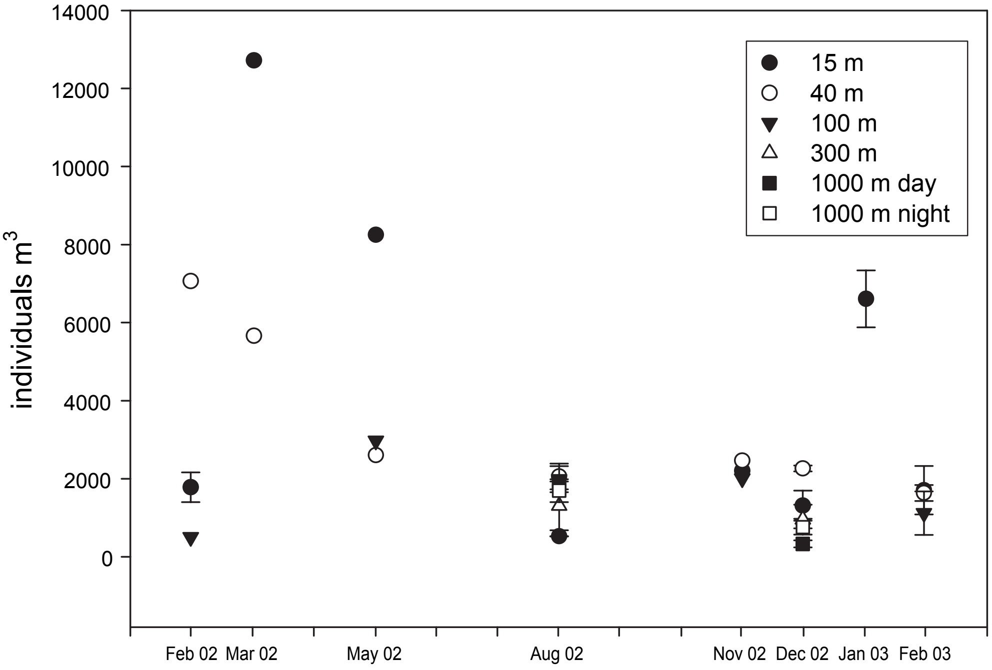

Fig. 3.21: Total abundance of mesozooplankton at the five stations along the Two Rocks Transect.

Most of the zooplankton consisted of copepods with abundances ranging from 300 to 10^{4} individuals m^{-3}. Peaks in copepod abundance occurred in late summer and autumn following diatom blooms. There was less difference in abundance between shelf and offshore stations in winter than in summer, opposite to the pattern exhibited by the phytoplankton. We observed that copepods offshore were more abundant in winter than in summer, consistent with the seasonal pattern of abundance of the phytoplankton. At all stations and all times nauplii and juvenile copepodites dominated numerically, followed by adult cyclopoids and calanoids (Fig. 3.22 and 3.23).

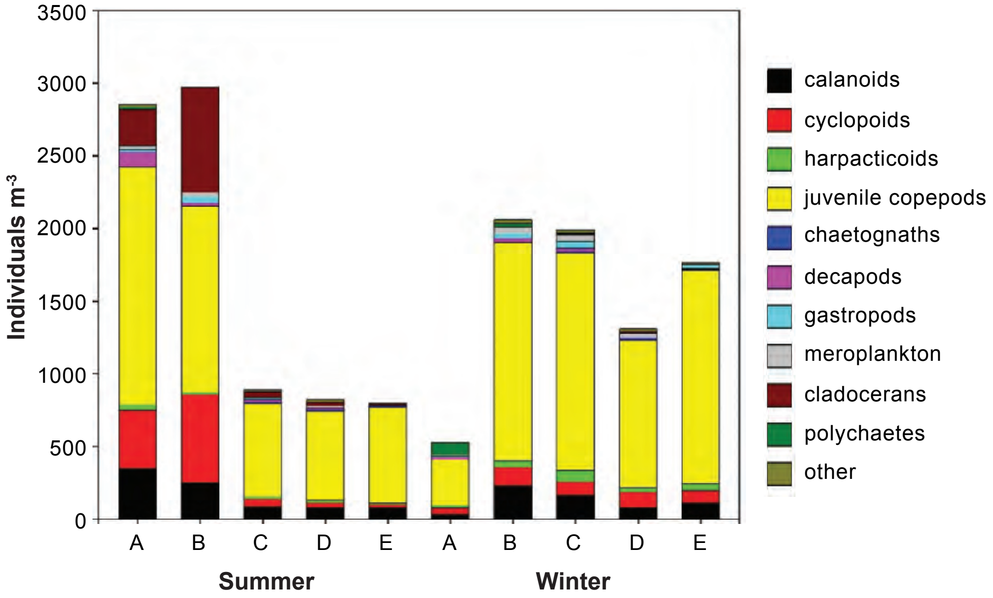

Fig. 3.22: Contribution of main groups of mesozooplankton (individuals m^{-3}) to abundance at stations A – E (Two Rocks Transect) in summer and winter.

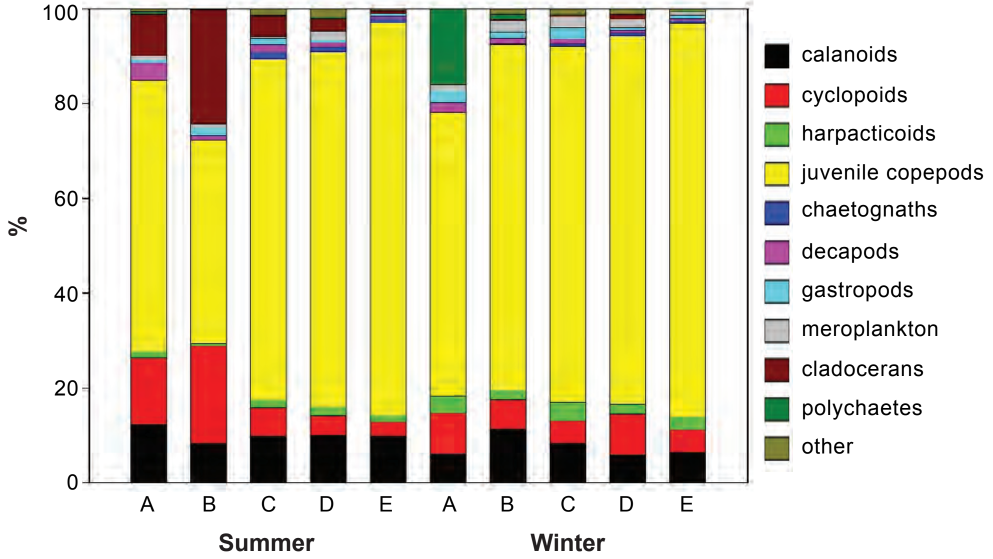

Fig. 3.23: Percent contribution of main groups of mesozooplankton (individuals m^{-3}) to abundance in stations A – E in summer and winter.

Cladocerans were important at nearshore stations A and B in summer and occurred in smaller numbers over the mid-shelf and shelf break (stations C and D). Polychaetes were common in winter in the lagoon (station A).

Acartia spp. and *Oithona* spp. dominated nearshore (stations A and B) in summer and at station A in winter (Fig. 3.24 and 3.25). Cyclopoid copepods were important at all stations at all sampling times. Small clausocalanidae were abundant at shelf and offshore stations (C – E). *Canthocalanus* spp and *Temora turbinata* were common in winter over the shelf (B and C). Harpacticoid copepods were present at all stations but were more common in winter.

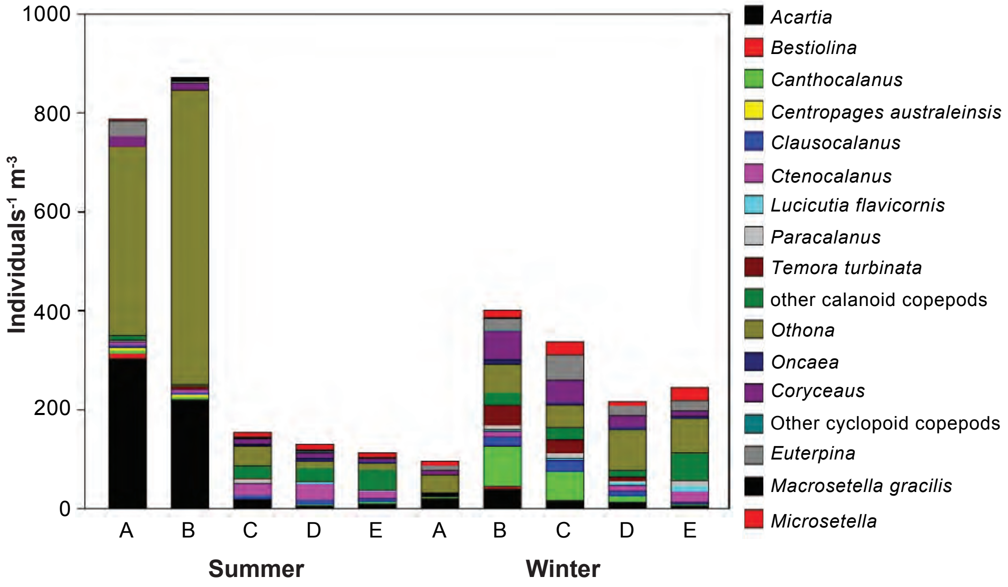

Fig. 3.24: Contribution of main groups of adult copepods (individuals^{-1}m^{-3}) to abundance in stations A – E (Two Rocks Transect) in summer and winter.

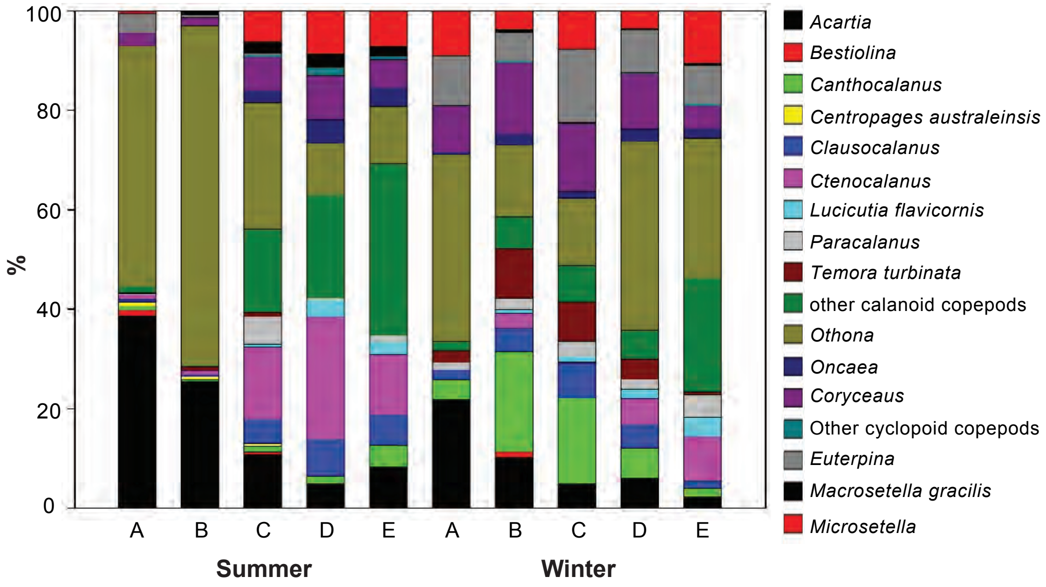

Fig. 3.25: Percent contribution of main groups of adult copepods (individuals^{-1}m^{-3}) to abundance in stations A – E in summer and winter.

Zooplankton biomass integrated over the water column was estimated as dry weight (Fig. 3.26). In general biomass of zooplankton was higher over the shelf than offshore. Biomass was higher offshore in winter than in summer, similar to the abundance of zooplankton.

The most nearshore station was excluded from the analysis. This station is located in about 10 m of water and it was impossible to exclude suspended sediment from the samples.

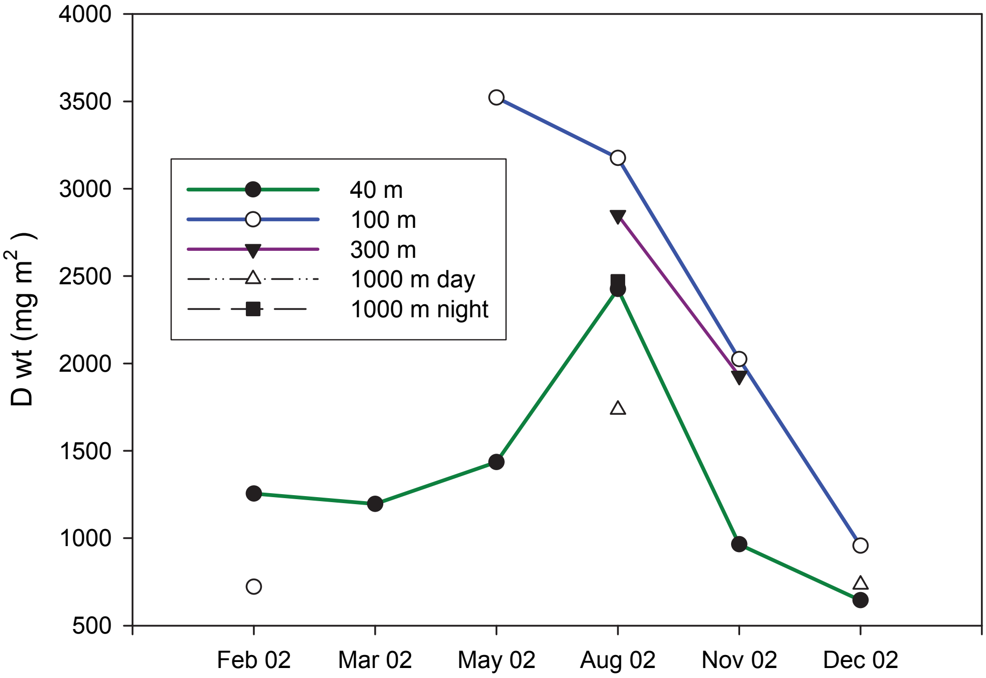

Fig. 3.26: Mesozooplankton biomass along the Two Rocks Transect.

Community composition

The mesozooplankton assemblages differed with distance offshore and between seasons (Fig. 3.27). Stations were significantly different to each other (PERMANOVA, p = 0.0002), and while seasons were not significantly different, there was a significant multivariate interaction between stations and seasons (PERMANOVA, p = 0.0002). Pair-wise a posteriori comparisons revealed that in summer the two nearshore stations A and B were not significantly different (PERMANOVA, p = 0.1) but they were significantly different from stations C, D and E (PERMANOVA, P<0.05), which did not differ significantly from each other (PERMANOVA, p = 0.3, 0.2 and 0.5 respectively). In winter all stations differed significantly from each other.

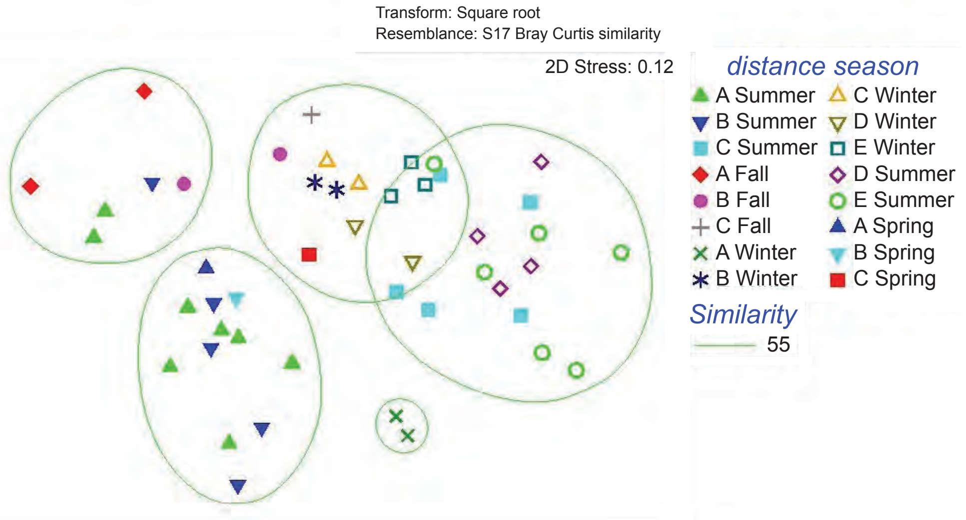

Fig. 3.27: Non parametric multidimensional scaling analyses showing associations of mesozooplankton assemblages between season and distance from shore with superimposed clusters from a dendogram at similarity levels of 55% (green line).

Station A had a consistent nearshore community; Station B consisted mostly of coastal species but some shelf species and a blue water copepod *Oncaea* occurred in winter. Station C had shelf and offshore species at all sampling times and stations D and E included offshore species most of the time. Some of the species that consistently contributed most to differences between nearshore and offshore assemblages were: *Oithona rigida*, *Acartia, Macrosetella*, *Microsetella, Temora turbinata,* (nearshore species) and *Pleuromammma*, *Euchaeta*, *Candacia*, *Eucalanus* (offshore species). These genera are cosmopolitan and are commonly observed to have such neritic or offshore distributions elsewhere (Boxshall and Halsey, 2004).). The cladocerans, *Evadne* sp and *Penila avirostris,* which occurred in large numbers in summer, contributed most to the seasonal pattern. *Penilia avirostris*, brachyuryan larvae and polychaete larvae were present mostly nearshore and contributed along with the copepods to the spatial patterns.

Mesozooplankton diversity based on the Shannon index increased from inshore to offshore and was higher in all stations in winter compared to summer, except at the lagoon station A (Table 3.5).

Table 3.5. Comparison of mesozooplankton diversity between stations along the Two Rocks Transect in summer and winter (Shannon index).

Station and Season	mean	standard deviation
A Summer	3.19	0.08
B Summer	3.13	0.06
C Summer	3.51	0.11
D Summer	3.55	0.06
E Summer	3.47	0.11
A Winter	3.10	0.03
B Winter	3.63	0.06
C Winter	3.57	0.06
D Winter	3.62	0.14
E Winter	3.74	0.00

Mesozooplankton grazing

Methods

Experimental studies of zooplankton grazing were conducted at sea during quarterly cruises from August 2002 to December 2004. The grazing experiments were conducted at Station A (15m water depth), Station C (100 m water depth) and Station E (1000 m water depth) along the Two Rocks transect. The experiments were carried out in 3L carboys maintained in a seawater bath at ambient sea surface temperature. Water from the surface collected by bucket was used as a food source, and three concentration levels of mesozooplankton were used, collected with gentle near-surface tows of the Bongo nets. Four replicates per treatment and four controls without mesozooplankton were prepared. An additional group of bottles was filled with surface seawater and filtered immediately to assess phytoplankton biomass at the start of the incubations.

The incubations were carried out for 24 hours. At the end of the incubations, mesozooplankton grazers were collected for identification and biomass determination, and a 200 ml subsample was collected from each replicate and preserved in 10% Lugol's for enumeration of microzooplankton food items. The remaining water was filtered through a GF/F filter for analysis of chlorophyll *a* concentrations. Grazing rates were calculated using a modification of the Frost (1972) equations that enabled phytoplankton productivity, microzooplankton grazing on the phytoplankton, and mesozooplankton grazing on both phytoplankton and microzooplankton to be estimated from the same set of experiments (Koslow *et al* in prep.).

Frost (1972) is a population growth equation that applies to a simple system of one predator and one prey:

$P_{24} = P_0 e\ (G\text{-}I)\Delta t$

where

P_{24} and P_0 – food concentrations at the beginning and end of experiment

Δt – duration of the experiment

G – growth rate

I – grazing rate.

Koslow *et al* (in prep.) allows determination of micro and mesozooplankton grazing rates from one set of experiments:

$P_{24} = P_0 \exp[(G_p - I_m M - I_{zp} Z)\Delta t]$

$M_{24} = M_0\ \exp[(G_m - I_{zm} Z)\Delta t]$

Where M and Z are the mean biomass of micro- and mesozooplankton, respectively, during the experiment. The grazing rate of the microzooplankton may be approximated from the control experiment, in which Z = 0, by assuming that $G_m = I_m/Ma$ where *a* is the growth efficiency of the microzooplankton, which is approximately 0.33 (Straile, 1997; Strom and Morello; 1998; Edwards *et al.* 2000).

Results and discussion

Calanoid and cyclopoid copepods dominated abundance and biomass of grazers except in the lagoon station A in summer where cladocerans, mainly *Penilia avirostris*, dominated both abundance and biomass and the 100 m and 1000 m stations in July where chaetognaths and siphonophores dominated biomass (Fig. 3.28) Heterotrophic dinoflagellates and ciliates dominated the prey, although diatoms were a major component of the biomass at the inshore station (A) in summer (Fig. 3.29). The size structure of grazers and prey was uniform across all three stations (Figs. 3.30, 3.31).

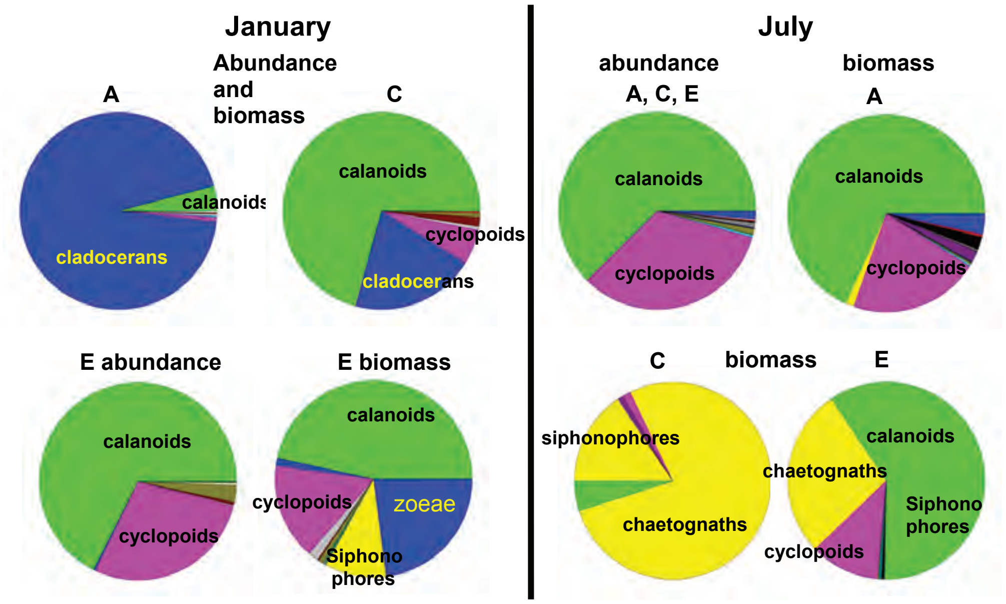

Fig. 3.28: Composition of mesozooplankton grazers.

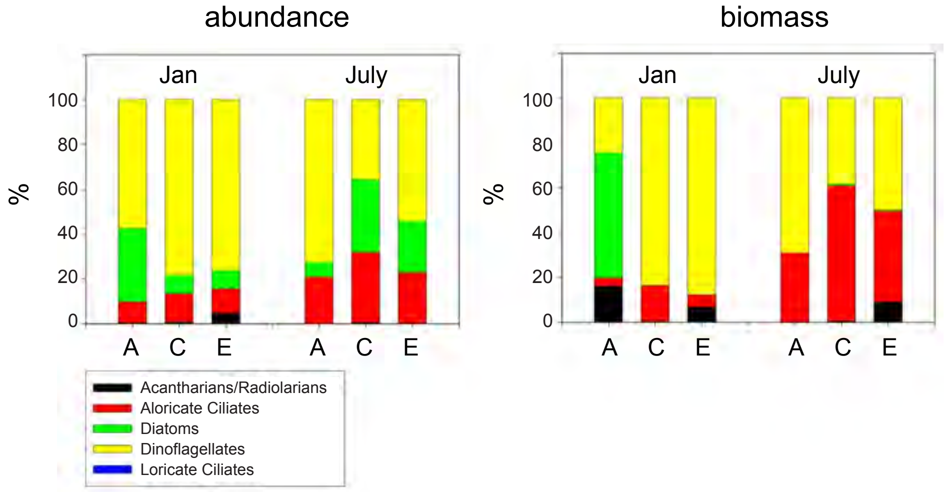

Fig. 3.29: Composition of prey (microzooplankton and diatoms) at stations A, C and E.

The size structure of grazers and prey was uniform across all three stations (Fig. 3.30).

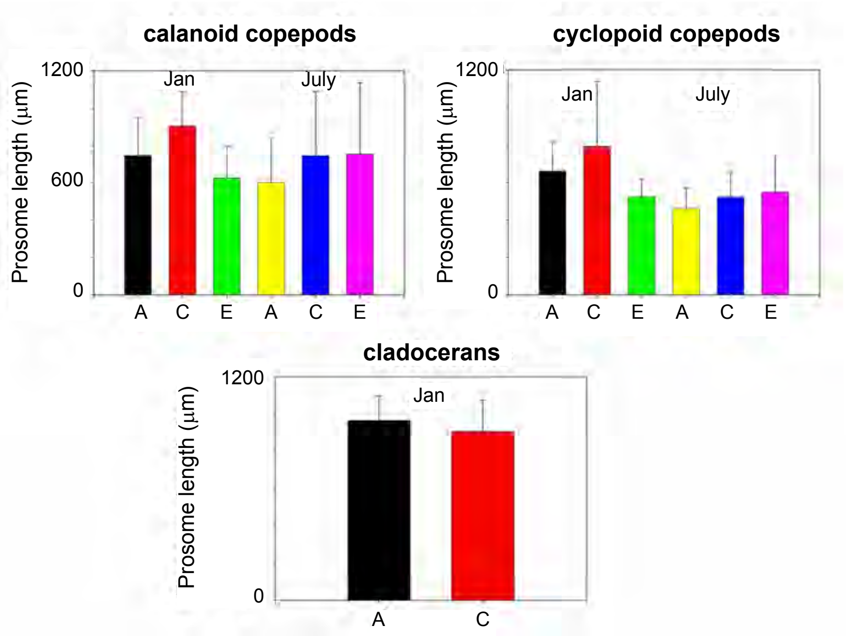

Fig. 3.30: Size structure of grazers.

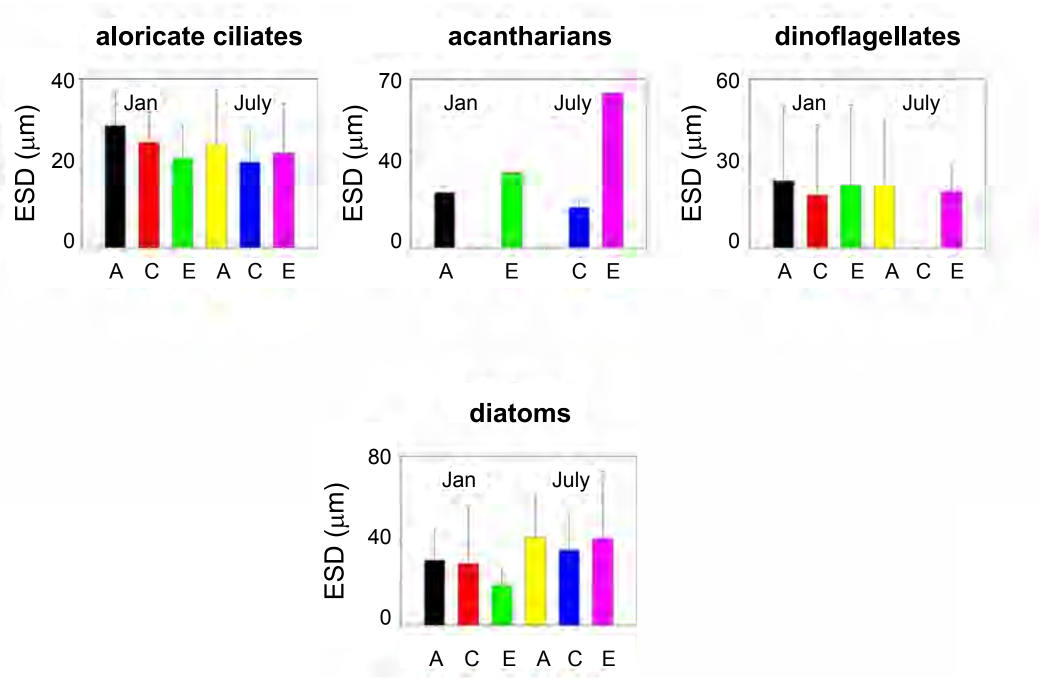

Fig. 3.31: Size structure of microzooplankton prey and diatoms (µm ESD).

We compared the mesozooplankton grazing rates on the microzooplankton calculated using the Frost equation and Koslow equation and obtained good agreement for all three stations (R^2 = 0.966, R^2 = 0.986 and R^2 = 0.978 for stations A, C and E respectively).

Mesozooplankton grazing on both total phytoplankton and on the microzooplankton was lowest at station A and increased with distance offshore (Fig. 3.38). The increased predation on the microzooplankton offshore was consistent with the smaller phytoplankton and increased role of microzooplankton grazing generally observed offshore (Paterson submitted). Grazing by mesozooplankton on phytoplankton was low: 0 (in 50% of experiments) to 12 % of primary production was removed. Grazing was higher in January than in July.

Mesozooplankton consumed between 0.5 and 1% of C body weight. This is at the lower end of literature values for copepods, which fall between 0.2 – 84% and about 20% is needed to sustain metabolism (Schultes, 2004 and references within). There is very little data available on feeding rates of mesozooplankton from oligotrophic warm waters and most of it covers only feeding on phytoplankton since it is based on the gut fluorescence technique. Recently, Paffenhöfer (2006) hypothesized that food availability is the most important factor limiting the abundance of copepods in warm oceanic waters. His measurements of ingestion rates and metabolic requirements of two abundant copepods from the subtropical open ocean indicated that the available food concentration was often insufficient to maintain metabolism and therefore limited reproduction.

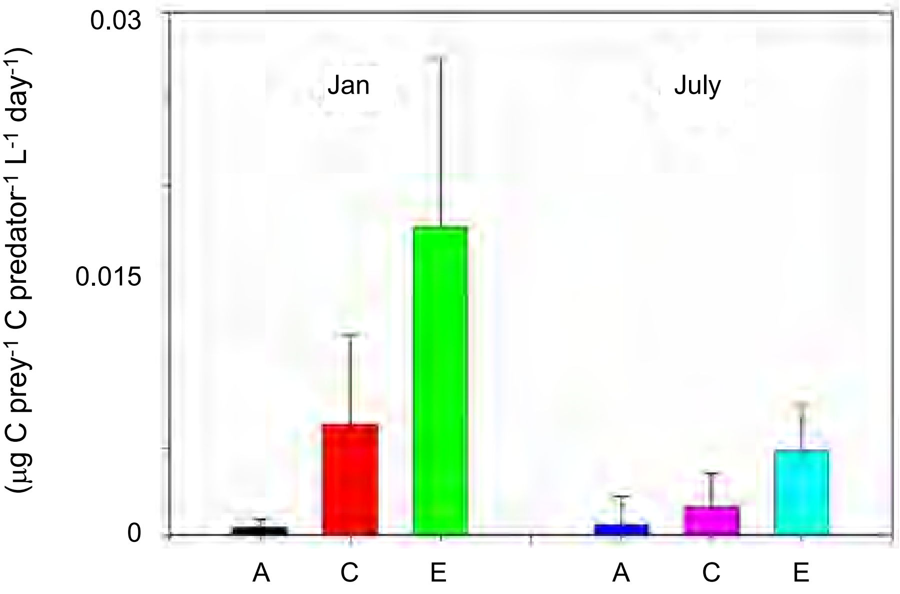

Fig. 3.32: Grazing of mesozooplankton on microzooplankton.

We detected coupling between the different trophic levels in our experiments. Mesozooplankton released small phytoplankton from grazing pressure by protozoa. The proportion of secondary production removed by mesozooplankton increased with increased biomass of predators, and the proportion of primary production decreased with increased biomass of mesozooplankton (Fig. 3.33).

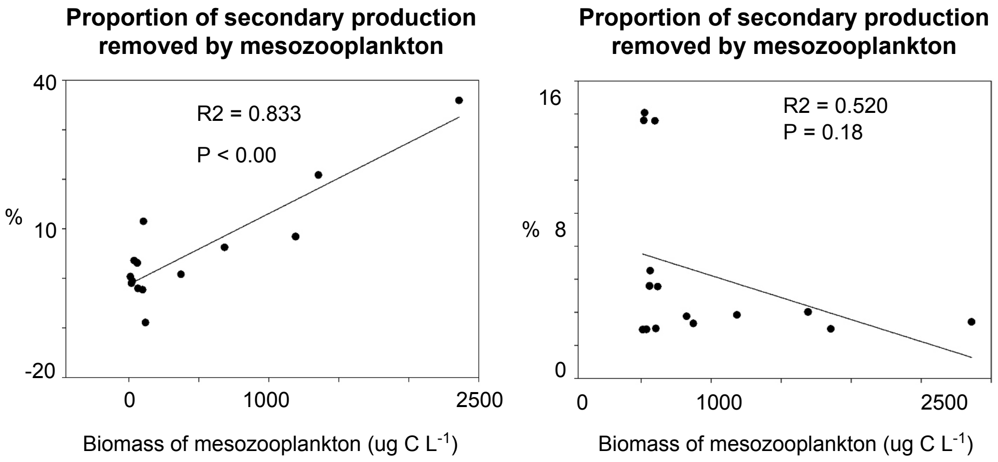

Fig. 3.33: The proportion of secondary production removed by mesozooplankton (left) and of primary production removed by microzooplankton (right) in relation to the biomass of mesozooplankton grazers. The decrease in microzooplankton grazing indicates the influence of mesozooplankton on microzooplankton grazing.

Mesozooplankton: estimation of secondary production

Methods

Secondary production experiments were conducted during two RV *Southern Surveyor* cruises in August 2003 (SS200307) and January 2004 (SS200401). Two field methods and two models were used to estimate secondary production. The egg production method is based on the fact that copepod somatic growth ceases in adult females, and the growth rate is therefore assumed to be equivalent to egg production. This method has good spatiotemporal resolution, because fecundity is both time and site specific. It reflects the integration by the adult female of environmental variables prevailing during accumulation of gonadal material. This method assumes that all stage specific instantaneous growth rates are equal. This was tested and found to be true in *Centropages, Acartia tonsa, Calanus pacificus, C. finmarchicus*. For many other species, rates decline with copepodite stage, and also food limitation may exist for the adult but not the juvenile. Rates of production can be estimated from the specific egg production rate, which equals the growth rate of females.

Copepods used for the egg production method were collected by slow vertical Bongo tows using 355 and 100µm solid codends. Individual females were placed in 70 ml plastic containers with particle free seawater. Females were incubated for 24 hours under a 12h dark:12 h light cycle and ambient temperature.

The second field method employed was a new amino acid method. Aminoacyl t-RNA synthetases (AARS) are a group of enzymes that catalyse amino acid ($\alpha\alpha$) activation and the transfer of activated amino acid to their tRNAs (Fig. 3.40). It is a first step in protein synthesis, and AARS activity is therefore directly related to protein synthesis. A significant relationship between protein synthesis and growth was observed in cephalopods and fishes. Chang *et al.* (1984) developed a continuous assay for AARS activity. They measured activity based on the release of pyrophosphate (PPi) during aminoacylation (incorporation of PPi into ATP) of tRNA assessed as oxidation of NADH by PPi. This method is inexpensive, using a commercial Sigma kit and a spectrophotometer (Yebra and Hernandez-Leon 2004).

We applied Ikeda and Motoda (1978) and Hirst and Lampitt (1998) models to our data. In the Ikeda and Motoda (1978) model, the growth rate is estimated from the respiration rate which is related to individual body weight and temperature. In the Hirst and Lampitt (1998) model, copepods are characterized according to spawning type (broadcast or egg carrying) and life stage. In adults, growth equals reproduction and in juveniles growth is reflected by weight gain, and production is a function of body weight and temperature. The models are similar, and both assume food is not limiting.

Results

Estimates of secondary production using the egg production method were found to be lower than estimates based on the AARS method and the empirical model (Fig. 3.34). At some times, there was a good agreement among the methods i.e. Station A and Stations C, D, E in winter and Station A in summer. The Hirst-Lampitt model and the AARS method showed good agreement in offshore stations in winter.

Copepod production estimated using the egg production method ranged from 0.4 to 10 mg C m^{-2} d^{-1}. This is comparable to copepod production measured in the North West Cape region of Western Australia (Mc Kinnon and Duggan, 2003), but was low compared to values from more productive coastal and shelf regions elsewhere in the world (Table 3.6).

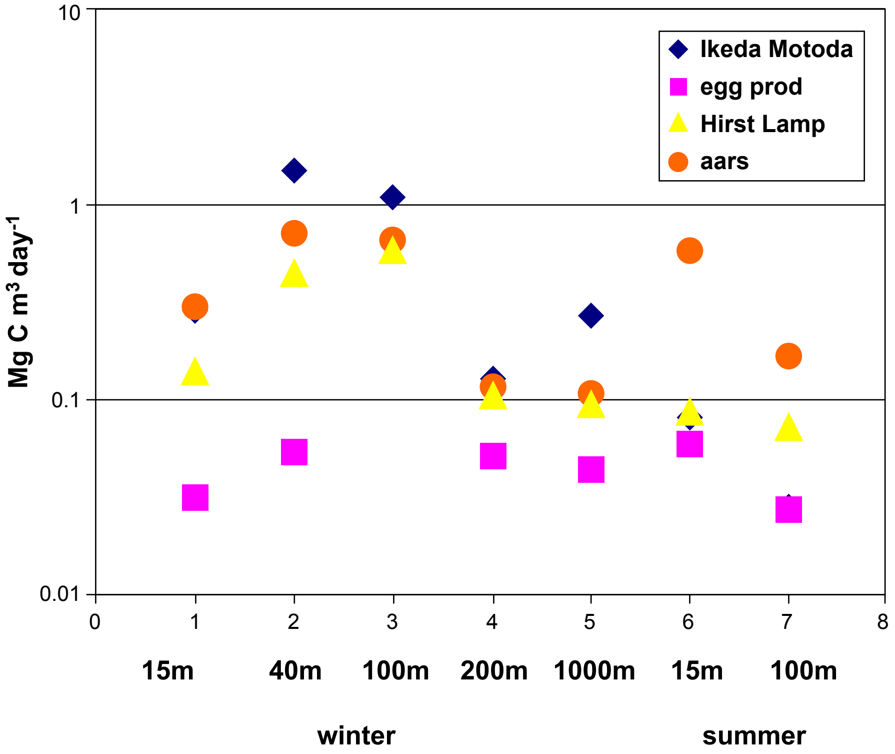

Fig. 3.34: Estimation of secondary production (in mg C m^{-3} day^{-1}) using the two field methods and models.

Table 3.6. Secondary production in different regions (McKinnon and Duggan, 2003).

Location	Production mg C m^{-2} d^{-1}	Environment
North West Cape, Western Australia	7.5	Subtropical shelf
North West Cape	11.5	Subtropical shelf
Kaneohe Bay, Hawaii	151	Tropical Bay
Western Port Bay, Victoria	7.5	Temperate Bay
Western Agulhas Bank, South Africa	40	Upwelling shelf
Western Agulhas Bank	400	Upwelling shelf

Secondary productivity is generally assumed to be related to primary production, on the order of 10% of primary production. We therefore examined the relationship between secondary production estimated using the enzyme and egg production methods and chlorophyll biomass (Fig. 3.35) and primary production (Fig. 3.36). There was no relationship between secondary production and either total or large phytoplankton biomass and between secondary production and either total or large phytoplankton production.

Only a small proportion of phytoplankton was utilized by copepods (Table 3.7).

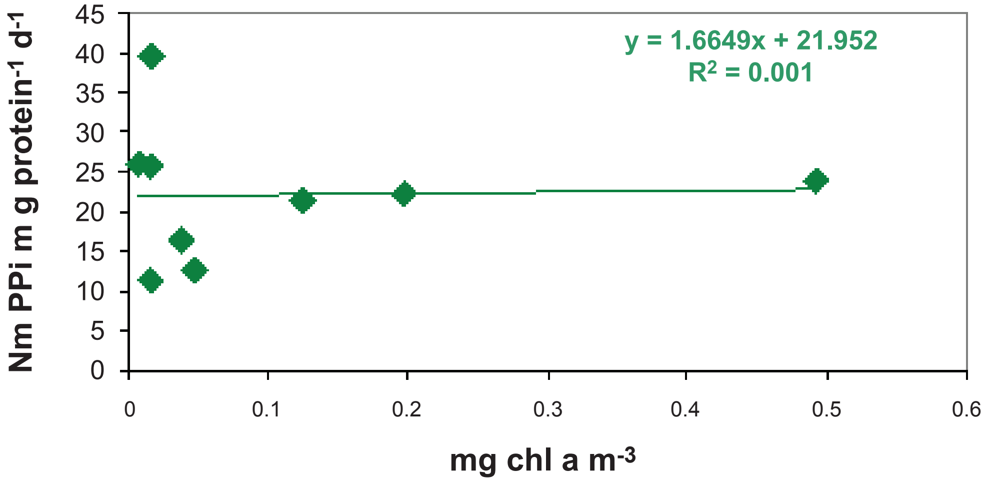

Fig. 3.35: Relationship between secondary production (AARS method) and large phytoplankton biomass

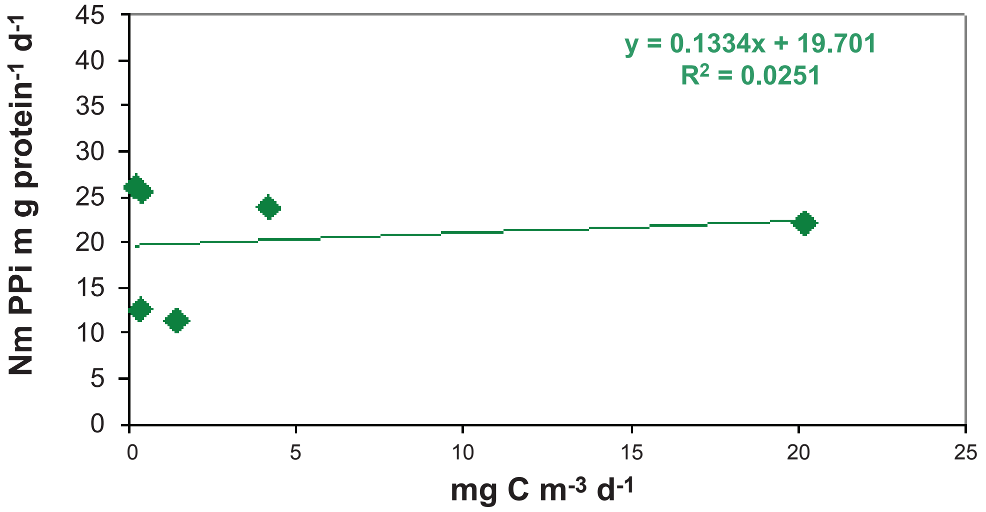

Fig. 3.36: Relationship between secondary production (AARS method) and large phytoplankton production

Table 3.7: Copepod production as a proportion of primary production.

Method	% total primary production	% large fraction of primary production
Egg production	0.2 – 1.6	0.6 - 52
AARS enzyme	1 – 25	1.7 - 250
Hirst and Lampitt model	0.8 – 24	1.61 - 267

Discussion

Secondary production was low in comparison with productive marine environments, but comparable to estimates off Australia's North West Cape. Our AARS enzyme and egg production method results were reasonably similar to the results predicted by the Hirst-Lampitt (1998) model. There was no correlation between phytoplankton biomass and secondary production. This is not surprising considering that most phytoplankton in our region are small and not heavily grazed by mesozooplankton. Between 0.2 and 44.9% of total primary production would sustain the estimated levels of secondary production (Table 3.7). However, secondary production was at times a large proportion of primary production if only the contribution by large phytoplankton was considered. Empirical size- and temperature-based models assume secondary production is not food limited, on the other hand, so they may overestimate *in situ* productivity, if copepods are food limited. In addition most copepods are omnivores eating protozoa (Boxshall and Halsey, 2004) and detritus; phytoplankton is only a portion of food available for copepods. In future, we will estimate zooplankton grazing and production as part of the SRFME biogeochemical model, which will incorporate realistic estimates of prey availability along with temperature- and size-based estimates of physiological processes.

Summary

The mesozooplankton assemblages across the Two Rocks transect showed apparent seasonality as well as onshore-offshore spatial structure. Assemblage differences were more pronounced in summer than in winter, when Leeuwin flow was stronger, driving greater offshore-inshore exchange. Nearshore assemblages were more variable in summer than in winter, and offshore station E showed the least seasonal difference. This corresponded to the greater seasonal variability inshore in temperature and salinity (section 3.2.1). Mesozooplankton diversity increased with distance offshore, however, consistent with the pattern observed in the microzooplankton (Section 2.2.9, vol. 1).

Mesozooplankton grazing on total phytoplankton was lowest nearshore and increased with distance offshore. Grazing rates were variable and the choice of prey varied within and among stations. Diatoms were grazed at all stations. An interaction between mesozooplankton and microzooplankton grazing was observed, with an increased impact of the mesozooplankton on the microzooplankton offshore, consistent with the trend toward increased microzooplankton grazing on the phytoplankton offshore (sec. 2.2.9, vol. 1).

Measured feeding rates were low. It is possible that the low food concentration is an important factor regulating the abundance of mesozooplankton in our region.

Secondary production was low in comparison with productive marine environments, but comparable to estimates off Australia's North West Cape. Our field method results were more similar to the results predicted by the Hirst-Lampitt (1998) than to other global models. There was no correlation between phytoplankton biomass and secondary production. Secondary production was at times a very high proportion of primary production, only in relation to the contribution by large phytoplankton alone.

3.2.5 Bioacoustics

Investigator / Institution

Nick Mortimer	CSIRO Marine and Atmospheric Research

Introduction

Acoustic methodologies can be applied to characterise the spatial and temporal variability of continental shelf marine life (McGehee *et al.* 2004; Warren *et al.* 2004). Acoustic remote sensing enables scientists to map a cross section of the ocean and view the interaction of marine life with seabed and oceanographic features (Sutor *et al.* 2005). It also has the potential to provide quantitative metrics within and between seasons on the densities of major trophic groups from plankton to fish (Swartzman *et al.* 2002).

To identify and quantify marine life from plankton (predominantly drifting small organisms 0.1 - 20 mm) to large nekton (organisms such as fish) that can move independently of currents) requires the use of many acoustic frequencies. In this study 9 frequencies were used ranging from 70 kHz to 3 MHz (Holliday and Pieper, 1995). The acoustic maps enable biological and physical samples to be better targeted and provide the necessary spatial and temporal context. Likewise the physical and biological samples are critical for the interpretation of the acoustic signatures and training of the multi-frequency remote sensing algorithms. To sample the marine life from phytoplankton to nekton, seawater pumps and variable meshed nets are used. These point samples of marine life can be used to ground-truth the acoustics and relate the samples to the across-shelf patches observed in the acoustics (Greene *et al.* 1998; Ressler *et al.* 2005;). It is often difficult to capture the organisms seen by the acoustics due to avoidance and difficulty in accurately targeting scattering layers. At 70 kHz the acoustic frequency is also selective towards larger organisms (macrozooplankton to micronekton). Current biological sampling methods using small meshed nets will under represent or undersample these animals. One way to assist in the identification and numbers of these species is to use multi-frequency acoustic methods (Korneliussen and Ona, 2003).

Low frequency bioacoustics

Aims/objectives

To develop and apply acoustic methods to map and monitor zooplankton and micronekton at low frequencies: 70, 120 and 200 kHz.

Methods

Nine voyages with acoustic transects along the Two Rocks transect have been completed using a specifically designed pole mounted three frequency echo sounder. The system was calibrated at the CSIRO Marine Research transducer calibration facility, and in the field using a standard tungsten carbide reference sphere method (Foote *et al.* 1987).

Results

The Two Rocks across-shelf acoustic transect (70 kHz on the 29th April 2003) provides unique insights into the spatial and temporal dynamics of inferred biota (Fig. 3.37). This acoustic map provides seabed attributes of depth and the inferred aggregations of biological life within the water column over the 90 km long transect. High acoustic reflectance was found inshore (A,B) associated with the cooler saltier and higher chlorophyll water mass (Fig. 3.43). Internal waves were observed on the outer shelf (C to D). Vertical migration of the deep scattering layer moving from ~600 m depth to 100 m depth at sunset is evident at station E. This cross sectional view of the water column provides a window into the subsurface marine life and its spatial relationships with oceanographic conditions and seabed features. There was a significant correlation between patches of high acoustic reflectance and high chlorophyll levels for this transect.

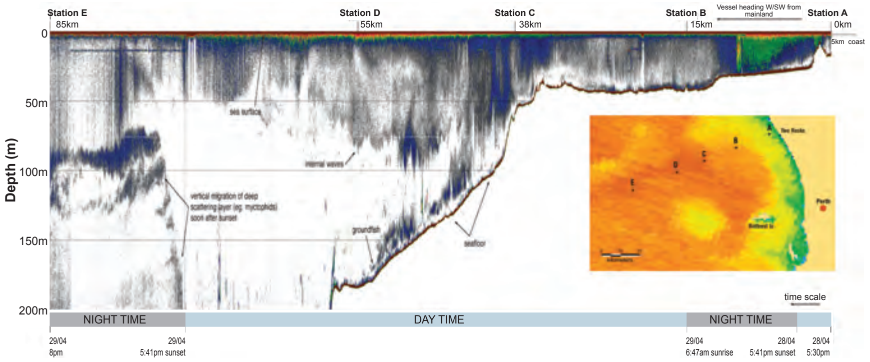

Figure 3.37: Acoustic echogram at one frequency (70 kHz April 2003) of the two rocks transect with vessel moving from Station A on the coast to Station E offshore. Low acoustic reflectance (volume reverberation) is shown in blue and high reflectance is red. The insert of a satellite image of ocean temperature variation of the Two Rocks transect with orange as high temperature and blue low temperature gives the sea surface context of the acoustic data.

Figure 3.38 illustrates the difference in spatial sampling between the acoustic data resolution and the physical, chemical and biological station data collected along the transects at quarterly and monthly intervals. Visually the vertical and horizontal resolution of the acoustic backscatter (inferred to be from large biological scatterers) provides a unique spatial context to complement the interpretation of the station data. In particular it highlights high gradients in backscatter that occur at bathymetric features close to sampling stations bc and c (Fig. 3.38c). Small changes in positioning of stations bc and c may result in large changes in biological, chemical and physical variables observed.

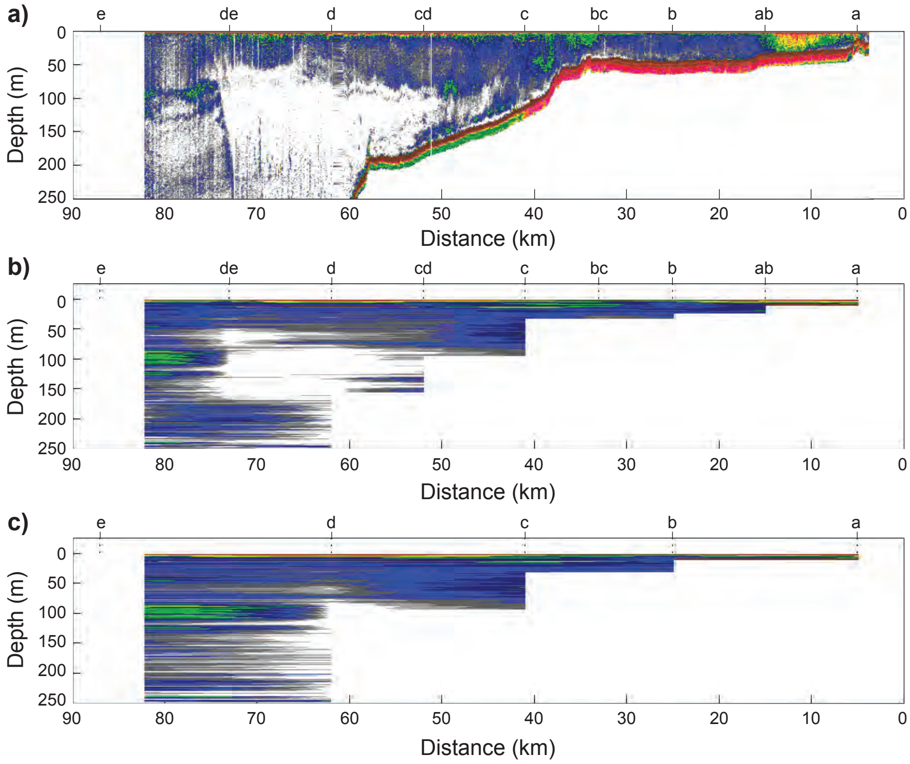

Figure 3.38: Calibrated acoustic transect data at 70 kHz (April 2003) shown in Figure 3.37 at (a) 10 m horizontal and 1 m vertical resolution, (b) re-sampled acoustic data with linear horizontal interpolation to simulate the collection of associated biological, chemical and physical data at the 9 quarterly stations and (c) similar re-sampling for the 5 monthly stations.

Figure 3.39 highlights the temporal variability within the acoustic data during the summer and autumn of 2003 and 2004 at 120 kHz. A large inter-season variation in backscatter was observed in summer (Fig. 3.39 a,b) and autumn (Fig. 3.39 c,d) that occurred over large spatial scales of 10 – 50 km for 2003 and 2004. Also, a large inter-annual change in backscatter is evident, with lower backscatter in 2003 than 2004 at large spatial scales from 20 to 30 km.

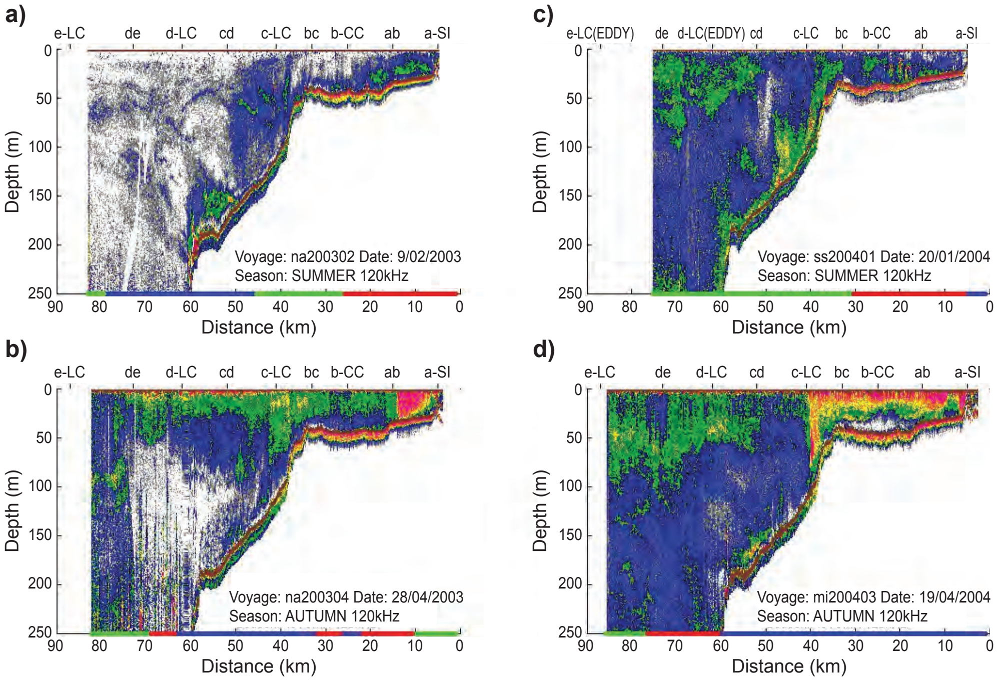

Figure 3.39: Volume reverberation (-85 dB minimum) at 120 kHz for between year comparison of Summer (a) 2003 and (b) 2004 and Autumn (c) 2003 and (d) 2004. At each station the water mass as interpreted from satellite imagery is identified where (LC = Leeuwin Current, WI == Winter Inshore water ,CC =Capes Current and SI = Summer Inshore water. Time of day is indicated with a blue bar (day), green bar (night) and twilight (red).

Principal component analysis was used to identify patterns of the acoustic reverberation along the Two Rocks transect. EchoView Ver 5.1 was first used to calculate the mean volume backscattering strength integrated from the surface to 5m above the bottom in 1 km horizontal bins, with a maximum integration depth of 150m. Small dense schools of fish were removed so the signal reflected large-scale features. The data were linear-transformed, with the original acoustic data expressed on a log scale (dB) and standardized by subtracting the transect mean and dividing by the standard deviation, before performing principal component analysis.

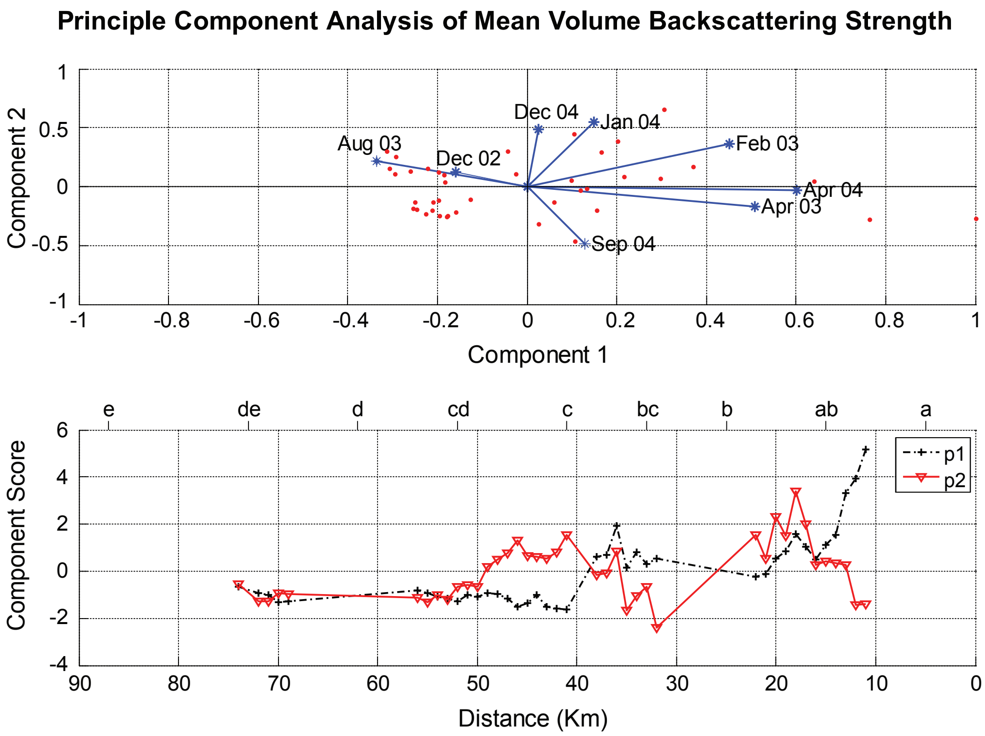

Principle Component Analysis of Mean Volume Backscattering Strength

Figure 3.40: (top) Principal component analysis of Mean Volume Backscattering Strength along the Two Rocks transect. (bottom) Component Scores along the Two Rocks Transect showing principal component 1 (p1 – black line) and principal component 2 (p2 – Red line).

Figure 3.40 shows a plot of the loadings for each cruise onto principal component 1 versus principal component 2 (top) combined with a plot of the scores of the first two principal components along the transect (bottom). Component 1 explains 31% of the variability. It highlights a cross-shelf gradient, with inshore scattering peaking in autumn (April 2003 and 2004) and also summer of 2003, with an opposite pattern in the winter (August) of 2003. Component 2 explains 19% of the variability, highlighting the inner and outer shelf. This area is influenced by the Capes Current in summer, a cool water current from the south that can cause localised upwelling. A pattern of increased backscattering on the inner shelf (15 – 20 km offshore) and on the outer shelf just offshore of the 100 m depth station (C) was observed on virtually all summer cruises, indicating a possible link between this current and enhanced backscatter in these regions (Fig.3.40). The pattern during summer was clearly differentiated from that during the spring (September) of 2004. Despite the limited data set, the available data suggest seasonal differentiation in the distribution of acoustic backscattering across the shelf.

Multi frequency

Distinguishing broad categories and associated numbers of marine life is possible using multiple acoustic frequencies in combination with acoustic scattering models (Kloser *et al.* 2002; Korneliussen and Ona, 2003). Figure 3.41 shows an example of such differentiation using our three frequency system of 70, 120 and 200 kHz. On the 200 kHz volume reverberation echogram a thin layer at 80 to 100 m depth stands out. This layer is characteristic of a non-gas bladdered animal (e.g. euphausiids), because such organisms have a higher reflectivity at 200 kHz (Fig. 3.41b) when compared to 70kHz (Fig. 3.41a). This feature is easier to visualise on the lower panel (Fig. 3.42c), which combines the frequencies using an amplitude-mixing algorithm. Of special note is the distinct depth layering of this feature and the need to accurately target these layers with biological sampling for identification.

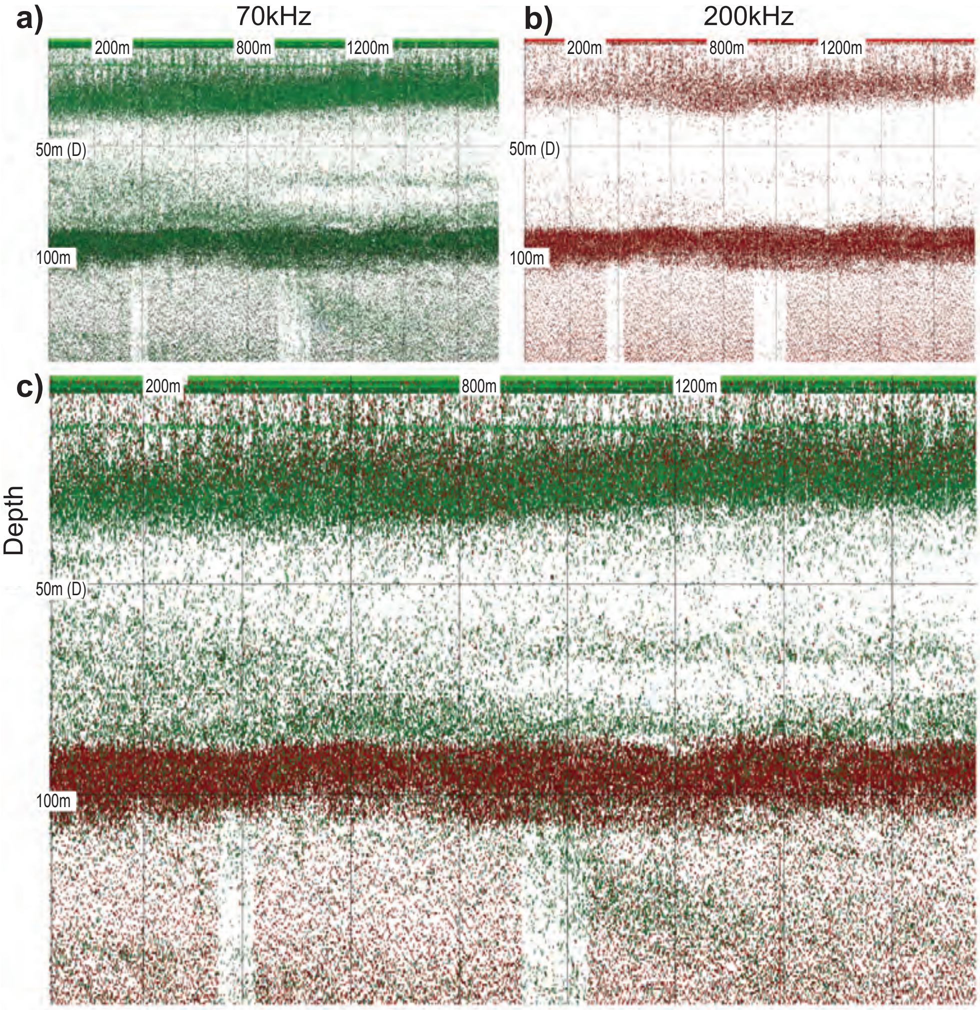

Figure 3.41: Acoustic species group identification example using two frequencies at a) 70 kHz (green), b) 200 kHz (red), and c) amplitude mixing of the two frequencies to highlight species differences (Kloser *et al.* 2002).

The multifrequency acoustic data can be used to explore the generic biological scattering type (solid, fluid or gas-filled) and size that is responsible for the calibrated volume reverberated backscatter. We consider four general classes of backscatter that relate to the size of the organisms equivalent radius (a) and the acoustic wave number (k); being Rayleigh ka<<1, resonance ka = 1, transition ka ~1 and geometric ka>>1 (Fig. 3.48). As an example, a fluid-filled organism in the Rayleigh scattering region at all frequencies requires the equivalent radius to be very much less than the 200 kHz wavelength of 7.5 mm. The volume backscattering strength (Sv dB re 1 m^{-1}) dB difference ($\Delta dB_{f_1-f_2}$) between frequencies f_1 and f_2 in the Rayleigh region can be approximated by:

$\Delta dB_{f_1-f_2} = 10\log 10\left(\frac{f_1}{f_2}\right)^4$ where $\Delta dB_{70-120} = -9.4$ and $\Delta dB_{70-200} = -18.2$ dB.

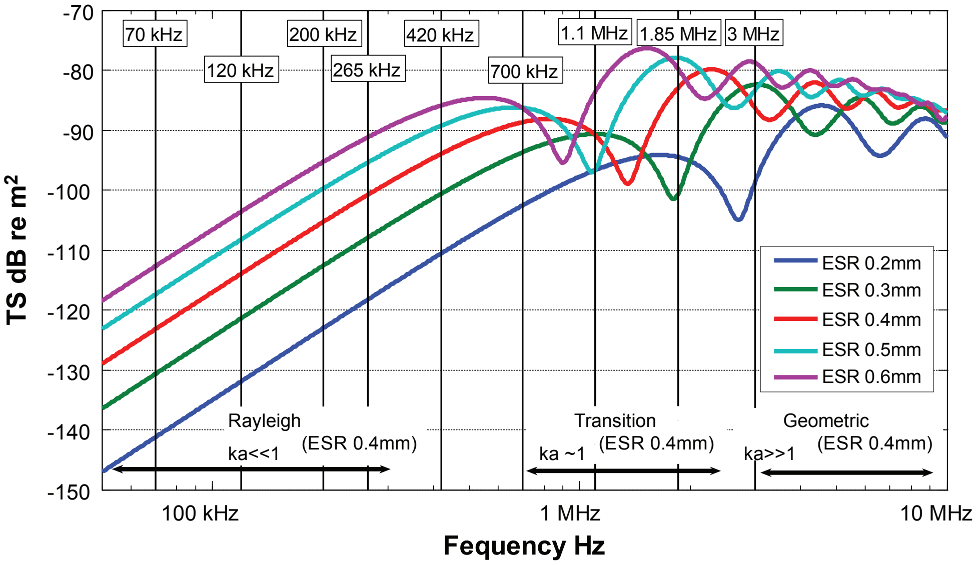

Figure 3.42: A plot of frequency versus target strength (TS) for organisms of equivalent spherical radius (ESR) from 0.2 – 0.6 mm). The frequencies used by SRFME are indicated along the top.

The volume reverberation data between 70 kHz and 120 kHz shows that there are clear areas of both significantly high (greater than 3 dB) and low frequency difference (Fig. 3.43). We hypothesise that the areas of low frequency difference are indicative of small scatterers within the Rayleigh scattering regime; fluid-filled organisms need to be very much less than an equivalent radius of 12.5 mm. When the frequency difference is very high (greater than 3 dB) the scattering is indicative of larger-bodied organisms or resonance gas bubble scatterers. This ability to segment the multi-frequency acoustic echogram into probabilistic scattering types is a first step toward understanding the spatial and temporal distribution and abundance of organisms. Acoustics provides a very high spatial (and potentially temporal) resolution of the marine environment and could form a complementary sampling tool in the evaluation of ecosystems and their natural and human induced changes. One aspect of the need to understand ecosystem function is for input into the ecosystem approach to fisheries management.

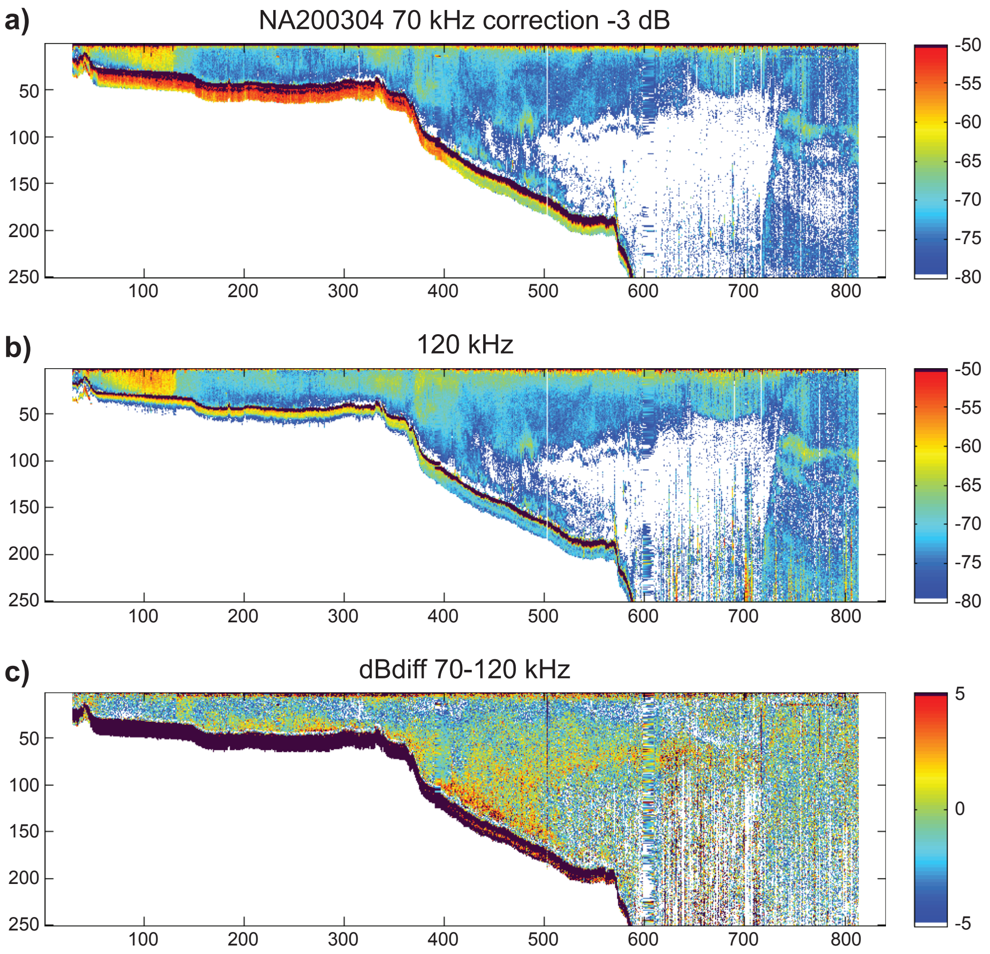

Figure 3.43: Example of the volume reverberation dB difference between a) 70 kHz and b) 120 kHz acoustic frequencies in c) ΔdB_{70-120} where blue indicates a low and red a high between frequency difference.

The sampling needs for ecosystem-based fishery management will depend on the overall management arrangements for the fishery, but acoustics can provide information on relative biomass, size and trophic spectra through the water column.

High frequency bioacoustics

Aims/objectives

The objective of this part of the project was to develop and apply acoustic methods to assess the fine-scale vertical distribution of mesoplankton at high frequencies ranging from 265 to 3000 kHz.

To use acoustics to investigate the distribution of mesoplankton (0.2 - 20 mm), higher frequencies must be employed than those normally used in fisheries. To determine both the size and abundance of zooplankton and micronekton, multiple frequencies are required (Holliday and Pieper, 1995). This study has been conducted using a Tracor Acoustic Profiler System (TAPS), in conjunction with a specially designed Discreet *In-situ* Plankton Sampler (DIPS). The DIPS unit can collect six discrete plankton samples from the water column, while TAPS collects concurrent acoustic data (Fig. 3.44).

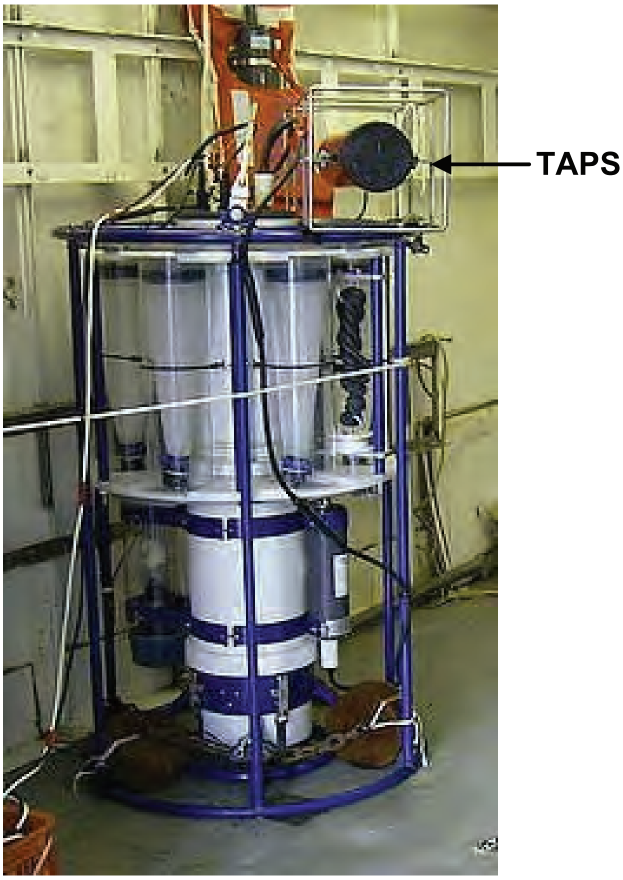

Figure 3.44: Picture of the specially designed Discreet *In-situ* Plankton Sampler (DIPS), that can collect six samples at targeted water depths, with the Tracor Acoustic Profiler System (TAPS) attached to the upper right of the frame.

The six TAPS frequencies were chosen to span the transition between Rayleigh to geometric scattering for fluid-filled animals such as copepods. The acoustic profiler has primarily been deployed in 'cast mode', where a finite volume of water (5 L) at a fixed range (1.5 m) from TAPS is sampled as the instrument is lowered through the water column. The DIPS unit is operated from the surface, combined with a real-time display of TAPS data that allows the operator to target features of interest in the water column.

Methods

Extensive trials and experiments have been undertaken during SRFME to develop the application of this technology and associated biological sampling, since this is an area of acoustic science new to Australia.

The TAPS and DIPS units were used extensively during the 2004 field season, with 50 vertical profiles and 120 plankton samples collected. These plankton samples are currently being digitized using a microscope fitted with a CCD camera. The digital pictures are then processed using ImageJ (Abramoff *et al.* 2004) to determine the volume and equivalent spherical radius (ESR) of each animal (Alcaraz *et al.* 2003). The ESR is the radius of a sphere that contains the same volume as the organism. Once dominant ESR size classes are known, backscatter models appropriate to organism shape and composition can be calculated to predict the frequency response (Holliday, 1992). Based on these backscatter models, the multi-frequency TAPS data can be inverted using non-linear least-squares to give estimates of biota size and abundance (Holliday and Pieper, 1995) (see Fig. 3.45).

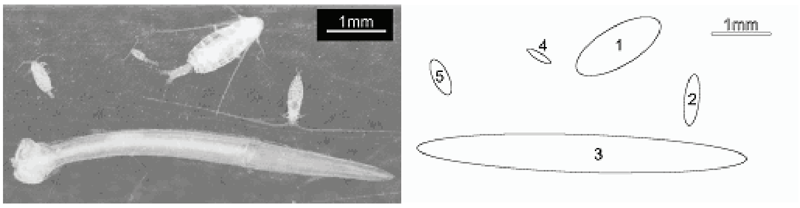

#	Taxa	Area (mm^2)	Major (mm)	Minor (mm)	Volume (mm^3)	ESR (mm)
1	copepod	0.821	1.605	0.652	0.357	0.440
2	copepod	0.168	0.865	0.248	0.028	0.188
3	chaetognath	2.755	5.542	0.633	1.163	0.652
4	copepod	0.041	0.451	0.114	0.003	0.090
5	copepod	0.134	0.654	0.260	0.023	0.177

Figure 3.45: Example of biota measured for acoustic truncated fluid sphere model development, showing the necessary simplifications of body shapes. The associated table quantifies the biota cross sectional area, major and minor axes, volume and equivalent spherical radius (ESR). The organisms were collected from 27 m water depth, with the frequency response as shown in Figure 3.48.

Results

Composition of pump samples varied in abundance, species and size classes. The abundance of zooplankton in pump samples was found to range between 145 m^{-3} and 6246 m^{-3}. Species composition changed with depth, station and time of day.

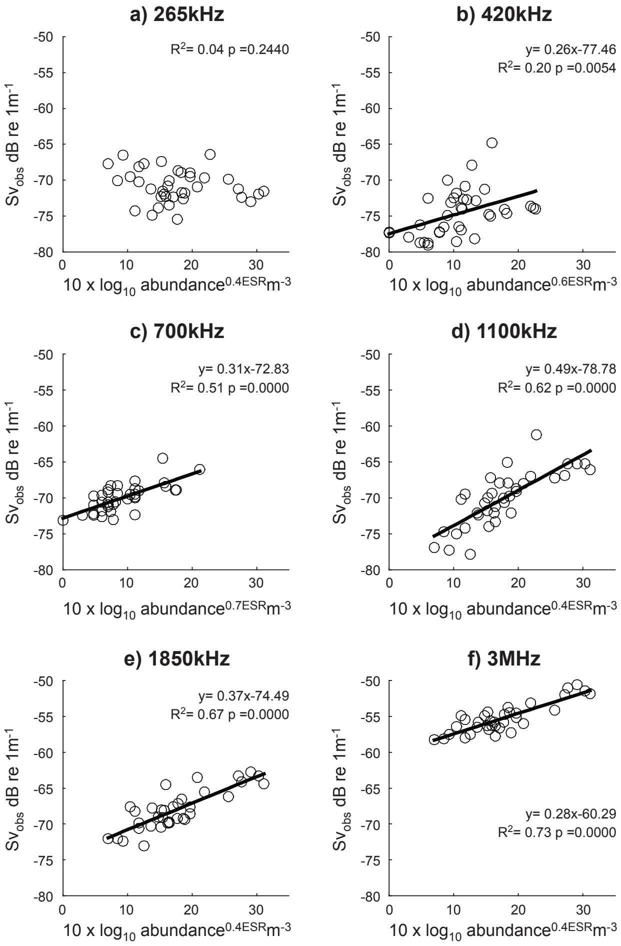

Figure 3.46: Stepwise Regression of measured TAPS Svobs to 10log10 (abundance) of dominant size class.

To evaluate our acoustic methodology we must determine a relationship between DIPS samples and TAPS-measured Sv. We assume the relationship between observed Sv and abundance of zooplankton is given by Equation 1.

$$S_{vobs} = \overline{TS} + 10\log_{10}(n_i) \quad [1]$$

Where Sv_{obs} is the mean volume backscatter in dB re 1 m^{-1}, *TS* is the mean target strength of the dominant scatterer in dB re 1 m^2 and *n* is the number of scatterers in the i^{th} sample (MacLennan *et al.* 2002). Thus doubling the abundance of zooplankton would lead to an increase of 3dB in Sv_{obs}. A stepwise linear regression against 10log abundance was performed to identify the most important ESR class for each frequency. A regression was performed against the dominant size classes (Fig. 3.46). The stepwise linear regressions indicate that there is a statistical relationship between the DIPS samples and the measured values of Sv ($p<0.05$) at all frequencies apart from 265 kHz. As has been shown before (Pieper and Holliday, 1984; Holliday and Pieper, 1995) there is a stronger correlation between larger copepods (ESR $\geq$ 0.4 mm) and higher frequencies than at lower frequencies.

The slope values for the regressions clearly indicate the presence of a low signal to noise ratio. This can be demonstrated by adding a noise term to Equation 1.

$$Sv_{pred} = 10\log_{10}\left(10^{(\overline{TS} + 10\log_{10}(n_i))/10} + 10^{\overline{NL}/10}\right) \quad [2]$$

Where *NL* is the mean noise level in dB re 1 m^{-1}. The noise level can be estimated from samples containing low abundances. Figure 3.46 shows TAPS measured Sv plotted against predicted Sv from Equation 2 for abundance values in the 0.4 mm ESR bin, the middle line indicating the regression function and the outer lines one standard deviation in the noise level. A target strength of –82 dB re 1 m^2 was assumed and estimates of noise level and noise standard deviation were made from data collected from low abundance samples. The value of R^2 has fallen from 0.73 to 0.68 but the slope is now much closer to the expected value of unity. This clearly shows that our ability to predict concentrations of zooplankton is limited by system noise, both the absolute noise level and its standard deviation.

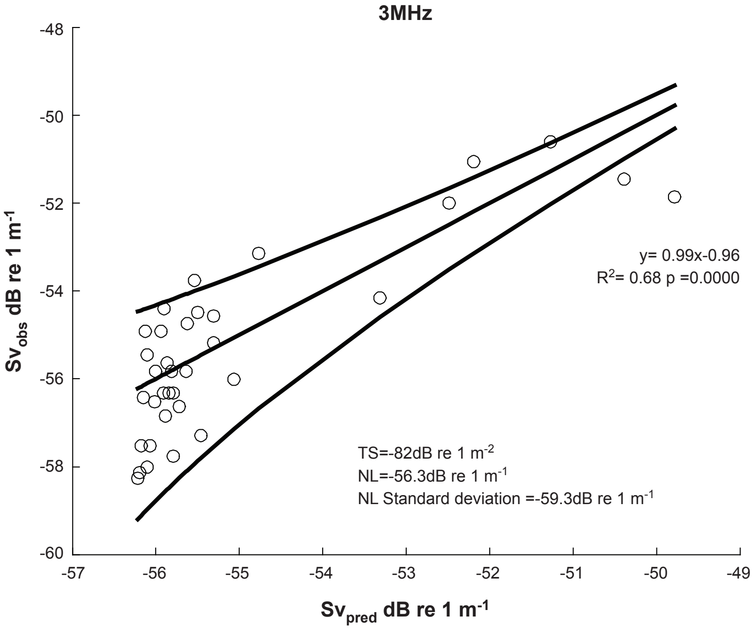

Figure 3.47: TAPS measured Sv_{obs} at 3 MHz vs Predicted Sv_{pred} including noise with an estimated target strength TS of -82 dB re 1 m^{-2}. The outer lines denote 1 standard deviation from the mean noise level.

Another key aspect of TAPS is the small sampling volume. The volume was chosen to exclude larger, less abundant creatures from the sample. We must be aware of the effects this can have when operating in a low abundance environment. It has been shown that reverberation from multiple scatterers is quite different to those from a single scatterer (Stanton, 1985). When a large number of randomly located scatterers are ensonified the resultant echo is dependent on the integral of the acoustic beam pattern, whereas with a single scatterer the result is a function of the beam pattern. Hence when the number of scatterers in the sample volume is large their position in the acoustic beam pattern can be ignored, but when numbers of scatterers approach one, their position in the beam becomes important. To get overlapping echoes there must be more than one scatterer in a given pulse resolution volume. The critical number of scatterers needed per m^3 assuming a random distribution can be calculated by dividing 1 by the sample volume in m^3. Typical values of critical density for TAPS ranges from 217 to 811 individuals per m^3 depending on range bin and frequency. Many of our samples approached or were within the range of that critical density.

Figure 3.48 highlights the effects of critical densities by comparing two samples taken from voyage SS200401. Sample 1 was taken during the day at a depth of 29 m in 40 m of water, 27 km off shore at station B. The highest abundance of zooplankton (6246 m^{-3}) during the voyage was recorded in this sample. Sample 2 was taken at night at a depth of 27 m in 1000 m of water, 85 km off shore at station E. A much lower total abundance (523 m^{-3}) was recorded in Sample 2, but with a higher concentration of larger zooplankton. A clear difference can be seen between the PDFs from the two samples. The high abundance Sample 1 is normally distributed in the log domain. Sample 2 shows two peaks which are probably related to two different scattering groups. As expected from a normal distribution, the mean and median of the acoustic Sample 1 are similar, unlike Sample 2. It was found that the median value of Sv correlated much better with the abundance of zooplankton in the DIPS samples than did the mean value. This is probably due to the median excluding less abundant larger scatterers. Identifying these distinct PDFs can improve our ability to predict plankton abundance from acoustic backscattering.

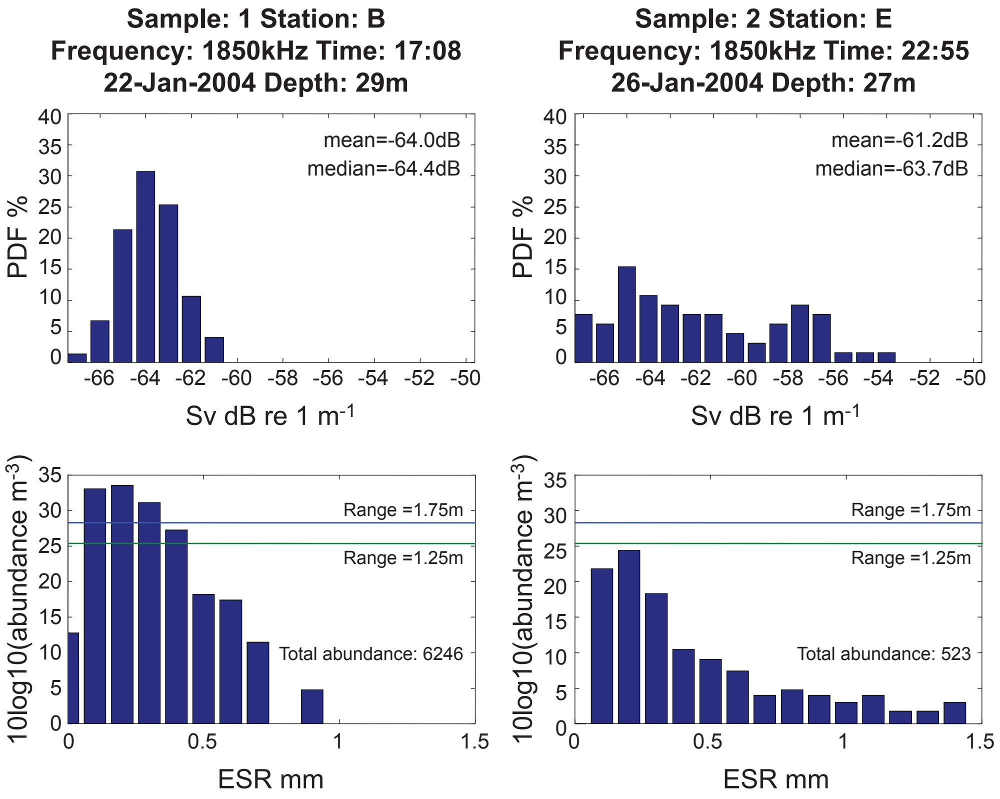

Figure 3.48: Comparison of the PDF from high and low abundance samples showing a) PDF of volume reverberation (Sv dB re m^{-1}) and b) The measured equivalent spherical radius (ESR) of the biota vs the 10*log10(abundance m^{-3}) . Lines indicate the critical number of scatters.

These results indicate that TAPS is limited by system noise but is still able to detect zooplankton in this region of low plankton abundance. Ideally a signal-to-noise ratio of 9-12 dB is required for reliable sampling of zooplankton populations (Greenlaw, 1983).

Derivations of Sv rely on two main assumptions: scatterers are randomly distributed in the sample volume; and the number of scatterers is statistically large. As a rule this can be taken to be 5-30 scatterers and with averaging 20 pings then the 95% confidence interval should be approximately ±2 dB (Greenlaw, 1983). The signal returned from the biota needs to be above the noise limit for all frequencies for inverse methods to work optimally. At typical density levels experienced along the Two Rocks transect the plankton density within the 3 L sample volume ranges from 0.4 to 18 plankton per sample volume.

Discussion

TAPS' utility could be greatly improved by increasing the signal-to-noise ratio. This could be done in a number of ways: increase the source level or the pulse length or reduce system noise. Perhaps the simplest of these methods would be to increase the pulse length. Doubling the pulse length would increase the signal-to-noise ratio by 3dB. TAPS currently uses a pulse length of 336 μs giving a sample interval of approximately 0.255 m in range. There are limits to the amount the pulse length can be increased. As pulse length increases range resolution decreases. Also the distance to the nearest sample range must be increased to avoid interference from the transducer ringing at the end of the pulse cycle. Increasing the pulse length will also decrease the number of statistically independent samples taken each ping, resulting in the need to increase the ping rate to compensate. Absorption at these high frequencies will also limit the maximum pulse length. The derivation of Sv assumes that absorption within the pulse length is negligible. At high frequencies such as 3 MHz absorption can be over 2.4 dB m^{-1} effectively limiting the pulse length to less than a meter. Signal-to-noise ratio could be improved using an FM slide (chirp) signal (Ehrenberg and Torkelson, 2000). Another way to tackle this problem is through noise reduction (Korneliussen, 2000) which could be achieved by monitoring distant range bins, and assuming that their return represents the noise level for that particular ping.

The detection of single targets versus multiple scatterers could be greatly improved by reducing the pre-averaging that TAPS performs and sampling the echo envelope at a higher frequency. Working with raw un-averaged data would be a distinct advantage. We hope to implement some of these strategies in the next round of field work to significantly improve our detection limits.

Summary and conclusion

Some major advances have been made in this project to understand the spatial and temporal dynamics of marine biota from zooplankton to micronecton using acoustics. Our studies have highlighted the limitations of existing equipment that is commonly used to study plankton at high frequencies. This advanced understanding is being fed back to equipment manufacturers to make instruments more suitable to the Western Australian environment. Our use of the low frequency instruments has highlighted the difficulties of using small vessels to collect high data quality at multiple frequencies at the same time of day.

The acoustic transect data in a qualitative sense provides a unique insight into the spatial structuring of marine biota that is impossible to obtain from coarsely-resolved sampling at fixed stations. In this way the acoustic data can assist in the extrapolation between sparse station sampling. Our use of multi-frequencies is in its infancy and we have demonstrated that by using simple scattering models we can segment the acoustic transect data into probable scattering groups. We see a clear path to improve the methods developed and applied so far in this project.

Improvements to existing use of acoustic data would probably require more emphasis on the partitioning into the various trophic groups with quantitative estimates of biomass, size and trophic spectra as well as integration with other environmental data. Ultimately, the objectives of data collection will determine the sampling protocols required and the best vessels (*e.g.*, industry, research, mooring, drifter or autonomous underwater vehicle (AUV)). The use of AUV's, gliders, moorings and ships of opportunity (e.g. ferries) can greatly increase the spatial and temporal coverage at potentially low data collection costs.

References

Abramoff, M. D., Magelhaes, P. J., and Ram, S. J. (2004). Image Processing with ImageJ. Biophotonics International 11, 36-42.

Alcaraz, M., Saiz, E., Calbet, A., Trepat, I., and Broglio, E. (2003). Estimating Zooplankton Biomass Through Image Analysis. Marine Biology 143, 307-315.

Alongi, D.M., McKinnon, A.D. (2005). The cycling and fate of terrestrially-derived sediments and nutrients in the coastal zone of the Great Barrier Reef shelf. *Mar. Poll. Bull*. 51, 239-252.

Arzayus, K.M., Canuel, E.A. (2004). Organic matter degradation in sediments of the York River estuary: Effects of biological vs. physical mixing. *Geochim. Cosmochim. Acta* 69, 455-463.

Babin, M., Stramski, D., Ferrari, G.M., Claustre, H., Bricaud, A., Obolensky, G. and Hoepffner, N. (2003). Variations in the light absorption coefficients of phytoplankton, nonalgal particles, and dissolved organic matter in coastal waters around Europe. *Journal of Geophysical Research*, 108, 3211-3230

Barlow, R., Stuart, V., Sessions, H., Sathyendranath, S., Lutz, V., Kyewalyanga, M., Clementson, L., Fukasawa, M., Watanabe, S., *in review*. Global pigment patterns in surface phytoplankton of the subtropical Southern Hemisphere. *Deep Sea Research I, in review*.

Berelson, W.M., Heggie, D., Longmore, A., Kilgore, T., Nicholson, G., and Skyring, G., (1998). Benthic nutrient recycling in Port Phillip bay, Australia. *Est. Coast. Shelf Sci*., 46, 917-934.

Boxshall, G.A and Halsey, S.H. (2004). An introduction to copepod diversity. The Ray Society, London.

Calbet, A. (2001). Annual zooplankton succession in coastal NW Mediterranean waters: the importance of the smaller size fractions.

Caputi, N., Chubb, C., Pearce, A. (2001). Environmental effects on recruitment of the western rock lobster, *Panulirus cygnus*. *Marine and Freshwater Research* 52: 1167-1174.

Clementson, L.A., Fearns, P.R.C.S., Majewski, L., Klonowski, W. and Harriden, T. (2004). Seasonal effects in the inherent optical properties of Western Australian coastal waters: impacts on the validation of ocean colour sensors in this region. Proceedings Ocean Optics XVII (CDROM).

Clementson, L. A., Parslow, J. S., Turnbull, A. R., McKenzie, D. C. and Rathbone, C. A. (2001). The optical properties of waters in the Australasian sector of the Southern Ocean. Journal of Geophysical Research, 106**,** 31611-31626.

Cook, P.L.M., Eyre, B.D., Leeming, R., and Butler, E.C.V. (2004a). Benthic fluxes of nitrogen in the tidal reaches of a turbid, high-nitrate sub-tropical river. *Est. Coast. Shelf Sci*., 59, 675-685.

Cook, P.L.M., Revill, A.T., Butler, E.C.V., Eyre, B.D. (2004b). Carbon and nitrogen cycling on intertidal mudflats of a temperate Australian estuary. II. Nitrogen cycling. *Mar. Ecol. Progr. Ser.,* 280, 39-54.

Cowan, J.L.W., Pennock, J.R., Boynton, W.R. (1996). Seasonal and interannual patterns of sediment-water nutrient and oxygen fluxes in Mobile Bay, Alabama (USA): regulating factors and ecological significance. *Mar. Ecol. Progr. Ser*., 141, 229-245.

Dam, H.G., Miller, C.A. and Jonasdottir, S.H. (1993). The trophic role of mesozooplankton at 47°N, 20°W during the North Atlantic Bloom Experiment. *Deep-Sea Research II*, 40, 197-212.

Dennison, W.C., Abal, E.G. (1999). The Moreton Bay Study: A Scientific Basis for the Healthy Waterways Campaign. South East Queensland Regional Water Quality Management Strategy, Brisbane, Queensland.

Douglas, D., Hamilton, D., Gerritse, R., Adeney, J., Coad, D. (1996). Sediment geochemistry, nutrient fluxes and water quality in the Swan River Estuary, Western Australia. In Davis, J.K. (ed), Outcomes from CSIRO's Multidivisional Blue-Green Algal Program. CSIRO Land and Water, Canberra.

Edwards, CA, Batchelder, HP and Powell, T.M. (2000). Modelling microzooplankton and macrozooplankton dynamics within a coastal upwelling system. *Journal of Plankton Research* 22, 1619-1648.

Ehrenberg, J.E. and Torkelson, T.C. (2000). Fm Slide (Chirp) Signals: a Technique for Significantly Improving the Signal-to-Noise Performance in Hydroacoustic Assessment Systems. *Fisheries Research* 47, 193-199.

Eslinger, D.L., O'Brien, J.J. and Iverson, R.L. (1989). Empirical orthogonal function analysis of cloud-containing Coastal Zone Color Scanner images of northeastern North American coastal waters. *Journal of Geophysical Research*, Vol. 94, No. C8. 10884-10890.

Eyre, B. D. and Ferguson, A. J. P. (2002). Comparison of carbon production and decomposition, benthic nutrient fluxes and denitrification in seagrass, phytoplankton, benthic microalgal and macroalgal dominated warm temperate Australian lagoons. *Mar. Ecol. Progr. Ser.*, 229, 43-59.

Fandry, C.B., Slawinski, D., Pender, L. (2006). Two-Rocks moorings data report. *CSIRO Marine and Atmospheric Research Paper* 005: 26pp.

Fanning, K.A., Carder, K.L., Betzer,, P.R. (1982). Sediment resuspension by coastal waters: a potential mechanism for nutrient re-cycling on the ocean's margins. *Deep-Sea Res.*, Part A 29, 953-965.

Fielding, S., Griffiths, G., and Roe, H. S. J. (2004). The Biological Validation of ADCP Acoustic Backscatter Through Direct Comparison With Net Samples and Model Predictions Based on Acoustic-Scattering Models. ICES Journal of Marine Science 61, 184-200.

Feng, M., Meyers, G., Pearce, A., Wijffels, S., (2003). Annual and interannual variations of the Leeuwin Current at 32°S. *Journal of Geophysical Research* 108(C11), 3355, doi:10.1029/2002JC001763.

Foote, K. G., Knudsen, H. P., Vestnes, G., MacLennan, D. N., and E.J. Simmonds (1987). Calibration of acoustic instruments for fish density estimation: a practical guide. ICES Cooperative Research Report.144 , 69.

Ferguson, A. J. P., Eyre, B. D., Gay, J. (2004). Benthic nutrient fluxes in euphotic sediments along shallow sub-tropical estuaries, northern NSW, Australia. *Aquat. Microb. Ecol.*, *37*, 219-235.

Forehead, H.I. (2006). The ecology and biogeochemistry of sandy sediments in the warm temperate coastal waters of Western Australia. PhD Thesis, University of Western Australia.

Fredericks, D.J., Heggie, D.T., Longmore, A., Palmer, D., Smith, C., Skyring, G.W.S. (1999). Nutrient recycling and benthic activity in a shallow coastal lagoon in Western Australia. AGSO Research Newsletter, No. 31.

Frost, B.W. (1972). Effects of size and concentration of food particles on the feeding behaviour of the marine planktonic copepod *Calanus pacificus*. *Limnology and Oceanography*, 17, 805-815.

Galienne, C.P. and Robins, D.B. (2001). Is Oithona the most important copepod in the world's oceans? *Journal of Plankton Research*, 23(12), 1421-1432.

Gasol, J.M. (1997). Biomass distribution in marine planktonic communities. *Marine Ecology Progress Series,* 42, 1353-1362.

Gaughan, D.J. and W.J. Fletcher, (1997). Effects of the Leeuwin Current on the distribution of carnivorous macrozooplankton in the shelf waters off southern western Australia. *Estuarine, Coastal and Shelf Science*, 45, 89-97.

Gaughan, D.J., Pearce, A.F. and P. Lewis. The Hillary's transect: influence on the dominant macrozooplankton and spawning of Sardinopsis sagax on the Continental Shelf off Perth, Western Australia. *Continental Shelf Research*. submitted.

Greene, C.H., Wiebe, P.H., Pershing, A.J., Gal, G., Popp, J.M., Copley, N.J., Austin, T.C., Bradley, A.M., Goldsborough, R.G., Dawson, J., Hendershott, R. and Kaartvedt, S. (1998). Assessing the Distribution and Abundance of Zooplankton: a Comparison of Acoustic and Net-Sampling Methods With D-Bad Mocness. *Deep Sea Research Part Ii: Topical Studies in Oceanography* 45, 1219-1237.

Greenlaw, C.F. (1983). Multiple-frequency Acoustical Estimation. *Biological Oceanography* 2, 3-4.

Hansen, J.A., Alongi, D.M., Moriarty, D.J.W., Pollard, P.C. (1987). The dynamics of benthic microbial communities at Davies Reef, Central GBR. *Coral Reefs*, 6, 63-70.

Hanson, C.E., Clementson, L.A., Koslow, J.A., *in prep*. Spatial and temporal dynamics in phytoplankton community composition off southwestern Australia.

Hanson, C.E., Waite, A.M., Thompson, P.A., Pattiaratchi, C.B., *in press*. Phytoplankton community structure and nitrogen nutrition in Leeuwin Current and coastal waters off the Gascoyne region of Western Australia. *Deep-Sea Research Part II*.

Harriden, T.D., Fearns, P.R.C.S. and Clementson, L.A. (2004). Remote sensing as a tool for marine managers. Proceedings Ocean Optics XVII (CDROM).

Havskum, H., Schluter, L., Scharek, R., Berdalet, E., Jacquet, S., (2004). Routine quantification of phytoplankton groups - microscopy or pigment analyses? *Marine Ecology Progress Series* 273**,** 31-42.

Helleren, S.K.R. and John, J., (1997). Phytoplankton and zooplankton dynamics in the southern metropolitan coastal waters, Perth. Technical Report Series: I Algal Research Group School of Environmental Biology, Curtin University.

Hill, V., Cota, G., Stockwell, D., (2005). Spring and summer phytoplankton communities in the Chukchi and Eastern Beaufort Seas. *Deep-Sea Research Part II-Topical Studies in Oceanography* 52 (24-26)**,** 3369-3385.

Holliday, D. V. (1992). Zooplankton acoustics. In 'Oceanography of the Indian Ocean'. pp. 733-40. (Oxford-IBH Publishing Co. Pvt. Ltd., New Delhi:

Holliday, D. V. and Pieper, R. E. (1995). Bioacoustical Oceanography at High Frequencies. ICES Journal of Marine Science 52, 279-296.

Irigoien, X., Meyer, B., Harris, R., Harbour, D., (2004). Using HPLC pigment analysis to investigate phytoplankton taxonomy: the importance of knowing your species. *Helgoland Marine Research* 58, 77-82.

Jeffrey, S. W. and Vesk, M. (1997). Introduction to marine phytoplankton and their pigment signatures, in Phytoplankton Pigments in Oceanography: guidelines to modern methods, edited by S.W. Jeffrey, R.F.C. Mantoura and S.W. Wright, pp. 37-84, UNESCO Publishing, Paris.

Jeffrey, S.W., Wright, S.W., (2006). Photosynthetic pigments in marine microalgae: insights from cultures and the sea. *In* Algal Cultures, Analogues of Blooms and Applications, Subba Rao, D.V., Ed., Science Publishers, pp. 33 - 90.

Keesing, JK and JN Heine (Eds.). Strategic Research Fund for the Marine Environment (SRFME): Interim Final Report, June 2005. CSIRO, 384 pp.

Kendrick, G.A., Langtry, S., Fitzpatrick, J., Griffiths, R., Jacoby, C.A., (1998). Benthic microalgae and nutrient dynamics in wave-disturbed environments in Marmion Lagoon, Western Australia, compared with less disturbed mesocosms. *J. Exp. Mar. Biol. Ecol*. 228, 83-105.

Kirk, J. T. O., (1983). Light and photosynthesis in aquatic ecosystems, 401 pp., Cambridge University Press, Cambridge.

Kirkman, H. (1981). The first year in the life history and the survival of the juvenile marine macrophyte, Ecklonia radiata (Turn.) J. Agardh*. J. Exp. Mar. Biol. Ecol*., 55, 243-254.

Kirkman, H., Kuo, J. (1990). Pattern and process in southern Western Australian seagrasses. *Aquat. Botany* 37, 367-382.

Klonowski, W.M., Majewski, L.J., Fearns, P.R.C.S., Clementson, L.A. and Lynch, M.J. (2004). Bottom type classification using hyperspectral imagery. Proceedings Ocean Optics XVII (CDROM).

Kloser, R. J. and Fulton, E. A. (2006). Model evaluation of acoustic monitoring requirements for the ecosystem approach to fisheries. ICES FAST working group presentation, March 2006, Hobart, Australia.

Kloser, R. J., Ryan, T., Sakov, P., Williams, A., and Koslow, J. A. (2002). Species Identification in Deep Water Using Multiple Acoustic Frequencies. Canadian Journal of Fisheries and Aquatic Sciences 59, 1065-1077.

Korneliussen, R.J. (2000). Measurement and Removal of Echo Integration Noise. *Ices Journal of Marine Science* 57, 1204-1217.

Korneliussen, R.J. and Ona, E. (2003). Synthetic Echograms Generated From the Relative Frequency Response. *Ices Journal of Marine Science* 60, 636-640.

Lennon, J.T., Pfaff, L.E. (2005). Source and supply of terrestrial organic matter affects aquatic microbial metabolism. *Aquat. Microbial. Ecol*. 39, 107-119.

Levitus, S., Boyer, T.P., (1994). World Ocean Atlas Volume 4: Temperature, NOAA Atlas NESDIS 4, U.S. Department of Commerce, Washington D. C., USA: 117pp.

Longmore, A.R., Abbott, B., Barry, J., Cowdell, R.A., Lourey, M., Nicholson, G. (1998). Effects of Water Quality on Black Bream Habitat in the Gippsland Lakes. First Report of the Fisheries Victoria Gippsland Black bream Habitat Assessment Program., MAFRI, Queenscliff, Victoria.

Lourey, M.J., Alongi, D.M., Ryan, D.A.J., Devlin, M.J. (2001). Variability of nutrient regeneration rates and nutrient concentrations in surface sediments of the Northern Great Barrier Reef shelf. *Cont. Shelf. Res.,* 21, 145-155.

Mackey, M.D., Mackey, D.J., Higgins, H.W., Wright, S.W., (1996). CHEMTAX - a program for estimating class abundances from chemical markers: application to HPLC measurements of phytoplankton. *Marine Ecology Progress Series* 144**,** 265-283.

Mackey, M.D. (1997). Chemtax user's manual: a program for estimating class abundances from chemical markers – application to HPLC measurements of phytoplankton pigments, CSIRO Marine Laboratories Report 229, Hobart, Australia, ISBN 0 643 06040 5, 47 p.

MacLennan, D.N., Fernandes, P.G. and Dalen, J. 2002. A consistent approach to definitions and symbols in fisheries acoustics. *ICES Journal of Marine Science*, 59: 365-369.

Majewski, L.J., Klonowski, W. M., Fearns, P.R.C.S., Clementson, L.A. and Lynch, M.J. (2004). Ocean colour product validation in Western Australian waters. Proceedings Ocean Optics XVII (CDROM).

McGehee, D.E, Demer, D.A., and Warren, J.D. (2004). Zooplankton in the Ligurian Sea: Part I. Characterization of their dispersion, relative abundance and environment during summer 1999. *Journal of Plankton Research* 26 (12):1409-1418. 0142-7873.

McKinnon, A. D. and Ayukai, T. (1996). Copepod egg production and food resources in Exmouth Gulf, Western Australia. *Marine and Freshwater Research* 47(4), 595-603.

McKinnon AD, Duggan S (2003). Summer copepod production in subtropical waters adjacent to Australia's North West Cape. *Marine Biology* 143:897-907

McKinnon AD, Duggan S (2001). Summer egg production rates of paracalinid copepods in subtropical waters adjacent to Australia's North West Cape. *Hydrobiologia* 1-12

Mitchell, B. G. (1990). Algorithms for determining the absorption coefficient for aquatic particulates using the quantitative filter technique. Ocean Optics X. **1302** , 137-148. The International Society for Optical Engineering.

Moore, T.S., Matear, R.J., Marra, J. and Clementson, L. (2006). Phytoplankton variability off the Western Australian Coast: Mesoscale eddies and their role in cross-shelf exchange, *Deep Sea Research*, submitted.

Morel, A. and Maritorena, S. (1977). Bio-optical properties of oceanic waters: A reappraisal. *Journal of Geophysical Research*, 106, 7163-7180.

Mueller, J.L., Fargion, G.S. and McClain, C.R. (eds.) (2003). Ocean Optics Protocols For Satellite Ocean Colour Sensor Validation, Revision 5, Volume V: Biogeochemical and bio-optical measurements and data analysis protocols, NASA, Maryland.

Murphy, L.S., Haugen, E.M., (1985). The distribution and abundance of phototrophic ultraplankton in the North Atlantic. *Limnology and Oceanography* 30**,** 47-58.

Olson, R.J., Vaulot, D., Chisholm, S.W., (1985). Marine phytoplankton distributions measured using shipboard flow-cytometry. *Deep Sea Research* 32**,** 1273-80.

Palacios, D.M., Bograd, S.J., Foley, D.G. and Schwing, F.B. (2006). Oceanographic characteristics of biological hot spots in the North Pacific: A remote sensing perspective. *Deep Sea Research II*. 250-269.

Parslow, J. and Rathbone, C. (1998). Temporal and spatial analysis of ocean chlorophyll distribution from the NASA CZCS monthly composites. Unpublished manuscript. 11pp.

Pearce, A.F., Helleren, S., Marinelli, M., (2000). Review of productivity levels of Western Australian coastal and estuarine waters for mariculture planning purposes. *Fish. Res. Rep. Fish. West. Aust.* No. 123.

Pearce, A.F., Lynch, M.J., Hanson, C.E. (re-submitted). The Hillarys Transect (1): seasonal and cross-shelf variability of physical and chemical water properties off Perth, Western Australia, 1996-98. Revised paper re-submitted to *Continental Shelf Research*.

Pearce, A.F., Phillips, B.F. (1988). ENSO events, the Leeuwin Current and larval recruitment of the Western Rock Lobster. *Journal du Conseil* 45: 13-21.

Pieper, R.E. and Holliday, D.V. (1984). Acoustic measurements of zooplankton distributions in the sea. *Journal du Conseil International pour l'Exploration de la Mer* 41, 226-238.

Precht, E., Franke, U., Polerecky, L., and Huettel, M. (2004). Oxygen dynamics in permeable sediments with wave-driven pore water exchange. *Limnol. Oceanogr*. 49, 693-705.

Redfield, A.C., Ketchum, B.H., Richards, F.A. (1963). The influence of organisms on the composition of seawater. In Hill, M.N. (ed), The Sea. Vol 2. Interscience, New York. pp. 26-77.

Ressler, P.H., Brodeur, R.D., Peterson, W.T., Pierce, S.D., Mitchell Vance, P., RřStad, A. and Barth, J.A. (2005). The Spatial Distribution of Euphausiid Aggregations in the Northern California Current During August 2000. *Deep-Sea Research Part Ii* 52 , 89-108.

Reynolds, R.W., Smith, T.M. (1994). Improved global sea surface temperature analyses using optimum interpolation. *Journal of Climate* 7: 929-948.

Rice, J. C., and Rochet, M. J., 2005. A framework for selecting a suite of indicators for fisheries management. ICES Journal of Marine Science, 62: 516-527.

Ryan, T. E. and Kloser, R. J. (2004). Quantification and correction of a systematic error in Simrad ES60 Echosounders. ICES FAST 2004 Gdansk, Poland Copy available from CSIRO Marine Research Library, Hobart, Australia. April 2004.

Rosich, R.S., Bastyan, G.R., Pailing, E.I., and van Senden, D.C. (1994). Sediment Nutrient Processes. Perth Coastal Waters Study, Project E3.4 Phase 2. Report No. SSB 15/94 Water Authority Perth Western Australia.

Schultes, S. (2004). The role of mesozooplankton grazing in the biogeochemical cycle of silicon and carbon in the southern Ocean. Dissertation, University of Bremen (Germany), 167 p.

Simon, N., Barlow, R.G., Marie, D., Partensky, F., Vaulot, D., (1994). Characterization of oceanic photosynthetic picoeukaryotes by flow cytometry. *Journal of Phycology* 30, 922-935.

Straile, D. (1997). Gross growth efficiencies of protozoan and metazoan zooplankton and their dependence on food concentration, predator-prey weight ratio, and taxonomic group. *Limnology and Oceanography*, 42, 1375-13185.

Stanton, T.K. (1985). Volume scattering:Echo peak PDF. *Journal of the Acoustical Society of America* 77, 1358-1366.

Stanton, T. K. and Chu, D. (2000). Review and Recommendations for the Modelling of Acoustic Scattering by Fluid-Like Elongated Zooplankton: Euphausiids and Copepods. ICES Journal of Marine Science 57, 793-807.

Strom, S.L. and Morello, T.A. (1988). Comparative growth rates and yields of ciliates and heterotrophic dinoflagellates. *Journal of Plankton Research*, 20, 571-584.

Sutor, M.M., Cowles, T.J., Peterson, W.T. and Pierce, S.D. (2005). Acoustic Observations of Finescale Zooplankton Distributions in the Oregon Upwelling Region. *Deep-Sea Research Part Ii* 52, 109-121.

Swartzman, G., Napp, J., Brodeur, R., Winter, A. and Ciannelli, L. (2002). Spatial Patterns of Pollock and Zooplankton Distribution in the Pribilof Islands, Alaska Nursery Area and Their Relationship to Pollock Recruitment. *Ices Journal of Marine Science* 59, 1167-1186.

Takashima, T., Rathbone, C. and Clementson, L. (2003). Atmospheric correction of SeaWiFS ocean colour data in the Southern hemisphere. Applied Mathematics and Computation, 141, 241-259.

Thompson, P., Waite, A., (2003). Phytoplankton responses to wastewater discharges at two sites in Western Australia. *Marine and Freshwater Research* 54, 721-735.

Tranter D.J. (1977). Further Studies of Plankton Ecosystems in the Eastern Indian Ocean. V. Ecology of the Copepoda. *Australian Journal of Marine and Freshwater Research* 28: 529-539.

Ullman, W.J., Sandstrom, M.W. (1987). Dissolved nutrient fluxes from the nearshore sediments of Bowling green Bay, Central BGBR Lagoon (Australia). *Est. Coast. Shelf Sci.*, 24, 289-303.

Utermohl, H., (1958). Zur Vervollkommnung der quantitativen Phytoplankton-Methodik. Mitt. int. Ver. theor. agnew. Limnol. 9, 1-38.

van Keulen, M., Borowitzka, M.A. (2003). Seasonal variability in sediment distribution along an exposure gradient in a seagrass meadow in Shoalwater Bay, Western Australia. *Est. Coast. Shelf Sci.,* 57, 587-592.

Wanstrand, I., Snoeijs, P., (2006). Phytoplankton community dynamics assessed by ships-of-opportunity sampling in the northern Baltic Sea: A comparison of HPLC pigment analysis and cell counts. *Estuarine Coastal and Shelf Science* 66 (1-2), 135-146.

Warren, J.D., Demer, D.A., McGehee, D.E., Di Mento, R. and Borsani, J.F. (2004). Zooplankton in the Ligurian Sea: Part II. Exploration of their physical and biological forcing functions during summer 2000. *Journal of Plankton Research* 26 (12):1419-1427. 0142-7873.

Webb, A.P., Eyre, B.D. (2004). Effect of natural populations of burrowing thalassinidean shrimp on sediment irrigation, benthic metabolism, nutrient fluxes and denitrification. *Mar. Ecol. Progr. Ser.* 268, 205-220.

Wenzhofer, F., Glud, R.N. (2004). Small-scale and temporal variability in coastal benthic O2 dynamics: Effects of faunal activity. *Limnol. Oceanogr.* 49, 1471-1481.

Witte, U. (2000). Vertical distribution of macrofauna within the sediment at four sites with contrasting food supply in the deep Arabian Sea. *Deep-Sea Res II,* 47, 2785-2804.

Willen, E., (1976). A simplified method of phytoplankton counting. 11 (265-278).

Zaker, N.H., Imberger, J., Pattiaratchi, C.B. (submitted). Dynamics of the coastal boundary layer off Perth, Western Australia. Submitted to *Continental Shelf Research*.

Zeitzschel, B. (1973). *The Biology of the Indian Ocean*. Springer-Verlag, New York, 1973

CHAPTER 4

4. COASTAL AND SHELF BIOGEOCHEMISTRY AND MODELLING

Contributing Investigators

Tony Koslow (Project Leader), Jim Greenwood, Martin Lourey, Uwe Rosebrock,
Karen Wild-Allen, Nugzar Margvelashvili

CSIRO Marine and Atmospheric Research

Stephane Pesant

The University of Western Australia

Outline

Executive Summary

The previous chapter examined the spatial structure and seasonal cycle of physical and chemical processes and the phytoplankton and zooplankton assemblages within the water column from the nearshore lagoon across the shelf and Leeuwin Current. The present chapter describes the plankton production cycle and the physical and chemical processes driving it, based upon a review and synthesis of regional nutrient data, the field study conducted from 2002 – 04 along the Two Rocks transect (see Chapter 3), and a range of modeling studies.

Several key questions are posed by the phytoplankton dynamics in this region:

- What is the relative influence across the shelf of offshore drivers, such as the Leeuwin Current, and nearshore influences, such as runoff and groundwater?
- How does the influence of the Leeuwin Current — the most energetic eastern boundary current, as well as one of the only ones that induces downwelling — manifest itself on the seasonal production cycle?
- Does the production cycle follow the spring bloom pattern observed in many temperate systems, as predicted by Longhurst (1995), or the winter bloom observed in many oligotrophic sub-tropical systems — or something else altogether?

Seasonal climatologies were generated from historical hydrographic data contained within the CSIRO Atlas of Regional Seas to identify spatial and seasonal characteristics of the nutrient environment on the southwestern Australian shelf. The surface waters of the shelf, the Leeuwin Current and offshore are all low in nitrogen (less than 0.5 μM) year round, suggesting that primary productivity is nitrogen limited. The shelf waters contain some dissolved phosphate, at relatively low levels (up to 0.25 μM), but diatom production may be as well limited by low levels of silicic acid (silicate). The Leeuwin Current is largely devoid of phosphate but contains

reasonably high levels of silicate (up to 4 μM) and may be a silicate source to surrounding waters. A cross-shelf gradient in chlorophyll *a* biomass suggests that terrestrial nutrient sources, or benthic regeneration and winter mixing processes, make an important contribution to primary productivity. Offshore, a winter increase in chlorophyll *a* biomass coincides with the deepening of the mixed layer and is presumably supported by mixing of nutrients or chlorophyll from their deep maxima into the euphotic zone.

The three-year field study along the Two Rocks transect indicated that the southwest region experiences an interesting variant on the typical sub-tropical production pattern. Primary productivity and concentrations of chlorophyll were particularly low in summer, when the water column was stratified, and most chlorophyll was concentrated in a layer above the nutricline at approximately 100 m depth. The phytoplankton bloomed in late autumn and winter, coinciding with the period of strongest Leeuwin flow. The bloom in winter was maintained by cooling and storms, which promoted convective mixing of the upper water column and a shoaling of the nutricline and chlorophyll maximum layer. However the late-autumn bloom coincided with the initial intensification of the Leeuwin Current. Eddies and meanders spin up just beyond the shelf break, and Leeuwin Current water was observed at this time to destratify the water column and flood the shelf with relatively nutrient-rich water. Several potential sources of these nutrients are proposed: advection of nutrient from the north, where the nutricline is shallower, the spinup of nutrients by the eddies along the shelf-break and subsequent 'pumping' across the shelf, and/or convective mixing. Eddy pumping of nutrients across the continental shelf has been observed in several regions of strong eddy activity, including off the southeastern USA, Brazil, and along the eastern Bering Slope, where there is another poleward-flowing eastern boundary current.

One-dimensional biogeochemical modelling of the water column indicated that the summertime deep chlorophyll maximum is a relatively stable feature that results from strong stratification of the upper water column during that season and a balance between vertical supply of deep water nutrients and sinking.

The simple one-dimensional model was unable, however, to simulate the rapid deepening of the mixed layer during autumn and the consequent bloom, indicating that the bloom is likely a result of non-local physical forcing. High rates of vertical mixing may partially account for the observed enhanced production and elevated surface chlorophyll often observed at this time. The influence of non-local nutrient supply (for example, by lateral advection) remains unclear and requires further investigation.

Three-dimensional numerical modelling highlighted the important role of mesoscale eddies in mixing deep nutrient into near-surface waters and the subsequent exchange of waters between the shelf and offshore.

A three-dimensional coupled physical-biogeochemical model was implemented for the region from Shark Bay to Cape Leeuwin. The seasonal evolution of the Leeuwin Current and eddy field is reproduced by the model; however, certain key features of the regional biogeochemistry are not yet adequately simulated, such as the high chlorophyll *a* concentrations adjacent to the coast and the development of a deep chlorophyll maximum layer in summer. The model will require improved representation of the vertical structure, and tighter constraint on the nutrient supply along the model boundaries and adjacent to the coast. Full calibration of the model against observations will allow the along-shore and cross-shelf supply of nutrients to coastal waters to be quantified.

4.1 Regional Nutrient Dynamics

Martin Lourey CSIRO Marine and Atmospheric Research

Introduction

The coastal waters off southwestern Australia are unique compared to the west coasts of other southern hemisphere continents. The Leeuwin Current (Cresswell and Golding, 1980; Chapter 2) transports nutrient poor water from the tropics southward along the coast suppressing the large-scale upwelling of cool, nutrient-rich deep water observed on the west coast of Africa and South America (Pearce, 1991). As a result, dissolved nutrient levels in the coastal waters are generally low (Johannes *et al.*1994) and pelagic primary productivity in southwestern Australia is lower than the western margins of the other southern hemisphere continents (Pearce, 1991). However, in somewhat of a dichotomy this shelf supports abundant seagrass beds (Kirkman and Kuo, 1990) and macroalgal communities (Kirkman, 1981; Chapter 5). The sources of nutrients that support this abundant benthic primary productivity are presently unclear as is the possible response of these communities to changes in anthropogenic nutrient loadings. Nutrient poor environments such as those influenced primarily by the Leeuwin Current, may be particularly susceptible to environmental nutrient increases.

The nearshore environment off southwestern Australia is subject to a range of terrestrial anthropogenic nutrient stressors derived from agricultural, industrial and urban land use. Sources of anthropogenic nutrients are mixed and include, direct waste water discharge (Thompson and Waite, 2003), contaminated ground water (Johannes, 1980), riverine discharge (Black *et al.*1981) and run off from agricultural drains and canals (McMahon and Walker, 1998). Increased nutrient loadings have the capacity to considerably influence shelf primary production and drive eutrophication in some systems. Unfortunately, investigations on the impacts of poor water quality on the Western Australian coastal environment are rare. Increased nutrient loadings stimulating enhanced epiphyte growth may have contributed to a large scale reduction in the extent of seagrass beds in Cockburn Sound (Cambridge *et al.*1986) and variations in phytoplankton community structure have been identified around metropolitan waste water discharges (Thompson and Waite, 2003). The circulation, mixing and stratification of the water column have been identified as important factors controlling the exposure of such communities to elevated nutrient concentrations during periods of enrichment (Thompson and Waite, 2003).

Management of marine resources requires that we first understand the natural distribution and sources of nutrients that presently sustain primary producers and distinguish these from the effects of anthropogenic sources. To achieve this we first review the current understanding of nutrient distribution and sources for the WA shelf. Second we examine how sediment chemistry and characteristics influences the way nutrients are recycled and released across the sediment water interface.

Objectives

The objectives of the SRFME study section are to:

- Describe the present understanding of the nutrient sources and sinks on the WA shelf to identify gaps that need filling and take the first step towards generating a nutrient budget.
- Describe broad scale temporal and seasonal variations in surface water nutrient concentrations compiled from a historical database of oceanographic measurements (the CSIRO Atlas of regional Seas).
- Measure seasonal and regional variations in the rates of sediment nutrient regeneration.

Preliminary nutrient budget and conceptual model of sources and sinks on the WA shelf

In order to quantitatively assess the impact of anthropogenic increases in nutrient supply to the shelf, we first need to understand the natural nutrient sources and sinks, particularly over large spatial (regional) and long temporal (seasonal) scales. Presently, our basic understanding of (and capacity to model) these processes in South Western Australian coastal waters is limited. As a first step, we have reviewed what is known about the regional shelf nutrient budget and identified key gaps in our knowledge. A conceptual model of the nutrient sources and sinks on the shelf is shown in Figure 4.1. We derive an annual flux rate for each of the sources and sinks. The budgets described here focus on the area between Yanchep and Mandurah (Fig. 4.2), where the source and sink terms are best known (Lord and Hillman 1995). It is also the region of major interest to the SRFME program.

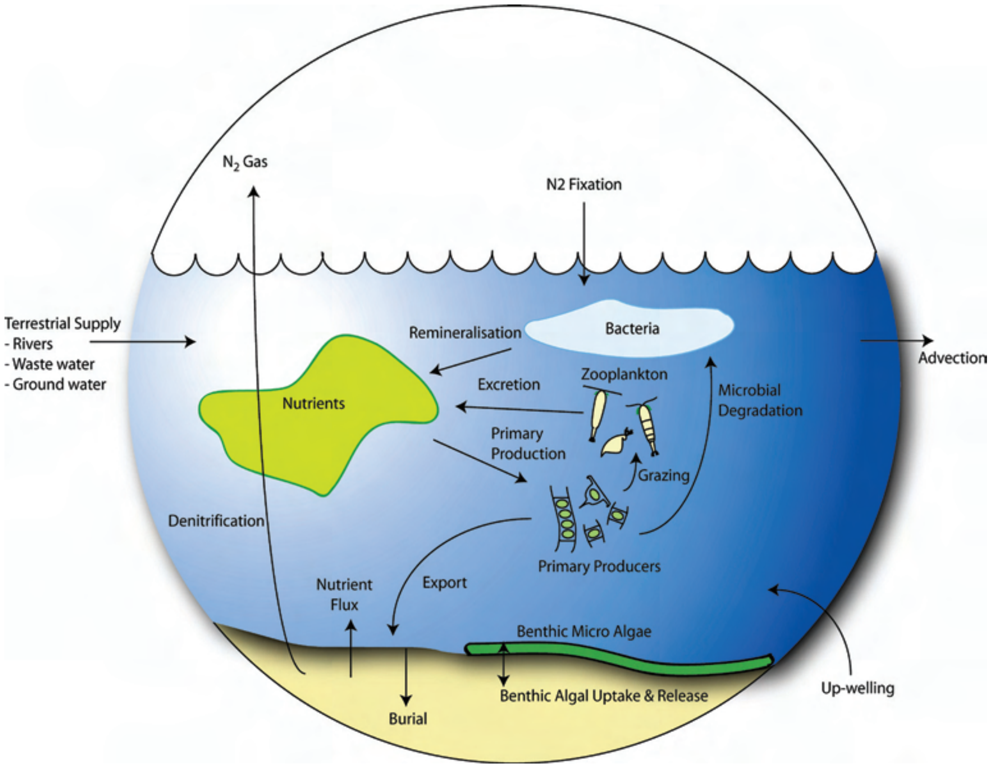

Figure 4.1: Schematic describing the major sources, sinks and cycling processes for the nutrient budget.

Nutrient Sources

Wastewater

Waste water discharged to the shelf in the Perth metropolitan region carries with it considerable nitrogen and phosphorous (Lord and Hillman, 1995; Thompson and Waite 2003) and is likely to be an important nutrient source on a regional basis. There are three major sewage outfalls in the Perth region: the Cape Peron outfall (4300m offshore in 20m of water), the Swanbourne outlet (1100m offshore, 10m depth) and the Beenyup outfalls (1600 and 1800m offshore at a depth of 10m) (Fig. 4.2), with discharges in 1993 of 85.0, 50.3, and 65.9 million litres day^{-1} respectively (Buckee *et al.*1994). Since then, due to population increases, discharge volumes have increased to 110, 55 and 100 million litres day^{-1} from these outfalls (Anon, 2003a). However, upgraded treatment facilities at the Woodman Point plant have resulted in a decrease in the nutrient loads discharged from the Cape Peron outfall from around 2400 tonnes of nitrogen year^{-1} in 2001 to 821 tonnes of nitrogen year^{-1} in 2003 (Anon, 2003b). In 2003, discharge of nitrogen to the marine environment from the Beenyup and Swanbourne outfalls was roughly 1000 and 550 tonnes of nitrogen year^{-1}, respectively (Anon 2003a), for a total of 2,371 tonnes of nitrogen yr^{-1}.

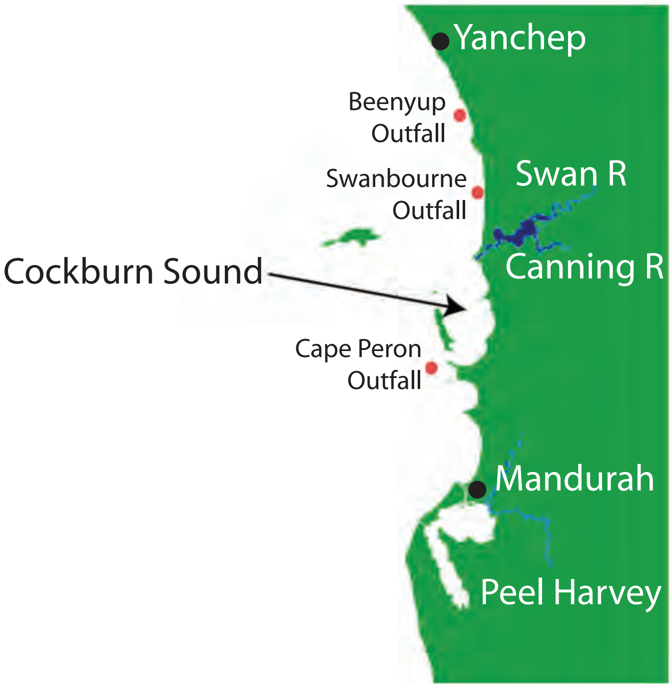

Figure 4.2: Map of the Perth metropolitan area with the location of the major sewage outfalls and river systems plotted.

High concentrations of nitrogen in the waste water generates extremely high nutrient concentrations immediately around the discharge points. At that time of the Perth Costal Waters Study, nitrate concentrations as high as 80 µg l^{-1} and ammonium concentrations reaching 47 µg l^{-1} were measured adjacent to the sewage outfalls (Buckee *et al.*1994). The Perth Coastal Waters Study aimed to determine the flushing and dilution about the outfalls and surveys close to the sewage outlets in the Perth region suggest that the nutrient signal was diluted and mixed away within around 4 km of the point of discharge (Buckee *et al.*1994; Lord and Hillman, 1995).

Rivers

Riverine discharge is a potentially important source of nutrients and carbon to shelf systems. There are only two major river systems located between Yanchep and Mandurah, the Swan – Canning and the Peel – Harvey (Figure 4.2). Short term studies on the Peel Inlet Estuary suggest that riverine nutrient supply to the shelf is seasonal and highest during periods of increased river flow (Black *et al.*1981). However, in southwestern Australia, rainfall and runoff are low and the contribution of rivers to nutrient supply is probably low compared to other regions (Johannes *et al.*1994). There are few published reports regarding the magnitude or seasonality of this type of nutrient supply to the shelf. Riverine discharge (Yanchep to Mandurah) was estimated to contribute 1,270 tonnes of nitrogen into Perth coastal waters during 1990 (Table 4.1, Lord and Hillman, 1995). A similar estimate (1300 tonnes of nitrogen and 160 tonnes of phosphorus) was made during the Southern Metropolitan Coastal Waters Study (Anon, 1996). This study partitioned estimates of nitrogen (and phosphorus) discharge at between 250 (30) and 900 (100) tonnes for the Swan – Canning Estuary and between 450 (60) and 900 (120) tones for the Peel - Harvey (Anon, 1996). It also suggests that blooms of nitrogen fixers in the Peel Harvey estuary had the potential to add a further 500 tonnes of nitrogen to the coastal system annually (Anon 1996). However, the long-term effect of the Dawesville channel on bloom and nutrient discharge dynamics was not well known at the time, and an updated estimate for this estuary is warranted. The Moore River is also a source of nutrients but is located well to the north of our Yanchep boundary (Figure 4.2).

In addition to major rivers, small creeks and drains can discharge considerable amounts of nutrients. A study investigating the supply of nutrients to support seagrass communities in Geographe Bay found that drains and small streams in the region supply 255 tonnes of nitrogen (total nitrogen) and 34 tonnes of phosphorus (total phosphorus) to the system each year (McMahon and Walker 1998). It is likely that similar drain systems also discharge nutrients in the Yanchep – Mandurah region although, given the more urban nature of the catchment, streams and drains are probably less important here than Geographe Bay. These estimates are likely to represent upper bounds for nutrients from this source.

Stormwater

The Perth Coastal Waters Study suggested 32 tonnes of nitrogen were discharged via surface drainage in the Yanchep – Mandurah region, which is unimportant compared with other nutrient sources.

Ground water

Groundwater discharge from aquifers with an outlet to the ocean is potentially a considerable source of nutrients to the shelf. Dated measurements in our region suggest nitrate levels in submarine groundwater discharge are at least 2 – 6 μM (Johannes, 1980) and that submarine ground water discharge contributes around 370 tonnes of nitrate to the coastal zone between the Moore River in the north and the Swan River in the South (around 80 km of coastline) each year. For the Perth region this may be a conservative estimate, firstly because of the uncertainties in the original calculation (see Johannes, 1980) and secondly because anthropogenic nutrient sources may have increased the ground water loading relative to the Johannes (1980) study. The estimate is, however, comparable to the 1990 estimate derived by the Perth Coastal Waters Study of 445 tonnes yr^{-1}.

Industry

Industrial discharge has the potential to contribute significantly to coastal nutrient budgets. This has been of particular concern in the heavily industrialized Cockburn Sound. Evidence of poor water quality and, particularly, seagrass stress has focused considerable attention on reducing anthropogenic nutrient loads to the Sound, from about 2000 tonnes yr^{-1} in 1978 to around 300 tonnes yr^{-1} in 2000 (Lord, 2001). Most of the remaining discharge is attributed to contaminated groundwater (Lord, 2001). Total nitrogen discharge into the Sound from licensed discharges is around 55 tonnes yr^{-1} (Lord, 2001). After dilution and uptake within the Sound, industrial nutrient export into the surrounding coastal waters is probably low.

Upwelling

The winds in the southwest are favorable for upwelling throughout the year, particularly during the summer when they are at their strongest (Fig. 4.3). Similar wind fields on the western margins of South America and Africa promote significant upwelling. The southwest of Western Australia is unique in that the southwards progression of the Leeuwin Current blocks this large scale upwelling. As a result, deep casts close to the shelf edge reveal higher nutrient concentrations in deep waters but the surface waters at the shelf break are nutrient depleted (Fig. 4.4). Despite this, upwelling and entrainment of deep water onto the shelf may still contribute nutrients to the system on a regional basis. Localized upwelling of cold deep water in the Capes region has been associated with the Capes Current (Gersbach *et al.*1999) and may transport some nutrients onto the shelf (Hanson *et al.*2005). Similarly, deep ocean upwelling has been proposed as a potential source of nitrogen to the Ningaloo region (Hanson, 2004) and the North-West Shelf (Holloway *et al.*1985).

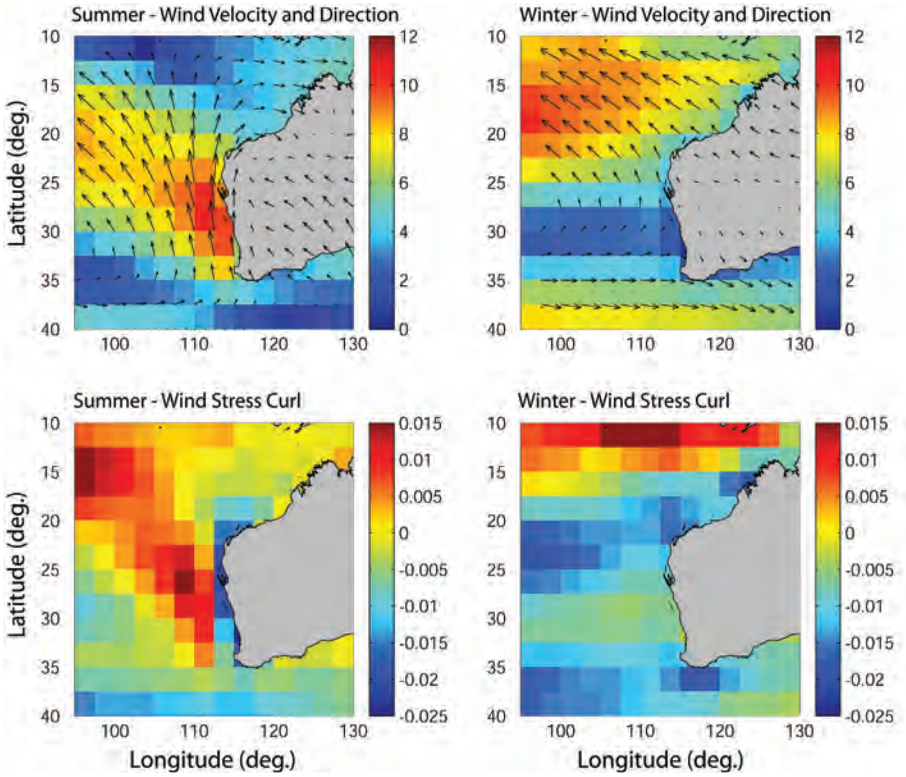

Figure 4.3: Summer and winter NCEP monthly averaged wind velocity (m s^{-1}) with direction vectors and the wind stress curl (N m^{-3}). Negative wind stress curl values highlight regions where winds favour upwelling.

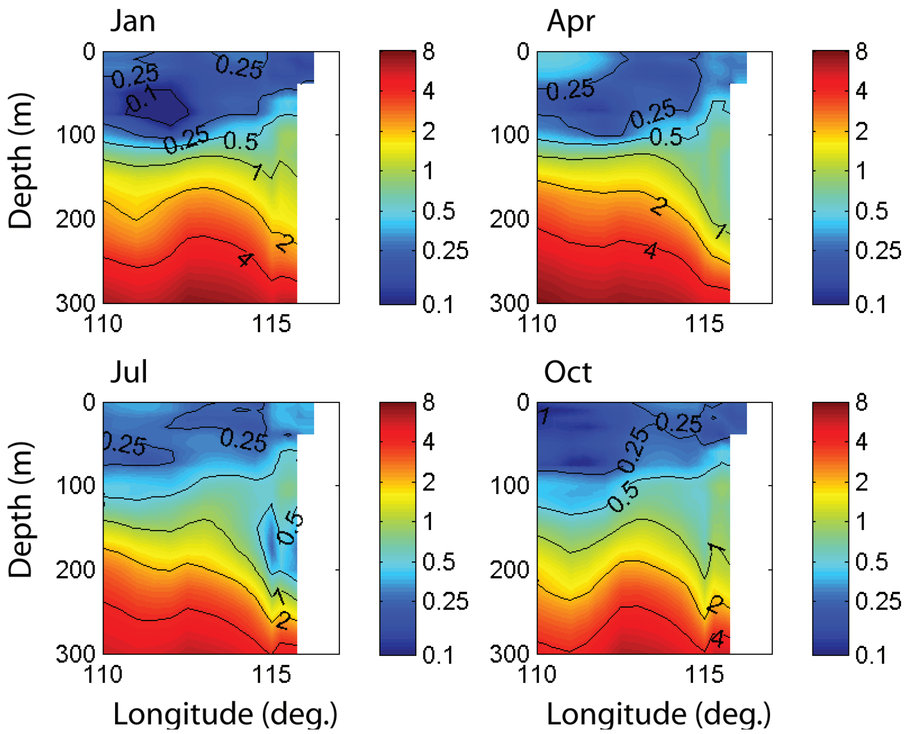

Figure 4.4: Cross shelf climatological nitrate (µM) section.

Eddies appear to play an important role in supplying nutrients to the shelf by promoting localised upwelling. In late autumn of 2003, the influence of an eddy located off shore of the SRFME transect appeared to weaken mixed layer stratification, resulting in localised upwelling of nutrient rich water onto the shelf. While this upwelling was only observed once on the

SRFME transect in 3 years of monthly sampling, suggesting that the process is temporally variable and of localised influence, it may still represent a significant nutrient source that warrants further investigation.

There is a seasonal deepening of the mixed layer in the climatology between summer (~30 m deep in December – February) and winter (75 to 100 m deep in June – September) (Fig. 4.5), a trend also reflected in the field data from the SRFME transect. At around 100m, the bottom of the deeper winter mixed layer approaches the depth of the nitricline (Fig. 4.4). This deepening of the mixed layer may mix nutrients (Fig. 4.4) up into the euphotic zone. However, the importance of this mixing is uncertain: the mixed layer is ill-defined and at its deepest appears to only approach the nitricline at its shallowest point and not mix below it.

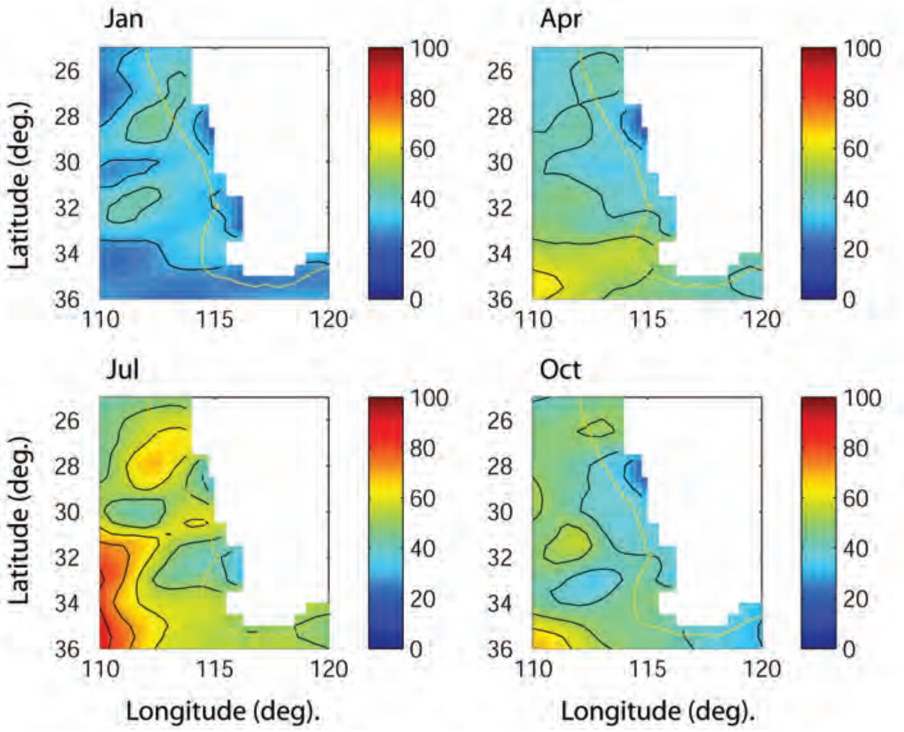

Figure 4.5: Monthly average mixed layer depth estimates. Here the mixed layer depth is defined as the minimum depth at which abs(T - T(10m)) > 0.4ºC or abs(S -S(10m)) > 0.03 (see Condie and Dunn, submitted). The yellow line marks the shelf break.

Atmospheric

Nitrogen fixation can make a significant contribution to the marine nitrogen cycle (Capone, 2001). The contribution of nitrogen fixation as a nitrogen source to the region is unclear. Cell counts & HPLC pigment analyses conducted during the SRFME program indicate that cyanobacteria are often significant components of the pelagic phytoplankton community, particularly from the shelf break and in the Leeuwin (and probably offshore). However, the first nitrogen fixation measurements made in these locations found that rates of pelagic nitrogen fixation are low (around 0.03 nmol l^{-1} h^{-1}), and sufficient to supply only a fraction of the nitrogen required to fuel observed rates of photosynthesis (Twomey *et al.*in press; Holl *et al.*in press). This disparity between the community composition and the field measurements may arise because nitrogen fixation is temporally and spatially patchy. Further nitrogen fixation measurements, supported by concurrent estimates of cyanobacterial biomass, will help determine whether the cyanobacterial communities observed during the SRFME program are important nitrogen fixers.

Nutrient Sinks

We know relatively little about the sink terms in the conceptual model relative to the more easily quantified source components. There are a number of sink terms that need to be quantified in order to achieve mass balance for a nutrient budget.

Carbon Export and Burial

We have not considered internal rates of production and remineralisation here because we assume these processes balance over seasonal timescales. However, this assumption requires testing as it is likely the process is not completely efficient. Some of the fixed carbon and nutrient remain in forms that are recalcitrant to remineralisation. Carbon and nutrients that are buried deep in the sediments are partitioned from diffusive and mechanical resupply processes. Carbon burial rates for the WA shelf have not been determined, although on the Great Barrier Reef loss due to this term is low, less than 1% (Brunskill *et al.* 2002). Wrack, detached seagrasses and macro algae deposited on the shore may be present there for extended periods and in some cases removed for aesthetic purposes. The deposition, break down and long-term accumulation of wrack is not well studied. Degradation is probably controlled by biotic factors such as microbial and grazing activity. This is an obvious gap in our understanding of coastal carbon and nutrient dynamics, and warrants further study.

Advection

While the deep ocean may be a substantial source of nutrients to the shelf there is also the potential for exchange between shelf and offshore waters to strip productive waters off the shelf. Elevated nutrient concentrations (up to 3.1 μM) measured in the Capes Leeuwin – Naturaliste region of the Leeuwin Current during winter are thought to result from entrainment of shelf water (Hanson *et al.* 2005).

Atmospheric

During the denitrification process nitrate is consumed and converted to N_2 gas which is lost to the atmosphere, making it a potentially important nitrogen sink. In some systems with high endogenous nutrient loads, efficient denitrification removes sufficient nitrogen to limit algal growth (Berelson *et al.*1998). Denitrification remains poorly studied in oceanic waters off WA and on the shelf, but is low in sediments of Cockburn Sound (Forehead PhD, see Vol. 1, sec. 2.2.12) and is unlikely to be important on the rest of the shelf.

Data quality

Sources of nutrients are best known for the Perth metropolitan area as most investigations have focused on urban land use pressures (particularly waste water discharge). The fact that good nutrient source estimates have been confined to the relatively unique (i.e. in terms of urban and industrial development) Perth region limits our ability to apply the loads implied here to other regions of the shelf, such as the other areas of interest to the SRFME project (Geographe Bay and Jurien Bay). In particular, the city of Perth is adjacent the Swan-Canning River system which has had significant nutrient-related water-quality problems in recent years Industrial activity is concentrated in this area, particularly around Cockburn Sound, and large amounts of treated sewerage are discharged to the coastal ocean. In regions without these urban pressures, different nutrient sources may be more relevant. Presumably, large scale waste water discharge and urban/industrial runoff will be unimportant in rural areas. In any case, in terms of nutrient stress, the area of shelf immediately adjacent to the coastline is most likely to be affected by anthropogenic nutrient inputs. That is the reason that most data have been compiled there.

In general, sufficient effort has been put towards quantifying nutrient sources to compile a preliminary nitrogen budget (Table 4.1) for inputs to the Perth region. However, many of the estimates were derived during the Perth Coastal Waters Study (Lord and Hillman 1995) and Southern Metropolitan Coastal Waters Study (Anon, 1996) and are somewhat dated. Point sources such as waste water discharge are routinely monitored and the data publicly available. These estimates take into account recent improvements to the sewage treatment process.

However, diffuse sources, such as for groundwater discharge, are more difficult to monitor. Estuarine nutrient loads may be better estimated from available data collected at upstream gauging stations. Improved sampling strategies and modelling approaches may yield superior nutrient load data in the near future (Degens and Donohue 2002).

Table 4.1. Magnitude of nitrogen sources (tonnes per year) to the WA shelf.

Source	PCWS	Updated	Notes
Waste water	2974	2370	Advanced treatment
Rivers	1270	1300	
Groundwater	445		
Creeks and Drains		225	PCWS not considered
Stormwater	32		
Deep ocean/upwelling	52000	??	

Summary

The conceptual model approach for compiling a nutrient budget is limited by a poor understanding of some of the seasonal flux terms (particularly sinks), large uncertainty due to poor temporal and spatial data coverage and the age of some of the data in light of recent land use changes. The annual discharge of nitrogen to the shelf can be best estimated, while nitrogen sinks remain largely unstudied. The efficiency and seasonality of production and recycling in the major organic matter pools will also contribute to our understanding of the persistence of nutrients in the environment. Advances in hydrodynamic and biogeochemical modelling will be essential for generating broad-scale seasonal supply and loss terms from the scant data available, particularly for quantifying the importance of cross-shelf supply and the role of localized up welling associated with eddy activity. Investigations that aim to improve our estimates of benthic primary productivity and cross shelf exchange will greatly improve our understanding of nutrient cycling, and ultimately yield a more quantitative nutrient budget.

Broad scale temporal and seasonal variations in surface water nutrient concentrations and phytoplankton biomass

Historical data sets can help generate broad-scale seasonal estimates for a number of parameters related to nutrient and production cycling. While this approach averages out the more dynamic features of the region (such as mesoscale eddies and meanders in fronts), these data represent broad averages over time and space and are particularly useful for isolating persistent seasonal and spatial patterns. Here we use a large scale database, the CSIRO Atlas of Regional Seas (hereinafter referred to as CARS), to construct monthly climatologies of nutrient concentration, and other oceanographic parameters (salinity, temperature, and mixed layer depth) for the Western Australian Shelf and Leeuwin Current waters. This provides an overview of the large-scale features of the regional dynamics, which complements the intensive field studies carried out during SRFME.

Methods

Data and climatology analyses

The region under consideration here is the section of the Western Australian Shelf extending from Shark Bay (25ºS) in the north to immediately south of Cape Leeuwin (36ºS) and out from the coast to 110ºE (Fig. 4.6). The section includes the coastal shelf, the continental shelf break, the offshore area occupied by the Leeuwin Current, and the waters of the eastern Indian Ocean (Feng *et al*. 2003). The CARS data set has been specifically developed for application to our region and includes data from the 1998 NODC World Ocean Atlas as well as the CSIRO archive of Australian hydrographic data. Data included in the atlas were collected between 1950 and 2001. The treatment of data and quality control procedures included in the CARS data set has been described elsewhere (Dunn and Ridgway, 2002; Ridgway *et al.*2002). Data from the CARS atlas has been used to generate the monthly sea surface height climatology. The mixed layer depth is defined as the minimum depth at which

$$|T - T(10m)| > 0.4^{\circ}C \quad \text{or} \quad |S - S(10m)| > 0.03$$

(Condie and Dunn, submitted). Most of the fields presented here focus on the near-surface (10m) depth interval rather than the surface value so that transient effects such as diurnal warming or local rain are unlikely to influence the calculations. Variability of the historical cast data in the CARS database away from the seasonal climatology estimates are presented in terms of the root-mean square (RMS) residuals.

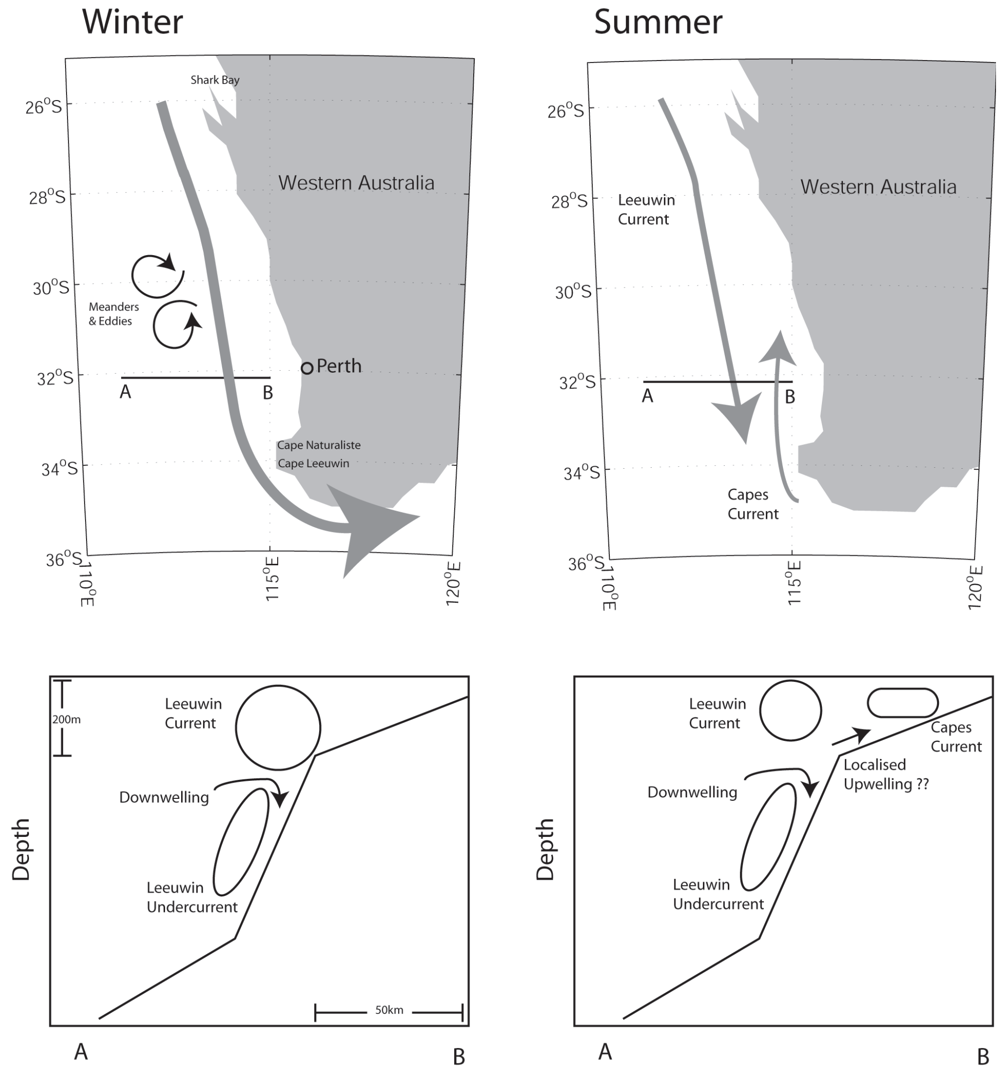

Figure 4.6: A schematic of the main circulation features off the coast of southwestern Australia during the austral winter (left) and summer (right). In the top panels, the large arrows represent the approximate path and the relative velocity of the Leeuwin and Capes Currents. The Leeuwin Current is at its strongest during the winter (left) (Feng *et al.*2003), while during the summer (right) a weak counter current (the Capes Current) flows from south to north on the inner continental shelf (Pearce and Pattiaratchi, 1999). Mesoscale meanders and eddies emanating from the Leeuwin Current are common along its entire length (Pearce and Griffiths, 1991). The lower panel represents a section across the shelf along the transect marked A to B in the upper panel. In winter (left), the strong Leeuwin current located at the shelf break blocks upwelling and net transport is downwelling. During the summer (right) the Leeuwin Current is weaker and located further offshore. A feature of the summer shelf not identified during winter is the Capes Current (Pearce and Pattiaratchi, 1999). Although net transport is still downwelling some localized upwelling may occur in the "Capes" region (Gersbach *et al.*1999).

The estimates of chlorophyll *a* concentration presented here are simple monthly averages compiled from 6 years of monthly global 9-km SeaWIFS ocean-colour products mapped onto a 0.1° grid (September 1997 – August 2004).

Climatology description

Mixed layer characteristics

The mixed layer depth climatology suggests a seasonal deepening in winter (Fig. 4.7). In summer (December – February) the mixed layer is shallow (~30 m) and relatively uniform spatially, but in the winter (June – September) there are sections on the shelf and offshore that are considerably deeper (75 to 100 m) (Fig. 4.7). There is considerable spatial variation during winter within the Leeuwin Current, for example, from 40 m at 25 ºS to 70 m at 27 ºS in July (Fig. 4.7). While it is possible that such spatial variations are realistic, two artefacts may also contribute. Firstly, the bottom of mixed layer may be difficult to define if the distinction between the surface and deep water masses is not sharp.

Secondly, where there are large inter-annual variations, or where the data are spatially patchy and temporally variable, some uncertainty can result from interpolation errors. For these reasons, we are cautious with our interpretation of some of the spatial variations in the mixed layer data presented here. We do note, though, that we are most interested in the well-sampled Leeuwin Current and shelf areas where interpolation errors are likely to be low.

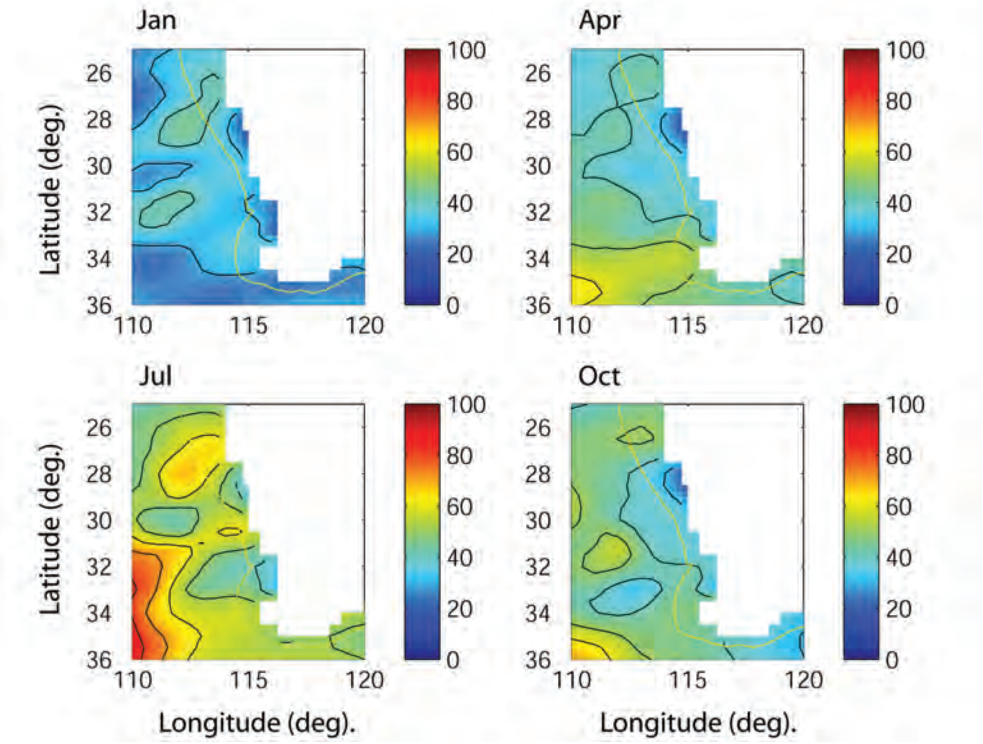

Figure 4.7: Monthly average mixed layer depth estimates from the CARS mixed layer depth atlas. Here the mixed layer depth is defined as the minimum depth at which |T - T(10m)| > 0.4ºC or |S -S(10m)| > 0.03 (see Condie and Dunn, submitted). The yellow line marks the shelf break.

Nutrient distribution

Productivity in the surface waters of the southwestern Australian shelf, Leeuwin Current and offshore region appears to be severely nitrogen limited. All the surface waters under study here are low in dissolved nitrate (<0.5 μM) throughout the year (Fig. 4.8). These low nitrate concentrations extend throughout the mixed layer down to around 100m at 31.5 ºS (Fig. 7.27). Deeper still (~300 m), nutrient concentrations are over 5 μM (Fig. 4.9) and may be a potential nutrient source to the surface waters. The seasonal progressions extracted from the climatology sections suggest that the seasonal variation in nitrate concentration is small, around 0.2 - 0.3 μM (Fig. 4.10) with the average ranging between 0.2 μM in February and 0.5 μM in June (Fig. 4.11). However, the variance in the nutrient observations about the mean is not negligible compared to the spatial and seasonal variations (Figs. 4.9 and 4.10). Although the nutrient climatologies average a very large number of observations to derive the seasonal signal, giving a better chance at isolating that signal from this substantial background variability, we must nonetheless be cautious in the interpretation of the seasonal progression of these highly variable parameters as they clearly fluctuate widely both spatially and temporally. The highest near surface concentrations of nitrate in our domain (around 0.8 μM) are in the absolute south (Fig. 4.8) and presumably represent the absolute northern extent of the Subtropical Front and the influence of the high nutrient, iron limited Subantarctic waters (Lourey and Trull, 2001). We would not normally expect the influence of the Subtropical Front to be captured in our domain as it generally lies further to south at ~40ºS (Belkin and Gordon 1996) but actual data points here are scarce, and this uncertainty in the location of the Subtropical Front arises from interpolation between distant data points.

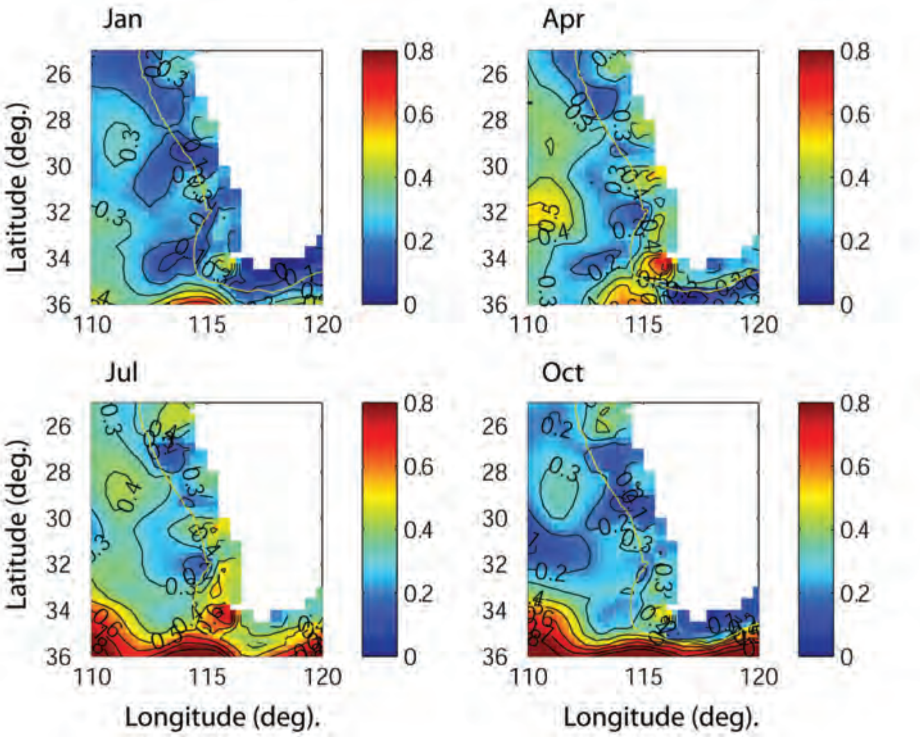

Figure 4.8: Monthly average distribution of nitrate (μM) at 10 m derived from the CARS climatology. The yellow line marks the shelf break.

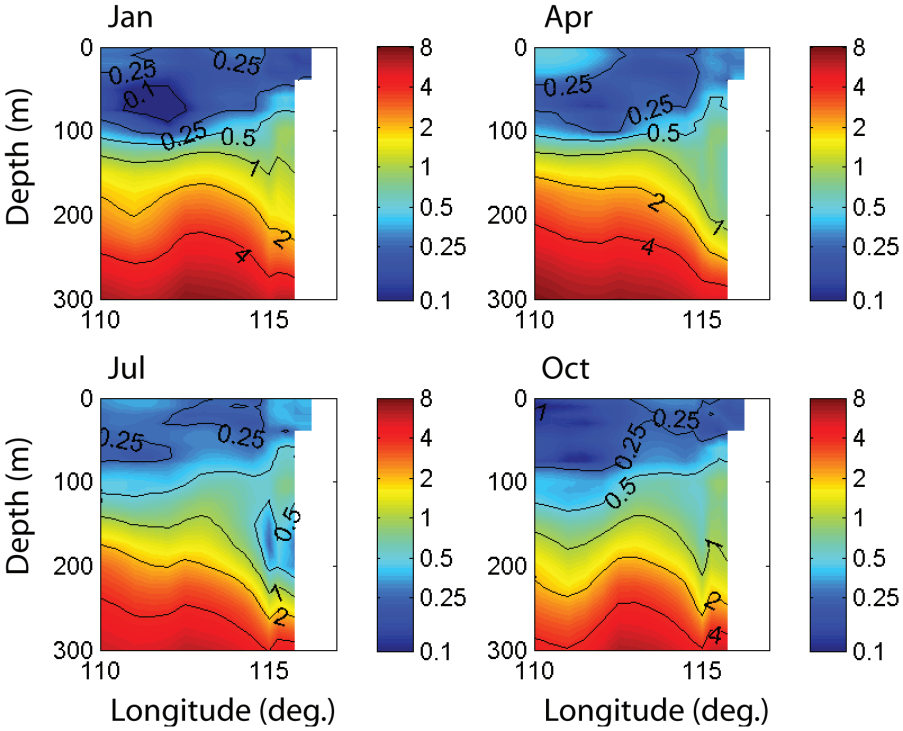

Figure 4.9: Cross shelf nitrate (μM) section (i.e., the A to B transect shown in Fig. 4.6) compiled from the CARS climatology. Higher concentrations of nutrients in deep waters compared to those at the surface were also a feature of the phosphate and silicate sections (not shown).

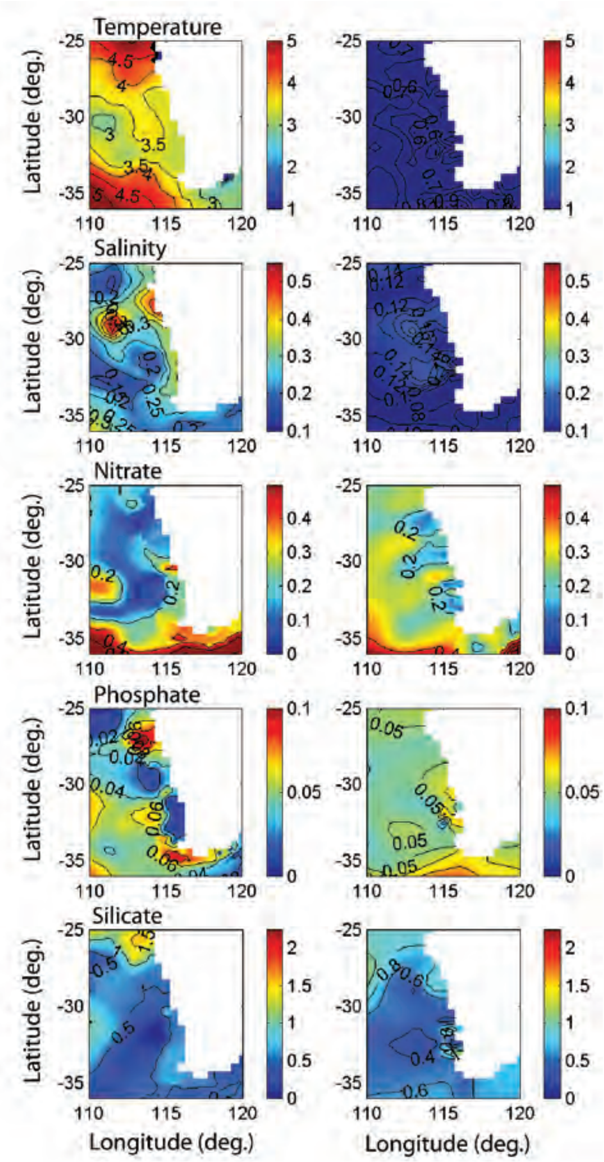

Figure 4.10: Magnitude of the seasonal variation in temperature, salinity, nitrate, phosphate and silicate at 10m in the Leeuwin Current and Perth Coastal waters derived from the CARS climatology (left). Included are the RMS residuals for each parameter (right).

Phosphate concentration inshore on the shelf (up to 0.25 μM) is higher (typically double) than in the Leeuwin Current and the waters further offshore (Fig. 4.11). The northern Leeuwin Current waters are lowest in phosphate concentration (<0.1 μM) but gradually increase as it makes its way south (Fig. 4.11) possibly due to mixing with the deeper waters at its base or water on the shelf. The low phosphate condition of the Leeuwin Current extends furthest to the south during the winter when transport is at its greatest (Fig. 4.11). On the shelf there are patches of elevated dissolved phosphate concentration during winter (Figs. 4.10 and 4.11), presumably accumulating because it is not limiting at any point during the year. As such, the shelf may be a source of phosphate to the Leeuwin Current as it travels southward, particular during its winter maximum.

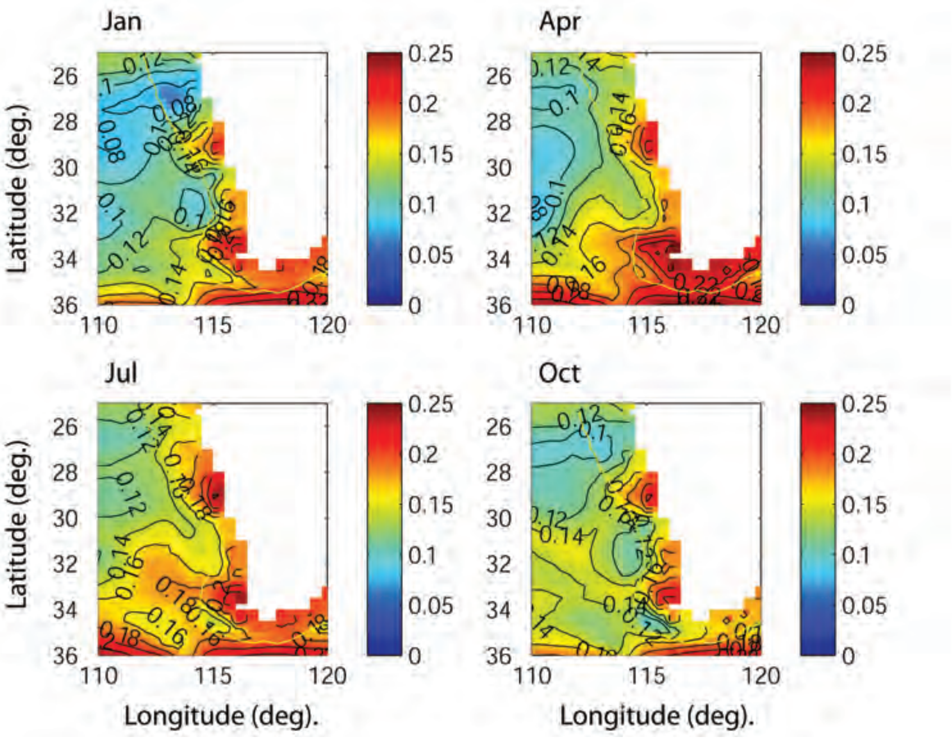

Figure 4.11: Monthly average distribution of phosphate (μM) at 10 m derived from the CARS climatology. The yellow line marks the shelf break.

Surface waters of most of the southern Western Australian shelf and offshore of the Leeuwin Current are generally low (<2 μM) in silicate while Leeuwin Current has slightly higher (~3-4 μM) levels of silicate (Fig. 4.12). The highest silicate concentrations (up to 4 μM) are in the very north of our domain, the source waters of the Leeuwin Current (Fig. 4.12). Moving south, these levels reduce rapidly (Fig. 4.12), probably due to a combination of the horizontal or vertical mixing already mentioned and utilization in the comparatively lower silicate region. Silicate concentration within the surface waters of the Leeuwin Current is highest in the winter, when the transport by the Leeuwin Current is at its strongest (Fig. 4.12). In the summer months, silicate concentrations in the Leeuwin Current are lower and close to those of the surrounding shelf and offshore waters (Fig. 4.12).

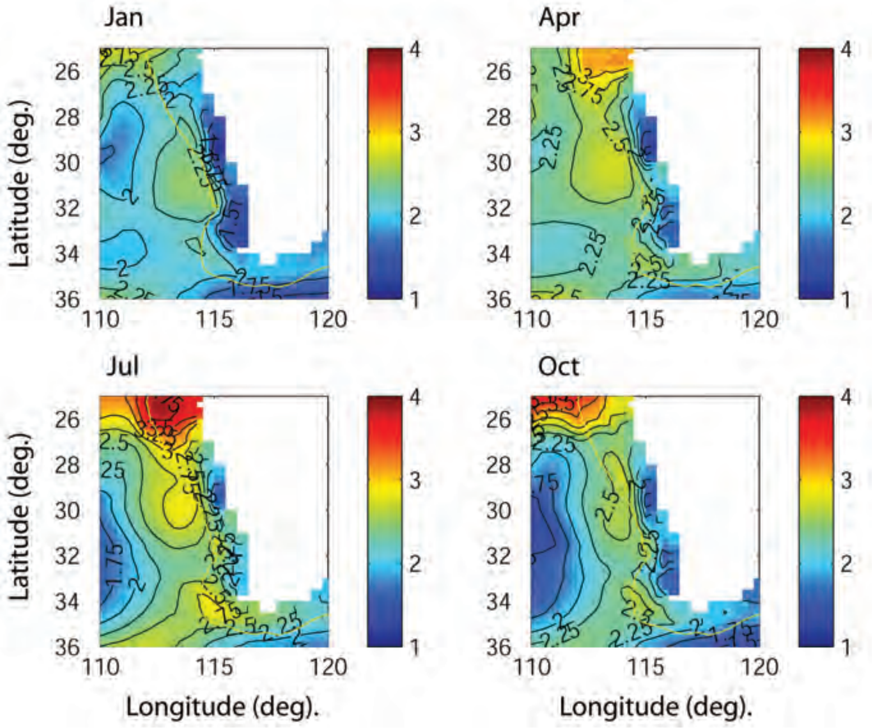

Figure 4.12: Monthly average distribution of silicate (μM) at 10 m derived from the CARS climatology. The yellow line marks the shelf break.

Chlorophyll *a* and biomass

Chlorophyll *a* concentration was highest, up to around 1 mg m^{-3}, inshore immediately adjacent to the coast (Fig. 4.13). On the outer shelf, chlorophyll *a* concentrations are lower than inshore (0.5 mg m^{-3}), but still elevated compared to the body of the Leeuwin Current and waters further offshore (0 – 0.25 mg m^{-3}) (Fig. 4.13). Seasonally, chlorophyll *a* concentrations inshore, on the shelf and offshore were higher in the winter than in the summer (Fig. 4.13). The summer to winter chlorophyll *a* increase is around 0.25 mg m^{-3} (from 0 – 0.25 mg m^{-3}) in the Leeuwin Current and offshore (Fig. 4.13). Inshore, the increase may be larger, possibly up to 0.75 mg m^{-3} (from 0.25 – 1 mg m^{-3}), between summer and winter (Fig. 4.13).

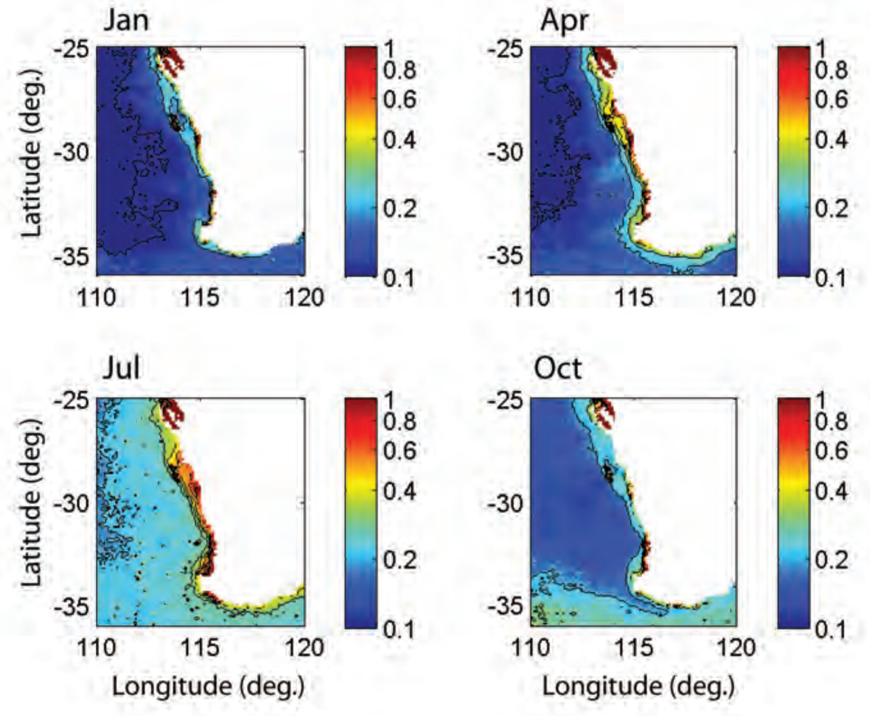

Figure 4.13: Monthly average distribution of chlorophyll *a* (mg m^{-3}) derived from six years of 9-km SeaWIFS data (September 1997 – August 2004).

Discussion

Variability, uncertainty and limitations of the approach

Combining a large number of historical data points in climatologies captures the long-term spatial mean and seasonal signal. However, the sections are smoothed temporally and spatially, so much of the short term and small scale variability inherent in the system may not be apparent, and it is important to include some estimate of this variation about the mean seasonal signal. To get a better understanding of the variability in the data about our calculated means we compare the RMS residuals with the seasonal and spatial variations given by the climatology. Residual fields are presented for all parameters (Fig. 4.10), but for brevity, we will focus on temperature (many underlying data points) and nitrate (typical of the nutrient fields with fewer underlying data points) residuals.

The most accurate representations (smallest residuals) are obtained for parameters that are not subject to small scale spatial and temporal disturbance relative to the temporal and spatial mean. Temperature residuals are small (up to around 1.0 ºC) compared to the magnitude of the seasonal variation (up to 5 ºC) (Fig. 4.10), suggesting the climatological fields are well matched by variations in the underlying data (Fig. 4.10). The close correlation of the temperature climatology with the observations demonstrates that the annual cycle is predictable both spatially and through the season.

On the other hand, the nutrient observations are highly variable compared to the CARS seasonal mean. Nitrate residuals were similar to the magnitude of the seasonal cycle, although for the Leeuwin Current and shelf waters the magnitude of the seasonal cycle is not large (Fig. 4.10). While this variance in the nutrient observations about the mean is not negligible compared to the spatial and seasonal variations, it is representative of the natural variability within the system. Large spatial and temporal variations in nutrient concentration are characteristic of this environment (Pearce *et al.*1985) and occur in response to the large range of factors that supply and remove nutrients. It is important to be aware of this substantial variability about the mean when considering the seasonal and spatial patterns identified by the climatology, particularly for the highly variable parameters.

In this region a chlorophyll maximum is generally present in deep water at the base of the euphotic zone and in close proximity to the nitracline (Hanson, 2004). Presumably this deep chlorophyll maximum delineates between abundant deep water nutrients and the onset of light limitation to the phytoplankton (Hanson, 2004). The deep chlorophyll maximum can represent a significant proportion of the depth integrated productivity in oligotrophic regions (Hanson, 2004). Unfortunately, the SeaWIFS sensor does not penetrate to the base of the euphotic zone, and therefore the analysis presented here does not capture the seasonal and spatial variations in this deep water feature.

Nutrient dynamics

The surface waters of the southwestern Australian shelf, Leeuwin Current and offshore region are all low in nitrate throughout the year (Fig. 4.8). This low new nitrogen condition, combined with a low N to P ratio (<4 compared to the ~16 required by phytoplankton (Redfield *et al*.. 1963)), suggests that all the near surface waters considered here are primarily nitrogen limited.

The shelf

By contrast with the low nitrate concentrations throughout our domain, phosphate concentrations on the shelf are higher than in the Leeuwin Current and offshore (Fig. 4.11). The major source of phosphorus to the inner shelf is probably terrestrial, delivered via rivers and drains, or possibly in ground water. The cross-shelf phosphorus gradient is consistent with a terrestrial nutrient source (Fig. 4.11) and there is a small (but variable) seasonal increase (up to 0.1 μM) in phosphate on the shelf during winter (Fig. 4.11), the period of highest rainfall and discharge. The seasonal increase in phosphate off the western margin of the Leeuwin Current may be driven by a reduction in mixed layer stratification in winter (promoting exchange between surface and deep waters, see next section) or seasonal variations in surface supply associated with the wintertime increase in the strength of the Leeuwin Current.

There is a small seasonal nitrate increase, around 0.3 μM (Fig. 4.10) but the observed seasonal increase in the limiting nutrient species does not necessarily reflect variations in supply to the shelf. A proportion, and possibly most, of the new nitrate and phosphate supplied during winter will be rapidly consumed by autotrophs. There is evidence for such a scenario in the surface SeaWIFS sections, where chlorophyll *a* concentrations are highest adjacent to terrestrial sources, and there is a considerable seasonal increase inshore during the winter (Fig. 4.13), when we would expect terrestrial supply to be at its highest.

Silicate is low year round (Fig. 4.12) on the shelf and may constrain diatom production in those waters. An increased dominance of diatoms at sites close to high silicate wastewater discharge in the Perth region tends to support the hypothesis that shelf diatom communities are co-limited (along with nitrate) by silicate (Thompson and Waite, 2003).

The Leeuwin Current

Although the general equatorward wind stress in the region is favorable for upwelling, it is counteracted by an alongshore steric height gradient driven by geostrophic transport from the Indonesian Throughflow which generates and drives the Leeuwin Current into the wind (Godfrey and Ridgway 1985). For the purposes of this discussion on nutrient dynamics, this downwelling circulation is of most significance as this limits the supply of nutrients to the surface waters. Consistent with this downwelling view and the tropical origins of its source waters, surface nitrate and phosphate concentrations in the Leeuwin Current are very low, <0.4 μM (Fig. 4.8) and <0.1 μM (Fig. 4.11) respectively.

By contrast, silicate is higher in the Leeuwin Current (3-4 μM) than surrounding shelf and open ocean (generally <2 μM) waters (Fig. 4.12) and the Leeuwin Current may be a source of silicate to these silicate-poor regions. Whether the Leeuwin Current is a source of silicate to the silicate-deficient shelf and open-ocean surface waters will be dictated by the magnitude of lateral exchange between the Leeuwin Current and these waters. Although the gradual decrease in silicate concentration (Fig. 4.12) as the Leeuwin Current travels south may be attributed to uptake, a similar increase in salinity (Fig. 4.8) suggests that there is exchange between the Leeuwin Current and gyre/shelf waters.

The high silicate concentration in the Leeuwin Current waters relative to those on the shelf may relate to differences in silicate supply, but may also be due to differences in uptake between the two water masses. Preliminary estimates suggest that there are considerable differences in the phytoplankton community structure between the Leeuwin Current and the shelf, with diatom communities rarer in the high silicate Leeuwin Current waters (Hanson, 2004). Although direct silicate uptake kinetics has not been studied, the difference in the importance of diatoms between the two water bodies may indicate that silicate uptake is lower in the Leeuwin Current.

It has been proposed that advection of water upwelled in the north of our domain by the Leeuwin Current may supply sufficient nutrients to the shelf to explain the seasonal increase in biomass (Moore, 2005). However, our sections suggest that nutrient concentrations in the Leeuwin Current are not high (silicate notwithstanding) compared to those on the shelf (see also Pearce *et al.*1985). As such, exchange between the waters of the Leeuwin Current and the shelf will most likely strip nutrients off the shelf. Localized high nutrient concentrations have been observed in the Leeuwin Current waters during winter in the Capes region (Hanson, 2004). This enrichment was attributed to entrainment of shelf waters into the Leeuwin Current (Hanson, 2004). A seasonal increase in mixed layer depth has been observed (Fig. 4.7) and is possibly a more likely source of nutrients to drive the seasonal variation in biomass (see section below).

Biomass

Chlorophyll *a* concentration is highest, up to around 1 mg m^{-3}, inshore immediately adjacent to the coast, and decreases with distance offshore (Fig. 4.13). This gradient is most likely sustained by terrestrial nutrient sources (but possibly resuspension and resupply from the sediments). Seasonally, the SeaWIFS sections presented here indicate considerable accumulation of biomass above summertime levels between May and August (Fig. 4.13). As this strong seasonal biomass accumulation occurs on the shelf, in the Leeuwin Current and offshore, it is not explained by variations in terrestrial supply. Both the SRFME field program and our climatology introduce variations in mixed layer depth as a possible driver for the summer – winter increase in biomass. The climatology suggests a seasonal deepening between summer (in December – February the mixed layer is ~30 m) and winter (in June – September there are areas on the shelf and offshore that are considerably deeper at 75 to 100 m) (Fig. 4.7). At around 100m, the bottom of the deeper winter mixed layer approaches the depth of the nitricline (Fig. 4.9). The SRFME field program also observed a seasonal weakening of mixed layer stratification during the winter. This deepening of the mixed layer into this region could have promoted chlorophyll *a* accumulation at the surface in two ways. Firstly, deep water nutrients (Fig. 4.9) may be mixed up into the euphotic zone. Secondly, there is a deep chlorophyll maximum located just above the nitracline and it is possible that this chlorophyll is mixed upward, resulting in a more even distribution through the water column and higher concentration evident at the surface. The field program observed both shoaling of the nitracline and chlorophyll maximum during their winter sampling cruises. See section 4.3 for a detailed analysis of the relative importance of vertical mixing of the chlorophyll maximum relative to vertical nutrient supply. The Leeuwin Current may be a source of energy that contributes to the reduced winter stratification and mixing of deep water nutrients towards the surface.

Conclusions

The waters of the southwestern Australian shelf, Leeuwin Current and offshore are primarily nitrogen limited, but diatom production in shelf waters may also be silicate limited. Compared to the shelf, the Leeuwin Current is high in silicate and exchange between the two water masses may supply silicate to the shelf. However, such exchange may also strip phosphate and possibly nitrate off the shelf. A cross-shelf (inshore to offshore) gradient in chlorophyll *a* biomass suggests that nutrients delivered from terrestrial sources play an important role in sustaining phytoplankton production on the shelf. A seasonal (summer – winter) increase in chlorophyll *a* biomass corresponds with a winter-time maximum in rainfall and discharge. However, the seasonal increase is ubiquitous across the shelf, occurring in areas well removed from terrestrial influence. As such, a further source of nutrients must contribute to this seasonal accumulation. The climatologies and the results from the SRFME field program suggest that a seasonal deepening of the mixed layer, and associated mixing of deep water nutrients or phytoplankton from the deepwater chlorophyll maximum towards the surface, is a likely candidate. Upwelling associated with mesoscale eddies likely makes an important contribution to the variability in the surface chlorophyll concentrations.

4.2 Phytoplankton Dynamics: Biomass and Production

Tony Koslow	CSIRO Marine and Atmospheric Research
Stephane Pesant	University of Western Australia

Introduction

A key objective of the SRFME Biophysical Oceanography Program was to determine spatial and temporal patterns of variability in phytoplankton biomass and production in relation to physical, chemical and biological forcing of the biogeochemical cycle. Our study was based on field observations along the Two Rocks Transect, supplemented by remote satellite observations of ocean colour and sea-surface temperature. A total of 102 stations were sampled in the course of 27 cruises along the Two Rocks Transect. At each station, up to 7 depths were sampled to describe the vertical distributions of these parameters, for a total collection of 508 water samples.

Methodology

Thermal infrared data from the NOAA Advanced Very High Resolution Radiometer (AVHRR) and ocean colour information from the Sea-viewing Wide Field-of-view Sensor (SeaWiFS) satellite were used to provide a larger-scale perspective (both spatially and temporally) to the study. Altimeter data were obtained from a 7-day temporal resolution altimeter sea level anomaly product on a 1/3º Mercator grid based on combined TOPEX Poseidon and ERS-1/ ERS-2 satellite missions from October 1992 to August 2002 from CLS Space Oceanography Division (Ducet *et al*., 2000).

Standard methods (JGOFS protocols (Knap *et al.* 1996)) were used to carry out size-fractionated measurements (< 5 µm and > 5 µm) of phytoplankton biomass, as both chlorophyll *a* and particulate organic carbon, and primary production, using the 24-hour ^{14}C-uptake method, based on deck incubations. The deck incubations were carried out in tubes, shaded to simulate *in situ* irradiance conditions. The different irradiance levels simulated by the incubator were 100, 63, 38, 15, 5, 1, 0.3 or 0% (dark) of sub-surface irradiance. Running seawater pumped from 2 – 5 meters below the surface was kept running through the tubes to regulate temperature within the incubator. ^{14}C incubations were all carried out from dawn to dawn to standardize potential day-night variability in productivity and respiration. Sampling was generally carried out in daylight hours, and no corrections were made for day-night variability in chlorophyll *a*.

A total of 102 stations were sampled in the course of 27 cruises along the Two Rocks Transect. At each station, up to 7 depths were sampled to describe the vertical distributions of these parameters, for a total collection of 508 water samples.

To examine the role of water column stratification on the vertical distribution of nutrients and primary production, we defined a ‘Gross Stratification Index’ (GSI) as the difference between the near-surface (5 m) and bottom densities divided by the depth interval and multiplied by 100 (effectively a modified mean density gradient).

Several methodological considerations which relate to the following were described in Keesing and Heine (2005) and will not be repeated here:

- the basis for our conversion of fluorescence to chlorophyll *a* concentration;
- our ^{14}C method of estimating primary production based on 24-hour deck incubations and key uncertainties associated with it;
- the relationship between particulate and dissolved production (i.e. production that is released back into the water during the course of the experiment);
- a comparison of our 24-hour ^{14}C incubations and primary production incubations carried out over shorter periods (e.g. 12-hour incubations); and
- the potential role of microzooplankton grazers in the incubation bottles on the primary production results.

Principal component analysis based on the correlation matrix was used to examine patterns in the cross-shelf seasonal cycle of chlorophyll *a* concentration. However, the dominant seasonal cycles are shown based on averaging data from the appropriate stations, rather than the derived principal components, because the offshore stations were sampled only quarterly, leading to a very 'gappy' record for the principal component time series.

Results

Remote sensing

As seen in Figure 4.14, SeaWiFS ocean colour data from 1998 – 2003 along the shelf break off the coast of WA shows a coherent seasonal cycle of chlorophyll fluorescence over a distance of approximately 700 km from the Abrolhos Islands (26˚ S) to Perth (32˚ S). Chlorophyll values were lowest in summer, peaked in late autumn/early winter, and remained relatively high through the winter. Averaging these data to obtain the climatological average, the phytoplankton bloom, which occurs broadly over the months of April through June, coincides closely with the peak in eddy kinetic energy of the Leeuwin Current, obtained from sea-height altimetry (Fig. 4.15). The region from the Abrolhos Islands to Perth also roughly corresponds to the region of peak eddy kinetic energy off WA (Fig. 4.16).

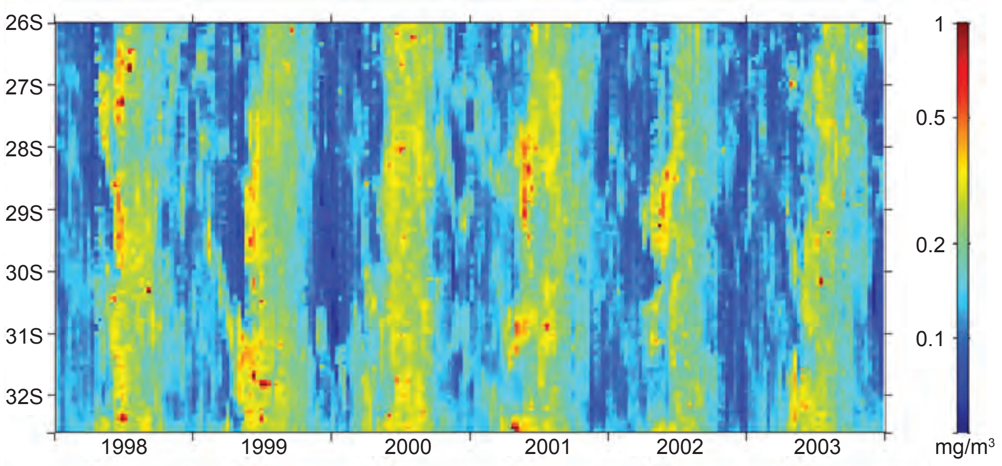

Figure 4.14: The concentration and distribution of chlorophyll estimated from SeaWiFS ocean colour data along the shelf break off the west coast of WA from 26˚ – 32˚ S from 1998 – 2003. A late autumn/early winter bloom extends along the coast, with relatively high chlorophyll levels maintained through much of the winter.

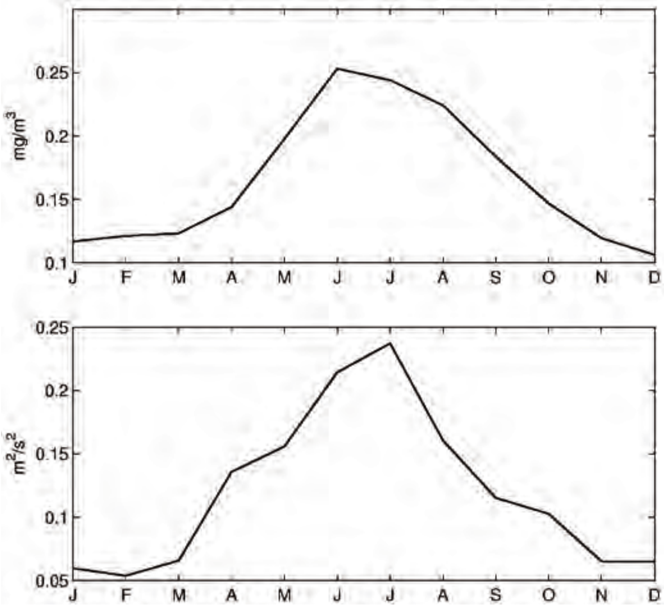

Figure 4.15: The climatological average for chlorophyll *a* concentration (upper panel) and eddy kinetic energy along (lower panel) along the slope off the coast of WA, estimated from satellite ocean colour and altimetry data.

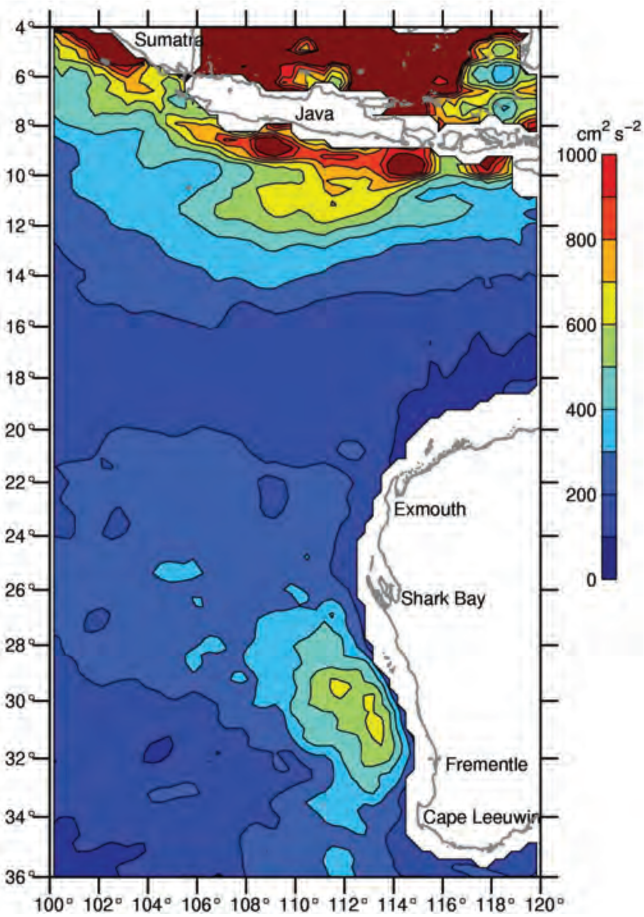

Figure 4.16: The distribution of eddy kinetic energy in the eastern Indian Ocean. Note the peak associated with Leeuwin Current eddies between the Abrolhos Islands, south of Shark Bay, and Cape Leeuwin.

The SeaWiFS ocean colour data from 1998 – 2004 indicated that the seasonal phytoplankton cycle was coherent onshore-offshore along the Two Rocks transect, with the exception of the inshore station (A), although it is unclear from the satellite data alone whether this is because, at 15 m depth, there are other contributors (such as suspended sediment and bottom reflection) to the colour (Fig. 4.17). Peak concentrations of chlorophyll also appeared to be higher at the inner shelf (40 m) station than farther offshore. The mean chlorophyll concentration at the inner shelf station in June was over 0.6 mg m^{-3}, falling to 0.2 mg m^{-3} in summer, whereas within the Leeuwin Current and at the offshore (stations D and E), the corresponding values were 0.3 – 0.4 mg m^{-3} in winter and about 0.1 mg m^{-3} in summer.

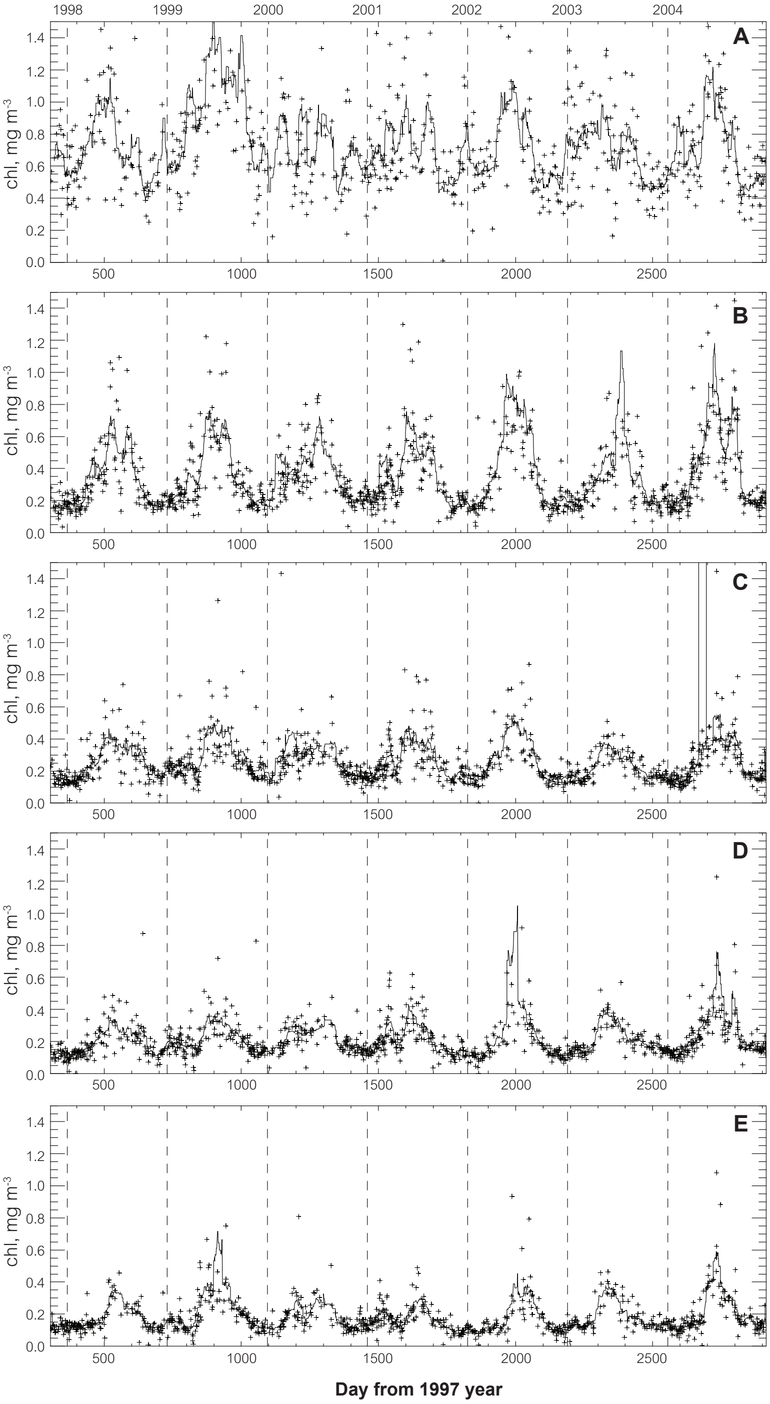

Figure 4.17: Daily SeaWiFS chlorophyll *a* concentrations at the stations along the Two Rocks Transect between 1998 and 2004. The solid line is a 31-day moving average.

Field observations: the seasonal cycle

Because of water column absorption of the visible wavelengths, the derived chlorophylls are only representative of the near-surface layer down to about 20 or 30 m depth. In summer, when the thermally stratified water column is nutrient depleted, chlorophyll concentrations in the near-surface layer are very low; in our region, most chlorophyll in summer is concentrated in a deep chlorophyll maximum layer at around 75 – 110 m depth, which cannot be detected from satellite observations. Field observations based on measurements of chlorophyll *a* through the water column were therefore required to ascertain the seasonal chlorophyll cycle. Satellite observations may also be biased inshore by re-suspended material.

With the exception of the nearshore 'lagoon' station, the seasonal cycle of chlorophyll *a* was reasonably coherent from the inner shelf to offshore stations (Fig. 4.18). Integrated chlorophyll *a* values over the study period were generally weakly (i.e. $0.05 < p < 0.10$) to significantly correlated from the inner shelf to slope stations (B – E), whereas the chlorophyll *a* concentrations at the 'lagoon' station were only significantly correlated with values at the adjacent inner shelf station (Table 4.2).

Table 4.2. Correlations (r) of the integrated chlorophyll *a* values at stations A – E (see Table 3.1), one-tailed probability levels (ρ), and number of data values (n). **: $p < 0.01$; *: $p < 0.05$; $p < 0.10$.

Station		**A**	**B**	**C**	**D**	**E**
A	r	1	.444(*)	.228	.082	.097
	ρ		.022	.154	.411	.376
	n	25	21	22	10	13
B	r	.444(*)	1	.566(**)	.393	.583(*)
	ρ	.022		.005	.131	.038
	n	21	21	20	10	10
C	r	.228	.566(**)	1	.599(*)	.824(**)
	ρ	.154	.005		.034	.000
	n	22	20	22	10	12
D	r	.082	.393	.599(*)	1	.497(?)
	ρ	.411	.131	.034		.072
	n	10	10	10	10	10
E	r	.097	.583(*)	.824(**)	.497(?)	1
	ρ	.376	.038	.000	.072	
	n	13	10	12	10	14

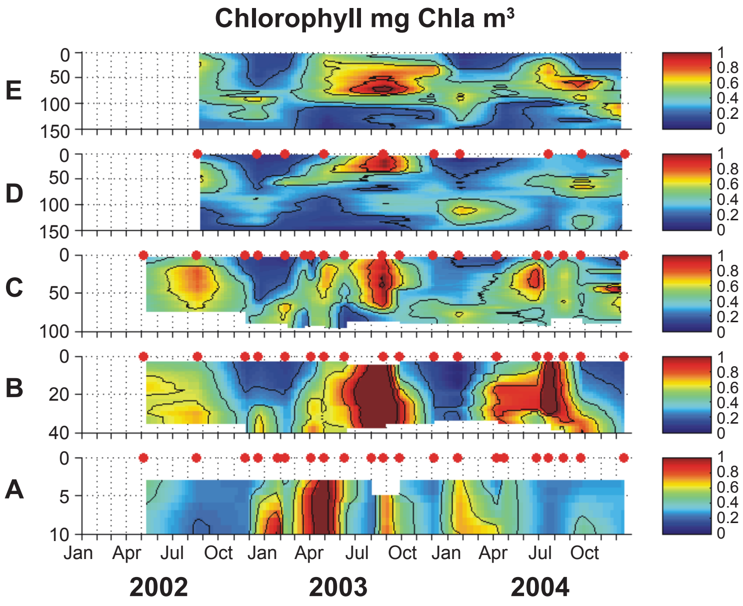

Figure 4.18: Time series of chlorophyll *a* through the water column at stations A to E along the Two Rocks Transect for the 2002 – 2004 field period. Note the coherence in the seasonal cycle from the inner shelf (station B) across the Leeuwin Current (station E). For station positions, see Figures 3.2 & 3.3, Table 3.1.

Principal component analysis (PCA) confirmed this pattern. The PCA was based on the matrix of correlations between the integrated chlorophyll *a* concentration at each station for all cruises in which all stations were sampled. The first two principal components explained 78% of the variance of the integrated chlorophyll *a* data set. The stations from the inner shelf to slope (B – E) all contributed strongly (> 0.7) to the first component, which explained 57% of the variance, whereas the second component consisted predominantly of the contribution of the nearshore station (A) (Table 4.3). No clear seasonal cycle of chlorophyll concentration was evident at the nearshore station.

Table 4.3. The contribution of each station to the first two principal components. The principal component analysis was based on the correlation matrix of integrated chlorophyll *a* values at each station along the Two Rocks Transect (see Table 4.2).

Station	**Principal Component**	
	1	**2**
A	.379	.874
B	.793	.333
C	.906	-.166
D	.712	-.320
E	.865	-.251

Integrated chlorophyll *a* across the Two Rocks transect from the inner shelf to the slope (stations B – E) shows a broad autumn and winter bloom period (March – August) with a minimum during the late austral spring and summer (November – February). There is approximately a factor of two difference in the integrated chlorophyll *a* concentration between these two periods (Fig. 4.19). The integrated chlorophyll concentrations were generally several-fold higher on the shelf and offshore, where values averaged from approximately 20 – 40 mg chl *a* m^{-2}, relative to the lagoon, where monthly values averaged between 5 – 15 mg chl *a* m^{-2}. However the difference was considerably reduced during spring and summer, when offshore biomass and productivity showed a considerably greater seasonal decline than the lagoon.

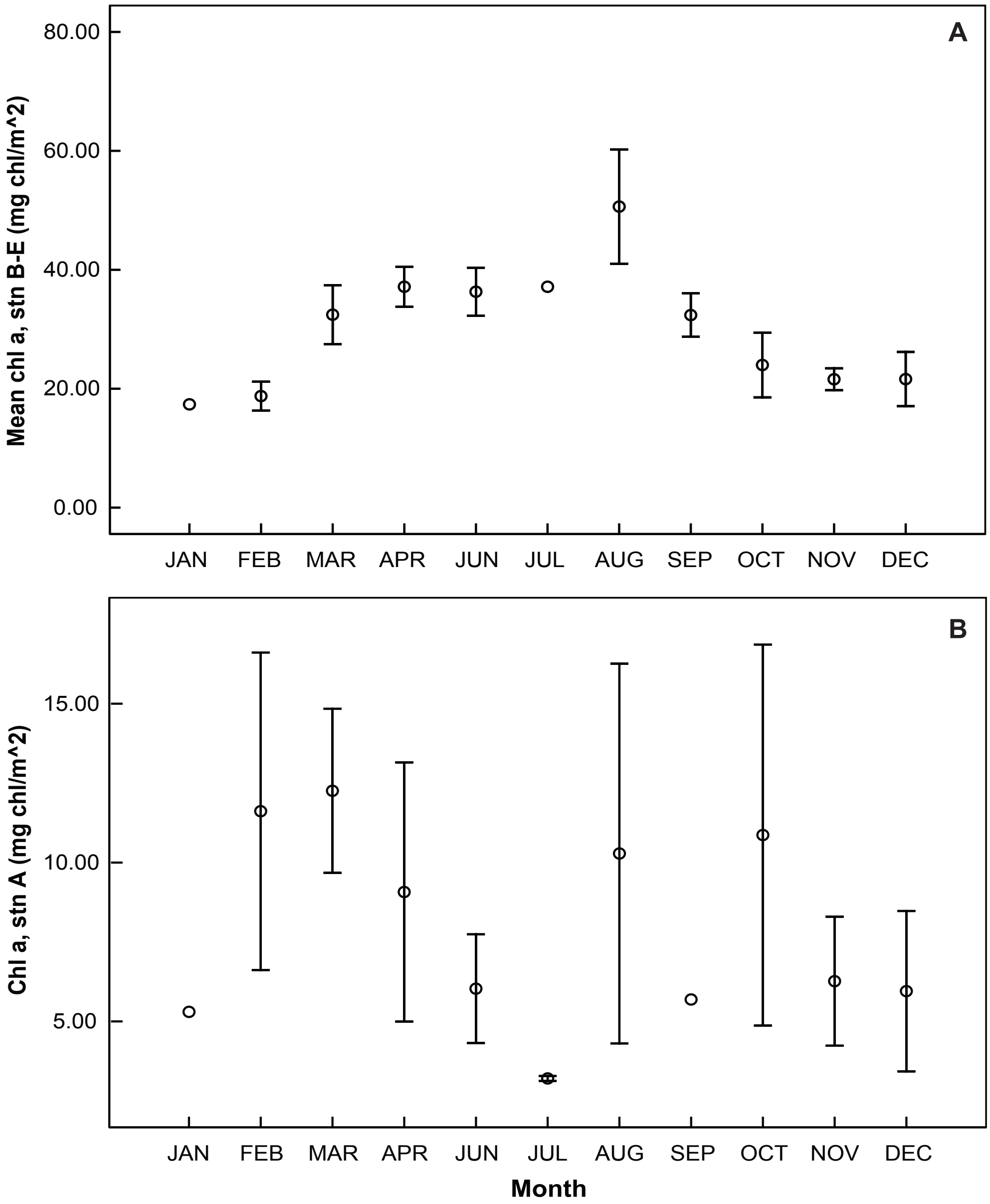

Figure 4.19: The mean integrated chlorophyll *a* from (a) stations B – E and (b) station A, across the Two Rocks transect, 2002 – 2004. Error bars are ±1 standard error. There were no data for May.

The seasonal patterns of primary production are similar but somewhat less clear (Fig. 4.20). Primary production at the outer shelf and slope stations (C and E) were weakly correlated (Kendall's tau = 0.42, $p < 0.05$), with highest primary production from late autumn to early spring offshore and extending into the summer on the shelf. There were spring and autumn peaks in production at the lagoon station, with a summer peak in primary production in 2004 as well. Primary production in autumn and winter was several-fold higher on the shelf and offshore than in the coastal lagoon, but productivity levels were comparable at all stations during spring and summer. These results are based on water column productivity only; benthic primary production would be considerably higher within the lagoon.

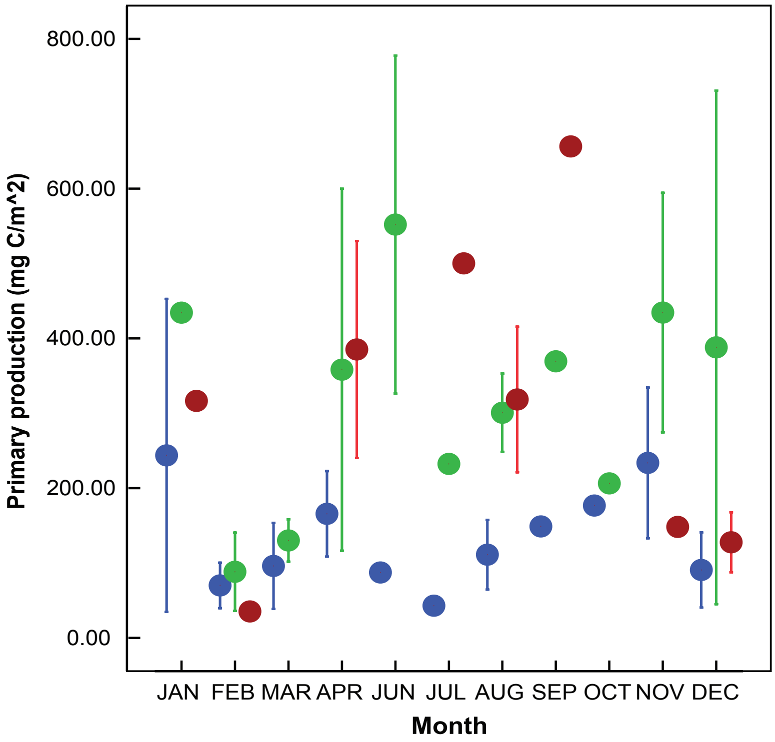

Figure 4.20: The average integrated primary production over the year at stations A (blue) (coastal lagoon), C (green) (mid-shelf), and E (red) (outer edge of the Leeuwin Current). The error bars are ±1 standard error. There were no data for May.

Vertical structure and stratification

Mixing of nutrients upwards into the photic zone is partly governed by the vertical stratification of the water column, which in turn depends on the temperature and salinity structure. In many studies, temperature alone is used to define the water column stability, but in our situation salinity changes may on occasion be sufficiently important that they should also be taken into account. We are accordingly analysing the vertical structure using the derived sigma-t profiles.

The CTD 1-m depth-averaged profiles were smoothed by a simple 5-point moving average to reduce small-scale variability, and the surface and bottom mixed-layer depths (MLD) have been defined as the top-most and bottom portions of the water column with a sigma-t gradient of < 0.002 m^{-1}. The pycnocline has been defined as a layer where the gradient exceeds 0.01 m^{-1}. The derived MLDs were visually compared with the plotted profiles to confirm the analysis. However, MLDs could not always be unambiguously defined if the density increased steadily with depth, and there were occasions where multiple pycnoclines and MLDs occurred down the water column. In many cases on the shelf, the water was effectively isopycnal right down to the bottom and so the surface MLD was equal to the water depth.

A simple indication of the strength of the vertical structure at each station was quantified by a ‘Gross Stratification Index’ (GSI), defined as the difference between the near-surface (5 m) and bottom densities (maximum 150 m) divided by the depth interval and multiplied by 100 (effectively a modified mean density gradient). While the GSI in the shallower water near the coast showed a mixed seasonality, from station C outwards the water column was clearly more strongly stratified during spring and summer (Fig. 4.21, 4.22).

There were appreciable differences in stratification between summer and winter, with important implications for nutrient profiles and resultant primary production. As an example of the summer situation, Fig. 4.22a shows the vertical structure in December 2002. The surface mixed layer was shallow, with a strong thermocline and well stratified water column so that the temperature at 150 m at the offshore station E was as low as 16°C. Salinity changes were by comparison insignificant. Chlorophyll *a* levels (derived from the fluorescence profiles using a regression relationship against extracted chlorophyll *a* measurements) were extremely low in surface waters (< 0.2 mg m^{-3}), with a weak deep chlorophyll maximum (DCM) of about 0.5 mg m^{-3} at 100 m depth. The bulk of the DCM was located between the 0.1% and 1.0% light levels, and shoaled towards the shelf break, with maximum chlorophyll levels found near the seabed at stations A and B. Nitrate was generally depleted (<0.2 µM) throughout the upper water column, with a distinct nitracline at 100 m water depth (coincident with the DCM).

In autumn by contrast, the offshore mixed layer extended down to 100 m with a (weaker) thermocline below this depth (Fig. 4.21, 4.22b). The chlorophyll maximum was located at ~ 50 m depth (well above the 1.0% light level), and chlorophyll levels on the shelf exceeded 1 mg m^{-3}. There was also an extensive tongue of high nitrate water (> 1 µM) intruding from offshore into the lower part of the water column towards the shelf, possibly an upwelling-like event associated with an eddy structure visible in the satellite image for this day. Similarly high nitrate levels were also noted on the shelf at station A.

Despite small-scale local variability, the seasonal relationships illustrated above tended to follow a similar pattern over the 3-year sampling period. For example, at station E (Fig. 4.21), the vertical stratification (as indicated by the gross stratification index) was generally highest in the summer months and weakest (with the deepest mixed layers) in autumn and winter. In winter, the DCM shoaled to 50-80 m from a summer depth of 100 m, with a concurrent increase in chlorophyll *a* concentrations from summer to winter. Volumetric particulate primary production at Station E was generally maximal at < 50 m water depth in fall and winter. However, in spring 2004, production peaked at ~ 75 m water depth, coincident with a strong nitracline located at 75 – 100 m depth. In general, nitrate was relatively low (< 0.2 µM) within surface waters, with the nitracline located near 100 m water depth. An unusual surface pulse of nitrate was measured in May 2003, coincident with a breakdown of the summer stratification.

The stratified conditions were largely restricted to the deeper offshore stations D and E (Fig. 4.21, 4.22). The shelf stations A and B (and even to a large extent C) were vertically mixed throughout the year, with some evidence of sporadic upwelling at station C e.g. in the spring of 2003. It appeared that the Leeuwin Current depressed the isotherms at station D (i.e. downwelling) as the 16° to 17°C water was much shallower at E than at D, and even reached the surface at station E in late winter 2003.

To compare with the vertical structure shown by the monthly CTD casts, vertical time-sections down to 300 m for the offshore station E have been extracted from the Levitus and Boyer (1994) climatology (Fig. 4.23). This reveals a phase shift between the warmest surface water (February to April) and that at 300 m (June/July) due to the deepening of the isotherms associated with the stronger Leeuwin Current during the autumn/winter months. The vertical temperature differential between the surface and 300 m dropped from about 11°C in summer to about 7°C in winter. The mixed layer depth increased from about 30 m in January/February to over 80 m in June. The salinity structure (Fig. 4.18) shows both the low-salinity of the Leeuwin Current tropical water near the surface in winter and the presence of high salinity (>35.9 psu) Indian Ocean Central Water at a depth of about 100 m in summer deepening to almost 200 m in winter.

Offshore phytoplankton dynamics: the late autumn and winter blooms

We examined the processes responsible for the seasonal productivity cycle at station E on the outer edge of the Leeuwin Current. From time series of temperature and vertical stratification, chlorophyll *a,* primary production, and nitrate + nitrite (NO_x) through the water column (Fig. 4.21), it is apparent that the two periods of peak primary production (late autumn 2003 and winter 2004) occurred during periods of minimal stratification. Detectable NO_x was observed in the upper water column during the late autumn, 2003 cruise - the only time this was recorded at this station during the study. During both of these periods, primary production attained carbon fixation levels of 10 - 20 mg C m^{-3} within the upper 50 meters of the water column.

Destratification of the water column thus appears to have enabled nutrient to mix into the upper water column, leading to heightened near-surface productivity and a shoaling of the chlorophyll through the water column. Light levels, even in winter, are sufficient to sustain peaks in seasonal production at this latitude.

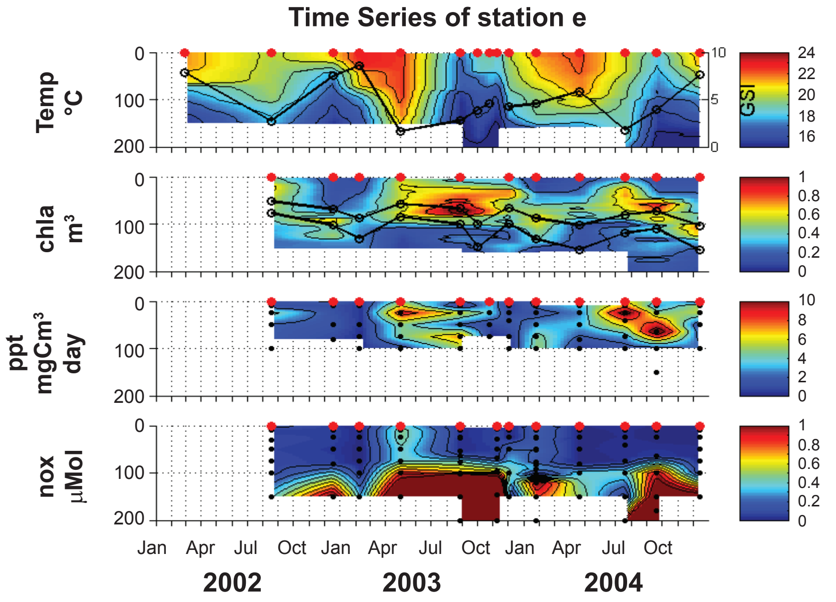
Time Series of station e

Figure 4.21: Time-series of temperature (upper panel), chlorophyll concentration (second panel), particulate primary productivity (third panel) and nitrate + nitrite (bottom panel) at station E derived from the quarterly CTD casts and bottle samples over the 3-year sampling period. The solid line in the temperature series is the Gross Stratification Index (defined in the methods), and the two lines in the chlorophyll panel show the depths of the 1% and 0.1% light levels from the PAR sensor. The solid dots in the lower 2 panels show the bottle sampling depths.

Interestingly, different mechanisms appear to be responsible for destratification of the water column in late autumn and winter. In late autumn (late April) of 2003, a Leeuwin eddy at the edge of the transect destratified the water column. Warm Leeuwin water extended to at least 150 m depth, as well as across the shelf. Although the Leeuwin Current is often assumed to be a low-nutrient water mass, measurable nutrient was found throughout the upper water column during this cruise, the only time this was observed in the field study at this outer station. There was evidence as well of upwelling of nutrient from offshore, indicating possible spinup of nutrients by the eddy (Fig. 4.22). The nutricline shoaled to about 50 m depth, leading to a shoaling of the maximum chlorophyll layer as well.

The other period of high productivity observed at this station was during the winter and early spring of 2004, when winter cooling appeared responsible for destratifying the water column, a phenomenon generally observed in oligotrophic subtropical regions (Fig. 4.21). In the winter of 2003 (Fig. 4.22C), the relatively warm, low salinity water of the Leeuwin Current is restricted to the shelf break (station D). Winter cooling has destratified the water column and the nitricline is again at 50 – 75 m depth, with relatively high chlorophyll concentrations (~1 mg/m^3) near the surface.

A

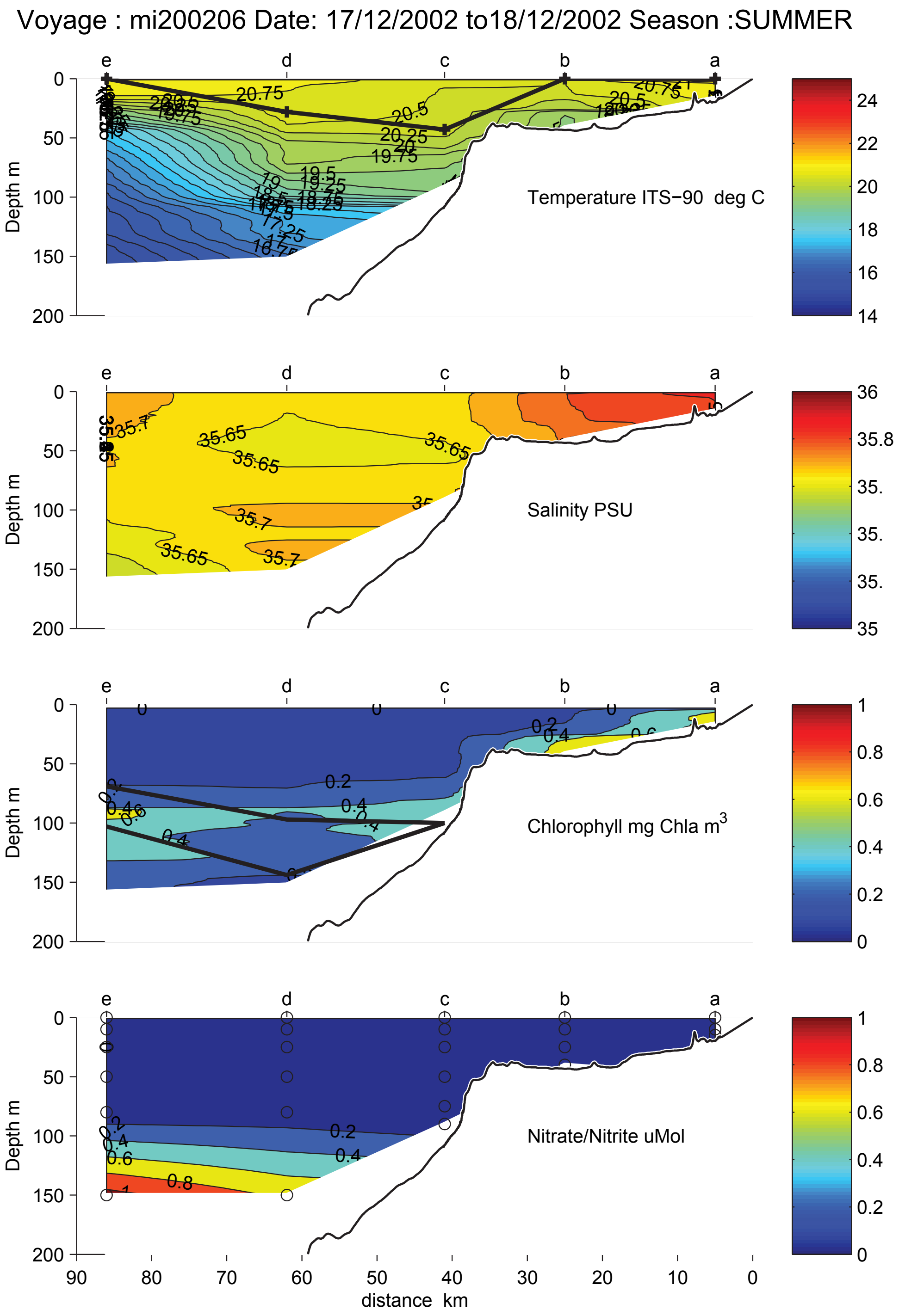
Voyage : mi200206 Date: 17/12/2002 to18/12/2002 Season :SUMMER
e
d
c
b
a
Depth m
Temperature ITS−90 deg C
20.75
20.5
20.25
20
19.75
19.5
19.25
18.75
18.25
17.25
16.75
24
22
20
18
16
14
Salinity PSU
35.7
35.65
36
35.8
35.
35.
35.
35
Chlorophyll mg Chla m3
0.2
0.4
0.6
1
0.8
0.6
0.4
0.2
0
Nitrate/Nitrite uMol
0.2
0.4
0.6
0.8
1
0
50
100
150
200
90
80
70
60
50
40
30
20
10
0
distance km

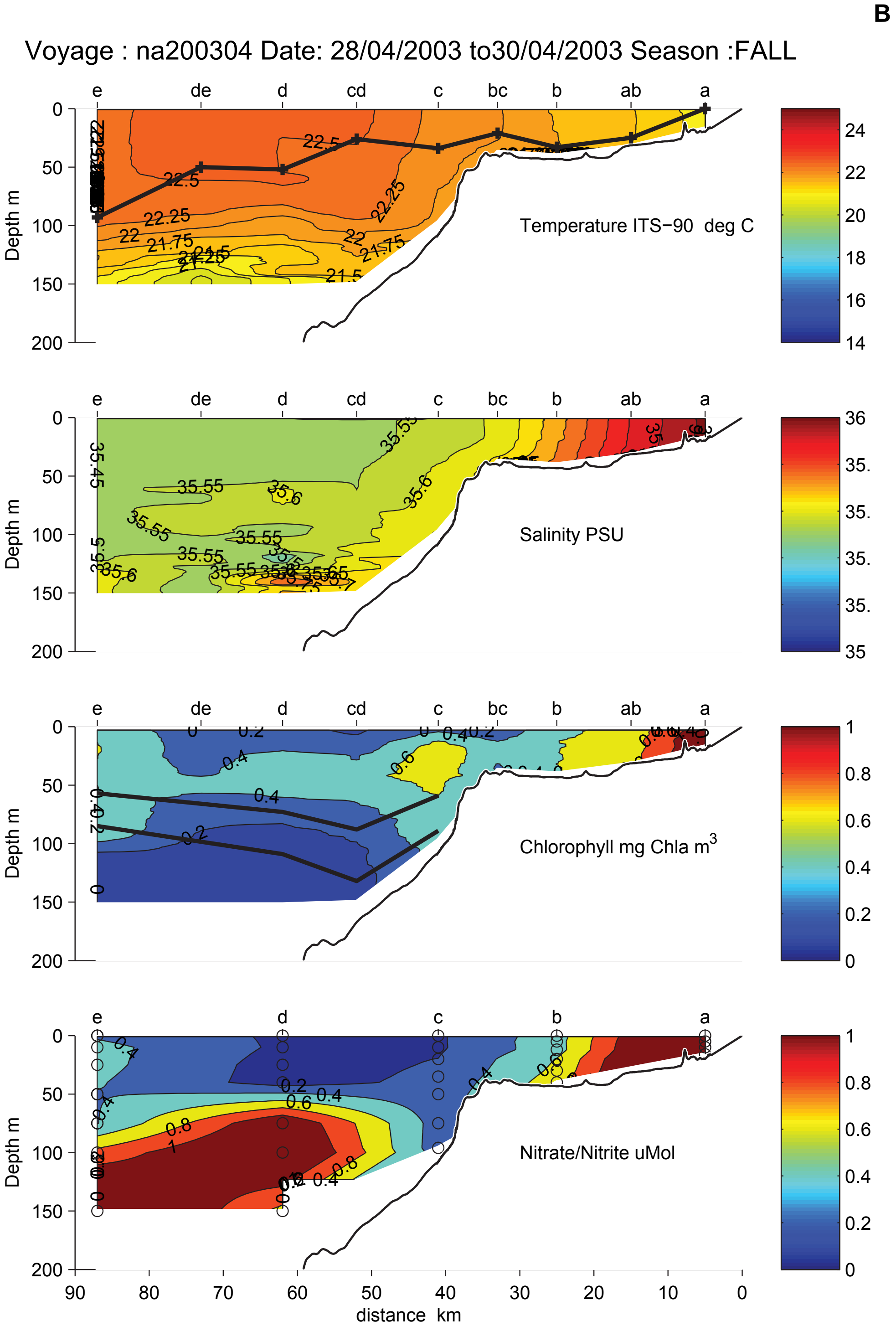
B
Voyage : na200304 Date: 28/04/2003 to30/04/2003 Season :FALL
e
de
d
cd
c
bc
b
ab
a
Depth m
0
50
100
150
200
Temperature ITS−90 deg C
22.5
22.25
22
21.75
21.5
21.25
24
22
20
18
16
14
Salinity PSU
35.45
35.5
35.55
35.6
35.65
35.7
36
35.
35
Chlorophyll mg Chla m3
0.2
0.4
0.6
1
0.8
0
Nitrate/Nitrite uMol
0.2
0.4
0.6
0.8
1
distance km
90
80
70
60
50
40
30
20
10
0

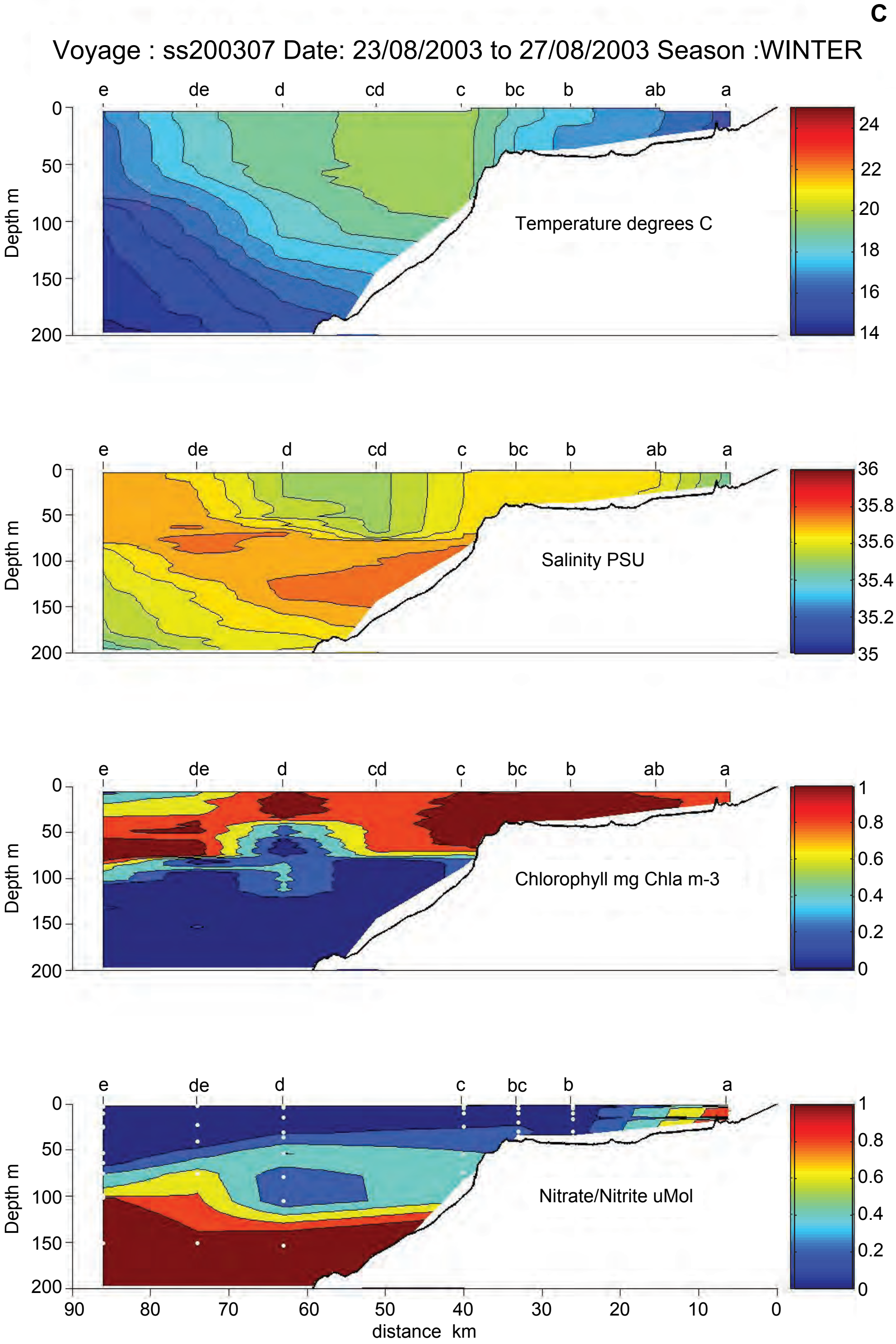

Figure 4.22: Vertical cross-sections of temperature (upper panel), salinity (second panel), chlorophyll (third panel) and nitrate + nitrite (bottom) across the Two Rocks Transect during (a) summer (December 2002), (b) late autumn (late April 2003), and (c) winter (August 2003). The solid line in the upper panel represents the upper mixed-layer depth (defined in the text), and the two lines in the chlorophyll panel show the depths of the 1% and 0.1% light levels from the PAR sensor.

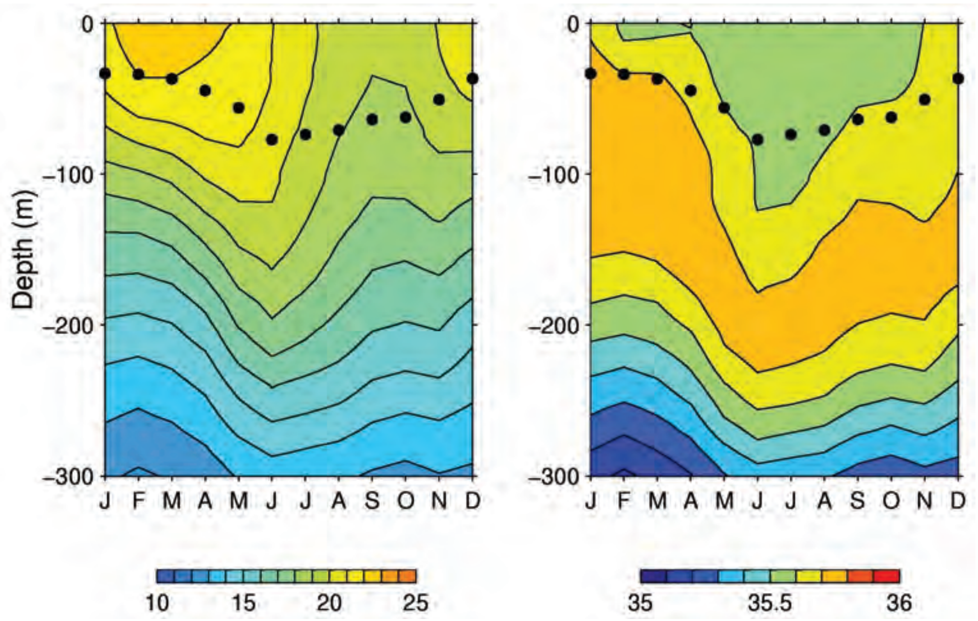

Figure 4.23: Vertical temperature and salinity sections for the upper 300 m at station E derived from the Levitus and Boyer (1994) climatology. The dots represent the monthly mixed layer depths.

Phytoplankton size structure

Most phytoplankton biomass and primary production was based on the small (< 5 µm) phytoplankton size-fraction (Fig. 4.24). There tended to be a higher contribution from the larger phytoplankton size fraction inshore, but there was no consistent seasonal pattern in the relative contribution of the larger size fraction; rather, significant contributions of the larger phytoplankton inshore occurred sporadically. The small phytoplankton size range (the nano- and picophytoplankton) typically dominate in relatively oligotrophic regions.

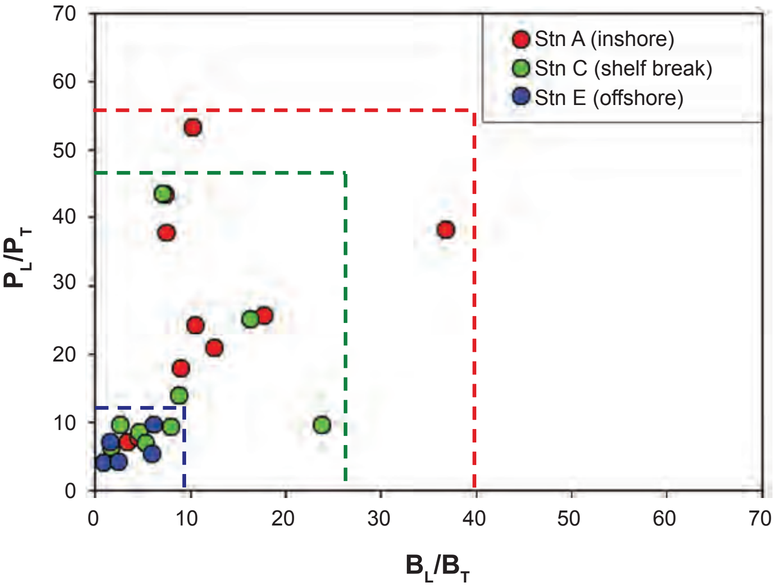

Figure 4.24: The relative proportion of biomass and particulate production contributed by 'large' phytoplankton (> 5 m) (B_L and P_L) and small phytoplankton (B_S and P_S) in relation to distance offshore.

Use of remote sensing to predict chlorophyll

We examined the relationship between remotely sensed chlorophyll fluorescence during the time of the cruises at the site of four shelf and slope stations and integrated chlorophyll through the water column to test our ability to use satellite data to predict total chlorophyll concentration. The relationships explained between 19% and 55% of the variance (see Fig. 4.25). Generally the relationship was better offshore. These results, however, are preliminary: further work is required to assess whether the relationship can be improved with additional information, such as from temperature related to the seasonal cycle,

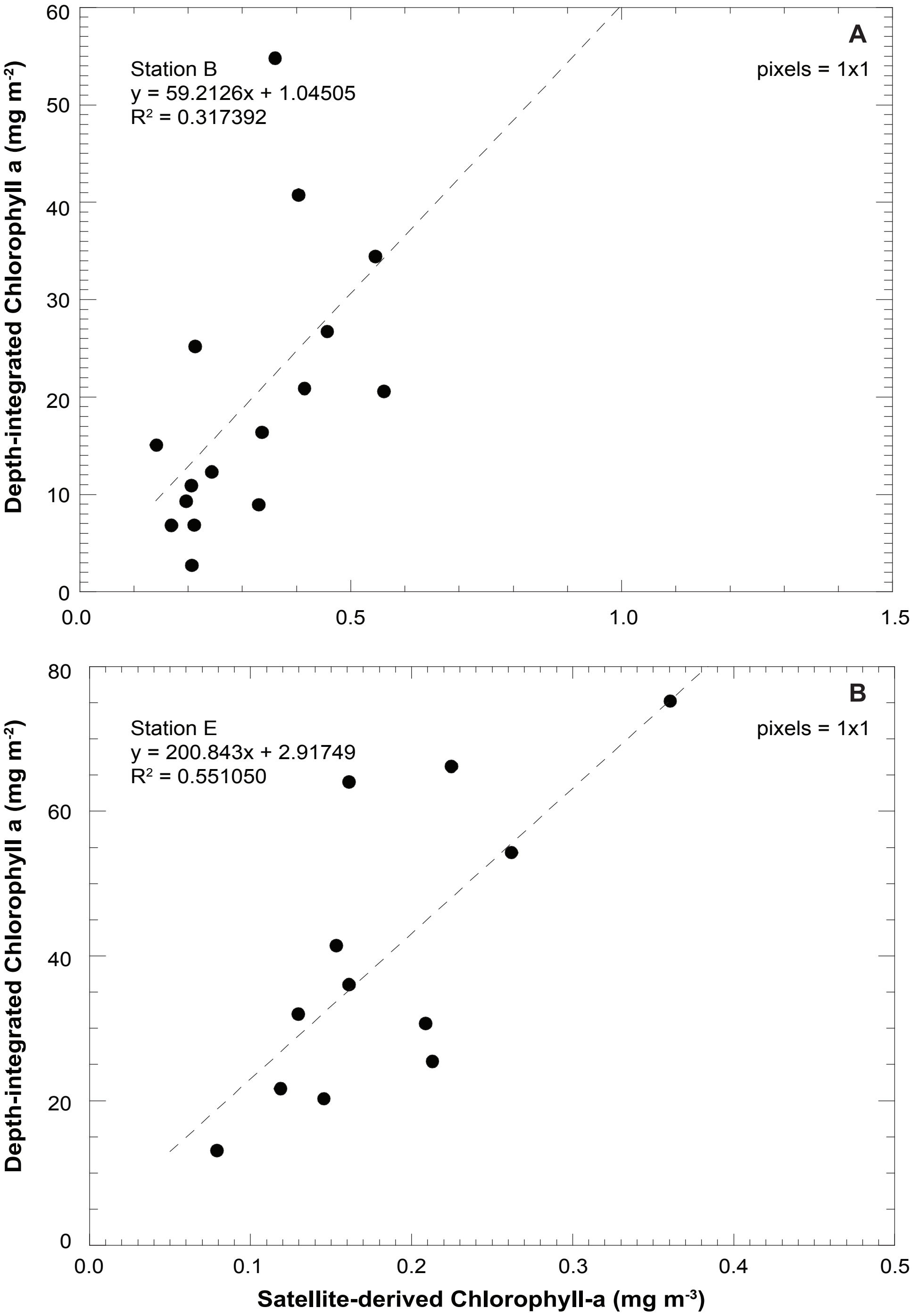

Figure 4.25: The relationships between chlorophyll fluorescence detected by the SeaWiFS satellite at the pixel covering the Two Rocks transect stations B and E and the integrated chlorophyll measured through the water column.

Discussion

The different seasonal cycles of chlorophyll concentration and primary production nearshore and across the shelf and slope reflect differences in nutrient budgets and physical forcing (see following section). The primary nutrient sources in the coastal lagoon are from runoff, groundwater, turbulent re-suspension of sediment, and re-mineralization of macroalgae and seagrasses; nutrient uptake is also likely dominated by the macroalgae and seagrasses in summer. Runoff and re-mineralization would lead to peak nutrient input during winter, but strong summer sea-breezes could resuspend benthic diatoms and sediment in the water column, possibly leading to the episodic peaks in summer chlorophyll.

Winter phytoplankton blooms are generally observed in oligotrophic sub-tropical marine systems, due to the breakdown of thermal stratification and convective mixing of nutrients into near-surface waters; there is still sufficient light in winter in the subtropics to maintain a bloom. The late autumn bloom, however, is less typical. Given that the Leeuwin Current is generally perceived as transporting low-nutrient water and promoting downwelling, how does enhanced flow of the Leeuwin in late autumn lead to nutrient enrichment and heightened primary production?

Several mechanisms may be responsible, which we propose to examine further during a focussed cruise of the *Southern Surveyor* in May, 2007:

- The spin-up of eddies beyond the shelf edge may promote upwelling;
- The Leeuwin Current may entrain nutrients in the tropics as it deepens in autumn, and transport them southward;
- Seasonal regeneration of nutrients within the shelf sediments may be mixed back into the water column with the autumn breakdown in stratification

The apparent relationship between enhanced flow of the Leeuwin Current and heightened primary production may explain the otherwise anomalous positive correlation between the strength of the Leeuwin and recruitment to the western rock lobster fishery. Griffin *et al.* (2001) observed, based on simulation modelling, that differential transport did not explain the correlation and hypothesized that it may be related to productivity. This conclusion is supported by our results.

There is considerable evidence of interannual variability in our study. The late autumn bloom, for example, occurred in 2003 but was not observed — or at least, not sampled — in 2004. This interannual variability points to the need for continued sampling and for sampling with greater temporal resolution. It also points to the need to increasingly integrate remote sensing, mooring and, if possible, glider observations with shipboard observations in the study of shelf-scale biogeochemistry and biophysical dynamics.

4.3 Phytoplankton dynamics: Investigating the Underlying Biophysical Mechanisms

Jim Greenwood, Nugzar Margvelashvili

CSIRO Marine and Atmospheric Research

Introduction

Observations at station E on the outer edge of the Leeuwin current described in the previous section show that destratification of the water column coincides with periods of peak primary production during late autumn and early winter. A number of biophysical mechanisms have been proposed to explain these observations. However, because this is a highly dynamic region strongly influenced by the Leeuwin Current and its associated features, it is difficult to confirm the mechanisms responsible for the observed seasonal trends in biological production from the observations made so far. In particular, the relative importance of vertical versus lateral nutrient input is difficult to judge. In this next section we examine results from some numerical experiments designed to help reinforce our understanding of some of these biophysical mechanisms and assess their relative importance in shaping the observed seasonal plankton production cycle.

One-dimensional model

In the first set of numerical experiments we test the ability of a one-dimensional (1-d) model to capture the three key seasonal biological features observed at station E on the outer edge of the Leeuwin Current during 2003 (Fig 4.21): the predominance of a summer-time deep chlorophyll maximum, the occurrence of a late-autumn maximum in surface chlorophyll and associated peak in production, and the appearance of a mid-water chlorophyll maximum and peak in production during winter. In simplifying the physics in this way we necessarily focus on vertical mixing and the supply of deep water nutrients to the upper water column, ignoring for the moment possible lateral advection of nutrients.

The slope and variability of the density profile of the upper water column is of primary interest as it strongly affects vertical mixing, and consequently plankton in the model (directly via light limitation, and indirectly via nutrient supply). In applying a 1-d representation of the ocean, it is hoped that the seasonal cycle in density can be approximated by inputs of heat, and perhaps to some extent freshwater, at the surface. However, we suspect that most of the local density changes off Western Australia are likely due to heat and salt advection by the Leeuwin current, and we must therefore expect unresolved advective fluxes. Here, we imitate these horizontal heat and salt fluxes by relaxation of modelled temperature and salinity to synTS (K. R. Ridgway and J. R. Dunn, CSIRO project report, 2002). This results in a variation in mixed layer depth that is constrained by observations, allowing an estimation of mixing rate and vertical nutrient supply. Additional turbulence generated as a result of horizontal current shear is ignored. It is also worth noting that while the unresolved heat and salt fluxes implicit in this approach do not generate significant artificial mixing (not shown), strong correction of the thermocline without a similar correction of the nitracline may lead to errors in the vertical nutrient flux.

Model set-up

The model is the same as that described in Greenwood *et al.*. (2006), representing the dynamics of nutrients, phytoplankton, zooplankton and sinking detritus. In the present application, it is designed to simulate the upper 200m of the water column at station E during 2003 with a vertical resolution of 2m. The lower boundary is left open to allow diffusive fluxes and sinking particles to cross the base of the model. The values of the biological scalars are fixed at the lower boundary implying a dissolved nitrogen flux into the model domain determined by the concentration gradient and the background diffusion coefficient. The biological model is initialised with small constant values for phytoplankton, zooplankton and detrital biomass, and a vertical profile of DIN measured during December 2002. The model is then run repeatedly with forcing for 2003 until a stable annual pattern is observed (reached after 10 years). The end condition of this ‘spin up’ run is then used as the initial condition of the main run.

Model Results

The model simulated temperature variation in the upper 150m is compared with satellite derived sea surface temperature, and five ship based depth profiles recorded at station E during 2003. The model compares well with the available data, capturing the overall seasonal variation in temperature throughout the upper 150m (Fig 4.26). The poorest result is found between the model and a depth profile measured at the end of August when the model over estimates temperature by up to 2.5 degrees throughout the entire 200m water column (Fig. 4.26). Satellite observation indicates that this occurs during a time of high temporal variability in sea surface temperature at this location (Fig. 4.26a). The cause of this observed variability and the mismatch with the model is discussed below.

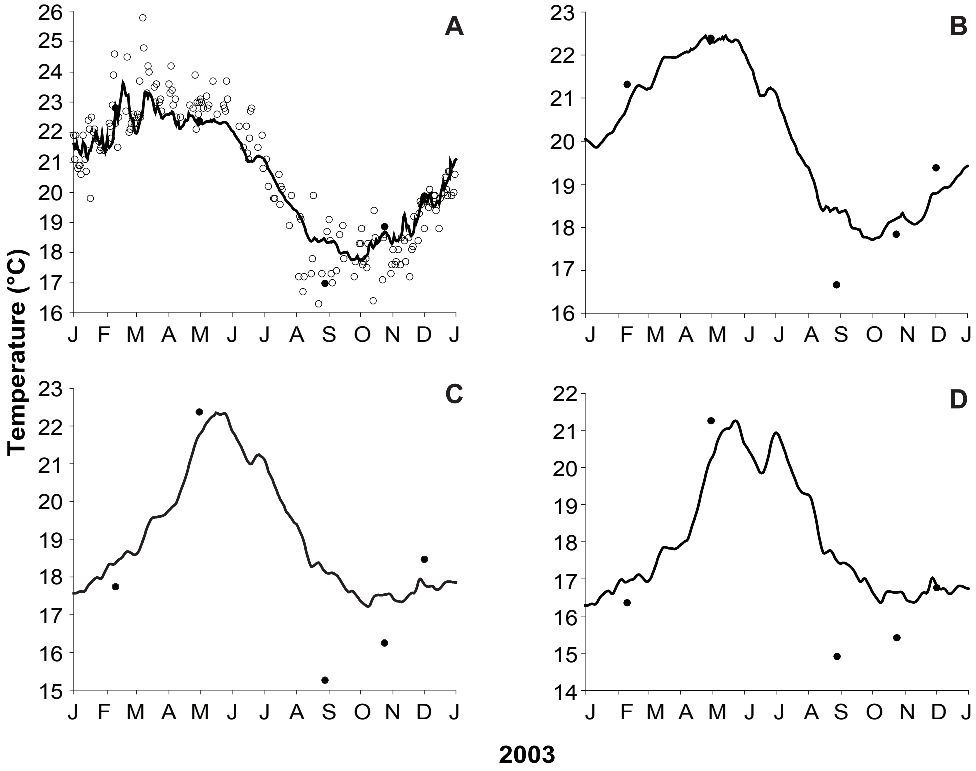

Figure 4.26: Seasonal variation in model simulated (solid line), measured (closed symbol) and satellite derived (open symbol) temperature at (a) the surface, (b) 50m, (c) 100m, and (d) 150m depth for station E during 2003.

Output from the biological model is compared with several sets of observations made at station E between December 2002 and December 2003. In order to characterize summer, autumn and winter conditions we compare three contrasting observed profiles of chlorophyll and dissolved inorganic nitrogen (nitrate+nitrite+ammonium) along with depth-integrated estimates of primary production from each season with average model output from the corresponding month.

Table 4.4. Comparison of measured and modelled estimates of depth integrated primary production at station E during 2003.

	Primary Production (mg C m^{-2} d^{-1})				
	measured	modelled			measured / modelled
		max	min	mean	
Summer	96	133	89	98	0.98
Autumn	530	340	73	162	3.27
Winter	416	186	77	105	3.96

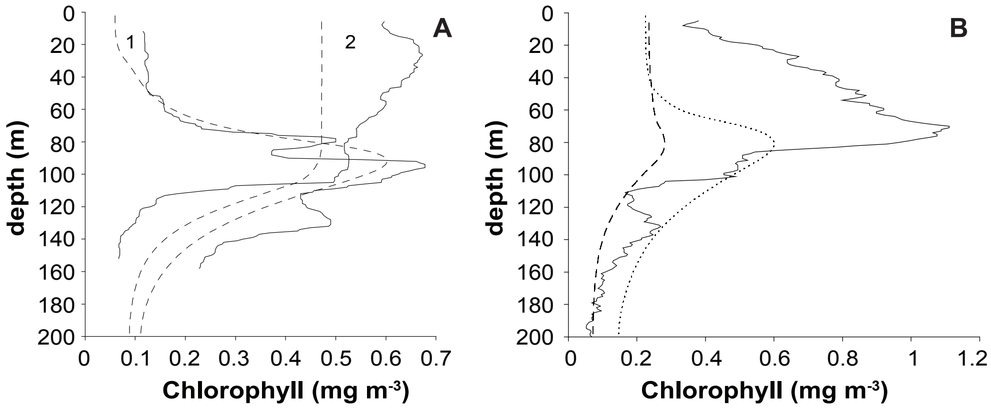

Figure 4.27: Vertical structure of chlorophyll in the upper 200m at station E predicted by the model (dashed line) and measured (solid line) during 2003 showing (a) the transition between summer (1) and autumn (2) conditions, and (b) the failure of the model to capture the deep chlorophyll maximum observed during early winter. The dotted line in (b) shows the improvement in model performance when the model temperature and salinity fields are relaxed to field observations.

Comparison of vertical profiles of chlorophyll show that the model performs surprisingly well in simulating the general vertical chlorophyll structure observed at Station E during both the summer and autumn (Fig. 4.27a). Summer biomass is dominated by a deep chlorophyll maximum and low surface concentrations consistent with observations. An important transition from this summer condition is captured by the model in early May that coincides with an increase in mixed layer depth and vertical mixing (not shown). This results in a relatively even distribution of biomass throughout the upper 100m and a marked increase in surface chlorophyll in accord with autumn observations. The best agreement, in terms of both biomass and vertical structure, is found for the summer. In the autumn the model accounts for 80% of the total observed chlorophyll biomass in the upper 100m. Model estimates of depth-integrated primary production follow a similar pattern, with low levels during summer that agree well with measurements, followed by an autumn increase (Table 4.4). The autumn increase simulated by the model is short lived and not well represented by the monthly mean, but at its maximum accounts for 65% of the measured rate. The magnitude of the model simulated autumn increase in production is very sensitive to the depth and slope of the nitracline at the time of mixed layer deepening. For example, a reduction of the initial summertime DIN concentration at 200m by 0.5 μM results in a 30% and 40% reduction in the simulated autumn peak in surface chlorophyll and primary production respectively. This highlights the potential sensitivity of the system to relatively small changes in nutrient concentration below the mixed layer. During summer, the predicted DIN profile compares well with observations having surface concentrations close to zero, and a nitracline at approximately 80m (Fig. 4.28a). At the onset of increased autumn production the model predicts a deepening of the nitracline. This result is consistent with a concomitant deepening of the mixed layer, but is surprisingly different to observations that suggest little change in the depth of the nitracline and elevated surface DIN concentrations (Fig. 4.28b).

Model output during winter compares poorly with observations with a large underestimation of production (Table 4.4), little sign of the mid-water chlorophyll maximum measured during August 2003 (Fig. 4.27b), and a 20m over-estimation of the depth of the nitracline (Fig. 4.28b).

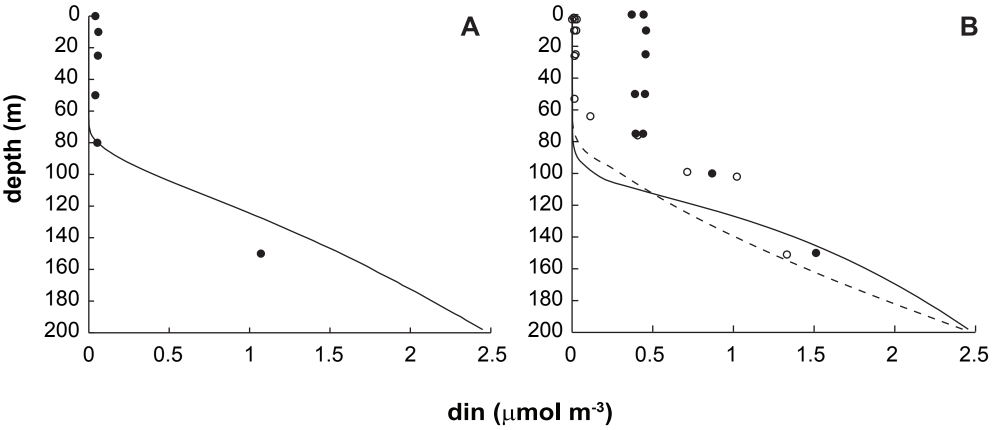

Figure 4.28: Comparison of model simulated (line) and measured (symbol) dissolved inorganic nitrogen at station E during 2003 showing (a) consistency between model and observations in the summer, and (b) mismatches in both the autumn (solid line, closed symbol) and winter (dashed line, open symbol).

Discussion

The model performs well in simulating the deep maximum and low surface concentrations of chlorophyll typical of summer months. The ability of the 1-d model to capture this summer feature is independent of any horizontal correction of temperature and salinity (not shown), but instead results from a net surface heat input during the summer months that maintains strong thermal stratification of the upper water column. This stratification weakens vertical mixing to the extent that production is only possible at the base of the euphotic zone (approx. 100m depth) where slow upward diffusion of nutrients is balanced by gravitational settling of phytoplankton and detritus.

In contrast to the summer condition, the simulated autumn deepening of the mixed layer relies strongly on the correction of temperature and salinity to allow for horizontal heat and salt transport. This supports speculation (see section 4.2) that non-local forcing associated with the Leeuwin Current, rather than local atmospheric conditions, are responsible for this autumn deepening of the mixed layer. The model demonstrates that a relatively rapid increase in mixed layer depth of this kind has the potential to trigger the enhanced production measured in May 2003 (Table 4.4). At the same time, an increase in the rate of stirring means that this production peak is characterised by an almost even vertical distribution of phytoplankton biomass throughout the upper mixed layer, and an associated increase in surface chlorophyll. This pattern is broadly consistent with both observations made at station E in May 2003 (Fig. 4.27a), and visual examination of satellite-derived surface chlorophyll. Over the three days up to and including the day of sampling in May 2003, the surface chlorophyll suggests a relatively sudden local increase in the vicinity of station E (Fig. 4.29).

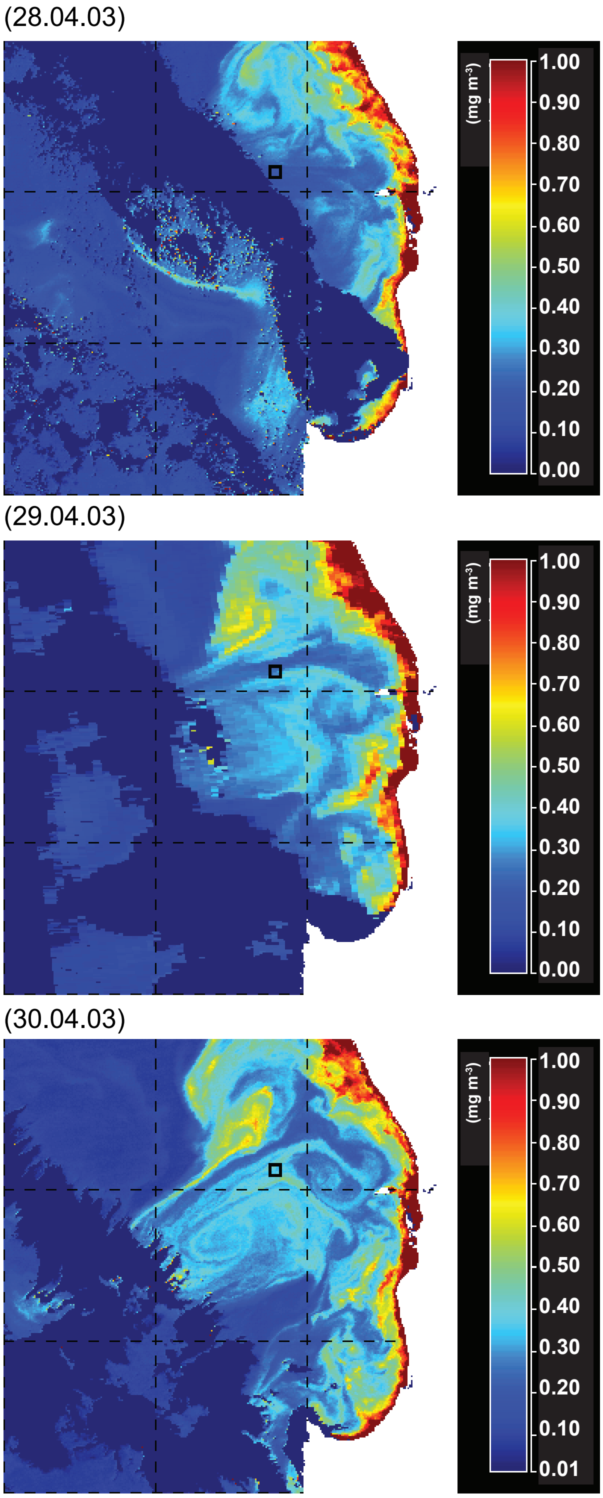

Figure 4.29: Three day sequence of surface chlorophyll (mg m^{-3}) derived from the MODIS satellite up to, and including, the day of sampling during autumn 2003. The image is overlaid with a 1^{0} grid (dashed lines) from 31 deg S, 113 deg E to 34 deg S, 116 deg E, and the location of station E (31.86 deg S, 114.79 deg E) is marked with a black square.

The evidence presented so far tends to support the theory that an increase in vertical mixing associated with the Leeuwin Current, and consequent entrainment of deep water nutrients is largely responsible for the observed peak in autumn production and chlorophyll biomass observed at station E during 2003. Notwithstanding this there are two mismatches between the model results and observations that warrant further investigation. Firstly, in an idealised 1-d ocean (and in our model simulation) entrainment of nutrients from below the mixed layer necessarily results in a deepening of the nitracline. There is no evidence of this in the data collected at station E during May 2003. We know that the slope and depth of the nitracline has a profound effect on the vertical nutrient flux, and that this model result occurs at a time when strong non-local forcing of the thermocline is necessary. This may indicate that similar forcing of the nitracline is needed. Secondly, the high levels of surface nitrate (~0.5μM) observed to accompany the autumn increase in production cannot be achieved via vertical nutrient supply in our model (Fig. 4.28b). Both results are inconsistent with the system being predominately one dimensional and suggest that the overall mechanism underlying the observed autumn increase in biomass and production is more complex.

The failure of the 1-D model to capture the observed mid-water chlorophyll maximum during winter is striking. The problem relates to the disparity between the modelled temperature field and the profile that was measured during winter 2003 (Fig. 4.26). Closer inspection of satellite imagery reveals that the August 2003 occupation of station E probably sampled cooler water from the edge of the Leeuwin Current (Fig. 4.30a). The comparison between measured and simulated surface temperature during winter (Fig 4.26a) suggests that this variability occurs on a time scale shorter than the temporal resolution of the background temperature field to which the model is constrained. Comparison with satellite images taken before and after this date (e.g. Fig. 4.30b) suggest that this may indeed have been a relatively short-lived feature (1-2 days) that resulted from a narrowing and eastward migration of the Leeuwin Current. Thus, while at times station E may have been within the warm surface waters of the Leeuwin Current (Fig. 4.30b), sometimes it may have been in cooler off-shore water (Fig. 4.30a). This could be the origin of some of the temporal variability seen in satellite sea surface temperature at station E during winter (Fig. 4.26a). It may also help explain the contrast in observed density structure and vertical chlorophyll distribution between stations E (location shown in Fig. 4.30) and D (31.77 deg S, 115.00 deg E) during August 2003 (see figures 4.18 and 4.22c) since, while station D appears to be well within the warm surface waters of the Leeuwin Current, station E is in cooler off-shore water.

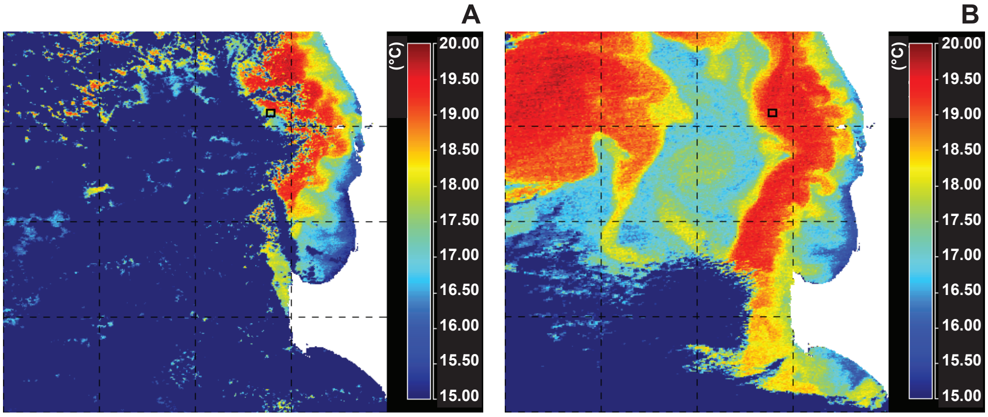

Figure 4.30: Location of station E (31.86S, 114.79E) (black square) in relation to spatial variability in sea surface temperature (colour map) from the MODIS satellite on (a) 29.08.03 and (b) 31.08.03. The maps are overlaid with a 1^0 grid covering the region 31S, 112E to 35S, 116E.

From this analysis it seem likely that the observed winter chlorophyll during 2003 is a feature that is advected into the vicinity of station E. Additional model simulations have shown that relaxation of the temperature and salinity fields to the profiles measured at station E during August (rather than the statistically derived profiles used so far) results in a vertical chlorophyll structure that more closely resembles the observations (Fig. 4.27b). While this does not resolve the issue, it does demonstrate the strong influence that changes in density structure can have on the vertical chlorophyll distribution, and highlights the difficulty in interpreting infrequent discrete measurements made at a fixed location in such a dynamic region.

Conclusions from 1-d modelling

1. The summertime deep chlorophyll maximum is a relatively stable feature that results from strong stratification of the upper water column during summer months and a balance between vertical supply of deep water nutrients and sinking.

2. Rapid deepening of the mixed layer during autumn, as a result of non-local physical forcing, and associated high rates of vertical mixing may partially account for the observed enhanced production and elevated surface chlorophyll often observed at this time. The influence of non-local nutrient supply (e.g. lateral advection) remains unclear and requires further investigation.

3. Mid-water chlorophyll maxima observed during winter at the shelf break cannot be reproduced from changes in local atmospheric conditions. Instead, they appear to be features that are more characteristic of cooler off-shore waters that are observed at times further inshore as a result of variability in water mass structure that occurs on a scale of 2-3 days.

Three-dimensional modelling

To further investigate the role of vertical mixing and upwelling in supplying deep offshore water to the surface mixed layer a number of 3-dimensional numerical experiments have also been carried out. The results are based on a one-year simulation of the transport of a dissolved conservative tracer using a 3-dimensional hydrodynamic model (see Herzfeld and Waring, 2005). Manipulation of the initial distribution and subsequent input of the tracer at the open boundaries has allowed a number of numerical experiments to be conducted.

Model Results

In the first scenario, the tracer was initially allocated everywhere in the model domain below 250m depth, the typical depth of the Leeuwin Current (Smith *et al.*1991), with a concentration of 100 units/m^3. The model was then run forward, forcing the open boundaries with the same vertical tracer profile. Figure 4.31 illustrates an example of an anticyclonic eddy simulated by the model during July 2003. During this event the tracer is mixed upward into the surface water resulting in an isolated plume with the tracer concentration within the eddy exceeding 1.8 % of the deep-water concentration (Fig. 4.32a). A sparse climatology for the nutrient distribution in the study area (Lourey *et al.*2006) indicates that nitrate concentrations in the surface layer may reach 10 % of the concentrations in the deep offshore water. The modelled ratio of the surface to deep-water concentrations of the dissolved tracer is comparable to the observed nitrate ratio, suggesting that anticyclonic eddies may play a significant role in delivering deep water nutrients to the surface mixed layer. Additional experiments with the tracer released only through the open sea-boundaries (not shown here) suggest that the water masses comprising the eddy consist of water from the Leeuwin Current (~50%), deep offshore water (~2%), offshore surface water (~20%), and inshore coastal water (~28%).

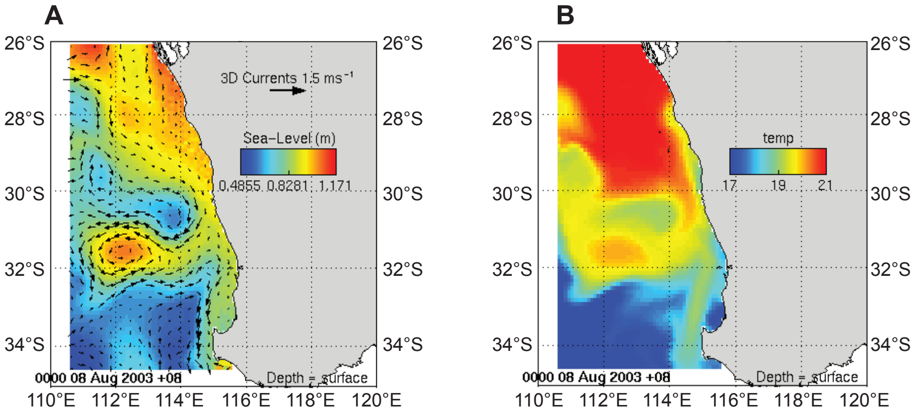

Fig. 4.31: Modelled (a) sea-surface elevation and currents (b) surface temperature.

Over the shelf area the simulated concentrations of the dissolved tracer in the first experiment do not exceed 0.4 % of the deep-water concentrations suggesting that there is no significant direct impact of water masses below 250 m depth on the shelf. Instead, it is suspected that shelf water is dominated by input from the Leeuwin Current and horizontal mixing with offshore surface water. Figure 4.32b shows a snapshot of surface concentrations of the dissolved tracer resulting from a separate experiment in which the tracer was released only through the surface section (upper 250m) of the northern boundary, representing input from the Leeuwin Current. The current follows the shelf edge in the northern part of the modelling domain and destabilises below 30S generating mesoscale eddies that propagate offshore. Due to enhanced horizontal mixing, up to 30 % of the water masses on the southern section of the shelf are represented by water masses from the Leeuwin Current, with the rest consisting of a mixture of offshore surface water and inshore coastal water.

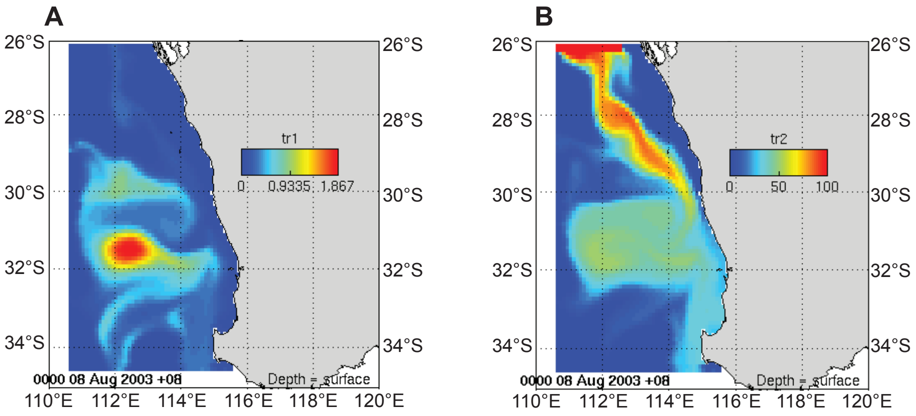

Fig. 4.32: Modelled surface concentration of the dissolved tracer (a) tracer initially allocated below 250 m depth and (b) tracer carried by Leeuwin Current.

Conclusions from 3-d modeling

The numerical experiments highlight the important role of mesoscale eddies in mixing deep and surface waters offshore, and suggest that there may be little direct impact of the deep water on the shelf during the simulation period. These modelling results are consistent with a general understanding of the regional oceanography.

4.4 A regional 3-D hydrodynamic-coupled biogeochemical model

Karen Wild-Allen and Uwe Rosebrock

CSIRO Marine and Atmospheric Research

Introduction

Dynamic mesoscale currents, jets and eddies occur along the continental shelf edge off western WA and mediate the biogeochemical interactions between coastal and oceanic waters. At the regional scale, remote sensing provides synoptic information on surface elevation, temperature and ocean colour; however it is not possible to determine reliable nutrient concentrations for the region or subsurface information from space. In-water observations are more difficult to obtain and existing data have limited spatial and temporal coverage. A 3D biogeochemical model provides a vehicle to synthesise our existing knowledge of the marine system off WA with simulations presenting an integrated hypothesis of the regional scale hydrodynamics, sediment and marine biogeochemistry, for validation against observations. The specific objective of this modelling exercise is to elucidate the transfer of nutrients between coastal and ocean waters off WA.

Model Description

The biogeochemical model (Baird *et al.* 2003; Wild-Allen *et al.* 2004) is dynamically coupled to a hydrodynamic model (Herzfeld and Waring 2005) and a sediment model (Margvelashvili 2003) which together form the CSIRO Environmental Modelling Suite (EMS). Within the biogeochemical model, processes such as phytoplankton growth and nutrient remineralisation are selected from a library of possible formulations. For the SRFME regional 3D biogeochemical model, the existing process library was extended to include formulations based on the model of Palmer and Totterdell (2001), which is simpler and therefore computationally more efficient than the existing EMS formulations. This allowed a 1 year simulation to be completed in <5 days compared with >20 days for the original EMS model (Fig. 4.33).

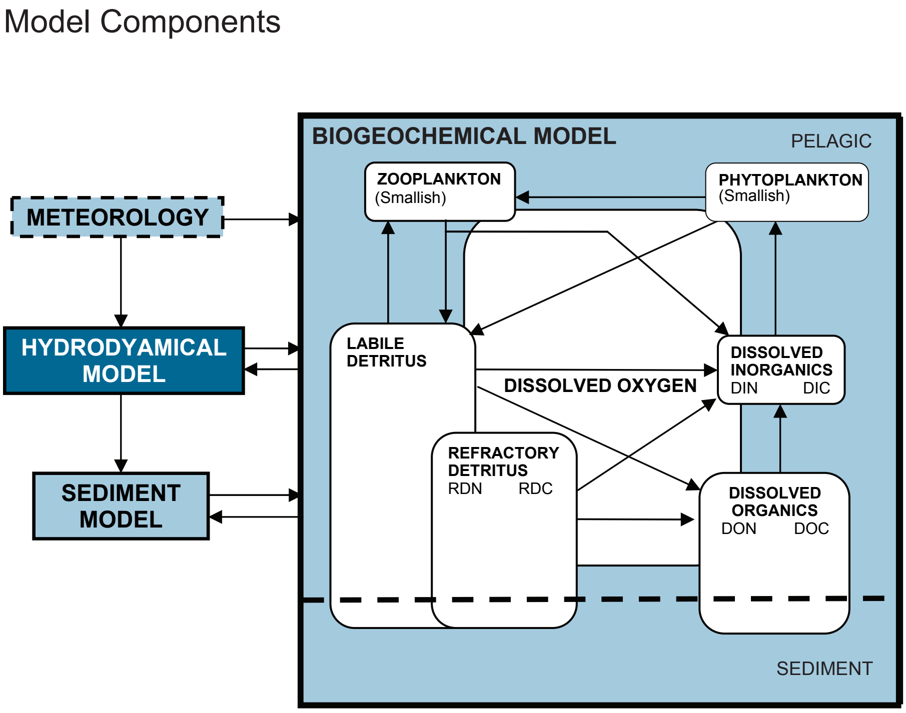

Figure 4.33: The main components of the biogeochemical model.

The biogeochemical model simulates the cycling of carbon, nitrogen and oxygen through dissolved and particulate phases. The single phytoplankton compartment represents small flagellates, and photoautotrophic pico- and nano-plankton which are prevalent off WA. Phytoplankton growth rate is calculated as a 24 hour mean, less respiration, from Michaelis-Menton formulations for light and nutrient controlled growth (Palmer & Totterdell 2001). Losses occur due to mortality, formulated as a quadratic above a threshold concentration, and zooplankton grazing (Palmer & Totterdell 2001).

The single zooplankton compartment represents microzooplankton less than 200µm in size such as *Tintinnids, Ciliates, Rotifers,* small copepod nauplii and polychaeta larvae. Zooplankton graze on phytoplankton and labile detritus proportional to their relative nitrogen biomass and according to a Holling Type 3 formulation (Holling 1965). This includes a threshold prey refuge and saturated grazing intensity at high prey concentrations. Of the ingested material portions are assimilated to zooplankton biomass, defecated to labile detritus, and released as DIN (Palmer & Totterdell 2001). In the SRFME model phytoplankton, zooplankton and labile detritus are assumed to have the Redfield elemental ratio of 106C:16N. Zooplankton mortality and predation by higher trophic levels are formulated as the sum of a linear and quadratic term and return labile detritus and DIN to the ecosystem.

Modelled labile detritus is remineralised, at rates mediated by bacteria, fungi and micro-organisms, into dissolved organic and inorganic material and refractory particulate detritus. These compartments have independent carbon and nitrogen pools as nitrogen is typically remineralised more rapidly than carbon. In addition to recycling of nutrient, detritus also contributes to the attenuation of PAR through the water column, along with optically active CDOM and plankton biomass.

Table 4.5. Biogeochemical model parameters.

Parameter	Value	Unit
Phytoplankton nominal radius	2.5E-6	m
Phytoplankton light absorption coefficient	50000	/m
Half saturation for phytoplankton N uptake	1.401	mgN/m3
Maximum photosynthetic rate @10˚C	0.8	/d
Phytoplankton initial slope of P-I curve	0.055	(W/m2)-1/d
Phytoplankton respiration	0.02	/d
Phytoplankton mortality (quadratic)	0.00357	/d /mgNm-3
Phytoplankton sinking rate	3.0	m/d
Phytoplankton N:Chl ratio	7.0	mg N/mg Chl
Zooplankton grazing prey threshold	0.1	mgN/m3
Zooplankton maximum grazing rate	1.0	/d
Half saturation for zooplankton grazing	10.5075	mgN/m3
Zooplankton growth efficiency	0.6	-
Fraction of growth inefficiency lost to detritus	0.5	-
Zooplankton mortality (linear)	0.0	/d
Zooplankton mortality (quadratic)	0.0143	/d /mgNm-3
Fraction of mortality lost to detritus	0.5	-
Pelagic labile detritus breakdown rate	0.1	/d
Refractory detritus breakdown rate	0.0036	/d
Dissolved organic matter breakdown rate	0.00176	/d
Fraction of labile detritus converted to DOM	0.01	-
Fraction of labile detritus converted to refractory detritus	0.19	-
Fraction of refractory detritus converted to DOM	0.05	-
Detrital sinking rate	-3.5e-05	m/s
Background attenuation of sea water	0.1	/m
Detrital nitrogen specific attenuation coefficient	0.0038	/m
TSS specific attenuation coefficient	30.0	/m/kg m-3
DON specific attenuation coefficient	0.0009	/m
O2 half saturation rate for aerobic respiration	500.0	mg O /m3
Temperature coefficient for rate parameters (Q10)	2.0	

Model Initialisation and Boundary Conditions

The Environmental Modelling Suite was implemented on a 10km grid (Fig. 4.34) with 34 layers in the vertical which gave a runtime ratio of ~70:1 [~5.5 days for 1 year simulation].

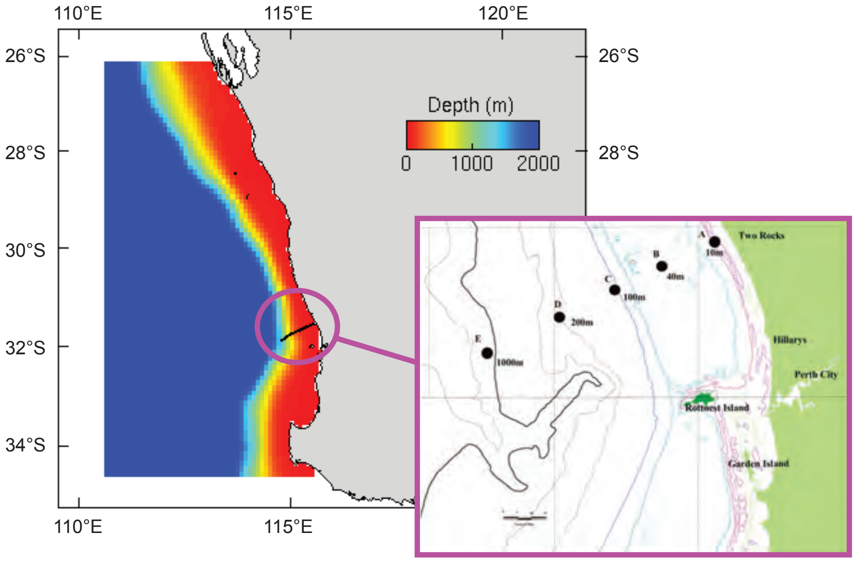

Figure 4.34: Bathymetry of 3D regional model domain with Two Rocks transect shown for scale.

The hydrodynamical model (see Herzfeld and Waring, 2005) was initialised on the 3-d grid with synTS temperature and salinity fields. SynTS is a routine CSIRO product (available on ftp.marine.csiro.au) that provides daily temperature and salinity fields derived, on a statistical basis, from sea-surface height and temperature. During the model runs, synTS also provides open boundary conditions at 'upstream' boundary points. Surface fluxes were specified from the NCAR Reanalysis data set (http://dss.ucar.edu/pub/reanalysis/). To reproduce the structure of the Leeuwin Current and its eddies, the model is constrained to (satellite-derived) sea-surface height on a 520-second relaxation time-scale.

Few observations are available throughout the region to initialise or provide boundary conditions for the biogeochemical model, so synthetic fields of dissolved inorganic nitrogen were constructed from proxy relationships between temperature, salinity and nitrogen. For nitrogen all available observations throughout the region were plotted against observed temperature and salinity (Fig. 4.35) and a curve fitted through the data (pers. comm. Thomas Moore, CSIRO).

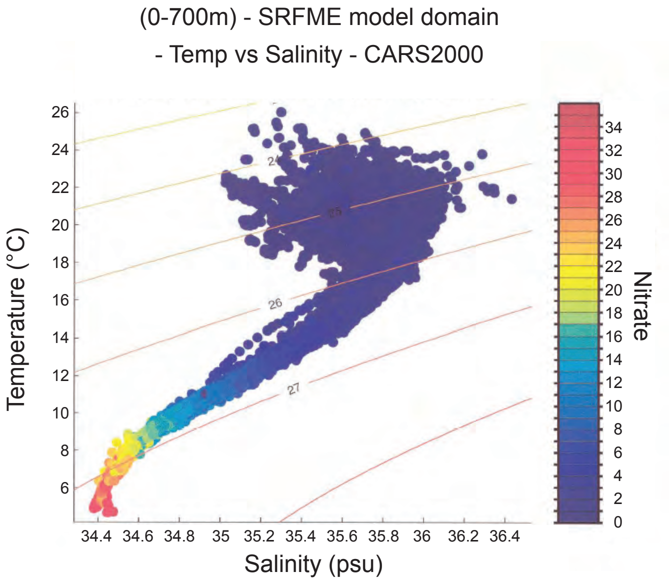

Figure 4.35: Concurrent observations of nitrogen concentration (µM), temperature and salinity from the surface to 700m throughout the SRFME regional model domain.

Above 200m there was considerable scatter in the data and the relationship between temperature, salinity and nitrogen was poorly constrained. This is likely due to episodic injection of nitrogen into surface waters and rapid assimilation by phytoplankton, giving a wide range of possible surface nitrogen concentrations. Further exploration of the relationship, with respect to season, biogeochemical provinces and recent mesoscale activity, proved inconclusive due to the relative sparse spatial and temporal data coverage. The relationships used to estimate DIN (in mgN/m3) from temperature and salinity are given for each depth layer in Table 4.6 with background concentrations constrained to 0.1 mgN/m3. [By this formulation the surface waters of the Leeuwin Current were synthesised to supply negligible surface nutrient concentrations (Fig. 4.36).]

Table 4.6 Relationships used to estimate dissolved inorganic nitrogen (DIN) as a function of temperature (T) and salinity (S) for 3 depth ranges

Variable	**Initial Concentration**		**Unit**
	Pelagic	**Sediment**	
Small phytoplankton biomass	0.8	0.0	mgN/m3
Small zooplankton biomass	0.2	0.0	mgN/m3
Labile detritus	0.0	200.0	mgN/m3
Refractory detrital nitrogen	0.0	2000.0	mgN/m3
Refractory detrital carbon	0.0	20000.0	mgC/m3
Dissolved organic nitrogen	10.0	20.0	mgN/m3
Dissolved organic carbon	100.0	200.0	mgC/m3
Dissolved inorganic nitrogen	Synthetic N	500.0	mgN/m3
Dissolved inorganic carbon	24000.	24000.	mgC/m3
Dissolved oxygen	8000.0	8000.0	mgO/m3

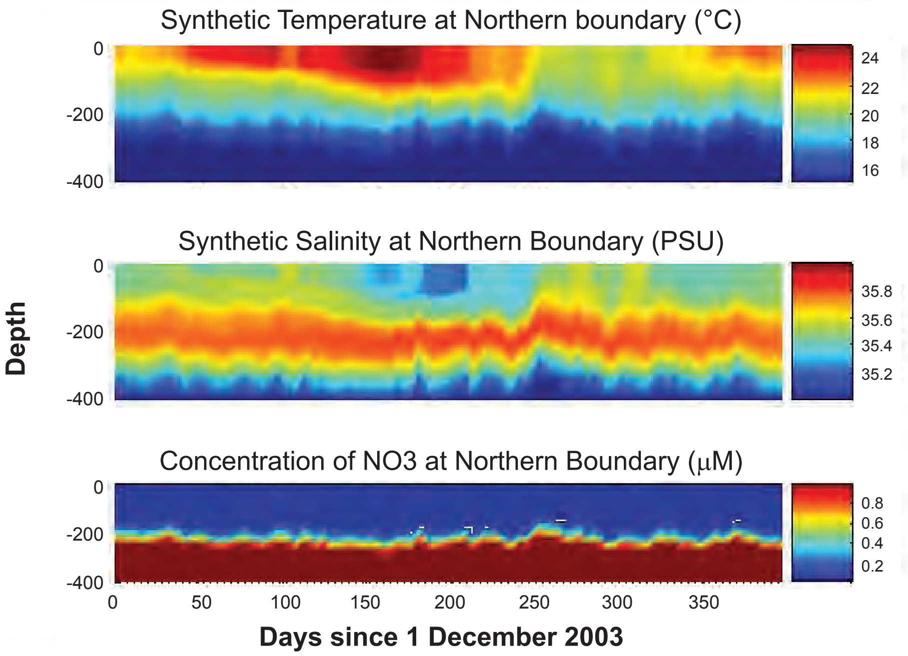

Figure 4.36: Time series of synthetic temperature, salinity and nitrogen at the mid-point of the northern boundary. The Leeuwin Current is shown as a winter pulse of warm low salinity surface water, with low nutrient concentration.

At the southern boundary profiles of nitrogen derived from synthetic temperature and salinity were found to have a significantly shallower nutricline than observations in the CARS database. Nutrient data from this sub-region were extremely sparse and therefore deemed insufficient to generalise a reliable synthetic temperature-salinity-nitrogen relationship. The upstream boundary condition was therefore specified with a spatial and temporal mean profile derived from observations (Fig. 4.37). Work is ongoing to source and collate more recent observations in the region to improve all three boundary conditions.

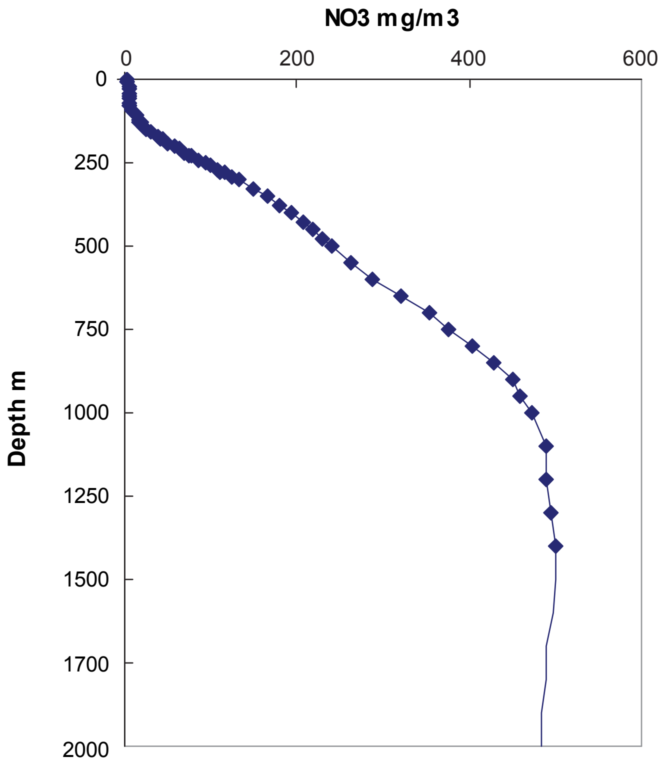

Figure 4.37: Spatial and temporal mean nitrate profile derived from observations (mostly along latitude 34˚S).

Model phytoplankton biomass was initialised and supplied along the model boundaries from images of remotely sensed sea surface chlorophyll. These were converted to nitrogen biomass by assuming a nitrogen to chlorophyll ratio of 7mg N/mg Chl. Near-shore values of remotely-sensed chlorophyll were found to be considerably higher than observed, so the model was initialised with the mean offshore value. Derived surface concentrations of phytoplankton biomass were assumed to represent the concentration throughout the surface mixed layer, (calculated from synTS temperature profiles) or to a maximum depth of 50 m. There were insufficient observations to estimate or infer any subsurface vertical structure in the distribution of phytoplankton biomass throughout the model region.

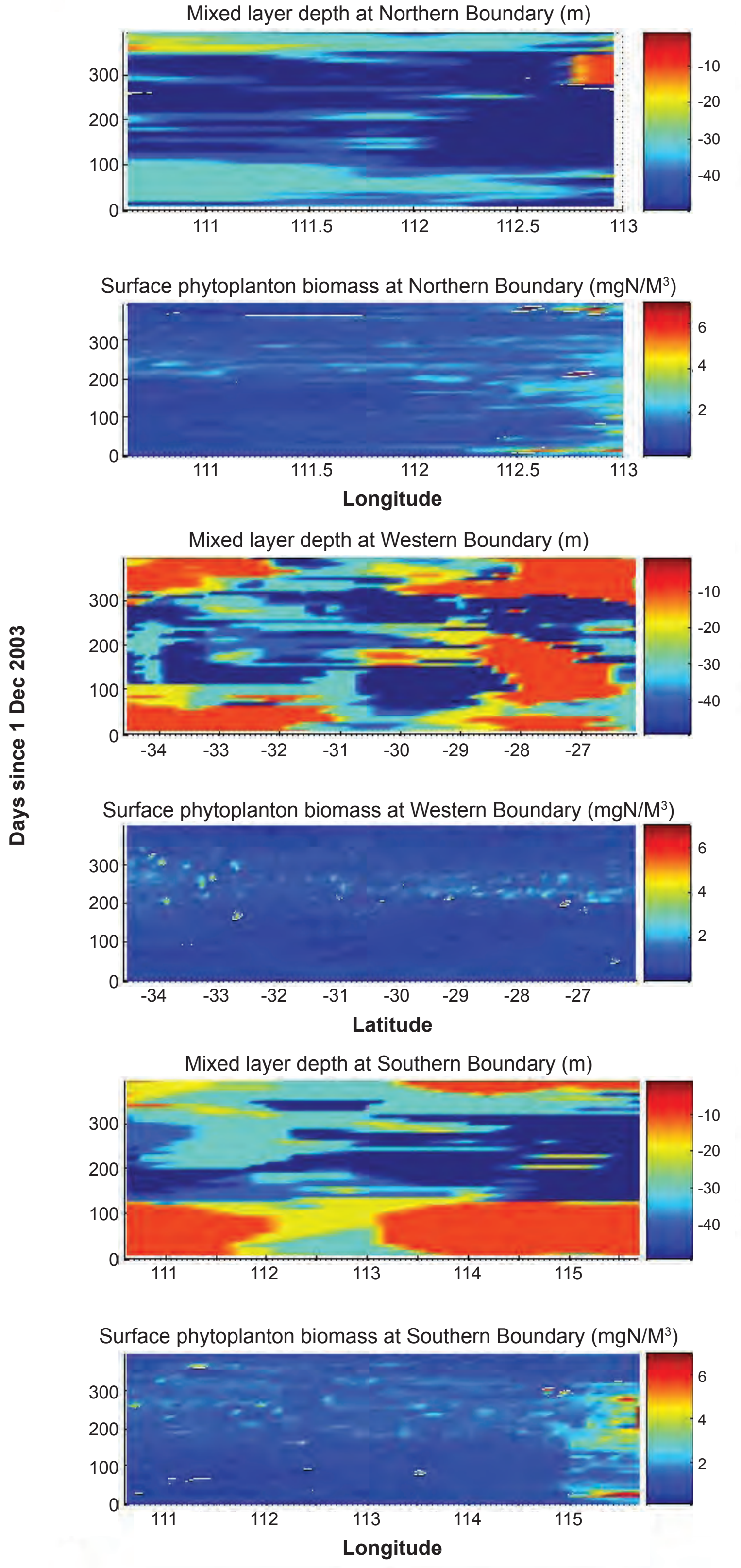
Mixed layer depth at Northern Boundary (m)

Surface phytoplanton biomass at Northern Boundary (mgN/M^3)

Mixed layer depth at Western Boundary (m)

Surface phytoplanton biomass at Western Boundary (mgN/M^3)

Mixed layer depth at Southern Boundary (m)

Surface phytoplanton biomass at Southern Boundary (mgN/M^3)

Figure 4.38: Time series of surface mixed layer depth (top panel) and derived phytoplankton biomass along the (a) northern, (b) western and (c) southern boundary.

All other biogeochemical model variables were initialised with spatially uniform nominal concentrations (Table 4.7) and parameterised at the model boundaries with a statistically adjusted no flux condition. During the first month of simulation the biogeochemical variables rapidly adjust to quasi-steady state concentrations determined by the ambient light, nutrient field and mixing. Results are shown for a year following the first month of simulation.

Table 4.7. Spatially uniform initial concentrations of biogeochemical variables.

Variable	**Initial Concentration**		**Unit**
	Pelagic	**Sediment**	
Small phytoplankton biomass	0.8	0.0	mgN/m3
Small zooplankton biomass	0.2	0.0	mgN/m3
Labile detritus	0.0	200.0	mgN/m3
Refractory detrital nitrogen	0.0	2000.0	mgN/m3
Refractory detrital carbon	0.0	20000.0	mgC/m3
Dissolved organic nitrogen	10.0	20.0	mgN/m3
Dissolved organic carbon	100.0	200.0	mgC/m3
Dissolved inorganic nitrogen	SynTSN	500.0	mgN/m3
Dissolved inorganic carbon	24000.	24000.	mgC/m3
Dissolved oxygen	8000.0	8000.0	mgO/m3

Model Results and Observations

Example model results and observations are presented from biogeochemical model run 24 which simulates Jan-Dec 2003. In this simulation, the hydrodynamical model is started with a stationary current field and synTS, and relaxed to surface elevation, derived from altimetry (as part of the synTS product), on a 520-second timescale. In the absence of strong relaxation the simulated hydrodynamics diverge from the observed fields after 7-10 days. Relaxation of the surface, but not internal, fields ensures consistent treatment of vertical mixing for physical, sediment and biogeochemical tracers, and gives an adequate representation of the spatial and temporal evolution of mesoscale fronts and eddies associated with the Leeuwin Current. Simulated temperature and salinity agreed well with observations made along the 'Two Rocks' transect except for salinity in inshore waters which was underestimated by the model between January and May (Fig. 4.39). This was probably due to the inadequate resolution of the bathymetry in the coastal reef and lagoon systems over the model 10 km grid and the necessarily poor representation of near-shore circulation and evaporation.

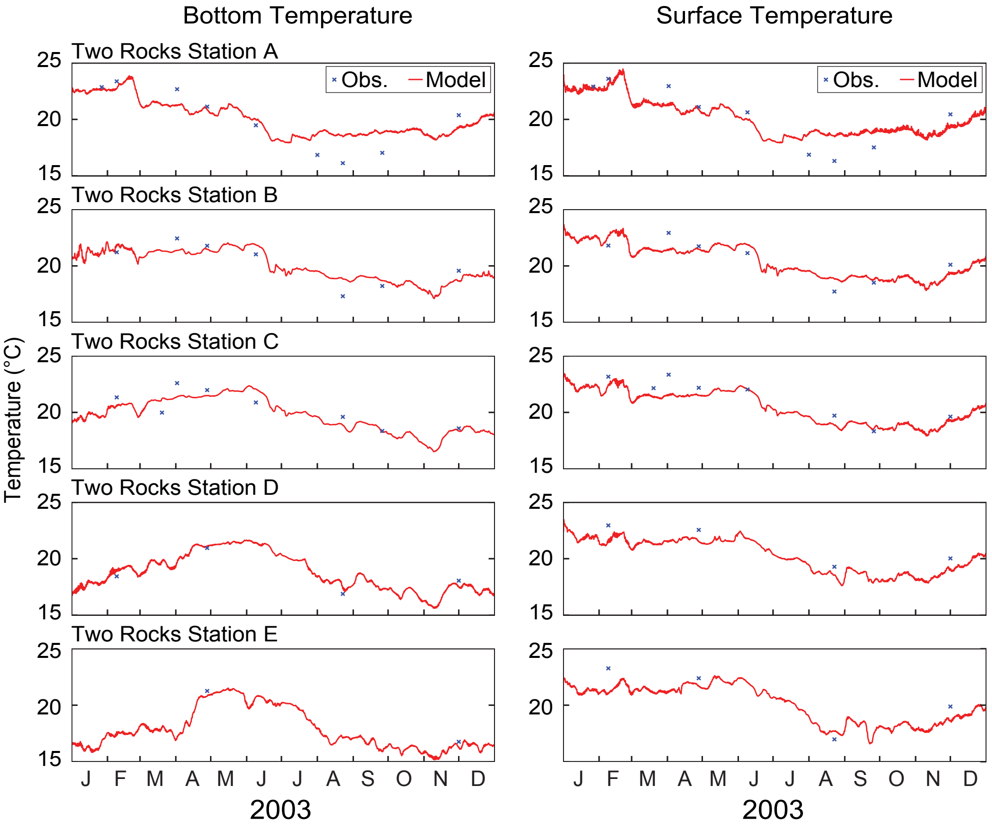

Figure 4.39: Modelled and observed surface (left) and bottom (right) water temperature at stations along the Two Rocks transect.

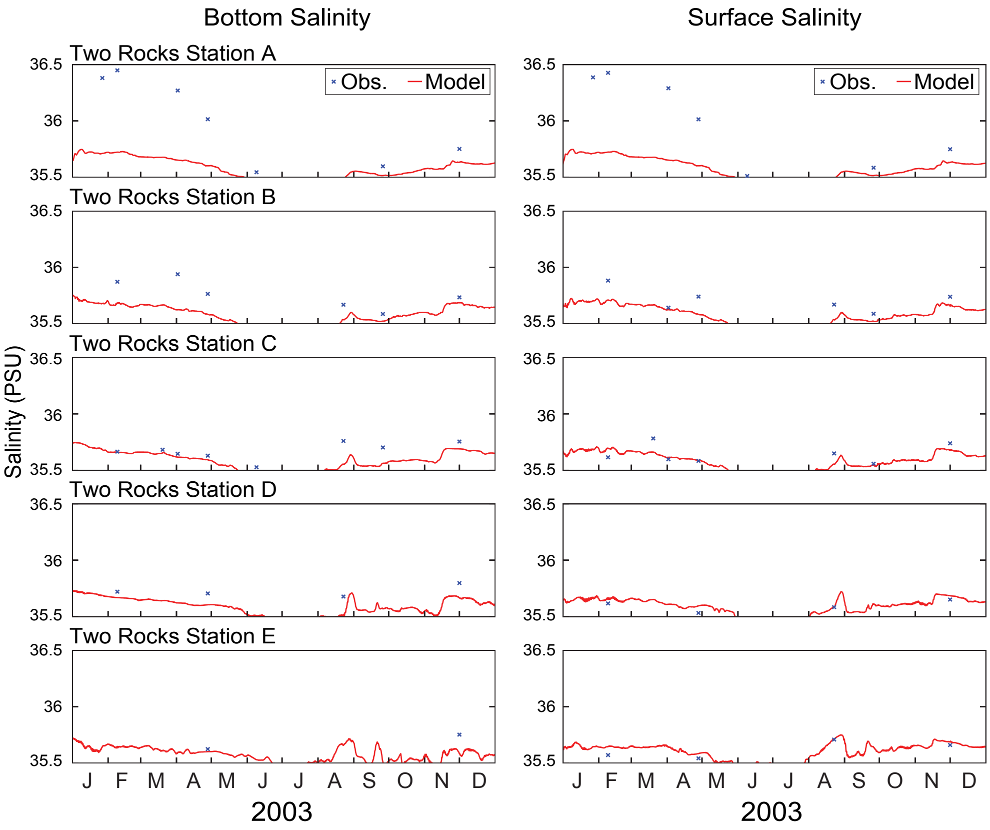

Figure 4.40: Modelled and observed surface (left) and bottom (right) water salinity at stations along the Two Rocks transect.

The vertical structure of temperature, salinity, chlorophyll and nitrate observed at Two Rocks are reasonably simulated by the model. Summer observations (Fig. 4.40) pre-date the model simulation, although the initial temperature, salinity, nitrate and surface chlorophyll fields have similar magnitude.

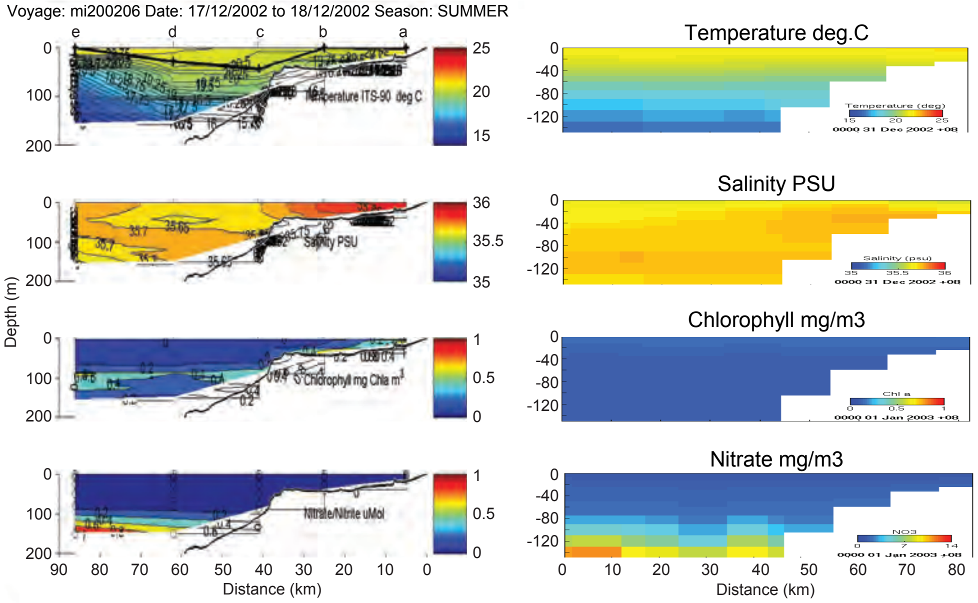

Figure 4.41: Summer observed (left) and modelled (right) vertical structure in temperature, salinity, chlorophyll and nitrate (note similar colour scale as 1μM=14mg/m3).

In autumn, the observed thermal and salinity structures show the Leeuwin Current as a warm, reduced salinity water mass located at the shelf break. Model representation is more diffuse with cooler temperatures across the whole transect and the absence of high salinity water on the shelf. Modelled nitrate and chlorophyll concentrations were similar in magnitude to those observed offshore although the modelled nutricline was ~100 m deeper and the observed inshore values of 1μM nitrate and 1mg Chl/m3 were not achieved.

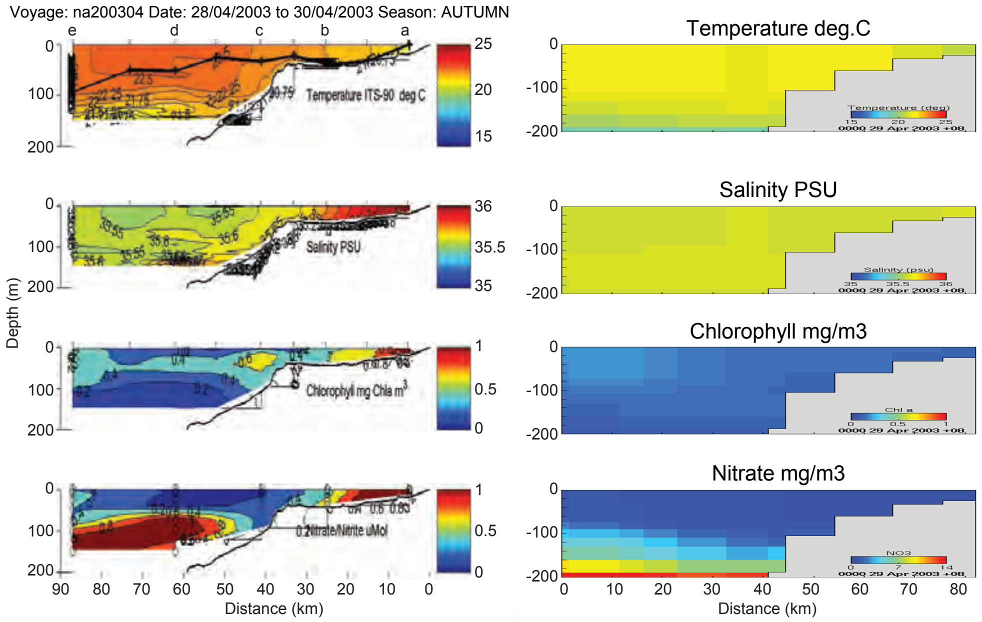

Figure 4.42: Autumn observed (left) and modelled (right) vertical structure in temperature, salinity, chlorophyll and nitrate (note similar colour scale as 1μM=14mg/m3).

Winter observations depict a cooler water column, with significant thermal and saline stratification bounding Leeuwin Current water at the shelf edge. Modelled fields show warm low salinity water flooding the whole shelf and fail to reproduce the observed subsurface salinity maximum at the shelf edge. Simulated nitrate and chlorophyll distributions are similar to the observed sections, although modelled chlorophyll concentration is less than observed and does not form a subsurface chlorophyll maximum offshore.

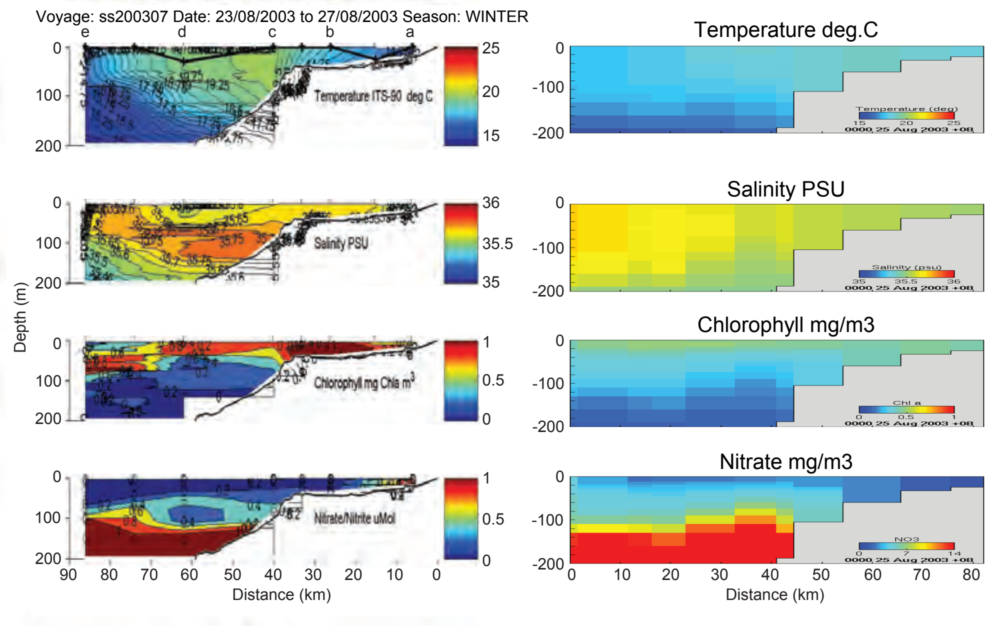

Figure 4.43: Winter observed (left) and modelled (right) vertical structure in temperature, salinity, chlorophyll and nitrate (note similar colour scale as 1μM=14mg/m3).

The observed temporal evolution of chlorophyll at stations along the Two Rocks transect shows a distinct seasonal cycle which is reproduced to some extent by the model. The model simulates elevated chlorophyll biomass in winter and spring up to 1mg Chl/m3 but does not reproduce the elevated concentrations observed at stations A, B and C in autumn. Periods of increased concentration are distinctly episodic, suggesting higher frequency variability than would have been captured by the sampling program. Simulated nitrate concentrations show similar episodic events which elevate the nutricline or mix deep water nitrate throughout the water column. Candidate mechanisms for intermittent perturbation of the nutricline include wind mixing, the breakdown of thermal stratification and, at offshore stations, interaction of mesoscale features such as Leeuwin Current fronts and eddies with the nutricline.

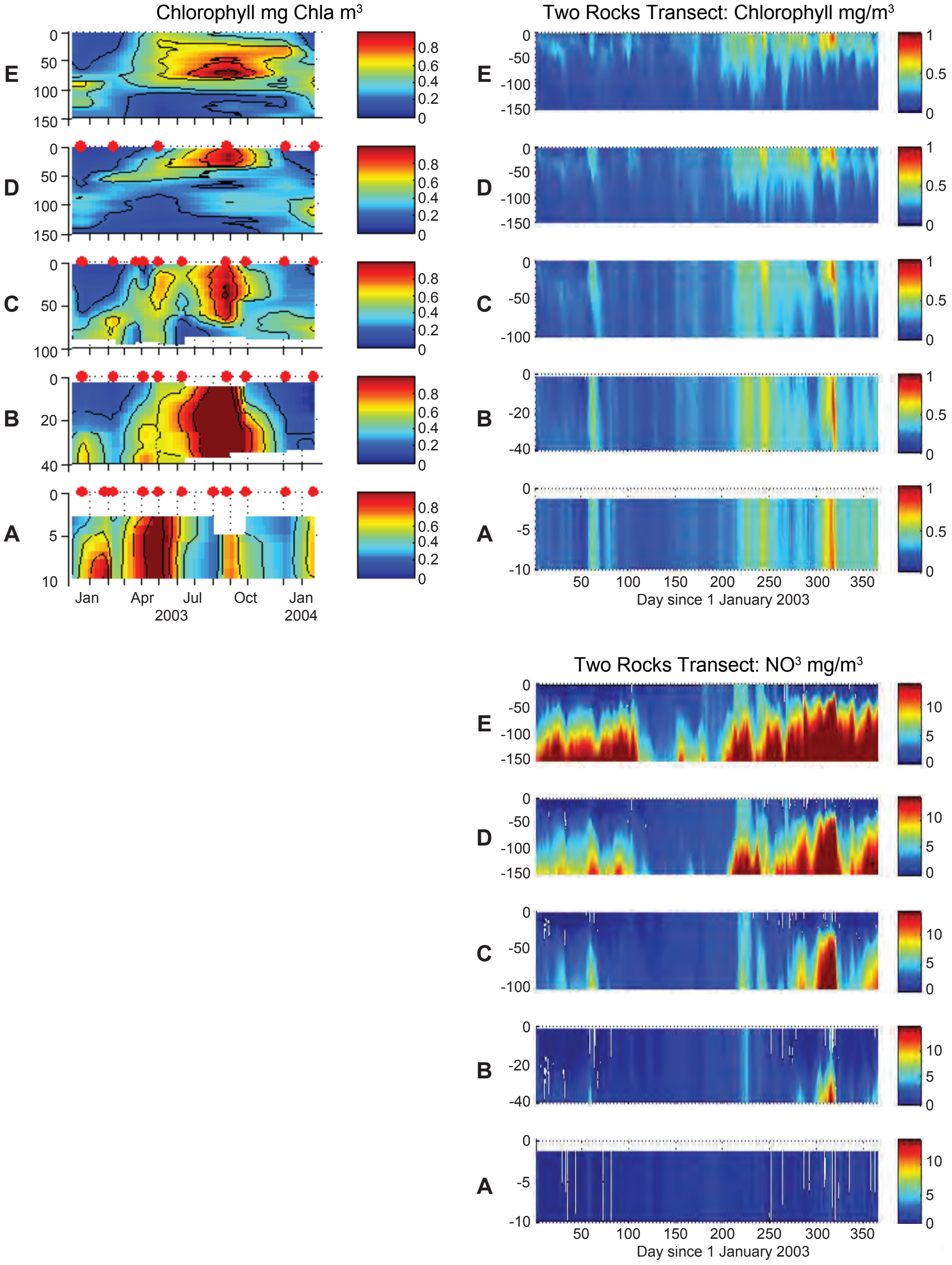

Figure 4.44: Observed (a) and modelled temporal evolution of the vertical distribution of chlorophyll (b) and DIN (c) at stations along the Two Rocks transect.

Surface chlorophyll concentrations derived from SeaWIFS remotely sensed data show a clear seasonal cycle with maximum concentration in winter. Elevated concentrations are also present along the coast for much of the year although this could be due in part to suspended sediment and or elevated CDOM. Modelled surface chlorophyll concentrations were of similar magnitude to the observed data but the spatial distribution was wrong as the model failed to simulate high concentrations adjacent to the coast. The model simulated a seasonal increase in chlorophyll in winter-spring which was greatest in the offshore eddy field and close to the south-west boundary of the model.

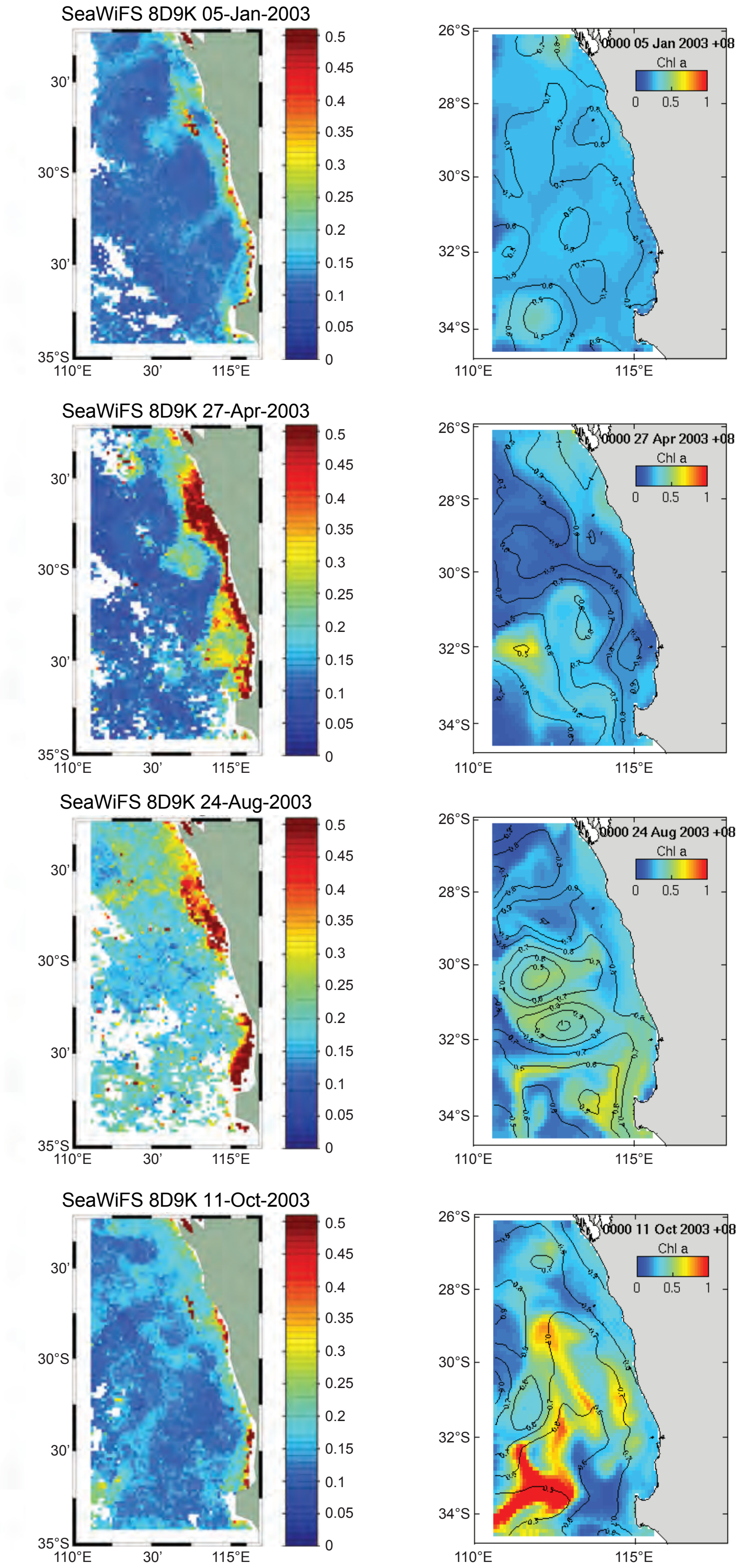

Figure 4.45: SeaWIFS sea surface chlorophyll (left) and modelled surface chlorophyll with surface elevation contours overlayed (right) for summer, autumn, winter and spring.

High resolution Seasoar observations through a warm core eddy in October 2003 show a pool of warm water depressing the thermocline to ~300m with elevated chlorophyll biomass on the perimeter. Model results along the equivalent sections (with necessarily coarser resolution) depict a similar structure, although the modelled thermocline is more diffuse and the chlorophyll biomass occurs at shallower depths.

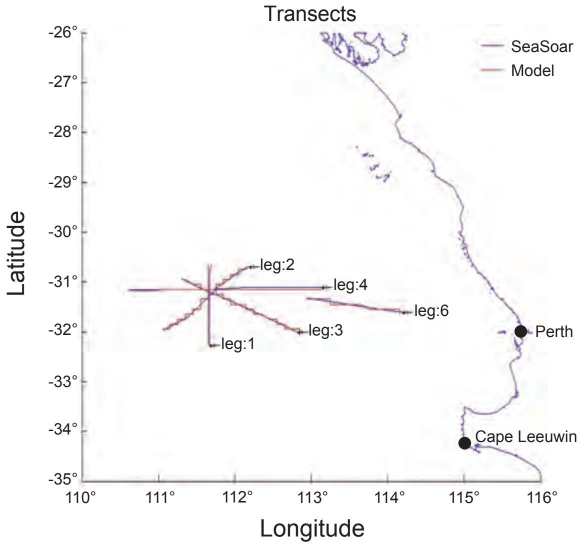

Figure 4.46: Seasoar transects 1, 2, 3, 4 & 6 (black), and equivalent model transects (red).

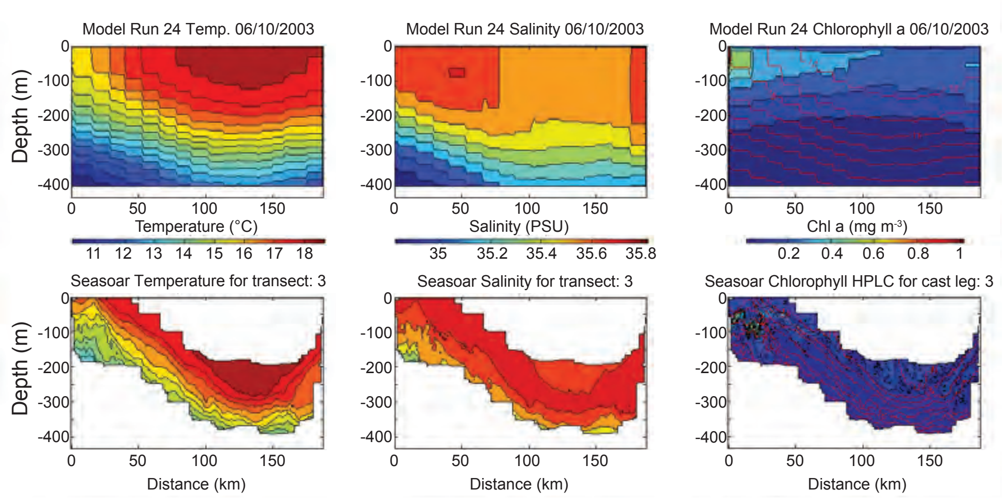

Figure 4.47: Model results (upper panels) and observations (lower panels) for temperature (left) salinity (middle) and chlorophyll with isotherms overlaid (right) along Seasoar leg 3.

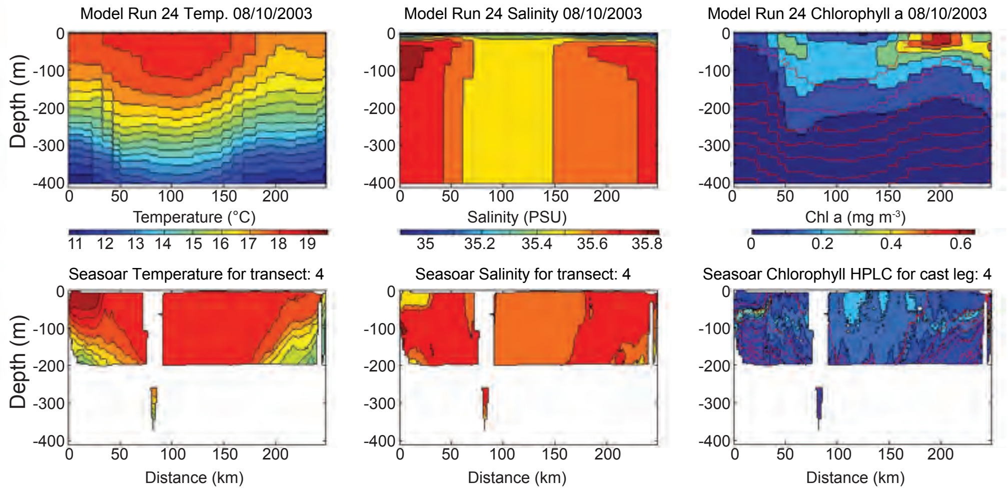

Figure 4.48: Model results (upper panels) and observations (lower panels) for temperature (left) salinity (middle) and chlorophyll with isotherms overlaid (right) along Seasoar leg 4.

Discussion

The biogeochemical model simulations to date have shown considerable potential to integrate our understanding of the hydrodynamical forcing, sediment dynamics and biogeochemical cycling active at the regional scale off WA. Comparison of the model against observations has raised important scientific questions associated with the validity of model relaxation schemes, the accuracy of synT/S and the interpolation of spatially (3D) and temporally sparse biogeochemical data onto a dynamic mesoscale field. This study has been hampered by the paucity of regional scale biogeochemical data and its achievements to date should be viewed in perspective of the assumptions necessary to initialise and force the model at the boundaries. Accordingly current model results are at best an hypothesis generated from estimations for many biogeochemical parameters and variables, and results are likely to change significantly as the model validation process progresses.

Model results to date have failed to demonstrate elevated chlorophyll concentrations adjacent to the coast. This is likely due in part to the omission of coastal nutrient sources in the model, which are thought to play a significant role in the inner shelf biogeochemistry. Candidate sources are rivers, runoff, sewerage discharge and groundwater and work is currently in progress to include these in the model. In addition, seasonally mediated resuspension of bottom sediments and nutrients by stormy weather could inject nutrients into the euphotic layer, particularly in shallow coastal regions, although this may not be well resolved on the current 10km grid. Future work includes the implementation of higher resolution models to simulate shelf and lagoon scale processes.

Offshore, modelled chlorophyll concentrations exceeded spatial fields observed in remote sensing and subsurface chlorophyll maxima were seldom simulated. This suggests that phytoplankton sinking may currently be under represented in the model and the depth of the euphotic zone could be too shallow. As the model calibration process proceeds, sensitivity of the simulated phytoplankton fields to parameters such as sinking rate will be assessed and the performance of alternative offshore boundary conditions will be evaluated. In the current version of the model phytoplankton growth is simulated, for efficiency, as a 24 hour mean rate. This is applied to a 24 hour mean light field which has a euphotic layer depth considerably shallower than would occur at noon each day. Further work is in progress, to include the diurnal resolution of phytoplankton growth and respiration in the EMS biogeochemical model which could better resolve the depth of phytoplankton growth in oligotrophic waters.

Following model validation existing tools will be used to identify the active biogeochemical pathways and evaluate the transfer of nutrients between coastal and oceanic waters off WA. Scenario simulations will enable a range of existing hypotheses to be tested and results will be available to direct further observations to target key unresolved issues.

References

Anon, 1996. Southern Metropolitan Coastal Waters Study – Final Report. Department of Environment Protection, Western Australia.

Anon, 2003a. A Partner in Sustainability. Wastewater Treatment Branch Annual Report 2002/2003. Water Corporation of Western Australia.

Anon, 2003b. Use of Cape Peron Outlet Pipeline to Dispose of Industrial Wastewater to Sepia Depression Kwinana. Public Environmental Review. Water Corporation of Western Australia.

Baird, M.E., S.J. Walker, B.B. Wallace, I.T. Webster, J.S. Parslow, 2003. The use of mechanistic descriptions of algal growth and zooplankton grazing in an estuarine eutrophication model. *Estuarine, Coastal and Shelf Science* 56:685–695.

Berelson, W. M., Heggie, D., Longmore, A., Kilgore, T., Nicholson, G., and Skyring, G. 1998. Benthic nutrient recycling in Port Phillip Bay, Australia. *Estuarine Coastal and Shelf Science*, 46, 917-934.

Black, R. E., Lukatelich, R. J., McComb, A. J., and Rosher, J. E. 1981. Exchange of water, salt, nutrients and phytoplankton between Peel Inlet, Western Australia, and the Indian Ocean. *Australian Journal of Marine and Freshwater Research* 32, 709-720.

Brunskill, G.J., Zagorskis, I., and Pfitzner J., (2002). Carbon burial rates in sediments and a carbon mass balance for the Herbert River Region of the Great Barrier Reef continental shelf, North Queensland, Australia. *Estuarine, Coastal and Shelf Science*, 54, 677-700.

Buckee, J., Rosich, R.S., and Van Senden, D.C., (1994). Water Quality Data.

Capone, D.G. 2001 Marine nitrogen Fixation: what's the fuss?

Condie, S.A., Dunn, J.R., 2006. Seasonal characteristics of the surface mixed layer in the Australasian region: Implications for primary production regimes and biogeography. *Marine and Freshwater Research,* 57, 569-590.

Cresswell, G.R., Golding, T.J., 1980. Observations of a south-flowing current in the southeastern Indian Ocean. *Deep-Sea Research* 27A, 449-466.

Dunn, J.R., Ridgway, K.R., 2002. Mapping ocean properties in regions of complex topography. Deep Sea Research I 49, 591-604

Feng, M., Meyers, G., Pearce, A., Wijffels, S., 2003. Annual and interannual variations of the Leeuwin Current at 32ºS. *Journal of Geophysical Research* 108, 2255, doi:10.1029/2002JC001763.

Gersbach, G.H., Pattiaratchi, C.B., Ivey, G.N., Cresswell, G.R., 1999. Upwelling on the south-west coast of Australia – source of the Capes Current. *Continental Shelf Research* 19, 363-400.

Godfrey, J.S., Ridgway, K.R., 1985. The large-scale environment of the poleward-flowing Leeuwin Current, Western Australia: Longshore steric height gradients, wind stresses and geostrophic flow. *Journal of Physical Oceanography* 15, 481–495.

Greenwood, J., Feng, M., Waite, A. (2006). The influence of vertical mixing on biological production in two contrasting mesoscale eddies in the south eastern Indian Ocean. *Deep-Sea Research*, in press.

Hanson, C.E., 2004. Oceanographic forcing of phytoplankton dynamics in the coastal eastern Indian Ocean. Ph.D. Thesis, University of Western Australia, Perth, Australia, unpublished.

Herzfeld, M & Waring, J.R. 2005. SHOC: Sparse hydrodynamic ocean code version 1.0: user manual. CMAR CSIRO Report, Hobart pp.113.

Holl, C.M., Waite, A.M., Pesant, S., Thompson, P., and Montoya, J.P., (in press). Unicellular Diazotrophy as a Source of Nitrogen to Leeuwin Current Coastal Eddies. *Deep-sea Research Part* 2.

Holling, C.S., 1965. The functional response of predators to prey density and its role in mimicry and population regulation. Memoirs of the Entomological Society of Canada No. 45, 61pp.

Holloway, P. E., Humphries, S. E., Atkinson, M., and Imberger, J. 1985. Mechanisms for nitrate supply to the Australian North West Shelf. *Australian Journal of Marine and Freshwater Research* 36, 753-764.

Johannes, R. E. 1980. The ecological significance of the submarine discharge of groundwater. *Marine Ecology Progress Series* 3, 365-373.

Johannes, R. E., Pearce, A. F., Wiebe, W. J., Crossland, C. J., Rimmer, D. W., Smith, D. F., and Manning, C. 1994. Nutrient characteristics of well-mixed coastal waters off Perth, Western Australia. *Estuarine, Coastal and Shelf Science* 39, 273-285.

Keesing, J.K. and J.N. Heine (Eds.) (2005). *Strategic Research Fund for the Marine Environment (SRFME): Interim Final Report.* 385 pp. Strategic Research Fund for the Marine Environment, CSIRO, Australia.

Large, W. G., Pond, S., 1981. Open ocean momentum flux measurements in moderate to strong winds. *Journal of Physical Oceanography* 11, 324-481.

Longhurst, A.R., 1995. Seasonal cycles of pelagic production and consumption. *Progress in Oceanography* 36, 77-167.

Lord, D.A., Hillman, K., 1995. Summary report. Perth Coastal Waters Study. Water Authority of Western Australia.

Lourey M., Dunn J., Waring J. (2006) A mixed-layer nutrient climatology of Leeuwin Current and Western Australian Shelf waters: Seasonal nutrient dynamics and biomass. *Journal of Marine Systems*, 59, 25-51.

Margvelashvili, N. 2003. MECOSED: Model for estuarine and coastal sediment transport. CMAR CSIRO Report, Hobart pp53.

McMahon, K., and Walker, D. I. 1998. Fate of seasonal, terrestrial nutrient inputs to a shallow seagrass dominated embayment. *Estuarine, Coastal and Shelf Science* 46, 15-25.

Moore, T.S., 2005. Physical oceanographic controls on phytoplankton distribution in the Banda Sea and Western Australian region. Ph.D. Thesis, University of Tasmania, Hobart, Australia, unpublished.

Palmer J.R. & Totterdell, I.J. 2001. Production and export in a global ocean ecosystem model. *Deep-Sea Research I* 48: 1169-1198.

Pearce, A.F., Lynch, M.J., Hanson, C.E., 2006. The Hillarys Transect (1): Seasonal and cross-shelf variability of physical and chemical water properties off Perth, Western Australia, 1996-98. *Continental Shelf Research* 26, 1689-1729.

Pearce, A.F., 1991. Eastern boundary currents of the southern hemisphere. *Journal of the Royal Society of Western Australia* 74, 35-45.

Pearce, A.F., Griffiths, R.W., 1991. The mesoscale structure of the Leeuwin Current: A comparison of laboratory models and satellite imagery. *Journal of Geophysical Research* 96, 16,739-16,757.

Pearce, A., Pattiaratchi, C., 1999. The Capes Current: a summer countercurrent flowing past Cape Leeuwin and Cape Naturaliste, Western Australia. *Continental Shelf Research* 19, 401-420.

Pearce, A.F., Johannes, R.E., Manning, C.R., Rimmer, D.W., Smith, D.F., 1985. Hydrology and nutrient data off Marmion, Perth, 1976-1982. CSIRO Marine Laboratories Report 167, 45pp.

Redfield, A.C., Ketchum, B.H., Richards, F.A., 1963. The influence of organisms on the composition of sea water. In: Hill, M.N. (Ed.), The Sea vol. 2. Interscience, New York, pp. 26-77.

Ridgway, K.R., Dunn, J.R., Wilkin, J.L., 2002. Ocean interpolation by four-dimensional least squares -Application to the waters around Australia. *Journal of Atmospheric and Oceanographic Technology* 19, 1357-1375.

Smith R., Huyer A., Godfrey S., Church J. (1991) The Leeuwin Current off Western Australia, 1986-1987. *Journal of Physical Oceanography,* 21, 323-345

Thompson, P., Waite, A., 2003. Phytoplankton responses to wastewater discharges at two sites in Western Australia. *Marine and Freshwater Research* 54, 721-735.

Twomey, L. J., Waite, A. M., Pez, V. and Pattiaratchi, C. B., (in press). Variability in nitrogen uptake and fixation in the oligotrophic waters off the south west coast of Australia. *Deep-sea Research* Part 2.

Wild-Allen, K., Parslow, J., Herzfeld, M., Sakov, P., Andrewartha, J. & Rosebrock, U. 2004. Biogeochemical Modelling of the D'Entrecasteaux Channel and Huon Estuary. Technical Report, CMAR CSIRO, Hobart pp113.

CHAPTER 5

5. BENTHIC ECOSYSTEM STRUCTURE: SPATIAL AND TEMPORAL VARIABILITY IN ANIMAL AND PLANT DIVERSITY

Contributing Investigators

Russ Babcock (Project Leader), Geordie Clapin, Phillip England, Nicole Murphy, Julia Phillips, Alison Sampey, Mat Vanderklift, Mark Westera

CSIRO Marine and Atmospheric Research

Outline

Executive Summary

The SRFME study found a strong seasonal signal in algal biomass in all regions, however processes underlying this pattern varied for different locations, or for particular sites within locations depending on the dominant algal habitat type. Most locations showed lowest biomass in winter (e.g. Jurien, Marmion, Two Rocks and Bunbury) but others showed summer minima where the majority of sites were dominated by *Sargassum*. The proximal factors that drive these variations also differ among locations. Erosion of biomass is most likely to be the factor driving changes in *Ecklonia* dominated sites (Marmion, Two Rocks, Perth) while light limitation is likely to be a major factor at Bunbury. Where *Sargassum* dominates sites (Green Head) algal phenology can explain changes in biomass. In contrast to the pattern for biomass, algal community structure showed no seasonal trend which was also the case for invertebrates.

Spatial trends in the data were apparent with both algae and invertebrates showing the highest number of species recorded at Jurien. Perth had the lowest numbers of species although

numbers were only marginally greater at Geographe Bay. Four new species of invertebrates were collected during the SRFME study. Algal community structure showed significant variation at the regional and location level, although much of this variation may be explained by site level variation within locations. Similar patterns were apparent for the invertebrates both for algal associated fauna and benthic fauna. Fish showed a contrasting pattern with a high level of variation among assemblages at the regional level and virtually none at the location level. However at site level there was once again significant variation in fish assemblages. We attribute this consistent variation in assemblages at the site level to definable algal habitat types that tend to dominate at particular sites. While assemblages dominated by canopy-forming large brown algae occurred at just over half the sites, nearly as many sites were instead characterised by diverse assemblages of foliose and filamentous red and brown algae.

The distribution of the different algal species assemblages is correlated with a range of environmental variables, but the relative importance of different variables differs from one region to the next. At Jurien 69% of the variation in assemblage structure was explained by a combination of bottom topography and wave-generated water motion at the sea floor. At other sites the explanatory power of environmental variables was lower, between 30% and 56% and a range of water quality parameters (nutrients and suspended sediments) were most highly correlated with assemblage structure. The distribution of invertebrates was in turn linked to the nature of the algal assemblages, with species number varying according to the algal habitat type. Total numbers of invertebrates also varied according to algal habitat with an inverse relationship being found between *Ecklonia* density and the density of both mobile invertebrates, and large sessile invertebrates, particularly sponges and corals.

Introduction

Western Australia is unusual in possessing high-biomass, high-productivity benthic ecosystems despite the relatively low-nutrient waters of this coastal region that result from the low-rainfall environment as well as the influence of the Leeuwin current. The drivers of productivity and spatial distribution of WA's coastal ecosystems are poorly understood, and there is increasing need for improved information on fundamental aspects of benthic community structure and variability in the wake of increasing pressures resulting from population growth and development (Department of Environmental Protection 1998). Improved understanding of benthic ecosystems can support efforts to manage growing human impacts, will better enable us to determine their likely response to human influences, and will help ensure their future health and sustainability.

The SRFME study focused on improving understanding of one major habitat type –coastal rocky reefs – that had previously received relatively little attention. Rocky reefs are an important habitat type in nearshore coastal waters, supporting a diverse assemblage of benthic macroalgae (Huisman & Walker 1990, Phillips *et al.* 1997) and associated fish and invertebrates. Aside from the biodiversity associated with rocky reef communities, they are also a key component of coastal productivity, provide habitat and food for marine fauna, contribute to biogeochemical cycles, and can exert influence over nearby habitats such as seagrass meadows (Van Elven *et al* 2004). Despite their recognised importance, comparatively little is known of the ecology of rocky reef habitats along the lower west coast of Western Australia. As a consequence, the SRFME study sought to address this gap in current knowledge of the mechanisms structuring rocky reef communities.

The approach taken in the SRFME study followed the only sound basis for future research which was to have a clear understanding of the distribution and abundance of major ecological components in the coastal ecosystem. The description of these patterns and their inter-correlations in space and time is the primary focus of Chapter 5. The dynamics of interactions between physical and biological processes, and of ecological interactions, is the focus of Chapter 6. The understanding of both pattern and process is essential to the achieving the ultimate goal of modelling the coastal ecosystem and gaining the ability to predict ecosystem behaviour.

Aims, objectives

Building meaningful ecosystem models, whether they are conceptual or ultimately numerical, is a complex process that must draw on many different areas of expertise. Within such a program, the task of ecology is particularly complex since it must deal with a sometimes bewildering array of biological complexity and attempt to distil this down to tractable concepts that can be dealt with in a cost effective manner. The usual approach applied to this problem, especially where there is relatively little prior research on the ecosystem, is to conduct a series of systematic observations in such a way that the patterns of variation in marine communities over space and time would inform us of the key processes and environmental factors influencing the structure and dynamics of the system. For this reason sampling was designed to cover as wide a range of coastal reef habitats as possible, in order to encompass the full range of variability in physical and biological variables, improving our ability to correlate physical parameters with biological responses. The study areas were replicated throughout the SRFME region between Jurien Bay and Geographe Bay in order to ensure that results would be representative of the region, rather than specific to just one location.

Additionally assemblages of plants and animals are patchy in space and time, complicating the process of discerning patterns in structure or process. Because ecologists' perception of the nature of patchiness is that it is not a nuisance but an important component of ecology influencing many processes from population abundances and rates of change to interactions among species and overall species diversity (Underwood *et al.* 2000). Sampling to investigate the scale and nature of variability in ecological systems usually employed a nested design, incorporating sites in a hierarchical structure. In our case there was both spatial and temporal nesting. Spatially, sampling was nested at scales of meters, kilometres, tens of kilometres and hundreds of kilometres (quadrats, sites, locations and regions – Fig. 5.2). Temporal sampling was structured to incorporate seasonal and annual variation. Thus all of this hierarchical or nested sampling was done at the same set of "core sites". This design also allowed us to establish baselines against which we will be able to assess whether trends or variation observed in the future are outside the range of spatial or temporal variation normally expected. Our ultimate goal was to lay the groundwork, with this reductionist approach, for scaling up estimates of distribution, abundance, biodiversity and so on, to broad scale synoptic evaluation of ecosystem values at a landscape scale. In order to do this we explored the use of remote sensing approaches to map and evaluate these ecosystem values.

The goal of the SRFME study was to characterise and understand the mechanisms underlying natural variability in diversity and dynamics of benthic community assemblages in selected southwestern Australian coastal marine ecosystems. The project focused mainly on reef habitats since these have been less intensively studied than the seagrass habitats of southwestern Australia. The geographic scope of the work included areas between Green Head in the north and Cape Naturaliste to the south. The range was not greater due in part to logistical constraints but also since all the sites fell within the temperate west coast region. At the same time they afforded a set of gradients in physical (latitude, temperature, bathymetry, fluvial inputs) as well as anthropogenic gradients (proximity to large urban centres, marine protected areas).

The specific SRFME goals addressed in this chapter were to:

- Characterise and quantify seasonal-scale temporal variation in algal and invertebrate assemblages
- Characterise and quantify region-, location- and site-level variation in algal, fish and invertebrate assemblages
- Characterise algal and invertebrate biodiversity and define identifiable algal community types
- Explore and identify environmental factors correlated with algal community structure variation at cross-shore, within location and within site levels
- Characterise and quantify correlations between algal community type and invertebrate assemblage structure and abundance
- Evaluate the use of remote sensing approaches for the mapping of shallow water habitats

Methods

Sampling sites

Sites for the SRFME project were chosen based upon representing spatial scales of meters, kilometres, tens of kilometres and hundreds of kilometres (as mentioned above). At the largest scale (hundreds of kilometres) three main 'regions' were selected, Perth in the centre of the project area, Jurien approximately 200 km to the north and Geographe Bay approximately 200 km to the south of Perth (Fig. 5.2). Within each region, 'locations' were selected at the northern and southern extent to represent a scale of tens of kilometres. The locations selected in the Jurien region are Green head and Jurien Bay, in the Perth region Two Rocks and Marmion and in the Geographe Bay region Bunbury and Cape Naturaliste. Nested within each location, 'sites' were chosen at a spatial scale of kilometres to represent a range of reefs in the area. At each site, a variety of sampling methods including quadrat samples, and transects represent the smallest spatial scale.

Sites from the SRFME regions of Jurien, Perth and Geographe Bay were sampled during the period winter 2003 to winter 2005. Within each location two 'core' sites were sampled each season in order to assess temporal variation. The core sites were chosen to be reasonably accessible during the expected range of seasonal weather conditions and were thus located on inshore reef, approximately 500m to 3 km from shore and within 12 km from the nearest safe boat launching ramp. Where possible, core sites were selected both inside and outside a marine reserve area.

Additional sites in each location were selected to address questions of spatial variability relating to variation in physical environment such as cross-shore position and depth. These sites were located on a variety of inshore, mid and offshore reefs in both exposed and sheltered aspects of the reef and due to limited accessibility were generally sampled only once during the summer or autumn seasons.

Fifty one sites were studied in the SRFME study; 9 sites from Green Head, 19 from Jurien Bay, 2 from Two Rocks, 9 from Marmion, 10 from Bunbury and 2 from Cape Naturaliste (Fig. 5.2 & Table 5.1). The average depth of reefs sampled ranged from 2.2 m at North Essex in Jurien Bay to 15.9 m at BBY15M at Geographe Bay. Most of the reefs sampled were less than 7 m but at least one deeper (>10 m) site was sampled in each region. The core sites were all inshore reefs of less than 7 m depth.

At a regional scale the sampling sites are spread over approximately 400 km of coastline from north to south and there are inherent differences in the physical influences on the three regions. Average sea surface temperatures (SST) for the regions range by approximately 1.5°C, with maximum temperatures during March to April from 21.8°C at Jurien, 21.6°C at Perth, 21.2°C at Eagle Bay and the lowest of 20.3°C at Bunbury. Minimum SST during September to October ranged from 18.5°C at Jurien, 18.4°C at Perth, 17.7°C at Eagle Bay and again the lowest average of 17.0°C at Bunbury (ref: SRFME DIVE database).

Human influences on water quality in the three regions are mainly dominated by proximity to large centres of population particularly at sites in the Marmion location and sites close to the Jurien, Bunbury and to a lesser extent Eagle Bay.

Influences on water quality in the three regions also include input from estuarine and river systems. In the Jurien region the only river system is the Hill River which is closest to sites at Booka Valley, however this river is only seasonally open and usually only for a few days or weeks (Brearley 2005). In the Perth region the nearest river inputs are the Swan River, 25 km south of sites at Marmion and the More River which is 12km north of sites at Two Rocks and only seasonally open to the sea (Brearley 2005). Sites in the Geographe Bay region are possibly influenced more by riverine input particularly at Bunbury with the Leschenault Inlet and Collie River only 6 km to the north and the Capel River and Wonnerup Inlet to the south. Sites in the Cape Naturaliste location may be influenced by the numerous small inlets to Geographe Bay such Toby Inlet, and the Vasse diversion drain (Brearley 2005). The closest site to these inlets is at Eagle Bay approximately 13 km from Toby Inlet.

The Jurien and Perth regions share similar topographic features of complex limestone reef systems with a range of offshore, midshore and nearshore reefs and islands although with a greater number of islands at Jurien. These complex systems present a range of sites with varying degrees of influence by wave action from highly exposed outer reef to very sheltered reef inshore and inside the islands. The topography was quite different in the Geographe Bay region with a mix of granite and limestone reef and lacking the complex offshore reef and islands. The west facing coast at the Bunbury location with no offshore reef is very exposed to wind and wave influence whereas at Cape Naturaliste, the sites face further to the north and although still very exposed, seemed to be more influenced by surge from large swell.

The majority of the reefs sampled were limestone; the exceptions to this are granite reefs located at Cape Naturaliste (Eagle Bay and Quarries) and basaltic reef at one Bunbury site (BBY08). The relief of core sites range from low relief limestone reefs at the Bunbury sites (South Bunbury and Dalyellup), through medium relief reefs at the Marmion sites (South Lumps and Whitford Rock) and Julia Rocks at Green Head, to high relief reefs at the remaining Jurien sites (Fisherman Island Sanctuary Zone 3, Wire Reef and Booka Valley Rocks) and the Two Rocks sites (Cook Lump and Map Reef). The Cape Naturaliste sites were medium to high relief granite boulders and cobbles interspersed with low relief sand covered patches of reef.

Sampling methods – environmental

Two measures of the physical characteristics of reefs were made; namely reef relief and rugosity (Table 5.1). The subjective measure of reef relief considered the elevation of the reef above the surrounding seabed, while the quantitative rugosity code measured the topography of the horizontal reef surface where sampling took place.

Chlorophyll *a*, total suspended solids (TSS), water column nutrients and light attenuation were measured at each site. Although the sampling frequency only provided a 'snapshot' of local environmental with no integration of temporal variability, measurements were useful for making relative comparisons between sites within seasons. Filtered water samples were analysed according to standard methods for chlorophyll *a*, TSS, N, P and Si. Available nitrogen was measured in the form of ammonium (NH_4) and total oxidised nitrogen (NO_x), which is the combination of nitrate (NO_3) and nitrite (NO_2). Light levels throughout the water column were measured using a Li-Cor LI 250 meter with 2-Pi sensor.

Carbon and nitrogen isotopes and content in the tissue of the kelp *Ecklonia radiata* were determined from reefs throughout the SRFME study area, to provide an indication of past nutrient availability and sources. Replicate plants were sampled from a number of reefs and samples were analysed using an ANCA-NT/20-20 stable isotope ratio mass spectrometer (Europa Scientific, Crewe, UK).

Sampling methods - biological

At each site sampling was conducted at both 1 m^2 and 0.25 m^2 scales using randomly placed 1 x 1 m quadrats which had a 0.5 x 0.5 m quadrat fixed in one corner. Sampling of the 1 m^2 quadrats included solitary or mobile invertebrates >10 mm in size, with the 0.25 m^2 quadrat typically providing data on invertebrates <10 mm in size. Algae were sampled by hand-collecting all macroalgae within the 0.25 m^2 quadrat. These were bagged for later identification and weighing. Invertebrates sampled incidentally with the algal collections were also identified in the lab. This fauna tended to be largely epifaunal, or associated with algal holdfasts. A photograph of each quadrat was then taken for later analysis of benthic cover, including various algal forms but also categories such as bare rock and sand. Photos were analysed using the JEHP (v 1.0.0.1, © James Wise, UWA/CoastalCRC), using a point intercept method. Fifty points were randomly selected by JEHP and assigned to benthic categories by an expert observer. Pilot analysis of data revealed little further gain in precision was achieved by sampling more than 40-50 points. Data were converted to the % cover of primary space occupied by various benthos components.

Where possible, specimens were identified to species level. Those that were not identified in the field were collected for follow up verification. An invertebrate reference collection for the

SRMFE region has also been established. Individuals in the 1 m^2 quadrat were counted and measured (max length and/or width in mm). Smaller individuals from the 0.25 m^2 quadrat were measured in a similar way and weighed.

Fish assemblages were characterised using underwater visual census (UVC) conducted by divers on SCUBA. Censuses were conducted within 25 x 5 m transects; three or four transects were conducted at each reef in the summer of 2005/2006. Multivariate analyses focussed on spatial patterns in fish assemblages. Patterns were visualised using non-metric multidimensional scaling (NMDS) ordination, and the significance of spatial patterns was tested using ANOSIM, with both analyses based on binomial deviance dissimilarity calculated from untransformed counts (Anderson & Millar 2004).

Abundance data from 0.25 m^2 and 1 m^2 quadrats recorded from the SRFME regions of Jurien, Perth and Geographe Bay was extracted from the SRFME ACCESS database. Only species with confirmed identity were used in analyses. Data were analysed using the software package PRIMER 6 (Plymouth Routines In Multivariate Ecological Research). The effect of physical factors including depth, relief, cross-shore position of the sampling site (inshore/offshore), algal habitat type and brown algal biomass were used in qualitative comparisons with invertebrate distribution within the SRFME region, in order to identify any patterns if present.

Overall square root transformation was applied to algae abundance (biomass) data and fourth root transformations were used for invertebrate abundance (count) data. A Bray-Curtis similarity resemblance matrix was then generated and data analysed through ordination by non-metric multidimensional scaling, with a restart value of 25. The factors of region, location, site, cross-shore position, depth, relief and algae habitat type were used in analyses with results displayed in the form of scatter plots. Analysis of Similarities (ANOSIM) was applied to these factors to test significance, and Similarity Percentages (SIMPER) used to assess contribution of species, to variation in assemblage structure between and within factors.

Habitat types were allocated to each quadrat using the % algal abundance (biomass). The species were ranked from most to least abundant and the species contributing most to overall community composition were used to assign *a posteriori* habitat types for each quadrat. Habitat categories were originally developed for use by divers to visually allocate habitat type based on algal cover. As such, the classification of individual quadrats, which were based on % biomass, may vary somewhat from classifications based on cover. However, analyses of classifications done using biomass or % cover showed close agreement between the two methods.

Remote Sensing of Shallow Water Habitat Data

The HyMap sensor is an airborne hyperspectral digital spectrometer that records reflected sunlight in 126 spectral channels between 450nm to 2500nm over a 512 pixel swath. Spatial resolutions are usually in the range 3 to 10 m (9 m^2 to 100 m^2). Two HyMap strips (26.1km and 23.1km by 1649m wide; 3.2m pixel width) were flown at Jurien Bay in April 2004 and processed by HyVista Corporation to correct for atmospheric absorption and scattering. These data were then processed using the shallow water reflectance model outlined below (see also Vol. 1, sec. 2.2.5).

Optical modelling

We have implemented a simple shallow water reflectance model applicable to the optical domain present in many Australian coastal waters. The model is typically tuned to local conditions by including spectral characteristics of commonly occurring local substrates. The model is based on the work of Lee *et al.* (1999). The remote sensing spectral reflectance, r_{rs}, is given by,

$$r_{rs} \approx r_{rs}^{dp}\left(1-\exp\left\{-\left[\frac{1}{\cos(\theta_w)}+\frac{D_u^{C}}{\cos(\theta)}\right]\kappa H\right\}\right)+\frac{1}{\pi}\rho\,\exp\left\{-\left[\frac{1}{\cos(\theta_w)}+\frac{D_u^{B}}{\cos(\theta)}\right]\kappa H\right\}$$

(**A**)

where, r_{rs}^{dp} is the remote sensing reflectance of an infinitely deep water column, θ and θ_w

relate to the illumination and viewing geometry, κ and D_u are light transmission functions and H is water depth. The light transmission functions may be expanded to include coefficients related to the optical properties of water column constituents, and these in turn related to concentration values for constituents such as chlorophyll and suspended sediment. The component of interest for this work is ρ, the substrate reflectance. For a pixel area that is uniformly covered in one substrate type, sand for instance, ρ is equal to,

$$r = P R'_{sand} ,$$

(**B**)

where R'_{sand} is a normalised sand reflectance spectrum and P is a scaling factor. The work of Lee *et al.* (1999) was developed for a single substrate, namely sand. We have expanded the applicability of the model to include mixed pixels. In theory, many substrate classes can be combined to model the total reflectance of a pixel. For this work we have chosen three commonly occurring, and spectrally distinct, substrate classes; sand, seagrass and brown algae. When the pixel contains a mixture of substrates, the total reflectance is modelled as a sum of reflectances,

$$r = P_1 R'_{sand} + P_2 R'_{seagrass} + P_3 R'_{algae} .$$

(**C**)

A constrained iterative optimisation scheme is employed to search the model space for coefficients providing the best fit to the measured reflectance spectrum. The retrieval process returns the three coefficients, P_1, P_2 and P_3[1] †, bathymetry (H in Eqn. **A**) and water column constituent properties. The three reflectance parameters, P_1, P_2 and P_3, are taken to represent the proportion of each substrate in a particular pixel. No account is made for variations in albedo (brightness) of substrates.

Collection of library spectra

Classification of benthic substrates by remote sensing techniques depends upon a-priori knowledge of the spectral nature of the substrates present. Typically, spectra are selected from a spectral library. This spectral library is built up from numerous field campaigns to undertake in-situ measurements of substrate spectral properties. CMAR have been involved in the collection of such spectra for a number of years, including campaigns measuring coral spectral properties on the Great Barrier Reef and spectral properties of numerous algae species in WA coastal waters. Reflectance spectra are measured with a dual channel Zeiss hyperspectral radiometer. The radiometer may be deployed by a diver to measure the reflectance spectrum *in situ*, or the diver may retrieve a sample of the benthic cover to measure the spectral reflectance in air. Reflectance spectra collected in Jurien Bay are shown in Figure 5.1. The spectra in each type may be normalised and averaged to create representative spectra for use in the inversion process. The sand spectrum is clearly very different to the algal spectra. The peak reflectance in the green substrate classes is around 550 nm. The peak reflectance in the brown and red/yellow algae occurs at longer wavelengths, and tends to exhibit a broader peak. For this work, the brown and red/yellow spectra have been combined to create the brown algae class. By combining and normalising spectra from a range of biotic substrate rather than treating them separately, we have opted for robust and reliable solutions for classification.

---

† P values don't necessarily add up to 1.0 because they represent reflectance scaling factors, not proportion of each substrate class. However, a larger P value can be related to a greater likelihood of a given substrate dominating a pixel's reflectance.

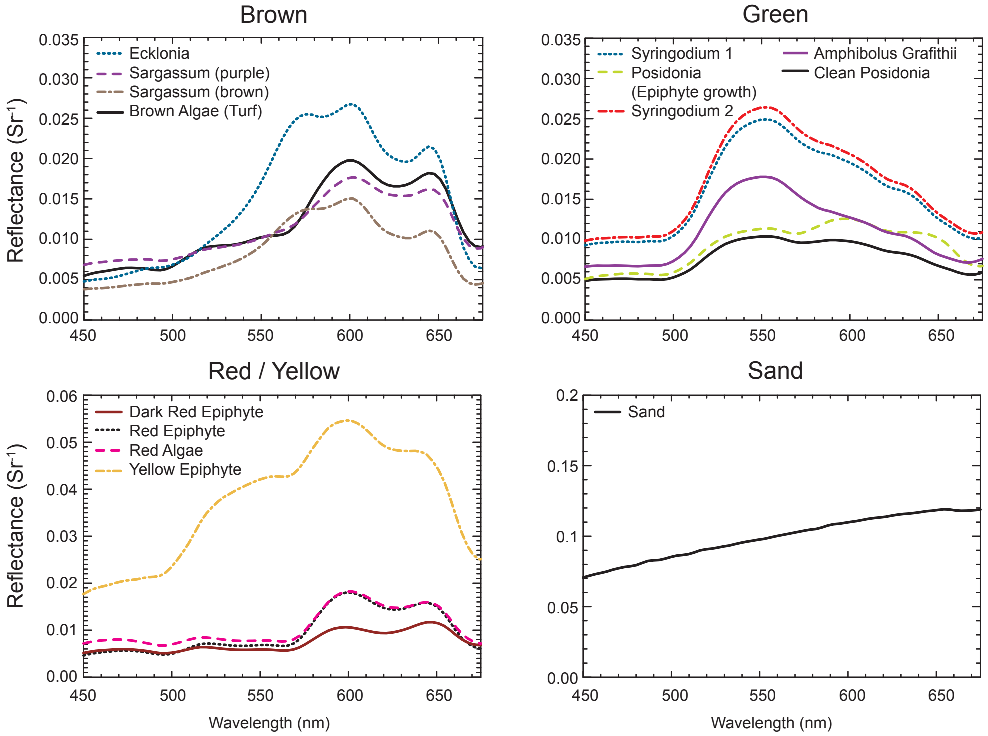

Figure 5.1: *In-situ* reflectance spectra of four different groups of substrate.

Ground Truthing

Approximately three hours of video footage was obtained during October, 2004. The underwater video camera was deployed in several regions of the HyMap strips. The boat's position was geolocated with a differential Global Positioning System (GPS). The filmed benthic cover was visually classified according to a habitat classification scheme based largely on the predominant canopy macrophyte species (Table 5.6, section 5.4) as well as sand, and two classes of seagrass (*Posidonia* and *Amphibolis*). For the validation work, these habitat types were collapsed into three classes: sand, seagrass and brown algae.

The method of video camera deployment was to suspend the camera from the boat and maintain a relatively constant position. The habitat maps below (Figure 5.36) show the locations of the video data indicated by white squares. Sites were chosen based on Klonowski (Vol. 1, sec. 2.2.5) to ensure that areas representative of each of the main spectral classes was sampled at approximately the same intensity. The substrate classification based on the video data provided approximately 1800 video frames.

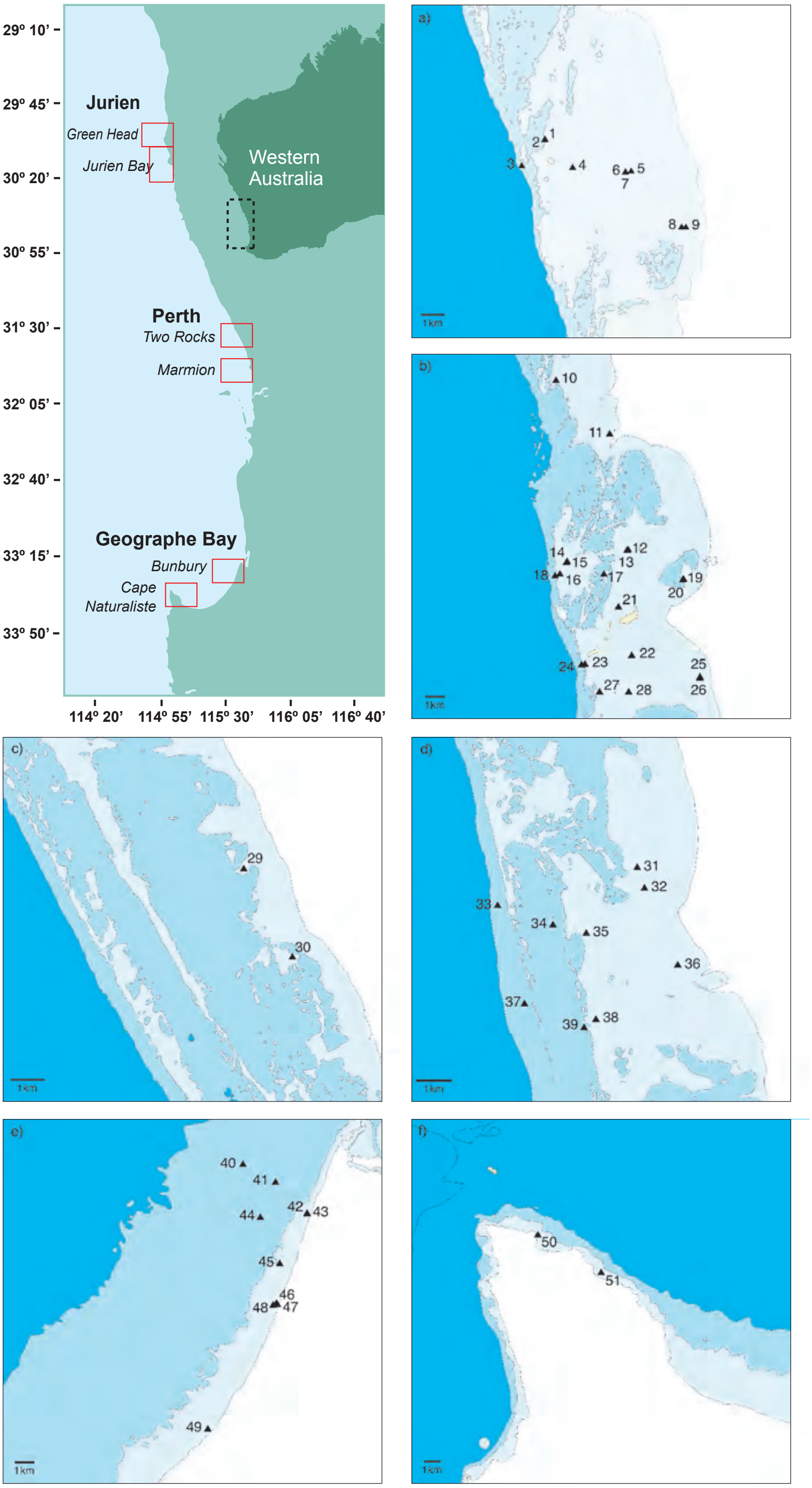

Figure 5.2: SRFME Coastal Ecosystems and Biodiversity Project study area showing the regions, locations and sites within each location a) Green Head, b) Jurien Bay, c) Two Rocks, d) Marmion, e) Bunbury and f) Cape Naturaliste. Site numbers are from Table 5.1. Colour shading on maps: white, mainland; yellow, islands; light blue, 0-10 m water depth; mid blue, 10-20 m; dark blue, 20-50 m.

Table 5.1: Sampling depths, reef relief and rugosity codes for all sampling sites. Core sites are indicated in bold. Reef relief, L – flat reef (0 – 10 cm above surrounding seabed), M – medium relief reef (10 – 100 cm), H – high relief reef (> 100 cm), B – boulders, C – cobbles, * - granite reefs. Higher rugosity values indicate greater change in topography, or roughness, of reef surfaces.

		Depth (metres)			Rugosity			
					Site		Quadrat	
No.	**Site Name**	**Mean**	**Range**	**Reef Relief**	**Mean**	**St Dev**	**Mean**	**St Dev**
	Jurien – *Green Head*							
1	WA Museum 12	8.6	8.3 - 9.1	H	1.3	0.2	1.2	0.1
2	WA Museum 11	5.6	5.2 - 5.8	L	1.5	0.8	1.2	0.1
3	Fisherman's Island 12m	12.8	12.5 - 13.2	M	1.0	0.1	1.1	0.1
4	Fisherman's Islands Sanctuary Zone 2	3.8	3.4 - 4.2		1.3	0.2		
5	Fisherman's Islands Sanctuary Zone 1	4.8	4.2 - 5.5	M	1.2	0.1		
6	WA Museum 15	7.0	7.0 - 7.1	L	1.0	0.0	1.0	0.0
7	**Fisherman's Islands Sanctuary Zone 3**	**4.1**	**2.5 - 5.8**	**H**	**1.4**	**0.2**	**1.4**	**0.2**
8	**Julia Rocks**	**2.9**	**1.0 - 4.4**	**M**	**1.3**	**0.1**	**1.3**	**0.2**
9	WA Museum 14	5.1	5.0 - 5.5	L	1.0	0.0	1.0	0.1
	Jurien – *Jurien Bay*							
10	WA Museum 9	4.8	4.7 - 5.0	M	1.6	0.3	1.2	0.1
11	North Head	4.6	4.3 - 4.9	H	1.3	0.0	1.4	0.2
12	Favourite Island	6.2	6.1 - 6.4	L				
13	WA Museum 3	5.4	4.5 - 5.9	H	1.3	0.2	1.3	0.2
14	Seaward Ledge East 06	6.5	5.8 - 6.8	LC	1.2	0.1	1.4	0.3
15	WA Museum 2	5.6	5.1 - 5.8	L	1.1	0.1	1.2	0.1
16	Seaward Ledge 6m	7.0	6.1 - 8.4	H	1.3	0.1	1.2	0.1
17	North Marker	9.7	9.0 - 10.2	L	1.3	0.1		
18	Seaward Ledge 13m	13.6	13.3 - 14.0	M	1.1	0.1	1.1	0.1
19	WA Museum 5a	7.7	7.5 - 8.0	L	1.0	0.0	1.2	0.1
20	**Wire Reef**	**5.2**	**3.8 - 6.3**	**H**	**1.6**	**0.1**	**1.6**	**0.3**
21	North Osprey	2.8	2.5 - 3.1	M	1.4	0.1		
22	North Essex	2.2	1.9 - 2.5	H	1.5	0.1		
23	WA Museum 7	6.8	6.3 - 7.8	M	1.4	0.1	1.2	0.1
24	WA Museum 6	11.8	11.4 - 12.0	H	1.2	0.1	1.2	0.1
25	WA Museum 4a	5.1	4.8 - 5.4	L	1.4	0.2	1.2	0.1
26	**Booka Valley Rocks**	**4.1**	**2.8 - 5.2**	**H**	**1.7**	**0.2**	**1.7**	**0.3**
27	WA Museum 8	7.7	7.0 - 8.6	H	1.2	0.1	1.5	0.2
28	WA Museum 1	3.1	2.6 - 3.8	H	1.4	0.1	1.4	0.3
	Perth – *Two Rocks*							
29	**Cook Lump**	**6.1**	**3.5 - 8.3**	**H**	**1.3**	**0.0**	**1.4**	**0.3**
30	**Map Reef**	**5.9**	**3.7 - 8.3**	**H**	**1.9**	**0.3**	**1.7**	**0.4**
	Perth – *Marmion*							
31	**South Lumps**	**5.5**	**4.4 - 7.2**	**L**	**1.2**	**0.1**	**1.4**	**0.2**
32	**Whitford Rock**	**4.4**	**2.9 - 5.7**	**M**	**1.5**	**0.2**	**1.6**	**0.3**
33	3 Mile Reef North	15.6	14.8 - 16.2	M	1.2	0.0	1.1	0.2
34	Little Island West 1	14.0	13.4 - 15.0	M	1.2	0.1		
35	Little Island	4.6	4.0 - 5.3	M	1.9	0.2		
36	Cow Rock	4.2	3.0 - 5.1	H	1.7	0.3	1.5	0.2
37	3 Mile Reef South	13.6	13.0 - 14.2	L	1.2	0.1	1.1	0.2
38	Outer Horseshoe Reef	6.5	6.2 - 6.8	L	1.1	0.0		
39	Horseshoe Reef West 1	13.8	13.4 - 14.2	L	1.1	0.0		
	Geographe Bay – *Bunbury*							
40	BBY15M	15.9	15.1 - 16.2	L	1.0	0.0	1.1	0.0
41	BBY08	10.8	10.4 - 11.0	L*	1.2	0.1		
42	**South Bunbury**	**7.2**	**6.5 - 8.0**	**L**	**1.4**	**0.2**	**1.3**	**0.2**
43	Bunbury 4							
44	BBY14M	13.7	13.2 - 14.2	L	1.2	0.1	1.1	0.1
45	BBY10B	9.4	9.2 - 9.5	L	1.1	0.1		
46	**Dalyellup 1**	**6.8**	**6.3 - 7.3**	**L**	**1.1**	**0.4**	**1.2**	**0.1**
47	Dalyellup North	5.8	5.6 - 6.0	L				
48	Bunbury 3							
49	Capel 5	2.1	1.5 - 2.6	M	1.4	0.1	1.7	0.1
	Geographe Bay – *Cape Naturaliste*							
50	**Quarries**	**5.2**	**3.8 - 7.4**	**L***	**1.2**	**0.1**	**1.5**	**0.5**
51	**Eagle Bay**	**5.7**	**2.3 - 6.7**	**L*BC**	**1.4**	**0.2**	**1.6**	**0.2**

Results

5.1 Environmental Parameters

Investigators / Institution

Alison Sampey, Geordie Clapin, Julia Phillips, Nicole Murphy, Russ Babcock,
Mat Kleczkowski

CSIRO Marine and Atmospheric Research

Nutrients

In the majority of samples NO_x made up a larger portion of available nitrogen than NH_4 (Fig. 5.3). Mean levels of available nitrogen were highest at Two Rocks and Jurien Bay during autumn 2004. Mean levels at Marmion were elevated above other sites on all other occasions. Mean phosphate (PO_4) levels at the majority of sites ranged from 0.3 to less than 0.01 μM^{-L}, and were highest at Marmion (0.28 μM^{-L}) and lowest at Bunbury (0.04 μM^{-L}) (data not shown here). There was little seasonal change in phosphate levels.

Chlorophyll *a*

Mean chlorophyll *a* levels were highest in Bunbury (5.4 μM^{-L}) and lowest at Green Head (0.5 μM^{-L}) (Fig. 5.3). Mean chlorophyll *a* levels did not vary much seasonally except at Bunbury, where they were much higher and more variable in winter compared to the other seasons. This is consistent with the trends in nutrient availability.

Light attenuation

Light attenuation coefficient showed a clear seasonal trend across most locations with attenuation increasing from autumn to winter and the highest attenuation recorded during spring then dropping off during summer (Fig. 5.4). Bunbury generally had the highest attenuation coefficient, which also corresponds to the high levels of chlorophyll *a* (and TSS, not shown here) particularly during winter and spring.

These trends were also quite apparent to the divers conducting sampling at each location as changes in underwater visibility. Visibility was very low at Bunbury sites during winter and spring, frequently with a distinct reduction to almost zero visibility within 1 to 2 m above the bottom. However, since water samples were collected near the surface this stratification of highly turbid water near the bottom is not fully reflected in the TSS samples.

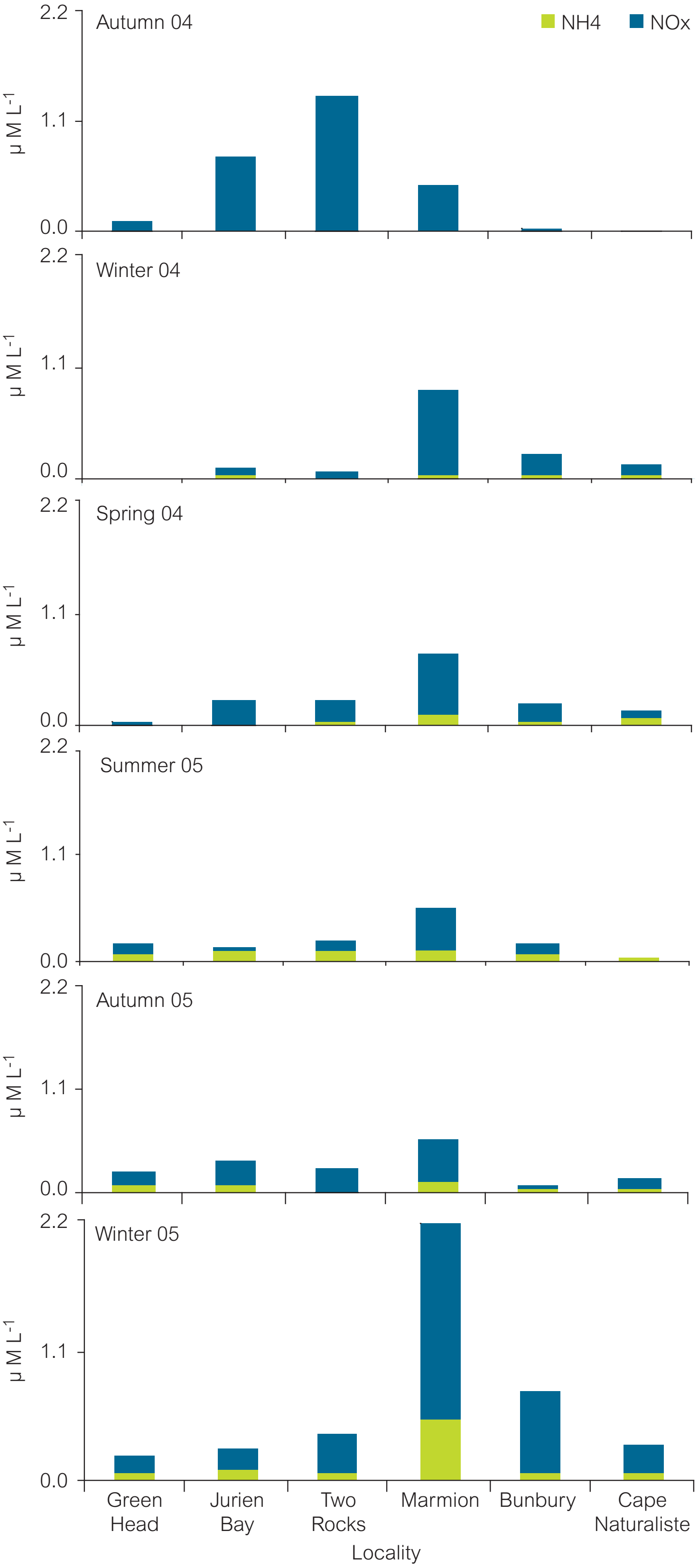

Figure 5.3: Mean total oxidized nitrogen (NO$_x$) and ammonium (NH$_4$) recorded from sites within each location.

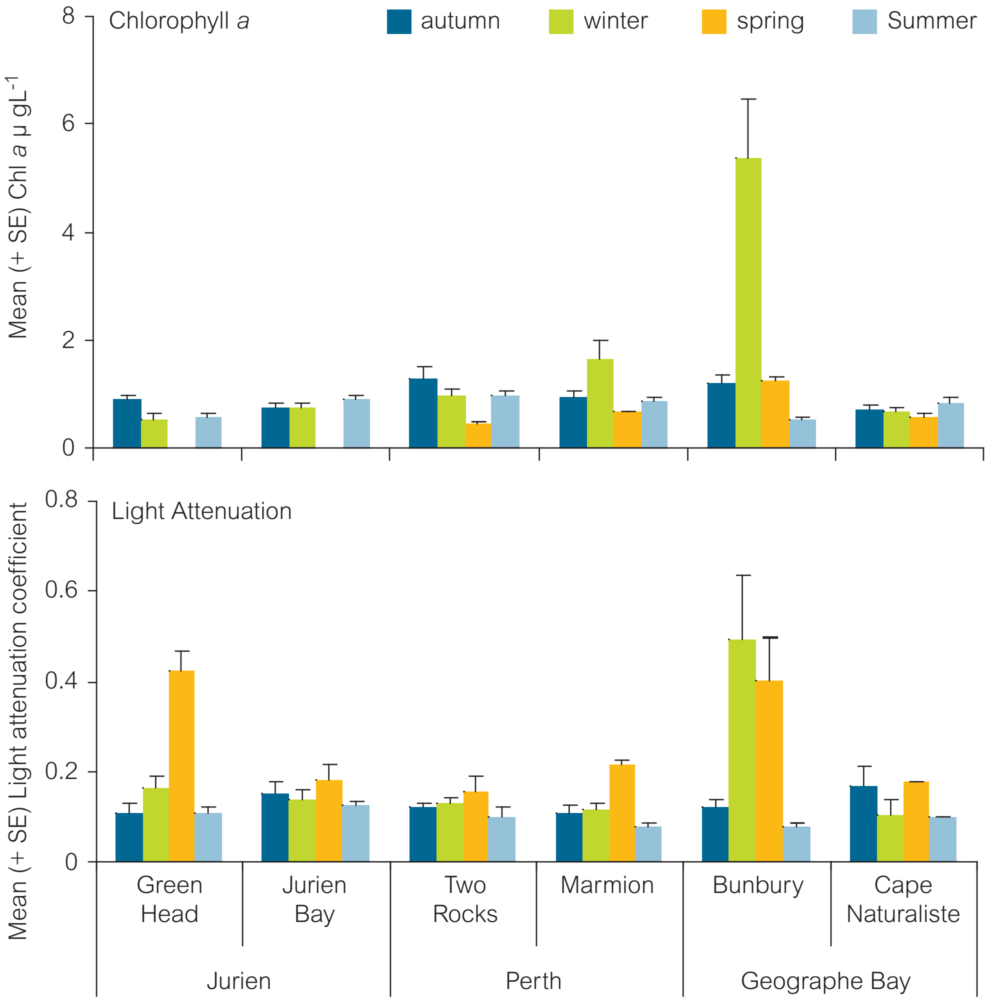

Figure 5.4: Seasonal variation in chlorophyll *a* (μg L^{-1}) and light attenuation for project sites during 2004-2005.

C and N content and isotopes

At a regional level, kelp from Perth reefs had elevated levels of $\delta^{15}N$, that were nearly twice as high as in kelp from Jurien and Geographe Bay ($p<0.001$), each of which had very similar levels (Fig. 5.5). The reverse was true of $\delta^{13}C$ and C:N ratios, with lower levels in Perth kelp compared to other regions ($p<0.001$). This is indicative of higher N availability in the Perth region. The elevated $\delta^{15}N$ signal suggests the source of this nitrogen is anthropogenic and effluent related.

Cross-shore variation in C and N isotopes and total C:N content was examined in kelps from reefs in Jurien Bay and in Marmion, in autumn 2004 and spring 2003 respectively. In Jurien Bay, $\delta^{15}N$ levels increased with increasing distance offshore ($p<0.001$) (Fig. 5.6). $\delta^{13}C$ was more variable among kelps across the shore, with similar levels in plants from mid and outer shore reefs ($p>0.05$). Lowest levels were in kelp plants from inner shore reefs. C:N ratios showed a general trend towards higher ratios with distance from shore and the lower levels in kelps from inner reefs ($p<0.001$) indicate a lesser degree of N-limitation compared to kelp from mid and outer reefs.

In Marmion Lagoon, $\delta^{15}N$ was significantly higher in kelp from inner shore reefs than from mid shore reefs ($p<0.001$) (Fig. 5.7), opposite to the trend at Jurien. $\delta^{13}C$ levels were variable and no patterns were discernible between inner and mid shore kelp populations ($p>0.05$) whereas C:N ratios were lower in inner reef kelps ($p<0.001$).

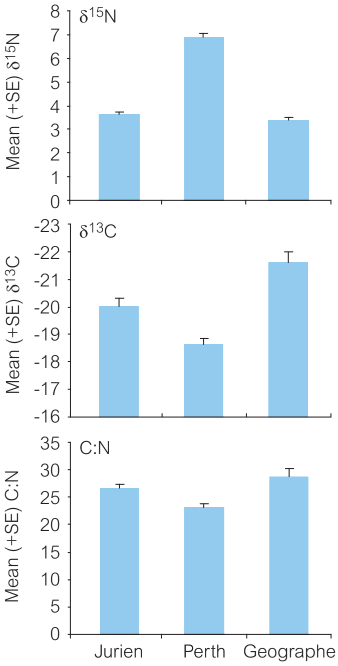

Figure 5.5: Regional variation in C and N isotopes and C:N ratio in the kelp *Ecklonia radiata*. n=25-80.

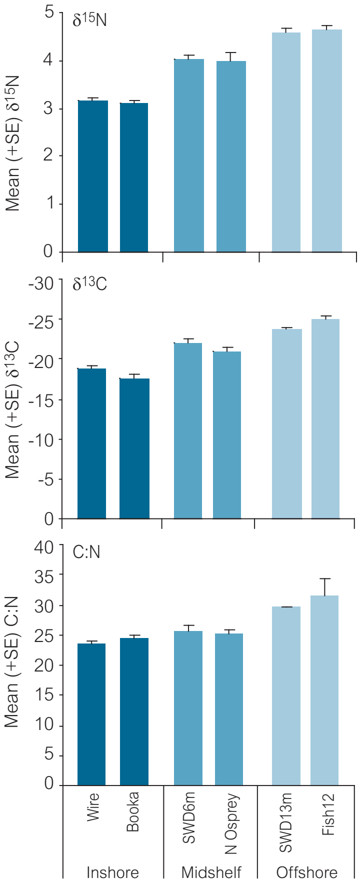

Figure 5.6: Cross-shore variation in C and N isotopes and C:N ratio in the kelp *Ecklonia radiata* from reefs in Jurien Bay during autumn 2004. n=3-8.

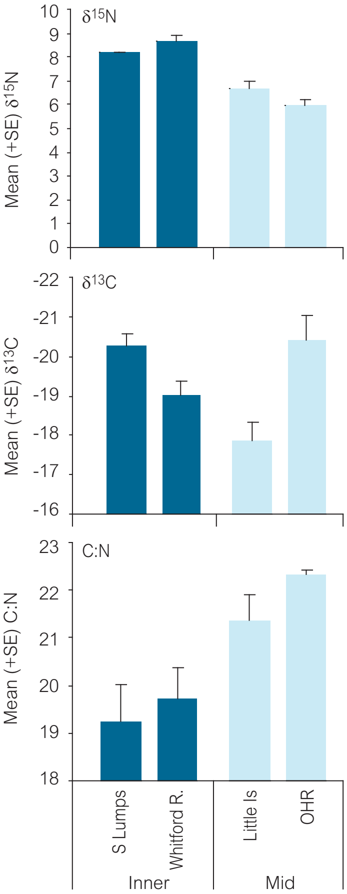

Figure 5.7: Cross-shore variation in C and N isotopes and C:N ratio in the kelp *Ecklonia radiata* from reefs in Marmion Lagoon during spring 2003. n=3.

5.2 Seasonal dynamics in reef algal communities

Investigators / Institution

Julia Phillips, Russ Babcock, Nicole Murphy, Geordie Clapin, Alison Sampey,
Mat Kleczkowski, Mark Westera

CSIRO Marine and Atmospheric Research

Abundance

Biomass of reef algae varied significantly among regions and seasons (2-way ANOVA, p<0.001, locations and sites pooled); furthermore, the biomass in each season differed according to the region (p=0.017, Table 5.2). In the Jurien and Perth regions, biomass was relatively high and seasonal variation followed predictable trends (e.g. Kirkman 1989) with lower biomass during winter, increasing to a spring-summer peak. Reef algal communities in the Geographe Bay region had lower biomass and deviated from the typical annual cycle of growth and erosion seen elsewhere, instead showing a trend of increasing biomass through the year to a spring maxima (Fig. 5.8). This deviation from the typical annual cycle of algal biomass may be largely explained by the particular environmental conditions that prevailed at Bunbury during the study, namely the reduced water clarity during winter and spring (discussed further in Section 5.8).

Table 5.2: Results of a two-way analysis of variance testing for differences in seasonal macroalgal biomass, using the fixed factors region and season.

	d.f.	MS	F	P
Region	2	11224540	17.77	<0.001
Season	3	3969191	6.28	<0.001
Region*Season	6	1636723	2.59	0.017
Residual	684	631631		
Total	695	685198		

Reef algal communities can be roughly divided into the understorey component and the overlying canopy, where such a canopy exists, and may have different ecological functions. The seasonal variation in understorey algal biomass was similar to that reflected in the total algal biomass (as shown in Fig. 5.8) with winter minima and spring/summer maxima (data not shown). Large canopy-forming brown algal species were a conspicuous and large component of the biomass on many reefs, and as such may contribute significantly to secondary production and the export of nutrients to adjacent habitats. Seasonal variation in the biomass of canopy-forming browns (Fig. 5.9) was related to the ecology of the dominant species at each location. Reefs at Jurien Bay, Two Rocks and Marmion were dominated by the kelp *Ecklonia radiata* and seasonal changes in biomass at these locations were consistent with the annual erosion of biomass during winter storms (Kirkman 1989). *Sargassum* is the dominant canopy-forming brown alga on reefs at Green Head, the seasonal variation in abundance is explained by its particular life history (phenology). *Sargassum* produces long branches bearing reproductive structures during mid-winter and spring, and plants then die back to a basal rosette of fronds in summer and autumn following the release of spores (Womersley 1987). This seasonal phenological cycle results in dramatic fluctuations in the biomass of *Sargassum* throughout the year, which is clearly reflected in Fig. 5.9.

Within locations at Geographe Bay there were contrasting seasonal patterns (Fig. 5.10) in total algal biomass. At Bunbury there was significant variation among seasons (p=0.002) with a significantly lower biomass in winter and spring (p<0.05) while at Cape Naturaliste there was no significant difference among seasons (p=0.46). This pattern is probably related to seasonal variation in light availability to the bottom which is restricted in winter by sediment resuspension and low attenuation coefficient (Fig 5.4 and Section 5.7).

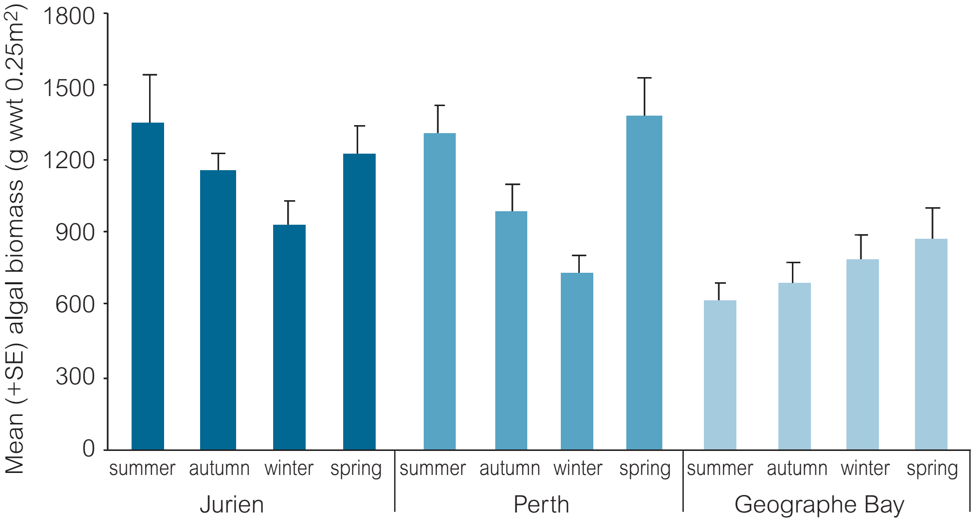

Figure 5.8: Seasonal variation in total biomass of reef algae within the SRFME regions.

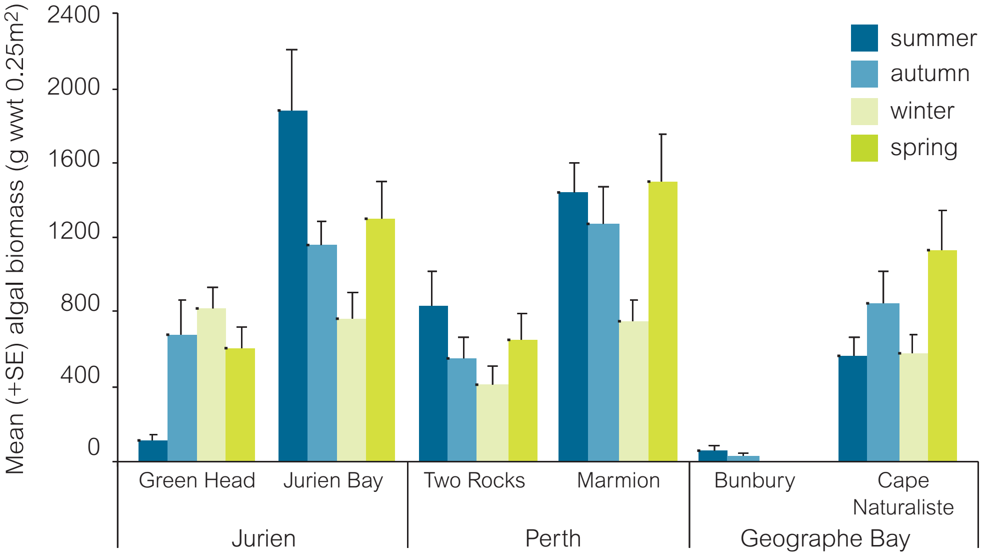

Figure 5.9: Seasonal variation in the biomass of large, canopy-forming brown algae on reefs in different locations within the SRFME regions.

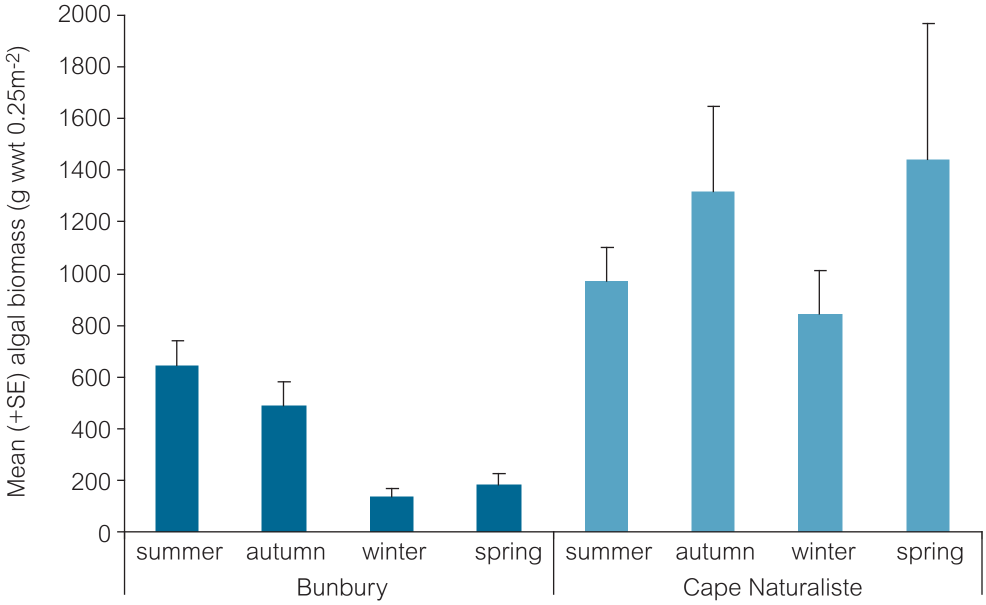

Figure 5.10: Seasonal variation in total biomass of reef algae within Geographe Bay.

In Geographe Bay the biomass of reef algae at South Bunbury and Dalyellup 1 was negatively correlated with light attenuation (-0.50 and -0.76, respectively; Fig. 5.11). Light attenuation coefficients increased during winter and spring seasons when a persistent and distinct nepheloid layer close to the seafloor was observed. This may be responsible for the subsequent dieback of low-light intolerant species.

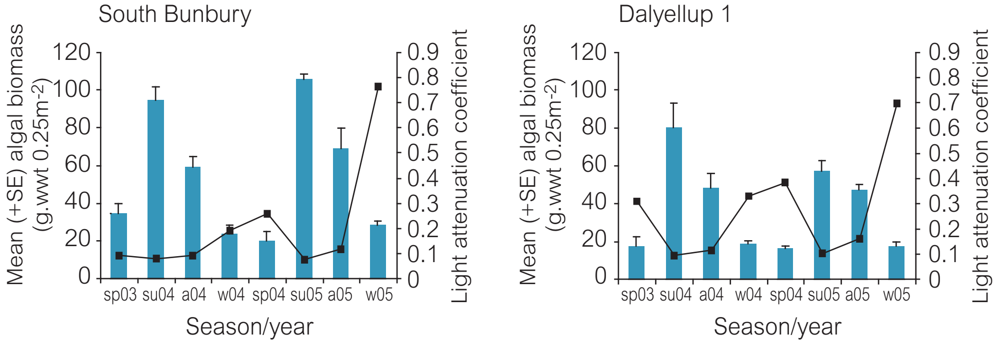

Fig. 5.11: Seasonal algal biomass and light attenuation coefficients at sites South Bunbury and Dalyellyup 1 within the Geographe Bay region.

Community structure

Seasonal dynamics in reef algal community structure was investigated at four sites within each region. These core sites were shallow (<7 m depth) and were sampled between two and four times in each season during the SRFME program. Overall, there was no seasonality in community structure at any of the core sites, as indicated by multivariate analyses of similarities of the communities (*R* = 0.009 – 0.339 for all sites). The lack of seasonal trends in reef algal community structure (species composition) within the SRFME area of interest demonstrated that communities as a whole on any given reef remain relatively stable, despite variations in the biomass of key taxa such as *Ecklonia* and *Sargassum*.

5.3 Regional trends in reef algal community structure

Investigators / Institution

Julia Phillips, Russ Babcock, Nicole Murphy, Geordie Clapin, Alison Sampey,
Mat Kleczkowski

CSIRO Marine and Atmospheric Research

Diversity and species richness

At the completion of the SRFME field program, a total of 373 marine plant taxa (macroalgae and seagrasses combined) had been identified. Over 99% of taxa have verified identifications to species level; voucher specimens have been prepared for lodgement with the Western Australian Herbarium and for inclusion on their *Naturebase* database. Numerous range extensions of species' distributions have been recorded, and the red alga *Gelidiella ramellosa* was 'rediscovered' after having not been recorded in WA for over 150 years.

The distribution of marine plant taxa among the three SRFME regions is represented in Figure 5.12. Species richness was comparable between Perth and Geographe Bay, with 230 and 237 taxa, respectively. Jurien had somewhat higher species richness (305 taxa) although it should be noted that sampling effort in terms of the number of sites visited was greater in this region and included both reef and seagrass habitats. Nevertheless, the number of species found in only one region appears high with 73 taxa recorded only at Jurien, compared with only 19 in Perth and 36 in Geographe Bay. Regional differences in the distribution of algal taxa will be driven by factors such as differences in environmental conditions (eg. water temperature) and biological constraints such as dispersal of spores, as well as sampling effort. Nevertheless, a large proportion of all taxa (over 40%, or 154 of 382 taxa) were present in all three geographic regions, indicating a broad geographic distribution along the lower west coast of Western Australia. Interestingly, although Jurien and Geographe Bay are geographically disjunct, these regions shared 34 taxa that were not found in Perth. This suggests that environmental conditions in the Perth region may be unfavourable to certain species.

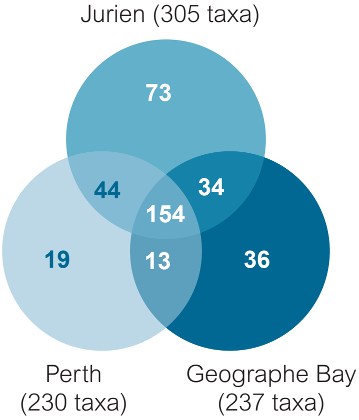

Figure 5.12: Distribution of marine plant taxa among the SRFME regions. Numbers in parentheses are the total number of taxa found in a region. Areas of overlap indicate the number of taxa shared between regions; the central region indicates the number that were found in all three regions.

Species accumulation plots were constructed for each region to determine the number of different species observed (*S*) with increased sampling effort (Fig. 5.13) and assess the extent to which these trends might be merely the result of sampling artifacts. Three non-parametric estimators of *S* were included as predictors of the true total number of species that would be observed in each region as the number of samples reaches infinity (Clarke & Gorley 2006). The jacknife technique depends on the number of samples seen only in 1 or 2 samples (Clarke & Gorley 2006) and reduces the bias in underestimating the true number of species in an assemblage (Colwell & Coddington 1994). The bootstrap estimator depends on the set of proportions of samples that contain each species (Colwell & Coddington 1994).

In all regions, the observed number of species (S_{obs}) was lower than that predicted by the *S* estimation techniques (Fig. 5.13), suggesting that the true number of species in each region is higher than that revealed by sampling to date. This is not entirely surprising since species-accumulation curves generated by permutations of *S* are typically negatively biased estimators of *S* due to averaging. Estimates of *S* for reef algae in the Perth region showed the greatest difference to S_{obs} at the maximum sample size, indicating that the biodiversity in this region is least well accounted for by the sampling effort. The S_{obs} curves for all regions also rose less steeply from the origin than either jacknife curve, indicating a high degree of heterogeneity in species composition (Colwell & Coddington 1994); again, this is to be expected given the range of reef habitats sampled. Importantly, the species accumulation plots show that variation in species richness is not simply related to sample size at the three sites. Based on the same number of samples for each region (e.g. 195 which was the total for Geographe Bay), both observed and modeled estimates of S are substantially higher at Jurien than they are at Perth and Geographe Bay, both of which had very similar estimated species counts (Table 5.3).

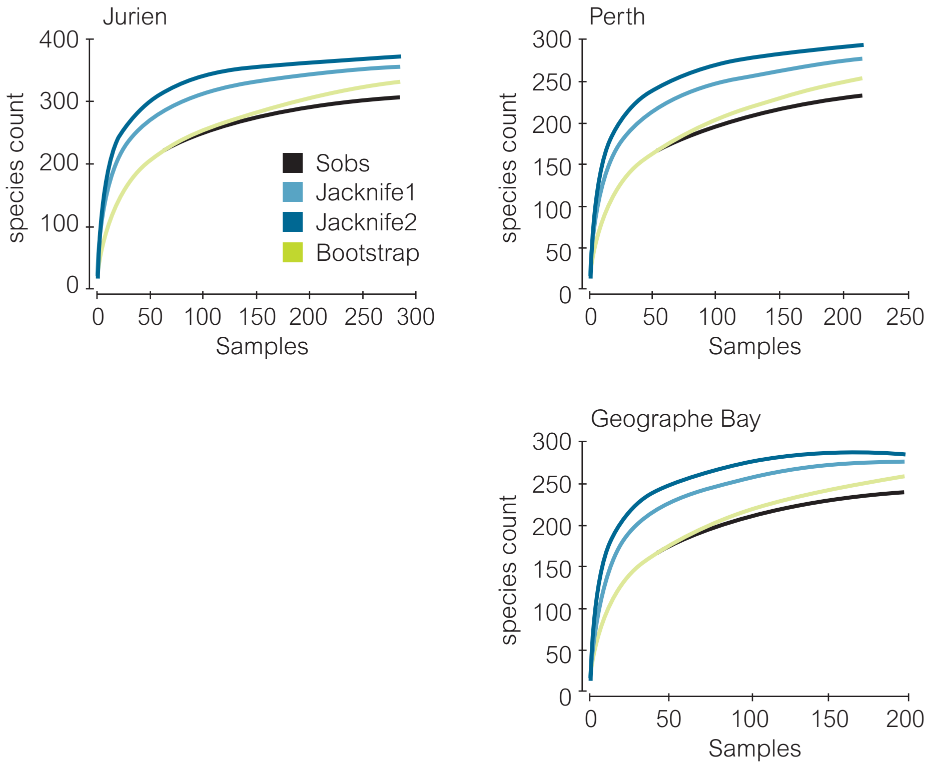

Figure 5.13: Species accumulation plots for algal richness in each SRFME region. Curves show the actual species observed (*S*obs) and three non-parametric estimators of *S* (Jacknife 1 and 2, Bootstrap). Jacknife techniques are based on functions of the number of species seen only in 1 or 2 samples; the Bootstrap technique depends on the set of proportions of samples that contain each species. For all curves each point is the mean of 999 randomisations of sample order.

Table 5.3 Comparisons of estimates of S for reef algae for a standard sample size using three non-parametric estimators.

	S_{obs}	Jacknife 1	Jacknife 2	Bootstrap
Jurien	288.3	343.6	363.1	303.5
Perth	228.6	273.3	291.4	247.3
Geographe Bay	239.6	277.7	285.2	258.5

In all three regions the species richness was dominated by red algae (Division Rhodophyta), which accounted for 65-72% of all species recorded (Figs 5.14-16). This did not translate to dominance in terms of biomass (or abundance) except on reefs at Bunbury, where red algae made up 77% of the total reef algal biomass (Fig. 5.16). This can be explained by the general lack of large, canopy-forming brown algae on reefs at Bunbury where reefs are instead dominated by red foliose algae. Elsewhere, the brown algae (Division Phaeophyta) were represented by relatively few species (only 15-24% of all species in any location) yet were by far the most abundant in terms of biomass (51-91% of total biomass). This is not surprising given the large size of the fucalean (eg. *Sargassum*, *Cystophora* and *Platythalia*) and laminarian (eg. *Ecklonia*) brown algae that are common on many nearshore reefs along the lower west coast of WA. In all regions, green algae (Division Chlorophyta) were a significant component of species richness yet contributed little to total biomass. An exception to this trend was seen on reefs at Two Rocks (Fig. 5.15), where large patches of *Caulerpa* spp. are common and can replace brown algae as the dominant benthic layer.

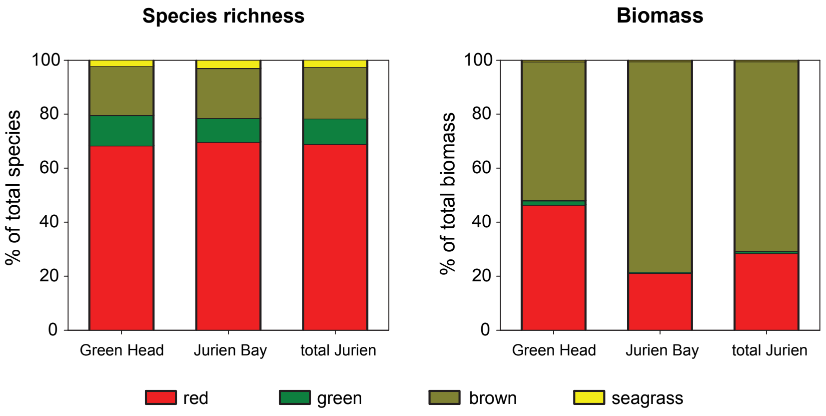

Figure 5.14: Contribution of different marine plant groups to total species richness and total biomass recorded from reef habitats at two locations in the Jurien region.

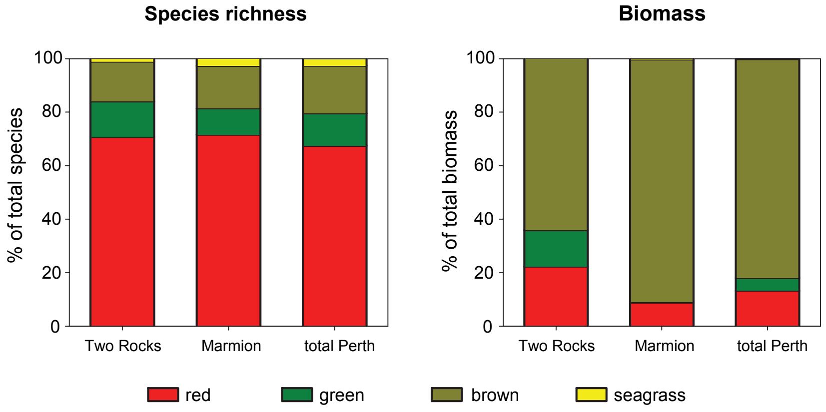

Figure 5.15: Contribution of different marine plant groups to total species richness and total biomass recorded from reef habitats at two locations in the Perth region.

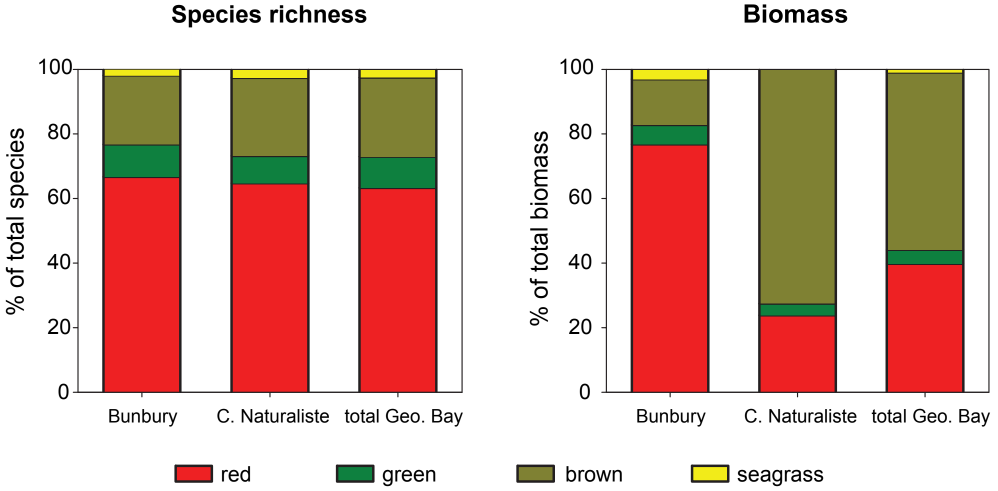

Figure 5.16: Contribution of different marine plant groups to total species richness and total biomass recorded from reef habitats at two locations in the Geographe Bay region.

5.4 Spatial variation in reef algal community structure

Investigators / Institution

Julia Phillips, Russ Babcock, Nicole Murphy, Geordie Clapin, Alison Sampey,
Mat Kleczkowski, Mark Westera

CSIRO Marine and Atmospheric Research

At the largest spatial scale (i.e. region), some pattern in algal community structure was evident. Although there was a substantial degree of overlap in community structure among the three regions (ANOSIM $R = 0.348$, $P = 0.001$), post-hoc pairwise comparisons showed Perth and Geographe Bay to have significantly different algal communities ($R = 0.668$, $P = 0.001$). The dissimilarity in communities was driven by abundance of the kelp, *E. radiata*; only 1.2% of samples in Geographe Bay contained *E. radiata*, compared to 24.5% in Perth (SIMPER).

Ecklonia radiata was also responsible for contributing to similarity between regions. As mentioned, the average abundance of *E. radiata* on Perth reefs was 24.5%, which accounted for 63.9% of the similarity between reefs in this region (SIMPER). *E. radiata* was fairly abundant in the Jurien region also (12.5% of samples and 33.5% contribution to similarity; SIMPER), and algal communities were similar in these two regions ($R = 0.131$, $P = 0.001$; ANOSIM).

When comparing within regions, locations in the Perth region (Fig. 5.17) had an average similarity of 27.6% in species composition (SIMPER). The similarity of species composition on reefs in the Jurien and Geographe Bay regions was considerably lower, at 17.2% and 15.2% respectively. The relatively high degree of similarity in species composition among reefs in the Perth region was again driven by the abundance of the kelp, *E. radiata*, on Perth reefs (SIMPER).

Comparison of algal communities within each location indicated statistically significant differences in algal communities between locations within Geographe Bay was large ($R = 0.665$, $p = 0.001$). Algal communities also varied significantly between locations within Jurien ($R = 0.359$, $p = 0.001$) and Perth ($R = 0.35$, $p = 0.001$) regions although this variation was lower than for locations in the Geographe Bay region. Algal species composition was most similar between sites within the Jurien Bay and Two Rocks ($R = 0.027$, $p = 0.285$), both of which have a number of sites dominated by *Ecklonia radiata* forest.

The clustering of data from Two Rocks and Marmion, and to a lesser extent Jurien Bay, in Fig. 5.17 can be explained by a common suite of species that typify algal assemblages in these areas. The brown algae *Ecklonia radiata* and *Sargassum* spp., along with several red algae including *Pterocladia lucida*, *Rhodymenia sonderi*, *Amphiroa anceps* and *Curdiea obesa*, were abundant at all locations and all species were among those with the highest contribution to the similarity in assemblage structure between reefs within these locations (SIMPER). The Cape Naturaliste data points that are clustered with those from Green Head (Fig. 5.17) were identified as being from the Eagle Bay site. These geographically separate areas both have *Sargassum* spp. (SIMPER) as the dominant canopy-forming brown algae on reefs, in contrast to *E. radiata* which dominates the canopy structure at Two Rocks and Marmion.

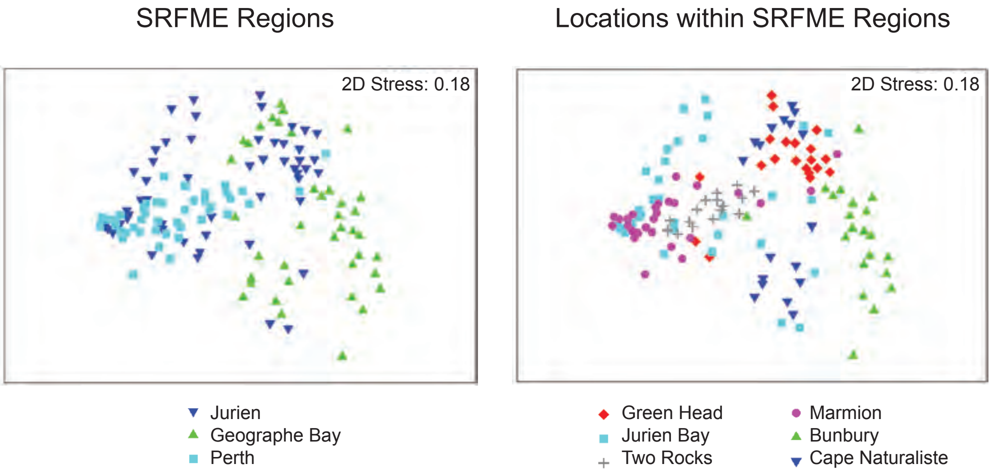

Figure 5.17: Regional and local variation in reef algal assemblages. Results of nMDS ordinations of mean abundance data per sampling event for sites within locations within each SRFME region.

Table 5.4: Results from a 1-way analysis of similarities (ANOSIM) of reef algal community structure among locations and post-hoc pairwise comparisons between locations.

	R statistic	**P**
Global test	0.467	0.001
Pairwise comparisons		
Bunbury vs. Cape Naturaliste	0.665	0.001
Bunbury vs. Jurien Bay	0.720	0.001
Bunbury vs. Greenhead	0.555	0.001
Bunbury vs. Marmion	0.851	0.001
Bunbury vs. Two Rocks	0.732	0.001
Cape Naturaliste vs. Jurien Bay	0.468	0.001
Cape Naturaliste vs. Greenhead	0.474	0.001
Cape Naturaliste vs. Marmion	0.791	0.001
Cape Naturaliste vs. Two Rocks	0.691	0.001
Jurien Bay vs. Greenhead	0.359	0.001
Jurien Bay vs. Marmion	0.062	0.027
Jurien Bay vs. Two Rocks	0.027	0.285
Greenhead vs. Marmion	0.724	0.001
Greenhead vs. Two Rocks	0.531	0.001
Marmion vs. Two Rocks	0.350	0.001

* calculated from rank similarities between groups: $R = 1$ indicates strong separation between groups; $R \approx 0$ indicates null hypothesis is true, that there is no difference between groups.

Variation at the site level (within locations) was much clearer than at either the regional or local level, with clustering often clearly apparent (Fig. 5.18) and highly significant (Table 5.5). The greatest degree of overlap in community composition was evident between the two sites at Two Rocks, while the highest degree of dissimilarity was between the sites at Cape Naturaliste (Table 5.5).

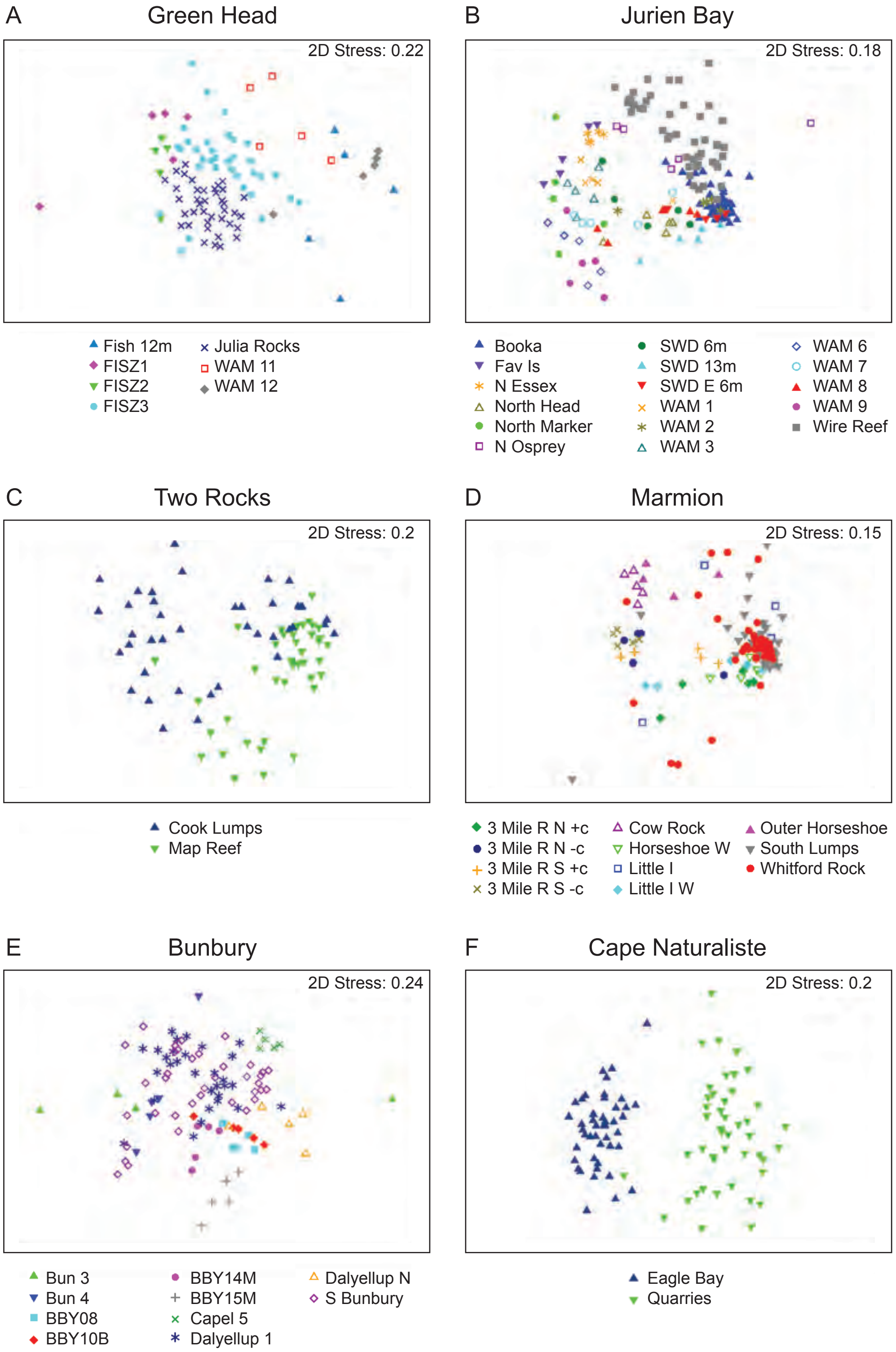

Figure 5.18: Site level variation in reef algal communities. Results of nMDS ordinations for sites within locations within the three SRFME regions.

Table 5.5: Site-level variation in algal communities. Results of ANOSIM for sites within locations at the three SRFME regions.

Location	Global R	Significance level (%)
Green Head	0.660	0.1
Jurien	0.675	0.1
Two Rocks	0.252	0.1
Marmion	0.391	0.1
Bunbury	0.365	0.1
Cape Naturaliste	0.788	0.1

Jurien region

The species composition of algal communities on reefs in Green Head and Jurien Bay showed only a small degree of overlap (Fig. 5.17) with an average dissimilarity of 87.8% (SIMPER). Differences were partly due to the presence of many foliose and turfing species of a more sub-tropical distribution being found on reefs at Green Head. Differences in community structure also resulted from shifts in the abundance of canopy-forming brown algal species: on reefs in Green Head, *Sargassum* spp. accounted for 19.1% of similarity between samples compared to *Ecklonia radiata* at only 1.3% of samples; in Jurien Bay *E. radiata* was the dominant canopy species and contributed 58.9% of similarity between samples while *Sargassum* spp. accounted for only 13.7% (SIMPER).

At Green Head, the algal community composition of sites grouping to the right of Fig. 5.18a are those which had an overlying canopy of large fucalean and/or laminarian brown species. Those grouping to the left were characterised by *Sargassum* spp. and associated red algae, or by communities dominated by red foliose algae and devoid of an overlying canopy of large brown algae.

The clustering of sites in Jurien Bay shown in Fig. 5.18b can be broadly divided in two according to their algal assemblages. Those sites grouping to the right of the diagram are characterised by *Ecklonia radiata* being the species having the highest contribution to similarity between samples from those sites, and these sites were classified as *Ecklonia* forest habitat (see text later in this Section). The sites ranged from those with a continuous canopy of *E. radiata* (>80% contribution to similarity between sites; SIMPER) to those with a mixed *E. radiata*-fucoid canopy (*E. radiata* contribution between 23-44%; SIMPER). Sites grouped to the left side were predominantly characterised by an abundance of *Sargassum* spp., which accounted for 15-82% of similarity in algal assemblages (SIMPER). Low turfing and foliose algae were also an important component of algal assemblages on these reefs.

Perth region

Geographic location of reefs in the Perth region did not affect species composition, with sites at Two Rocks and Marmion having similar, and overlapping, overall algal community structure (Table 5.4 and Fig. 5.17). Within locations, the Two Rocks sites of Map Reef and Cook Lump had very similar algal communities (Table 5.5) and any dissimilarity was attributed to differences in the relative abundance of *Ecklonia radiata* on each reef (SIMPER). *E. radiata* was also responsible for the tight clustering of a number of sites in the centre-right of Fig. 5.18d. Algal communities at Whitford Rock, South Lumps and Horseshoe West all had particularly high abundances of *E. radiata*, which accounted for between 67-79% of similarity of samples from these reefs (SIMPER).

Geographe Bay region

Algal communities at different locations in the Geographe Bay region showed a reasonable degree of separation, with communities from Bunbury reefs differing from those found on Cape Naturaliste reefs ($R = 0.665$, $P = 0.01$; Fig. 5.17). Unlike other locations in the SRFME study area, *E. radiata* was uncommon and instead red algae were the most important components of community structure on reefs in Bunbury, with individual species (eg. *Husseya rubra*, *Spyridia dasyoides*, *Vidalia spiralis*, *Dictyomenia tridens* and *Amphiroa anceps*) contributing as much as 69% to the similarity within a reef (SIMPER).

The two reefs sampled within the Cape Naturaliste location were well separated (Fig. 5.18F and Table 5.5) in terms of their algal communities. The Quarries site was characterised by the abundance of large brown algae belonging to the Cystoseiraceae (eg. *Platythalia, Cystophora*), which was unique among all reefs in the entire SRMFE study area (SIMPER). At Eagle Bay, the most common species were *Sargassum* spp., *Lobophora variegata*, *Cystophora monilifera* and *Botryocladia sonderi* although all these species occurred in less than 8% of all samples (SIMPER). The remaining component of the algal community at Eagle Bay was characterised by a suite of low-stature, mainly red algal species with uniformly low abundances.

Algal habitat types

The sampling and analyses above indicated that much of the variation observed among locations, and particularly among sites within locations, was related to the presence of distinct algal habitat types which often dominated particular reefs. Therefore, moving beyond a species-level approach, sites on reefs in the SRFME study area were classified into algal habitat types based on whole-assemblage structure and composition. A site-level classification chosen as it was the relevant scale at which data could be related to wave modelling and habitat mapping (see Chapter 6) and is the scale at which the effects of many structuring forces operate are thought to manifest themselves (eg. wave energy, nutrient availability, light regime, etc). Next, a set of habitat categories were defined based on existing knowledge and observations of broadly recognizable reef algal habitats, and are described in Table 5.6. Following this, species abundances for each site within a region were input into a similarity of percentages analysis (SIMPER) run in PRIMER, using a Bray-Curtis similarity measure. This procedure allowed the determination of the contribution of each species to the similarity of algal assemblages within a site. Using the % contribution of the highest ranking species (or suite of species) to similarity within a site, the sites were then categorised into one of the habitat types listed in Table 5.6. This classification approach can also be applied at the quadrat level, or at larger spatial scales and has the potential to be used in broad-scale visual habitat classifications.

Ordinations (nMDS) of algal communities within each region based on these *a priori* habitat categories showed fairly good clustering by habitat type, particularly in the Jurien and Perth regions (stress < 0.2, Fig. 5.20). Ordination stress was higher for Geographe Bay (stress = 0.23), yet algal communities still showed clustering by algal habitat although it should be noted that only three habitats were recognised in this region. Ordinations for all regions were not improved by using presence-absence data.

The Jurien region was most diverse in terms in number of habitats (Fig. 5.20), with reefs classified into six different algal habitats. Eight of the 25 reefs at Jurien were classified as *Ecklonia* forest habitat, with *Sargassum* and red foliose the next most common habitats (5 reefs each). Reefs in Perth and Geographe Bay regions were less diverse and could be classified into one of 3 or 4 habitat types. Both regions had a large proportion of reefs that could be classified as low algal habitats, although red foliose habitat was more common in Geographe Bay. Notably, Geographe Bay lacked any reefs that could be considered *Ecklonia* forest. It should be noted, however, that the number of reefs surveyed in Perth and Geographe Bay was around half that for Jurien, which may account for both reduced habitat complexity and apparent absence of certain habitats. Habitat dominated by green algae of the genus *Caulerpa* was commonly observed in small patches (up to ~5 m^2) but not at the reef scale.

Table 5.6: Algal habitat types used in classification of reef habitats in the SRFME study area. Habitat types marked with an asterix (*) indicate those with an overlying canopy of large brown algae. Unmarked habitat types are those without an overlying canopy. Photographs showing examples of each habitat type are shown in Fig. 5.17

Habitat Type	Habitat Code	Description Of Habitat Structure/Composition
Ecklonia forest	E	Canopy consists of only *Ecklonia*, or >50% in canopy with <20% fucoids
Mixed brown canopy	MB	Mix of large brown algae comprising canopy: >20% fucoids in canopy, some *Ecklonia*
Sargassum	S	*Sargassum* >50% of canopy, <20% *Ecklonia*/other large brown algae
Fucoid	F	Fucoids >50%, <20% *Ecklonia*
Red foliose	RF	>70% foliose (upright) red algal species
Coralline/foliose	CF	>70% non-crustose corallines/foliose algae
Low algae	LA	>70% turf/epiphytes/foliose/cover other than algae, <30% of categories above
Turf	T	>70% turf only (algae <10 cm high)
Caulerpa	C	>70% *Caulerpa* spp.

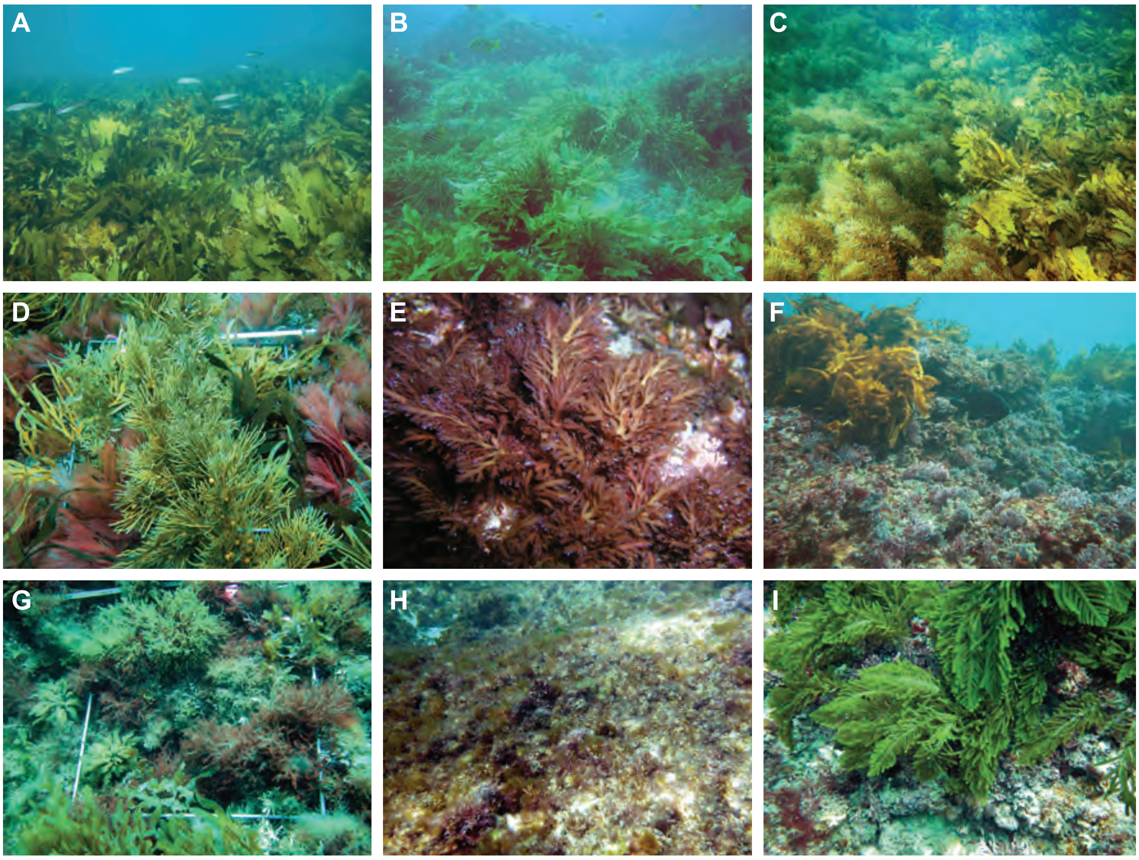

Figure 5.19: Photographs showing examples of the algal habitat categories described in Table 5.6 and used to classify sites

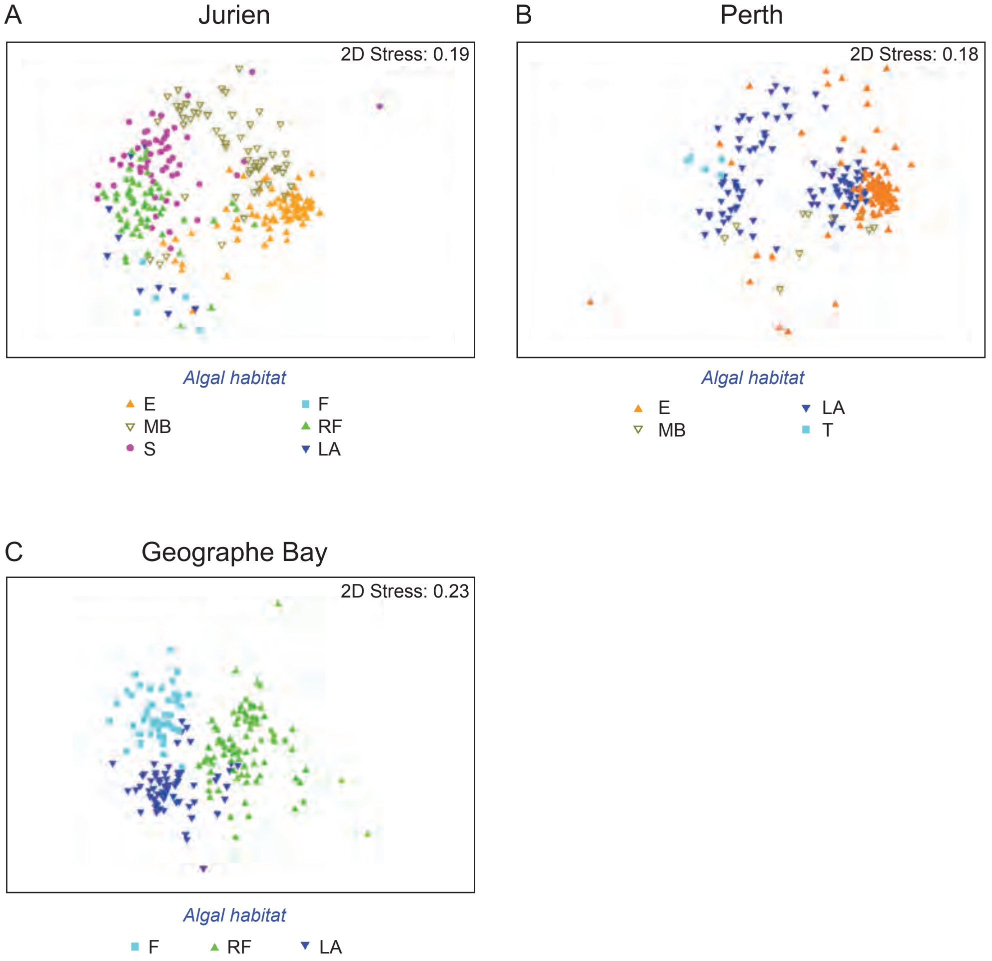

Figure 5.20: nMDS ordination of reef algal community structure within assigned algal habitat categories

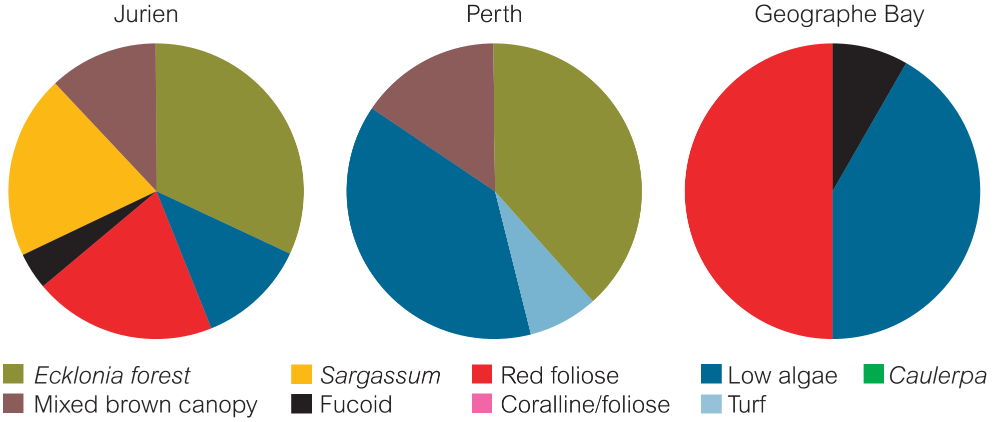

Figure 5.21: Proportion of each of the algal habitat categories assigned to sites on reefs in the Jurien, Perth and Geographe Bay regions using SIMPER analyses. Refer to Table 5.6 for descriptions of each algal habitat.

The success of habitat classification was independently tested using a canonical analysis of principal coordinates (CAP). The ordination was constrained using the *a priori* algal habitats assigned following SIMPER analyses, and untransformed mean species abundances at each site were randomly permuted 999 times on the basis of a Bray-Curtis dissimilarity measure.

The CAP analysis revealed an overall allocation success of 72%. Habitats with a canopy of large brown algae had a higher allocation success rate (Table 5.7) with any errors due to differences in the abundances of understorey species. Habitats lacking a canopy of large browns, namely red foliose, low algae and turf habitats, were more problematic and the success of correctly distinguishing these structurally similar, low-stature habitats was relatively low. This is related to the fact that a suite of species are common across all these habitat types, thus masking the defining characteristics of each. There were very few turf and fucoid dominated sites and it was not possible to draw meaningful comparisons about classification success for these habitats. The classifications are retained for future testing as these habitat types are known to be more common in other regions of WA.

Table 5.7: Allocation success of algal habitat classification of reefs in the SRFME study area. Results are from a canonical analysis of principal coordinates (CAP) which uses a canonical discriminant analysis based on *a priori* habitat types assigned to each reef (site). Numbers in bold type represent correctly allocated habitat types.

	Classification by discriminant analysis								
Original classification	**RF**	**LA**	**E**	**S**	**MB**	**F**	**T**	**Total # of sites**	**% correct**
Red foliose (RF)	8	3	0	0	0	0	0	11	72.7
Low algae (LA)	4	7	1	0	1	0	0	13	53.8
Ecklonia forest (E)	0	0	11	0	2	0	0	13	84.6
Sargassum (S)	0	0	0	5	0	0	0	5	100
Mixed brown canopy (MB)	0	2	0	0	3	0	0	5	60
Fucoid (F)	0	2	0	0	0	0	0	2	0
Turf (T)	0	1	0	0	0	0	0	1	0

5.5 Spatial trends in reef invertebrate communities

Investigators / Institution

Nicole Murphy, Geordie Clapin, Russ Babcock, Alison Sampey, Julia Phillips.

CSIRO Marine and Atmospheric Research

Overview of invertebrate assemblages from the SRFME region

A total of 431 invertebrate taxa were recorded from the SRFME regions of Jurien, Perth and Geographe Bay. Of the 431 taxa, 290 were recorded from Jurien, 243 from Perth and 249 from Geographe Bay (Fig. 5.22). Within regions, 86 taxa were only recorded for Jurien, 47 from Perth and 65 from Geographe Bay (Fig. 5.22). Between regions, 49 taxa were shared between Jurien and Perth, 37 taxa between Jurien and Geographe Bay and 29 taxa between Perth and Geographe Bay, with 118 recorded from all three regions (Fig. 5.22).

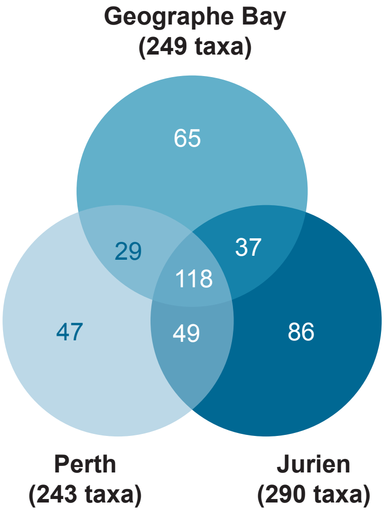

Fig. 5.22: Invertebrate species relationships from the SRMFE regions of Jurien, Perth and Geographe Bay (782 taxa). Numbers in parentheses represent the total number of species found within a region. Areas of overlap show the number of species shared between regions, with the central region showing the number of species common to all three regions.

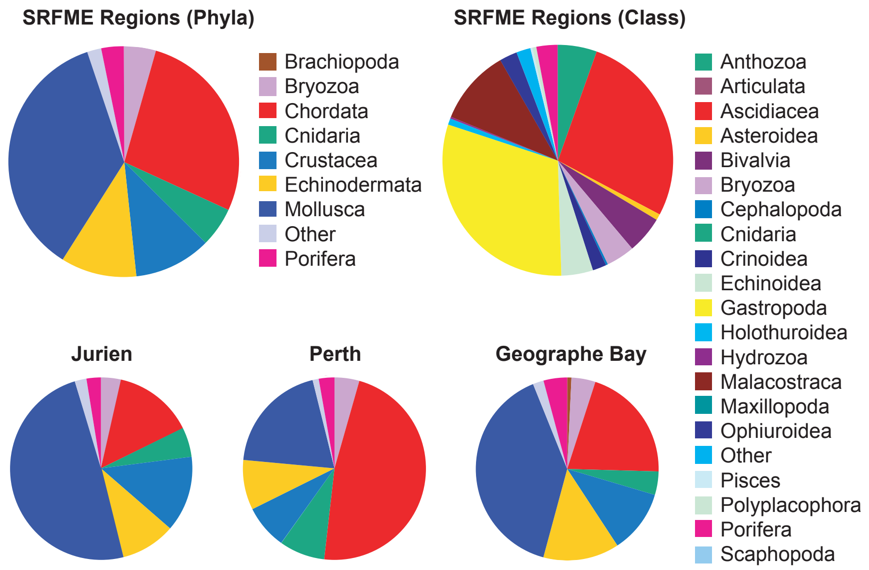

Fig. 5.23: Composition of invertebrate assemblages from the SRMFE region (phylum and class level) and within the SRFME regions of Jurien, Perth and Geographe Bay (phylum).

The phyla Mollusca and Chordata were found to be the two numerically dominant taxa of invertebrate assemblages from the SRFME regions of Perth, Jurien and Geographe Bay. The Echinodermata and Crustacea, as the third and fourth dominant taxa, were roughly equal in their contribution, followed by the Cnidaria, Bryozoa, Brachiopoda and Porifera. The majority of the Chordata was comprised of the class Ascidiacea, with Gastropoda comprising the majority of the Mollusca (Fig. 5.23).

Within the SRFME regions, variation in the contribution of the Chordata (Ascidiacea) and Mollusca (Gastropoda) represented the main differences between Jurien, Perth and Geographe Bay. The Echinodermata, Crustacea, Cnidaria, Bryozoa, Brachiopoda and Porifera were found to contribute equally in each region (Fig. 5.23).

Species identification to date has recognised four new invertebrates, an ophiuroid, cf. *Ophiocomina australis* and three crustaceans, barnacle 2 – juv. cf. nov. sp. on *Sargassum, Hippolyte* sp. nov. and *Juletta* sp. nov. (Hale 1927, Poore 2004). Range extensions for two species have also been recorded for the ophiuroid, *Macrophiothrix spongicola*, from the Ashmore Reef (northern WA) and the crustacean, *Cryptocnemus vincentianus*, from the Gulf of St Vincent, South Australia.

The two types of sampling methods used at each quadrat targeted distinct groups of invertebrates; the 0.25m^2 quadrat samples were collected as part of the algal sampling procedure and were useful in sampling small (<1cm) epifauna associated with the algae. The larger 1m^2 samples targeted sessile or solitary fauna larger than 1cm. Consequently, within each site data were examined separately at the 0.25 m^2 and 1 m^2 levels, to examine broad scale relationships between the core sites at the SRFME regions of Jurien, Perth and Geographe Bay and their locations.

Epifauna (0.25 m^2 quadrat data) showed significant but weak differences among the regions of Jurien, Perth and Geographe Bay (R=0.16, p=0.001) and their locations (R=0.11, p=0.001) (ANOSIM). At the site level a similarly weak separation was found among the sites of Jurien (R=0.15, p=0.001), Perth (R=0.08, p=0.001) and Geographe Bay (R=0.11, p=0.001) (ANOSIM). Consequently we do not interpret these results as representing strong patterns in epifaunal distribution at these spatial scales (1, 10, 100 km). There were no seasonal trends in invertebrate assemblage structure at either for epifauna or for the larger sessile and solitary mobile fauna.

Larger sessile and solitary fauna (1 m^2 quadrat data) displayed a stronger separation among the regions Jurien, Perth and Geographe Bay (R=0.25, p=0.001) and at locations within these regions (R=0.29, p=0.001) (Fig. 5.24). The MDS ordination suggests a continuous, though overlapping, transition between regions and locations along a north-south gradient.

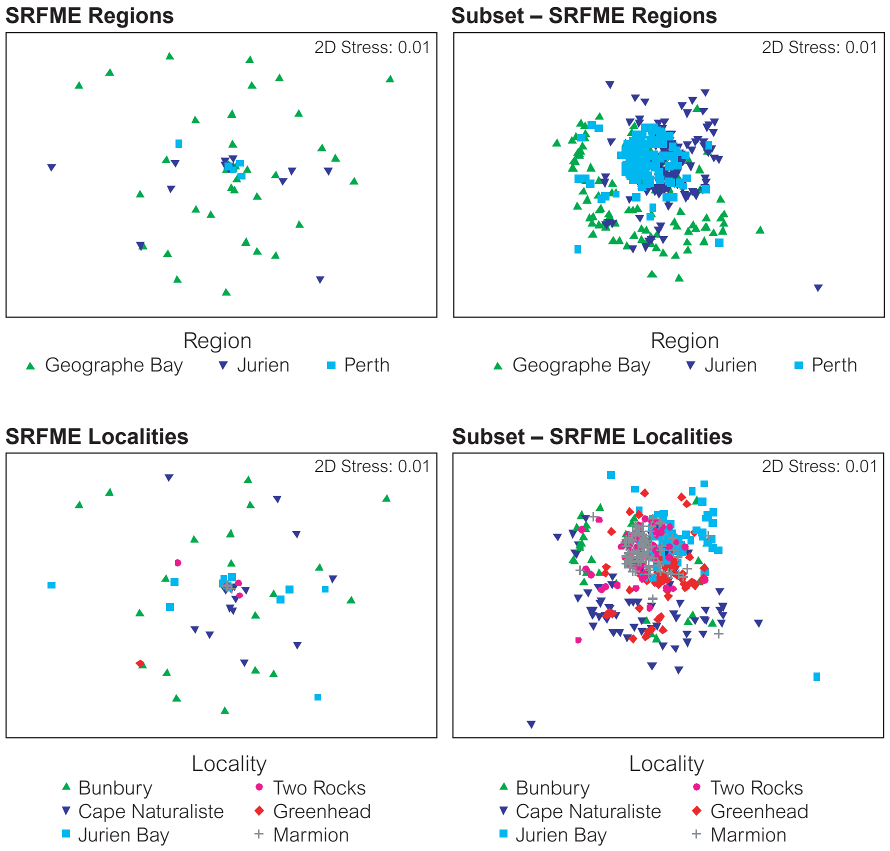

Fig. 5.24: MDS plots for Invertebrate assemblages examined at the level of the factors region and location (1 m^2 quadrat) (subset represents centre cluster from original plot).

Ascidians were found to dominate sessile faunal assemblages in all three regions, with *Polycarpa* sp. 5 (blue and yellow throated), dominating assemblages in Geographe Bay and *Herdmania momus*, dominating assemblages in Jurien and Perth (SIMPER) (Table 5.8).

Table 5.8. Dominant invertebrate species at core SRFME sites. Species listed represent top ranking species from SIMPER analysis and their contribution to within site sample similarity (%) (1 m^2 quadrat).

Region	Location	Site	Species	Average Abundance (% of samples)	Contribution (% similarity between samples)
Jurien	-	-	*Herdmania momus*	0.76	44.37
Perth	-	-	*H. momus*	1.89	52.94
Geographe Bay	-	-	*Polycarpa* sp. 5	0.78	24.24
Jurien	Green Head	FISZ3	*H. momus*	0.84	30.62
		Julia Rocks	*Serpulorbis* sp.	0.93	28.50
	Jurien Bay	Booka	*H. momus*	0.97	45.04
		Wire Reef	*Serpulorbis* sp.	0.79	41.76
Perth	Two Rocks	Cook Lump	*Polycarpa* sp. 5	2.12	43.10
		Map Reef	*H. momus*	0.93	63.03
	Marmion	Whitford Rock	*H. momus*	3.17	69.05
		South Lumps	*Polycarpa* sp. 5	2.54	42.28

Region	Location	Site	Species	Average Abundance (% of samples)	Contribution (% similarity between samples)
Geographe Bay	Bunbury	Dalyellup 1	*Plesiastrea versipora*	0.27	41.96
		South Bunbury	*Polycarpa* sp. 5	3.08	83.20
	Cape Naturaliste	Eagle Bay	*P. versipora*	0.48	25.59
		Quarries	*Polycarpa* sp. 5	0.71	71.81

The species influencing dissimilarity in assemblages, varied between pairs of locations. Numbers of the ascidian, *Polycarpa* sp. 5, were found to drive dissimilarity between the locations of Bunbury and Cape Naturaliste, Bunbury and Jurien Bay, Bunbury and Green Head, Jurien Bay and Marmion, Bunbury and Two Rocks, Jurien Bay and Two Rocks and Green Head and Two Rocks. Between the locations of Cape Naturaliste and Jurien Bay, Jurien Bay and Green Head, Bunbury and Marmion and Cape Naturaliste and Marmion, another ascidian, *Herdmania momus*, drove dissimilarity, with numbers of the gastropod, *Serpulorbis* sp. driving dissimilarity between Cape Naturaliste and Green Head (SIMPER) (Table 5.9, Fig. 5.26).

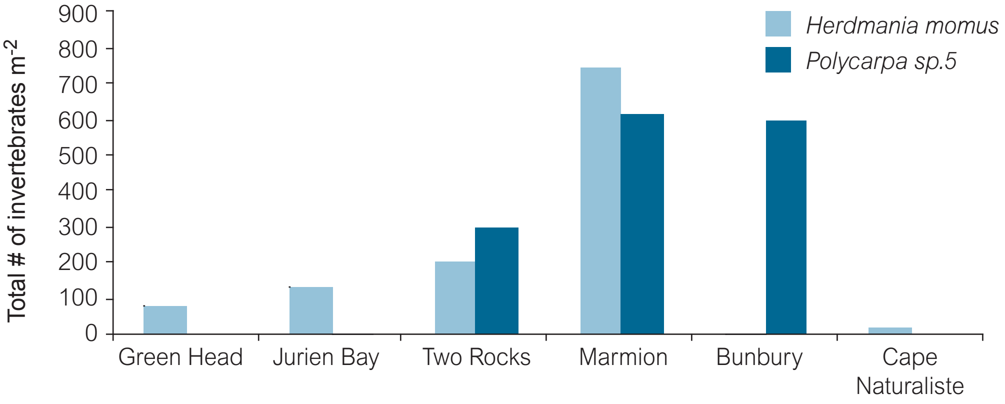

Fig. 5.25: Relative abundance of key invertebrate species found to drive dissimilarity between the SRFME locations of Jurien, Perth and Geographe Bay (1 m^2 quadrat).

Table 5.9. Contribution of invertebrate species found to drive dissimilarity between assemblages in the SRFME regions of Jurien, Perth and Geographe Bay from SIMPER analysis (%) ($1m^2$ quadrat).

Species	Location comparison	Average Dissimilarity (%)	Contribution (%)
Polycarpa sp. 5	Bunbury v Cape Naturaliste	19.86	20.64
	Bunbury v Jurien Bay	17.96	17.71
	Bunbury v Green Head	14.86	15.54
	Jurien Bay v Marmion	15.85	19.28
	Bunbury v Two Rocks	20.59	22.66
	Jurien Bay v Two Rocks	12.16	14.26
	Green Head v Two Rocks	10.47	12.12
	Marmion v Two Rocks	12.97	17.68
Herdmania momus	Cape Naturaliste v Jurien Bay	12.69	13.13
	Jurien Bay v Green Head	10.04	11.51
	Bunbury v Marmion	21.75	24.82
	Cape Naturaliste v Marmion	20.14	21.45
	Green Head v Marmion	14.08	16.34
	Cape Naturaliste v Two Rocks	14.73	15.71
Serpulorbis sp.	Cape Naturaliste v Green Head	10.54	11.36

Species	Site comparison - Jurien	Average Dissimilarity (%)	Contribution (%)
H. momus	Booka v FiSZ3	11.45	14.12
	Booka v Julia Rocks	10.57	11.67
	Booka v Wire Reef	12.17	16.19
	FISZ3 v Wire Reef	9.20	11.18
Serpulorbis sp.	FiSZ3 v Julia Rocks	10.28	12.78
	Julia Rocks v Wire Reef	9.32	10.23

Species	Site comparison - Perth	Average Dissimilarity (%)	Contribution (%)
Polycarpa sp. 5	Cook Lump v Map Reef	15.36	19.86
	Cook Lump v South Lumps	12.23	18.52
	Map Reef South Lumps	18.47	23.27
	South Lumps v Whitford Rock	12.39	18.56
H. momus	Cook Lump v Whitford Rock	11.98	17.30
	Map Reef v Whitford Rock	18.71	23.85

Species	Site comparison – Geographe Bay	Average Dissimilarity (%)	Contribution (%)
Plesiastrea versipora	Dalyellup 1 v Eagle Bay	11.15	11.74
Cenolia trichoptera	Dalyellup 1 v Quarries	20.93	21.11
	Eagle Bay v Quarries	13.92	14.83
Polycarpa sp. 5	Dalyellup 1 v South Bunbury	43.29	45.35
	Eagle Bay v South Bunbury	28.68	29.32
	Quarries v South Bunbury	35.71	36.70

Solitary and sessile invertebrates also showed significant pattern at the among-site level (Jurien, R= 0.23; Perth, R=0.21; Geographe Bay, R=0.26; p=0.001) (ANOSIM), than at the location or regional level. The ascidian, *Herdmania momus*, was found to dominate species assemblages at the sites of Jurien Bay, Green Head, Marmion, Two Rocks, Bunbury and Cape Naturaliste, with another ascidian, *Polycarpa* sp. 5 also dominating assemblages at Marmion, Two Rocks, Bunbury and Cape Naturaliste. The gastropod, *Serpulorbis* sp., was found to dominate assemblages at the sites of Jurien Bay and Green Head, with the cnidarian, *Plesiastrea versipora* and the crinoid, *Cenolia trichoptera*, dominating assemblages at Bunbury and Cape Naturaliste (Table 5.8, Fig. 5.26).

Comparisons between SRFME sites, showed dissimilarity was driven by numbers of *Herdmania momus* at Jurien Bay, Green Head, Marmion, Two Rocks, Bunbury and Cape Naturaliste, with *Polycarpa* sp. 5 also driving dissimilarity at Marmion, Two Rocks, Bunbury and Cape Naturaliste. The gastropod, *Serpulorbis* sp., was found to drive dissimilarity at Jurien Bay and Green Head, with the cnidarian, *Plesiastrea versipora*, and crinoid, *Cenolia trichoptera*, driving dissimilarity at Bunbury and Cape Naturaliste (SIMPER) (Table 5.9, Fig. 5.26).

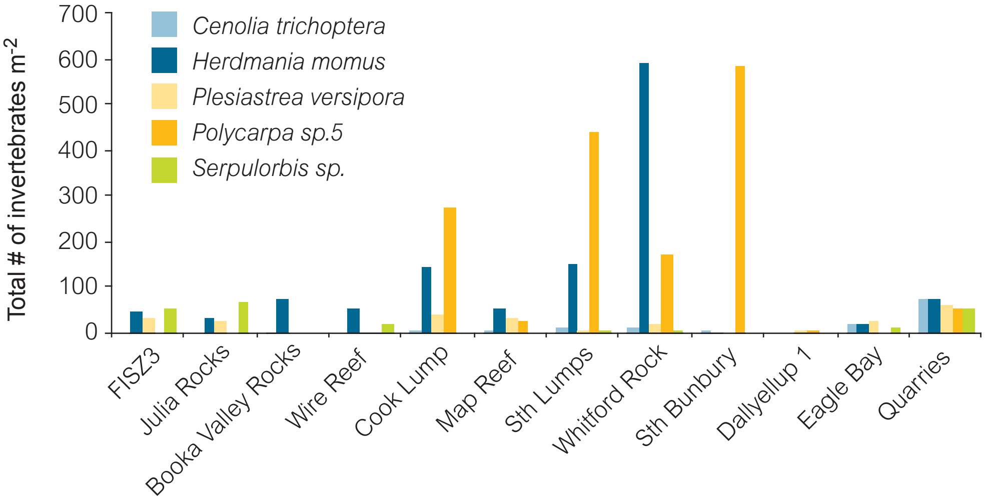

Fig. 5.26: Relative abundance of key invertebrate species found to drive dissimilarity between the SRFME sites of Jurien, Perth and Geographe Bay (1 m^2 quadrat).

5.6 Regional trends in fish communities

Investigator / Institution

Mat Vanderklift CSIRO Marine and Atmospheric Research

Overview of invertebrate assemblages from the SRFME region

A total of 56 species of reef fish were recorded during SRFME surveys. This relatively low number reflects that the fish surveys were done at a more limited number of sites than the algae and invertebrate surveys, and that fish surveys were done once only. Of the 56 species, 34 were recorded from Jurien, 32 from Perth and 26 from Cape Naturaliste (Fig. 5.27).

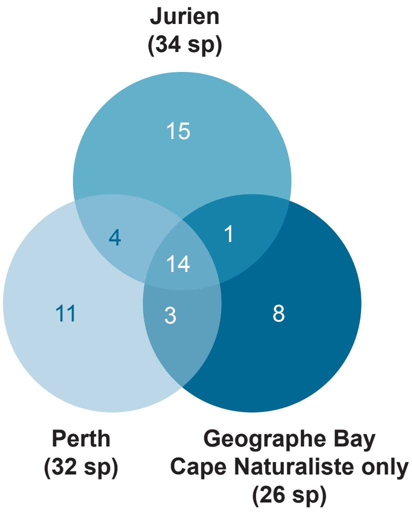

Fig. 5.27: Invertebrate species relationships from the SRMFE regions of Jurien, Perth and Geographe Bay (782 taxa). Numbers in parentheses represent the total number of species found within a region. Areas of overlap show the number of species shared between regions, with the central region showing the number of species common to all three regions.

All three regions were characterised by a similar suite of dominant species (Table 5.10). The large damselfish *Parma* spp (mainly *Parma mccullochi*) was characteristic of all three regions, but was especially abundant at Jurien and Perth. Two species of wrasses (*Notolabrus parilus* and *Halichoeres brownfieldii*) were characteristic of more than one region. The same species contributed most strongly to differences among regions. The western king wrasse *Coris auricularis* distinguished sites at Jurien from those at Cape Naturaliste and Perth: *C. auricularis* was more abundant at Jurien. The western chromis *Chromis klunzingeri* distinguished sites at Cape Naturaliste from sites at Jurien and Perth, *C. klunzingeri* being more abundant at Cape Naturaliste.

Table 5.10. Dominant fish species at core SRFME sites. Species listed represent top ranking species from SIMPER analysis and their contribution to within site sample similarity (%).

Region	Location	Site	Species	Average Abundance	Contribution (% similarity between samples)
Jurien	-	-	*Parma* spp	5.09	35.86
			Coris auricularis	7.18	32.09
			Notolabrus parilus	1.85	13.14
Perth	-	-	*Parma* spp	5.23	42.37
			Notolabrus parilus	3.19	33.78
			Halichoeres brownfieldii	0.61	4.07
Cape Naturaliste	-	-	*Chromis klunzingeri*	6.56	31.97
			Parma spp	1.11	25.02
			Halichoeres brownfieldii	2.44	11.11

Table 5.11. Contribution of fish species to dissimilarity between regions.

Species	Location comparison	Average Dissimilarity (%)	Contribution (%)
Coris auricularis	Cape Naturaliste v Jurien	13.36	15.15
Chromis klunzingeri	Cape Naturaliste v Jurien	10.51	11.92
Parma spp	Cape Naturaliste v Jurien	9.13	10.36
Chromis klunzingeri	Cape Naturaliste v Perth	10.74	12.34
Parma spp	Cape Naturaliste v Perth	9.56	10.98
Notolabrus parilus	Cape Naturaliste v Perth	7.33	8.42
Coris auricularis	Perth v Jurien	12.38	16.06
Pempheris klunzingeri	Perth v Jurien	8.78	11.40
Parma spp	Perth v Jurien	8.66	11.24

Fish assemblages showed distinct differences among the three regions studied (Fig. 5.28). Substantial differences were indicated by a large *R* statistic (0.75) from a two-way ANOSIM , although the significance of this could not be tested due to the low number of permutations possible (only 15 permutations). Differences among locations within the regions were negligible ($R = 0.1$, $P > 0.05$). Perth reefs were characterised by higher overall abundances of brown-spotted wrasse (*Notolabrus parilus*) and silver drummer (*Kyphosus cornelii*); Jurien reefs were characterised by higher overall abundances of western king wrasse (*Coris auricularis*) and western buffalo bream (*Kyphosus sydneyanus*); Cape Naturaliste reefs were characterised by higher overall abundances of Brownfield's wrasse (*Halichoeres brownfieldii*) and black-headed puller (*Chromis klunzingeri*).

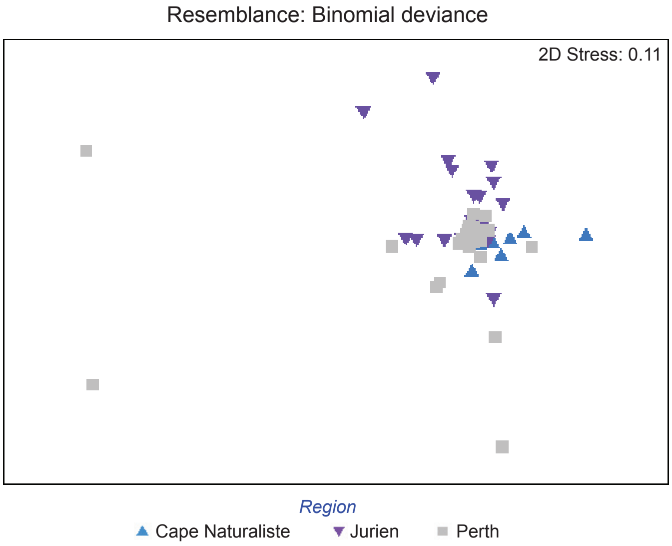

Figure 5.28: Multidimensional scaling of fish assemblages found on reefs in the SRFME study area, grouped according to the three main regions studied.

Within each of the regions, there were clear differences in the fish assemblages of individual sites (Fig. 5.29), but not between locations. These patterns were reflected by ANOSIM: differences among sites were statistically significant for Perth ($R = 0.26$, $P < 0.01$), Jurien ($R = 0.41$, $P < 0.01$) and Cape Naturaliste ($R = 0.26$, $P = 0.05$).

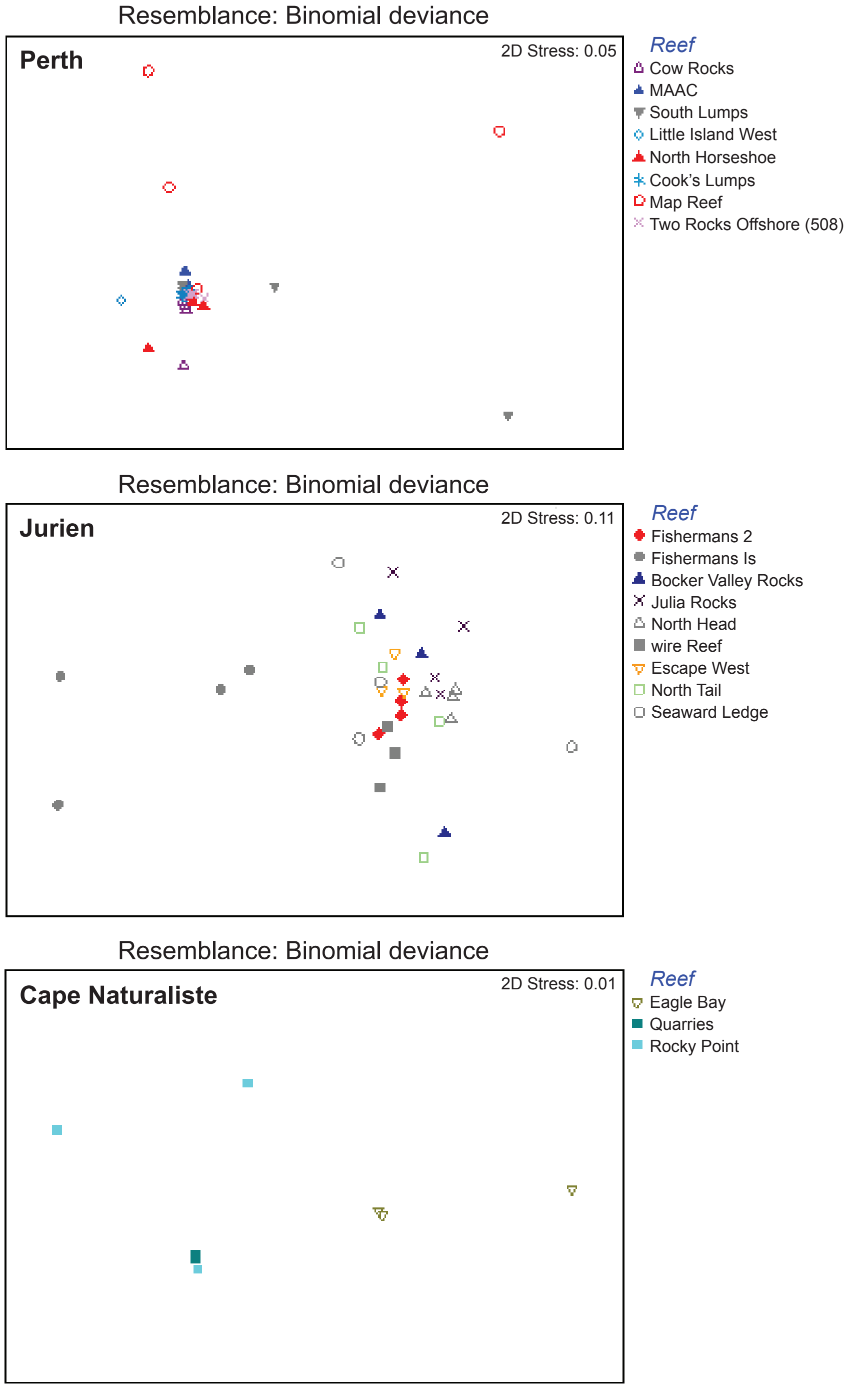

Figure 5.29: Multidimensional scaling of fish assemblages found on reefs in the SRFME study area, grouped according to reef separately for the three main regions studied.

5.7 Environmental correlates of reef algal community structure

Investigators / Institution

Julia Phillips, Russ Babcock, Phillip England, Geordie Clapin,
Alison Sampey, Nicole Murphy

CSIRO Marine and Atmospheric Research

As the largest number of sites sampled were from the Jurien region, and because Jurien was the only region from which modelled wave-driven orbital velocity at the sea floor was available, the correlation of algal community structure with environmental variables was restricted to this region. The extent to which environmental variables explained the patterns observed in reef algal community structure was investigated, as a means of better understanding and ultimately modelling important factors influencing reef ecosystems. Variables considered included nominal categories of depth of reef (≤6 m, 6.1-10m, >10 m), cross-shore position (inner, mid or outer shore) and reef relief (high, medium or low relief), while light attenuation, water column nutrients (Si, PO_4, NO_x, NO_2, NH_4), water column particulates (chl-*a*, total suspended solids (TSS)), as well as depth and rugosity of each quadrat were directly measured. Additionally, wave modelling was used to derive a number of parameters relating to the orbital motion experienced at each reef; namely cumulative, minimum, maximum and mean orbital motion (refer to Chapter 6.1).

Using square-root transformed biomass data, ordinations (nMDS) of algal communities based on depth category, cross-shore position, or reef relief, did not reveal definitive patterns in community structure that could be related to these reef properties, and plots are not included here ($R<0.3$, $p<0.06$; ANOSIM). A similar lack of patterns resulted when presence-absence species data was used instead, indicating that this suite of reef descriptors are not important in structuring algal communities, at least across the range of environmental variation encountered in this study.

For the remaining, directly measured or modelled environmental variables, the approach taken was to analyse the algal data and then determine how well the environmental variables, either singly or in combination, was correlated to algal community structure. This was achieved using the BIOENV procedure in PRIMER, whereby a Bray-Curtis dissimilarity measure among samples was used for the algal data. Log($0.1+x$) transformation was applied to the phosphate and nitrogen concentrations before all environmental data was normalised prior to analysis. Euclidean distances were used as the measure of dissimilarity among environmental data and Spearman rank correlations were used as the measure of agreement between the algal and environmental resemblance matrices. Rank correlation coefficients (ρ) were generated from 99 random permutations of the data and compared to the true value of ρ to determine the statistical significance of the BIOENV procedure. Since environmental data were missing for some sites or variables, linking of algal and environmental variables was restricted to those sampling events for which full datasets existed. The BIOENV procedure was repeated using both biomass (square-root transformed) and presence/absence algal data: in all cases, stronger correlations with environmental variables existed when presence/absence data was used and only these results are presented here.

In the Jurien region, surface complexity of reefs (ie. quadrat rugosity) and orbital motion explained a large and significant proportion ($\rho=0.686$, $p=0.01$) of the variation in reef algal communities based on the presence/absence of species (Table 5.12). The four orbital motion parameters used in this analysis – cumulative, minimum, maximum and mean orbital motion – are naturally highly auto-correlated so any attempt to identify which is more important as an algal structuring force should proceed with caution. Nevertheless, it is clear that algal communities in Jurien are strongly influenced by both reef rugosity and exposure to wave forces, since the best eight results from BIOENV contain no other environmental variables either singly or in combination (Table 5.12). At this point, NOx was included in the combination of important environmental variables. Nitrogen is accepted as the most limiting nutrient in the marine environment (Lobban & Harrison 1994) and further investigation into the role of N in regulating algal community structure is recommended.

Table 5.12: Results from linking multivariate algal community analysis to environmental variables for reefs in the Jurien region. Rank correlations (ρ) were determined using the BIOENV procedure in PRIMER following 99 random permutations of presence/absence algal data and normalised environmental data. Global ρ=0.686, p=0.01.

			Best results	
	Variables	**No. of variables**	**ρ**	**Variable #'s**
1	Light attenuation coeff.	3	0.686	10, 11, 13
2	Mean Si	4	0.683	10 -13
3	Mean PO_4	2	0.675	10, 13
4	Mean NO_x	5	0.673	10 -14
5	Mean NO_2	4	0.673	10, 11, 13, 14
6	Mean NH_4	4	0.671	10, 11, 13, 15
7	Mean Chl-*a*	3	0.668	10, 12, 13
8	Mean TSS	3	0.668	10, 13, 14
9	Mean quadrat depth	4	0.666	10, 12–14
10	Mean quadrat rugosity	5	0.665	10, 11, 13–15
11	Mean site rugosity			
12	Cumulative orbital motion			
13	Minimum orbital motion			
14	Mean orbital motion			
15	Maximum orbital motion			

5.8 Relationships between algal communities and faunal diversity and biomass

Investigators / Institution

Nicole Murphy, Geordie Clapin, Russ Babcock, Alison Sampey, Julia Phillips

CSIRO Marine and Atmospheric Research

Algal habitat type and invertebrate assemblage distribution

To measure the relationship between algal communities and their associated fauna, invertebrate assemblages were related to algal community (habitat) type (classified at the quadrate level) (Table 5.6). Comparisons included all quadrat data (0.25 m^2 and 1 m^2 separate or combined) and belt transects designed to measure larger or rarer invertebrates (25 ×1 m).

For the purposes of exploring relationships between algal communities and invertebrates, the structurally similar habitat classes of coralline/foliose (CF) and red foliose (RF) habitat were combined as were the fucoid (F) and mixed brown algae (MB) habitats. Previous analyses have shown these classes to be difficult to separate (Table 5.6). In both instances the latter habitat name (i.e. red foliose and mixed brown algae) has been used hereafter.

Over the three SRFME Regions, *Ecklonia* was found to be the single most dominant algal habitat type at Jurien, Perth and Geographe Bay, with low algae comprising the second most common group (Fig. 5.30). Based on the classifications above, mixed brown algae and *Sargassum* habitats formed an equal proportion of the total quadrats to that of red foliose, with the habitat type fucoid representing the smallest overall proportion (Fig. 5.30). Overall, those habitats dominated by large brown algae comprised slightly more than half of all habitats.

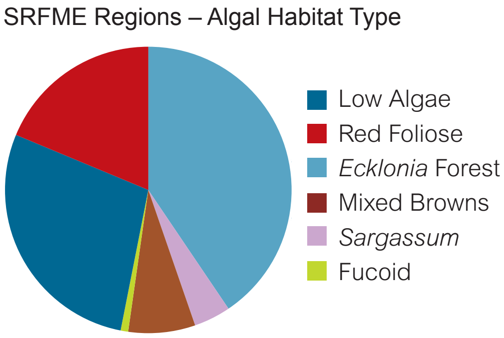

Fig. 5.30: Relative abundance of algal habitat types from the SRFME regions of Jurien, Perth and Geographe Bay.

When invertebrate density (combined 0.25m^2 and 1m^2 quadrat data) from the SRFME regions of Jurien, Perth and Geographe Bay was assessed against algal habitat type, a weak separation was found between invertebrate assemblages and algal habitat type (R=0.26, p=0.001) (ANOSIM) (Fig. 5.31).

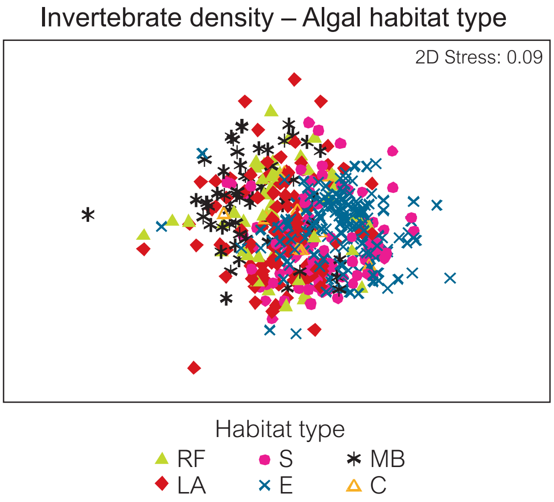

Fig. 5.31: Invertebrate assemblage as a function of algal habitat type. MDS plot for the SRFME regions of Jurien, Perth and Geographe Bay (combined 0.25m^2 and 1m^2 quadrat data). Refer to Table 5.6 for algal habitat definitions.

For the 0.25 m^2 quadrat data, a higher number of invertebrate taxa were found to be associated with turf (T) habitats, followed by *Caulerpa* (C), *Ecklonia*, *Sargassum*, low algae, red foliose and mixed brown algae (Fig 5.31). Data from the 1 m^2 quadrat, found a higher number of taxa associated with low algae and red foliose, followed by mixed brown algae, turf, *Sargassum*, *Ecklonia* and *Caulerpa* habitats (Fig. 5.32).

Generally, higher numbers of invertebrate taxa were identified from habitats without a canopy (*Caulerpa*, red foliose, low algae, and turf), compared to canopy dominated habitats (*Ecklonia*, mixed brown algae and *Sargassum*), with this pattern becoming stronger when invertebrates collected off the algae were examined (Fig. 5.32).

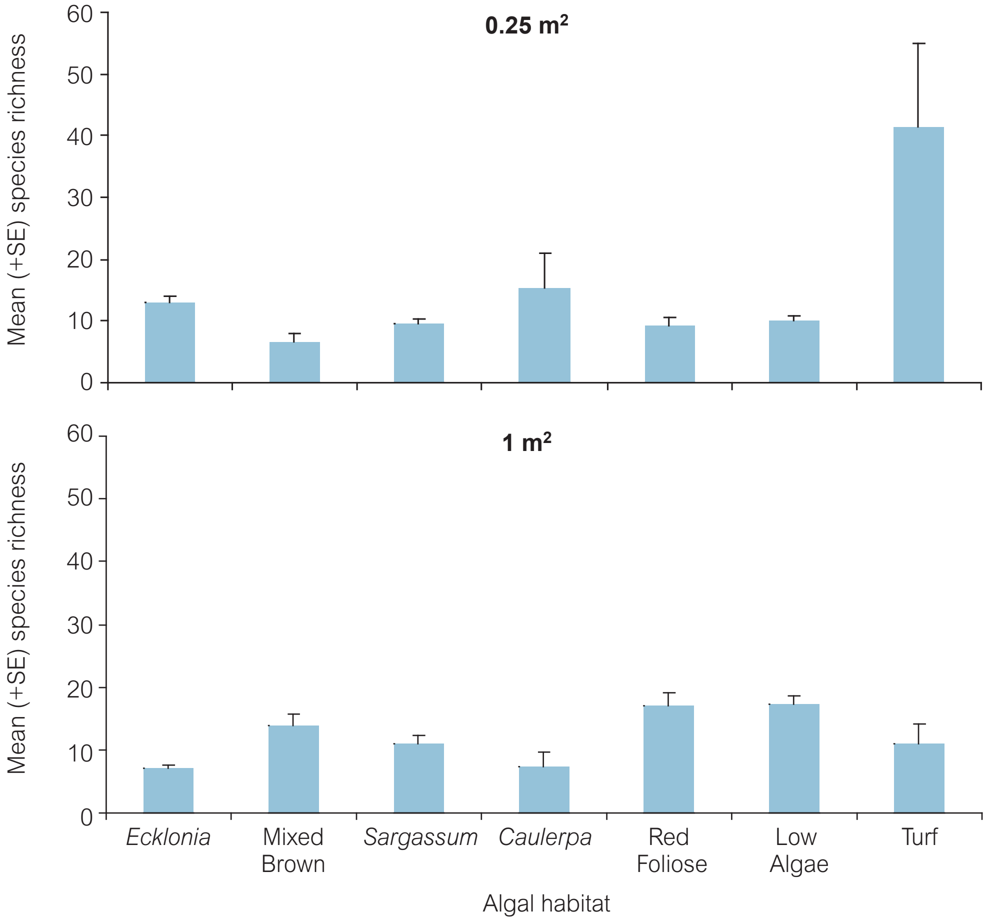

Figure 5.32: Species richness of invertebrates collected from 0.25 m^2 and 1 m^2 quadrats per algal habitat type.

SIMPER analysis of habitat type for the 0.25 m^2 quadrat data showed the top ranking species of *Pyrene bidentata* was primarily associated low algae, *Ecklonia* and *Sargassum* habitats; *Mitrella austrina* with low algae, fucoid and *Caulerpa*; *Muricopsis planilirata* with red foliose; and *Hippolyte caridina* with mixed brown algae (Fig. 5.33). For the 1 m^2 quadrat, data showed the top ranking species of *Herdmania momus* was primarily associated with low algae, *Ecklonia* and *Sargassum* habitats; *Polycarpa* sp. 5 with red foliose and *Caulerpa*; and *Cenolia trichoptera* with fucoid habitat (Fig. 5.33).

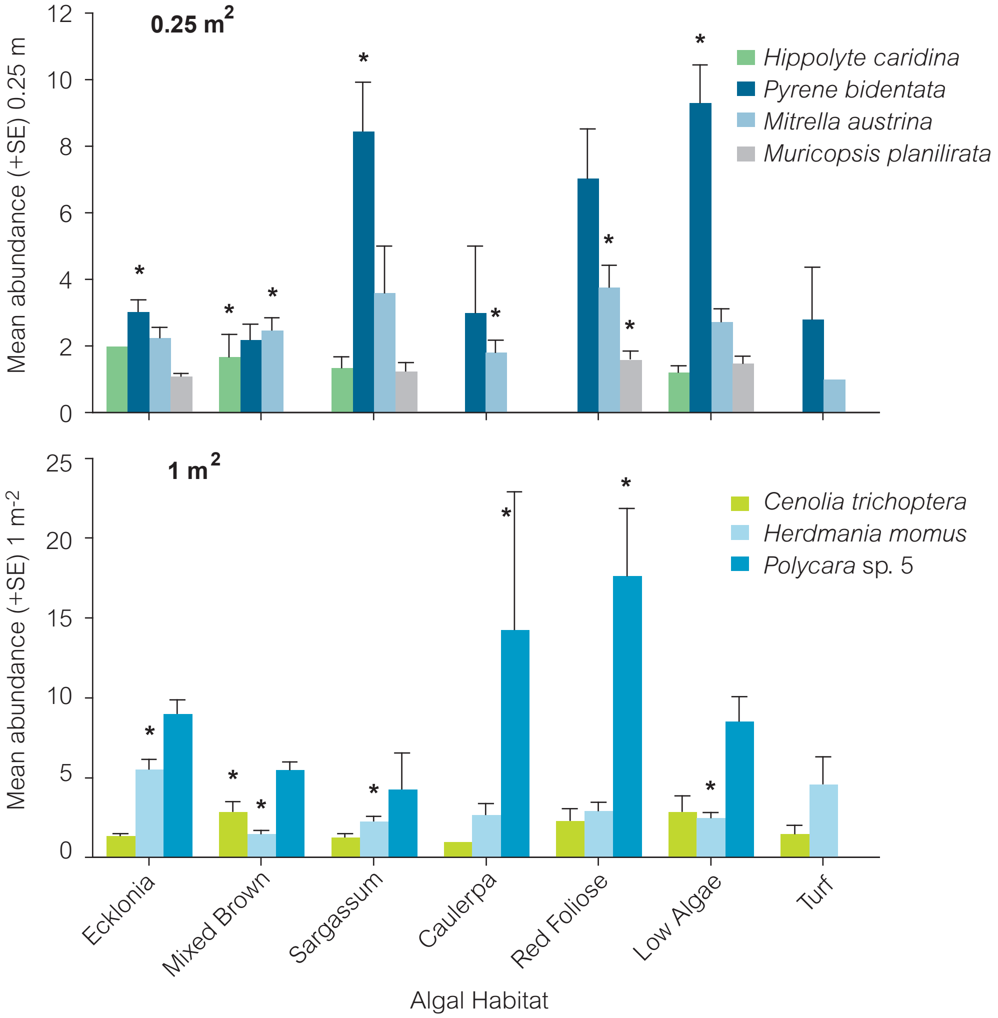

Figure 5.33: Mean abundance of taxa from 0.25m^2 and 1m^2 quadrats per algal habitat type (as assigned to individual quadrats). Marked taxa (*) represent top ranked species from SIMPER analysis of algal habitat type.

The number of mobile inverts (0.25 m^2 and 1m^2 quadrats combined) from the SRFME regions of Jurien, Perth and Geographe Bay, representing the Mollusca, Echinodermata and Crustacea, was assessed in relation to those algal habitat sites classified as *Ecklonia* forest. Not only were higher numbers of taxa present in non-canopy habitats, the number of individuals was also correlated with habitat type. As kelp density increased, invertebrate number was seen to decrease across all size classes of Mollusca, Echinodermata and Crustacea (Fig. 5.34). This trend was significant at both Jurien and Perth, but not at Geographe Bay where *Ecklonia* is a relatively rare component of reef algal assemblages.

Table 5.13. Mobile invertebrate density as a function of *Ecklonia* canopy density. One Way ANOVA on total density of gastropods, crustaceans and echinoderms,) (Combined 0.25 m^2 and 1m^2 quadrat data).

	R^2	***df***	***SS***	***MS***	***F***	***Significance F***
Jurien	0.412	1.0	156874.9	156874.9	51.8	0.0
Perth	0.113	1.0	23003.1	23003.1	7.0	0.0
Geographe Bay	0.001	1.0	543.7	543.7	0.1	0.8

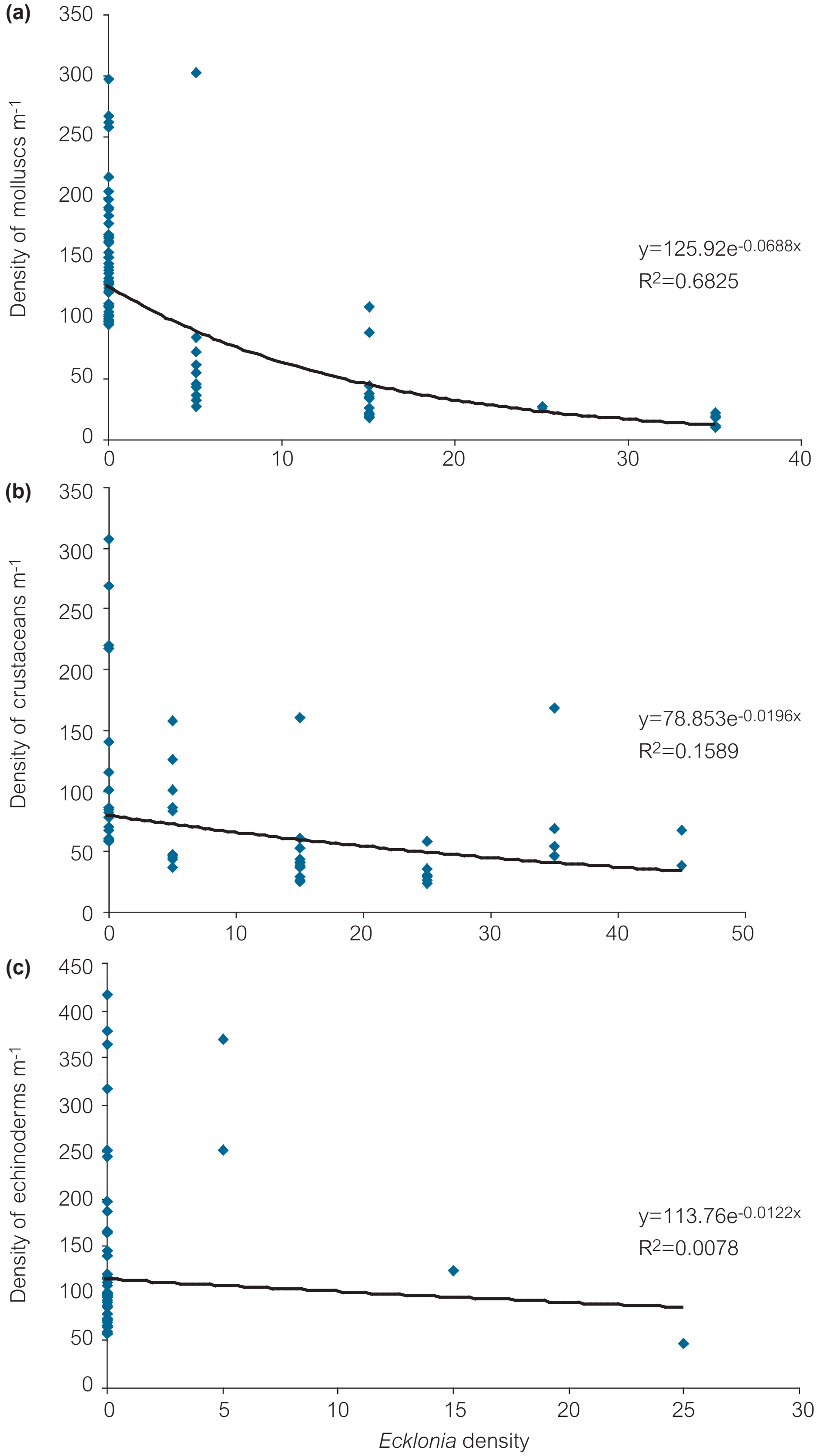

Figure. 5.34: Relationship between density of *Ecklonia radiata* and a) molluscs, b) crustaceans and c) echinoderms across the SRFME study area. Data was pooled in bins of 10, with the upper quartiles plotted for regression (Combined 0.25 m^2 and $1m^2$ quadrat data).

There were also strong relationships between algal community composition and the abundance of larger sessile invertebrates. Belt transects revealed strong trends among algal habitats in the abundance of corals and sponges. Brown algal dominated habitats totalled 53% of habitats covered by transects at Marmion, yet for these same transects only 22% of sponges and 7% of corals were recorded from brown algal dominated habitats (Fig. 5.35). Note that *Caulerpa* habitat was not recorded along belt transects. The transects also gave an indication of the spatial scale of the patches. Canopy and non-canopy patches were approximately the same average length (canopy 2.4 ±2.1m, non-canopy 2.5 ±2.1m) and the maximum patch sizes recorded were also approximately the same for canopy and non-canopy patches (9 and 11 m respectively).

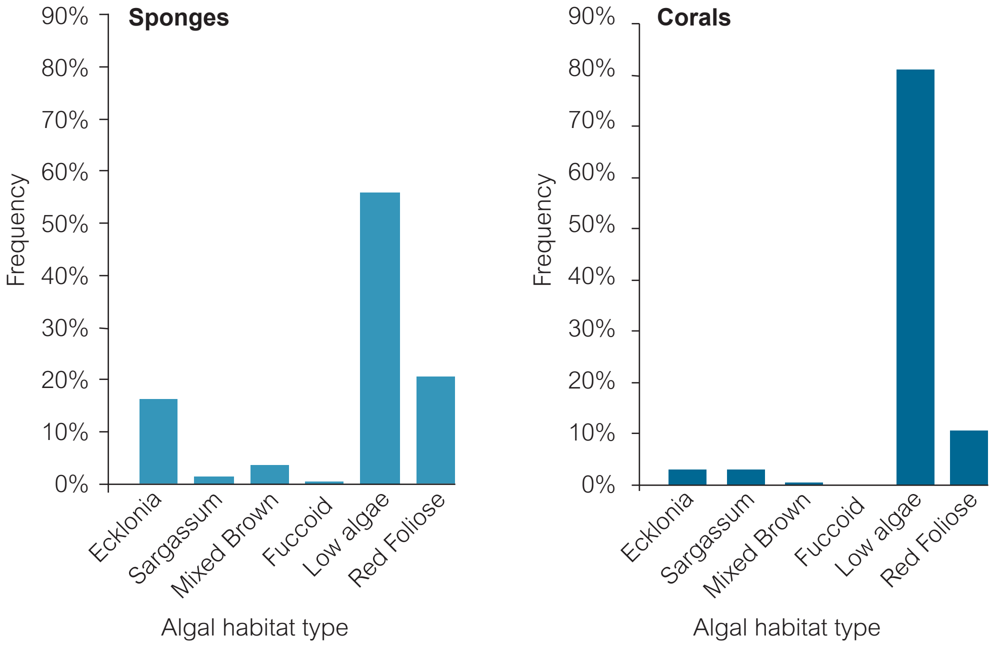

Fig. 5.35: Algal habitat associations of sessile invertebrates (sponges and corals). The proportion of invertebrates from belt transects in six major algal habitat types at Marmion.

5.9 Shallow water habitat mapping

Investigators / Institution

Peter Fearns, Dirk Slawinski, Phillip England, Geordie Clapin,
Julia Phillips, Russ Babcock.

CSIRO Marine and Atmospheric Research

Wojciech Klonowski

Curtin University of Technology

In SRFME we aimed to advance the science of hyperspectral remote sensing for application as a mapping and monitoring tool in shallow Western Australian coastal environments. Here we describe initial efforts to map benthic habitat in the Jurien Bay region using the airborne sensor, HyMap (Hyvista Corporation, Sydney). We present results of analysis of the northern section of one of the HyMap strips; chosen because it had good representation of each habitat type. The remote sensing-derived results are validated by comparison with video-based ground truthing information. This work represents the first of its kind undertaken in WA.

Video data

The total number of video frames was 1807. For the HyMap validation exercise the number of classes of substrate was limited to three; sand, seagrass and brown algae. Table 5.14 shows the number of video frames for each class of substrate where at least 10% of the frame contained that class. Note that each video frame can contain more than one class of substrate, so the sum of all frames from all classes amounts to more than 1807.

Table 5.14. The number of video frames that contained at least 10 percent cover for each substrate class. The total number of video frames was 1807. Some frames contained more than one substrate type and are therefore counted more than once.

Substrate class	Number of video frames
Sea grass	523
Sand	598
Algae	1111

Comparison of video and remote sensing data

Achieving a useful outcome from hyperspectral habitat classifications is a matter of setting thresholds for reflectance parameters that result in the optimal trade-off between accurate classification of the substratum and minimize the number of cells that are not classified. For Jurien these optimal reflectance parameter values were; sand=0.015, seagrass=0.006 and brown algae=0.002. These parameters produced validation percentages of sand = 52%, seagrass = 48%, and brown algae = 88% for ground truthed sites which were judged to have at least 10% cover of one of these habitat types. Validation percentages were calculated as the percentage of video-classified pixels of a particular class for all pixels that were classified by HyMap at the chosen threshold.

Judging where to set the balance between accuracy and coverage will in part be determined by the intended application of the habitat map as some uses will require higher levels of certainty than others. Brown algae was the most accurately classified of the three habitat types as this category achieved the highest reliability with respect to the pixels for which ground truth data were available. This seems counter-intuitive as sand appears to be the brightest and most distinctive bottom type in remote images of shallow water. This result may be related to the problems associated with accurately identifying sand when seagrass is present at low to medium densities, as it often is at Jurien Bay. It may also be related to water depth, which is lowest over raised reef where algae mostly occur, reducing water column effects on the bottom reflectance and thereby improving accuracy for this habitat class.

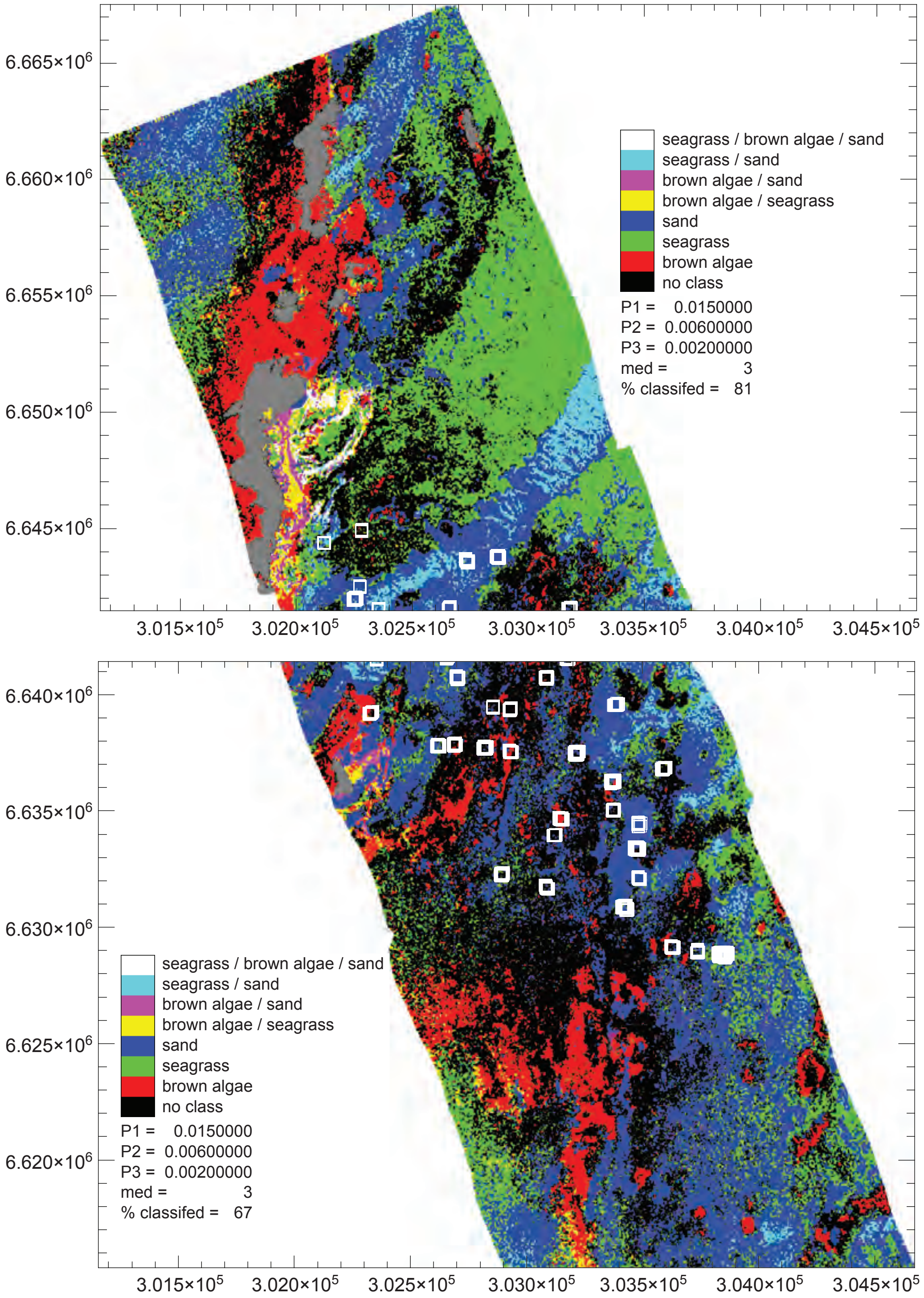

Fig. 5.36: Habitat map of the Fishermans Island area of Jurien Bay Marine Park using optimised reflectance thresholds.

Benthic plant communities at Jurien Bay are highly biodiverse (Section 5.4) and there is likely to be a corresponding diversity of spectral signatures among the dominant species represented in the bottom reflectance signal. Furthermore, the conspicuous spatial patchiness in reef habitats occurs on a scale which corresponds closely to that of HyMap (~1-5m). Continued field campaigns to build the spectral library of substrates should lead to better understanding of the spectral variability of substrates, and therefore improved estimates of substrate cover from remote sensing data.

One can envisage a classification technique based on statistical information related to such factors as spatio-temporal variations in spectral nature, patch scale dynamics, depth, rugosity, wave exposure, local and historical knowledge. The output of the model outlined here lends itself to such probabilistic methods, where products are delivered at every pixel in an image, and each pixel also contains information which may be interpreted as a confidence estimate.

A key to the difference between *in situ* ecological data collection and remote sensing methods is that *in situ* methods are often assessed by some form of statistical sampling theory. *In situ* results are analysed with the understanding that a small sample (a number of quadrats) of a population (a complete reef structure) is being measured. The results might be analysed using ANOVA techniques to report, say, the ability to classify a particular characteristic (such as 10% change in coral cover) with a high (> 90%) statistical power. However, remote sensing methods sample the complete population (the complete reef). The power of the remote sensing data is therefore in its spatial coverage.

One of the products determined from the remote sensing data is water depth. Figure 2.20 in Vol. 1, sec. 2.2.5 shows model-derived bathymetry compared to hydro-acoustical bathymetry data (WA Department of Planning and Infrastructure). For 1500 data points the RMS error was less than 7%. The model-derived substrate map may be overlayed on the model-retrieved bathymetry. This provides a very powerful tool for improving the accuracy of habitat classifications, as contextual information can greatly increase classification success but these clues have usually have to be obtained through independent sources (e.g. Ong *et al* 1998). Figure 5.37 shows the habitat class data extracted from the northern (top) portion of Figure 5.36 overlaid on the retrieved bathymetry. Brown algae (red) is situated along the sides of the raised reef structure. Sand (blue) occurs in the low lying channel running across the middle of the region (and mega-ripple structures of partially vegetated sand substrata can be seen). Sea grass (green) covers the broad low lying and relatively smooth area to the right of the scene. The unclassified (black) pixels atop the mounds in Figure 5.37 are the result of breaking waves and islands. Areas of mixed algal/sand or algal/seagrass habitat form a relatively small proportion of the total area, but interestingly they are all located in a very concentrated area of the landscape, in the shallow wave sheltered area behind Fisherman Is. and its associated reefs. In general the congruence of the geomorphological aspects of the map and the biological classifications provide a significant level of validation of the overall classification success of the approach.

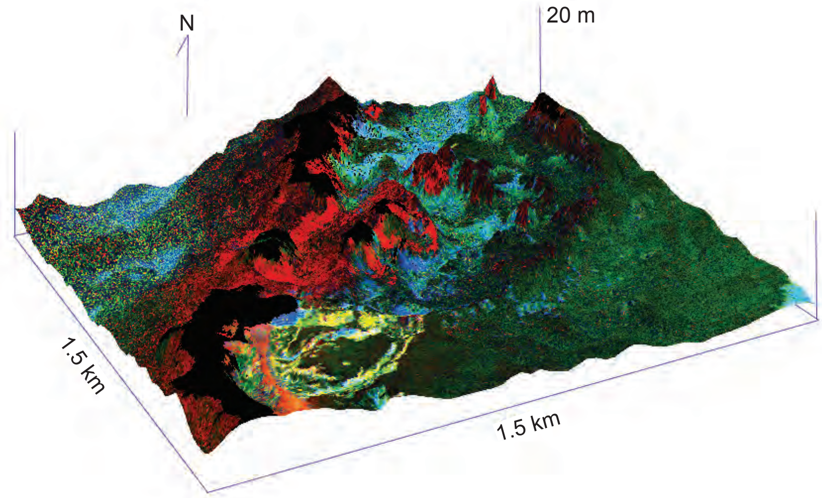

Figure 5.37: Substrate classes (red – brown algae, green – sea grass, blue – sand, yellow – algae/sand, purple – algae/seagrass, turquoise – sand/seagrass, white – sand/seagrass/algae) overlayed on model derived bathymetry. Maximum water depth is approximately 15 m. The spatial extent of the image is approximately 1.5 km x 1.5 km. The region portrayed is the northern most section of the HyMap flight line shown in Figure 5.36. The vertical resolution is exaggerated to emphasise the variability in bathymetry across the scene.

This work represents the first application of a physically based optical model to the processing of hyperspectral remote sensing data for coastal mapping undertaken in Western Australia. We are confident that hyperspectral remote sensing can be a valuable tool in monitoring and mapping shallow coastal waters in WA. Challenges include overcoming signal to noise ratio in deeper water and over dark substrates. Future advances in sensor technology will improve this state. The optical model is, we believe, valid for the range of optical conditions typically experienced in SW WA coastal waters.

While there is a perceived high cost of HyMap data, it presents significant opportunities for shallow water habitat mapping and classification since it can produce high resolution bathymetry at the same time as habitat data. While its use is limited to relatively shallow waters these are precisely the areas where hydroacoustic methods lose their power because of the reduction in acoustic swath width in shallow water. The combination of shallow water hyperspectral mapping and multibeam acoustic mapping and habitat modelling techniques in deeper waters promises to provide a seamless picture of habitats across the continental shelf. These data will for the basis for bioregional planning and more process orientied studies such as biogeochemical modeling, trophodynamic modeling.

Discussion

The SRFME study found a strong seasonal signal in algal biomass in all regions, however processes underlying this pattern varied for different locations, or for particular sites within locations depending on the dominant algal habitat type. Most locations showed lowest biomass in winter (e.g. Jurien Bay, Marmion, Two Rocks and Bunbury) but others showed summer minima, where the majority of sites were dominated by *Sargassum*. The proximal factors that drive these variations also differ among locations. Erosion of biomass is most likely to be the factor driving changes in *Ecklonia* dominated sites (Marmion, Two Rocks, Perth) (Kirkman 1981) while light limitation is likely to be a major factor at Bunbury, most likely due to seasonal re-suspension of particulate matter and sediment in eastern Geographe Bay by winter and spring storm events and long-period swells. In the case of Bunbury these effects appear to occur across the entire algal community which is largely made up of foliose red and brown algae. Where *Sargassum* dominates sites (Green Head), algal phenology can explain reduced algal biomass in summer (Kendrick 1993). In contrast to the pattern for biomass, algal community structure showed no seasonal trend, which was also the case for invertebrates.

Among the study regions the overall number of algal species recorded was similar. While variations in number were not large, there were more species recorded at the lower latitude sites, and fewer recorded in the Perth region. In this regard it is worth noting that this may be explained by variation in the relative dominance of large brown algae in the different regions. In all the regions, by far the largest contribution to overall species diversity was made by the red algae (Figs. 5.13-5.15). The highest densities of *Ecklonia* were found at reefs in the Perth region (Fig. 5.20) and since there is an inverse relationship between *Ecklonia* biomass and that of red algae (Figs. 5.13-5.15), it is perhaps not surprising that fewer species were recorded around Perth where *Ecklonia* appears to be particularly dominant. At this point we can only speculate on the underlying cause of the dominance of *Ecklonia* at some sites in the Perth region. The potential for anthropogenic nitrogen sources (Fig 5.3) to enhance the growth of *Ecklonia* may provide one explanation worthy of further investigation. Nutrient levels seem to be elevated in the area and to carry a high level of $\delta^{15}N$ (Fig. 5.6), a sign of terrestrial effluent origins for this nitrogen. Other Laminarian algae are known to be nitrogen limited (Davison *et al.* 1984, Brown *et al.* 1997, Hepburn & Hurd 2005) however it is not known if this is actually the case for *Ecklonia* on the WA coast.

Macroalgal community structure of varied at all the spatial scales we examined, but was strongest at the site level. In fact, site level variation is likely to be largely responsible for the patterns observed at larger scales. Regional trends were due to the separation of Geographe Bay sites from more northern sites, and this difference could be attributed to a lack of sites dominated by *Ecklonia radiata*. Similarly there were even clearer differences at the location level, except between sites at Jurien and the Perth region dominated by *Ecklonia*. In fact, at the site level, the differences among sites, even within locations, was greater than the differences between sites at the most widely separated regions. This strongly suggests that for algal community structure, processes operating or varying across relatively small scales may be responsible for much of the variation observed on west coast reefs. Assemblages not dominated by *Ecklonia* or other canopy species were most often composed of a diverse mixture of medium to small sized foliose algae, mainly red and brown algae, though green algae were occasionally dominant. Our study has shown that for the study area these habitats can on average form almost 50% of all algal communities, and are likely to be of greater importance than previously assumed in WA, although other recent studies in temperate Australia have shown that on rocky reefs algal habitats that are not dominated by a closed kelp canopy are a characteristic and important feature of reefs on the WA south coast, South Australia and southern New South Wales (Fowler-Walker and Connell 2002).

Since the nature of this variation was often associated with clear qualitative differences in community structure, e.g. presence or absence of a canopy, we developed a method to classify algal communities based on a semi-quantitative mix of structural and taxonomic attributes. The system was 75% reliable and offers a means of classifying algal assemblages for use in higher level analysis of patterns at the landscape scale and as a rapid system for visual quantification of habitats for mapping and ground truthing.

A statistical model relating algal assemblage structure to physical environmental variables in the Jurien region showed that the two factors most strongly associated with community structure were sea bed roughness at the 1 m and 10 m scales, and modelled seabed orbital velocity. Wave generated water movement across the seabed and small scale seabed topography are likely to interact very strongly, further reinforcing the conclusion that small scale variations in ecological processes are likely to be of prime importance in determining the structure of benthic reef assemblages. Processes controlled by interactions of topography and water motion include physical disturbance (dislodgement), diffusive processes (gas and nutrient exchange) and sediment transport (scour and burial) (Hurd 2000). It is important for us to understand the implications of this small scale variation in algal assemblages for several practical reasons. Ecological studies, whether long term monitoring or extensive mapping surveys, need to be explicit about what sorts of habitats they are describing. To fail to do so will create a high level of uncertainty for subsequent research.

For invertebrates weaker patterns were present, particularly for the algal-associated epifauna. Some pattern was present in the larger sessile and solitary fauna, but levels of similarity/dissimilarity did not vary markedly across scales. The lack of pattern suggests that the spatial scales encompassed in the sampling (regions, locations, sites), which was designed primarily to quantify algal assemblages, was not adequately capturing variation in the invertebrate assemblages.

When examined at different spatial scales however, informative patterns did emerge. Species number varied according to the algal habitat type with epifuanal invertebrate species richness (at the scale of 0.25 m^2 quadrats) higher for turf habitats, followed by *Caulerpa*, *Ecklonia* forest, *Sargassum*, low algae, red foliose and mixed brown habitats. A higher number of solitary and sessile invertebrates (1 m^2 quadrat) were found to be associated with low algae and red foliose habitats, followed by mixed brown, turf, *Sargassum*, *Ecklonia* forest and *Caulerpa* habitats. As for the algae, the highest number of invertebrate species was recorded at Jurien, and Perth had the lowest numbers of species although numbers were only marginally greater at Geographe Bay. While the magnitude of the differences is relatively small, it is once again interesting that the region with the most *Ecklonia* dominated sites had the lowest number of species.

For larger sessile invertebrates, belt transects revealed strong trends for coral and sponge abundance, for low algae and red foliose algal habitat types. Brown algal dominated habitats totalled 53% of habitats covered by transects at Marmion, yet for these same transects only 22% of sponges and 7% of corals were recorded in these areas. These patterns essentially reflect algal habitat structure and coverage, and its patchiness or variability not just at the site level but within sites. Interestingly one of the coral species (*Plesiastrea*) was one of the taxa most responsible for dissimilarity among sessile and solitary invertebrate assemblages at the site level (Fig. 5.25). Sessile invertebrates such as corals and sponges, may achieve a higher larval settlement rate and/or higher subsequent survival and growth, in habitat that is lower and sparser in comparison to the typically dense, canopy forming brown algae species. Physical abrasion by kelp is a likely explanation for this since mechanical damage by large kelps is known to influence the distribution of other invertebrates. While the coral species in question are hermatypic species and do require light, which is also lower under kelp canopies, these same species are also found in nearby overhangs and walls associated with sciaphilous filter feeder assemblages (sponges, colonial ascidians, bryozoans, gorgonians; R. Babcock pers. obs.) therefore light is less likely as an explanation for their relative absence under kelp.

At the scale of individual quadrats there were significant patterns in the overall abundance of mobile invertebrates, particularly molluscs and crustaceans. Most of these animals are relatively small and likely to be key contributors to secondary production in the reef ecosystem (Edgar 1990). Interestingly this pattern resulted from a significant negative correlation between invertebrate abundance and the biomass of *Ecklonia radiata*, which in this case turns out to have a key indirect influence on invertebrate assemblages.

Fish assemblages showed a contrasting pattern to those of algae and invertebrates, with a high level of variation among assemblages at the regional level and virtually none at the location level. However at the site level there was once again significant variation in fish assemblages. We attribute this consistent variation at the site level to the association of fish assemblages with definable algal habitat types that tend to dominate at particular sites. While assemblages dominated by large brown algae dominated at just over half the sites, nearly as many were characterized by a canopy of large brown algae and were instead characterized by a diverse assemblages of foliose and filamentous red and brown algae.

Across all three major groups we have studied, algae, invertebrates and fish, we see the importance, even dominance, of processes operating at relatively small scales (meters to tens of meters) for structuring variation in benthic assemblages. This variation has important implications for ecological processes which will be explored in Chapter 6. Some aspect of wave action, coupled with the nature of the substratum, interact to determine the characteristics of the algal community. The characteristics of the algal community in turn appear to strongly determine the nature of invertebrate assemblages. For fish, these aspects of habitat also appear to be important, although in their case there may also be stronger large-scale biogeographic factors influencing distribution across the west coast region. At the regional level some locations have physical characteristics that mean larger scale processes play a more important role. Variation in water quality in eastern Geographe Bay creates conditions that result in a seasonal change in algal biomass quite distinct from other parts of the west coast. The implications of this unusual pattern merit further exploration. It is possible that elevated nitrogen levels in Perth metropolitan waters are linked in some way to the abundance of *Ecklonia* dominated habitats at Marmion. For most of the coast smaller scale studies focused on the way in which environmental factors impact at the site or even quadrat scale are likely to lead to a broader general understanding of key ecological processes. The role of such small scale processes, and of nutrients in coastal reef systems, will be explored as part of a 5 year program beginning in 2006.

This small-scale understanding will have to be applied from the bottom-up to larger scale pictures of ecological processes across the coastal ecosystem as a whole. Remotely sensed habitat mapping shows significant promise as a tool in the scaling up process to the landscape level and integrating information at a range of scales

Acknowledgments

Dr John Huisman (Murdoch University).

References

Anderson, M.J., Millar, R.B. (2004). Spatial variation and effects of habitat on temperate reef fish assemblages in northeastern New Zealand. *J. Exp. Mar. Biol. Ecol.* 305(2): 191-221.

Brearley A., (2005). Ernest Hodgkin's Swanland: The Estuaries and Coastal Lagoons of South-Western Australia. UWA Press.

Brown MT, Nyman MA, Keough JA, Chin NKM (1997) Seasonal growth of the giant kelp *Macrocystis pyrifera* in New Zealand. *Marine Biology* 129:417-424

Clarke, K. R., Gorley, R. N. (2006). PRIMER v6: User Manual/Tutorial. PRIMER-E Ltd, Plymouth.

Colwell, R. K., Coddington, J. A. (1994). Estimating terrestrial biodiversity through extrapolation. *Philosophical Transactions of the Royal Society of London. Series B* 345: 101-118.

Davison IR, Andrews M, Stewart WDP (1984) Regulation of growth in *Laminaria digitata*: use of *in-vivo* nitrate reductase activites as an indicator of nitrogen limitation in field populations of *Laminaria* spp. *Marine Biology* 84:207-217

Edgar GJ (1990). Predator-prey interactions in seagrass beds. I. The influence of macrofaunal abundance and size-structure on the diet and growth of the Western Rock Lobster *Panulirus cygnus* George. *J. Exp. Mar. Biol. Ecol.* 139:1-22

Fowler-Walker MJ, Connell SD (2002). Opposing states of subtidal habitat across temperate Australia: consistency and predictability in kelp canopy-benthic associations. *Marine Ecology Progress Series* 240:49-56.

Hepburn CD, Hurd CL (2005) Conditional mutualism between the giant kelp *Macrocystis pyrifera* and colonial epifauna. *Marine Ecology Progress Series* 302:37-48.

Huisman J.M., Walker D.I. (1990). A catalogue of the marine plants of Rottnest Island, Western Australia, with notes on their distribution and biogeography. *Kingia* 1:349-459.

Hurd CL (2000) Water motion, marine macroalgal physiology, and production. *Journal of Phycology* 36:453-472.

Keesing, J and Heine J. (2005). Strategic Research Fund for the Marine Environment: Interim Final Report CSIRO Marine and Atmospheric Research Perth. ISBN 1 921061 04 9.

Kendrick, GA (1993) *Sargassum* beds at Rottnest Island: species composition and abundance. In: The Marine Flora and Fauna of Rottnest Island, Western Australia, Wells, FE, Walker, DI, Kirkman, H, Lethbridge, R, (Eds.), WA Museum, pp. 455-472.

Kirkman H (1981) The first year in the life history and the survival of the juvenile marine macrophyte, *Ecklonia radiata* (Turn.) J. Agardh. *J .Exp. Mar. Biol. Ecol.* 55:243-255

Kirkman H (1989) Growth, density and biomass of *Ecklonia radiata* at different depths and growth under artificial shading off Perth, Western Australia. *Australian Journal of Marine and Freshwater Research* 40:169-177

Lobban, C. S., Harrison, P. A. (1994). Seaweed Ecology and Physiology. Cambridge University Press, Cambridge.

Phillips JC, Kendrick GA, Lavery PS (1997) A test of a functional group approach to detecting shifts in macroalgal communities along a disturbance gradient. *Mar. Ecol. Progr. Ser.* 153:125-138.

Underwood AJ, Chapman MG and Connell SD (2000). Observations in ecology: you can't make progress on processes without understanding the patterns. *J. Exp. Mar. Biol. Ecol.* 250:97-115.

Van Elven B.R., Lavery P.S., Kendrick G.A. (2004). Reefs as contributors to diversity of epiphytic macroalgae assemblages in seagrass meadows. *Marine Ecology Progress Series* 276:71-83.

Womersley, H. B. S. (1987). The Marine Benthic Flora of Southern Australia. Part II. South Australian Government Printer, Adelaide, Australia.

CHAPTER 6

6. BENTHIC ECOSYSTEM DYNAMICS

Investigators / Institutions

Russ Babcock (Project Leader), Geordie Clapin, Phillip England, Matt Kleczkowski,
Martin Lourey, Nicole Murphy, Julia Phillips, Alison Sampey, Mat Vanderklift, Jason Waring,

CSIRO Marine & Atmospheric Research

Kylie Cook, Catriona Stuart-Andrews, Kris Waddington

University of Western Australia

Thomas Wernberg Edith Cowan University

Outline

Executive Summary

Human activities can affect coastal ecosystems strongly, particularly the biological communities of the shallow sea floor. The goal of the SRFME study into benthic (sea floor) ecosystem dynamics was to advance the understanding of human impacts on these ecosystems and communities through a set of focussed studies addressing the relative influences of exposure to wave action (the dominant physical disturbance) and fishing by humans (i.e. direct and indirect trophic interactions).

Several discrete studies addressed the influence of wave action. One approach compared modelled wave-induced forces with species richness of macroalgae collected as part of the coastal ecology programme. A key finding was that diversity of assemblages of reef algae was related to the wave-energy regime they experience. Quadrat level species diversity was highly correlated with wave exposure, with much of the variance in species composition explained by wave exposure.

Other correlates of exposure to waves are seen in differences in patterns and processes across the lagoons, that become evident as differences between reefs close to the shore (sheltered from waves) and reefs far from the shore (exposed to waves). This was found to be the case for the biomass of detached macrophytes (drift, or wrack), densities of sea urchins (higher densities inshore) and magnitudes of drift grazing by sea urchins (higher inshore), and the importance of ammonium, derived from the breakdown of wrack, as a source of nitrogen to kelps at Jurien. Analyses of the morphology of drift kelps accumulating at one location showed that a large proportion of drift kelps originate from the reefs further offshore, providing evidence for large-scale trophic linkages across the lagoon that are a direct result of wave action. Inconsistent trends were found for cross-lagoon patterns in primary productivity and recruitment of sea urchins. For primary productivity, both direct and indirect methods (i.e. tagging of individual kelp and estimates based on biomass, respectively) found that productivity was higher offshore at Jurien, but not at Marmion. These inconsistent patterns suggest that we do not yet fully understand the main factors influencing rates of primary productivity of reef algae.

Trophic interactions can also have a considerable influence on patterns of reef benthos, so an additional component of the research focussed on an initial assessment of the influence of predators on the structure of reef assemblages, including the first assessment of the effects of a 16-year fishing closure at Kingston Sanctuary (Rottnest Island). The overall abundance of fish, and the abundance of predatory fish and western rock lobster (*Panulirus cygnus*), were higher inside the Kingston Sanctuary than at adjacent fished reefs. These differences in abundances of predatory fishes and lobsters were reflected by patterns of predation, with higher predation on tethered sea urchins in the sanctuary. However there were no simple trends in the abundances of prey: the abundance of one species of sea urchin (*H. erythrogramma*) was lower in the area protected from fishing, consistent with the pattern predicted if predation was a strong influence, but the abundance of a second species (*C. tenuispinus*) was higher in the area protected from fishing. The species composition of assemblages of reef algae did not differ between sanctuary and fished areas, suggesting that although we experimentally measured indirect cascading effects of fishing on predation, these did not manifest themselves strongly as a trophic cascade that affected herbivores or primary producers in a discernable way.

Introduction

The Western Australian coast encompasses one of the world's marine biodiversity hotspots, and contains high species richness and endemism (Roberts *et al.* 2002). The lower west coast (roughly, Geraldton to Cape Leeuwin), that was the geographic focus of SRFME research, is a region of overlap between tropical and cool temperate biotas (Wilson and Allen 1987). The area is unusual because it features high-biomass, high-productivity benthic ecosystems despite relatively low-nutrient waters. The lower west coast also hosts the majority of Western Australia's human population, with the majority living near the coast around Perth (Department of Environmental Protection 1998). The pressures associated with human use will continue to increase as the population of Western Australia is predicted to rise from 2 to 2.7 million by 2029 (Department of Environmental Protection 1998).

Pressures on the environment therefore impact most heavily on coastal benthic ecosystems. Understanding ecological patterns and processes in these ecosystems will be increasingly important as managers strive to minimise these impacts. The State of the Marine Environment Report (Zann 1995) highlighted the poor state of understanding of ecological processes, and the limited data for much of the coast, as well as the limited application of existing knowledge in management.

Much of the practical focus of SRFME benthic ecology studies was directed at understanding spatial and temporal variability in diversity and composition of reef benthos (Chapter 5). But the overall goal of SRFME research into benthic ecosystem dynamics (this chapter) was to investigate some of the mechanisms underlying this variability, and the potential for fishing by humans to alter food webs. The research was implemented as a number of discrete components, each designed to evaluate specific mechanisms thought to be important in shaping patterns in reef communities, in particular wave action (physical disturbance) and fishing by humans.

Exposure to waves is known to influence community structure (Goldberg & Kendrick 2004), intraspecific morphological variation (Stewart & Carpenter 2003), nutrient uptake (Larned 1999) and patch dynamics (Menge *et al.* 2005). Our understanding of the importance of waves was improved through various methods. A combination of observations and modelling was used to test associations between (modelled) wave-induced forces and species richness of macroalgae (Section 6.1). Because practical constraints make it difficult to obtain data with good spatial or temporal coverage of the hydrodynamic forces operating throughout an extensive reef system, numerical wave modelling is a widely used alternative means of quantifying hydrodynamic forces, especially in regions for that comprehensive meteorological and oceanographic data are available. To our knowledge, investigations of ecologically significant hydrodynamic forces as estimated from numerical models are rare and performed at coarse spatial resolutions (e.g. Hemer in press). While there are limitations to the use of numerical wave modelling at ultra-fine spatial scales (< ~5m) where turbulence induced non-linearity is exhibited, applying wave modelling in and around coastal reef systems to investigate ecologically important processes is an under-exploited approach.

If waves are a dominant influence on reef benthos, one prediction is that patterns would be different across the lagoon - between reefs close to the shore (sheltered from waves) and reefs far from the shore (exposed to waves). An additional component of the research therefore examined whether rates of three key ecological processes (primary production, herbivory and recruitment) varied between these two broad types of reefs (Section 6.3). As part of this, research also included a component that examined the magnitude of exchange of drift kelp between these two reef strata.

Trophic interactions can also have a considerable influence on patterns of reef benthos. For example, in several parts of the world, hunting and fishing has reduced predators of sea urchins to ecologically trivial abundances, resulting in increases in sea urchin abundance, followed by landscape-scale decreases in canopy-forming primary producers due to grazing (Babcock *et al.* 1999, Estes *et al.* 2004). Grazing is therefore another process that could create and maintain patches of different habitats. A fourth component of the research therefore focussed on an initial assessment of the influence of predators on the structure of reef assemblages, taking advantage of a protected area at Rottnest Island (Section 6.3).

Methods

Wave modelling and patterns of diversity

This study focussed on Jurien Bay. The coast in this region consists of shallow limestone reefs interspersed with sand. Shelf bathymetry is complex, with depths ranging between 0 and 20 m out to the steep shelf edge about five kilometres offshore (Fig. 6.1). The coastal geography and bathymetry at Jurien Bay is representative of much of the coast stretching from Perth to Geraldton and it is therefore a useful model region to understand the ecology of the shallow subtidal habitats of much of Western Australia and the impacts of human activities on them.

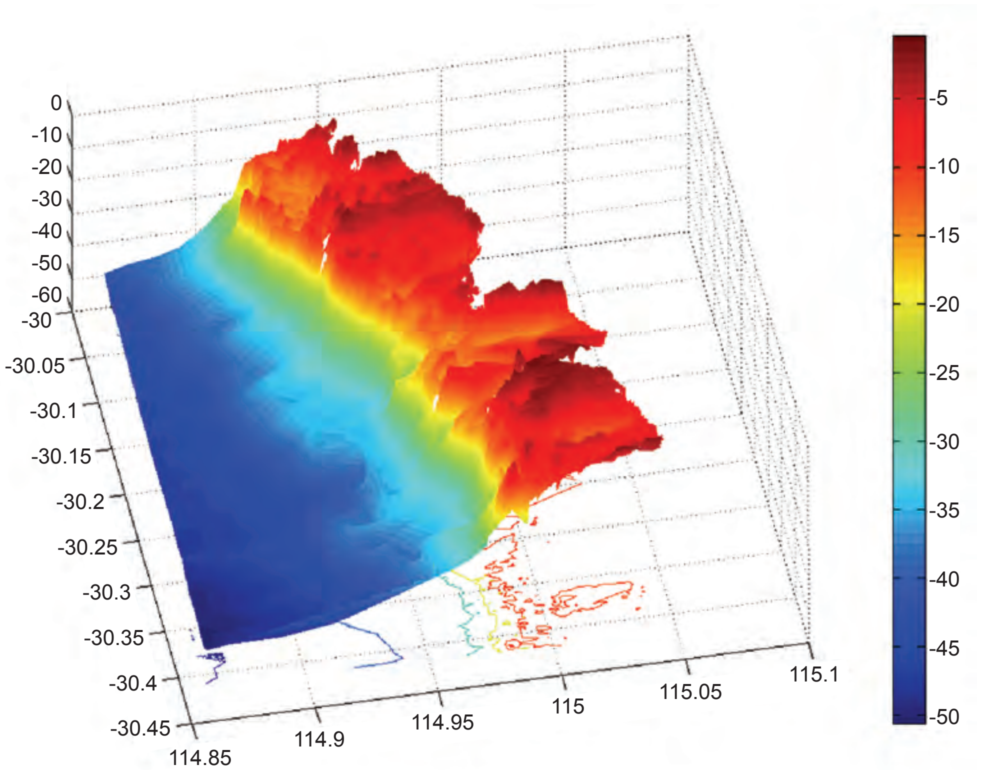

Figure 6.1: Representation of bathymetry in the vicinity of Jurien Bay based on depth soundings gridded to 30m resolution. Colourbar shows the depth in metres and the horizontal scales are degrees of latitude and longitude. The bathymetrically complex coastal lagoon where ecological sampling was performed is clearly evident above about the 20m isobath (yellow band).

To model wave conditions we used SWAN v40.41 (Ris *et al.* 1994), a spectral wave model that uses the shallow-water equation to estimate orbital water motion at the bottom boundary layer (seabed) in a gridded domain of bathymetry. Given wave conditions at the domain boundaries, SWAN models wave propagation in time and space, shoaling, refraction due to current and depth, frequency shifting due to currents and non-stationary depth, wind-generated waves, wave interactions, white-capping, bottom friction and depth-induced breaking, transmission through and reflection by obstacles, and diffraction.

The modelling domain consisted of two nested grids: an outer domain of 300 m resolution gridded bathymetry and an inner domain of 30 m resolution. Boundary conditions for model runs using the outer grid were based on several data sources: offshore wave buoy data and NOAA Wavewatch III global wave model data. Boundary conditions for the inner domain were taken from the SWAN results in the grid bounding cells of the outer grid.

We took two approaches to quantify disturbance experienced at the field sites. First, the full range of wave conditions known to occur throughout the year was simulated and the range of orbital speeds experienced at each site was compared with ecological data.

Second, a time series of extreme events, defined as the periods when significant wave heights at the Jurien Bay wave buoy exceeded the 90th percentile of observations over an 8 year period (this was the total period of available data from the Jurien wave buoy) was extracted. Modelled orbital speeds obtained at each time step in the time series were summed to approximate the area under the extreme event curve. This was used to evaluate the accumulated exposure to high energy conditions at a site in the two years preceding the collection of the benthic community data.

On each sampling visit five 0.25 m^2 quadrats were placed randomly within an area of approximately 20 m radius at each of 26 reef sites. The positions of sites were accurately recorded using differential GPS to allow seasonal sampling at the same location. All but encrusting macroalgae were harvested from the quadrat for later identification and weighing. Sampling at some sites occurred seasonally (quarterly) for two years, but most sites were sampled less often. See more detailed methods in Chapter 5.

Export of detached macroalgae from offshore to inshore reefs

The methods for this study are described in detail in Vanderklift & Wernberg (submitted manuscript). Briefly, four morphological measurements were made on laterals of attached pieces of kelp collected in December 2003 from five reefs offshore of Fremantle, and on drifting pieces of kelp from one reef: width (cm), thickness (mm), rugosity (number of corrugations cm^{-1}) and spinosity (number of surface spines mm^{-2}). Spatial patterns in morphology were analysed by principal coordinates analysis, to characterize cross-shore spatial differences in morphology. The characteristic differences in morphology could then be use predict the origin of each piece of drifting kelp using linear discriminant analysis.

Productivity and herbivory at inshore versus offshore reefs

Productivity and herbivory was measured in several ways: fish and invertebrates were censused, detached and attached macrophytes were collected, and consumption (C) of tethered kelp was measured at three reefs at each of the inshore and offshore positions at both Marmion and Jurien. Productivity (BA) of *E. radiata* was measured at two reefs at each of the inshore and offshore positions at both Marmion and Jurien.

Abundances of herbivorous fishes were counted by visual census in three 25 × 5 m transects per reef. Abundances of invertebrates (focussing mainly on sea urchins) were censused by recording densities in five 5 × 1 m belt transects per reef.

Productivity of kelp *Ecklonia radiata* was measured following a method described by Larkum (1986). Briefly, a hole was punched into the central lamina, 5 cm from the junction between the stipe and the lamina, of 5 individual *E. radiata*. These individuals were collected 20-22 days later, and in the laboratory the distance of the hole from the junction between stipe and lamina was measured (allowing the extension to be calculated by subtraction). The first 20 cm of the thallus was then cut into 5 cm strips, that were oven-dried at 60ºC for 48 hours. The strip with the maximum biomass was then used to calculate biomass accumulation BA (g^{-1} ind^{-1} d^{-1}) as $BA = xw/5d$, where x is the distance moved by the hole (cm), w is the dry weight of the strip (in grams), and d is the number of days between punching the hole and collecting the kelp.

Consumption of kelp *Ecklonia radiata* was measured following a method described by Vanderklift & Wernberg (submitted manuscript). Clean (i.e. free of epiphytes), uneroded laterals were collected, placed between two sheets of Perspex (the top sheet clear and the bottom sheet white), and photographed. Lateral were secured by a clothes peg and assigned to one of four treatments: caged (enclosed in a cage of plastic mesh to exclude all large herbivores), drift (clothes peg attached to a ~50 cm length of monofilament fishing line), and fixed-canopy (clothes peg attached to a float, that was tied to a ~50 cm length of nylon line). The 'drift' treatment was intended to mimic the action of detached kelps, and estimate consumption of sedentary herbivores; the 'fixed-canopy' treatment was intended to mimic kelp at the level of the canopy, and estimate consumption by herbivorous fish. After 2-3 days, the lateral were collected and rephotographed. The consumption C (% loss d^{-1}) of each lateral was then calculated.

Recruitment of sea urchins to different areas of the shelf

Recruitment collectors were deployed at three positions along an east-west transect from inshore coastal areas to Rottnest Island, with two sites per position. Recruitment collectors were deployed by SCUBA diving from a boat. Collectors were deployed at approximately 7 m depth at all sites except one (Radar Reef) where they were deployed at approximately 11.5 m depth. At all sites the habitat was mainly limestone reef dominated by *Ecklonia radiata*. At each site, three replicate collectors were deployed in an equilateral triangle formation. Collectors were retrieved at approximately six-week intervals from early autumn 2005 to late winter 2005, and at approximately 5 to 20 week intervals from early summer 2005 to winter 2006, This yielded six periods of data from autumn 2005 to winter 2006 observation.

Recruitment collectors were made from 50 cm long sections of 90 mm PVC pipe. A rectangle of artificial turf (23 cm by 29 cm) was secured to each end of the PVC pipe by three plastic cable ties. Collectors were hung vertically in the water column near the reef surface, attached to a rope with a subsurface float. After retrieval, each piece of artificial turf was washed down with a high-pressure hose. The material from the collectors was then rinsed through a series of four sieves of decreasing size: 2.8 mm, 1.7 mm, 500 µm, and 355 µm, and sorted under a microscope. Counts of sea urchin recruits were converted to a per day recruitment rate to account for the different numbers of days that collectors were deployed.

Patterns in densities of invertebrates and fish, biomasses of detached macrophytes, biomass accumulation of *Ecklonia radiata* and daily numbers of sea urchin recruits were analysed by mixed effects analysis of variance.

Role of predators in structuring benthic communities

Research into the role of predators in structuring benthic communities focussed on contrasts of patterns and processes inside the Kingston Reef Reserve — a small (126 ha) reserve located at Rottnest Island — and in fished areas in the vicinity of the reserve. Measurements of abundances of fishes, abundances of large benthic invertebrates (focussing particularly on spiny lobsters and sea urchins), and relative rates of predation on sea urchins were taken from high relief rocky reefs.

Surveys of spiny lobsters (*Panulirus cygnus*) were conducted in late spring of 2003 and repeated later in the winter of 2004. The study used a blocked design such that it compared lobster populations on reefs with varying management status (STATUS) on two different occasions (TIME). Spatial variability was examined by dividing both the marine sanctuary and the adjacent coastal habitats into four areas of approximately equal size, giving four fished and four unfished areas (AREA) within each block. Within each of these areas replicate 50 x 5 m belt transect surveys were conducted to determine the density, size and sex of resident lobster populations. Transects were run parallel to depth contours at depths between 4 and 8 m in habitats that had the potential to hold lobsters (medium to high relief reef with caves, ledges or overhangs). Lobsters were recorded and their size (carapace length: CL) and sex estimated visually to the nearest 5 mm (MacDiarmid 1991). All transects were conducted in November to December 2003, and July and August of 2004 by three divers trained to estimate lobster size prior to commencing surveys. Calibration of diver visual estimates involved visually estimating the CL of a lobster, then capturing and measuring the lobster with vernier callipers. Additional calibration checks were made opportunistically throughout each survey period. Calibration data obtained in this way can be used to correct size estimates for any bias. Where possible the sex of each lobster was also determined. Where size or sex could not be positively determined, these were recorded as unknown. There was a close relationship between estimated and actual measures of CL ($r^2 = 0.81$, $F = 396$, $P < 0.001$) however the slope of the regression was significantly different from 1:1 ($t = -6.24$, $P < 0.001$) and had a y-intercept of 21.481 ($t = 19.9$, $P < 0.001$), indicating that the size of small animals was often underestimated, while the size of larger animals was often overestimated. Part of this bias may be due to pronounced allometric changes in the relative leg length of large male *P. cygnus*. Estimates were corrected using the appropriate relationship to remove systematic bias in size estimates. For the second survey raw values were used as estimates of size did not differ significantly from 1:1.

Spiny lobsters are social animals, often aggregating for mating or to utilize available shelter. Because of this, count data are non-normally distributed and so the data were analysed using a mixed-effects log-linear model to fit the data using the GLIMMIX macro (Little *et al.* 1996, Millar and Willis 1999) using SAS v.8. The model treated STATUS, AREA and TIME as fixed effects. The blocking factor was random and treated as a co-variate in the analysis. Data were analysed for all lobsters combined, and separately for legal sized animals (> 77 mm CL), and for those less than legal size. Lobster sizes in fished and unfished areas were tested using

ANOVA. In order to assess the effects of fishing on lobster biomass, CL was converted to biomass using the equations:

$$W = 0.0016068\ CL^{2.8682} \text{ males}$$

$$W = 0.0025053\ CL^{2.778} \text{ females}$$

where W = weight in g, and CL = carapace length in mm (Hall and Chubb 2001). Where sex could not be determined the animals were randomly assigned a sex for estimating biomass in the analysis. Similarly CL estimates were used to estimate egg production using the relationship:

$$E = 2(1.92)\ CL^{2.69}$$

where E = the number of late stage eggs borne by a female lobster larger than the size at maturity (95 mm CL in the southern zone, Hall and Chubb 2001). Rather than make any assumptions about the egg production of lobsters where their sex could not be positively determined, lobsters of unknown sex were excluded from the comparison. Data for biomass and fecundity were summed for each transect and analysed as for the density data.

Abundances of fishes were quantified using underwater visual census (UVC), and two methods using video — baited underwater video (BUV) and baited remote underwater video (BRUV). In the UVC method (12 sites in 2005), predatory fishes were counted in 50 × 10 m transects, and abundances of all other species of non-cryptic fishes were counted in 25 × 5 m transects nested inside the larger transects. Male western king wrasse (*Coris auricularis*), brown-spotted wrasse (*Notolabrus parilus*) and maori wrasse (*Opthalmolepis lineolatus*) were censused using the larger transect, while female and juvenile wrasses were censused using the smaller transect. Abundances of invertebrates (focussing mainly on sea urchins) were censused by recording densities in 5 × 1 m belt transects. Fish were censused in three transects per site, and invertebrates were censused in five transects per site.

BUV was used in 2003 (27 videos, 14 in the sanctuary and 13 outside) and BRUV was used in 2004 (31 videos, 15 in the sanctuary and 16 outside). Video systems were set at least 200m apart to avoid attracting the same individual fish from visiting multiple camera stations. Cameras were not set within an hour of dusk, or an hour after dawn, to avoid biases due to the crepuscular feeding behaviour of some species (Hobson *et al.* 1981).

The BUV system used in 2003 consisted of a pencil camera mounted on a stainless steel stand 115 cm above the substrate and facing straight down (Willis & Babcock 2000, Willis *et al.* 2003). A bait jar containing 4 whole pilchards was mounted on the triangular base of the stand so that it lay in the centre of the camera's field of view. The bottom frame was marked with tape at measured increments to allow spatial calibration of digitized images. This permitted accurate and precise length estimates of fish entering the field of view. The BUV system was lowered from an anchored vessel. Live imagery was recorded onto Hi-8 digital video tapes using a Hi8 DV recorder at the surface. The BRUV system used in 2004 was similar in construction to the BUV, the main difference being that a housed video camera (Sony TRV 19) was mounted on the frame facing the seafloor, and video was recorded onto digital tape. Each system was allowed to record for 30 minutes. In the laboratory video footage was analysed in real time to determine the relative abundance of all reef fish greater than 5cm in length entering the field of view. Relative abundance was estimated using MaxN, the maximum number of individuals of a species in any given frame (Ellis and DeMartini 1995). This eliminated repeat counts of the same fish that would have violated univariate assumptions of independence. The lengths of selected recreational and by-catch species were measured from calibrated still images using Sigma Scan Pro™ image analysis software. Biomass for selected species was estimated using published length-weight regressions where available or from those given on www.fishbase.org. For species where no data were available, relationships from other species similar in morphology were used as substitutes.

Relative predation intensity between the sanctuary and fished areas was assessed by measuring the survival of tethered sea urchins over 24 hours. We used the two main species of sea urchins (the purple sea urchin *H. erythrogramma* and the grey sea urchin *C. tenuispinus*). Sea urchins were measured (test diameter in mm), and tethered by inserting a monofilament line through the test using a hypodermic needle, and then tying the line to form a loop. The other end of the line (approximately 20 cm long) was tied to metal chain. Usually at least ten tethered individuals of each species were deployed at each reef. We retrieved the tethers after 24 hours and scored the sea urchins as alive or eaten (empty loop of line, or loop with fragment of test remaining) or uncertain (entire line missing or cut, or dead urchin showing signs indicating a cause of death other than predation).

Benthic macroalgae were sampled to assess whether gradients in predator density and size, or grazer density, or both might have resulted in any cascading trophic effects, including reduced algal biomass and the development of urchin barrens. Within each AREA surveyed for lobsters five haphazard 0.25 m^{-2} quadrats were sampled and all algae collected, identified and weighed.

Results

6.1 Wave Modelling and Patterns of Diversity in Benthic Communities

Investigator / Institution

Phillip England, Julia Phillips, Russ Babcock, Geordie Clapin,
Alison Sampey, Nicole Murphy

CSIRO Marine and Atmospheric Research

Wave Modelling

Modelled orbital motion varies in complex ways throughout the shelf (Fig. 6.1). Annual maxima experienced at the 26 different sites (Fig. 6.2) varied between 0.38 and 1.85 ms^{-1} and minima varied between 0.02 and 0.21 ms^{-1}. The highest values (1.85 ms^{-1}) occurred on the outer edge of the lagoon where prevailing ocean swells first encounter shallow water. Lower values (<0.5 ms^{-1}) were observed in the more sheltered regions behind islands and close to the shore. The most exposed sites also experienced the greatest range of orbital motion values, consistent with the accessibility of these locations to the largest swell waves. Where outer reef crests are deeper or absent, waves penetrate further into the lagoon and orbital motion values are elevated closer to shore. The penetration of elevated values close to shore depends on swell direction and the presence and characteristics of protective outer reefs.

Figure 6.2: Asterisks show the locations of macroalgal sampling sites in the vicinity of Jurien Bay. The green 20m isobath shows the approximate location of the lagoon edge. The blue 10m isobath highlights the complexity of the lagoon's bathymetry. Grey lines indicate the low water mark. The horizontal distance from Jurien Bay inlet to the 20 isobath is 7.5 km.

The 90th percentile of observed significant wave heights was 3.17 m and the 10% of records that exceeded this were used to construct a time series of extreme events. The predominant direction of these waves was south-westerly (range 200-250 degrees). While the ratio of the upper limit of orbital motion experienced at the most and least exposed sites was 4.5:1; the ratio of two years of cumulative exposure from the time series of extreme events at these same sites was over 10:1.

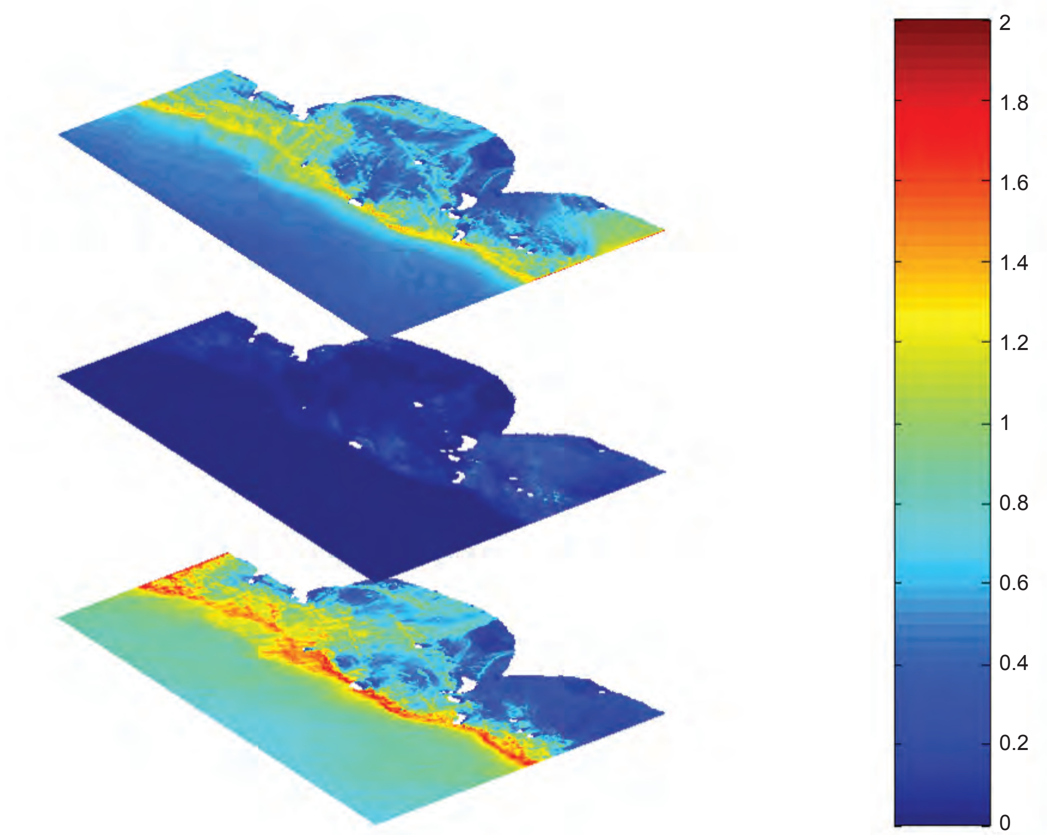

Figure 6.3: Maps of modelled orbital motion (ms^{-1}) under three contrasting scenarios at Jurien Bay. Upper map: north-westerly storm; middle map: calm conditions; lower map: south-westerly storm.

Macroalgal species diversity

Approximately 280 species of macroalgae were recorded at Jurien Bay. The number of species recorded per 0.25 m^2 ranged from 1-56 with a mean of 19.3, a median of 19 and a mode of five. Species accumulation curves suggest that for sites at that only a small number of quadrats were collected, site diversity might be underestimated by an unknown amount. Average quadrat diversity per site ranged from 5.2 to 34.6 with a median of 21.8.

Orbital motion versus species richness

There was a significant positive correlation between macroalgal species diversity and exposure. Similar results were observed when diversity was compared with various summary statistics of the likely annual range of orbital water motion or with the cumulative extreme event timeseries. Here we present results from the latter comparisons. The number of species present in a quadrat (S) was related to cumulative extreme event orbital motion (U) by the linear regression $S = 8.05 + 0.012U$, adj. $r^2 = 0.27$, $p<0.0001$. The goodness of fit of the data is better with a non-linear regression of the quadratic form $S = 6.36 + 0.043U + (1.3x10^{-5})U^2$, adj. $r^2 = 0.434$, $P<0.0001$ (Fig. 6.4). This analysis used the diversity data from each quadrat individually. Because many sites were sampled in different seasons and years, different extreme event time series applied at the same site and it was therefore not possible to take the mean of quadrat diversity across all quadrats from a site. However, the correlation was stronger when replicate quadrats sampled on the same field trip were pooled (because they experienced identical extreme event histories) to derive site/time average diversities. Natural log transformation of diversity and cumulative extreme event orbital motion normalised the data and yielded the linear regression $\log S = -3.02 + 0.86 \log U$, adj. $r^2 = 0.523$, $p<0.0001$ Fig. 6.4). The quadratic non-linear regression had the same goodness of fit.

There is a clear relationship between diversity and our index of disturbance due to wave exposure. The shape of this relationship differs according to how the diversity data are summarised. The linear regression achieved when quadrat data were averaged to estimate site-wide diversity is stronger than without averaging but this operation is potentially problematic as it relies on untested assumptions relating to scale, patchiness and diversity in reef macroalgal habitats.

Relationships between diversity and disturbance have been observed in many species-rich communities where there is competition for limited resources and spatially heterogeneous (patchy) disturbance regimes including intertidal rocky reefs, coral reefs, rainforests and grasslands (reviewed in Shea *et al.* 2004). When this relationship is curvilinear and highest at intermediate disturbance levels it has been called the intermediate disturbance hypothesis (IDH) (Connell 1978). Model studies of the IDH (Tilman 1994; Bampfylde *et al.* 2004) show that, in a system consisting of a mosaic of patches in different states of recovery from localised disturbance, highest diversity is supported in the system as a whole at intermediate levels of disturbance, whether the degree of disturbance be described in terms of intensity, frequency of occurrence or duration.

Although noisy, the curvilinear relationship in Fig. 6.4 is consistent with intermediate values of orbital motion correlating with higher macroalgal species diversity, as expected under the IDH. We did not sample at the most exposed parts of the lagoon edge where orbital velocities are substantially higher (>2 ms^{-1}). A testable prediction of the IDH is that estimates of species diversity at these locations would be lower than ~30 species per 0.25m^2. If the relationship is linear, substantially higher estimates of diversity should be obtained. Even if our data are more indicative of a positive and linear relationship than a hump-shaped one the results lend support to the view that wave-induced forces are a dominant factor in the ecology of shallow water benthic communities.

It is yet to be determined exactly how the index of exposure we chose to use manifests itself as disturbance in benthic habitats, but it is known that oscillatory motion of water at the bottom boundary layer due to waves passing overhead exerts a drag force on sessile benthic organisms known to cause breakage of algal stipes and fronds or complete dislodgement from the substrate (Denny *et al.* 1998, Thomsen *et al.* 2004). As these forces are greatest during extreme events when wave energies are at their peak, it is reasonable to assume that biomass reduction and canopy gap formation occurs in proportion to the severity and duration of extreme events. Thomsen *et al.* (2004) estimate that bed orbital velocities >2 ms^{-1} would be sufficient to dislodge *E. radiata.* This is close to the 1.85 ms^{-1} experienced at our most energetic sites during times when significant wave height exceeded the 90th percentile. Since by definition the maximum wave heights of such times would be significantly higher, orbital velocities greater than 1.85 ms^{-1} would be likely on a regular basis. Integration of the two year time series of orbital motion generated during extreme events to produce a cumulative index of exposure is a valid way of estimating a time-averaged likelihood of a disturbance event occurring at a given place.

Alternative phenomena may explain the observed relationship. One of the prerequisites of the IDH is that ecological succession operates in the system. While there is some suggestion that macroalgal communities in the west coast of Western Australia exhibit succession, it remains unverified and difficult to test. Significant questions remain regarding whether different exposure regimes support different diversity levels reflecting adaptive differences among species or niche diversity, or whether the observed pattern is being driven by ecological interactions among a few key species in reef habitats. Canopy-forming species, including the dominant canopy forming species at Jurien Bay, *Ecklonia radiata*, are known to influence community dynamics in macroalgal forests (Kennelly 1989; Emmerson & Collings 1998; Kendrick *et al.* 1999). We found a significant negative correlation between the presence of *Ecklonia radiata* and species diversity of macroalgae ($\tau = -0.24$, $P<0.001$), and the diversity of key invertebrate taxa (Chapter 5).

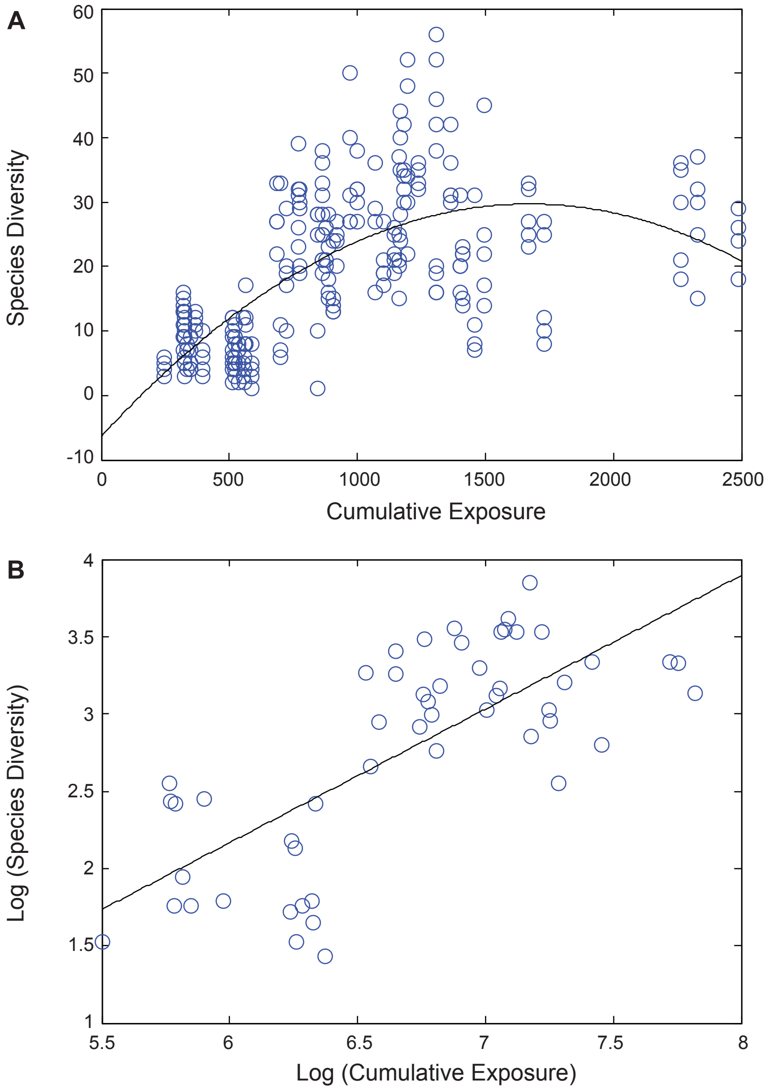

Figure 6.4: Number of macroalgal species (per 0.25m^2 quadrat) versus cumulative exposure to extreme events in the two years prior to sampling. A: Diversity for each quadrat versus cumulative exposure with the regression of best fit (quadratic). B: Log transformed average quadrat diversity at sampling sites on each field trip versus log transformed cumulative exposure with the regression of best fit (linear).

6.2 Inshore Versus Offshore Trends in Key Ecological Processes

Investigators / Institutions

Mat Vanderklift, Geordie Clapin, Alison Sampey, Julia Phillips, Russ Babcock
CSIRO Marine and Atmospheric Research

Kylie Cook, Catriona Stuart-Andrews, Kris Waddington
University of Western Australia

Thomas Wernberg Edith Cowan University

Cross-lagoon variation in standing crop and productivity

Overall biomass of macroalgae, and productivity rate of one key indicator species was measured to determine levels of spatial variation that might ultimately be related to environmental factors. Cross-lagoon variation in standing crop (g C m^{-2}: a rough proxy for rates of primary productivity) of reef algal communities was examined within each SRFME region. Overall, standing crop was higher in the Jurien region than other regions ($P<0.001$) although differences were not significant between Jurien and Perth ($P=0.1$) (Fig. 6.5). Reef algal communities in the Jurien region showed a trend of higher standing crop with increasing distance from the shore, while the opposite trend was apparent for Perth reefs, although differences were not significant in either region ($P>0.1$). Productivity on reefs in Geographe Bay showed no variation with position on lagoon.

Productivity of the kelp *Ecklonia radiata*, directly measured as grams wet weight of biomass accumulated per day, was significantly higher (F=144.6, p=0.001) at offshore than inshore reefs at Jurien (2.2 ± 0.35 g^{-1} d^{-1} SE offshore; 1.0 ± 0.19 g^{-1} d^{-1} SE inshore), but there was little difference at Marmion (1.0 ± 0.12 g^{-1} d^{-1} SE offshore; 0.9 ± 0.20 g^{-1} d^{-1} SE inshore; Fig. 6.6) and inshore offshore variation was not significant (F=0.48 p=0.53).

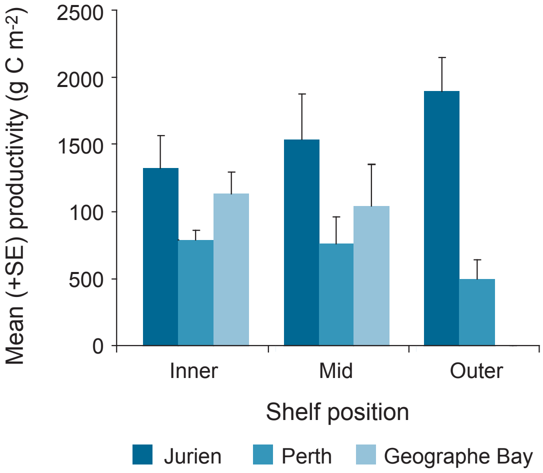

Figure 6.5: Cross-lagoon variation in standing crop of reef algal communities.

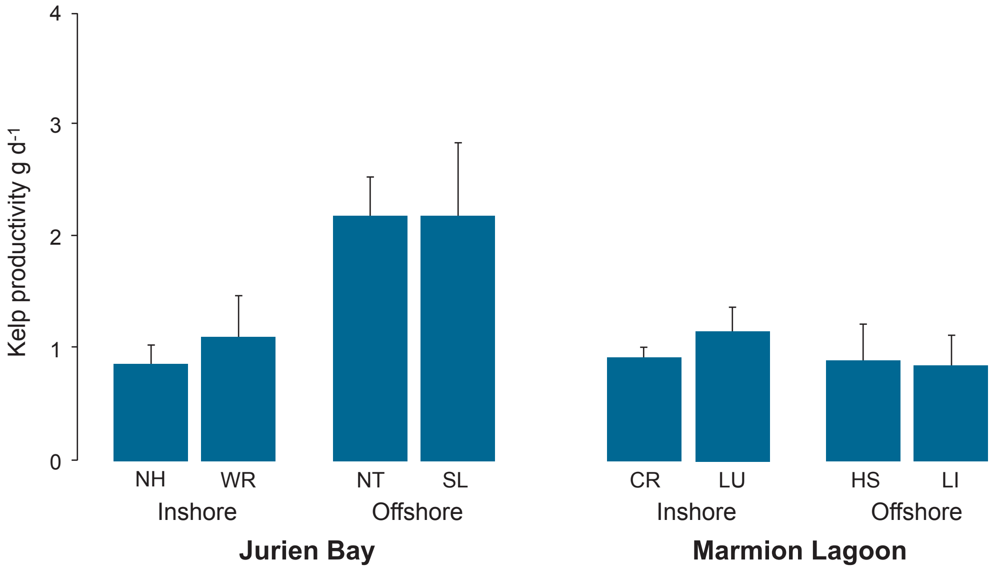

Figure 6.6: Productivity of tagged individuals of *Ecklonia radiata* (measured in g^{-1} dry weight d^{-1} at inshore and offshore reefs in Jurien Bay and Marmion Lagoon. NH = North Head, WR = Wire Reef, NT = North Tail, SL = Seaward Ledge, CR = Cow Rocks, LU = Lumps, HS = Horseshoe Reef, LI = Little Island.

Herbivory at inshore versus offshore reefs

Consumption of tethered pieces of kelp *Ecklonia radiata* varied among the tethering treatments at some reefs (significant Reef × Treatment interaction: $F = 3.81$, $P = <0.001$). Consumption that was consistent with grazing by sea urchins (significant consumption of the 'drift' treatment) was significant at Booka Valley (Fig. 5.2 site 26), Wire Reef (Fig. 5.2 site 20), and North Head (Fig. 5.2 site 11), in Jurien, and at South Lumps (Fig. 5.2 site 32), in Marmion (Fig. 6.7). Consumption that was consistent with fish grazing (significant consumption of the 'fixed-canopy' treatment) was significant at Cow Rocks (Fig. 5.2 site 36), in Marmion (Fig. 6.7). All these reefs were inshore reefs — no consumption was recorded on any of the offshore reefs. No consumption was recorded in any of the caged individuals.

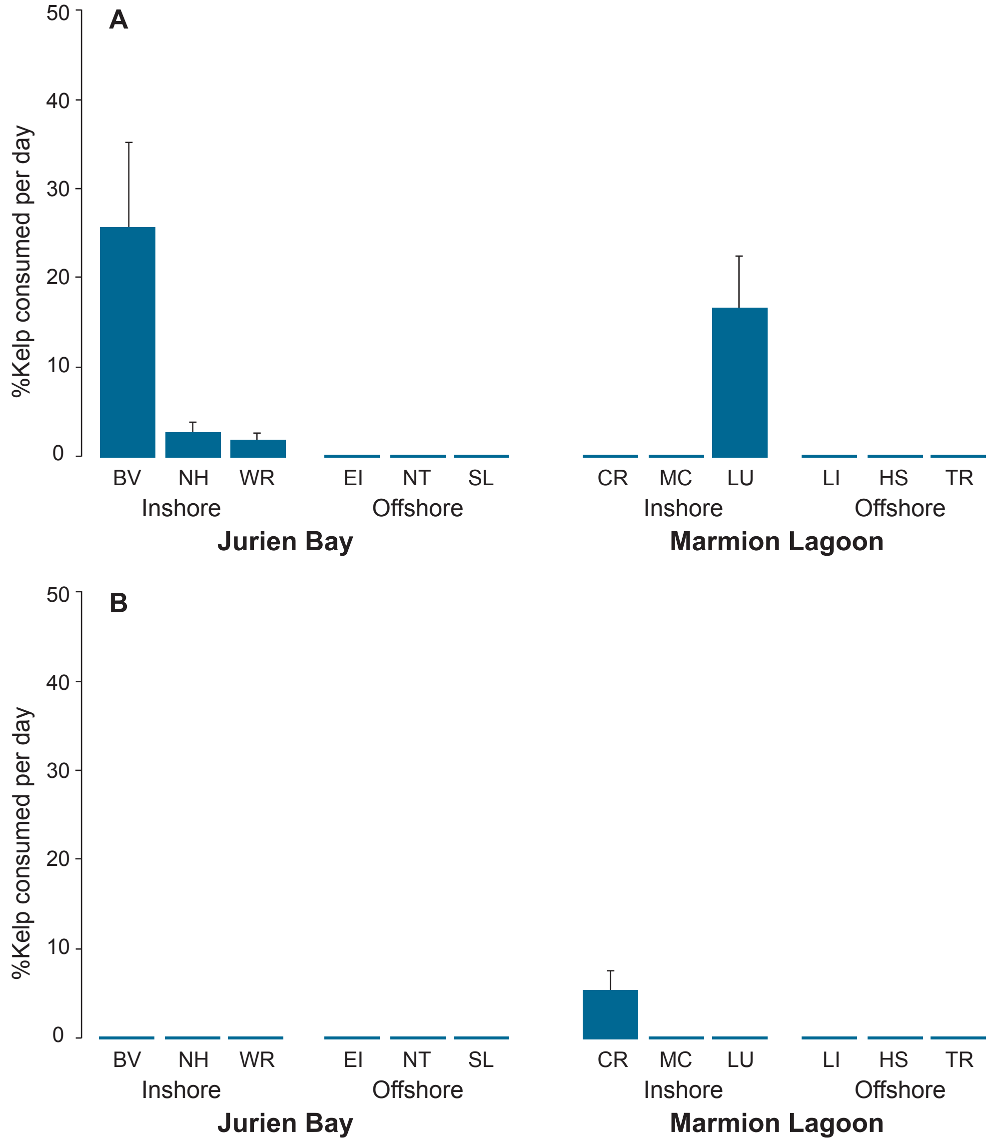

Figure 6.7: Consumption of tethered pieces of *Ecklonia radiata* at inshore and offshore reefs in Jurien Bay and Marmion Lagoon to estimate (a) consumption by sea urchins and (b) consumption by fish. NH = North Head, WR = Wire Reef, NT = North Tail, SL = Seaward Ledge, CR = Cow Rocks, LU = Lumps, HS = Horseshoe Reef, LI = Little Island.

The main large herbivorous fauna recorded at the study reefs that could be responsible for the observed consumption were sea urchins and herbivorous fishes. Two species of sea urchins were recorded: *Heliocidaris erythrogramma* and *Phyllacanthus irregularis*; most were the *H. erythrogramma.* Densities of sea urchins were significantly higher in Jurien Bay than in Marmion Lagoon ($F = 6.93$, $P = 0.03$; Fig. 6.8) (2.83 individuals·transect^{-1} ±0.54 versus 0.80 individuals·transect^{-1} ±0.35, n=30). Densities were also significantly higher on inshore reefs than offshore reefs ($F = 1\ 088$, $P = 0.02$; Fig. 6.8) (2.37 individuals·transect^{-1} ±0.38 versus 1.27 individuals·transect^{-1} ±0.43, n=30). Four species of herbivorous fishes were recorded: the most abundant was *Parma* spp., followed by the kyphosids *Kyphosus sydneyanus* and *K. cornelii*, and the odacid *Odax cyanomelas.* No trends were evident to suggest differences in total abundance between locations, or between positions in the respective lagoons (both comparisons $F < 1$, $P > 0.5$). There was significant variability among reefs ($F = 4.42$, $P = 0.002$; Fig. 6.9), indicating substantial small-scale spatial variability.

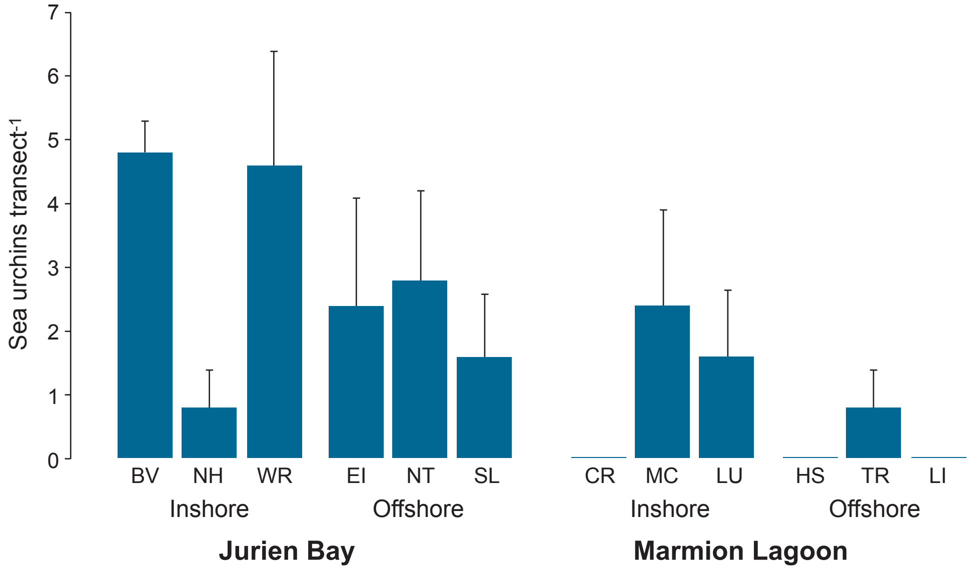

Figure 6.8: Densities of sea urchins (*Heliocidaris erythrogramma* and *Phyllacanthus irregularis*) at inshore and offshore reefs in Jurien Bay and Marmion Lagoon. BV = Booka Valley, NH = North Head, WR = Wire Reef, EI = Escape Island, NT = North Tail, SL = Seaward Ledge, CR = Cow Rocks, MC = MAAC, LU = Lumps, HS = Horseshoe Reef, TR = Two Rocks, LI = Little Island.

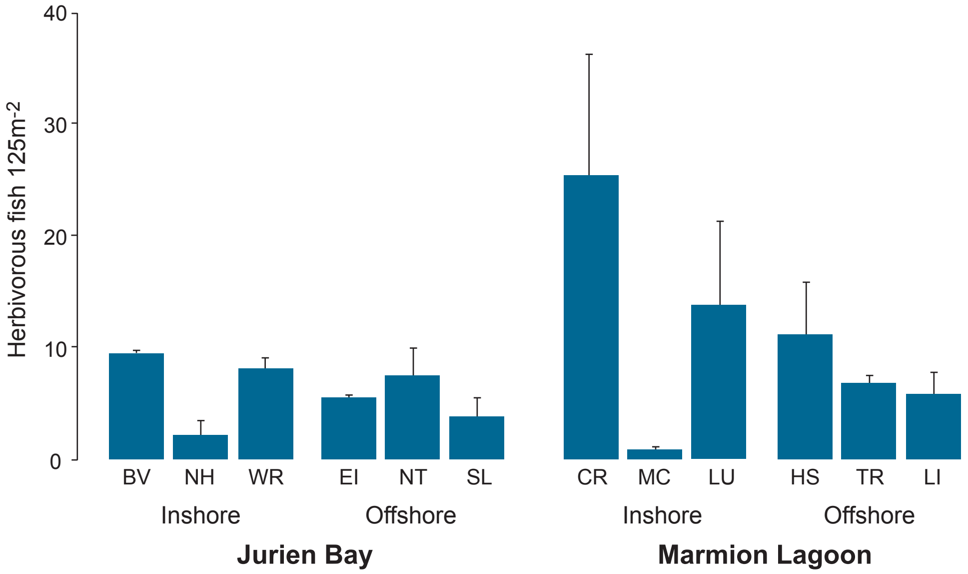

Figure 6.9: Densities of herbivorous fish at inshore and offshore reefs in Jurien Bay and Marmion Lagoon. BV = Booka Valley, NH = North Head, WR = Wire Reef, EI = Escape Island, NT = North Tail, SL = Seaward Ledge, CR = Cow Rocks, MC = MAAC, LU = Lumps, HS = Horseshoe Reef, TR = Two Rocks, LI = Little Island.

Recruitment of sea urchins to different areas of the shelf

The main species of sea urchin recorded from the recruitment collectors was the purple sea urchin *Heliocidaris erythrogramma*. Daily rates of recruitment of *H. erythrogramma* showed considerable spatial and temporal variability, with a significant Position × Season interaction ($F = 3.1$, $P = 0.03$), and a significant Site × Season interaction ($F = 3.7$, $P = 0.04$). Despite this variability, there was a trend for higher rates of recruitment during autumn 2005 (Fig. 6.10).

No consistent spatial trend was evident, indicating that sea urchin recruitment was spatially variable, and suggesting that cross-shelf gradients in density of adults were not related directly to recruitment.

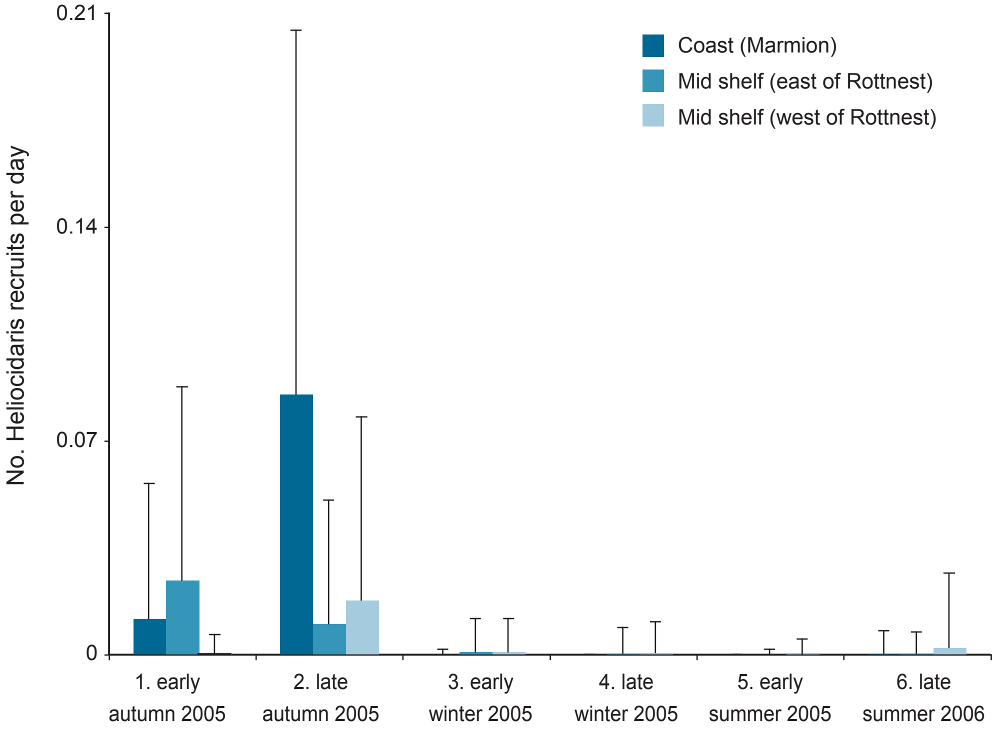

Figure 6.10: Daily rates of settlement (± SE) of the purple sea urchin *Heliocidaris erythrogramma* at three different positions on the shelf, from six different seasons over the year 2005-2006.

Export of detached macroalgae from offshore to inshore reefs

Based on their morphology individual attached kelps (*Ecklonia)* could be broadly categorised into three main morphological groups: offshore group (Seaward Reef and Casuarina Shoal), central group (two reefs that were located further inshore,The Roarers and Straggler Rocks), and a third inshore group (represented by an isolated reef (Mewstone). At the same time as the attached kelps were measured drift kelp was also measured. Most of the drift kelps collected inshore at Mewstone were morphologically most similar to the two groups of reefs further offshore (Fig. 6.11). Overall, linear discriminant analysis indicated that, 30% of the drift kelps were most similar to attached kelps from the group of reefs furthest inshore, while 50% of the drift kelps were most similar to attached kelps from the next group of reefs, and only 20% of drift kelps were most similar to attached kelps from the reef at that they were collected. These results imply that drift kelps at Mewstone, for example, had originated at a range of different sources, and that many had drifted for distances of 2-8 kilometres before arriving there.

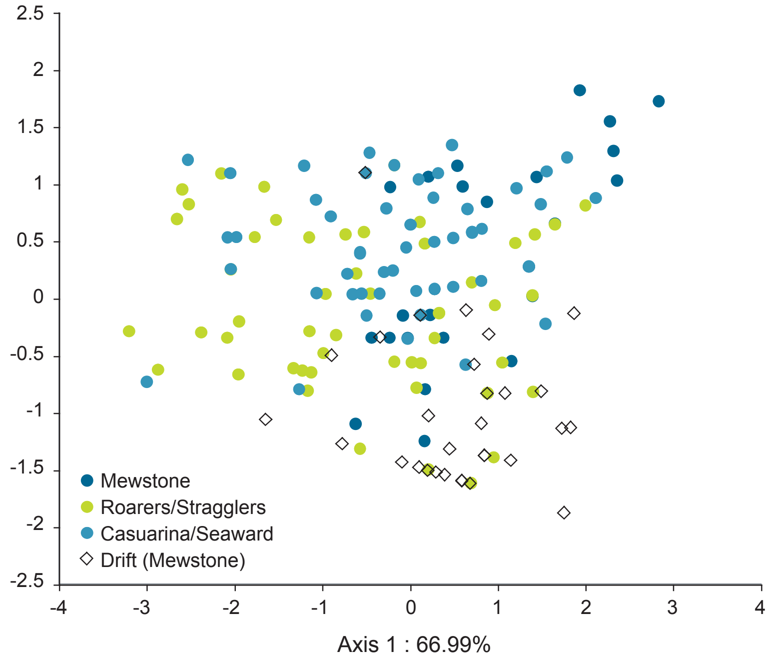

Figure 6.11: Two-dimensional principal coordinate plot of individual attached kelps from different reefs, and drift kelps from one reef, based on four morphological characteristics. The plot shows that the morphology of drift kelps at Mewstone is most similar to the morphology of kelps from further offshore.

6.3 Role of Predators in Structuring Benthic Communities

Investigator / Institution

Russ Babcock, Mat Vanderklift, Geordie Clapin, Julia Phillips, Matt Kleczkowski, Alison Sampey, Martin Lourey, Nicole Murphy

CSIRO Marine and Atmospheric Research

Kylie Cook University of Western Australia

Determining whether trophic interactions such as predation or grazing have a strong determining role in coastal ecosystem process and structure is often difficult because in many areas important predators or grazers have been removed by fishing. Consequently attempts to manipulate these interactions through caging experiments for example may fail because there is nothing left for the cages to exclude. Recent experience has shown that one of the most effective ways to investigate these interactions, given such depleted populations, is to compare fished and unfished areas as a means of exploring the contrasting processes and patterns in systems with or without key organisms or groups of organisms. A well defined set of steps is required to implement such an approach.

1. Contrasts in predator abundance must be established. If they do not exist the comparison will be meaningless.
2. Other components in the ecosystem that may be affected either directly by the predators (e.g. grazers) or indirectly by their prey (algae) can be contrasted across the same gradients.
3. The rates of key processes assumed to be responsible for the differences in abundance should be quantified to account for the possibility that the spatial patterns observed are due to some other unanticipated factor.

This is the approach that was taken in studies at Rottnest Island using the Kingston sanctuary zone.

Lobsters

During the two surveys the abundance and size distribution of lobsters (*Panulirus cygnus*) differed markedly between sanctuary and non-sanctuary areas (Fig. 6.12) with a greater proportion of lobsters above minimum legal size inside the sanctuary zone. Another feature of the sanctuary zone population was the presence of large males (over 115 mm CL) that were virtually absent from the fished areas. Mean size (CL) was 8.4 mm larger in the sanctuary zone ($F = 72.21$, $P <.0001$). While there was a slightly higher abundance of male lobsters overall the ratio of females to males (0.89:1) was not significantly different from 1:1. Due to the cryptic behaviour of the lobsters it was not possible to positively determine the sex of 53% of the lobsters observed. While this is a high proportion it is unlikely to have biased the results of the overall comparison since very similar proportions of lobsters of unknown sex were recorded in both fished (47%) and unfished areas (53%).

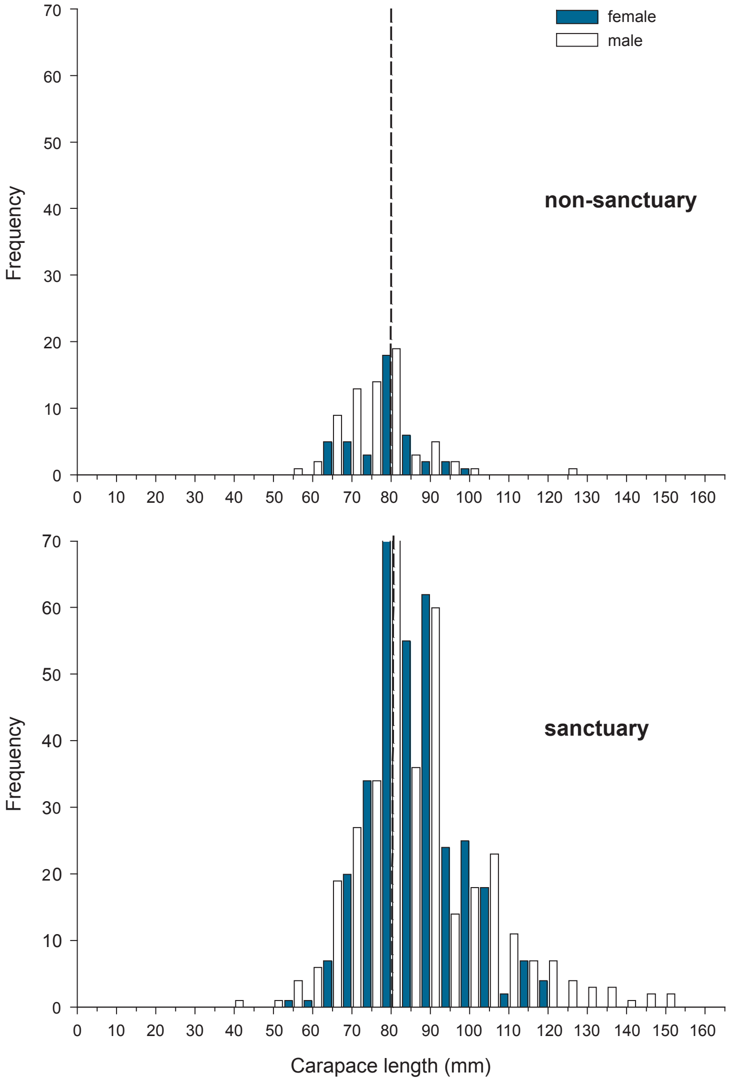

Figure 6.12: Population structure of spiny lobsters *Panulirus cygnus* in the Kingston Marine Sanctuary and in adjacent fished areas

The overall density of rock lobsters was higher within the sanctuary than in adjacent fished areas (STATUS t = -3.38, $P<0.004$) with an estimated density of 17.7 lobsters per transect inside the sanctuary and 0.5 lobsters per transect in adjacent fished areas — a ratio of 34.4

(Table 6.1). The density of lobsters also varied with TIME (t = 4.73, *P*<0.001) but did not vary significantly among areas or blocks (Table 6.2) or in any interactions between factors. The density of legal- (t = -2.96, *P*<0.004) and sublegal- (t = -3.44, *P*<0.001) sized lobsters was higher inside the sanctuary (Table 6.2), though this difference was much more pronounced for legal-sized lobsters, that were estimated to be 50.4 times more abundant inside the sanctuary (Table 6.1). Lobsters below the legal size limit were estimated to be 21.7 times more abundant inside the sanctuary. The arrangement of areas within the blocks made it possible to test whether lobster densities varied significantly with distance from the centre of the sanctuary (AREA) (Table 6.2). Overall, and for both legal and sub-legal sized lobsters, densities were highest at the centre of the sanctuary, intermediate at the edges, and uniformly low in areas outside the sanctuary (Fig. 6.13).

Table 6.1: Density, biomass and egg production of spiny lobsters in the Kingston Reef Marine Sanctuary and adjacent fished areas.

	Sanctuary mean	Fished mean	Sanctuary: Fished ratio
Total density (250 m^{-2})	17.7	0.5	34.4
Legal density (250 m^{-2})	12.7	0.25	50.4
Sublegal density (250 m^{-2})	4.5	0.2	21.7
Biomass (kg.ha^{-1})	180.1	0.6	313.7
Fecundity (eggs ha^{-1})	4.4×10^7	4.4×10^5	101.1

Table 6.2: Generalised Linear Mixed Model Analyses of variation in density of spiny lobsters in and around the Kingston Reef Marine Sanctuary.

		All lobsters		Legal lobsters		Sublegal lobsters		All lobster biomass		All lobster fecundity	
Source	**df**	**F**	**P**	**F**	**P**	**F**	**P**	**F**	**P**	**F**	**P**
Status	1	50.7	<0.0001	41.8	<0.001	31.97	<0.001	12.16	0.0006	31.57	<0.001
Time	1	13.5	0.0003	4.47	0.036	21.87	<0.001	3.87	0.051	4.27	0.040
Area	1	1.1	0.294	0.9	0.343	0.36	0.55	1.09	0.29	1.29	0.26
Status × time	1	1.2	0.28	0.22	0.64	2.5	0.12	0.68	0.41	0.03	0.87
Status × area	1	5.82	0.017	5.78	0.017	7.52	0.007	2.57	0.11	2.55	0.11
Time ×area	1	0.01	0.91	0.01	0.917	0.18	0.67	0.26	0.61	0.04	0.85
Status × time × area	1	0.09	0.76	0.5	0.482	0.04	0.83	0.31	0.58	0.00	1.00
block	1	3.02	.	5.41	.	2.58	.	7.84	.	4.36	.

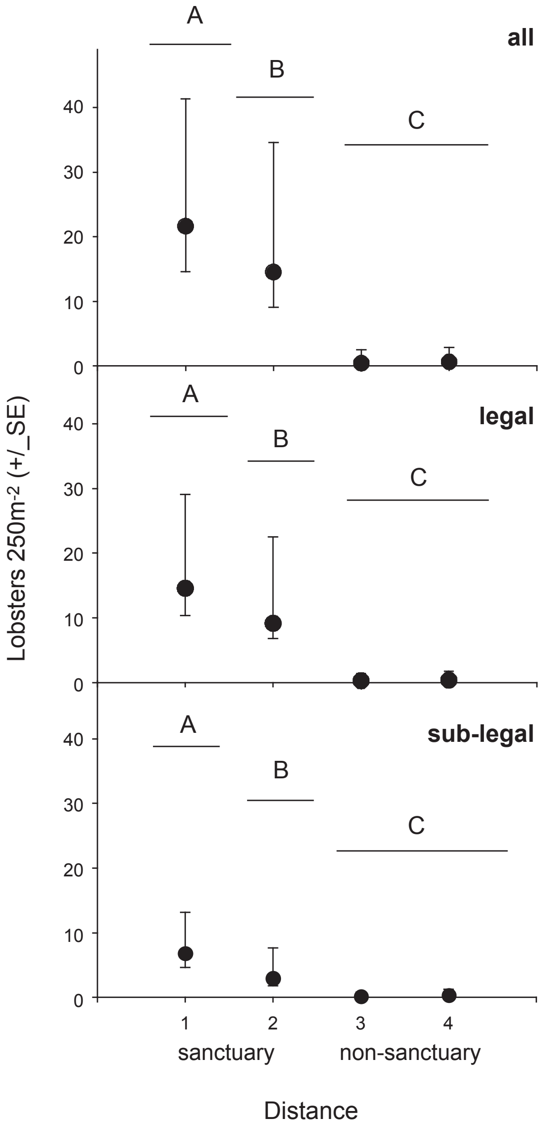

Figure 6.13: Density of lobsters as a function of distance from the centre of the Kingston Reefs Marine Sanctuary. 1=centre of sanctuary zone, 4=most distant non-sanctuary area. 2 & 3, boundary zones inside an outside the sanctuary respectively.

Fish

Pooled densities of all fishes recorded during UVC were significantly higher in the sanctuary (ANOVA: $F = 7.66$, $P = 0.05$). Fish were approximately twice as abundant inside the sanctuary (40.9 individuals·transect ± 4.17, mean ± se) than outside (20.4 ± 2.36). Densities of the five species of fishes that were observed to prey on sea urchins were also significantly higher inside the sanctuary (ANOVA: $F = 11.12$, $P = 0.03$), being approximately twice as abundant inside (2.9 ± 0.42) than outside (1.4 ± 0.41).

Video methods yielded a significant difference in the relative density of one key target species *Glaucosoma hebraicum* (ANOVA: $F = 4.53$, $P = 0.04$), but not a second species *Epinephelides armatus* (ANOVA: $F = 0.56$, $P = 0.46$). Relative density of *G. hebraicum* was ten times more abundant in the reserve (MaxN = 0.3) than in fished areas (MaxN = 0.03). Biomass of both these species was significantly higher inside the reserve (ANOVA: $F > 4$, $P < 0.05$ in each case). Some bycatch species, including terminal phase *Ophthalmolepis lineolatus*, and *Meuschenia hippocrepis* were found in significantly greater relative densities within the reserve

(ANOVA: $F > 4$, $P < 0.05$ in each case), with these patterns also reflected by a greater biomass (ANOVA: $F > 7$, $P < 0.01$ in each case).

Sea urchins were typically present in low densities ($<1 \cdot 5m^{-2}$). Densities of the two main species of sea urchins (the purple sea urchin *H. erythrogramma* and the grey sea urchin *C. tenuispinus*) differed significantly between the sanctuary and fished 'zones' (*H. erythrogramma*: $F = 14.97$, $P = 0.003$; *C. tenuispins*: $F = 15.77$, $P = 0.003$). Densities of *H. erythrogramma* were significantly lower inside the sanctuary (Fig. 6.14), consistent with the pattern expected if predators were influencing abundance. However, *C. tenuispinus* showed the opposite pattern, as densities were significantly higher inside the sanctuary (Fig. 6.14).

Rates of predation on both species of sea urchins were significantly higher inside the sanctuary than outside (*H. erythrogramma*: Deviance = 5.51, $P = 0.02$; *C. tenuispinus*: Deviance = 21.03, $P = <0.01$). Tethered *C. tenuispinus* were 8.0 times more likely to survive outside the sanctuary than inside, while *H. erythrogramma* were 2.7 times more likely to survive outside the sanctuary than inside.

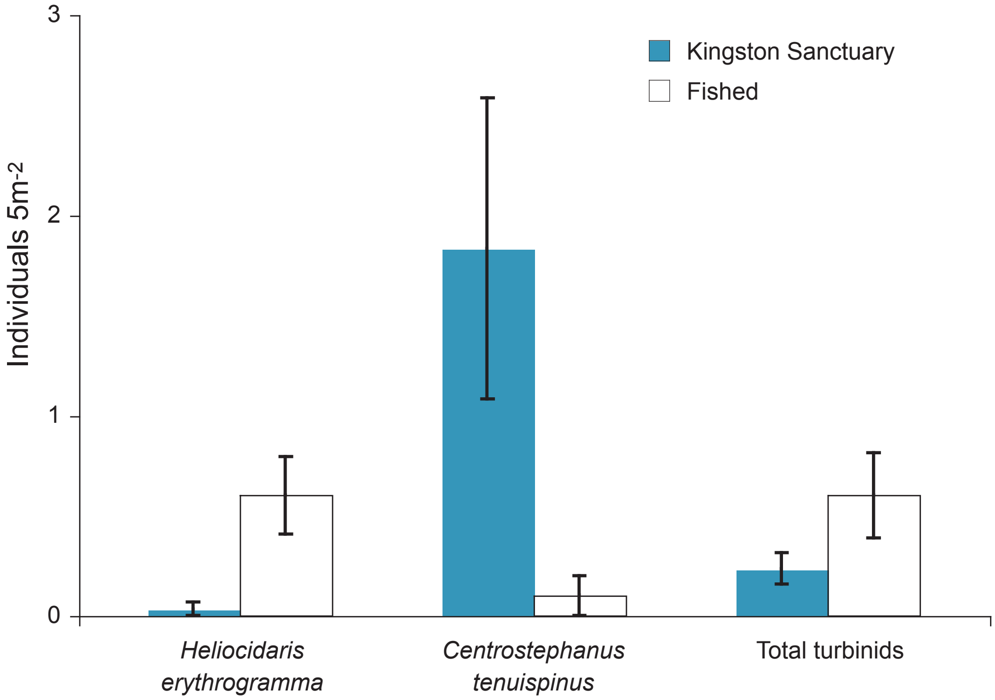

Figure 6.14: Abundance of the two main species of sea urchins, and of turbinid gastropods (± SE, n=30) inside and outside (Fished) the Kingston Sanctuary.

There was significant spatial variation in the species composition of reef algae at Rottnest island, but these spatial patterns explained little of the overall spatial variation (Global $R = 0.173$, $P = 0.007$). There was no significant overall difference in macroalgal composition between sanctuary and fished areas (Global R -0.552, $P = 1.00$). This result is visually evident in Fig. 6.15 in that quadrats from sanctuary and fished areas are well intermingled. There was significant clustering present within the data, but this compositional similarity, that corresponds to previously described habitats types that occur in patches on reefs throughout the region, was not spatiall correlated with conservation status.

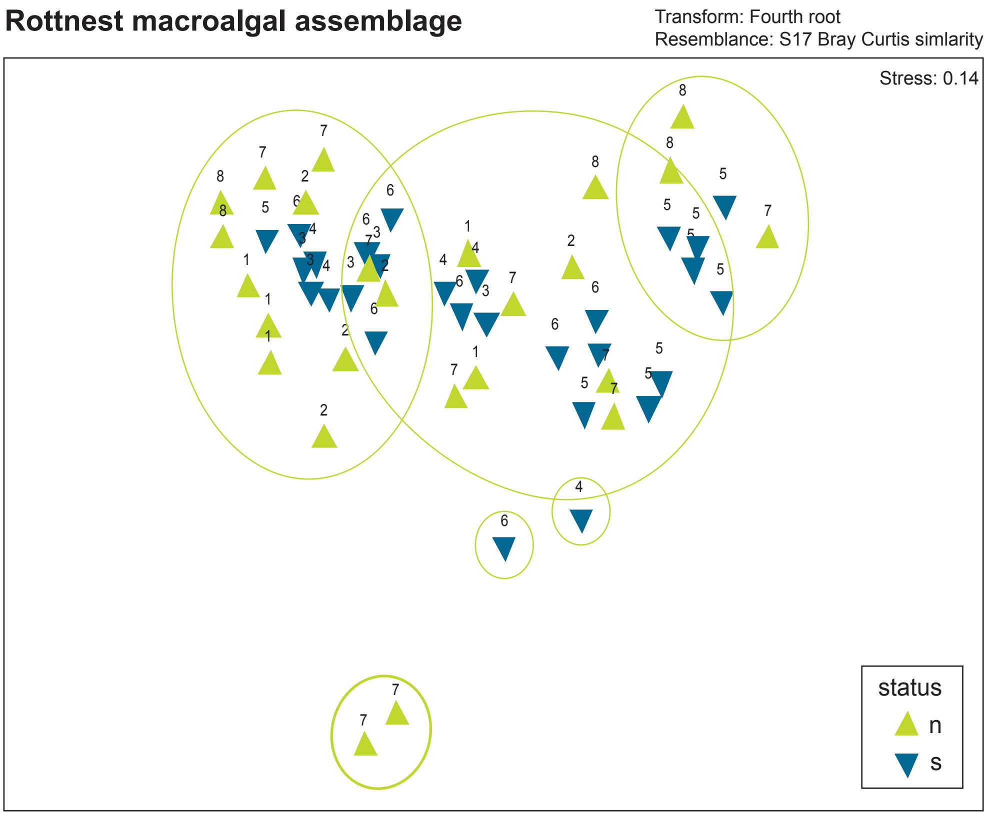

Figure 6.15: Non-metric multidimensional scaling ordination of sites at Rottnest Island based on species composition of assemblages of reef algae. There was no significant pattern related to conservation status, however there was significant clustering due to the presence of patches dominated by characteristic algal taxa E: *Ecklonia;* S: *Sargassum,* T: *"turf"*. The lines constrain clusters of quadrats with similarity values greater than 30%. n = non-sanctuary, s = sanctuary.

Discussion

SRFME research on benthic ecosystem dynamics incorporated the first quantitative, broad-scale investigations of the effects of several key ecological processes on the reef benthos of south-western Australia. Key general findings were that spatial gradients in wave exposure were significantly correlated with spatial patterns in the species richness and composition of macroalgae, that the rates of some ecological processes and the abundances of some fauna vary significantly between inshore and offshore reefs, and that consumers (including humans) might exert a significant influence on some reef-associated biota.

Physical disturbance by waves and cross-lagoon patterns in benthic patterns and processes

Using a model-based index of disturbance by wave action, we found evidence that biodiversity in assemblages of reef algae might be related to wave disturbance. Number of species per quadrat was highly correlated with orbital wave energy, and much of the variance in species composition could be explained by orbital wave energy. Wave energy decreases as waves are attenuated and diffracted by reefs, and this relationship provides another key explanatory variable that we used to test some aspects of assemblage structure. Importantly, accumulated wave exposure over an 8 year period provided a significantly better explanation of species patterns (number of species per quadrat) than wave energy over a single year (P. England unpublished data). This suggests that species richness of macroalgae might be the result of integration of processes occurring over years, as well as short-term responses to disturbance.

The consequences of wave action for an individual alga include detachment from the substrate on that it grows. Our research showed that, once detached, kelps may drift for many kilometres. Substantial accumulations of detached reef algae occurred at an inshore reef, coinciding with high densities of sea urchins, that mainly eat detached fragments of algae (Vanderklift & Kendrick 2005). Analyses of the morphology of individual kelps at this location indicate that a large proportion originate from the reefs several kilometres further offshore. A similar result was found by Kirkman & Kendrick (1997), who calculated that 78% of *Ecklonia radiata* tagged in Marmion Lagoon had been transported distances greater than 2 km. These results indicate that there are large-scale trophic linkages across the lagoon that are a result of wave action, and they imply even longer distance transport of this primary production both into and out of this area.

These linkages might have profound implications for how these ecosystems function at broad scales. For example, differences between inshore and offshore reefs were observed for densities of sea urchins (higher densities inshore) and grazing on drift kelp by sea urchins (higher inshore). This overall trend might be a result of the gradient in wave action as well as gradients in other ecological processes that occur due to physical disturbance by waves such as detachment and export of reef algae. Our measurements of rates of urchin recruitment to collectors indicated that while rates were higher inshore, they were highly variable. This suggests that densities of adult urchins inshore did not seem to be due to higher recruitment, but to the higher availability of food (drifting fragments of algae) and adult mobility.

Trends for primary productivity of *Ecklonia* were not consistent with predictions from the C:N ratios of *Ecklonia* radiata tissue (high C:N ratios indicate lower levels of available nitrogen). At a regional level, direct and indirect methods of estimating primary production (i.e. tagging of individual kelp and estimates based on biomass, respectively) indicated that productivity was greater at Jurien than in the Perth Region. In addition both methods found that productivity was higher offshore at Jurien, but not in the Perth Region. These results suggest that nitrogen *per se* might not be limiting for growth of macroalgae on this coast since these patterns are directly opposite to the C:N trends found in *Ecklonia* plants from these sites (see Chapter 5). The C:N values were far lower at Perth, than at Jurien — yet standing biomass (and most likely production; Coppertino *et al* 2005) was higher at Jurien. In addition, C:N ratios of kelps from both regions were lower inshore than offshore — yet production tended to be higher offshore, at least at Jurien. The most common paradigm for marine algae of all types is that their growth is nitrogen limited, yet our data contradict this assumption. The idea that availability of nitrogen might not be limiting growth of macroalgae requires investigation, and other potential influences on the rate of N uptake, such as light availability, and the role of wave-driven turbulence, must also be investigated.

Little of the *Ecklonia* primary productivity was directly consumed. The only direct grazing was by herbivorous fish. However, densities of herbivorous fish, and rates of grazing by herbivorous fishes, varied from reef to reef, and showed no broad trends. The highest rates of consumption of tethered kelps were on drifting fragments, and this was mainly due to sea urchins. This suggests that detached macroalgae play a key role in sustaining reef food webs. Together with observations that detached macroalgae are important in seagrass and intertidal habitats in the region (Lenanton & Caputi 1989, Wernberg *et al.* 2006), this further suggests that the importance of detached macroalgae in sustaining coastal food webs is prominent on this coast.

Trophic interactions and the potential for 'top-down' control of reef assemblages

Humans can exert a strong influence on the structure of communities through harvesting of key species. For example, in several parts of the world, hunting and fishing has reduced predators of sea urchins to ecologically trivial abundances, resulting in increases in sea urchin abundance, followed by landscape-scale decreases in canopy-forming primary producers due to grazing (Babcock *et al.* 1999, Estes *et al.* 2004). Similar processes are possible in WA, and are a potential explanation for variation in the structure of assemblages of reef algae. SRFME research included the first assessment of the effects of a 16-year fishing closure (the Kingston Sanctuary at Rottnest Island) on assemblages of fish and invertebrates. Researchers found that the overall abundance of fish, abundance of predatory fish and western rock lobster

(*Panulirus cygnus*) was higher inside the Kingston Sanctuary than at adjacent fished reefs. For fish the research found significant differences for two popular angling species and four bycatch species, while some bycatch species showed opposite patterns.

These differences in abundances of predatory fishes and lobsters were also reflected in patterns of predation on small and medium size invertebrates. The intensity of predation on tethered sea urchins was higher in the sanctuary. Thus the observed patterns in the relative rates of key processes were as expected given the differences in predator density. However, there were no simple trends in the abundances of prey: the abundance of prey species. One species of sea urchin (*H. erythrogramma*) was found at lower in the area protected from fishing, consistent with the pattern predicted if predation was a strong influence, but the abundance of a second species (*C. tenuispinus*) was higher in the area protected from fishing. Given the ambiguous findings for urchins, and the fact that *H. erythrogramma* is mainly a drift feeder (Vanderklift and Kendrick 2005), it is perhapst to be expected that there was no evidence of trophic cascade effects on algae occurring as a result of lower abundances of predators, with assemblages of macroalgae showing no difference in structure between the sanctuary and fished areas.

The experiments and observations at Kingston sanctuary were a complement to previous experiments that also addressed the potential for grazing urchins to influence benthic community structure. Even when densities of urchins were greatly increased above ambient densities, there was no measurable effect of urchins on benthic algal communities (Vanderklift and Kendrick 2005). This might be because the prominent herbivores in the system, sea urchins, rely on drifting macroalgae rather than attached macroalgae for food. In contrast the correlation between wave energy and both number of algal species per quadrat and community structure (Chapter 5) plus the heterogenous (patchy) nature of macroalgal assemblages suggests that physical disturbance may have stronger or much more pervasive and important influences on benthic communities than do top down effects resulting from variations in predation. Curiously, bottom-up effects (supply of nutrients) also appear to have less influence on the structure of benthic assemblages than might be predicted in what has been assumed to be a nutrient limited coastal ecosystem. The dynamics of patches and the influence of varying nutrient availability require more detailed investigation before we can be certain of how these factors interact with the dynamics of WA coastal ecosystems.

Acknowledgements

Nugzar Margvelashvili and Dirk Slawinski assisted with the wave modelling. Druime Nolan (CSIRO Graduate Fellowship), Julian Neurauter, Adrian Wiley, Lisa Moloney (Curtin University work experience program) and Grant Nosworthy (Tafe Work Experience program) helped process the settlement collectors.

References

Acosta, C.A. (2002). Spatially explicit dispersal dynamics and equilibrium population sizes in marine harvest refuges. *ICES Journal of Marine Sciences.* 59, 458-468.

Babcock RC, Kelly S, Shears NT, Walker JW, Willis TJ (1999) Changes in community structure in temperate marine reserves. *Mar. Ecol. Progr. Ser.* 189:125-134.

Bampfylde, C.J., Brown, N.D., Cavaghan, D.J., Maini, P.K. Modelling rainforest diversity: The role of competition. *Ecological Modelling* 188: 253-278.

Butler, M.J. IV, MacDiarmid, A.B., and Booth, J.D. (1999). The cause and consequence of ontogenetic changes in social aggregation in New Zealand spiny lobsters. *Mar. Ecol. Progr. Ser.* 188, 179-191.

Childress, M. J. and Hernkind W.F. (1997). Den sharing by juvenile Caribbean spiny lobsters (*Panulirus argus*) in nursery habitat: cooperation or coincidence? *Mar. and Freshw. Res.* 48**,** 751-758.

Chubb, C.F. (1994). Reproductive biology: Issues for management. In 'Spiny Lobster Management' (Eds B.F. Phillips, J.S. Cobb, J. Kittaka), pp. 181-212. (Blackwell Scientific Publications: London).

Chubb, C.F., Barker, E.H. (2003). The western rock lobster fishery 1997/98 to 1998/99. Fisheries research report no. 140 (Department of Fisheries: Western Australia). 47pp.

Chubb, C.F., Rossbach, M., Melville-Smith, R., Cheng, Y.W. (1999). Mortality, growth and movement of the western rock lobster. (*Panulirus cygnus*). Australian Fisheries Research and Development Corporation, Final Report of Project No 95/020. 42 pp. ISBN 0 7309 1936 6.

Connell, J.H. (1978). Diversity in tropical rainforests and coral reefs. *Science* 199: 1302-1310.

Copertino, M., Connell, S.D., Cheshire, A.D. (2005). The prevalence and production of turf-forming algae on a temperate subtidal coast. *Phycologia* 44: 241-248.

Denny, M., Gaylord, B., Helmuth, B., Daniel, T. (1998) The menace of momentum: Dynamic forces on flexible organisms. *Limnology & Oceanography* 43(5):955-968.

Department of Environmental Protection (1998) Environment Western Australia 1998: State of the Environment Report. Government of Western Australia, Perth.

Edgar, G.J. and Barrett, N.S. (1999). Effects of the declaration of marine reserves on Tasmanian reef fishes, invertebrates and plants *J. Exp. Mar. Biol. Ecol*. 242, 107-144.

Ellis, D.M. & DeMartini, E.E. (1995). Evaluation of a video camera technique for indexing abundances of juvenile pink snapper, *Pristipomoides filamentosus*, and other Hawaiian insular shelf fishes. *Fishery Bulletin* 93, 67-77.

Emmerson L.M. & Collings G.J. (1998) Macroalgal recruitment in artificially disturbed areas: interactive effects of temporal and spatial scale. *Mar. Freshw. Res.* 49:541-546.

Estes JA, Danner EM, Doak DF, Konar B, Springer AM, Steinberg PD, Tinker MT, Williams TM (2004) Complex trophic interactions in kelp forest ecosystems. *Bull. Mar. Sci.* 74:621-638.

Goldberg, N.A., Kendrick, G.A. (2004). Effects of island groups, depth, and exposure to ocean waves on subtidal macroalgal assemblages in the Recherche Archipelago, Western Australia. *Journal of Phycology* 40 (4): 631-641.

Goni, R., Renones, O., and Quetglas, A. (2001). Dynamics of a protected western Mediterranean population of the European spiny lobster *Palinurus elephas* (Fabricius, 1787) assessed by trap surveys. *Mar. Freshw. Res*. 52, 1577-1587.

Hall, N. and Chubb, C. (2001). The status of the western rock lobster, *Panulirus cygnus*, fishery and the effectiveness of management controls in increasing the egg production of the crop. *Mar. Freshw. Res*. 52, 1657-1667.

Hall, N., Cao, L., Chubb, C., Caputi, N, Cheng, H., Melville-Smith, R and Shanks, S. (2000). Modelling to explore management strategies to optimize the value of the rock lobster fishery of Western Australia. Australian Fisheries Research and Development Corporation, Final Report of Project No 97/104. 170 pp. ISBN 0 7309 8442 7.

Hemer, M.A. The magnitude and frequency of combined flow bed shear stress as a measure of exposure on the Australian continental shelf. *Continental Shelf Research* (In press).

IRC Environment. (2003). Western Rock Lobster Ecological Risk Assessment. 121 pp. (Department of Fisheries: Western Australia).

Kelly, S. Scott, D., Macdiarmid, A.B. Babcock, R.C. (2000). Spiny lobster, *Jasus edwardsii*, recovery in New Zealand marine reserves. *Biological Conservation*. 92, 359-369.

Kendrick, G.A., Lavery, P. J., Phillips, J.C., (1999). Influence of *Ecklonia radiata* kelp canopy on structure of macro-algal assemblages in Marmion Lagoon, Western Australia. *Hydrobiologia* 398/399: 275-283.

Kennelly, S.J. (1989) Effects of kelp canopies on understory species due to shade and scour. *Mar. Ecol. Progr. Ser.* 50:215-224.

Kirkman H, Kendrick GA (1997) Ecological significance and commercial harvesting of drifting and beach-cast macro-algae and seagrasses in Australia: a review. *J. Appl. Phycol.* 9:311-326

Kramer, D.L. and Chapman, M.R. (1999) Implications of fish home range size and relocation for marine reserve function. *Environmental Biology of Fishes*, 55, 65-79.

Lafferty, K. D., and D. Kushner. (2000). Population regulation of the purple sea urchin, *Strongylocentrotus purpuratus*, at the California Channel Islands. In 'Fifth California Islands Symposium' (Eds D. R. Brown, K. L. Mitchell, and H. W. Chang). Pp. 379-381. (Minerals Management Service: Santa Barbara, California).

Larned, S.T. Nitrogen- versus phosphorus-limited growth and sources of nutrients for coral reef macroalgae. (1998) *Mar. Biol.* 132 (3): 409-421.

Lenanton, R.C.G. & Caputi, N. (1989) The roles of food supply and shelter in the relationship between fishes, in particular *Cnidoglanis macrocephalus* (Valenciennes) and detached macrophytes in the surf zone of sandy beaches. *J. Exp. Mar. Biol. Ecol.* 128: 165-176.

Littell, R. C., Milliken, G. A., Stroup, W. W. & Wolfinger, R. D. (1996). 'SAS system for mixed models'. (SAS Inst. Inc.: North Carolina).

Lüning, K. (1990). *Seaweeds: Their Environment, Biogeography, and Ecophysiology*. Edited by C. Yarish and H. Kirkman. John Wiley & Sons, New York.

MacDiarmid, A.B. (1991). Seasonal changes in depth distribution, sex ration and size frequency of spiny lobster *Jasus edwardsii* on a coastal reef in northern New Zealand. *Mar. Ecol. Progr. Ser*. 70**,** 129-141.

Mayfield, S, Atkinson, L.J. and Branch, G.M. (2000). Reserves for rock lobsters: are they just a bureaucratic blunder? In '10th Southern African Marine Science Symposium (SAMSS 2000): Land, Sea and People in the New Millenium'. p.1.

McGarvey, R. (2003). Assessing the impact of proposed marine protected areas on South Australian Rock Lobster catches. Australian Fisheries Research and Development Corporation, Final Report of Project No 2000/195. 96 pp. ISBN 0 7308 5293 8.

Menge, B.A., Allison, G.W., Blanchette, C.A., *et al.* (2005). Stasis or kinesis? Hidden dynamics of a rocky intertidal macrophyte mosaic revealed by a spatially explicit approach. *J. Exp. Mar. Biol. Ecol.* 314 (1): 3-39.

Millar, R.B., Willis, T.J., (1999). Estimating the relative density of snapper in and around a marine reserve using a log-linear mixed effects model. *Australian and New Zealand Journal of Statistics* 41**,** 383-394.

Nevitt, G. Pentchett, N.D., Lohmann K.J., and Zimmer R.K. (2000). Den selection by the spiny lobster *Panulirus argus*: testing attraction to conspecific odors in the field. *Mar. Ecol. Progr. Ser.* 203**,** 225-231.

Parsons, D.M., Eggleston, D.B. 2005. Indirect effects of recreational fishing on behaviour of the spiny lobster *Panulirus argus. Mar. Ecol. Progr. Ser.* 303**,** 235-244.

Ris, R.C., Holthuijsen, L.H., Booij, N., (1994). A spectral model for waves in the near shore zone. Proceedings of the 24th International Conference on Coastal Engineering, Kobe, Japan, pp. 68-78.

Roberts CM, McClean CJ, *et al.* (2002) Marine biodiversity hotspots and conservation priorities for tropical reefs. *Science* 295, 1280-1284.

Rowe, S. (2002). Population parameters of American lobster inside and outside no-take reserves in Bonavista Bay, Newfoundland. *Fisheries Research* 56, 167-175.

Russ, G.R. (2002). Marine Reserves as reef fisheries management tools: yet another review. In 'Coral Reef Fishes: Dynamics and Diversity in a complex system'. (Ed P.F. Sale). pp 421-443. (New York USA: Academic Press).

Shea, K., Roxbourgh, S.H., Rauschert, E.S.J. (2004). Moving from pattern to process: coexistence mechanisms under intermediate disturbance regimes. *Ecology Letters* 7: 491-508.

Stewart, H.L., Carpenter, R.C. (2003). The effects of morphology and water flow on photosynthesis of marine macroalgae. *Ecology* 84 (11): 2999-3012.

Thomsen, M.S., Wernberg, T. Kendrick, G.A. (2004). The effect of thallus size, life stage, wave exposure and substratum conditions on the forces required to break or dislodge the small kelp *Ecklonia radiata*. *Botanica Marina* 47: 454-460.

Tilman, D. (1994). Competition and biodiversity in spatially structured habitats. *Ecology* 75(1):2-16.

Vanderklift MA, Kendrick GA (2005) Contrasting influence of sea urchins on attached and drift macroalgae. *Mar. Ecol. Progr. Ser.* 299:101–110.

Wernberg T, Vanderklift MA, Lavery PS, How J (2006) Export of detached macroalgae from reefs to adjacent seagrass beds. *Oecologia* 147:692-701

Willis, T.J., Millar, R.B. & Babcock, R.C. (2000). Detection of spatial variability in relative density of fishes: Comparison of visual census, angling, and baited underwater video. *Mar. Ecol. Progr. Ser.* 198, 249-260.

Willis, T.J., Millar, R.B. & Babcock, R.C. (2003). Protection of exploited fish in temperate regions: high density and biomass of snapper *Pagrus auratus* (Sparidae) in northern New Zealand marine reserves. *Journal of Applied Ecology* 40, 214-227.

Willis, T.J., Millar, R.B., Babcock, R.C. and Tolimieri, N. (2003). Burdens of evidence and the benefits of marine reserves: putting Descartes before des horse? *Environmental Conservation* 30**,** 97-103.

Wilson BR, Allen GR (1987) Major components and distribution of marine fauna. In Fauna of Australia. Volume 1A. General articles. pp. 43-68. (Australian Government Publishing Service: Canberra).

Zann LP (1995) Our sea, our future: major findings of the State of the Marine Environment Report for Australia. Great Barrier Reef Marine Park Authority, Townsville.

CHAPTER 7

7. VISUALISATION AND DATA DELIVERY

Investigators / Institution

Jason Waring, Hiski Kippo and Irshad Nainar

CSIRO Marine and Atmospheric Research

7.1 Introduction

Recognising the importance of data archiving and data accessibility, SRFME has developed software tools that will allow WA marine managers, and the broader researcher community to interactively explore and visualise SRFME datasets and datasets from other projects. The four products that have been developed are:

- Argo website
- Aus-Connle website
- WebOLIVE
- Data Interrogation and Visualisation Environment

Data Management Functions

- To maintain the existing SRFME database and extend to support new types of observational and modelled datasets.
- To develop web tools to allow the Research Scientists to directly import data into the database.

The SRFME database can be found at:

SRFME-DB (http://www.marine.csiro.au/datacentre/srfme)

- This relational database contains a quality controlled observational and modelled dataset created as part of the SRFME project.

Argo website

The Argo website provides an interactive data explorer to display tracks and vertical profiles from over 100 Argo vertical profiling floats which have been deployed in the Indian and Southern Oceans (see Fig. 7.1).

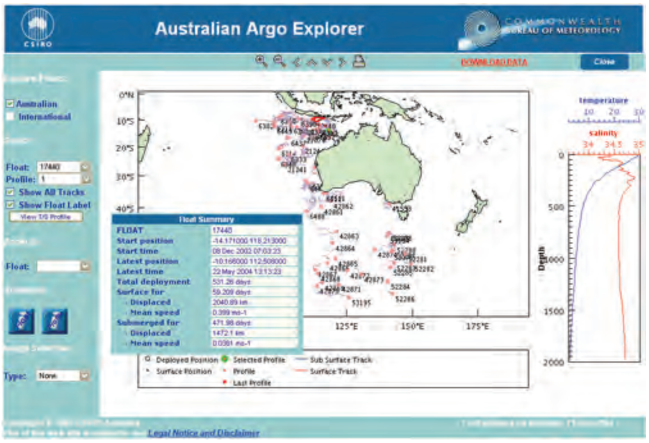

Float Summary	
FLOAT	17440
Start position	-14.171000 118.213000
Start time	08 Dec 2002 07:03:23
Latest position	-10.166000 112.508000
Latest time	22 May 2004 13:13:23
Total deployment	531.26 days
Surface for	59.209 days
- Displaced	2040.89 km
- Mean speed	0.399 ms-1
Submerged for	471.98 days
- Displaced	1472.1 km
- Mean speed	0.0361 ms-1

Fig. 7.1: The ARGO web explorer showing the drift tracks of over 100 floats.

The Argo website is located at http://www.per.marine.csiro.au/argo. It builds on a pre-existing website developed as part of the *Cooperative Ocean Observing Experiment* (COOE). The Argo website was developed under a collaborative agreement with the Bureau of Meteorology.

Aus-ConnIe website

The *Australian Connectivity Interface* (Aus-ConnIe) is a web-based tool developed to allow environmental scientists and managers to investigate the large-scale patterns of spatial connectivity around Australia (see Figs 7.2 and 7.3). It provides the user with an estimate of the probability that any two regions are connected by ocean circulation over a specified dispersion period (10, or 20 days for monthly averaging or 30, 40, 60 or 80 days for quarterly averaging). It is expected to find applications in areas such as larval dispersion and recruitment studies, and the development of scenarios and risk assessments for contaminant dispersion.

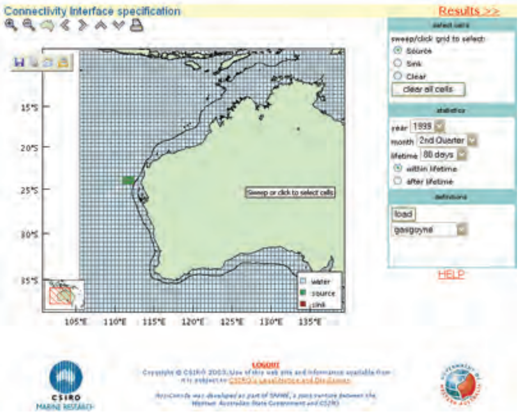

sweep/click grid to select:
● Source
○ Sink
○ Clear

year 1999
month 2nd Quarter
lifetime 80 days
● within lifetime
○ after lifetime

gascoyne

Fig. 7.2: Aus-ConnIe specification page – Selected source cells are shown in dark-green

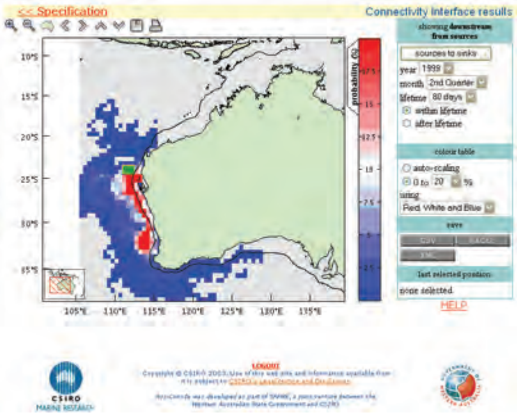

showing **downstream from sources**

year 1999
month 2nd Quarter
lifetime 80 days
● within lifetime
○ after lifetime

○ auto-scaling
● 0 to 20 %
using
Red, White and Blue

last selected position
none selected

Fig. 7.3: Aus-ConnIe results page. Note the Leeuwin current.

The *Aus-ConnIe* website is located at http://www.per.marine.csiro.au/aus-connie. Aus-ConnIe builds on the *JEMS-ConnIe* website developed as part of the *North West Shelf Joint Environmental Management Study* (NWSJEMS).

WebOLIVE

WebOLIVE is a web-based visualisation tool developed to allow users to explore gridded datasets (such as hydrodynamic model output and climatology atlases) using a standard web browser. Features include the ability to visualise selected variables for a given time and depth as coloured, contoured or vector maps, as well as interactively select a time-series and vertical profile for a specific location. Some controls are provided to permit refinement of the graphics (e.g. colour ranges and colour tables).

WebOLIVE has been integrated into the SRFME modelling website, allowing users to explore the CARS climatology and hydrodynamic model datasets (see Fig 7.4).

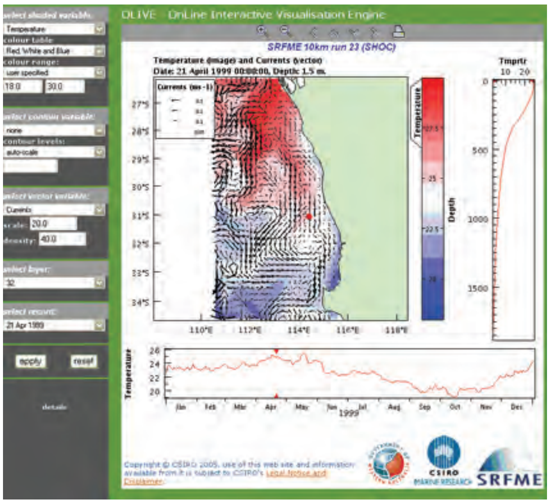

select shaded variable: Temperature
colour table: Red, White and Blue
colour range: user specified
18.0 30.0
select contour variable: none
contour levels: auto-scale
select vector variable: Currents
scale: 20.0
density: 40.0
select layer: 32
select record: 21 Apr 1999

Fig. 7.4: Hydrodynamic model output displayed using WebOLIVE

Data Interrogation and Visualisation Environment (DIVE)

A large number of datasets have been accumulated within SRFME through field programs, remote sensing and numerical model runs. Not only are these datasets large in volume but they are also diverse in nature. They range from 1-dimensional point data (e.g. species biomass) to 4-dimensional time-varying volumetric datasets (e.g. model output).

These large diverse datasets are not easily understood without the aid of visualisation tools. A web enabled graphical tool would be the most effective means of delivering the data to our partners and collaborators.

The *Data Interrogation and Visualisation Environment* (DIVE) is a graphical tool to interactively explore and visualise these diverse datasets. It provides users with the ability to view and inter-compare datasets in space and time (e.g. Fig 7.5). DIVE supports the display of data as spatial maps, time-series plots and vertical profiles. The spatial data is represented as coloured maps, contoured plots, vector arrows, or as habitat maps (Fig 7.6).

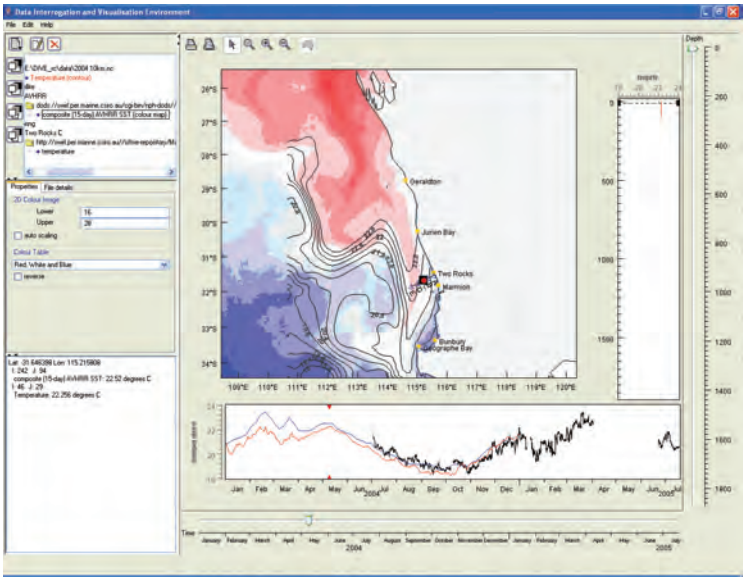

```
Lat: -31.646398 Lon: 115.215808
 I: 242  J: 94
 composite (15-day) AVHRR SST: 22.52 degrees C
 I: 46  J: 29
 Temperature: 22.256 degrees C
```

Fig. 7.5: Comparison of Remote Sensing, Hydrodynamic model output & data from moored instrument

DIVE has the capability to access datasets stored in the SRFME data repository. It allows for data residing remotely on the repository to be visualised and downloaded.

DIVE support the following file formats:

- NetCDF files that conform to commonly used formats within the oceanographic community such as COARDS, CF-1.0, etc.
- ASCII files conforming to the CMAR Column File Format (CFF). This format was designed specifically to capture observational datasets such as vertical profiles and time-series.
- ASCII files conforming to the CMAR Shape File Format (SFF). This format was designed to flexibly define geometric shapes.
- Shape files conforming to the ESRI shapefile format.

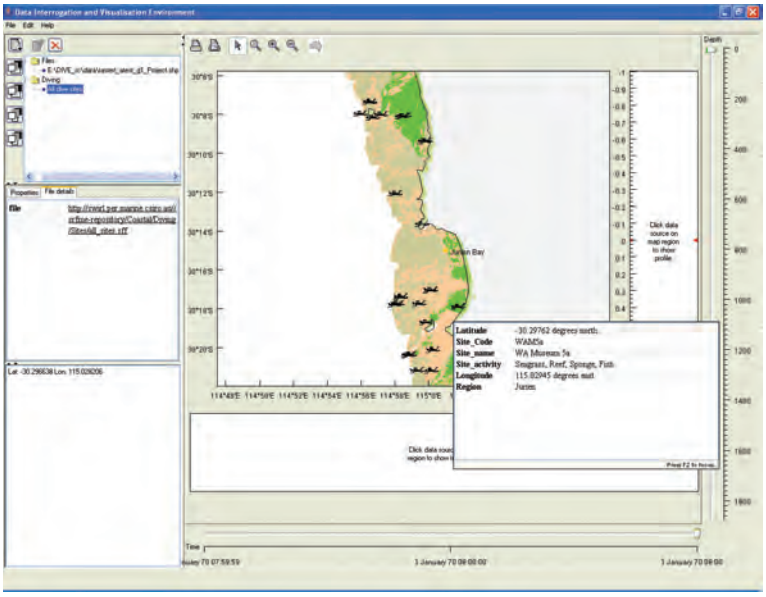

```
Latitude       -30.29762 degrees north
Site_Code      WAM5a
Site_name      WA Museum 5a
Site_activity  Seagrass, Reef, Sponge, Fish
Longitude      115.02945 degrees east
Region         Jurien
```

Fig. 7.6: Habitat map of Jurien bay with dive sites overlaid

DIVE supports the following types for data-streams:

- Model outputs
  - –Hydrodynamic model
  - –Biogeochemical model
  - –Wave model
- Climatological datasets.
- Remote sensing data.
  - –AVHRR datasets
  - –SeaWIFS datasets
- Benthic habitat data.
- Underway time-series data (Fig 7.7).
- Temperature/salinity profile data (CTD casts) (Fig 7.7).
- Data measured by moored instruments.

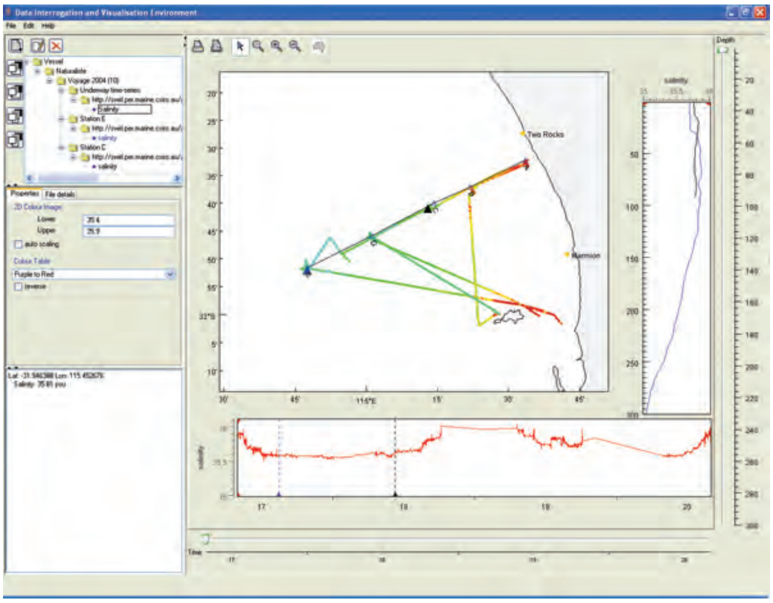

Lower 35.4
Upper 35.9

Fig. 7.7: Underway time-series & vertical profiles

DIVE provides a hierarchical view of the datasets in the SRFME data repository. The navigation model employed within DIVE allows the data to be accessed using different views (Fig 7.8). Currently DIVE supports three types of views:

- *Platform* view – This view lists the platforms used for data collection. Selecting a platform and navigating through its hierarchy displays the datasets associated with that platform.
- *Device* view - This view lists the devices and instruments used for the data collection. Selecting a device and navigating through its hierarchy displays the datasets associated with that device.
- *Data-stream* view - This view lists the different streams of data that has been collected. Selecting a data-stream and navigating through its hierarchy displays the datasets that conform to that stream.

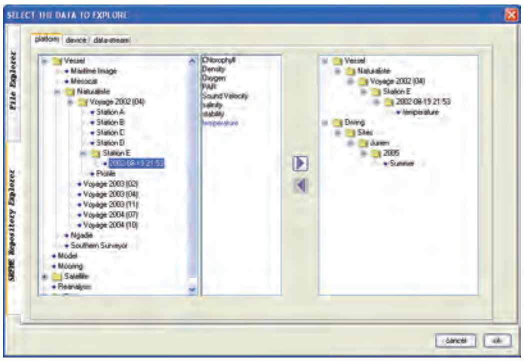

Fig. 7.8: Data Selection Dialog in DIVE

7.2 Data Repository

Data Management Overview

The SRFME program has generated data from a wide range of sources, disciplines and organizations that has resulted in the assembly of a multitude of data formats and data types.

To manage these data sets, a data repository was established that served as a central data distribution point and is supported by a repository web site (http://www.marine.csiro.au/datacentre/srfme/) and a publicly accessible metadata tool called MarLIN (http://www.marine.csiro.au/marlin/). MarLIN is linked to both the Australian Spatial Data Directory and Ocean Biogeographic Information System (OBIS). Both these external metadata search services provided international online access to SRFME metadata records. Metadata records are published in the public domain, while access to datasets in the data repository and the SRFME data repository web site are restricted to SRFME participants only.

Data Repository

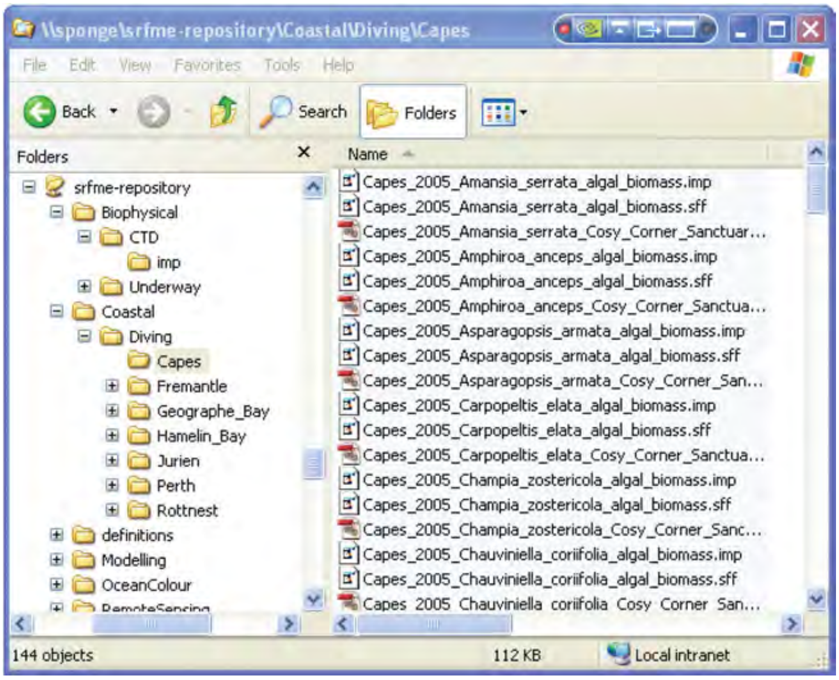

Fig 7.9 Data repository structure

The data repository is mounted on a CSIRO divisional computer with appropriate firewall restrictions to limit access to SRFME participants only. The repository consists of a directory structure that mirrors the major project components of the SRFME program.

To maintain the integrity of data, only data that has been quality assured by scientific staff is included in the repository. Quality standards are maintained by and are the responsibility of individual projects.

Data Repository Integration with DIVE

The DIVE visualization tool provides a flexible method of viewing data sets from three perspectives based on platform, device and data-stream. DIVE utilises a MySQL data base (SRFMEDB) to serve datasets from the SRFME data repository based on DIVE generated database queries. Data is then displayed appropriately as graphical layers based on the type of data.

Tools written in the Java programming language were developed to simultaneously validate and load standard data sets into SRFMEDB.

Figure 7.10 illustrates the main components that constitute the SRFME data management system.

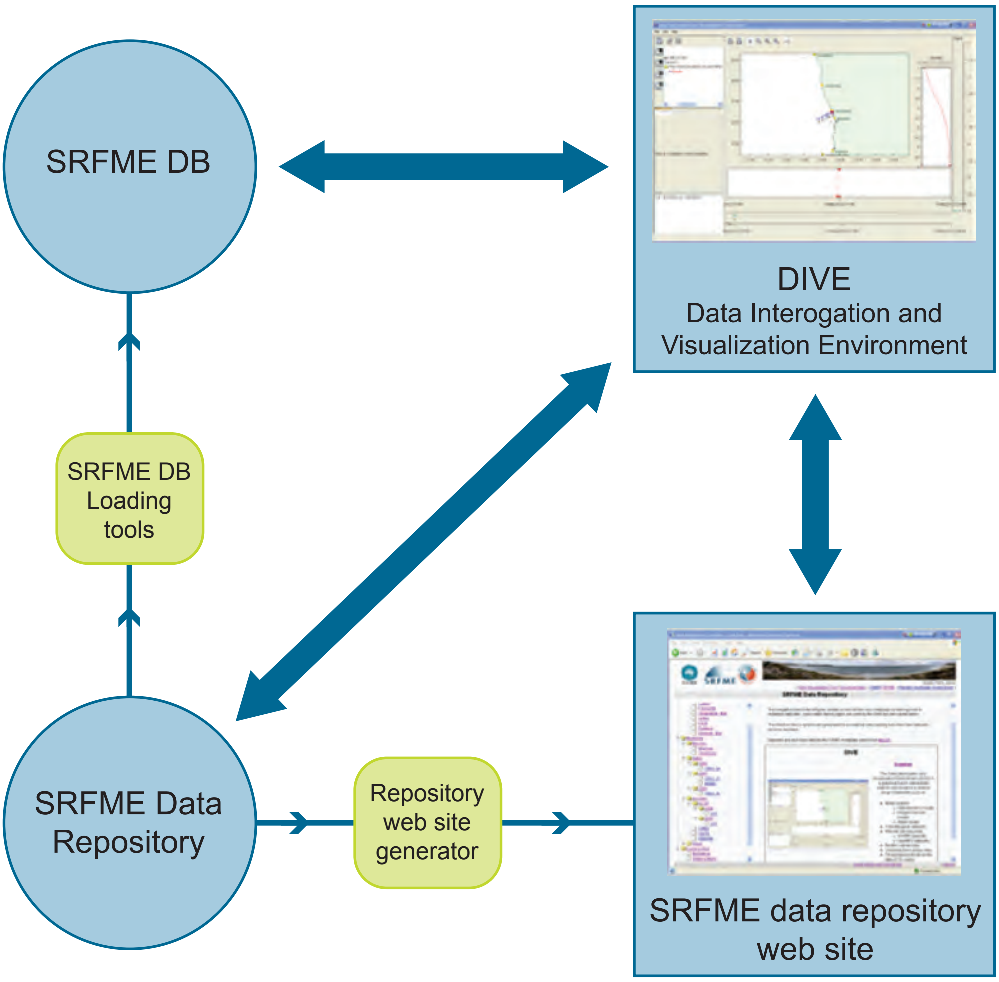

Fig 7.10 Data repository tools

To facilitate the operation of DIVE, data was converted to one of three standard formats as described in Table 7.1

Table 7.1 Standard file types used by DIVE

Data Type	Description	File extension
Column File Format (CFF)	A text based tabular file including a metadata header Ref: http://www.per.marine.csiro.au/srfme-repository_dev/docs/CMAR-CFF-v2.pdf	.cff
Network Common Data Format (NetCDF)	A machine-independent format for representing scientific data. Ref: http://www.unidata.ucar.edu/software/netcdf/docs/	.nc
Shape File Format (SFF)	Two-dimensional geo-referenced point, polyline, graph and grid geometric data as ASCII text http://www.per.marine.csiro.au/srfme-repository_dev/docs/CMAR-SFF-v3.doc	.sff

Data Repository Metadata

Metadata for datasets is located within each directory of the data repository, and is accessible via DIVE and from the Data Repository website.

A comprehensive metadata set is maintained within the SRFME Data Repository website (Fig. 7.11). This metadata set is ANZLIC compliant and is also registered within the CMAR metadata tool MarLIN (http://www.marine.csiro.au/marlin).

Through the use of the MarLIN metadata data base, SRFME metadata records are searchable through the Australian Spatial Data Directory (http://asdd.ga.gov.au/) and OBIS Australia (http://www.obis.org.au/). Access to SRFME metadata records is also possible through the international OBIS site (http://www.iobis.org/).

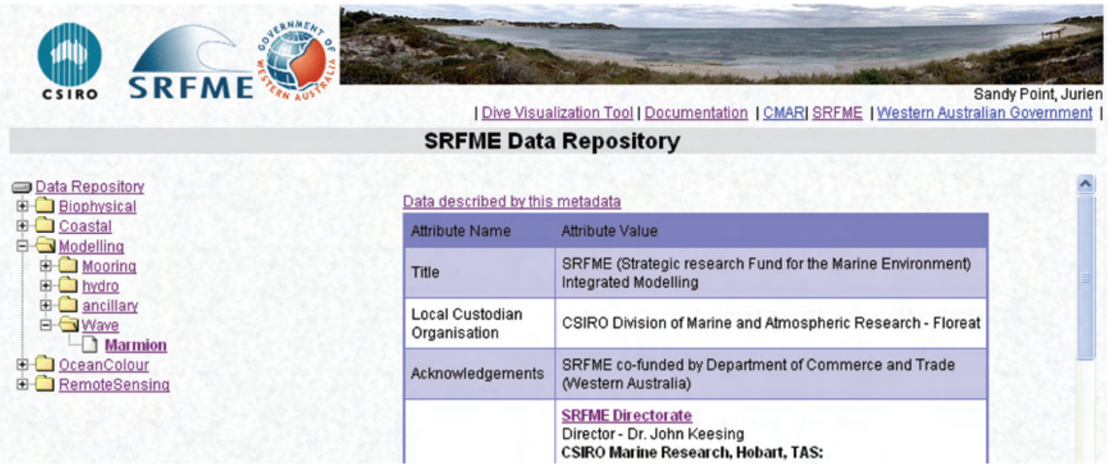

SRFME Data Repository

Data described by this metadata

Attribute Name	Attribute Value
Title	SRFME (Strategic research Fund for the Marine Environment) Integrated Modelling
Local Custodian Organisation	CSIRO Division of Marine and Atmospheric Research - Floreat
Acknowledgements	SRFME co-funded by Department of Commerce and Trade (Western Australia)
	SRFME Directorate Director - Dr. John Keesing **CSIRO Marine Research, Hobart, TAS:**

Fig 7.11 SRFME data repository web site showing metadata

ISBN 1 921061 92 8

SRFME is a joint venture between CSIRO and the Western Australian government

Wealth from Oceans
NATIONAL RESEARCH
FLAGSHIPS

CSIRO

Department of
Fisheries

Fish for the future

Department of
Environment and Conservation

Department of
Industry and Resources